

Design, Synthesis and Applications of new cationic ligands of the 15th main group elements

Dissertation

zur Erlangung des mathematisch-naturwissenschaftlichen Doktorgrades

"Doctor rerum naturalium"

der Georg-August-Universität Göttingen

im Promotionsprogramm Chemie

der Georg-August University School of Science (GAUSS)

vorgelegt von

Hendrik Tinnermann

aus Ahlen

Göttingen, 2017

Betreuungsausschuss:

Prof. Dr. Manuel Alcarazo (Institut für Organische und Biomolekulare Chemie, Tammannstr. 2, 37077 Göttingen)

Prof. Dr. Dietmar Stalke (Institut für Anorganische Chemie, Tammannstr. 4, 37077 Göttingen)

Mitglieder der Prüfungskommission:

Referent: Prof. Dr. Manuel Alcarazo (Institut für Organische und Biomolekulare Chemie, Tammannstr. 2, 37077 Göttingen)

Korreferent: Prof. Dr. Dietmar Stalke (Institut für Anorganische Chemie, Tammannstr. 4, 37077 Göttingen)

Weitere Mitglieder der Prüfungskommission:

Prof. Dr. Franc Meyer (Institut für Anorganische Chemie, Tammannstr. 4, 37077 Göttingen)

Prof. Dr. Sven Schneider (Institut für Anorganische Chemie, Tammannstr. 4, 37077 Göttingen)

Dr. Shoubhik Das (Institut für Organische und Biomolekulare Chemie, Tammannstr. 2, 37077 Göttingen)

Dr. Franziska Thomas (Institut für Organische und Biomolekulare Chemie, Tammannstr. 2, 37077 Göttingen)

Hiermit versichere ich, dass ich die eingereichte Dissertation selbständig erfasst und keine anderen als die angegebenen Quellen und Hilfsmittel benutzt, sowie Zitate kenntlich gemacht habe.

(Ort, Datum)

(Unterschrift)

Die vorliegende Arbeit entstand unter Anleitung von Herrn. Prof. Dr. Manuel Alcarazo in der Zeit von November 2012 bis Dezember 2015 am Max-Planck-Institut für Kohlenforschung in Mülheim an der Ruhr und in der Zeit von Januar 2016 bis September 2016 an der Georg-August-Universität zu Göttingen. Diese Arbeit wurde in folgenden Beiträgen veröffentlicht:

H. Tinnermann, C. Wille, M. Alcarazo, *Angew. Chem. Int. Ed.* **2014**, *33*, 8732.

E. Haldón, Á. Kozma, H. Tinnermann, L. Gu, R. Goddard, M. Alcarazo, *Dalton Trans.* **2016**, *45*, 1872.

~ für meine Eltern ~
Danke für die Unterstützung und
die Geduld in allen Lebenslagen

Danksagung

Mein herzlichster Dank gilt Prof. Dr. Manuel Alcarazo für die Aufnahme in seinen Arbeitskreis und die Vergabe des interessanten Promotionsthemas. Des Weiteren danke ich Prof. Manuel Alcarazo für seine große Hilfe, die mir erlaubte mich sowohl auf fachlicher und persönlicher Ebene stark zu entwickeln. Ich bin zutiefst dankbar für all die Motivation zu der Prof. Dr. Manuel Alcarazo angeregt hat, sowie für seine kompetente Beratung. Herrn Prof. Dr. Manuel Alcarazo und Herrn Prof. Dr. Dietmar Stalke danke ich für die freundliche Übernahme des Referats und Koreferats.

Weiterhin möchte ich der Max-Planck-Gesellschaft und im Besonderen dem Max-Planck-Institut für Kohlenforschung, sowie der Georg-August Universität zu Göttingen für die Bereitstellung meines Arbeitsplatzes und die finanzielle Unterstützung danken.

Allen Mitgliedern der Arbeitsgruppen Fürstner und Alcarazo danke ich für die gute Zusammenarbeit, das angenehme Arbeitsklima und die schönen Stunden innerhalb und außerhalb des Laboralltags. In den vielen gemeinsam verbrachten Laborstunden seid Ihr mir alle ans Herz gewachsen, vielen Dank dafür. Für die in Mülheim verbrachte Zeit möchte ich mich besonders bei Sigrid Holle, Gerlinde Mehler, Agnes Kozma, Elisa Gonzales, Christian Wille und Angus Rocha für die großartige Arbeitsatmosphäre sowie für Ihre Hilfsbereitschaft bedanken. Für die große Hilfe bei organisatorischen Angelegenheiten danke ich recht herzlich Frau Lickfeld. Für die in Göttingen verbrachte Zeit möchte ich mich besonders bei Kai Aversch und Katja Grube aus meinem Labor sowie allen weiteren Mitgliedern der Arbeitsgruppe bedanken. Mein Dank geht an die Mitarbeiter aller analytischen Abteilungen für die zuverlässige und schnelle Durchführung und Auswertung zahlreicher Analysen. Besonders bedanke ich mich bei Herrn Kochius, Herrn Dr. Farès aus der NMR-Abteilung, bei Herrn Kampen, Frau Blumenthal und Herrn Klein aus der MS-Abteilung. Prof. Dr. Christian W. Lehmann, Dr. Richard Goddard, Jörg Rust, Nils Nöthling, Herrn Dr. Mondal, Frau Dreier, Frau Schucht und Frau Dreher aus der Kristallographie-Abteilung möchte ich besonders für die herzliche und angenehme Atmosphäre während meines Aufenthalts danken. Mein Dank geht an die Mitarbeiter der theoretischen Abteilung für die gute Berechnung und hilfreichen Informationen zur Aufklärung der Mechanismen. Besonders bedanke ich mich bei Dr. Yiyang Zheng und Prof. Walter Thiel. Für umfangreiche Cyclovoltammetrie- Messungen möchte ich mich des Weiteren bei Herrn Christian Wille und Herrn Leo Nicholls aus der Arbeitsgruppe Alcarazo bedanken.

Für das gründliche Korrekturlesen danke ich Prof. Manuel Alcarazo, Dr. Christophe Werlé und Kai Aversch. Ich möchte allen Freunde besonders für die gemeinsam verbrachte Zeit in Mülheim und in Göttingen danken. Auch möchte ich mich bei meiner Familie für die Unterstützung in allen Lebenslagen bedanken.

We are indeed a blind race, and the next generation, blind to its own blindness, will be amazed at ours.

- Lancelot Law Whyte, *Accent on Form: An Anticipation of the Science of Tomorrow* **1955**, 33.

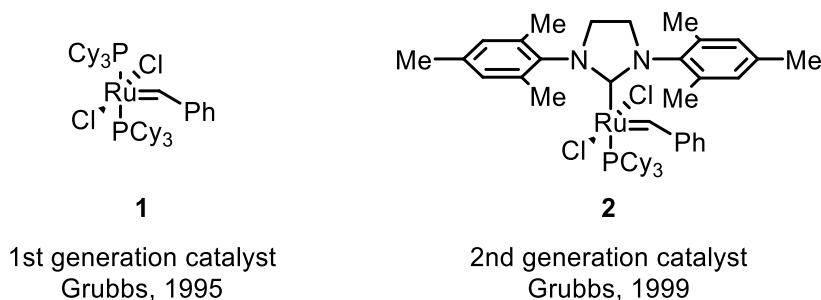
Table of contents

1. The importance of ligand design in catalysis	14
<u>1.1 Utility of phosphines in ligand design</u>	
2. Ligand design in π-acid catalysis	22
<u>2.1 Generalities, mechanism and scope</u>	
<u>2.2 Influence of the ancillary ligand in π-acid catalysis</u>	
<u>2.3 Applications of phosphines in π-acid catalysis</u>	
3. Ligand design in Cross Coupling Reactions	33
<u>3.1 Generalities, mechanism and scope</u>	
<u>3.2 Influence of the ancillary ligand in cross coupling reactions</u>	
<u>3.3 Application of phosphines in cross coupling reactions.</u>	
4. A new strategy to modify the donor properties of phosphines	40
<u>4.1 α-monocationic phosphines</u>	
<u>4.2 α-polycationic phosphines</u>	
<u>4.3 Evaluation of the stereo electronic properties</u>	
<u>4.4 Applications of cationic phosphines</u>	
5. Motivation	59
6. Objective	60
7. Results and Discussion	61
<u>7.1 Synthesis of pyridinium phosphines</u>	
<u>7.2 Synthesis of metal complex derivatives</u>	
<u>7.3 Applications in catalysis</u>	
<u>7.4 Applications of other cationic ligands in catalysis</u>	
8 Synthesis, structure and applications of arene pyridinium phosphines	88
<u>8.1 Strategies for the synthesis of N-aryl substituted pyridinium phosphines</u>	
<u>8.2 Synthesis of gold complexes</u>	
<u>8.3 Applications in gold catalysis</u>	
<u>8.4 Applications in palladium chemistry</u>	
9. Summary and Outlook	113
10. Experimental Part	114
<u>10.1 General procedures</u>	
<u>10.2 Experimental procedures and characterizations</u>	
<u>10.3 Solid State Structures</u>	

1. The importance of ligand design in catalysis

Ligands significantly alter the properties of the metals they coordinate. Therefore, ligand design can have an enormous impact on the selectivity and reactivity of a given transformation and consequently, has found broad applications in the synthesis of new molecules and materials. The design of new ligand structures and their applications in metal catalysis can even enable completely new reactivities or selectivities. Amongst other prominent examples are the Grubbs catalysts for olefin metathesis, awarded with the Nobel Prize in 2005 (together with Schrock and Chauvin).¹

The Grubbs catalysts are a great example of the importance of ligand design in catalysis. While the first well defined Grubbs catalyst was prepared 1992 from $\text{RuCl}_2(\text{PPh}_3)_4$ and diphenylcyclopropene, its low accessibility limited its use.² Therefore, the first generation Grubbs³ catalyst **1** has been developed that is accessible in an easy one pot synthesis starting from $\text{RuCl}_2(\text{PPh}_3)_4$, phenyldiazomethane and tricyclohexylphosphine. This catalyst is already highly stable towards air and compatible with a broad range of functional group. However, due to the low life time of the catalyst ring closing reaction for larger ring sizes only limited conversions were observed.⁴ Therefore Grubbs further exploited ligand design to accelerate the activation of the catalyst that proceeds via dissociation of one phosphine moiety. Substituting one phosphine with a cyclic bis-amino carbene ligand increased the dissociation rate of the remaining phosphine unit and therefore the metathesis activity, leading to the nowadays most used metathesis catalyst **2**⁵



Scheme 1: ligand designs by Grubbs.

This pronounced effect of ligand design - here shown with the development of Grubbs 2nd generation catalyst - towards the reactivity and selectivity of any metal catalysed reaction fostered the development of a broad range of different ligand classes as well as many

¹ "The Nobel Prize in Chemistry 2005". *Nobelprize.org*. Nobel Media AB 2014. Web. 24 Apr 2017. <http://www.nobelprize.org/nobel_prizes/chemistry/laureates/2005/>

² S. T. Nguyen, L. K. Johnson, R. H. Grubbs, J. W. Ziller, *J. Am. Chem. Soc.* **1992**, *114*, 3974.

³ P. Schwab, M.B. France, J.W. Ziller, R.H. Grubbs, *Angew. Chem., Int. Ed.* **1995**, *34*, 2039.

⁴ P. Schwab, R.H. Grubbs, J.W. Ziller, *J. Am. Chem. Soc.* **1996**, *118*, 100.

⁵ M. Scholl, T.M. Trnka, J.P. Morgan, R.H. Grubbs, *Tetrahedron Lett.* **1999**, *40*, 2247.

variations within the ligand class. Nowadays a number of ligands have been developed, outstanding examples being the ligand design of carbenes and of phosphines.

1.1 Utility of phosphines in ligand design

The phosphines advanced as a ligand class of high importance, because they can easily be prepared and modulated. This modularity allows the ligands to control the steric and electronic properties of the metals they coordinate, therefore, enabling control over selectivities and yields of a vast number of different transformations. One of the most common examples of phosphines being the triphenylphosphine, which is applied in all fields of catalysis for example in π -acid catalysis as well as in cross coupling reactions. Another positive aspect that proved beneficial from a synthetic point of view was the possibility to examine the phosphines by simple ^{31}P NMR to ensure any modifications made. Phosphines obviously allow to be tuned in their electronic and steric parameters and this high modularity has been used to optimize the ligands in several processes, either to increase or to deplete the electron density of the metal or to modulate its steric environment.

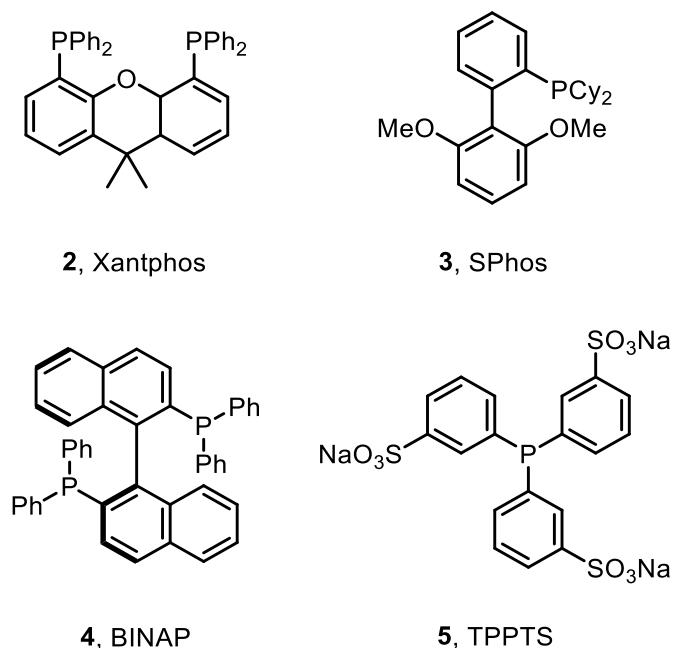
Prominent examples are amongst others:

- Xantphos (**2**)⁶, ensuring a coordination mode between *cis* and *trans*,
- Buchwald's ligands, (e.g. SPhos **3**), highly efficient in palladium catalysed aminations,
- BINAP (**4**)⁷, used by Noyori as catalyst for asymmetric hydrogenations, and
- TPPTS (**5**)⁸, used for hydroformylation in the Ruhrchemie/Rhône-Poulenc-process.

⁶ M. Kranenburg, Y. E. M. van der Burgt, P. C. J. Kamer, P. W. N. M. van Leeuwen, K. Goubitz, J. Fraanje, *Organometallics* **1995**, *14*, 3081.

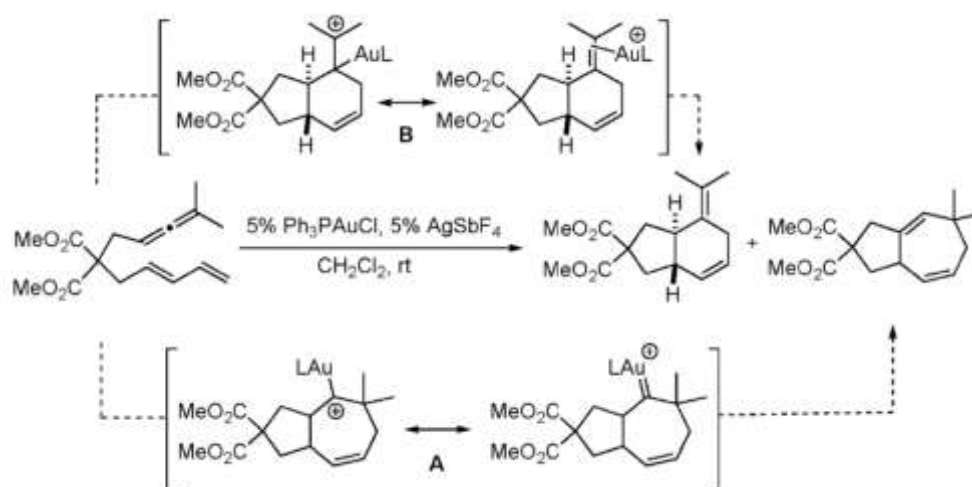
⁷ A. Miyashita, A. Yasuda, H. Takaya, K. Toriumi, T. Ito, T. Souchi, R. Noyori, *J. Am. Chem. Soc.* **1980**, *102*, 7932.

⁸ W. A. Herrmann, C. W. Kohlpaintner, *Inorg. Synth.* **1998**, *32*, 8.



Scheme 2: prominent phosphines.

The possibility to tune the stereo electronic properties of phosphines increases their importance and utility in a number of transformations: For example if ligands with high π -accepting properties are needed, instead of phosphines, phosphite or polyfluorinated phosphines can be used to improve yields and selectivities. For example Toste *et al.*⁹ reported the use of a phosphite ligands in a highly selective Au-catalysed [4+2] cycloaddition in excellent yields. The enhanced π -accepting properties of the phosphite decrease the stability of the carbocation intermediate **A** of the competing [4+3] cycloaddition, therefore improving the selectivity (100:0) and the yield (91%) of the [4+2] process.

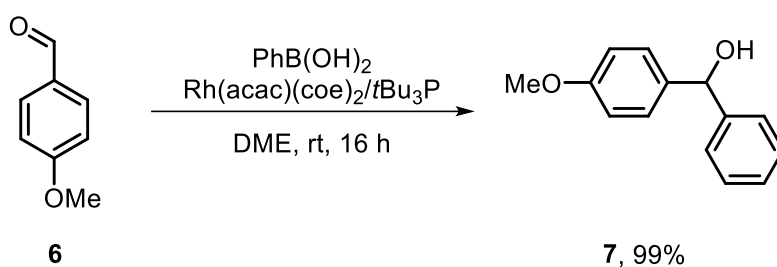


Scheme 3: competing pathways of the gold catalysed cycloaddition reported by Toste.

⁹ P. Mauleón, R. M. Zeldin, A. Z. González, F. Dean Toste, *J. Am. Chem. Soc.* **2009**, *131*, 6348.

Obviously, the electronic structure of the employed phosphine can as well be tuned to be more σ -donating. Formal substitution of the phenyl groups of triphenylphosphine with *tert*butyl groups leads to tris(*tert*butyl)phosphine, a highly σ -donating ligand.

Miyaura *et al.*¹⁰ reported a large accelerating effect in the rhodium catalysed addition of aryl boronic acids to aldehydes using tris(*tert*butyl)phosphine as ligand. Increasing the σ -donor properties of the used phosphine, – from triphenylphosphine over tricyclohexylphosphine to tris(*tert*butyl)phosphine – improved the yields of the rhodium catalysed additions at 50°C from 33% over 50% to full conversion. Tris(*tert*butyl)phosphine was even reactive enough to achieve full conversion at room temperature.



Scheme 4: rhodium catalysed addition of phenylboronic acid to 4-methoxybenzaldehyd.

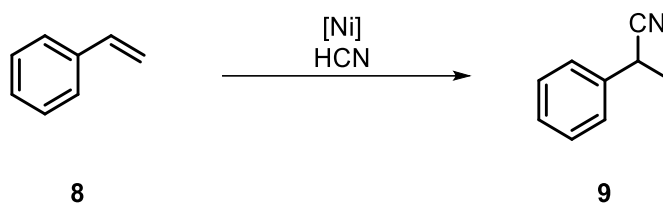
Steric parameters also significantly modulate the reactivity of the catalyst. As mentioned before, tris(*tert*butyl)phosphine is particularly successful in reactions, in which high σ -donor capabilities are needed. One prominent example being palladium catalysed cross coupling reactions, in which the steric bulk of tris(*tert*butyl)phosphine ensures a di-ligation of the palladium centre, avoiding, or at least slowing down, its deactivation.¹¹

For bidentate ligands besides the steric and electronic parameters, the bite angle is of tremendous importance. Among others, Keim *et al.*¹² showed an enormous effect for the hydrocyanation of styrene (**8**) after optimisation of the bite angle of the employed ligands. For this particular transformation an optimal bite angle around 104 to 105° was found, ensuring high yields and selectivity of the desired hydrocyanated product, while only small changes in the bite angle significantly reduced the yield of the desired product. The authors conclude that the bite angle of 105° forces the nickel catalyst to adopt a tetrahedral geometry, beneficial for the reductive elimination, underlining the importance of ligand design.

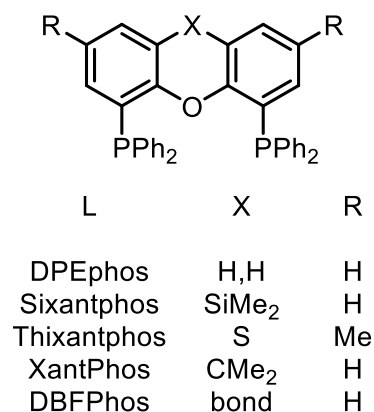
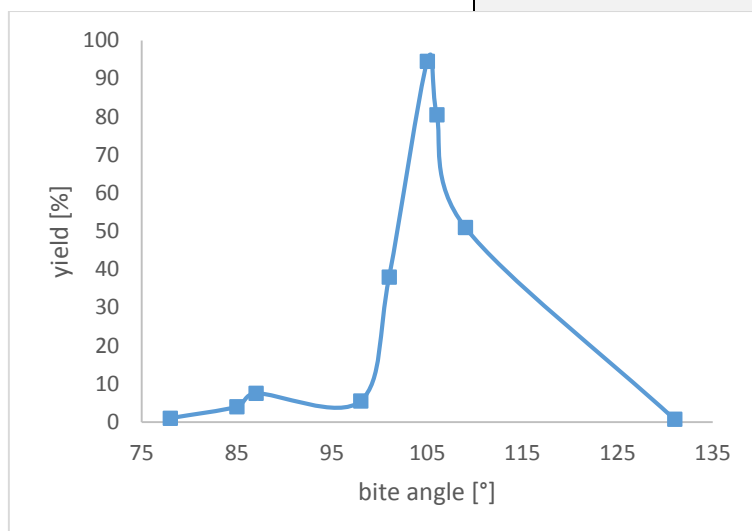
¹⁰ M. Ueda, N. Miyaura, *J. Org. Chem.* **2000**, *65*, 4450.

¹¹ M. Matsumoto, H. Yoshioka, K. Nakatsu, S. Otsuka, *J. Am. Chem. Soc.* **1974**, *96*, 3322.

¹² M. Kranenburg, P. C. J. Kamer, P. W. N. M. van Leeuwen, D. Vogt, W. Keim, *J. Chem. Soc., Chem. Comm.* **1995**, *21*, 2177.

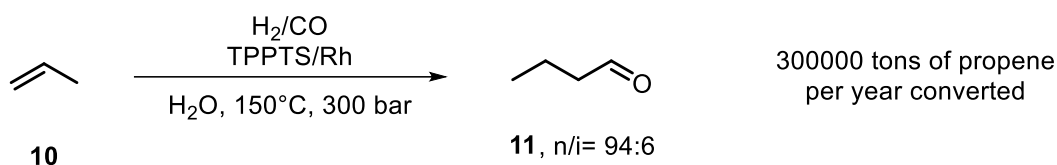


Ligand	Bite angle [°]	Yield [%]
Ph ₂ P(CH ₂) ₂ PPh ₂	78	1
BINAP	85	4
Ph ₂ P(CH ₂) ₃ PPh ₂	87	7,5
Ph ₂ P(CH ₂) ₄ PPh ₂	98	5,5
DPEPhos	101	38
SiXantPhos	105	94,5
ThiXantphos	106	80,5
Xantphos	109	51
DBFPhos	131	0,7



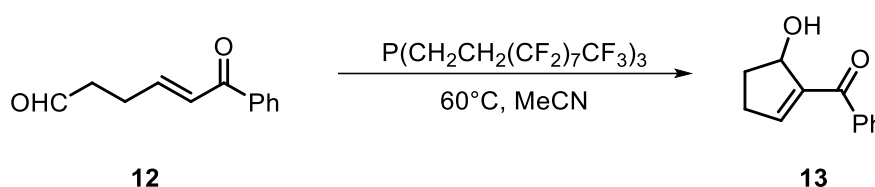
Scheme 5: effect of the bite angle of the employed ligand on the yield of the hydrocyanation of styrene.

The possibility to modulate the solubility was as well investigated, with the most famous example being the Ruhrchemie/Rhône-Poulenc-process mentioned before. Here the phosphine is modified by the introduction of three sulfonate groups to be highly soluble in an aqueous phase (>1kg/l) and insoluble in the organic product phase.⁸ This allows easy recovery of the catalyst just by separation of two phases. TPPTS is applied since 1984 in the rhodium catalysed hydroformylation of propene (**10**) in the Ruhrchemie/Rhône-Poulenc process on a multi-ton scale.



Scheme 6: Ruhrchemie/Rhône-Poulenc process.

This concept then was first extended to systems based on fluorous biphasic hydroformylations.¹³ While at lower temperatures hydrocarbons and fluorocarbons form two phases, they mix at higher temperatures. This allows reactions to perform in one phase at high temperatures and at the same time allowing easy catalyst. While the fluorination alters the electronic and steric parameters of the employed phosphine as well, the main focus of this section lies within the changed solubility. Gladysz *et al.*¹⁴ reported the applications of an analogous fluorous phosphine in the Morita–Baylis–Hillman reaction. This catalyst due to its lowered solubility in hydrocarbons (not soluble at rt, soluble at 60°C) could be recycled up to 5 times without significant loss of reactivity.



Scheme 7: Morita-Baylis-Hillman reaction employing fluorous phosphine.

Despite the high success of phosphines in catalysis alternative ligand systems have been developed as well, for example carbenes. These ligands classically possess a singlet state at the central carbon atom, which is stabilized through the p-orbitals of the neighbouring atoms usually being nitrogen. This results in a high net electron density on the central carbon atom. This atom donates electron density to the metal via σ - and π -donation. While only little backdonation from the metal towards the carbenes occurs.

The steric parameters of carbenes and phosphines are largely different. While phosphines usually bend away from the metal, the carbene substituents form a pocket around it.¹⁵ This orientation enables NHCs to perform with remarkable selectivity in asymmetric catalysis as the stereo information is brought closer to the reactive centre (figure 1).

¹³ I. T. Horvath, J. Rabai, *Science* **1994**, 266, 72.

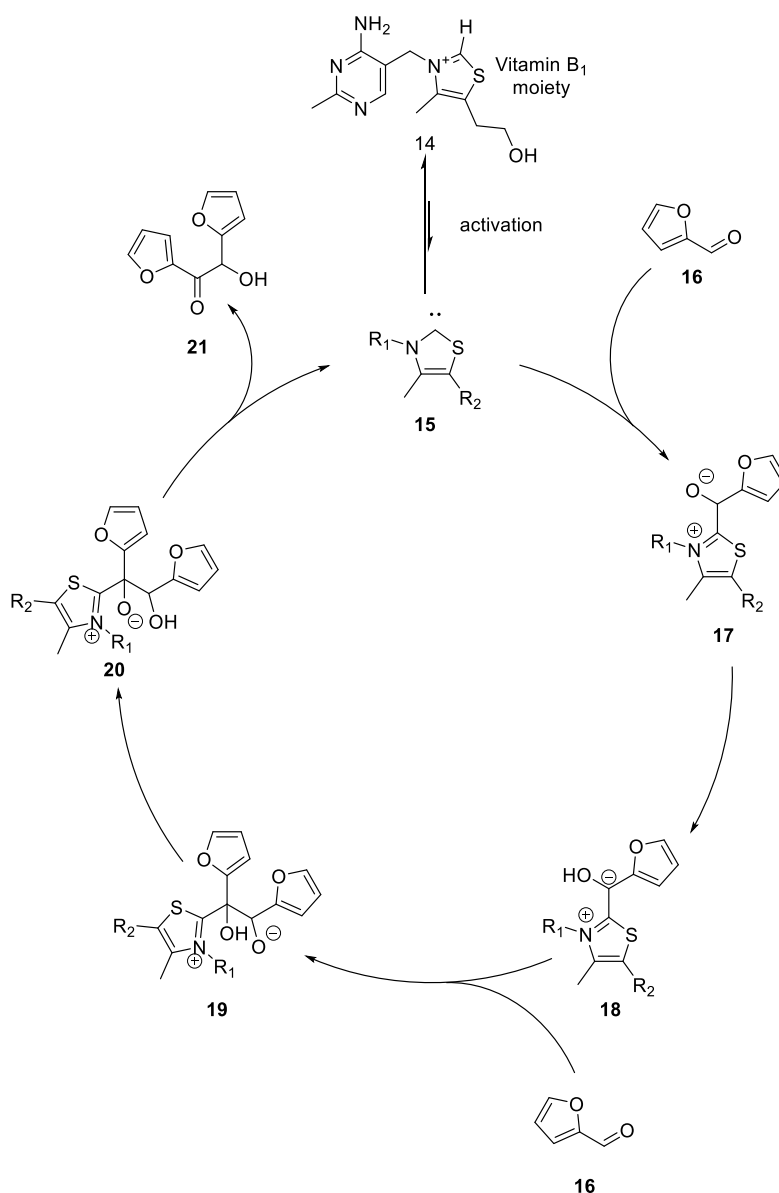
¹⁴ F. O. Seidel, J. A. Gladysz, *Adv. Synth. Catal.* **2008**, 350, 2443.

¹⁵ F. Glorius *N-Heterocyclic Carbenes in Transition Metal Catalysis* Berlin, Springer, **2007**, print.



Figure 1: shape of phosphines and NHCs.¹⁵

Early evidence of the existence of carbenes was proposed 1957 by Breslow¹⁶ for the catalytic cycle of vitamin B1 transforming fuoin (**21**) from furfural (**16**) (scheme 8). He based his hypothesis on an experimental fact: when the reaction was performed in deuterated water, instead of a proton at the C₂ position a statistical mixture of hydrogen and deuterium was found, indicating the presence of a deprotonated species - the carbene **15**.

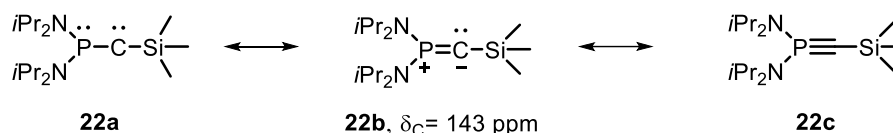


Scheme 8: generation of fuoin proposed by Breslow based on the formation of a carbene.

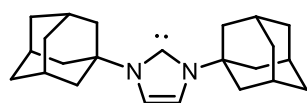
¹⁶ R. Breslow, *Chem. Ind. London* **1957**, 26, 893; R. Breslow *J. Am. Chem. Soc.* **1958**, 80, 3719.

The first isolated carbene phosphinocarbene **22** was prepared by Bertrand¹⁷ in 1988 and as no solid state structure was obtained the carbenic nature was initially doubted. The first structural proof has been achieved by Arduengo¹⁸ in 1991 preparing diaminocarbene **23**.

Bertrand:

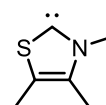


Arduengo:



23, NHC

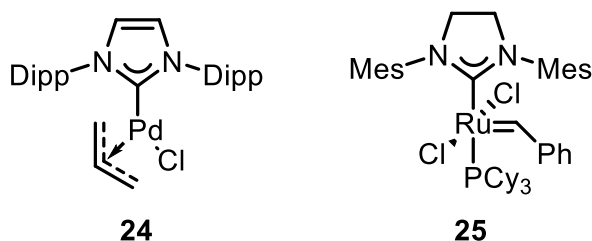
Breslow:



15, proposed intermediate

Scheme 9: proposed and synthesized carbenic structures.

Carbenes from their discovery on have been applied extensively as ligands in metal catalysis and several new processes based on carbenes have been developed. Important examples include NHC palladium complexes¹⁹ like **24** used in Suzuki-Miyaura²⁰, Negishi²¹, Sonogashira²² or Heck-Mizoroki²³ couplings and the Hoveyda-Grubbs catalyst **25** used in alkene metathesis, even incorporating a NHC and a phosphine.



Scheme 10: NHC palladium complex 24 and Hoveyda-Grubbs catalyst 25.

Realizing the advantages of carbene and phosphine ligand systems one can easily realise, that both systems are complementary. For instance, the already discussed Tolman electronic parameter (TEP) and the average CO stretching frequencies of NHCs and phosphines can be compared. Where extreme σ -donating ligands are needed only few electron rich phosphines

¹⁷ A. Igau, H. Grutzmacher, A. Baceiredo, G. Bertrand, *J. Am. Chem. Soc.* **1988**, *110*, 6463.

¹⁸ A. J. Arduengo, R. L. Harlow, M. Kline, *J. Am. Chem. Soc.* **1991**, *113*, 361.

¹⁹ G. Fortman, S. Nolan, *Chem. Soc. Rev.* **2011**, *40*, 5151.

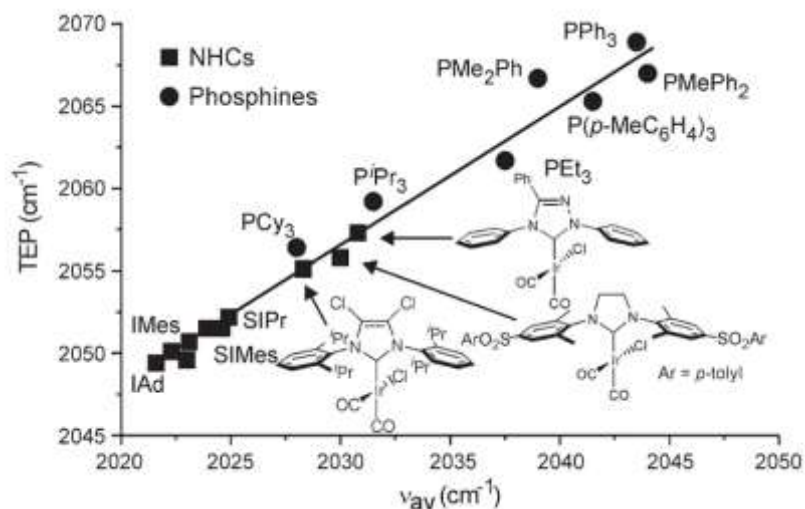
²⁰ C. Gstöttmayr, B. Volker, E. Hardtweck, M. Grosche, W. Herrmann, *Angew. Chem. Int. Ed.* **2002**, *41*, 1363.

²¹ J. Nasielski, N. Hadei, G. Achonduh, E. A. B. Kantchev, C. J. O'Brien, *Chem. Eur. J.* **2010**, *16*, 10844.

²² R. Batey, M. Shen, A. Lough, *Org. Lett.* **2002**, *14*, 1411.

²³ M. Taige, A. Zeller, S. Ahrens, S. Goutal, E. Hardtweck, *J. Organomet. Chem.* **2006**, *692*, 1519.

are available, but his lack of σ -donation can be achieved by carbenes.²⁴ This fostered the coexistence of phosphines and NHCs as important ligand classes in all fields of catalysis.



Scheme 11: Tolman electronic parameter (TEP) versus the average CO stretching frequencies for NHCs and phosphines.²⁴

2. Ligand design in π -acid catalysis

2.1 Generalities, mechanism and scope

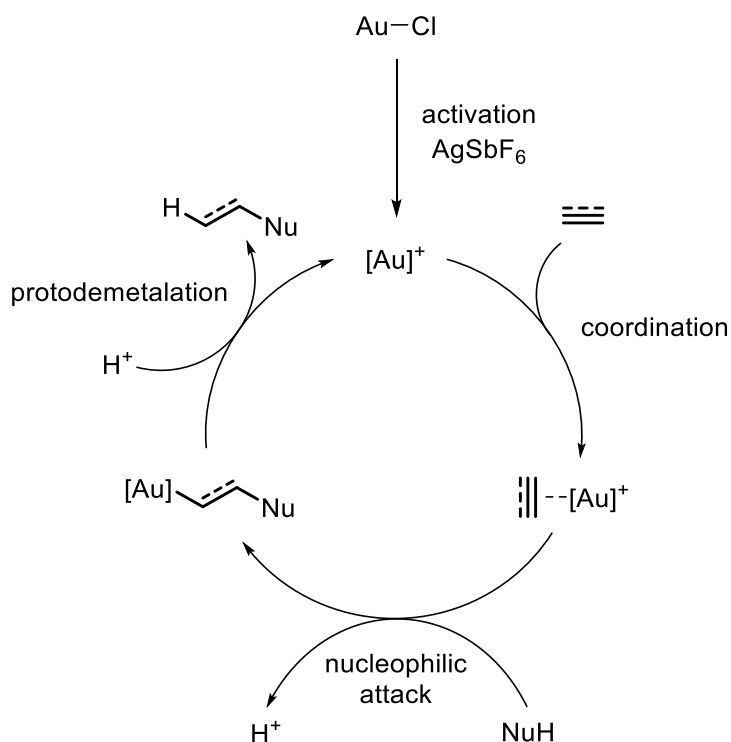
π - acid catalysis evolved in the last years to a highly active area of research in organometallic chemistry. π - acids selectively bind to unsaturated C-C double and triple bonds allowing powerful and atom-economic transformations to obtain complex products from rather simple starting material.

In general π -acid catalysed reactions consist of an activation step, coordination of the substrate, nucleophilic attack and protodemetalation.²⁵

After activation of a suitable metal precursor, the catalytically reactive species is generated (here: $[\text{Au}]^+$). The activated metal centre is then coordinated by a π -system, generally, an alkene or alkyne, which upon coordination following the Dewar-Chatt-Duncanson model (see next page) is activated towards the following nucleophilic attack leading to a metal alkyl/vinyl intermediate. Upon protodemetalation the product of the hydrofunctionalisation is realised and the reactive metal species regenerated. Besides productive pathways catalyst deactivation can occur generating metal⁰ and bisligated metal⁺, furthermore geminal digold formation for gold catalysis might as well lead to a resting state of the catalyst.

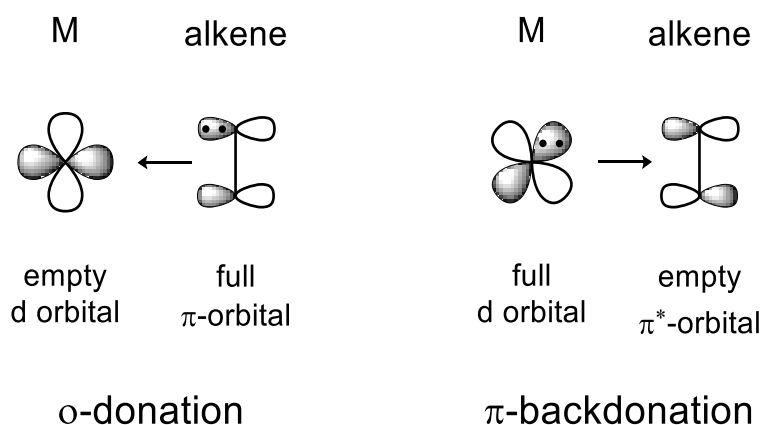
²⁴ S. J. Cazin *N-Heterocyclic Carbenes in Transition Metal Catalysis and Organocatalysis* St Andrews, Springer, **2011**, print.

²⁵ C. J. V. Halliday, J. M. Lynam, *Dalton Trans.* **2016**, 45, 12611.



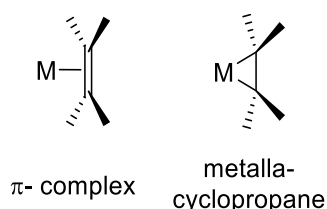
Scheme 12: π -acid catalysis: simplified catalytic cycle of a gold catalysed hydrofunctionalisation.

The unique reactivity of these metals in catalysis can be explained considering the interaction between the metal centre and the associated π -system. This interaction consists of σ -donation of the π -systems (for example an alkyne) towards an empty d- or s-orbital of the metal and of π -backdonation from a full d- orbital of the metal towards the empty π^* -orbital of the π -system. For example for alkynes this results in a neat reduction of electron density of the π -system enhancing its reactivity towards nucleophiles, while at the same time owed to the π -backbonding, the bond order of the π -system decreases.



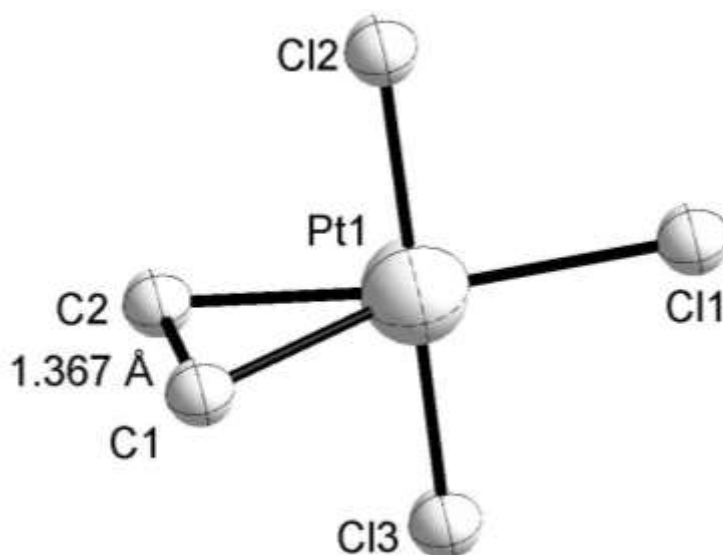
Scheme 13: schematic representation of the Dewar-Chatt-Duncanson model.

The model to describe these interaction was first reported by Dewar *et al.*²⁶ in 1951 and expanded by Chatt and Duncanson²⁷ in 1953 on the basis of olefin coordination towards platinum and is therefore named the Dewar-Chatt-Duncanson model. Due to the high amount of backbonding and the resulting weakening of the bond order a bending of the idealized geometry of a π -complex can as well be understood as a metallacyclopropane. However Hoffmann *et al.*²⁸ showed in 1979 that the real bonding situation lies between these two forms.



Scheme 14: extreme resonance forms of alkene metal complexes.

The first alkene metal structure - the well-known Zeise's salt $[\text{PtCl}_3(\text{C}_2\text{H}_4)]^-$ - which was already prepared in 1827²⁹ (even though the solid state structure was only implied in 1954³⁰ and verified in 1970³¹), evidences the presence of the before mentioned interactions. Although the alkene bond is only marginally elongated to 1.37 Å compared to 1.35 Å in free ethylene.



Scheme 15: solid state structure of the anion in Zeise's salt.

The first structural evidence of a gold alkyne interaction was reported by Dias *et al.*³² in 3-hexyne gold chloride complexes. As mentioned before the σ -donation of the alkyne towards the metal and the π -backbonding result in a bending of the idealized linear geometry of an

²⁶ M. Dewar, *Bull. Soc. Chim. Fr.* **1951**, 18, 79.

²⁷ J. Chatt, L. A. Duncanson, *J. Chem. Soc.* **1953**, 1, 2939.

²⁸ B. E. R. Schilling, R. Hoffmann, *J. Am. Chem. Soc.* **1979**, 101, 3456.

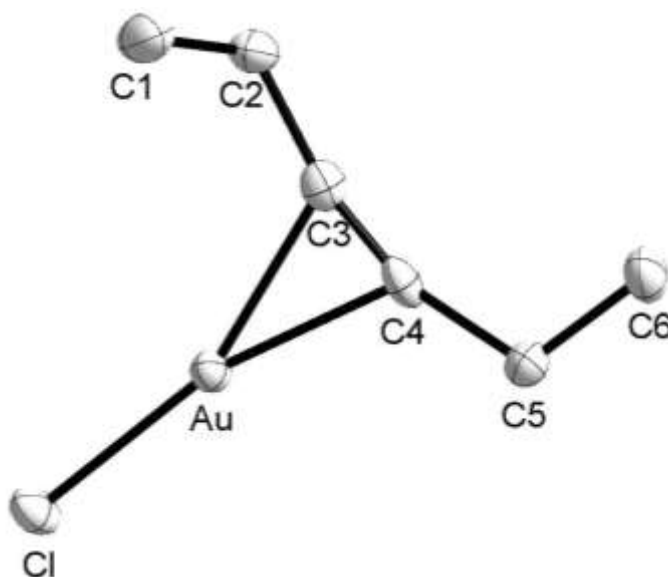
²⁹ W. C. Zeise, *Ann. Phys.* **1827**, 85, 632.

³⁰ J. A. Wunderlich, D. P. Mellor, *Acta Crystallogr.* **1954**, 7, 130.

³¹ J. A. J. Jarvis, B. T. Kilbourn, P. G. Owston, *Acta Cryst. Sect. B* **1971**, 27, 366.

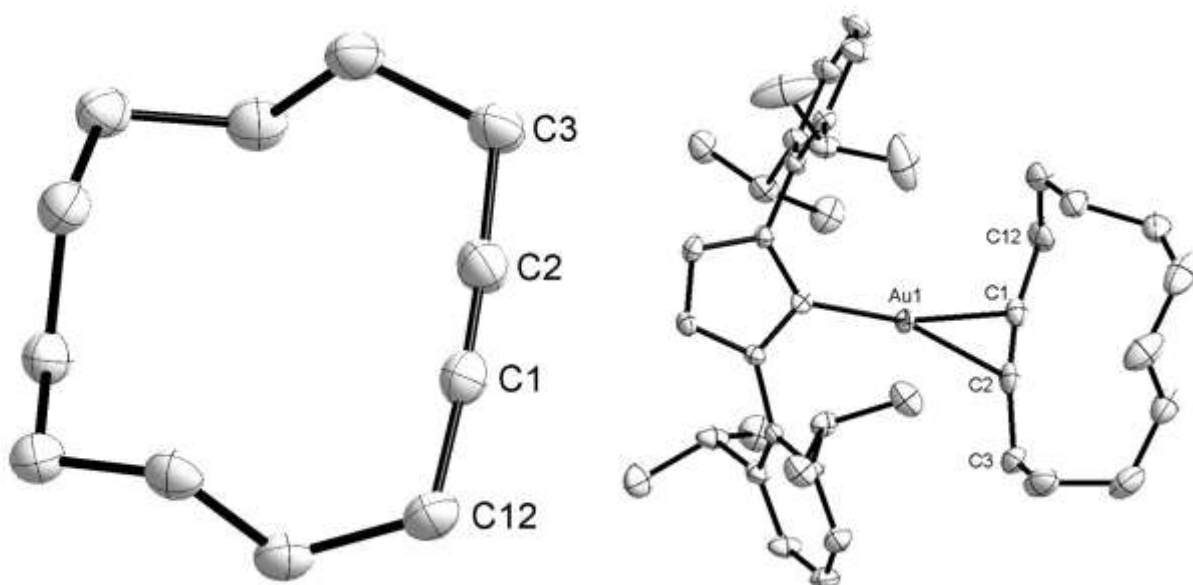
³² J. Wu, P. Kroll, H. V. R. Dias,

uncoordinated alkyne (180°) towards a metallacyclopropene structure (120°), resulting in bond angles of 167° and 163° .



Scheme 16: solid state structure of 3-hexyne gold chloride complex.

In the gold complex reported by Fürstner³³ this concept was extended to catalytically applied NHC gold cyclododecyne complexes.



Scheme 17: solid state structures of free cyclododecyne and the NHC gold cyclododecyne complex **27**.

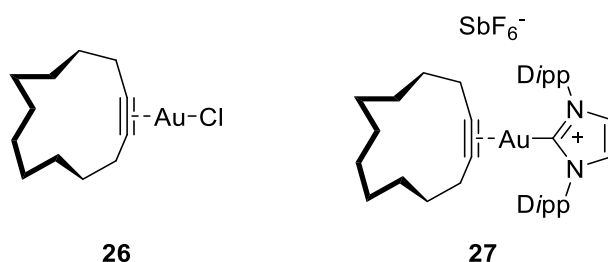
The coordinated alkyne shows significant bending away from 175.9° in free cyclododecyne to an average bond angle of 168° in the NHC gold dodecyne complex **27** underlining the importance of the interactions between gold and π -systems for catalysis. This trend is also

³³ S. Flügge, A. Anoop, R. Goddard, W. Thiel, A. Fürstner, *Chem. Eur. J.* **2009**, *15*, 8558.

observed in the carbon NMR shifts of the alkyne: While in free cyclododecyne the alkyne signal is at 81.7 ppm, in the coordinated complexes the alkyne carbon is shifted significantly down field in complexed cyclododecyne gold chloride **26** (86.4 ppm) and in gold NHC complex **27** (88.0 ppm).

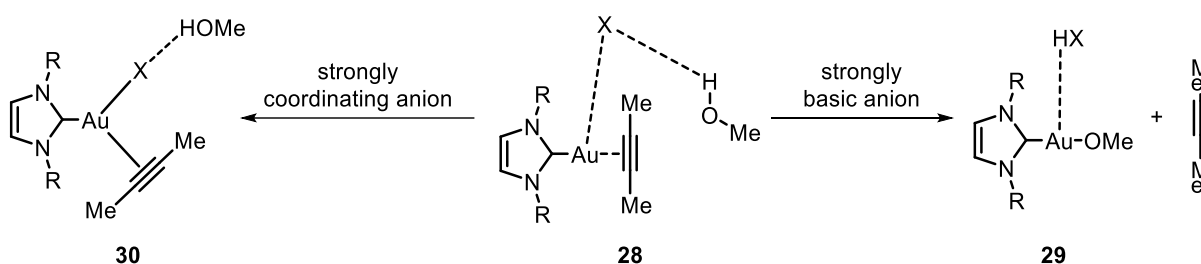
Compound	δ_{C} [ppm] in CD_2Cl_2
cyclododecyne	81.7
26	86.4
27	88.0

Table 1: carbon NMR shifts of cyclododecyne and its corresponding gold complexes **26** and **27**.



Scheme 18: alkyne complexes **26** and **27** prepared by Fürstner *et al.*

This interaction renders then the nucleophilic attack to occur easier, generating the aforementioned metal alkyl/vinyl intermediates. The nucleophilic attack itself is highly sensitive towards the nature of the counter anion.³⁴ Two major catalyst deactivation pathways can occur depending on the nature of the anion. Strongly coordinating anions can decoordinate the alkyne and regenerate the precursors or eventually form a tricoordinated complex **30**, while strongly basic counter anions can deprotonate the nucleophile (here methanol) and thereby form a catalytically inactive gold nucleophile adduct **29**.



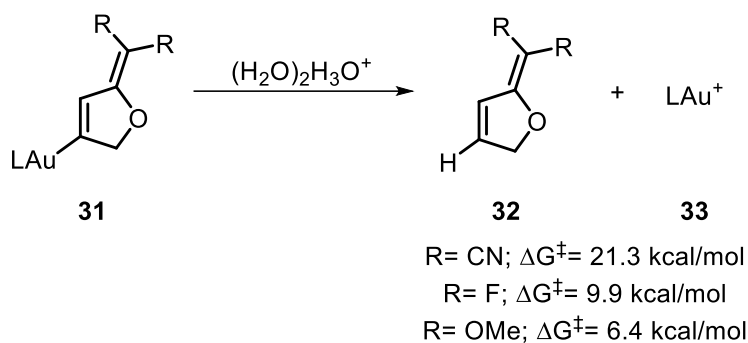
Scheme 19: catalyst deactivation steps during the nucleophilic attack.

Besides the later on discussed ligand effect in the protodemetalation step, the effect of substrate substituents should be considered as well. While in general the protodemetalation is considered fast, specific substitution pattern may slow down the rate of this elementary step. Theoretical studies by Ariafard *et al.*³⁵ showed that for the protonolysis of alkenyl complexes

³⁴ G. Ciancaleoni, L. Belpassi, D. Zuccaccia, F. Tarantelli, P. Belanzoni, *ACS Catalysis* **2015**, *5*, 803.

³⁵ R. B. Ahmadi, P. Ghanbari, N. A. Rajabi, A. S. K. Hashmi, B. F. Yates, A. Ariafard, *Organometallics* **2015**, *34*, 3186.

31. The reaction rate is mainly dependent of the substitution pattern and of the ligand within the same substitution pattern. The stronger the Au carbon bond is, the higher the activation barrier will be. Therefore protodemetalation is faster, when π -donating substituents (e.g. –OMe) are present, while protodemetalation is significantly slower, when π -accepting substituents (e.g. –CN) are present.



Scheme 20: theoretical investigation of the substitution effect for the protodeauration step in π -acid catalysis.

The counter anion plays a major role in the protodemetalation step as well, because it greatly lowers the activation barrier of this elementary reaction acting as a proton shuttle. Belanzoni *et al.*³⁴ calculated the proton migration step in the alkoxylation of alkynes to be highly depended of the counter anion. Much lower activation energies were calculated for BF_4^- or OTf^- assisted protodemetalation (2.4 kcal/mol for BF_4^- and 4.7 kcal/mol for OTf^-) in comparison to the protodemetalation without an anion (11.0 kcal/mol).

π -acid catalysis has found extensive applications in chemistry. A few noteworthy examples include for gold and platinum catalysis enine cyclisations,^{36,37} cycloadditions,^{38,39} hydroadditions,^{40,41} Meyer-Schuster-rearrangement^{42,43} and applications in natural product synthesis.^{44,45}

³⁶ C. Nieto-Oberhuber, M. P. Muñoz, E. Buñuel, C. Nevado, A. M. Echavarren, *Angew. Chem. Int. Ed.* **2003**, *43*, 402.

³⁷ A. Fürstner, C. C. Stimson, *Angew. Chem. Int. Ed.* **2007**, *46*, 8845.

³⁸ B. F. Straub, *Chem. Commun.* **2004**, 1726.

³⁹ N. Asao, H. Aikawa, Y. Yamamoto, *J. Am. Chem. Soc.* **2004**, *126*, 7458

⁴⁰ N. Morita, N. Krause, *Org. Lett.* **2004**, *6*, 4121.

⁴¹ Z. Zhang, C. Liu, R. E. Kinder, X. Han, H. Qian, R. A. Widenhoefer, *J. Am. Chem. Soc.* **2006**, *128*, 9066.

⁴² Y. Fukada, K. Utimoto, *Bull. Chem. Soc. Jpn.* **1991**, *64*, 2013.

⁴³ D. A. Engel, G. B. Dudley, *Org. Lett.* **2006**, *8*, 4027.

⁴⁴ E. Jiménez-Núñez, K. Molawi, A. M. Echavarren, *Chem. Commun.* **2009**, 7327.

⁴⁵ A. Fürstner, E. K. Heilmann, P. W. Davies, *Angew. Chem. Int. Ed.* **2007**, *46*, 4760.

2.2 Influence of the ancillary ligand in π -acid catalysis

The ancillary ligand significantly controls the reactivity and selectivity as well as the rate of a chosen transformation. While the electronic properties possess a strong influence towards the reactivity and selectivity of the corresponding reaction, in many cases and especially for the Buchwald type ligands the rate of the reaction is as well modulated by the stability of the catalyst. Bulkier ligand can lead to a better steric shielding of the metal centre, therefore stabilizing the complexes and slowing down decomposition reactions.

The electronic properties of the ancillary ligands strongly influences the rate of the nucleophilic attack and of the protodemetalation. In π -acid catalysis weak σ -donor and good π -acceptor ligands reduce the electron density of the metal and therefore, a coordinated alkyne donates more electron density towards the metal resulting in a higher partial positive charge, promoting the nucleophilic attack. This, at the same time slows down the rate of the protodemetalation, as the metal with a good π -accepting ligand already is rather electron poor. On the other hand if a good σ -donor is used, the rate of the nucleophilic attack is reduced, as the metal backdonates more electron density towards the alkyne, at the same time accelerating the rate of the protodemetalation.

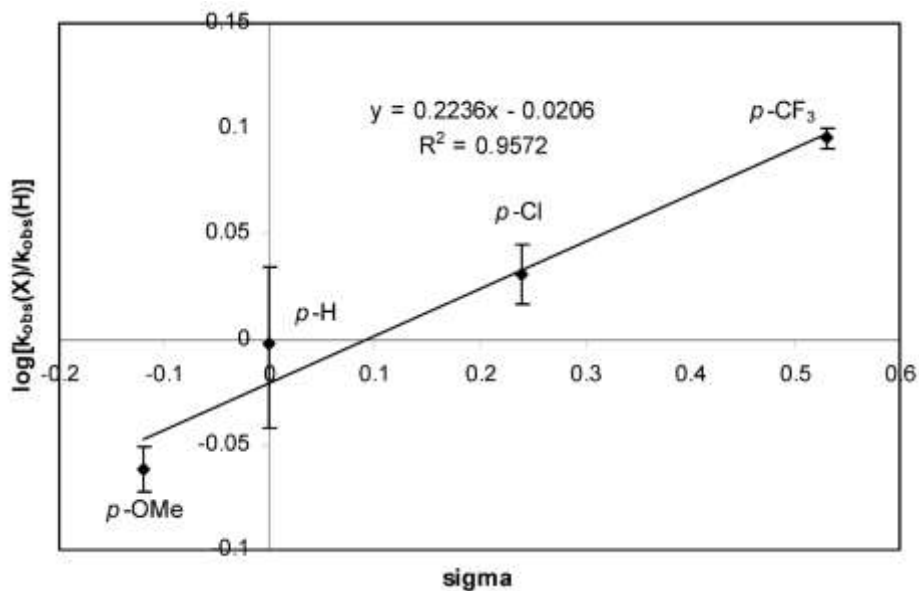
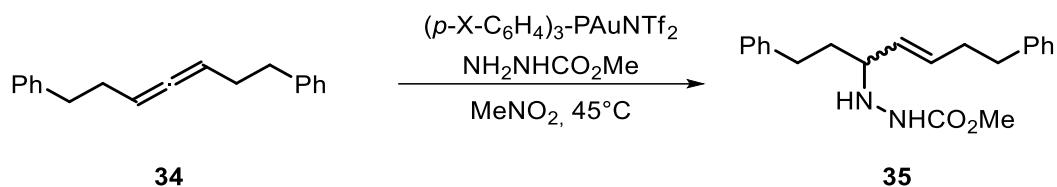
The electronic and steric effects of ligands in Au-catalysis have been studied by Xu *et al.*⁴⁶ amongst others. They showed that proper ligand design can lead to increased reaction rates if the rate determining step and the rate of catalyst deactivation are considered.

If the activation of the alkyne, alkene or allene towards nucleophilic attack is the rate determining step, strong electrophilic activation of the metal should enhance the reaction rate. Employing a weak nucleophile, like electron poor hydrazides and utilizing less electrophilic π -systems like allenes, the rate determining step would become the nucleophilic attack. This low reaction rate then could be enhanced by the use of electron poor phosphine ligands, which would generate a more π -acidic metal, resulting in a stronger activation of the π -system and a higher overall reaction rate.

Toste *et al.*⁴⁷ showed that for the intermolecular hydroamination of allene **34** the rate determining step is the activation of the allene towards nucleophilic attack and therefore the use of an electron poor ligand (*p*-CF₃ substituted PPh₃) leads to a 10-fold increase in reaction rate compared to classical triphenylphosphine.

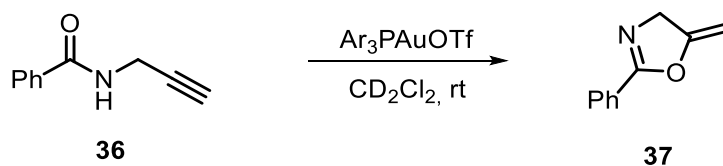
⁴⁶ W. Wang, G. B. Hammond, B. Xu, *J. Am. Chem. Soc.* **2012**, *134*, 5697.

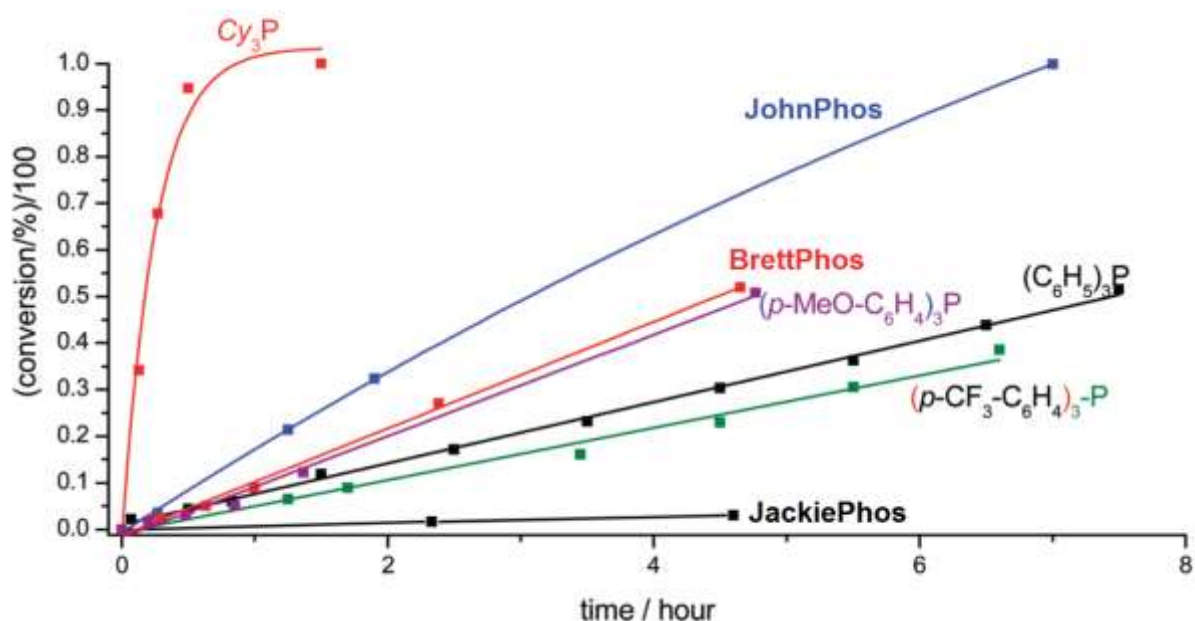
⁴⁷ Z. J. Wang, D. Benitez, E. Tkatchouk, W. A. Goddard, F. D. Toste, *J. Am. Chem. Soc.* **2010**, *132*, 13064.



Scheme 21: Hammett plot of k_{obs} for hydroamination of **34** in the presence of $\text{Ar}_3\text{PAuNTf}_2$ reported by Toste *et al.*⁴⁷

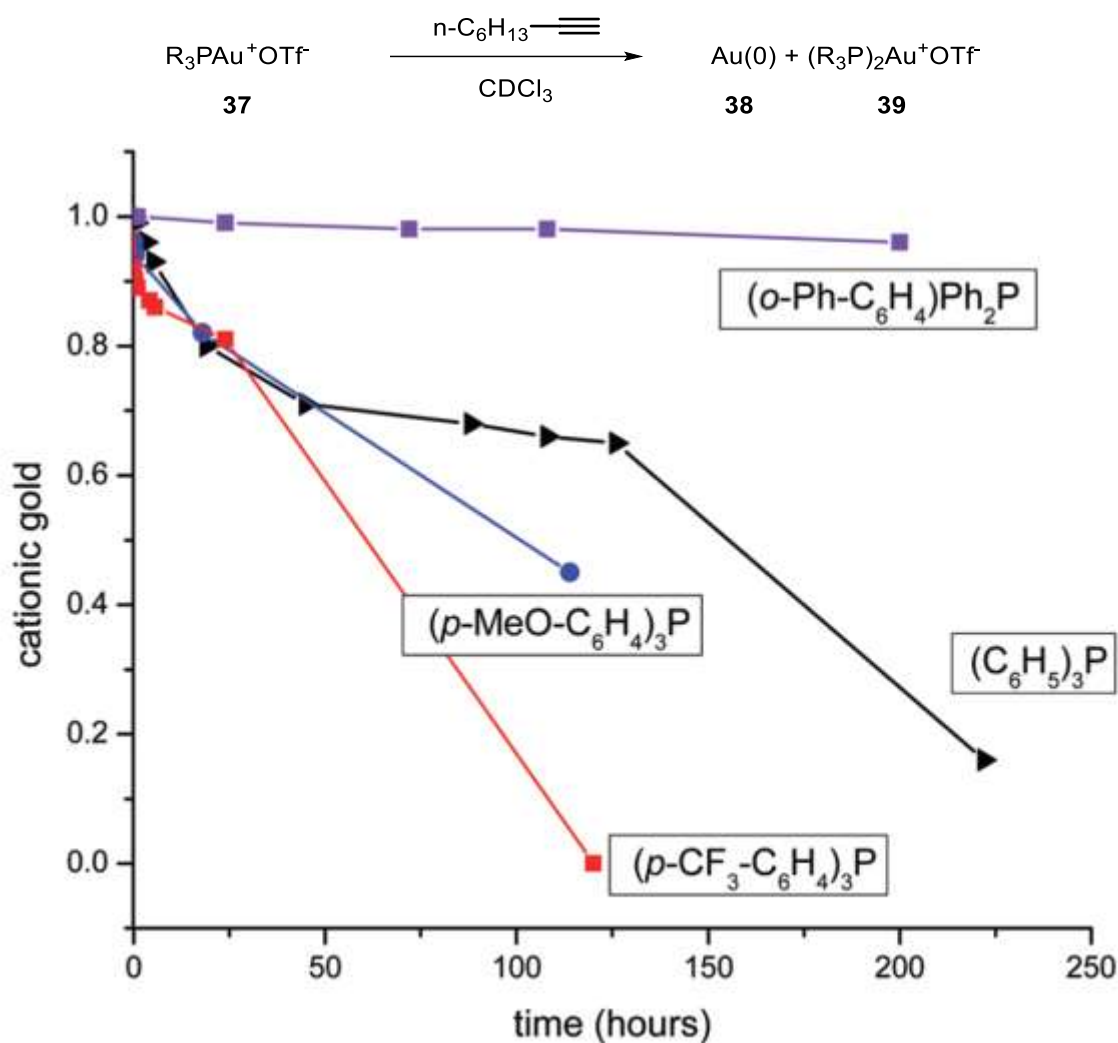
On the other hand protodeauration can be rate determining as well and then the use of an electron poor ligand would slow down the reaction rate. This is the case for the intramolecular hydroamination of propargylamide **36**.⁴⁶ Therefore the use of electron rich phosphines proved to be beneficial and full conversion could be obtained with tricyclohexylphosphine within one hour.





Scheme 22: ligand effect on the transformation of propargylamide **36** to oxazole **37**. Reagents and conditions: **36** (0.5 M), gold precatalyst (5 mol%), CD₂Cl₂, rt.

If catalyst deactivation occurs during the desired transformation, then this is also an important factor to consider during the catalyst design process. For example to avoid catalyst deactivation the biphenyl systems first reported by Buchwald proved to be useful, as due to the additional arene gold interaction and the steric bulk of the phosphine ligand, the aforementioned catalyst deactivation pathways (formation of digeminal gold complexes or formation of Au⁰ and bisligated Au⁺) are less likely to occur. As shown by Xu *et al.*⁴⁶ the decomposition of gold complexes **37** to elemental gold (**38**) and dicoordinated gold species **39** occurs for ortho substituted phenyl triarylphosphine at a much slower rate than the one of even electronically different triarylphosphines.



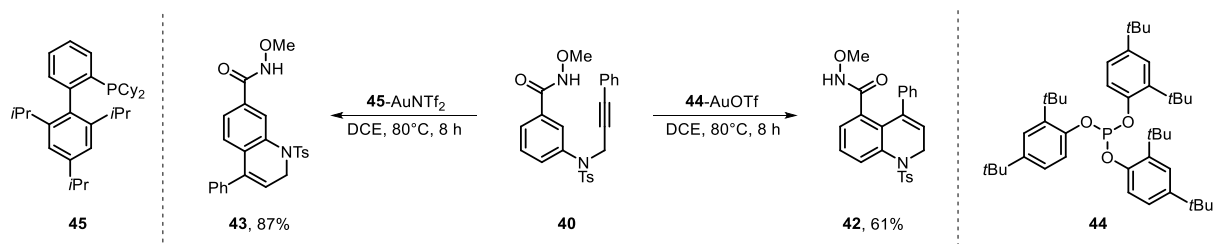
Scheme 23: ligand effect toward to catalyst decomposition.

The possibility to tune the stereo electronic properties of the phosphines, enabled the broad applicability of these ligand class.

2.3 Applications of phosphines in π -acid catalysis

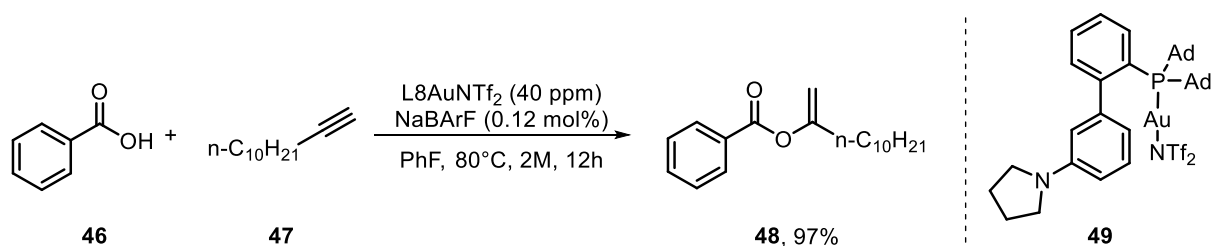
Jiang *et al.*⁴⁸ reported in 2016 a π -acid catalysis, in which depending on the applied ligand *ortho* or *para* selective cyclization can exclusively be obtained. While XPhosAuNTf₂ (**45**-AuNTf₂) leads to dihydroquinoline **43** (*para* selective cyclisation, 87%), the use of phosphite ligand **44** results in selective *ortho* cyclization to dihydroquinoline **42** (61%). This ligand controlled reactivity could be broadened to 50 substrates.

⁴⁸ D. Ding, T. Mou, M. Feng, X. Jiang, *J. Am. Chem. Soc.* **2016**, *138*, 5218.



Scheme 24: ligand controlled ortho or para selective cyclization of phenyl propargyl amine **115** to dihydroquinoline **42** or **43**.⁴⁸

Another impressive example was published by Zhang *et al.*⁴⁹ in 2014 controlling the anti-nucleophilic attack of alkynes through ligand design. Zhang *et al.* as well used the additional stability of ortho phenyl substituted phosphines and combined their beneficial effect with an additional directing group to enable the anti-nucleophilic attack of alkynes through precoordination of the nucleophile. Zhang *et al.* reported the addition of benzoic acid (**46**) to 1-dodecyne (**47**) with low catalyst loadings (40 ppm) yielding the desired 2-dodecenylbenzoate (**48**) in excellent yield (97%) after only 12 h of reaction time, once more demonstrating the power and utility of ligand design.



Scheme 25: ligand controlled anti addition of benzoic acid to dodecyne reported by Zhang *et al.*⁴⁹

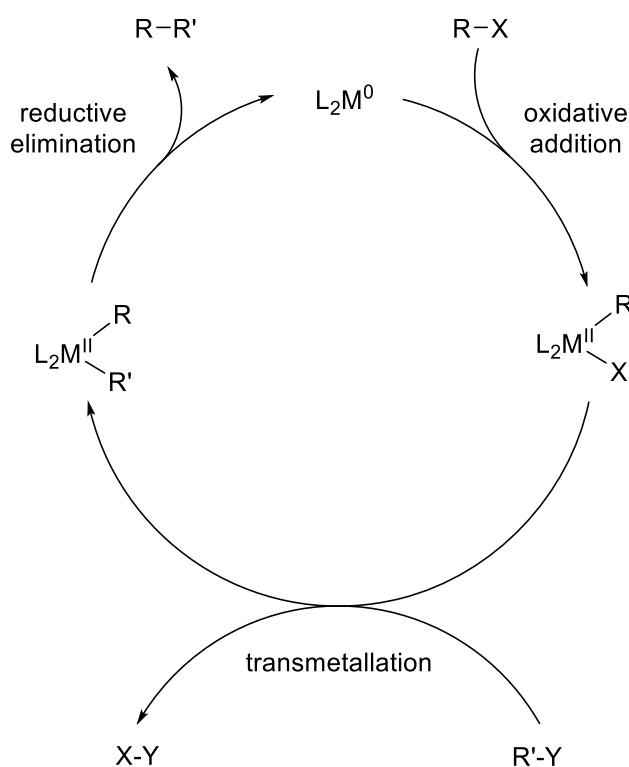
⁴⁹Y. Wang, Z. Wang, Y. Li, G. Wu, Z. Cao, L. Zhang *Nature Communications* **2014**, *5*, 3470.

3. Ligand design in Cross Coupling Reactions

3.1 Generalities, mechanism and scope

A cross coupling reaction is a reaction, in which two substrates are coupled in the presence of a metal centre. It is one of the most important reaction for the creation of new carbon-carbon bonds. Homo- (e. g. Glaser coupling) as well as heterocoupling reactions (e. g. Sonogashira reaction) are known and both types are applied in modern chemistry.

In general a cross coupling reaction starts with the generation of the active metal⁰ source. This metal undergoes an oxidative addition with a suitable organic halide generating a metal^{II} centre. Subsequently the second reaction partner is transferred to the metal via transmetalation reaction. Reductive elimination then releases the product and regenerates the catalyst.



Scheme 26: schematic catalytic cycle of a cross coupling reaction.

Besides the ligand effect the oxidative addition is highly dependent on the nature of the used aryl halide. Amongst other^{50,51} Maseras *et al.*⁵² showed experimentally and by calculations, that more labile aryl halides undergo oxidative addition at a higher rate, decreasing from PhI over PhBr and PhCl to PhF. Experimentally, this was proven using mass spectroscopy. The mass spectra clearly showed higher amounts of addition products for more labile aryl halides

⁵⁰ L. J. Goossen, D. Koley, H. L. Hermann, W. Thiel, *Organometallics* **2005**, *24*, 2398.

⁵¹ H. M. Senn, T. Ziegler, *Organometallics*, **2004**, *23*, 2980.

⁵² K. Vikse, T. Naka, J. S. McIndoe, M. Besora, F. Maseras, *ChemCatChem* **2013**, *5*, 3604.

(ArI: 100%, ArBr: >99%, ArCl: 97%, ArF ~10%). This general trend was then confirmed by DFT calculations.

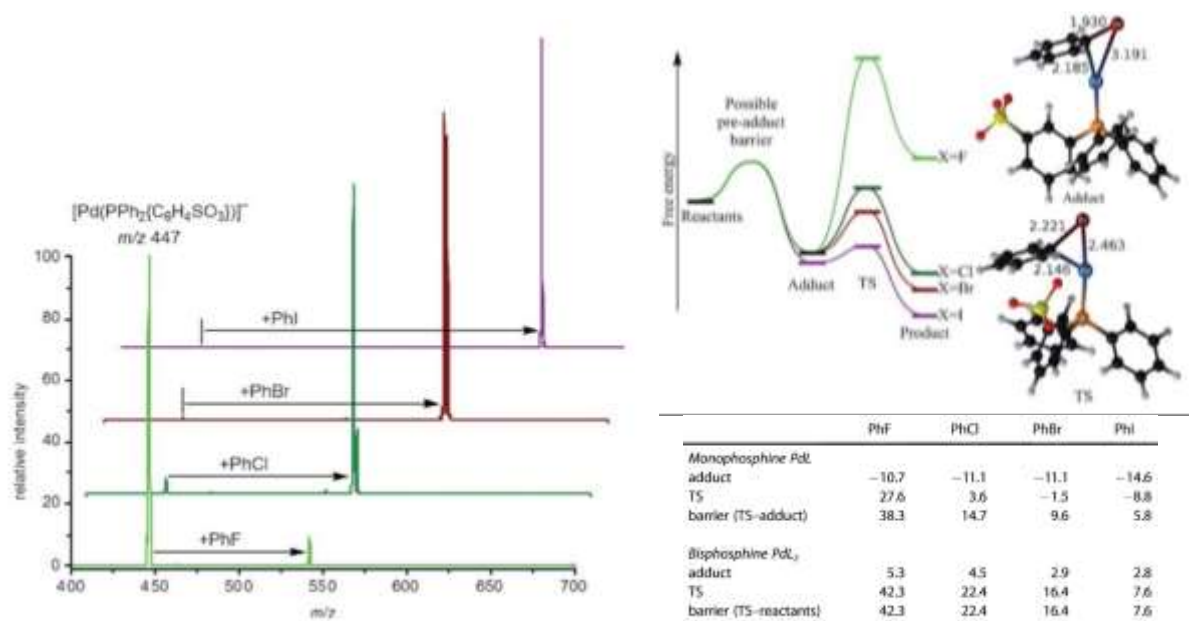


Figure 2: experimental and theoretical investigation of the oxidative addition performed by Maseras et al.⁵²

The relative rate of different aryl residue should as well be considered and is roughly proportional to the relative rate in S_NAr transformations of these substrates.⁵³ This trend can be easily rationalized considering the reactivity of for example 2,5-dibromopyridine in Pd-catalysed reactions. These take place regioselectively at the C2 position,⁵⁴ whereas palladium-catalysed reactions of 2,4- or 2,6-dichloropyrimidines take place at C4 and C6 more readily than at C2.⁵⁵

The rate of the transmetalation step is strongly influenced by the concentration of the base that is used.⁵⁶ While higher concentrations in [OH⁻] promote the transmetalation step due to the formation of formation of [ArPd(OH)(PPh₃)₂], which reacts faster with Ar'B(OH)₂ (for example in the Suzuki reaction). At the same time to high concentrations of OH⁻ lower the reaction rate due to the deactivation of the transmetalation reagent (here the boronic acid is deactivated to the boronate). Further the rate of the transmetalation step is decreasing in the order of Cl > Br > I, which is the reverse order of the oxidative addition.⁵⁷ The electronics of the transmetalation reagent matter as well. More electron rich fragments are often faster transmetalated, while at

⁵³ J. J. Li, G. W. Gribble *Palladium in Heterocyclic Chemistry, Volume 26, Second Edition: A Guide for the Synthetic Chemist*. Oxford: Elsevier, 2007. Print.

⁵⁴ J. W. Tilley, S. Zawoiski *J. Org. Chem.* **1988**, *53*, 386.

⁵⁵ N. M. Simkovsky, M. Ermann, S. M. Roberts, D. M. Parry, A. D. Baxter, *J. Chem. Soc., Perkin Trans. 1* **2002**, 1847.

⁵⁶ C. Amatore, A. Jutand, G. Le Duc, *Chem. Eur. J.* **2011**, *17*, 2492 – 2503.

⁵⁷ N. Miyaura, *J. Organometallic Chemistry* **653** (2002) 54.

the same time the steric bulk of the coupling partners slows down the rate of the transmetalation step.⁵⁸

The reductive elimination step is as well promoted by the presence of base through the generation of a pentacoordinated anionic palladium complex.⁵⁶ This can be attributed to a general steric effect, which as well promotes the reductive elimination, if enough steric bulk is present on the two coupling partners and the ligands. The electronic structure of the coupling partners significantly increases the rate of the reductive elimination as shown by Hartwig *et al.*⁵⁹ on the basis of platinum complexes. While this elementary step is considered facile for coupling partners with different electronic structures (e.g. one electron rich and electron poor one), the reductive elimination is more difficult for electronically similar coupling partner (e.g. two electron rich or two electron poor ones).

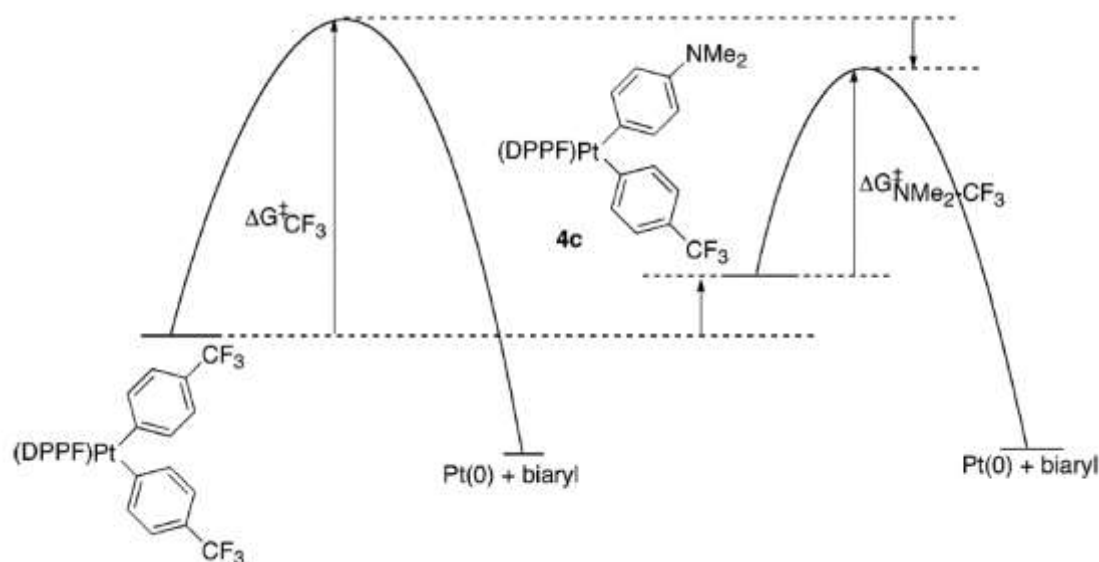


Figure 3: Qualitative energy diagram for the comparison of the rates of reductive elimination from (DPPF)Pt(C₆H₄-4-CF₃)₂ and (DPPF)Pt(C₆H₄-4-CF₃)-(C₆H₄-4-NMe₂) reported by Hartwig.⁵⁹

In some cases the rates of all elementary steps in the catalytic cycle can be improved through ligand design. For example with bulky, electron rich ligands the oxidative addition is promoted electronically, while the reductive elimination is facilitated by the steric repulsion of the metals ligand and the substrate residues.⁶⁰

A Nobel Prize was even attributed to Heck, Negishi and Suzuki for their development of palladium catalysed cross coupling reactions in 2010.⁶¹ While classically aryl halides and boronic acids had been used for the cross coupling reaction (for example Suzuki reactions)⁶²,

⁵⁸ P. Espinet, A. M. Echavarren, *Angew. Chem. Int. Ed.* **2004**, *43*, 4704.

⁵⁹ S. Shekhar, J. F. Hartwig, *J. Am. Chem. Soc.* **2004**, *126*, 13016.

⁶⁰ U. Christmann, R. Vilar, *Angew. Chem. Int. Ed.* **2005**, *44*, 366.

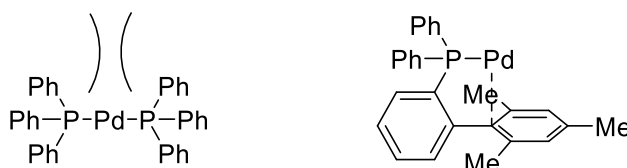
⁶¹ "The Nobel Prize in Chemistry 2010". *Nobelprize.org*. Nobel Media AB 2014. Web. 19 Apr 2017. <http://www.nobelprize.org/nobel_prizes/chemistry/laureates/2010/>

⁶² N. Miyaura, K. Yamada, A. Suzuki, *Tetrahedron Lett.* **1979**, *20*, 3437.

the general reactivity could amongst other be expanded to organohalides with organozinc compounds (Negishi coupling)⁶³, organotin compounds (Stille coupling) or organosilicon (Hiyama coupling) compounds, to alkenes with aryl halides (Heck coupling) or even to aryl halides with amines (Buchwald-Hartwig amination). Therefore nowadays cross coupling reactions allow access to a broad range of different products. Not surprisingly the ligand design plays as well a prominent role to tune the metal properties and reactivity to exclusively yield the desired compounds.

3.2 Influence of the ancillary ligand in cross coupling reactions

The ligand plays an important role in all elementary steps necessary for a given transformation and its influence to each step will be discussed later on. Besides the electronic influence the ligand also acts via its steric effects, which in general stabilize the metal centre, shielding it from other molecules (e.g. water) to avoid side reactions. This additional stabilisation achieved through ligand design can easily be realized, comparing the reactivity of palladium acetate, tetra triphenylphosphine palladium and SPhos palladium salts. While in palladium acetate the ligand shields the metal only minorly from undesired reactivity, in the triphenylphosphine palladium complex a better shielding can be obtained through the steric bulk of the ligand. The shielding can even be further improved as realized by Buchwald type ligand, which shield the metal centre through their steric bulk and a secondary arene metal interaction avoiding almost all side reaction. This results in a net improvement of the catalytic activity of the metal systems employed and impressive high turnover numbers can be obtained for those systems. However, if the steric bulk is increased even further at a certain point the substrate is not able to add to the metal centre and thereby the reactivity is completely blocked. Therefore, the steric bulk of the employed ligand system needs to be optimised with care.

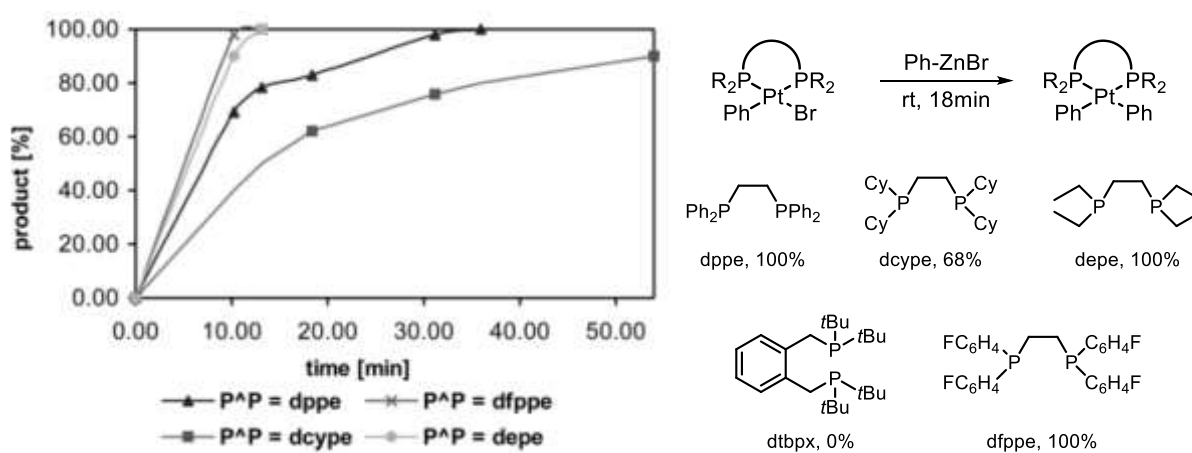


Scheme 27: steric protection of palladium⁰.

Besides the steric bulk the electronic properties of the used ligands play a tremendous role as well, because for each elementary step the ligand can either be beneficial or detrimental. For example while the oxidative addition is promoted by electron rich ligands for example carbenes, those will be unfavourable for the reductive elimination, where electron poor ligands

⁶³ A. O. King, N. Okukado, E.-I. Negishi, *J. Chem. Soc. Chem. Comm.* **1977**, 19, 683.

are beneficial. For the transmetalation step studies from Farina⁶⁴, Espinet⁶⁵, Amatore and Jutand⁶⁶ suggest, that for phosphine ligands an indirect electronic effect is observed due to the loss of one ligand before or during the transmetalation step and therefore it is more a steric, than an electronic effect. This trend was further underlined by Clarke *et al.*⁶⁷ They tested the influence of bidentate ligands in the transmetalation of phenyl zinc bromide to platinum complexes. While changing the electronic nature of the ligands from more electron rich phosphine (depe) to more electron poor ligands (dppe) no significant influence (both 100% yield after 18 mins) was observed, increasing the steric bulk significantly inhibits the reactivity (dcype: 62% yield and dtbpx: 0% yield after 18 mins).



Scheme 28: influence of the ligand to the transmetalation step in cross coupling reactions.

A steric influence to the reductive elimination was as well reported by Buchwald *et al.*⁶⁸ They realized that by the extended steric bulk of the ligand the rate of the reductive elimination is increased as both residue at the metal centre are pushed away. Overall, to successfully tune the rate of a given transformation all elementary steps need to be considered. If this concept is applied successfully high reactivities and selectivities are achieved in cross coupling reactions. Therefore, we can find a broad range of highly developed ligands for different types of cross coupling reactions, once more demonstrating the power of ligand design.

3.3 Application of phosphines in cross coupling reactions.

Phosphines in general and for instance triphenylphosphine are applied in a broad range of coupling reaction amongst others in the Heck-, Stille-, Suzuki-Miyaura-, and Kumada coupling. Additional noteworthy ligands based on the dialkylbiaryl phosphines used in palladium

⁶⁴ B. Krishnan, V. Farina, *J. Am. Chem. Soc.* **1991**, *113*, 9585.

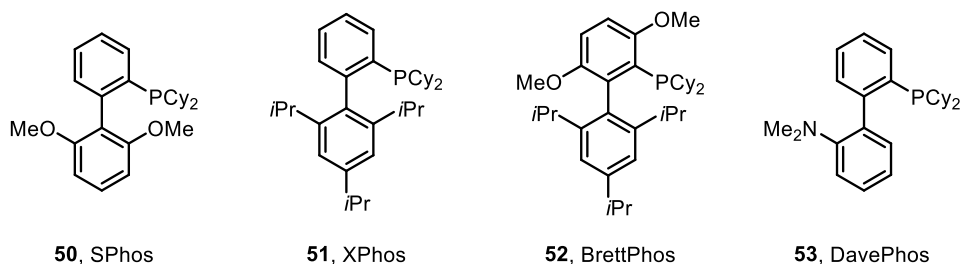
⁶⁵ A. L. Casado, P. Espinet, *J. Am. Chem. Soc.* **1998**, *120*, 8978.

⁶⁶ A. A. Bahsoun, A. Jutand, G. Meyer, A. N. Ntepe, L. Ricard, C. Amatore, *J. Am. Chem. Soc.* **2003**, *125*, 4212.

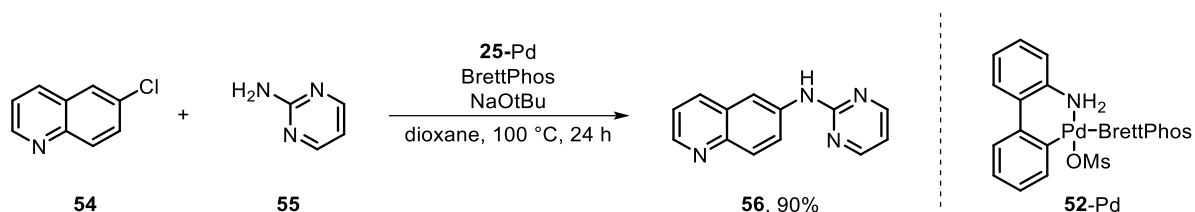
⁶⁷ M. Heydt, M. L. Clarke, *Organometallics* **2005**, *24*, 6475.

⁶⁸ N.C. Bruno, M. T. Tudge, S. L. Buchwald, *Chem. Sci.* **2013**, *4*, 916.

chemistry were reported by Buchwald *et al.*⁶⁸ and applied in C-N bond formations. Buchwald *et al.*⁶⁸ reported the preparation of SPhos (**50**), XPhos (**51**), BrettPhos (**52**) and DavePhos (**53**) as well as their application in palladium catalysed C-C and C-N bond formations.

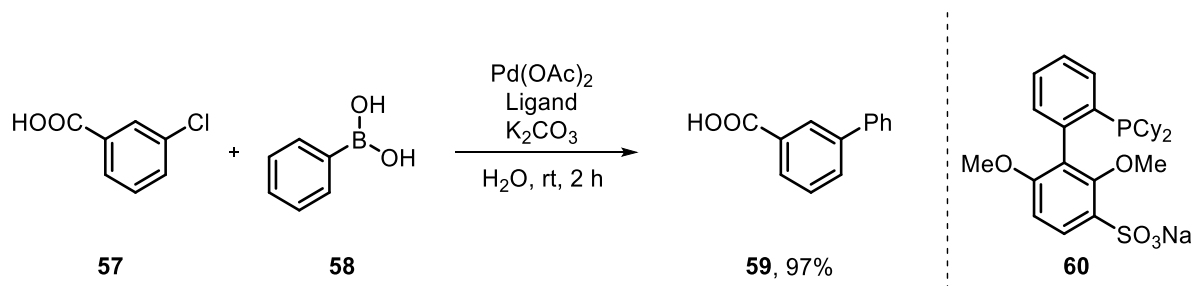


Scheme 29: ligands developed by Buchwald *et al.*⁶⁸



Scheme 30: C-N bond formation reported by Buchwald *et al.*⁶⁸

Suzuki-Miyaura and Sonogashira coupling reactions in water were reported with the anionic Buchwald type ligands in excellent yields for a broad range of substrates (over 25 examples) and even at room temperature an impressive Suzuki-Miyaura coupling could be performed in water with low catalyst loading (2 mol%) converting chloroarene **57** to biphenyl **59** in excellent yield (97%) within 2 hours.



Scheme 31: Suzuki-Miyaura coupling in water with anionic ligand.

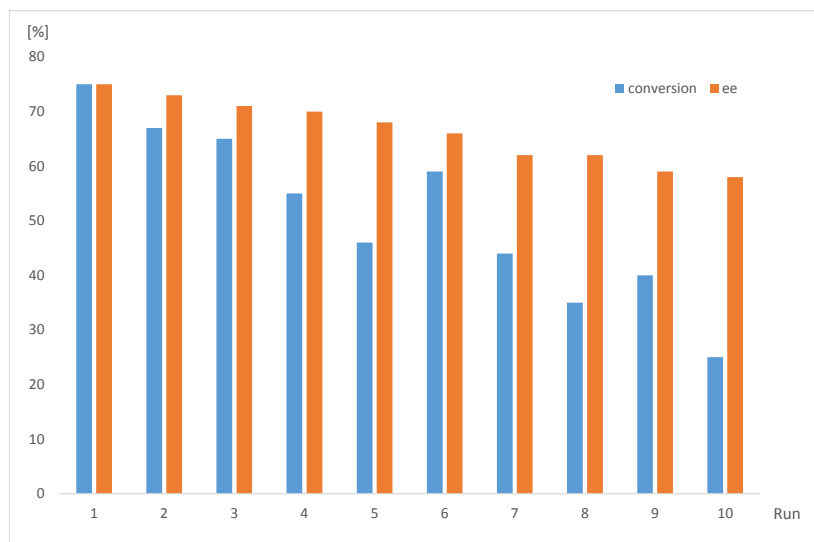


Figure 4: recycling effect on the enantioselective nucleophilic substitution with an imidazolium tagged chiral diamidophosphate ligand. Fehler! Textmarke nicht definiert.

4. A new strategy to modify the donor properties of phosphines

Our group reported a new strategy to modify phosphine ligands. Although charged phosphines are already reported in literature, these usually bear the cationic charge at a remote position having low influence on the donor and acceptor properties of the corresponding phosphines. Direct attachment of the positive charge α to the phosphine was first reported by Kuhn *et al.*⁷⁰, but the systematic applications of their donor properties were largely overlooked. The strong inductive effect of the introduced positive charge, significantly reduced the σ -donor abilities of α -cationic phosphines. At the same time, the energy of the $\sigma^*(\text{P}-\text{C}^+)$ orbitals is further decreased, increasing their π -acceptor character, and as consequence, the global electron donation of these ligands to the metal is quite low. Only polyhalogenated phosphines such as PF_3 , $\text{P}(\text{CF}_3)_3$, or PCl_3 depict similar electronic properties, but are, because of the labile phosphorus–halogen bond, much more sensitive to moisture and water and therefore, more difficult to handle. Hence, α -cationic phosphines are in this regard superior to the hereto known electron poor, but sensitive ligands. The effect, caused by the introduction of different α -cationic residues, to the frontier orbital on phosphines was reported by our group (Figure 5: frontier orbital for cationic phosphines.) The introduction of a cationic charge significantly lower the energy of the corresponding HOMOs in comparison to triphenylphosphines. However, for the different cationic phosphines the energy of the corresponding HOMOs is relatively close to each other (-9.05 eV to -9.85 eV), indicating, that the σ -donation of the different cationic phosphine is similar. Conversely the LUMOs are diminished in a much wider range (-4.1 eV to -6.34 eV), confirming, that the neat reduction of global electron density is a result of the enhanced π -acceptor properties.

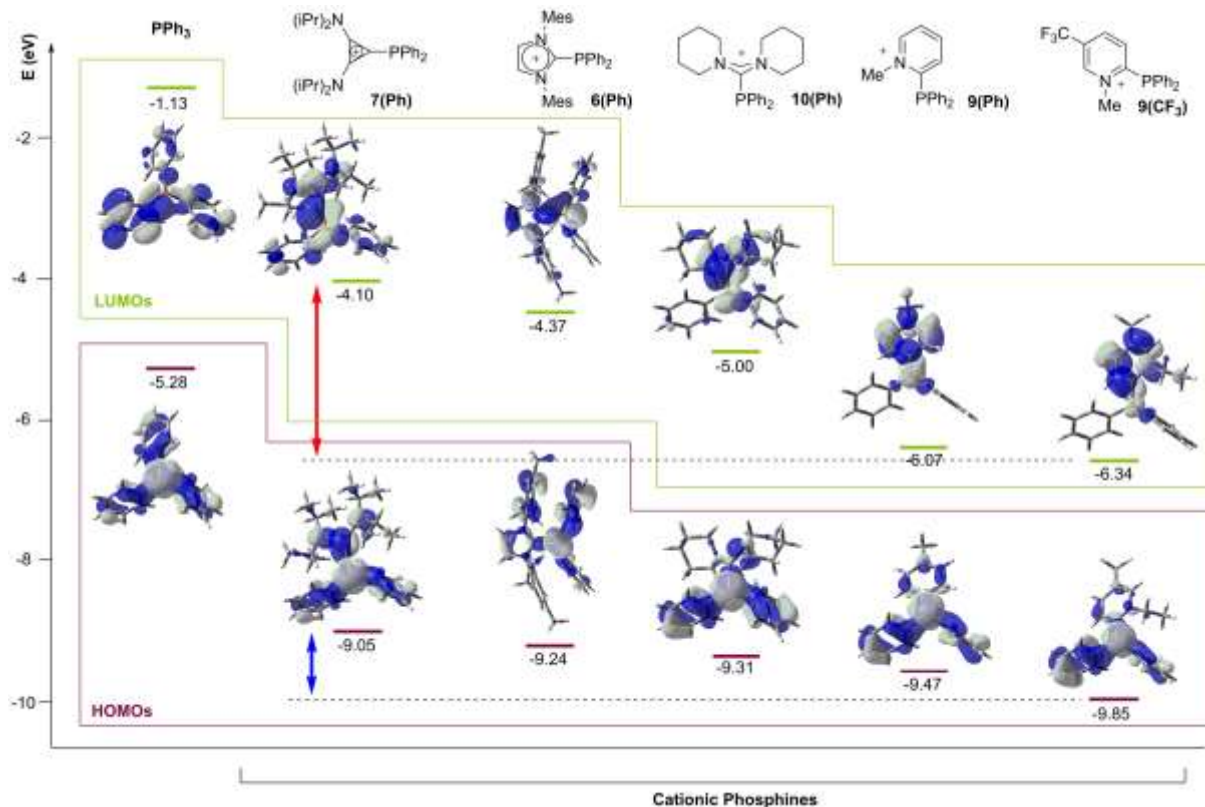
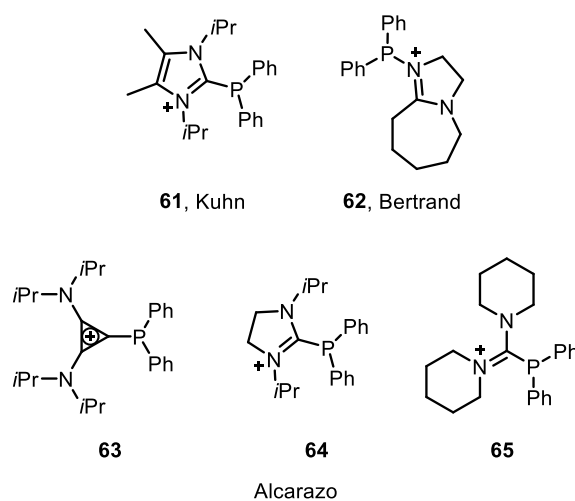


Figure 5: frontier orbital for cationic phosphines.

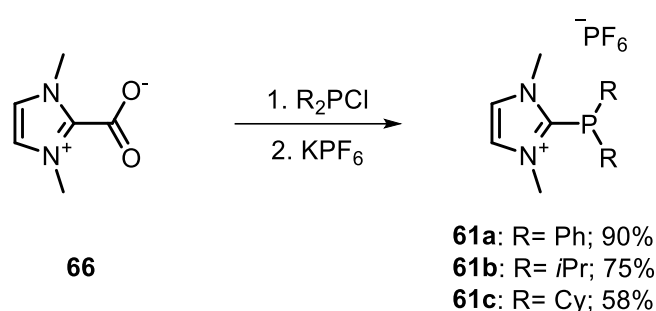
4.1 α -monocationic phosphines

As mentioned before our group and others developed α -cationic phosphines.



Scheme 32: developed α -cationic phosphines.

The first α -cationic phosphine **61**, which was based on an imidazolium moiety, was reported by Kornilov⁶⁹ and further developed by Kuhn,⁷⁰ Wasserscheid⁷¹ and Tkatchenko.⁷² Through generation of the carbene by decarboxylation of imidazolium zwitterion **66** and attack towards different disubstituted phosphine chlorides the corresponding imidazolium phosphines **61a-c** were obtained in moderate to good yields (58-90%). This synthetic strategy however could not be extended towards the preparation of other cationic phosphines as the generation of the corresponding carbene is difficult or the attack towards the phosphine does not occur in the desired selectivity.



Scheme 33: generation of imidazolium phosphines **61a-c**.

For this reason our group⁷³ developed a more general synthetic strategy consisting of direct condensation of a secondary phosphine with a Vilsmeier-type salt and could extend the scope of cationic phosphines to cyclopropenium-⁷⁴, imidazolinium-⁷⁵ and formamidinium phosphines.

Cyclopropenium phosphines **63a-f** with different substitution patterns at the phosphorus atom were obtained in good to excellent yields (76-96%) through direct condensation of chlorocyclopropenium salt **67** followed by anion exchange. This reaction allows the preparation of cyclopropenium phosphines on a multiple gram scale as white and air stable solids.

⁶⁹ I. V. Komarov, M. Y. Kornilov, *Tetrahedron* **1995**, *51*, 11271.

⁷⁰ H. Bohnen, G. Henkel, N. Kuhn, *Z. Naturforsch. B* **1994**, *49*, 1473.

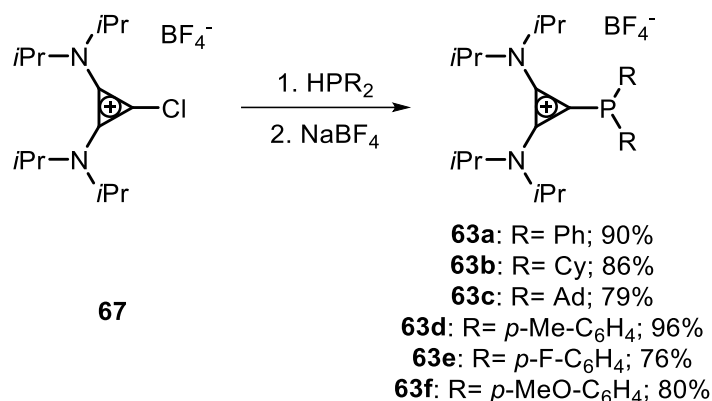
⁷¹ D. J. Brauer, K. W. Kottsieper, C. Liek, O. Stelzer, H. Waffenschmidt, P. Wasserscheid, *J. Organomet. Chem.* **2001**, *630*, 177.

⁷² M. Azouri, J. Andrieu, M. Picquet, P. Richard, B. Hanquet, I. Tkatchenko, *Eur. J. Inorg. Chem.* **2007**, *31*, 4877.

⁷³ Compare: M. Alcarazo, *Acc. Chem. Res.* **2016**, *49*, 1797.

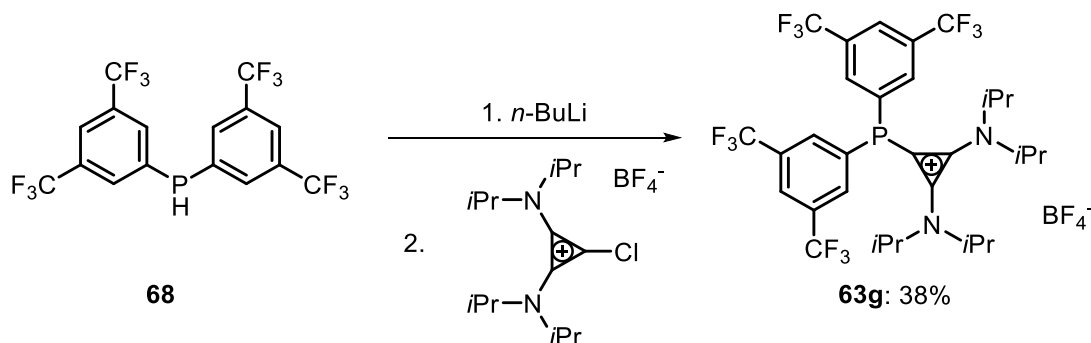
⁷⁴ J. Petuškova, H. Bruns, M. Alcarazo, *Angew. Chem., Int. Ed.* **2011**, *50*, 3799.

⁷⁵ E. Haldón, E. A. Kozma, H. Tinnermann, L. Gu, R. Goddard, M. Alcarazo, *Dalton Trans.* **2016**, *45*, 1872–1876.



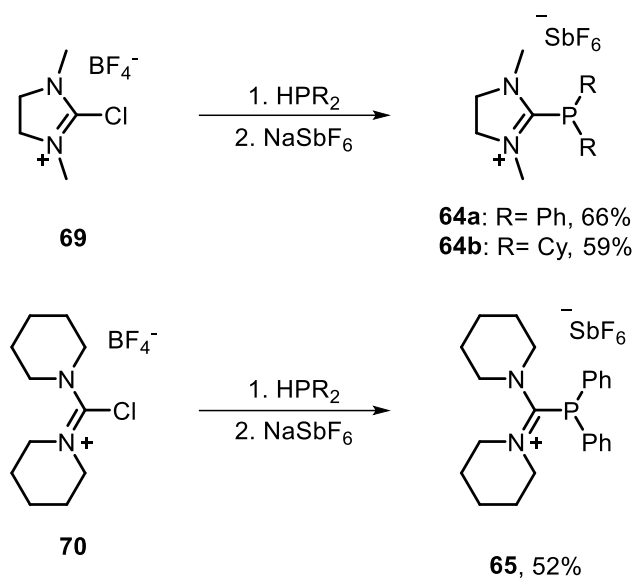
Scheme 34: generation of cyclopropenium phosphines.

Introducing the electron poor polyfluorinated phosphine **68** via the aforementioned condensation failed, due to the low nucleophilicity of the phosphine. Therefore, deprotonation is necessary to achieve the condensation reaction to the corresponding cyclopropenium salt **63g**⁷⁶.

Scheme 35: condensation of phosphine **68** with cyclopropenium salt **67**.

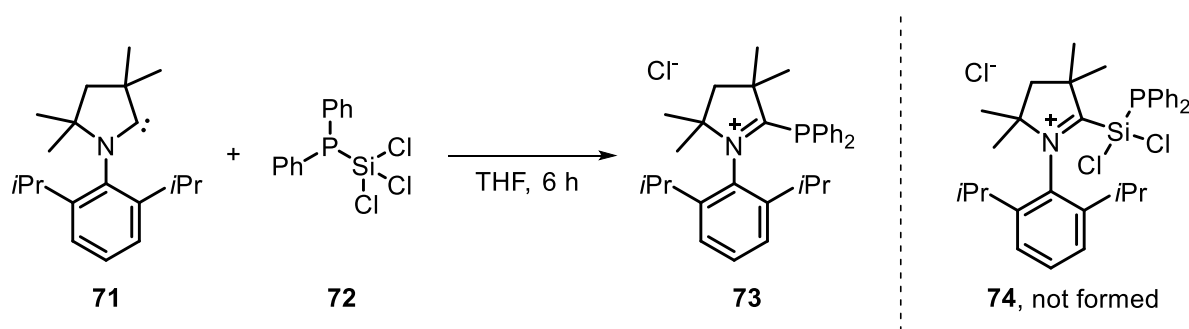
In addition to the modification of the phosphine moiety, an alteration of the cyclopropenium substituent is possible and formamidinium and imidazolium residues can be introduced, yielding the corresponding cationic phosphines **64a-b** and **65**.

⁷⁶ Á. Kozma, T. Deden, J. Carreras, C. Wille, J. Petušková, J. Rust, M. Alcarazo, *Chem. Eur. J.* **2014**, *20*, 2208.



Scheme 36: preparation of imidazolinium- and formamidinium phosphines.

A report by Roesky *et al.*⁷⁷ mentions CAAC based cationic phosphine **73** obtained as by-product instead of the desired formation of silaphosphine **74**, however, applications of phosphine **73** are until now not reported.

Scheme 37: formation of CAAC phosphine **73**.

4.2 α -polycationic phosphines

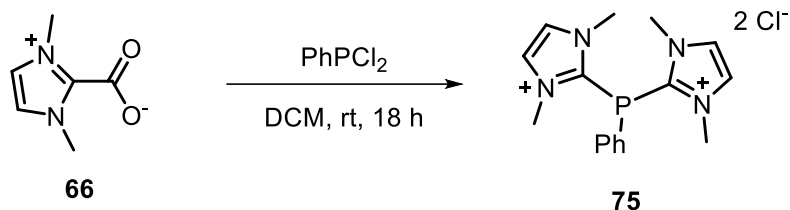
To increase the influence of the positive charge, not only monocationic, but di- and even tricationic phosphines have been prepared.

Cathey *et al.*⁷⁸ reported the preparation of dicationic imidazolium substituted phosphine **75**, which was prepared through addition of the corresponding carbene towards phenylphosphinedichloride. Unfortunately, purification of this compound proved to be difficult

⁷⁷ S. Roy, A. C. Stückl, S. Demeshko, B. Dittrich, J. Meyer, B. Maity, D. Koley, B. Schwederski, W. Kaim, H. W. Roesky, *J. Am. Chem. Soc.* **2015**, *137*, 4670.

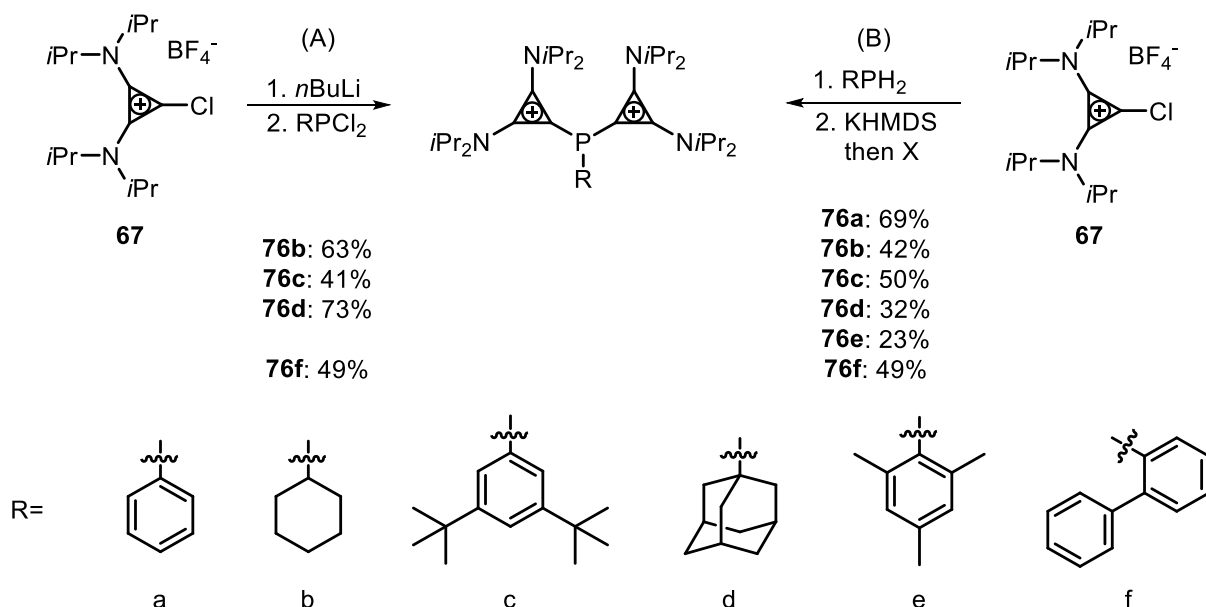
⁷⁸ M. Azouri, J. Andrieu, M. Picquet, H. Cathey, *Inorg Chem.* **2009**, *48*, 1236.

and the product was still contaminated with 10% of starting material even after extensive washing.



Scheme 38: preparation of dicationic phosphine **75**.

Alcarazo *et al.*⁷⁹ reported the preparation of dicationic cyclopropenium phosphine **76a** and its derivatives⁸⁰ and could prepare several new dicationic cyclopropenium phosphines **76b-f** in moderate to good yields. Their synthesis strategy either consisted of halogen/lithium exchange followed by addition towards the dichlorophosphine similar to Cattey *et al.*⁷⁸ or through a stepwise condensation of primary phosphines with chlorocyclopropenium salts.

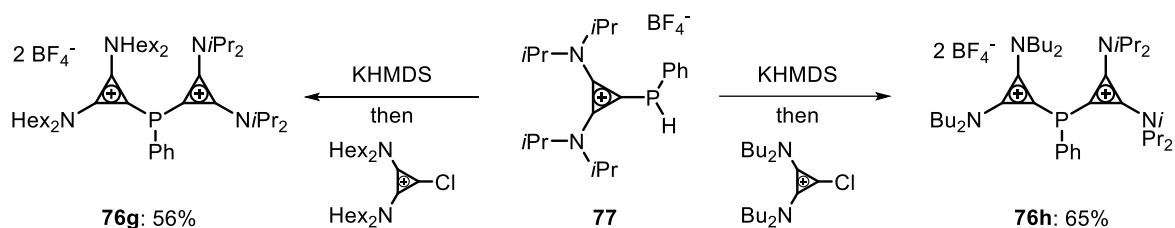


Scheme 39: preparation of dicationic phosphine **62a-f**

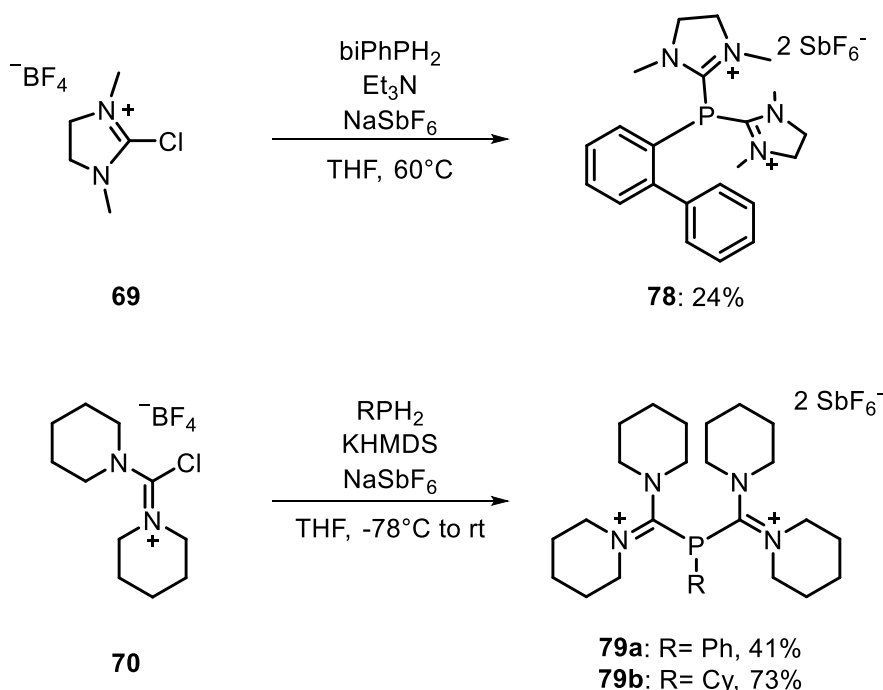
In addition to the modification of the phosphine substituents this reliable synthesis plan tolerates modification of the amine substituents as well as allowing fine tuning of the solubility properties of the resulting phosphines. For example the preparation of butyl and hexyl substituted dicationic phosphines **76g** and **76h** is reported⁸⁰ as well, employing the same preparation method.

⁷⁹ J. Carreras, G. Gopakumar, L. Gu, A. Gimeno, P. Linowski, J. Petrušková, W. Thiel, M. Alcarazo, *J. Am. Chem. Soc.* **2013**, *135*, 18815.

⁸⁰ G. Mehler, P. Linowski, J. Carreras, A. Zanardi, J. W. Dube, M. Alcarazo, *Chem. Eur. J.* **2016**, *22*, 15320.

Scheme 40: preparation of dicationic phosphines **76g** and **h**.

Furthermore the synthetic strategy could be extended to bis-imidazolium- and bis-formamidinium phosphines **78** and **79a-b** in moderate to good yields (24-73%).

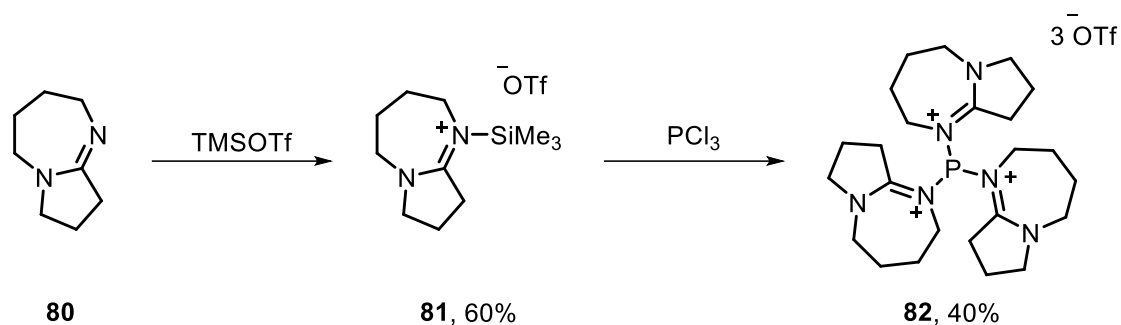
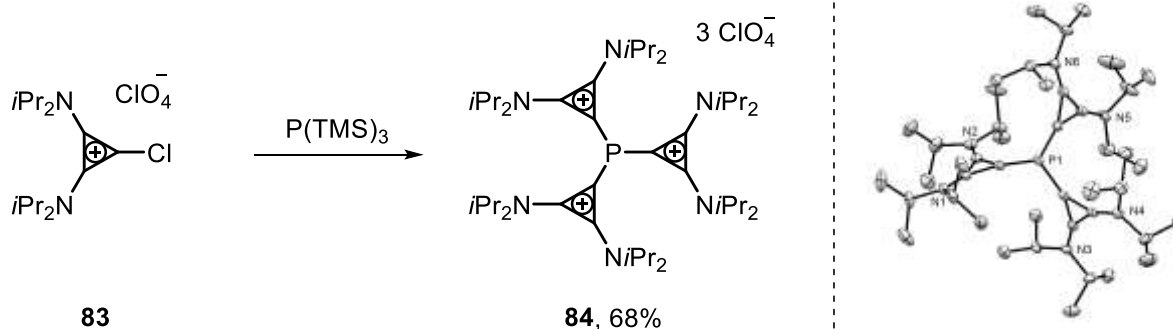
Scheme 41: synthesis of bis-imidazolium and bis-formamidinium substituted phosphines **78** and **79a-b**.

The most extreme π -acceptor phosphines prepared so far were reported by Bertrand *et al.*⁸¹ (based on DBU - **82**) and Alcarazo *et al.*⁸² (based on cyclopropenium - **84**), and are tricationic ones. The syntheses are based on the “onium” and reversed “onium” strategy⁸³, a direct condensation of a cationic residue with the release of trimethylsilylchloride. Both structures could be verified by solid state analysis, however only Alcarazo reported further applications of the tricationic system.

⁸¹ G. Bouhadir, R. W. Reed, R. Reau, G. Bertrand, *Heteroatom Chem.* **1995**, *6*, 371.

⁸² J. Petuškova, M. Patil, S. Holle, C. W. Lehmann, W. Thiel, M. Alcarazo *J. Am. Chem. Soc.* **2011**, *133*, 20758.

⁸³ K. G. Wagner, C. Priesner, J. Macheleid, R. Weiss, *J. Am. Chem. Soc.* **1985**, *107*, 4491.

Scheme 42: synthesis of DBU based tricationic phosphine **82**.Scheme 43: synthesis of cyclopropenium based tricationic phosphine **84** and its solid state structure. Anions and hydrogen atoms are omitted for clarity. Ellipsoids set at 50% probability.

4.3 Evaluation of the stereo electronic properties

To understand why the additional positive charge is beneficial in terms of reactivity and reaction rate, one needs to understand the nature of the interactions between the phosphine and the metal as well as the influence of the cationic charge towards the interactions. A model is introduced to explain the interactions between phosphine and metal. Furthermore, the phosphine's electronic and steric parameter are categorised using different models. This discussion then led to the interactions between metal and substrate depending on the employed phosphines, which explains the observed reaction rates and selectivities.

The ligands interact with the metal by σ -donation from the phosphorus lone pair to an empty d-orbital of the metal, while at the same time a metal's full d-orbital interacts by π -backdonation to the three σ^* -orbital of the phosphorus and the phosphorus substituents bonds.

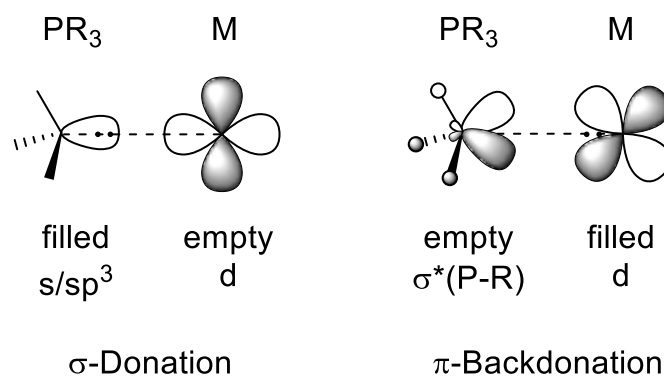


Figure 6: interactions between metals and phosphine ligands, σ -donation and π -backdonation.

Depending on the electronic properties of the phosphine, the amount of σ -donation and π -backdonation differs. It has been shown by calculations, that the main interaction is usually the σ -donation.⁸⁴ Only for the most electron poor phosphines for example tricationic phosphines or PF₃ the π -backdonation is the main interaction between the phosphine and the metal, because of the more efficient orbital overlap between the σ^* orbital (which lies lower in energy) and the metal d-orbitals.⁹⁷

On the other hand, electron rich phosphines show stronger σ -donation, for example in PtBu₃ the phosphorus-metal interaction is strengthened by the inductive effect of the *tert*-butyl groups.

To classify the electronic structure of different phosphines, Tolman *et al.*⁸⁵ introduced an electronic parameter in 1970 measuring the CO stretching frequencies of the corresponding nickel carbonyl complexes, which was later named Tolman electronic parameter (TEP). Despite the high toxicity of nickel tetra-carbonyl, these complexes were chosen as model for the TEP being easily prepared by mixing the ligand and Ni(CO)₄ in a 1 to 1 ratio. Furthermore the A₁ band of the carbonyl group is sharp and therefore can be measured with high accuracy. Depending on the aforementioned effect of σ -donation and π -backdonation of the employed phosphine the electron density of the metal changes, resulting in different interactions of the metal with the carbonyl group causing the C-O stretching frequencies to shift. The interaction between the metal and the carbonyl group consist of σ -donation and π -backbonding. As both fragments – the phosphine moiety as well as the carbonyl ligand - compete for the electron density of the metal, the electronic characterisation of the carbonyl unit through infrared analysis corresponds to the electronic nature of the phosphines as well. Therefore, the CO stretching frequency is relevant for the quantification of the ligands donor and acceptor properties. More π -backdonation from the metal towards the carbonyl group leads to a higher

⁸⁴ D. Zuccaccia, L. Belpassi, A. Macchioni, F. Tarantelli, *Europ. J. Inorg. Chem.* **2013**, 24, 4121.

⁸⁵ C. A. Tolman, *J. Am. Chem. Soc.* **1970**, 92, 2953.

population of the antibonding π^* orbital of the carbonyl group and hence, the carbonyl bond order decreases, leading to higher CO stretching frequencies. This results in lower CO stretching frequencies for better σ -donor ligands, while higher CO stretching frequencies are observed for better π -acceptor ligands. Consistent with this trend a few examples of phosphine ligands reported by Tolman⁸⁶ and their TEPs are shown in table 1.

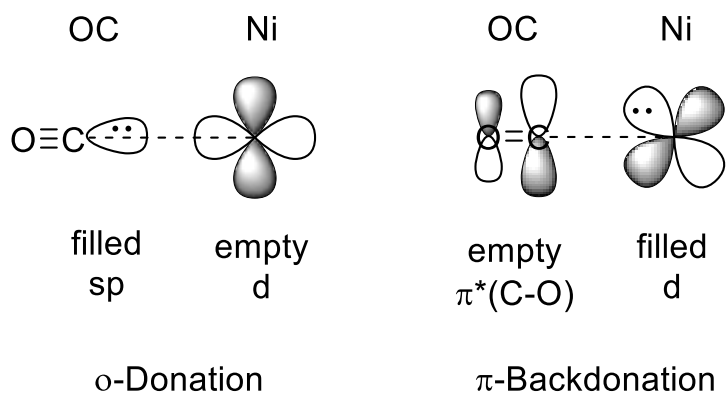


Figure 7: interactions between nickel and carbonyl ligands, σ -donation and π -backdonation.

Ligand	$\nu_{\text{CO}}(A_1)$ [cm ⁻¹]	Ligand	$\nu_{\text{CO}}(A_1)$ [cm ⁻¹]
P(<i>t</i> Bu) ₃	2056.1	P(OEt) ₃	2076.3
P(<i>i</i> Pr) ₃	2059.2	PPh ₂	2077.0
PBu ₃	2060.3	P(OMe) ₃	2079.5
PEt ₃	2061.7	PPh ₂ Cl	2080.7
PMe ₃	2064.1	P(OPh) ₃	2085.3
P(<i>p</i> -tolyl) ₃	2066.7	P(C ₆ F ₅) ₃	2090.9
PPh ₃	2068.9	PCl ₃	2097.0
PPh ₂ H	2073.3	PF ₃	2110.8
P(O <i>i</i> Pr) ₃	2075.9		

Table 2: Tolman electronic parameter of a range of ligands.⁸⁶

In addition to the TEPs of phosphines their steric environment needs to be considered as well. Thus, Tolman defined the steric parameter θ , nowadays known as the Tolman angle.⁸⁶ The Tolman angle is defined as the weighted apex angle to the outermost atom of each substituent of the phosphorus of a cone, centred 2.28 Å from the centre of the phosphorus atom (see Equation 1 and Figure 8). Consistent with the expectations, a few examples of the Tolman angle for more established ligands are shown.

$$\theta = 2/3 \sum_{i=1}^3 \theta_i / 2 \quad (\text{Eq.: 1})$$

⁸⁶ C. A. Tolman, W. C. Seidel, L. W. Gosser, *J. Am. Chem. Soc.* **1974**, 96, 53.

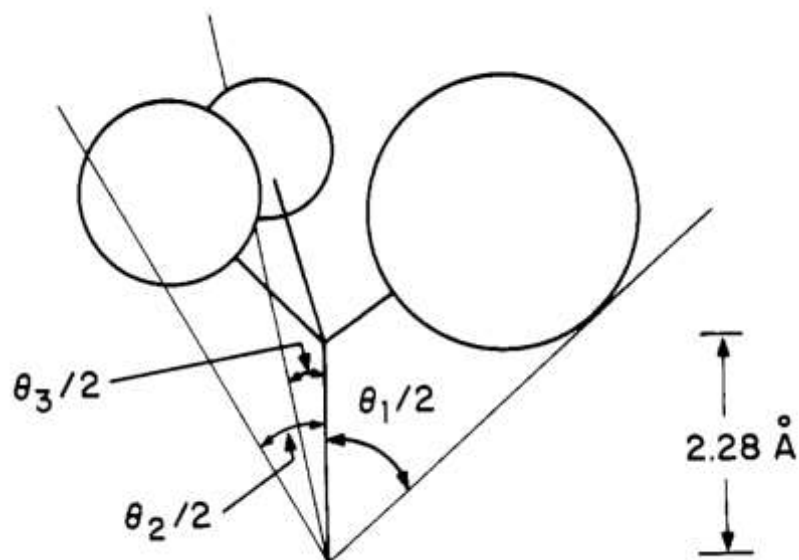


Figure 8: Tolman cone angle determination of unsymmetrical phosphines.

Ligand	θ [°]	Ligand	θ [°]
PH ₃	83	PPh ₃	145
PF ₃	104	PBn ₃	165
PMe ₃	118	PCy ₃	170
PCl ₃	124	P(<i>t</i> Bu) ₃	182
P(OPh) ₃	128	P(C ₆ F ₅) ₃	184
P(CF ₃) ₃	137	PMes ₃	212

Table 3: Tolman angle of a range of phosphine ligands.⁸⁶

Combining the electronic and steric effect of all examined ligands then led to a stereo electronic map⁸⁶ – nowadays known as Tolman stereo-electronic map. This map allows to design new ligands, with the necessary electronic or steric properties, or to choose among the already established ligands for a particular transformation for example to enhance reactivity or to improve selectivity.

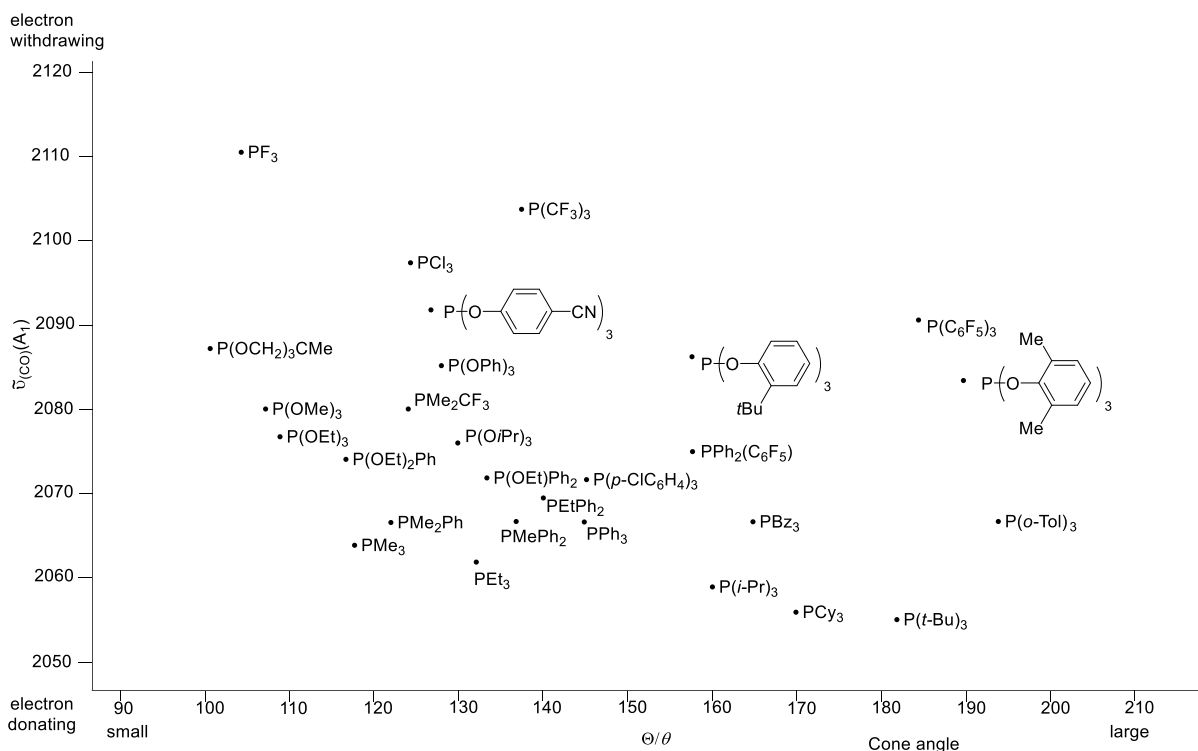
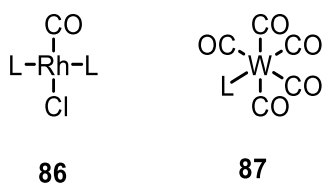


Figure 9: Tolman stereo electronic map.

Due to the high toxicity of nickel tetra-carbonyl numerous alternatives besides the Tolman stereo electronic map have been developed to characterise the donor and acceptor properties of phosphine ligands. Analogously to the nickel carbonyl stretching frequencies rhodium or tungsten carbonyl stretching frequencies can be measured to characterise the ligands. The rhodium or tungsten carbonyl complexes are as easily prepared and do not stem the high toxicity of nickel tetracarbonyl. Unfortunately, the analysis of their corresponding CO stretching frequencies shows a strong dependency upon the applied method (e. g. dissolved or solid)⁸⁷ and the used solvent. In case of the rhodium carbonyl frequencies measurements even non-linear effects⁸⁸ were observed. Therefore, the CO stretching frequencies of the corresponding complexes can be compared, but with care.



Scheme 44: carbonyl complexes of rhodium and tungsten used for the determination of the ligands donor and acceptor properties.

⁸⁷ A. Roodt, S. Otto, G. Steyl *Coordination Chemistry Reviews* **2003**, 243, 121.

⁸⁸ R. J. Angelici, *Inorg. Chem.* **1967**, 6, 1731.

Another method to measure the donor/acceptor properties of ligands is the cyclic voltammetry⁸⁹. In cyclic voltammetry the reduction and oxidation potential of the molecule under study, is measured and referenced against a standard potential (for example ferrocene). Comparing these potentials then allows to rank the donor and acceptor properties of the examined ligands. The advantage of this method is the independence of the steric bulk of the examined system, while the disadvantage is that additional functional group could easily get reduced or oxidized. These are not relevant for the coordination process, but still result in signals in the cyclic voltammogram, which might lead to misassignments. Furthermore, through cyclic voltammetry the reversibility of the reduction and oxidation processes is measured as well, yielding additional information about the radicals generated during the measurement. In Figure 10 a typical cyclic voltammogram is shown.

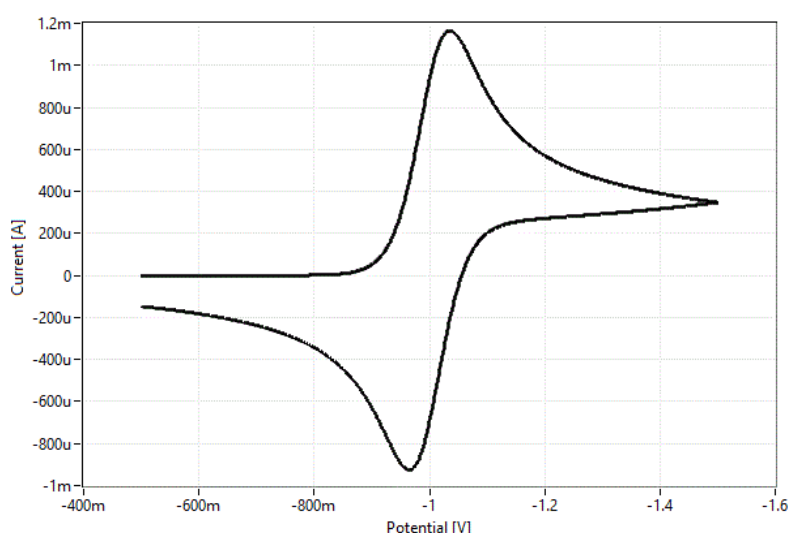


Figure 10: typical cyclic voltammogram of a reversible reduction.

In the literature apart from the Tolman angle the buried ligand volume $\%V_{\text{bur}}$ was introduced by Nolan *et al.*⁹⁰ to access the steric parameter, which allows the characterisation of the steric bulk of all types of ligands including phosphine ligands. The buried ligand volume is defined as the volume of a sphere occupied by the ligand. The sphere has a radius of 3 Å and is centred 2 Å next to the ligand with a metal at its centre. $\%V_{\text{bur}}$ shows an excellent correlation with the Tolman angle for a broad range of phosphines ($R=0.981$)⁹¹ and can further be extended to chelating phosphines or even carbene systems, which could not be characterised well with the Tolman angle. However it should be noted, that the Tolman angle and $\%V_{\text{bur}}$ are not correlating the phosphites as good as the phosphines.

⁸⁹ A. J. Bard, L. R. Faulkner, *Electrochemical Methods: Fundamentals and Applications (2 ed.)* Wiley. **2000**.

⁹⁰ A. C. Hillier, W. J. Sommer, B. S. Yong, J. L. Petersen, L. Cavallo, S. P. Nolan, *Organometallics* **2003**, *22*, 4322.

⁹¹ H. Clavier, S. P. Nolan, *Chem. Commun.* **2010**, *46*, 841.

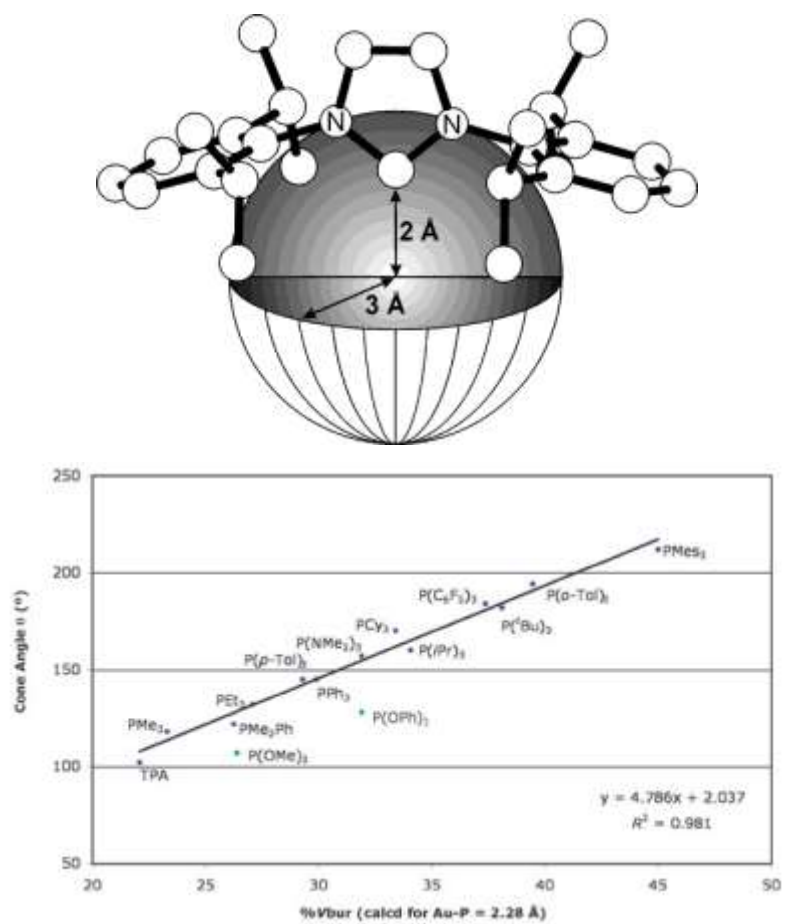
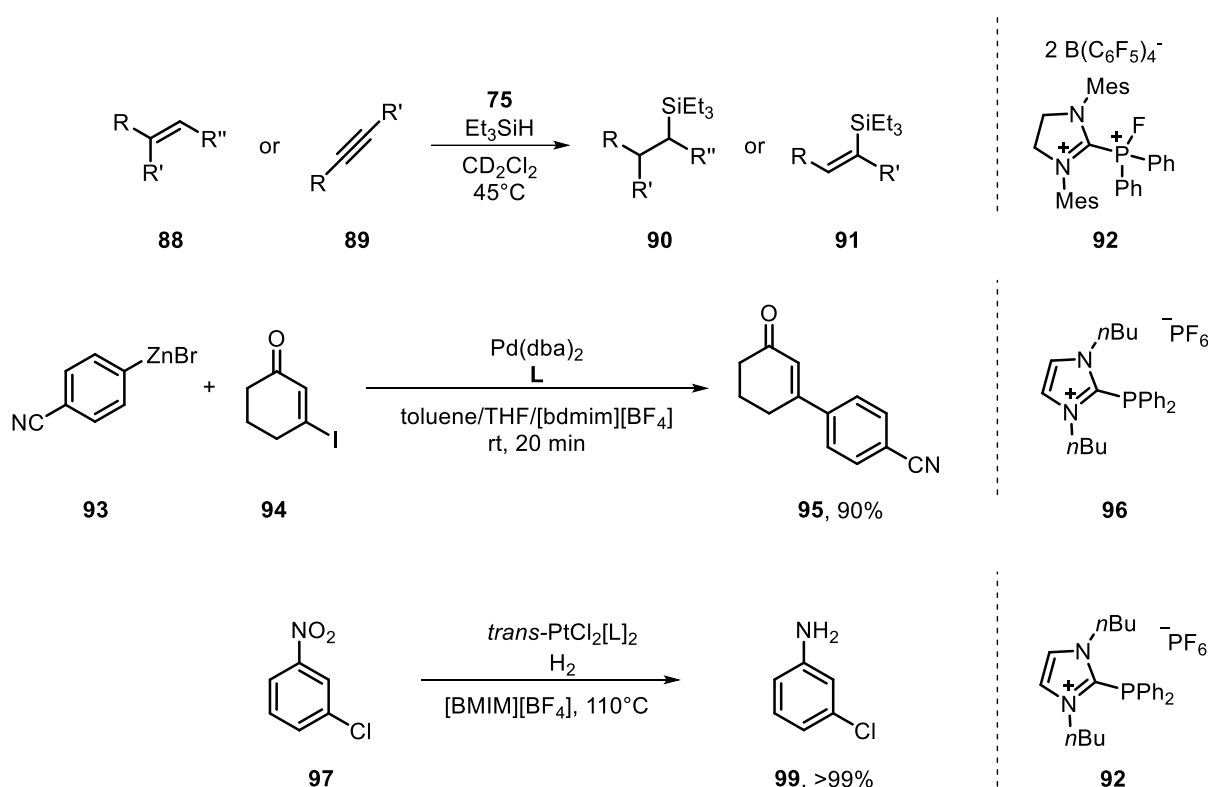


Figure 11: sphere dimension for the determination of %V_{bur} and the correlation of the Tolman angle and the %V_{bur}.⁹¹

4.4 Applications of cationic phosphines

The new cationic phosphines showed great potential and therefore, the metal complexes of the cationic phosphines were applied in a vast amount of π -acid catalysis systems. The phosphines themselves after quaternisation as reported by Stephan *et al.*⁹² show reactivity in hydrodefluorinations of fluoroalkanes and in hydrosilylation of alkenes and alkynes. Further applications of cationic phosphines include Negishi coupling (Knochel *et al.*⁹³), Sonogashira coupling, hydrogenations (both by Picquet *et al.*⁹⁴) and hydroformylations (Wasserscheid *et al.*⁹⁵).



Scheme 45: applications of cationic phosphines.

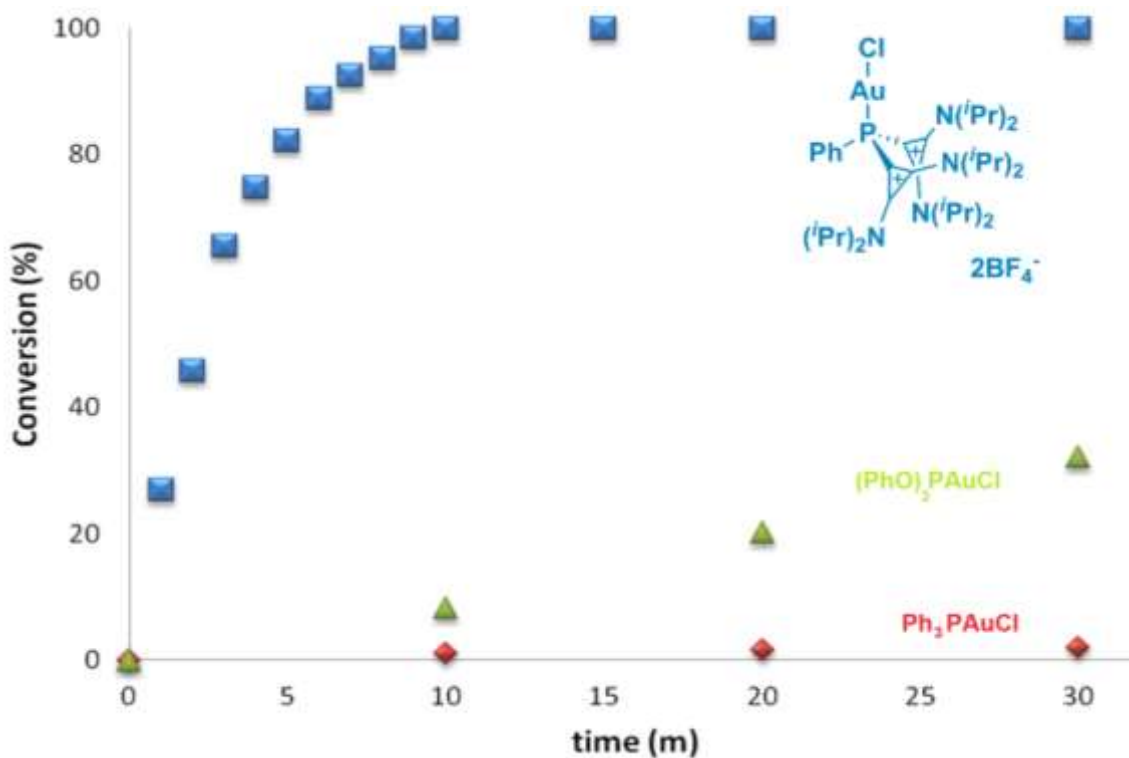
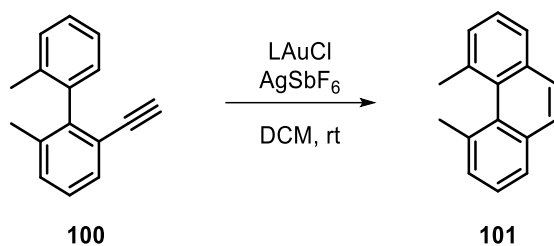
Alcarazo *et al.*⁷⁹ showed, that the application of cationic phosphines in π -acid catalysis after coordination to gold or platinum sources enhances the reaction rate of some transformations tremendously. A strong beneficial ligand effect was present in the hydroarylation of strained biphenylsystem **100** towards phenanthrene moiety **101**. A broad range of different phenanthrenes (over 15 examples) could be prepared by this newly developed method, including some natural products (Coeloginin (**102**), Epimedoicarisoside A (**103**) and Calanquinone C (**104**)).⁷⁶

⁹² M. H. Holthausen, M. Mehta, D. W. Stephan, *Angew. Chem., Int. Ed.* **2014**, *53*, 6538.

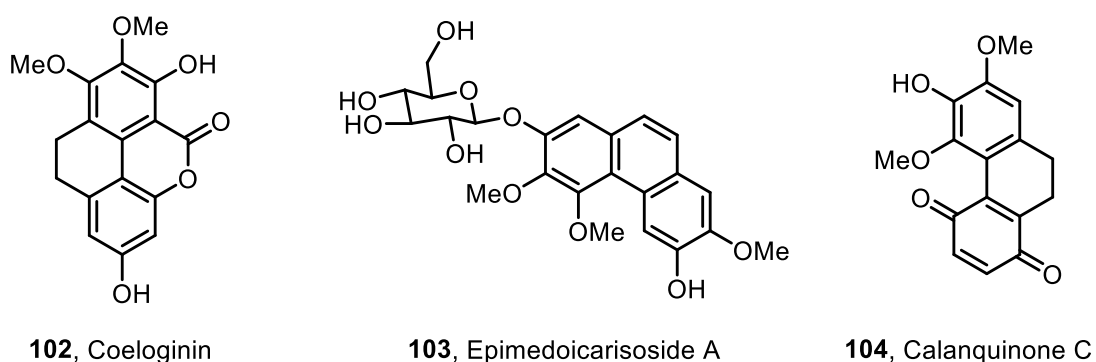
⁹³ J. Sirieix, M. Oßberger, B. Betzemeier, P. Knochel, *Synlett* **2000**, *2000*, 1613.

⁹⁴ S. Saleh, E. Fayad, M. Azouri, J.-C. Hierso, J. Andrieu, M. Picquet, *Adv. Synth. Catal.* **2009**, *351*, 1621.

⁹⁵ C. C. Brasse, U. Englert, A. Salzer, H. Waffenschmidt, P. Wasserscheid, *Organometallics* **2000**, *19*, 3818.



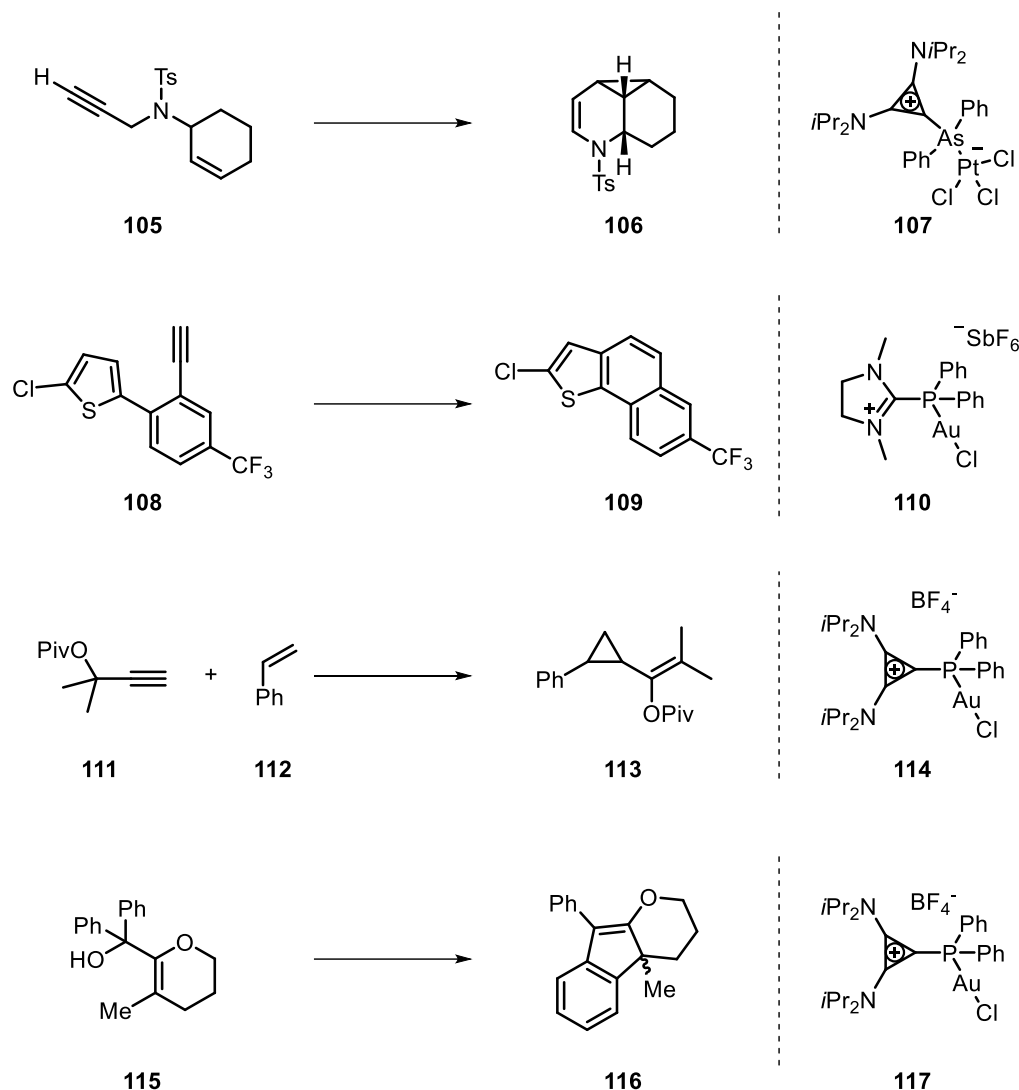
Scheme 46: ligand effect in the cyclization of biphenyl **100** to phenanthrene **101**.⁷⁶



Scheme 47: natural products synthesised employing cationic phosphines.

The aforementioned cationic phosphines proved to catalyse a broad range of different gold(I) and platinum(II) catalysed reactions, for example the enine cyclisation of amine **105** to tricyclic

system **106**⁹⁶, the hydroarylation of **108**⁷⁹, the cyclopropanation of styrene (**112**)⁷⁴ and the hydroxyl abstraction of **115**⁷⁴.



Scheme 48: applications of cationic phosphines/arsines in gold and platinum catalysis.

Despite their high reactivity towards moisture the tricationic phosphines showed great rate enhancement in platinum catalysis⁹⁷. An example is the cyclisation of 2-ethynyl-1,1'-binaphthalene (**118**) into [5-carbo]helicene (**119**). While classical ligands still catalyse the cyclisation reaction, better π -acceptor ligands lead to a rate acceleration. While triphenylphosphine only converts 25% of the starting material, $P(C_6F_5)_3$ (**120**) already converts 50% of the starting material. The use of tricationic ligand platinum complexes **121** and **122** further enhances this beneficial effect and resulted in full conversion within 90 min. and proves

⁹⁶ J. W. Dube, Y. Zheng, W. Thiel, M. Alcarazo, *J. Am. Chem. Soc.* **2016**, *138*, 6869.

⁹⁷ J. Carreras, M. Patil, W. Thiel, M. Alcarazo, *J. Am. Chem. Soc.* **2012**, *134*, 16753.

the positive influence of cationic charges in π -acid catalysis. The tricationic phosphine **84** was also applied in the synthesis of 21 additional phenanthrene derivatives.

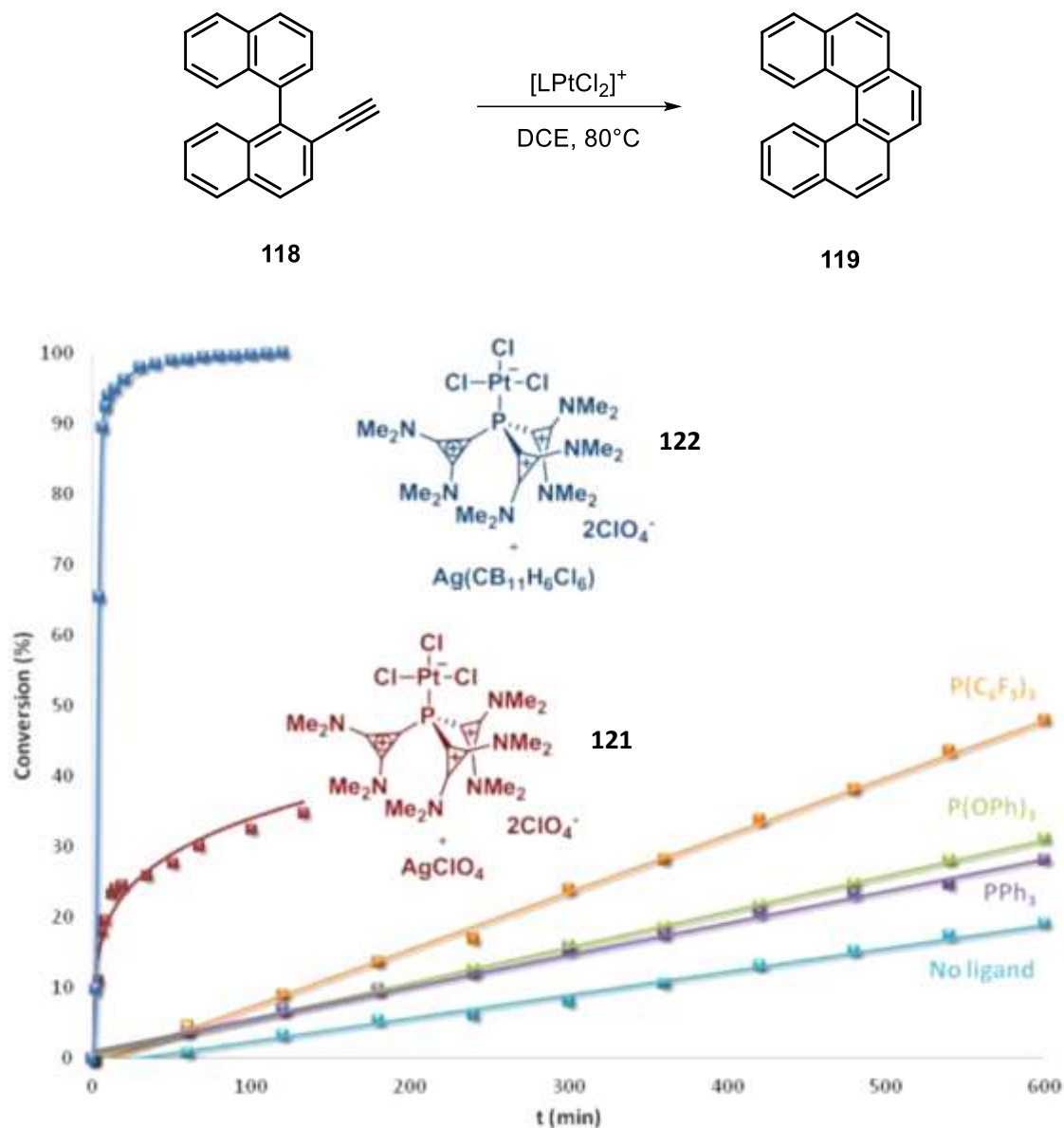
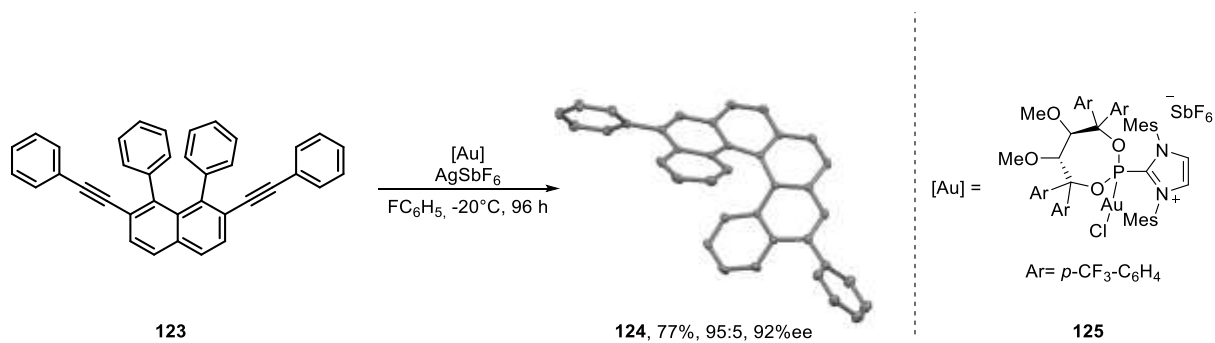


Figure 12: ligand effect on the hydroarylation of biphenyl derivative **118** to pentahelicene **119**. Reagents and conditions: biphenyl **118** (0.05 M), platinum precatalyst (5 mol%), $AgSbF_6$ (5 mol%), $(CH_2Cl)_2$, 80°C.

Alcarazo *et al.*⁹⁸ reported the cyclization of diynes (e.g. **123**) to [6]carbohelicenes (e.g. **124**). While classically used phosphoramidites could not perform this transformation at -20°C (no conversion), the newly developed cationic phosphonites (e.g. **125**) allowed to achieve for multiple enyne substrates excellent yields (up to 98%), selectivities (up to 99:1) and

⁹⁸ E. González-Fernández, L. D. M. Nicholls, L. D. Schaaf, C. Farès, C. W. Lehmann, M Alcarazo, *J. Am. Chem. Soc.* **2017**, *139*, 1428.

enantioselectivities (up to 99%ee) for this hydroarylation reaction. Once more demonstrating the beneficial influence of an additional positive charge to established ligand frameworks.



Scheme 49: enantioselective cyclization promoted by α -cationic gold phosphine complex.

5. Motivation

The previously described cationic phosphines, despite their impressive reactivity, carry several disadvantages as well. First, to achieve better reactivities than commercial phosphite or polyfluorinated phosphines the introduction of two cationic charges is necessary. This renders the phosphines very insoluble. Therefore, the corresponding complexes can be rarely used in common, less polar solvents. Due to the number of charges the phosphines and the corresponding complexes are not as stable as monocationic phosphines and undergo side reactions with nucleophiles, limiting the scope of reactions employing dicationic systems. Moreover, the high number of steps for the preparation of dicationic systems further renders modifications of the dicationic systems rather difficult and time consuming. While the alternative introduction of polyfluorinated phosphines avoids the disadvantages of dicationic systems at the same time and similar reactivities to dicationic systems can be achieved, the polyfluorinated systems themselves carry several disadvantageous as well. For example the difficult introduction and high price of these phosphines, limiting once again the scope and flexibility of the prepared cationic phosphines. Furthermore, polyfluorinated phosphines are not environmental benign and therefore should as well be avoided if possible. Therefore, the development of new, highly reactive phosphines is necessary.

6. Objective

This dissertation focuses on the development of new π -acceptor ligands, based on the pyridinium moiety, and their applications in gold, platinum and palladium chemistry.

The pyridinium system are not only easily accessible, but are as well easy to modify, allowing a broad range of modifications and fine tuning for a specific reaction or reaction class. For example the pyridinium phosphines can be modified at the nitrogen, the five position of the pyridinium ring and the phosphine moiety rather easily, while up to now reported systems are not as easily modifiable and would rely on a multistep synthesis for modifications as mentioned before. Although pyridinium phosphines only incorporate one charge, they are expected to be highly reactive in π -acid catalysis, as was shown by calculation of the lowest unoccupied molecular orbital discussed before. Therefore, even though the pyridinium phosphines will show as high reactivities as dicationic systems, they will not incorporate their disadvantages of lowered solubility. In addition, their easy modulation should further allow the fine tuning and improvement of the pyridinium phosphine complexes to outperform even dicationic systems in catalysis.

After the development of those phosphines we then aim to characterize their donor/acceptor properties through classical CO-stretching frequency analysis, solid state analysis and cyclic voltammetry.

Furthermore, we want to apply the newly developed pyridinium phosphines in gold, platinum and palladium catalysis and show their beneficial effect towards the reaction rate of a given transformation.

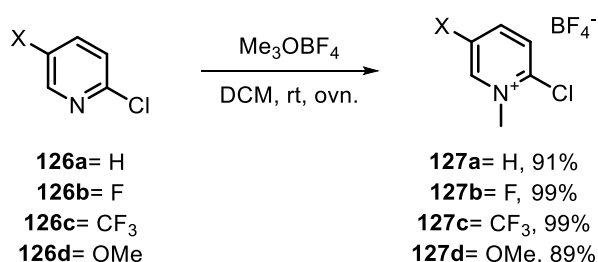
7. Results and Discussion

7.1 Synthesis of pyridinium phosphines

The cationic pyridine residue renders the phosphine a better π -acceptor even in comparison to the dicationic cyclopropenium substituted phosphines. Therefore, allowing the access to a more reactive catalyst without the disadvantages of dicationic systems (low solubility and a less stable phosphine metal bond).

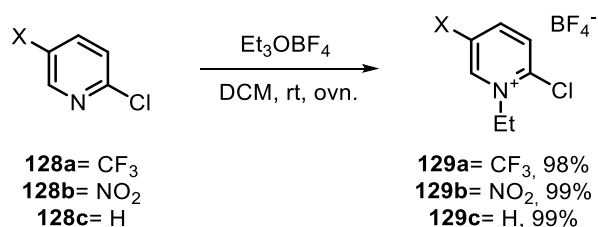
The synthesis of pyridinium substituted phosphines was achieved in good to excellent yields in only two steps – direct methylation of 2-chloropyridine with Meerwein salt followed by phosphination with the corresponding phosphine.

Starting from the readily available chloropyridines **126a-d** electron rich and electron poor pyridinium salts **127a-d** (methoxy, fluoro and trifluoromethyl substituted) were obtained by N-alkylation with trimethyl oxonium tetrafluoroborates in excellent yields (89-99%).



Scheme 50: methylation of chloropyridins.

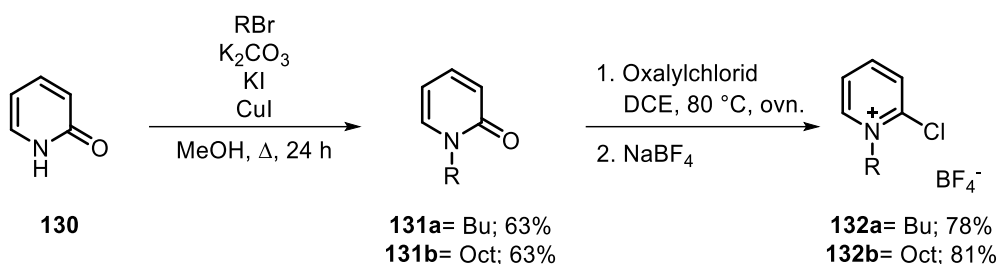
Besides N-methylation the strategy could be extended towards ethylation of 2-chloro-5-(trifluoromethyl) pyridine, 2-chloro-5-nitro pyridine and 2-chloro pyridine in excellent yields (98-99%). The ethyl group increases the solubility of the obtained products **129a-c** and that of the final phosphines.



Scheme 51: ethylation of 2-chloro-5-(trifluoromethyl) pyridine.

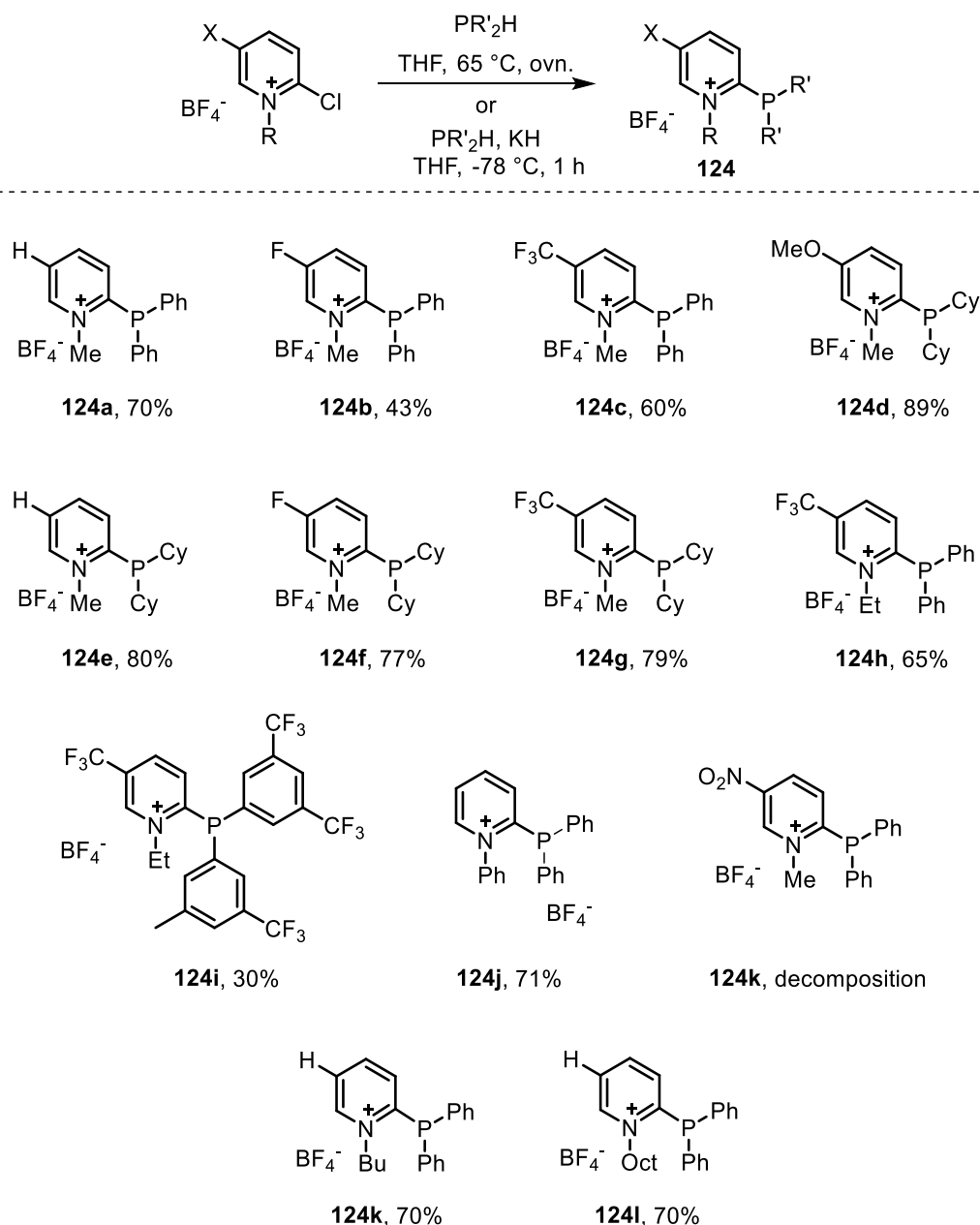
Even better solubility was obtained introducing butyl- and octyl chains. This was achieved through a copper catalysed coupling⁹⁹ of pyridone with butyl- or octylbromide (both 63%) followed by chlorination (78-81%).

⁹⁹ Compare: S. McN. Sieburth, C.-H. Lin, D. Rucando *J. Org. Chem.* **1999**, *64*, 950.



Scheme 52: synthesis of butyl and octyl substituted pyridinium salts.

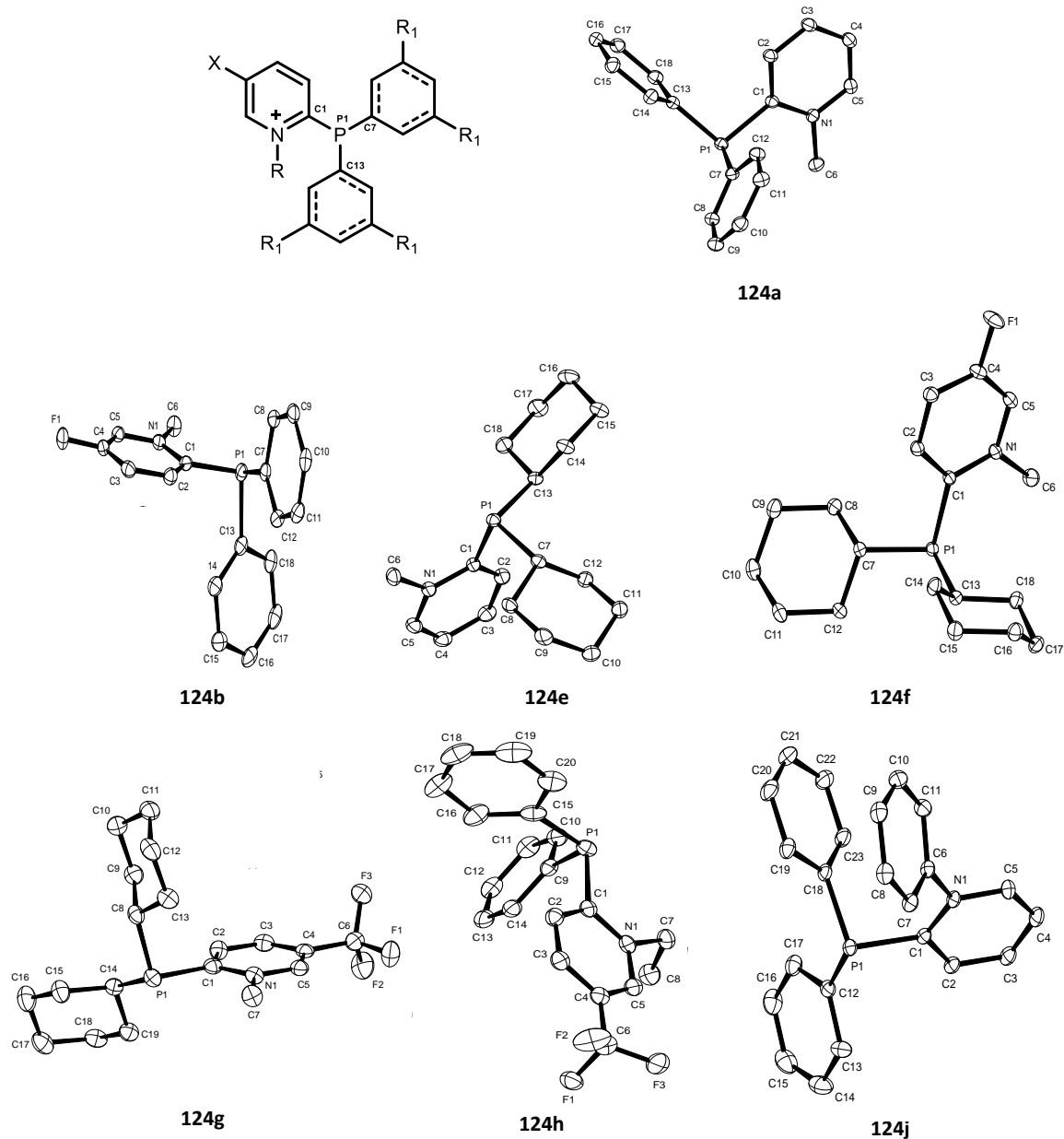
With all the chloropyridinium precursors in hand, the direct nucleophilic aromatic substitution was performed with different secondary phosphines yielding a broad range of cationic phosphines in moderate to excellent yields (30-89%). Despite the different electronic structures of the chloropyridinium salts, good yields were obtained for electron poor and electron rich precursors upon direct phosphination (**124a-h,k,l**; 43-89%), only in case of the nitro substituted pyridinium salt **124k**, no product could be isolated and a complex mixture was obtained. This undesired reactivity is most likely caused by the additional redox-active nitro group reacting with the employed phosphines. The synthesis of the cationic phosphine **124i** showed to be more difficult - although the crude NMR showed high conversion (90%) – removal of potassium salts as well as anion exchange proved to be difficult, leading to a rather low yield (30%).



Scheme 53: synthesis of pyridinium phosphines.

The newly developed phosphines are in case of the diphenylphosphine derivatives crystalline, white and air stable solids, which were easy to handle. The new phosphines are in comparison to dicationic systems more soluble in common solvents and even stable towards water.

To confirm the structure, a few of the phosphines prepared were crystallized and examined by X-ray crystallography, confirming the desired connectivity. The bond lengths (1.852-1.865 Å) between the phosphorus atom and the carbon C1 of the pyridinium moiety suggest, that significant charge density resides on the phosphorus atom and nicely illustrates, that the phosphorus lone pair still is available for coordination. This is further underlined through the significant pyramidal environment around the central phosphine atom (303.79°- 304.87°).



Scheme 54: crystal structures of **124a, b, e, f, g, h** and **j**. Hydrogen atoms, anions and solvent molecules were omitted for clarity; ellipsoids are set at 50% probability.

phosphine	d(P-C1) [Å]	d(P-C7) [Å]	d(P-C13) [Å]	pyramidalization [°]
124a	1.855	1.826	1.824	304.87
124b	1.862	1.833	1.829	303.45
124e	1.858	1.873	1.849	303.79
124f	1.865	1.872	1.854	304.55
124g	1.858	1.872	1.854	304.08
124h	1.852	1.831	1.824	304.84
124j	1.854	1.831	1.829	304.29

Table 4: chosen bond distances and pyramidal environment around the phosphorus atom of crystallised cationic phosphines.

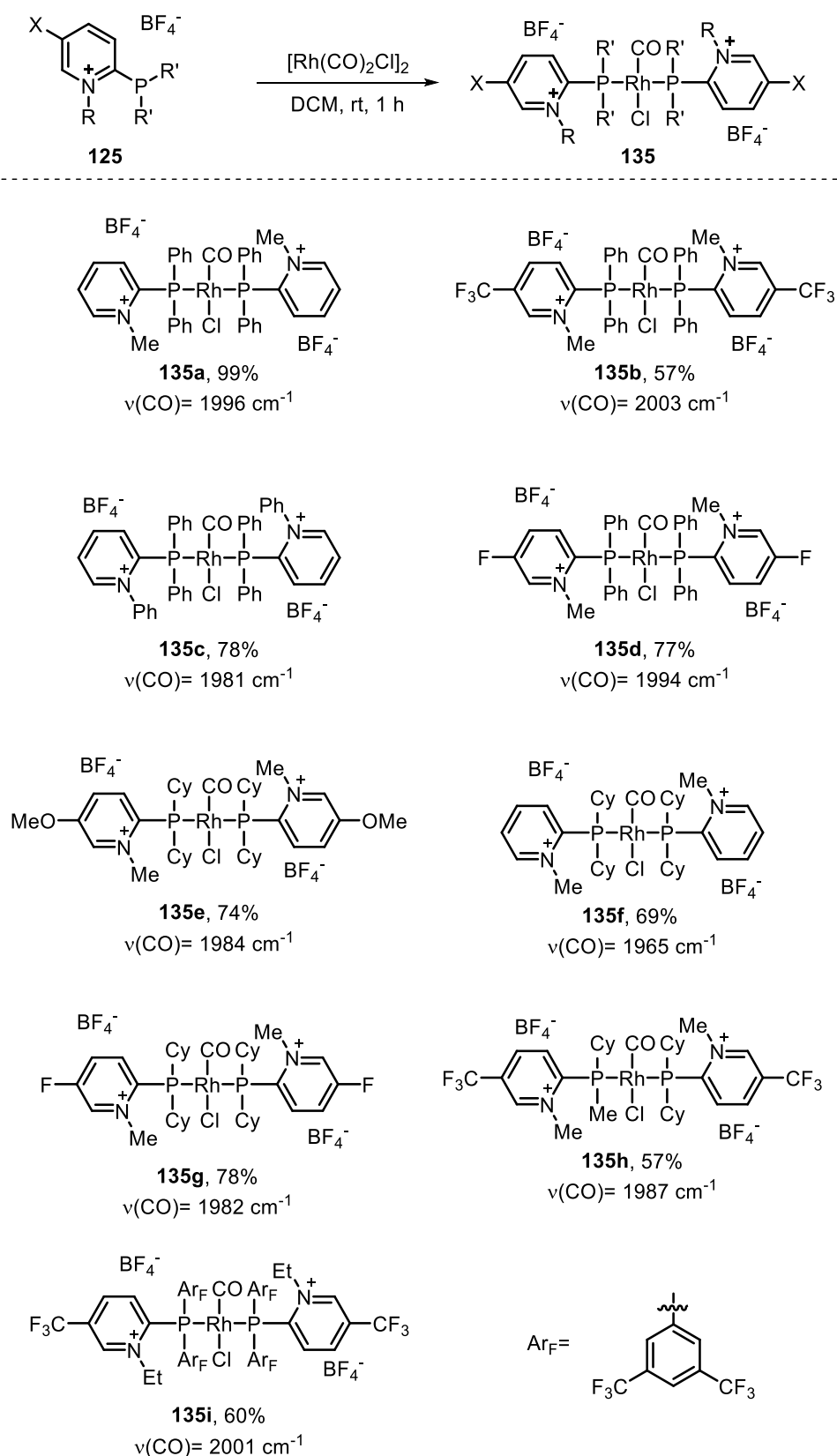
Next we evaluated the stereo electronic properties of the prepared phosphines. As before mentioned this can be done comparing the Tolman angle and the Tolman stereo-electronic parameter of the corresponding phosphines. Despite the high toxicity of nickeltetracarbonyl we attempted the synthesis of the corresponding nickel carbonyl complexes. However these could not be prepared, as they probably decomposed upon removal of the solvent.

As the preparation of the nickel carbonyl complexes failed, we instead prepared the rhodium(I) Vaska type complexes **135a-f** in good to excellent yields (57-99%). A simple quadratic function (Eq. 1.0) then allows as described by Roodt *et al.*¹⁰⁰ to correlate the carbonyl stretching frequencies to Tolman electronic parameter.

$$y = ax^2 + bx + c \text{ (Eq.: 1.0)}$$

*Equation 1: correlation between $\nu(\text{CONi})$ and $\nu(\text{CORh})$
with $a=(2.77\pm0.44)\times10^4$, $b=(-2.65\pm0.45)\times10$ and $c=(6.8\pm1.1)\times10^{-3}$*

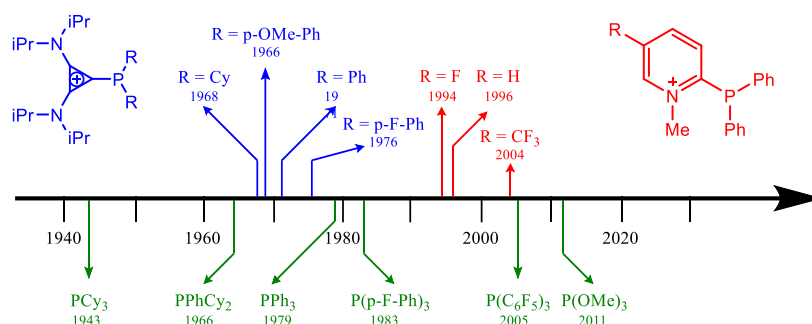
¹⁰⁰ G. Steyl, S. Otto, A. Roodt, *Coordination Chemistry Reviews* **2003**, 245, 121.



Scheme 55: preparation and structures of the rhodium carbonyl complexes and their corresponding CO stretching frequencies.

For the prepared complexes the CO stretching frequencies directly correlates with the π -acidity of the corresponding phosphines. As more π -acidic phosphines deplete more electron density from the metal, less backdonation from the metal to the carbonyl groups antibonding π -orbital can occur and therefore the CO bond is stronger, resulting in higher CO stretching values for more π -acidic phosphines.

The CO stretching frequencies of the new pyridinium phosphines (1994 to 2004 cm^{-1}) clearly show their enhanced π -acidity in comparison to the previously reported cyclopropenium phosphines (1968 to 1976 cm^{-1}). Furthermore, the pyridinium phosphines even reach CO stretching frequency values comparable to the good π -acceptor ligands $\text{P}(\text{C}_5\text{F}_6)_3$ and $\text{P}(\text{OMe})_3$. However, within the pyridinium phosphines this general trend is not followed and for example the more electron deficient polyfluorinated pyridinium phosphine **135i** shows a lower CO stretching ($\nu(\text{CO})= 2001 \text{ cm}^{-1}$) frequency than the trifluoromethyl substituted pyridinium phosphine **135b** ($\nu(\text{CO})= 2003 \text{ cm}^{-1}$).



Scheme 56: comparison of the carbonyl stretching frequencies of commercial, known and newly prepared phosphine Vaska type complexes.

As suspected, that spatial restrictions cause the inconsistency between the CO stretching frequencies and the electronic structures of the pyridinium phosphines, we crystallized rhodium complex **135c**.

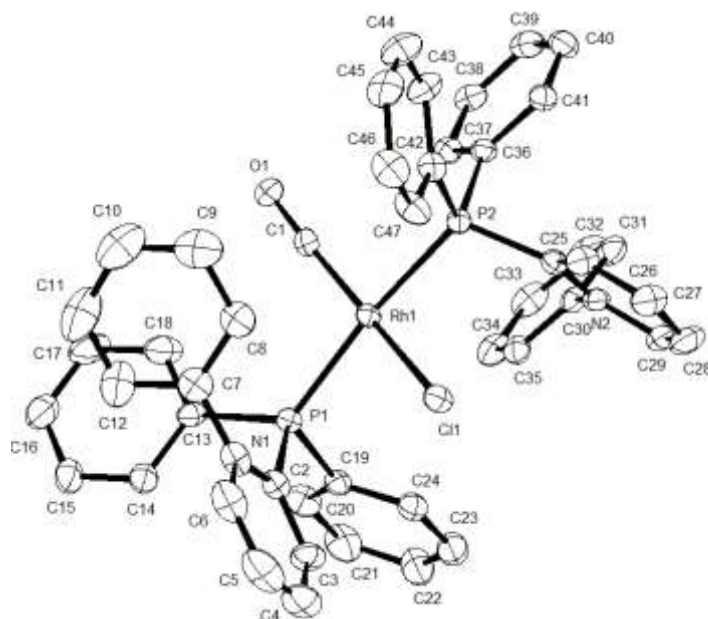


Figure 13: molecular structure of **135c** in the solid state. Hydrogen atoms and anions are omitted for clarity. Anisotropic displacement parameter are shown at 50% probability level.

The analysis of the crystal structure directly reveals a distortion from the ideal square planar geometry at the rhodium atom ($\angle \text{ClRh}(\text{CO})=163.3^\circ$ and $\angle \text{P1RhP2}=172.8^\circ$), that strongly influences the back bonding of the phosphine ligand towards the metal and, in return, from the metal towards the carbonyl group, as the orbital overlap due to this distortion is less efficient. This is the origin of the misleading CO stretching values as observed¹⁰¹.

We therefore did not calculate the TEP based on the carbonyl values of the Vaska type complexes as described before, but instead calculated the carbonyl stretching frequencies of L-Ni(CO)₃ complexes by DFT (blue dots) and measured the carbonyl stretching frequencies of the stable cationic phosphine nickel carbonyl complexes (red dots).¹⁰² Combined with the measured cone angle of the phosphine metal complexes, we were able to add the newly prepared cationic phosphines to the Tolman stereo electronic map.

¹⁰¹ D. A. Valyaev, R. Brousses, N. Lugan, I. Fernández, M. A. Sierra, *Chem. A. Europ. J.* **2011**, *24*, 6602.

¹⁰² M. Alcarazo, *Chem. Eur. J.* **2014**, *20*, 7868.

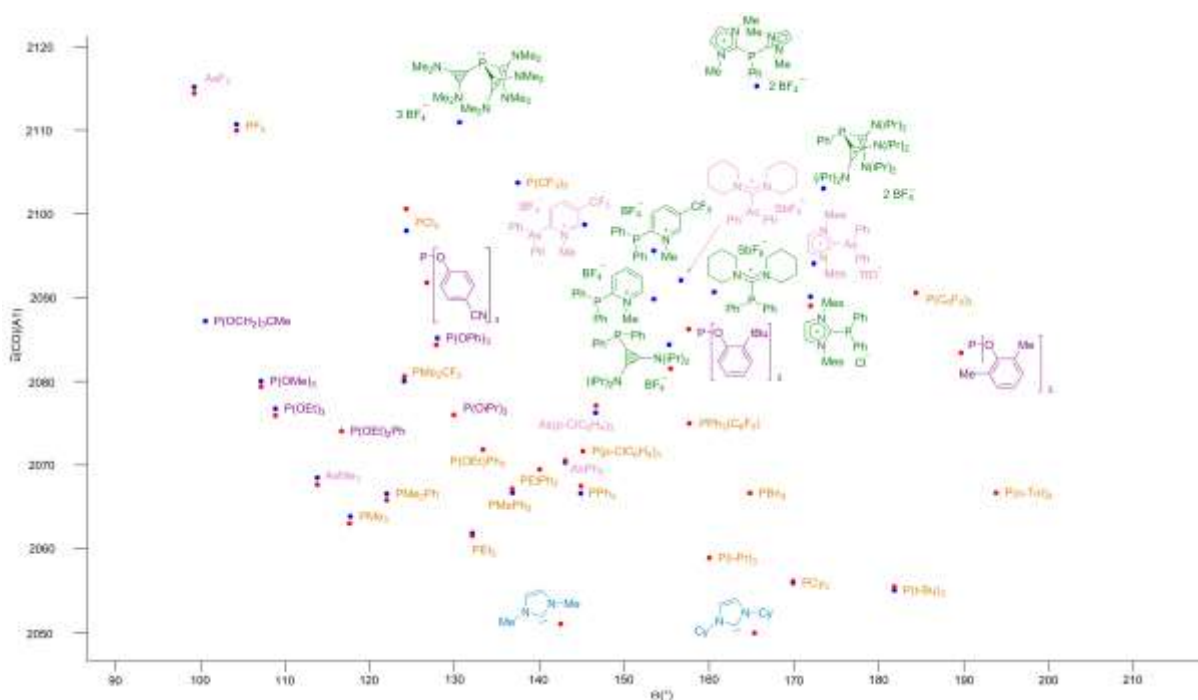


Figure 14: Tolman stereo electronic map with additional α -cationic phosphines.

The nickel carbonyl stretching frequencies both calculated and experimental ones are in good agreement with the expectation. This confirms a higher π -backdonation towards the newly prepared pyridinium phosphines in comparison to the previously published monocationic cyclopropenium phosphines. The pyridinium phosphines reach π -acceptor properties of dicationic cyclopropenium phosphines and are better π -acceptors than polyfluorinated phosphines or even phosphites.

Besides theoretical calculations we also used cyclic voltammetry to measure the electrochemical properties of the prepared pyridinium phosphines to get experimental proofs for the predicted high π -acidity.

In cyclic voltammetry the potential to remove one electron from the examined compound is measured (the so called oxidation potential). The oxidation potential directly correlates with the phosphines σ -donor properties. The more difficult it is to remove the electron from the phosphine (higher oxidation potential), the worse σ -donor this ligand is. Besides the oxidation potential, the reduction potential (adding one electron to the examined compound) is measured as well and this can be correlated with the π -acceptor properties. Furthermore the reversibility of the oxidation and reduction process at different scan rates can be examined, indicating the life times of the corresponding radicals.

Entry	Ligand	$\tilde{\nu}_{\text{Co}}^{[a]}$ [RhCl(CO)L ₂]	E _p (ox) ^[b]
1	124a , X = H; R = Me; R' = Ph	1996	1.398
2	124b , X = F; R = Me; R' = Ph	1994	1.355
3	124c , X = CF ₃ ; R = Me; R' = Ph	2004	1.436
4	124f , X = F; R = Me; R' = Cy	1982	1.297
5	124d , X = OMe; R = Me; R' = Cy	1974	1.269
6	124i , X = CF ₃ ; R = Et; R' = 3,5-di(CF ₃)Ph	2001	1.578 ^[c]
7	63a	1971	1.207
8	84	-	1.541
9	Ph ₃ P	1979	0.687
10	(MeO) ₃ P	2011	1.287

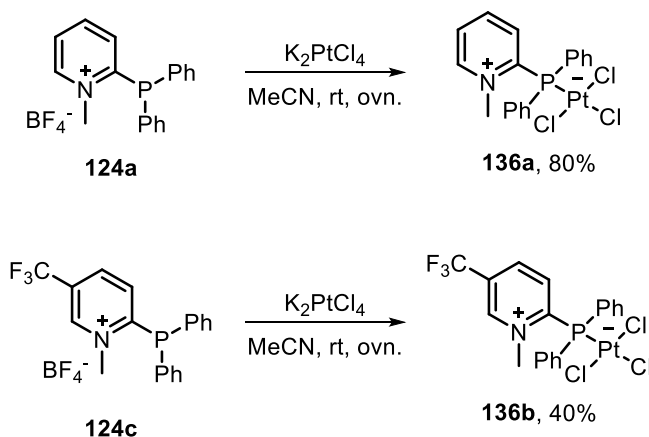
Scheme 57: oxidation potentials of commercial, cyclopropenium and pyridinium substituted phosphines, [a] Values in cm^{-1} . [b] Oxidation peak potentials reported in V. Calibrated versus ferrocene/ferrocenium ($E_{1/2} = 0.24\text{V}$), Bu_4NPF_6 (0.1 M) in CH_2Cl_2 , [c] measured in CH_3CN .

By comparison of the obtained oxidation potentials the expected trend of reduced σ -donation from phosphine ($E_{\text{ox}} = 0.697\text{ V}$) to phosphite ($E_{\text{ox}} = 1.287\text{ V}$) and cyclopropenium phosphine ($E_{\text{ox}} = 1.207\text{ V}$) to pyridinium phosphine ($E_{\text{ox}} = 1.398\text{--}1.578\text{ V}$) could be validated. Furthermore, the effect of different substitution patterns (-OMe, -F, -CF₃) and their electronic effects in cyclic voltammetry line up well, confirming, for example that the CF₃ substituted phosphine **124c** ($E_{\text{ox}} = 1.578\text{ V}$) is even more electron poor than the dicationic cyclopropenium phosphines ($E_{\text{ox}} = 1.541\text{ V}$). Therefore, during the catalytic experiments the newly developed system should show a superior reaction rate compared to classical phosphine ligands, like triphenylphosphine and triphenylphosphite, or even dicationic cyclopropenium phosphines.

7.2 Synthesis of metal complex derivatives

7.2.1 Platinum complexes

The new zwitterionic platinum complexes were prepared by addition of the corresponding phosphine to K_2PtCl_4 in acetonitrile. The desired platinum complexes **136a,b** were obtained as white air stable solids in moderate to good yields (40 and 80%).



Scheme 58: synthesis of platinum complexes.

Comparison of their structure to the one of the PtCl_4^{2-} unit in K_2PtCl_4 allowed us to evaluate the strength of the trans-effect of our ligands compared to chloride. Although we would expect - as cationic phosphines are weak σ -donors - a weaker trans influence compared to chloride, we did observe the opposite as revealed by the elongated Pt1-Cl2 bond (2.351 Å) for the cationic system **136a** in comparison to Pt-Cl (2.308 Å) in K_2PtCl_4 . Thus, the cationic phosphine possesses a stronger trans effect, which should enable easy abstraction of the Cl^- anion during catalysis. This strong trans influence is caused by the short bond distance between Pt and P1 (2.219 Å), probably due to electrostatic interactions between the cationic phosphine and the anionic platinum atom. This short distance facilitates π -back donation due to the more efficient orbital overlap and therefore, it renders the metal more π -acidic and more reactive in catalysis.

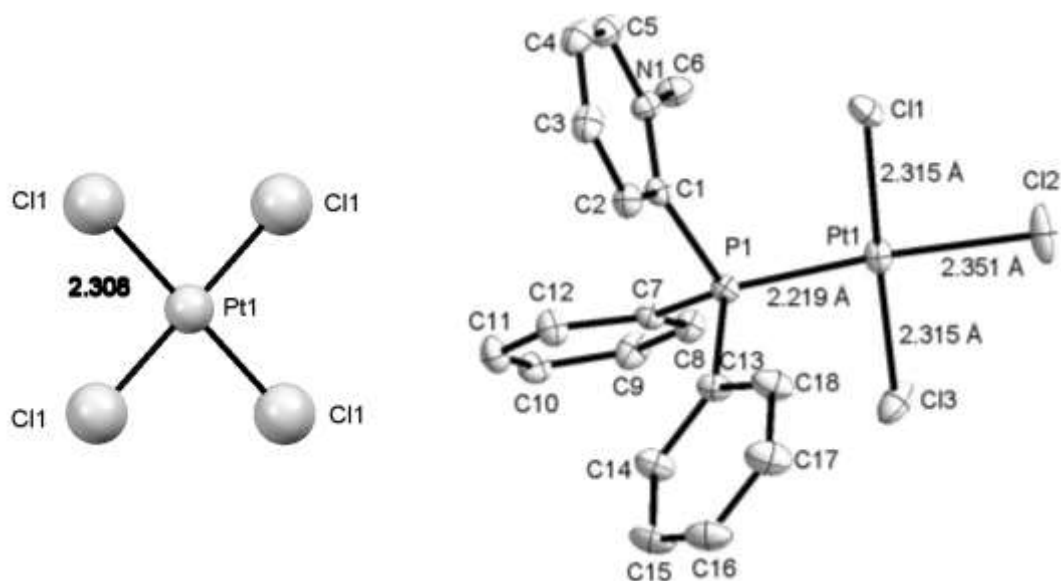
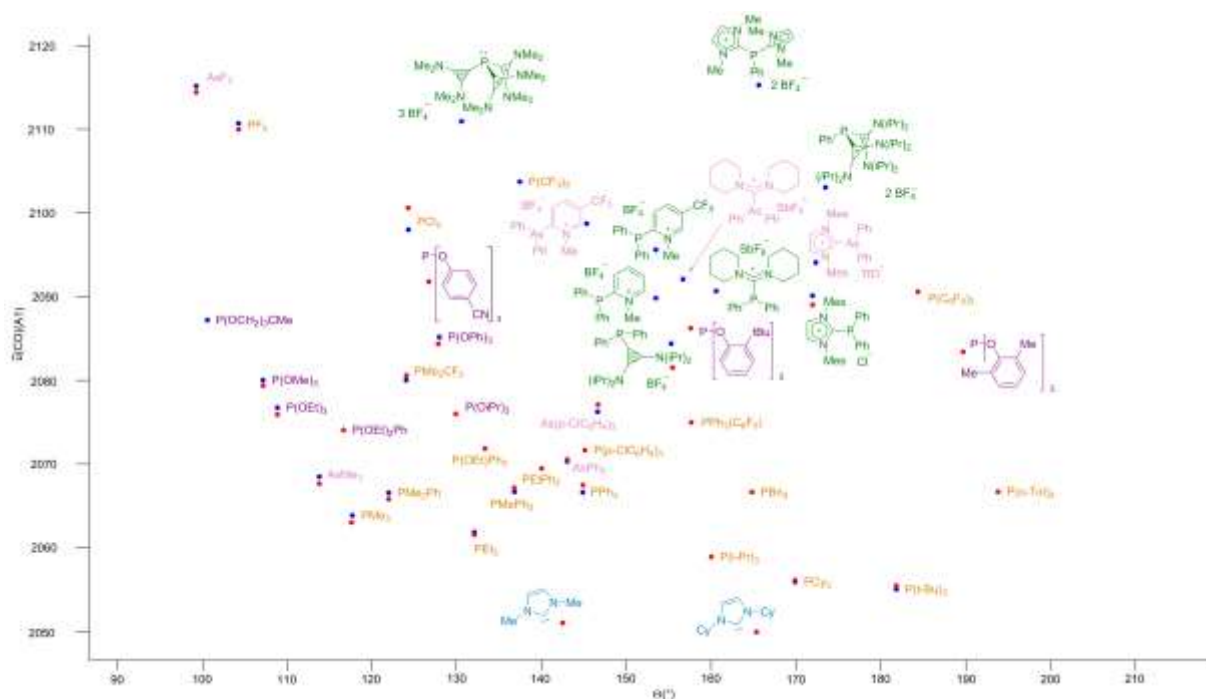
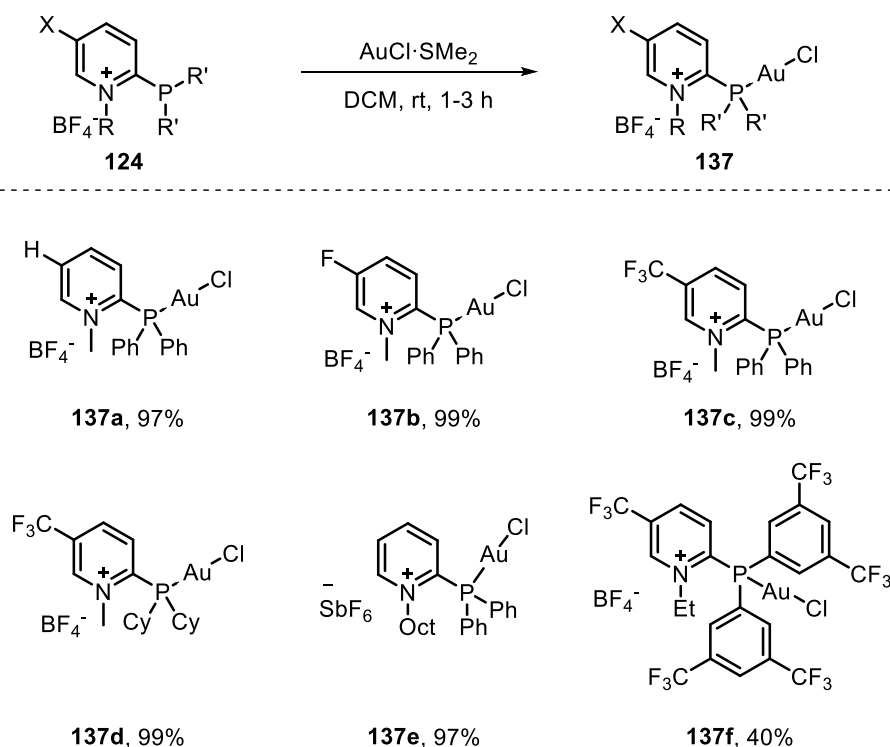


Figure 15: molecular structure of K_2PtCl_4 and **136a** in the solid state. Hydrogen atoms and cations are omitted for clarity. Anisotropic displacement parameter are shown at 50% probability level.

7.2.2 Synthesis of gold complexes

Gold complexes were prepared by reaction of $Me_2S \cdot AuCl$ with the desired ligand in DCM for one to three hours. The desired gold complexes **137a-c,f-g** were obtained in excellent yields (97-99%) independently of their stereo electronic properties. Only the preparation of the gold complex **137e** proved due to the high reactivity of the corresponding phosphine to be more challenging (40% yield).



Scheme 59: synthesis of gold complexes **137a-e**.

7.3 Applications in catalysis

With all these complexes in hand, we next examined the possible application of platinum complexes **136a** and **b** in catalysis. We chose the hydroarylation of propargyl ether **138** to chromene **139** published by Sames *et al.*¹⁰³ As they showed, up to 32% conversion can be obtained with the more π -acidic PtCl_4 , while the less π -acidic PtCl_2 only converts 3% of the starting material to the desired product. Because the nucleophile is an arene unit, which is a relatively bad nucleophile, the rate determining step should be the nucleophilic attack. Both arguments predict higher reactivity with electron poor phosphines like the newly prepared pyridinium phosphines.

While all tested ligand are stable within the examined timeframe (linear regression) only highly π -acidic phosphines are reactive enough to fully convert the starting material to the desired chromene **139**. Classical ligands like PPh_3 or $\text{P}(\text{C}_6\text{F}_5)_3$ only increase the conversion up to 10%. Apart from the tuning of the π -acidity of the ligand, that coordinate the platinum metal, also the acidity of the metal itself can be enhanced to promote the reaction. Using platinum at a higher oxidation state $\text{Pt}(\text{IV})\text{Cl}_4$ lead to 30% within the examined timeframe. However, the highly π -acidic pyridinium ligands promote much faster reactions. Full conversions are obtained within minutes. The non-substituted pyridinium phosphine platinum complex **136a** leads to full

¹⁰³ S. J. Pastine, S. W. Youn, D. Sames, *Org. Lett.* **2003**, *5*, 1055.

conversion within 25 min., while the CF₃-substituted pyridinium phosphine platinum complex **136b** accelerates the reaction rate even more, resulting in 100% conversion after 2 mins.

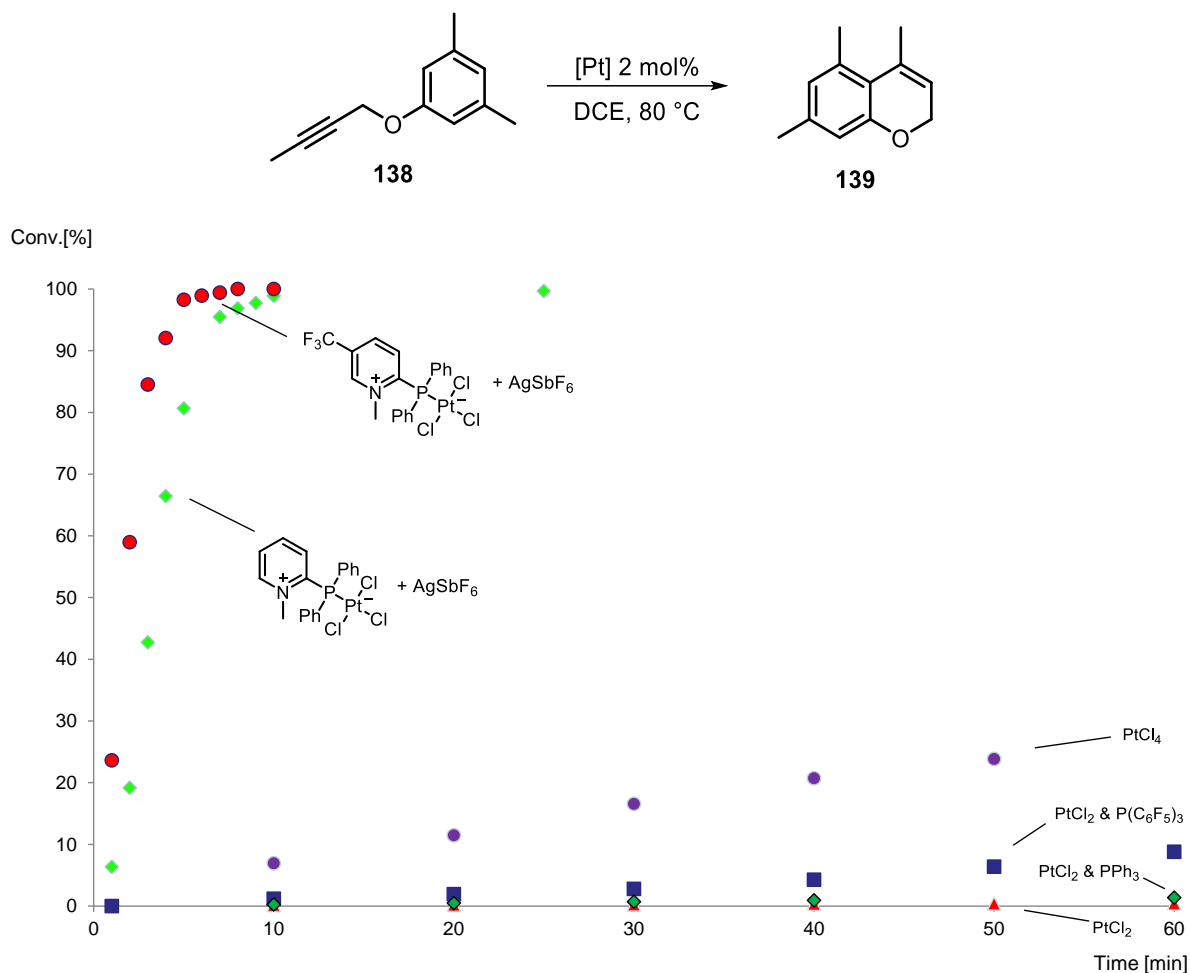


Figure 16: ligand effect on the Pt-catalysed hydroarylation of propargyl aryl ether **138** to chromene **139**. Reagents and conditions: a) **138** (0.05 m), Pt precatalysts (2 mol%), AgSbF₆ (2 mol%), (CH₂)₂Cl₂, 80 °C. Conversions determined by gas chromatography.

To further prove the generality of this effect, we performed an additional platinum catalysis. In this case enine **140** was converted to cyclobutene **141**.¹⁰⁴ We chose this transformation from Fürstner *et al.*¹⁰⁴ as it is known to respond to the strong π -acceptor properties of the ligands. In comparison to classical ligands PPh₃ (2% conversion), P(OPh)₃ (15% conversion) or even the archetypical π -acceptor ligand CO (20% conversion), our cationic ligands vastly outperformed the known reaction rates and could achieve full conversion within 5 min. (with catalyst **136a**) or even within 2 min. (with the CF₃-substituted analogue **136b**). This proves the superiority of our newly designed ligand class.

¹⁰⁴ A. Fürstner, P. W. Davies, T. Gress, *J. Am. Chem. Soc.* **2005**, *127*, 8244.

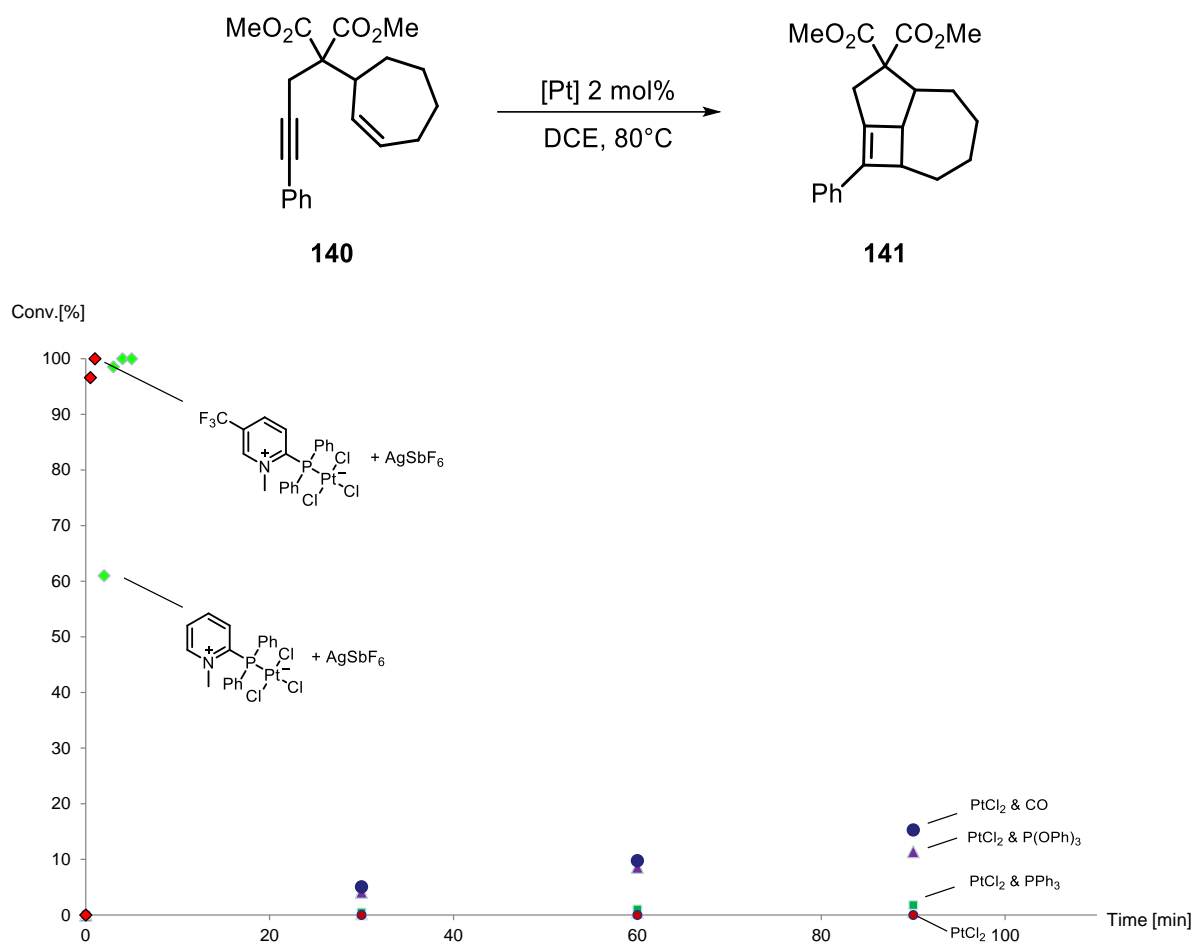


Figure 17: ligand effect on the Pt-catalysed cycloisomerisation of enyne **140** to cyclobutene **141**. Reagents and conditions: **140** (0.05 M), Pt precatalysts (2 mol%), AgSbF₆ (2 mol%), (CH₂Cl)₂, 80 °C. Conversions determined by gas chromatography.

Apart from platinum catalysis phosphine ligands find a lot of applications in gold catalysis as well. Therefore, we next tested the effect of our ligands in gold catalysis, performing an intermolecular hydroarylation of phenyl acetylene at 60 °C in 1,2-dichloroethane.

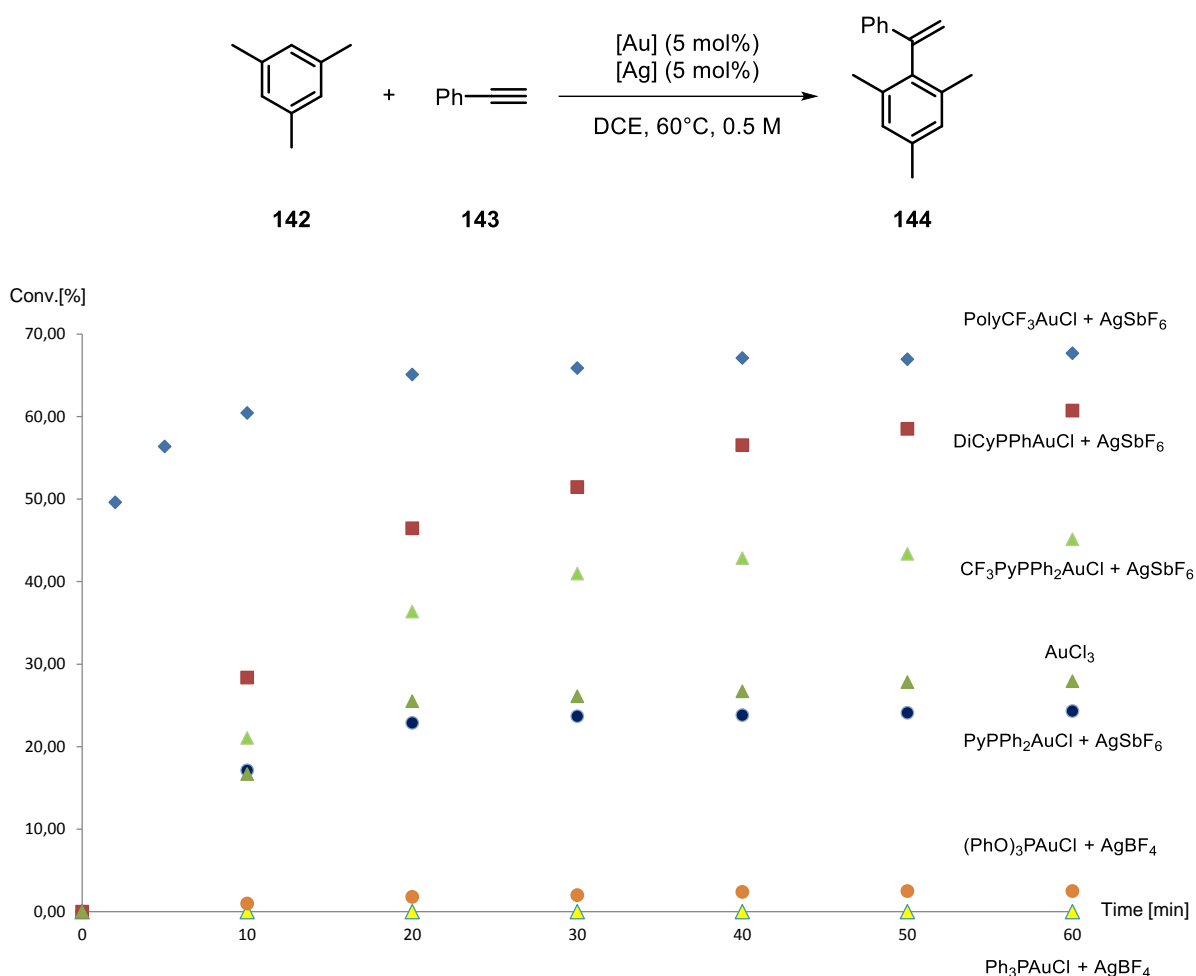


Figure 18: ligand effect on the Au-catalyzed hydroarylation of alkyne **143** with arene **142**. Reagents and conditions: **143** (0.05 m), **142** (4 equiv; 0.2 m), Au' precatalysts (5 mol%), AgBF₄ or AgSbF₆ (5 mol%), (CHCl₂)₂, 60 °C. Conversions determined by gas chromatography.

This reaction was reported by Reetz *et al.*¹⁰⁵ with a catalytic mixture of AuCl₃ and 3 equiv. AgSbF₆ to generate highly electrophilic gold(III) cations. Our newly developed cationic phosphines should enable gold(I) to be tuned as highly electrophilic as the reported gold(III) catalysts. Therefore, we tested the effect of our pyridinium phosphines in the mentioned transformation.

As expected, with the classical gold phosphine systems (PPh₃AuCl and P(OPh)₃AuCl) very low conversions were obtained, because the electrophilicity of the gold atom is not high enough to promote the intermolecular attack of mesitylene towards phenylacetylene. Using the pyridinium substituted phosphine gold complex **137a**, moderate yields (up to 25%) were

¹⁰⁵ M. T. Reetz, K. Sommer, *Eur. J. Org. Chem.* **2003**, 3485.

achieved within 60 mins; already reaching the high turnovers of gold(III) chloride (up to 27%). Enhancing the π -acidity of the phosphine further (using the CF_3 substituted phosphine **137c**) 45% conversion to the desired product **144** could be obtained. This high reactivity was surpassed by the dicationic cyclopropenium system **62a**, which lead to a conversion of 60% within 60 mins. The best conversion (70%) observed, was achieved with the highly electrophilic polyfluorinated pyridinium phosphine gold complex **137e**. However, in all the cases - even with the commercial systems - a major drawback is the deactivation of the catalytic mixtures when prolonged reaction times are necessary. Probably this is caused by decomposition of the gold complexes towards gold nanoparticles and free phosphines.

Next we examined the effect of the counter ions used during catalysis employing the trifluoromethyl substituted pyridinium phosphine **137c**. While the tetrafluoroborate anion is accounted as non-coordinating, the hexafluoroantimonate anion is even less coordinating, thus, it should lead to slightly increased reaction rates. As expected the reaction rate is significantly lower with two BF_4^- anions (15%), while the substitution of one BF_4^- unit towards a SbF_6^- anion increases the conversion: A 1:1 mixture of BF_4^- and SbF_6^- yields 45% conversion, while two SbF_6^- units convert up to 65% of the starting material to the product, confirming a strong effect of the used counter anions. Another rational to understand the effect of the employed counter anions consist on considering the enhanced solubilities achieved with larger, less coordinating anions in polar solvents.

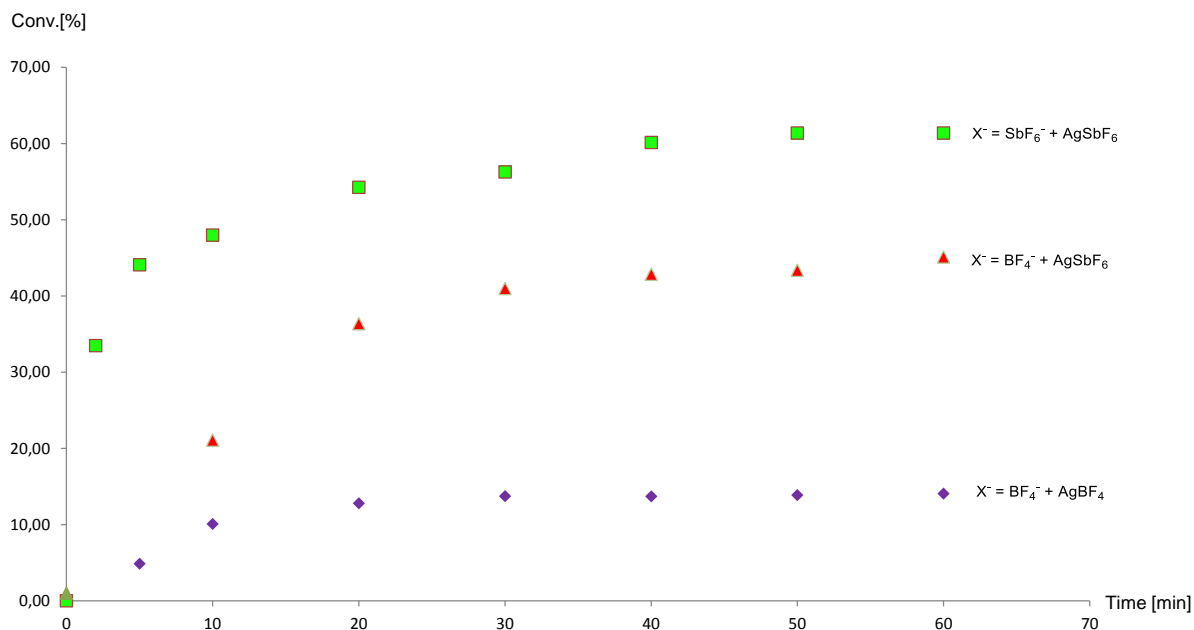
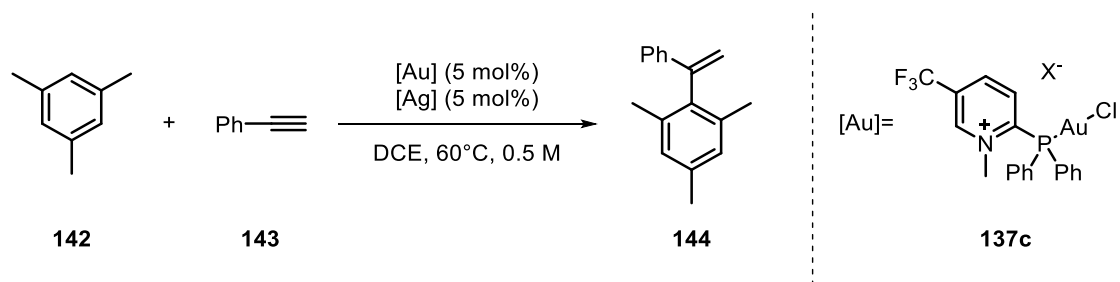
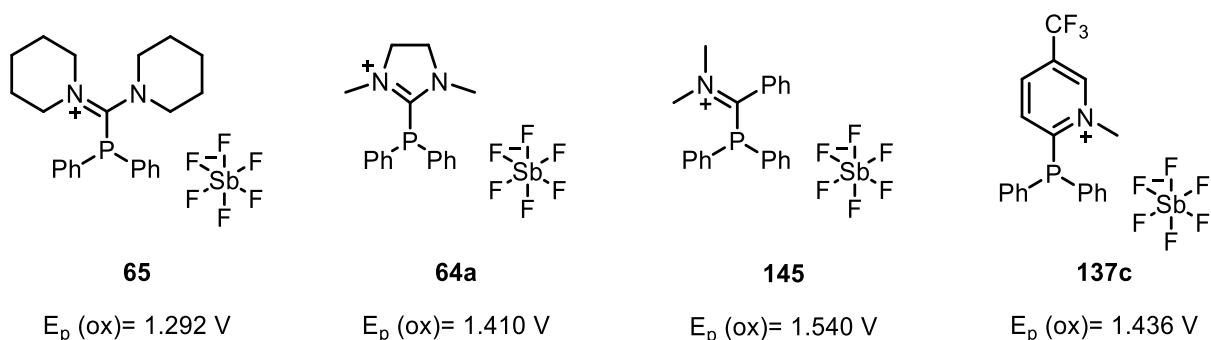


Figure 19: counter anion effect on the Au-catalyzed hydroarylation of alkyne **143** with arene **142**. Reagents and conditions: **142** (0.05 m), **143** (4 equiv; 0.2 m), Au^I precatalysts (5 mol%), AgBF₄ or AgSbF₆ (5 mol%), (CH₂Cl)₂, 60 °C. Conversions determined by gas chromatography.

Comparison of the kinetic data for the three examined reactions shows good agreement of the measured oxidation potentials by cyclic voltammetry and the reactivity during catalysis. In all cases, a higher oxidation potential led to an increased reactivity independent of the examined reaction, allowing predictions of the reactivity of new compounds by simple measurement of their oxidation potentials.

Besides the pyridinium phosphine and the aforementioned mono-, di- or tricationic cyclopropenium phosphines, we previously reported the synthesis of bis-piperidinium-, imidazolium- and amidinium phosphines.⁷⁵ While the formamidinium system **65** and the dihydroimidazolium phosphine **64a** show lower oxidation potential and therefore should possess a lower reactivity during catalysis, the amidinium phosphine **145** shows an even higher oxidation potential, indicating that improved reactivity might be obtained.

Scheme 60: oxidation potential of cationic phosphines **64a**, **65**, **137c** and **145**.

To prove the predicted reactivities, we then applied the aforementioned phosphines in the hydroarylation of propargyl ether **138** to chromene **139** as well.

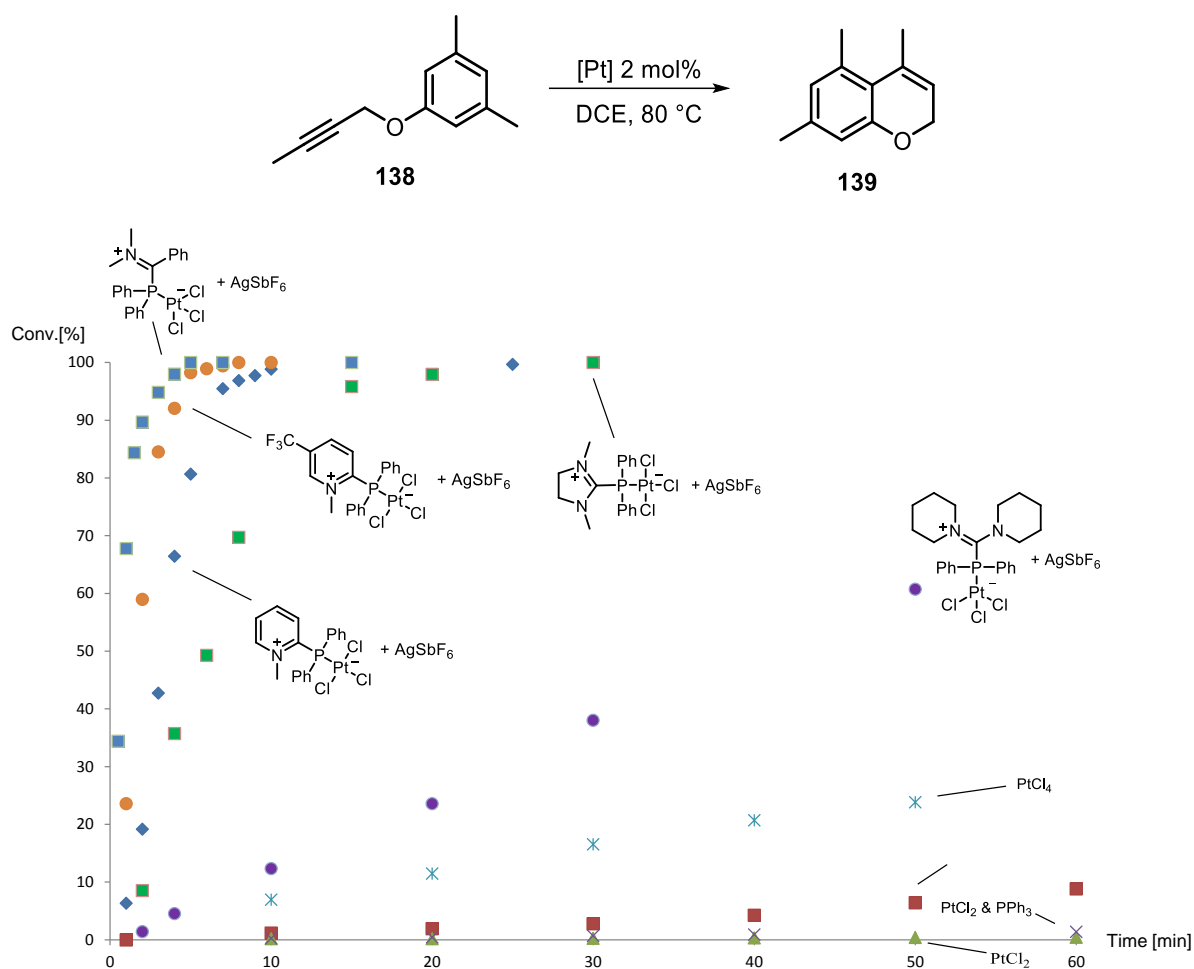


Figure 20: ligand effect on the Pt-catalysed hydroarylation of propargyl aryl ether **138** to chromene **139**. Reagents and conditions: a) **138** (0.05 m), Pt precatalysts (2 mol%), AgSbF₆ (2 mol%), (CH₂Cl), 80 °C. Conversions determined by gas chromatography.

The observed kinetic is in excellent agreement with the corresponding oxidation potentials as well as their calculated respective frontier orbital, which increase from formamidinium- over dihydroimidazolium- to amidinium-phosphine.⁷³

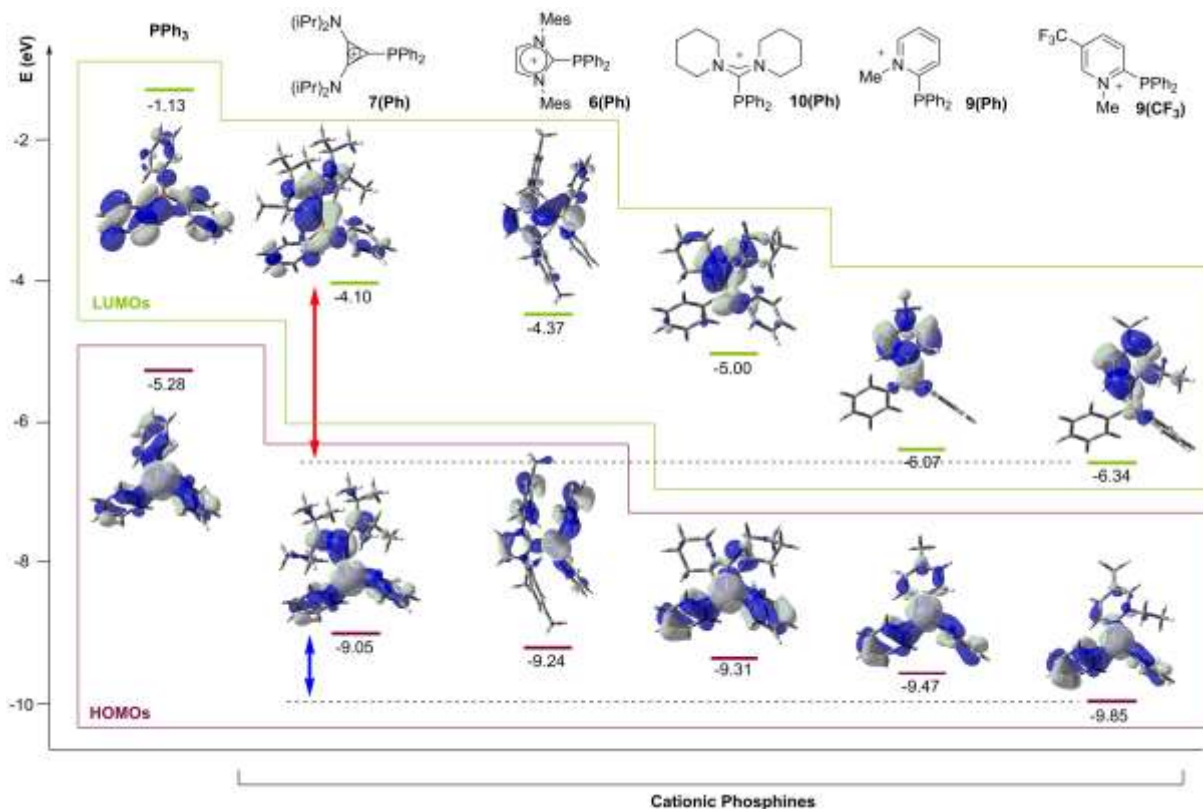
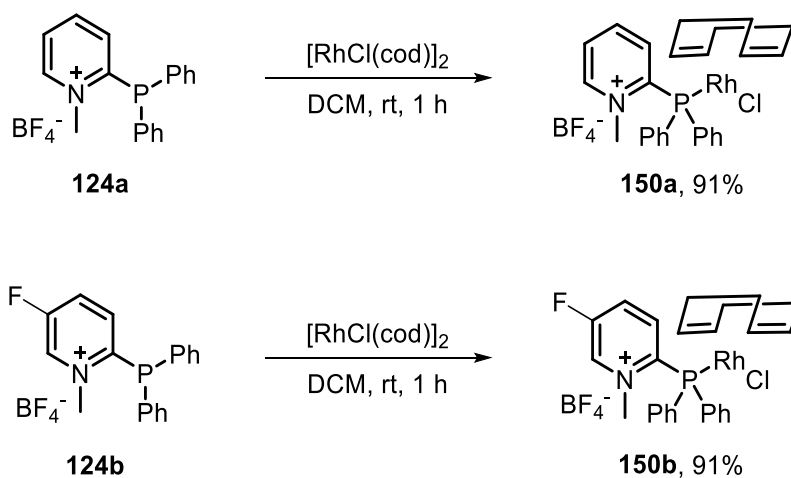


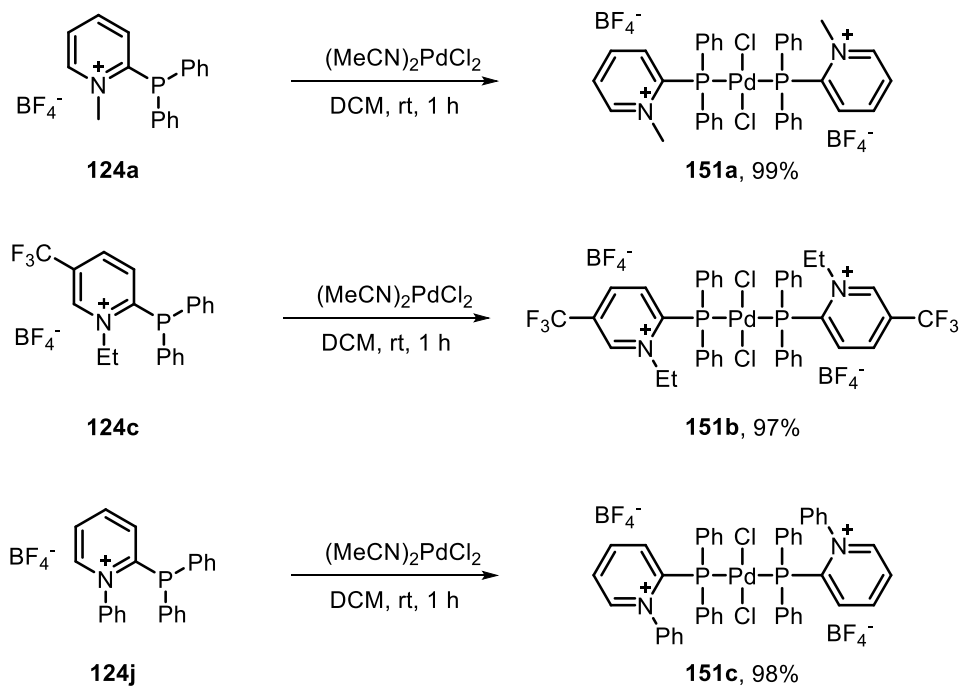
Figure 21: frontier orbitals of commercial and cationic phosphines.

Apart from the applications in gold and platinum catalysis further coordination chemistry to other metals sources was tested. As described before, we could successfully coordinate rhodium sources and use the corresponding complexes for the evaluation of the electronic properties of the corresponding phosphines. Applying this knowledge we also examined the coordination of cationic pyridinium phosphine **124a** and **124b** to $[\text{Rh}(\text{COD})\text{Cl}]_2$ and were pleased to see, that the corresponding complexes **150a** and **150b** were obtained in excellent yields.



Scheme 61: synthesis of the rhodium complexes **150a-b**.

We also tested the coordination chemistry of pyridinium ligands to Pd(II) sources. The corresponding complexes **151a-c** were obtained in excellent yields.



Scheme 62: synthesis of palladium complexes **151a-c**.

Crystallisation of palladium complex **151c** confirmed the square planar geometry around the palladium centre ($\angle\text{Cl1PdCl1}^* = 180^\circ$ and $\angle\text{P1PdP1}^* = 180^\circ$) as well as the trans-assembly of the two phosphine residues.

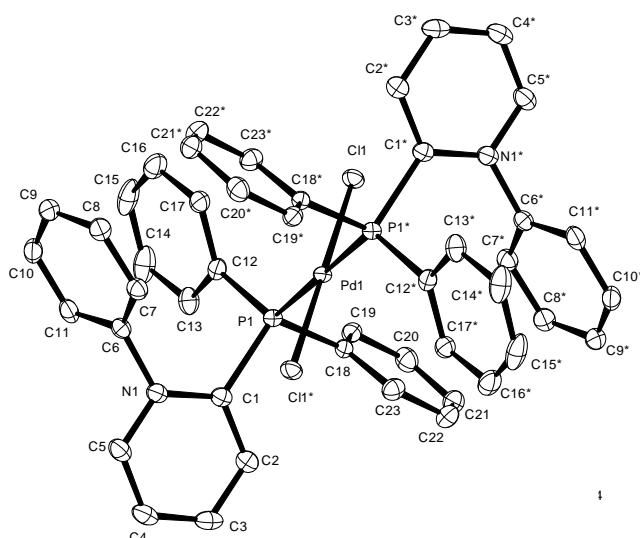
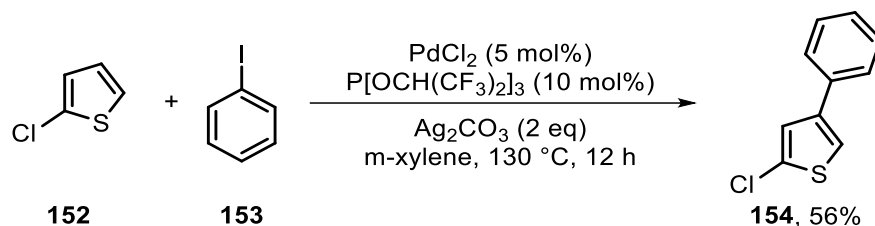


Figure 22: Molecular structure of **151c** in the solid state. Hydrogen atoms and cations are omitted for clarity. Anisotropic displacement parameter are shown at 50% probability level.

Next we tested the newly prepared palladium complexes in direct arylation reported by Itami *et al.*¹⁰⁶ selectively phenylating thiophene **152** at the β -position.



Scheme 63: Direct arylation of thiophene published by Itami.

This reaction is reported to be faster by employment of electron poor phosphine ligands and therefore cationic ligands should be beneficial for this transformation. To minimize the lower α/β selectivity caused by cationic ligands we changed the silver salt from Ag_2CO_3 to AgBF_4 ¹⁰⁷ obtaining good β selectivity with our cationic phosphines as well.

As shown by kinetic experiments in the presence of weak π -accepting ligands like PPh_3 only traces of the starting material are converted to the desired product, while stronger π -acidic ligands like P(OPh)_3 or $\text{P(O}i\text{PrF}_6)_3$ already convert up to 30% of the starting material within six hours. Using the cationic palladium complexes, we could further accelerate the reaction to gain conversion of up to 55% within 6 hours. Unfortunately the catalytic mixture lost its reactivity with prolonged reaction times., probably caused by degradation of the catalyst.

¹⁰⁶ K. Ueda, S. Yanagisawa, J. Yamaguchi, K. Itami, *Angew. Chem.* **2010**, 122, 9130.

¹⁰⁷ Compare to: S. Yamaguchi, K. Itami, *Tetrahedron* **2011**, 67, 4425.

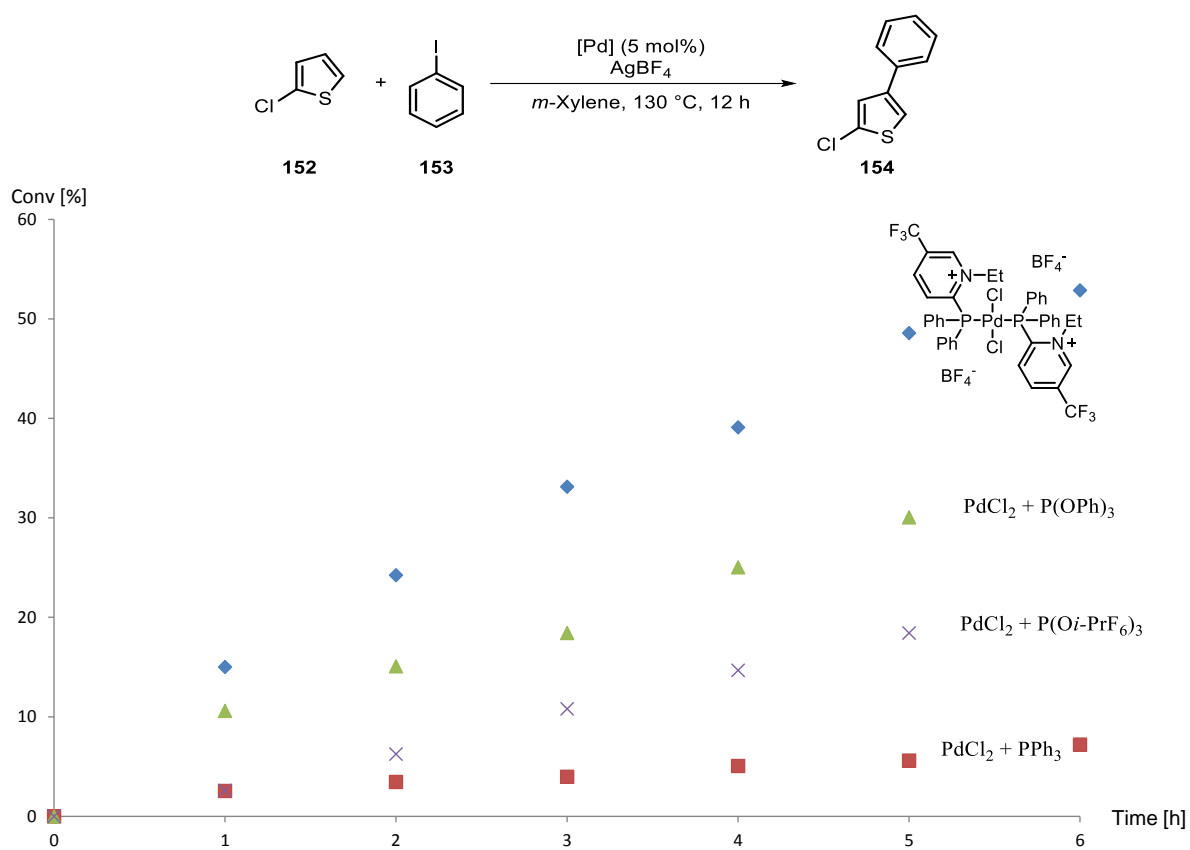


Figure 23: ligand effect on the C-H activation of thiophene. Reagents and conditions: **152** (0.5 M), **153** (0.75 M), palladium precatalyst (5 mol%), AgBF₄ (1.5 eq), PhI (1.5 eq), *m*-Xylene, 130°C. Conversions determined by gas chromatography.

7.4 Applications of other cationic ligands in catalysis

We next examined, if the reaction conditions of the hydroarylation of **138** to chromene **139** could be tuned to allow lower reaction temperatures – possibly enhancing the functional group tolerance – and a lower catalyst loading. Decreasing the temperature from 80°C to rt and reducing the catalyst loading to 1 mol% still allowed the reaction to be finished within 60 mins for the more reactive catalytic systems (**64a**, **65**, **126a**, **145**). Whilst the amidinium system only achieved 5% conversion, the dihydroimidazolium and the pyridinium substituted catalytic mixtures converted up to 90% within 60 min. The amidinium system turned out to be the most reactive system (full conversion within 10 mins). For the imidazolium and the pyridinium systems a sigmoid correlation (S- shape)¹⁰⁸ is observed, indicating low solubility of the precatalyst (lower reaction rate at the beginning), high reactivity once all catalyst is activated and diffusion controlled lowered reactivity at the end of the reaction.

We tried to further improve the reaction conditions for the most reactive catalyst system **145** lowering the catalyst loading to 0.5 mol%, however under these reaction conditions only 93% conversion was obtained.

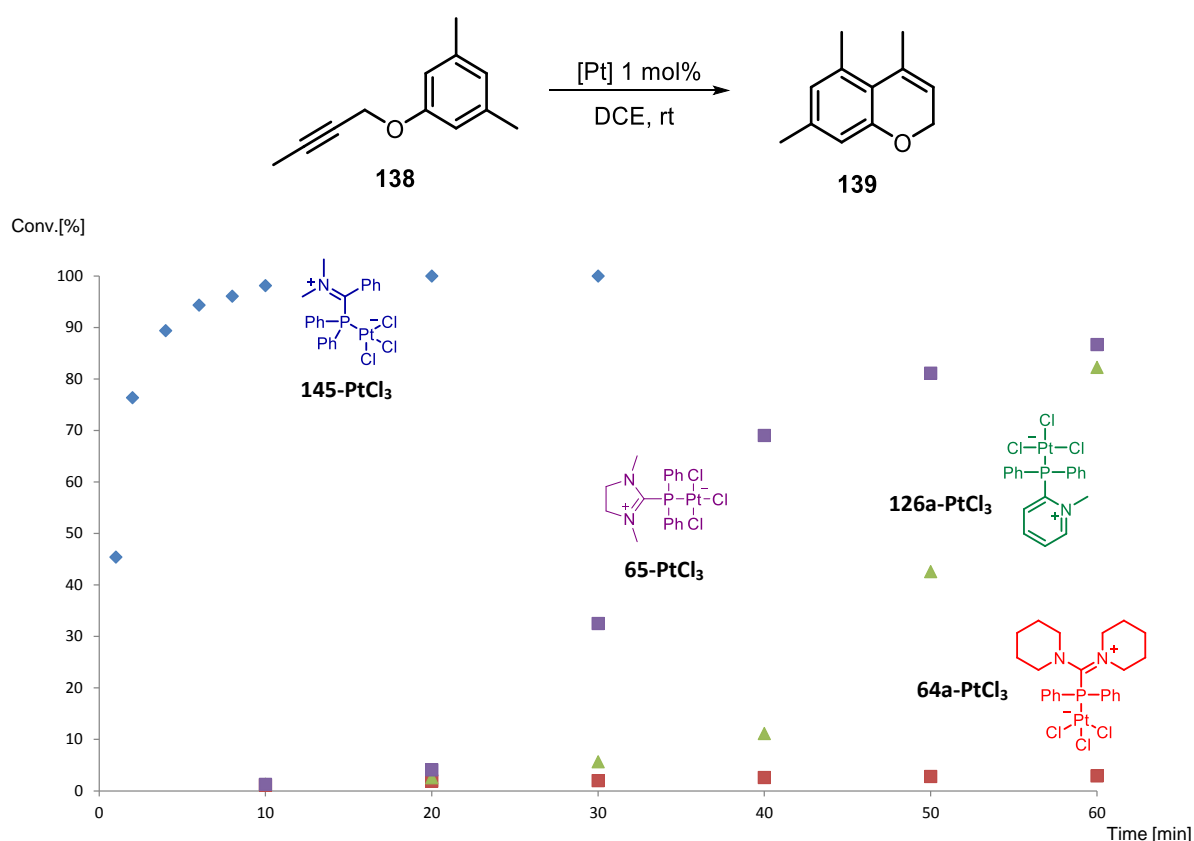
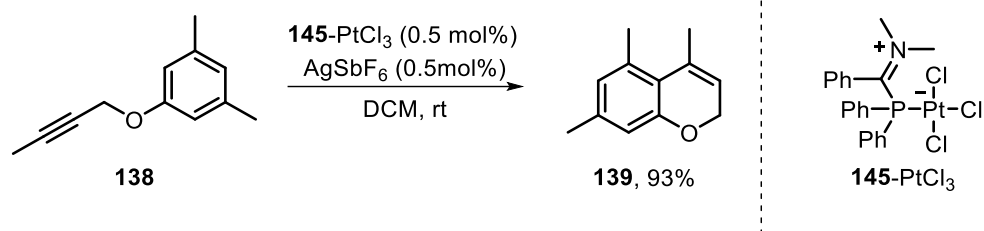


Figure 24: ligand effect on the Pt-catalysed hydroarylation of propargyl aryl ether **35** to chromene **36**. Reagents and conditions: a) **35** (0.05 m), Pt precatalysts (1 mol%), AgSbF₆ (1 mol%), CH₂Cl₂, rt. Conversions determined by gas chromatography.

¹⁰⁸ W. Xu, J. S. Kong, P. Chen, *J. Phys. Chem. C* **2009**, *113*, 2393.



Scheme 64: platinum catalysed hydroarylation at 0.5 mol% catalyst loading.

Hydroaminations¹⁰⁹ and hydroalkoxylations¹¹⁰ reported by Widenhofer *et al.* were also investigated. However, in the hydroalkoxylation of alcohol **146** to ether **147** instead of the expected trend of reactivity all catalyst systems performed equally well, indicating a case of hidden acid catalysis is faced. We therefore tested triflic acid as catalyst, which converted the examined systems as good as the π -acids into the product. Further we noted, that the addition of a sterically hindered non-coordinating base stops the reaction, which also corroborates the hypothesis of hidden acid catalysis. Instead of activating the alkene function of molecule **146** as a π -acid the gold complexes are coordinated by the hydroxyl group and act as a σ -acid. The released proton then catalyses the hydroalkoxylation, resulting in nearly the same reactivity for all gold complexes.

¹⁰⁹ C. F. Bender, R. A. Widenhofer *J. Am. Chem. Soc.* **2005**, *127*, 1070.

¹¹⁰ H. Qian, X. Han, R. A. Widenhofer, *J. Am. Chem. Soc.* **2004**, *126*, 9536.

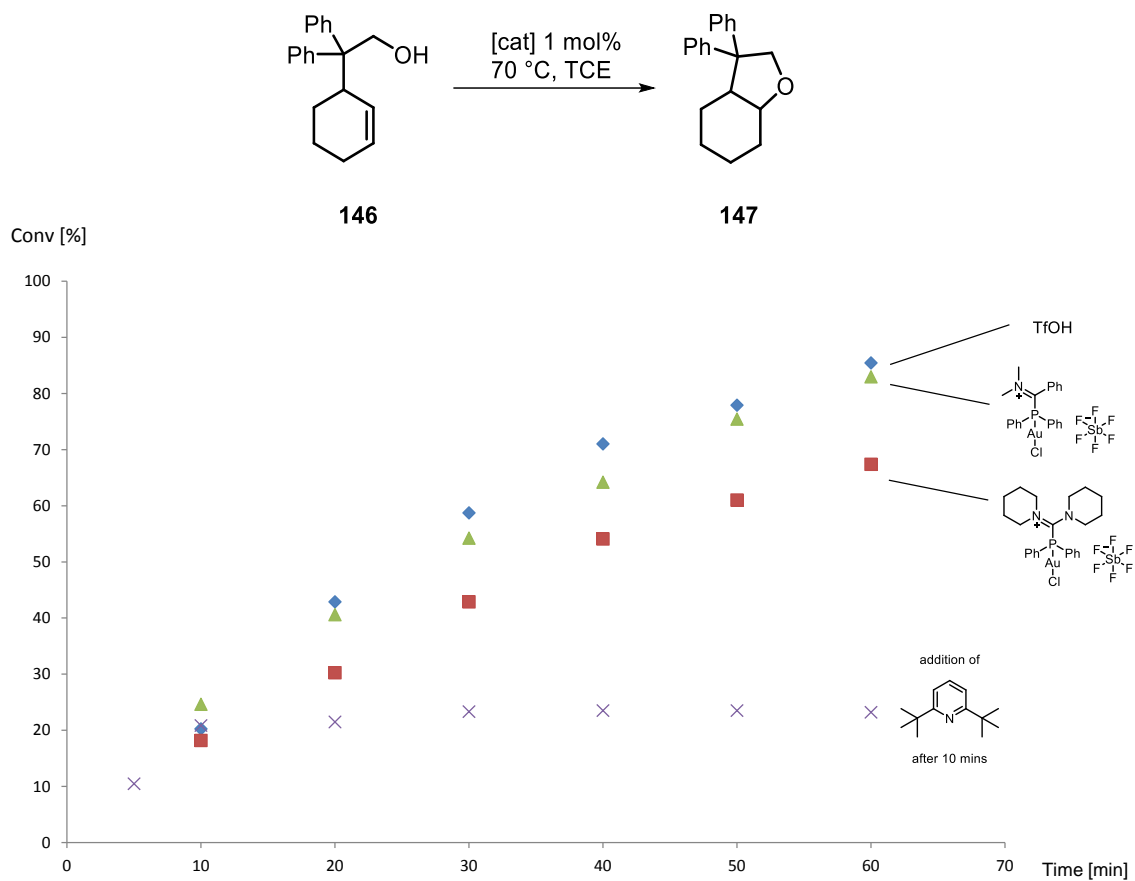


Figure 25: ligand effect on the hydroalkoxylation of alcohol **146** to tetrahydrofuran **147**. Reagents and conditions: **146** (0.05 M), Au precatalysts (1 mol%), AgSbF₆ (1 mol%), (CHCl₂)₂, 70°C. Conversions determined by gas chromatography.

In the exo cyclisation of alkynyl biphenyl system **148** to fluorene **149** the tested gold complexes PPh_3AuCl , **48**-AuCl and **49**-AuCl performed equally well. The additional ester function reduces the electron density of the alkyne function and therefore instead of π activation of the alkyne σ activation is again observed. The gold complex coordinates the ester function and generates a partial positive charge at the alkyne, this results in the exo cyclisation of **148**.

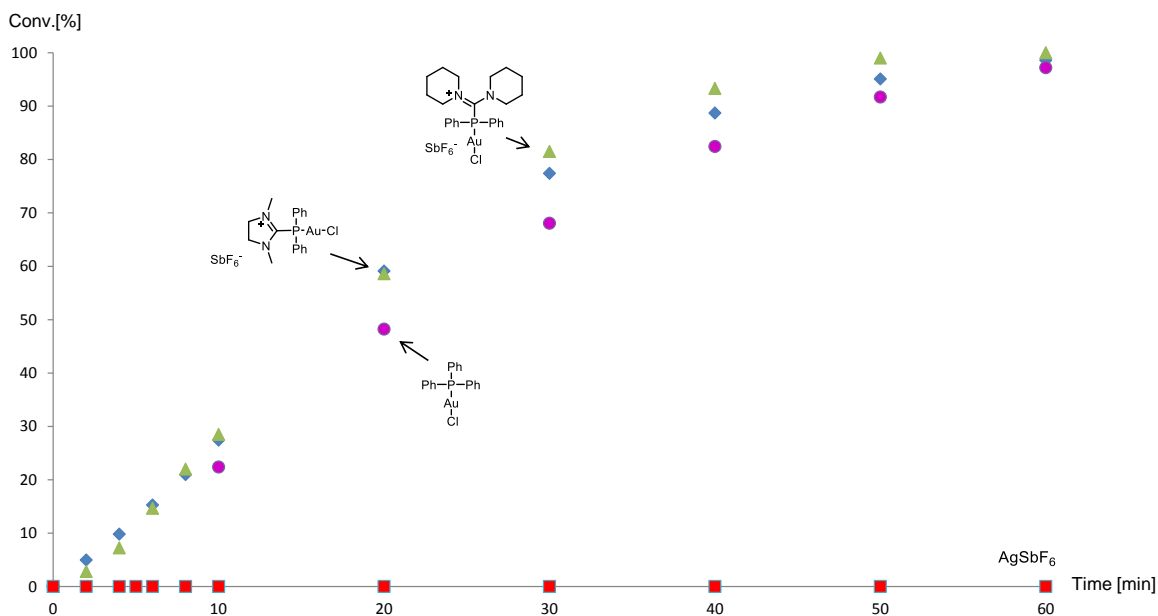
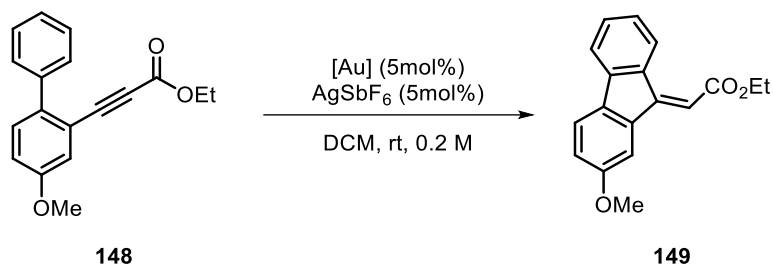


Figure 26: ligand effect on the hydroalkoxylation of biphenyl system **148** to fluorene **149**. Reagents and conditions: **148** (0.05 M), Au precatalysts (1 mol%), AgSbF_6 (1 mol%), $(\text{CHCl}_2)_2$, 70°C . Conversions determined by gas chromatography.

8 Synthesis, structure and applications of arene substituted pyridinium phosphines

After the successful application of N-alkyl phosphine in catalysis, we tried to further improve this system. As mentioned before the catalytic mixtures of gold(I) precursors and the pyridinium phosphines undergo slow decompositions. Therefore we aimed to develop more stable pyridinium substituted phosphines.

One way to enhance the stability of the reactive gold(I)-catalyst is as shown by Echavarren¹¹¹, Xu⁴⁶ and others to introduce a biphenyl unit to the phosphorus atom, allowing a secondary stabilizing interaction between the gold atom and the additional arene ring. For example biphenyldiphenylphosphine gold triflate does not decompose to Au⁰ and bisligated gold triflate within 200 h, while triphenylphosphine gold triflate decomposes up to 80%.⁴⁶ Furthermore the beneficial effect of biphenyl gold catalyst was shown along a vast amount of transformation in gold chemistry. For example as reported by Echavarren in the methoxycyclisation of enyne the use of XPhos as ligand allowed long reaction times and high yields (18 h, 94%), while more reactive ligands like AsPh₃ (48%) or the classically used PPh₃ (70%) only gave lower yields of the desired product within the same time.¹¹²

The mentioned biphenyl unit is as well advantageous in palladium chemistry: Buchwald *et al.* showed, that the presence of the biphenyl unit facilitates the oxidative addition, as only one ligand can coordinate the Pd(0) generated, and at the same time facilitates the reductive elimination process through the steric bulk employed. Furthermore, the additional aryl unit retards oxidation by O₂ and stabilises the Pd centre through secondary interactions. The large substituents at the additional arene unit themselves avoid the cyclometalation of the palladium centre.

All this beneficial effects and the broad applications of the structural related and commercial phosphine ligand SPhos (**22**) and XPhos (**23**) encouraged us to attempt to synthesize a related class of pyridinium phosphines **168**. This should be achieved through the introduction of an aryl unit to the nitrogen of the pyridinium generation N-aryl substituted pyridinium phosphines.

¹¹¹ P. Pérez-Galán, N. Delpont, E. Herrero-Gómez, F. Maseras, A. M. Echavarren *Chem. Eur. J.* **2010**, *16*, 5324.

¹¹² C. Nieto-Oberhuber, S. López, E. Jiménez-Núñez, A. M. Echavarren, *Chem. Eur. J.* **2006**, *12*, 5916.

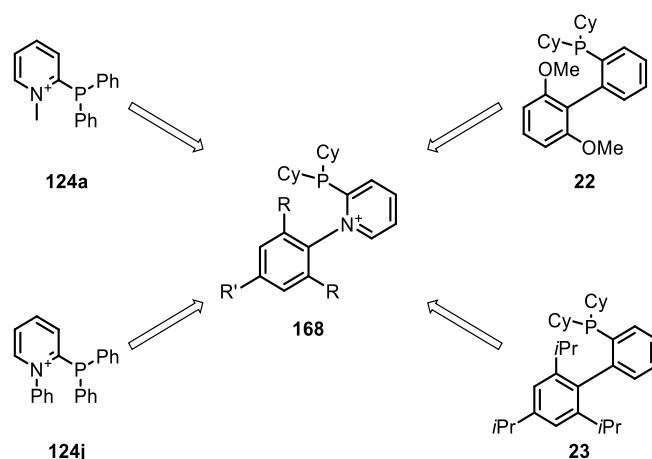
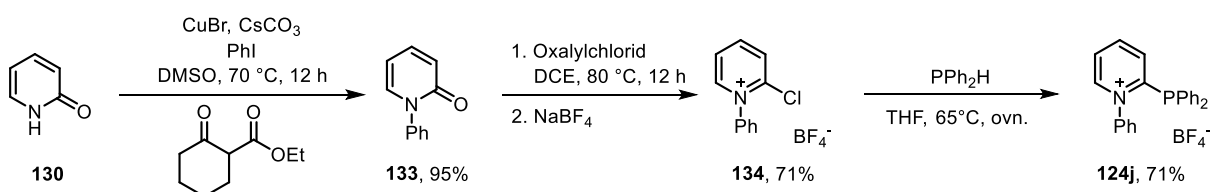


Figure 27: Development of arene substituted pyridinium phosphines.

8.1 Strategies for the synthesis of N-aryl substituted pyridinium phosphines

8.1.1 Direct N-arylation

The synthesis of 1-aryl substituted pyridinium phosphines was accomplished in three steps. Ullmann coupling of pyridone **130** with phenyl iodide gave the corresponding 1-phenylpyridone (**133**) in excellent yield (95%).¹¹³ After chlorination with oxalyl chloride to obtain the 2-chloro-1-phenyl-pyridinium salt **134** in good yield (71%) N-aryl pyridinium phosphine **124j** was prepared by nucleophilic aromatic substitution with diphenylphosphine in good yield (71%).

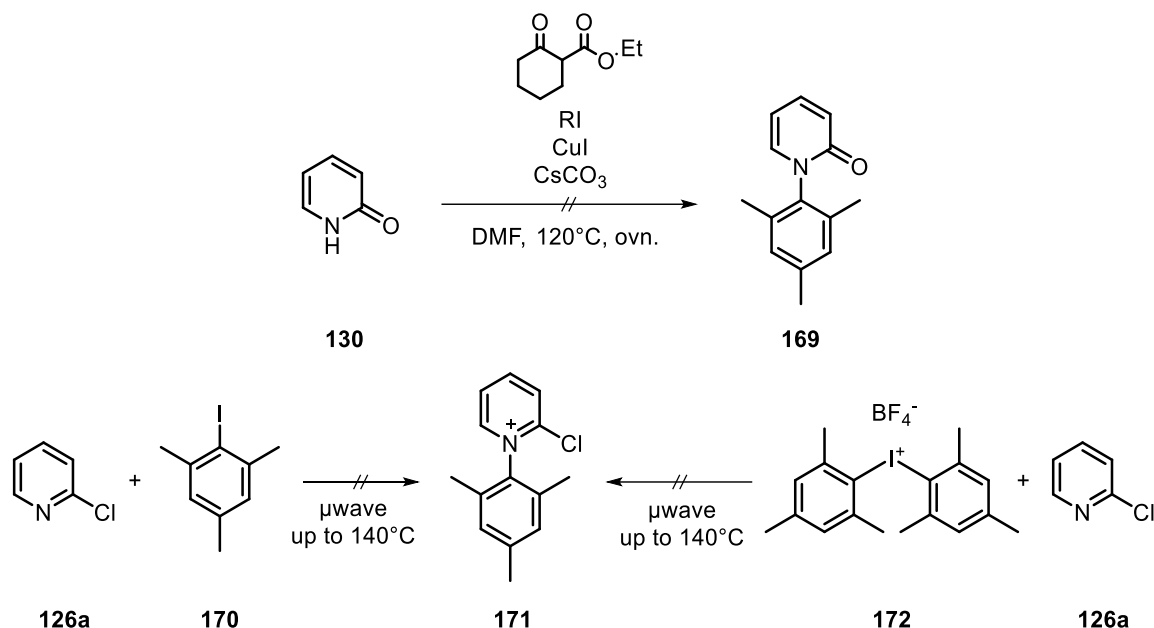


Scheme 65: preparation of **134** by Ullmann coupling and chlorination with oxalyl chloride.

Similarly to the N-phenylation of the pyridinium ring, we tried to introduce the mesityl or the dimethoxy arene unit by Ullmann coupling with pyridone and the corresponding aryl iodide. However, due to the increased steric demand no product formation was observed. Direct coupling of chloropyridine **126a** and the corresponding iodide at reaction temperature of up to 140 °C, either heating in an oil bath or by μ wave irradiation, failed. The same occurs when the coupling is attempted with dimesityl iodonium salt **172**. These limitations most likely are caused

¹¹³ K. H. Müller, M. W. Drewes, P. Dahmen, D. Feucht, DE 100 24 938 A 1

by the vastly increased steric bulk of the employed iodide in comparison to phenyl iodide. Therefore we decided to attempt another approach.

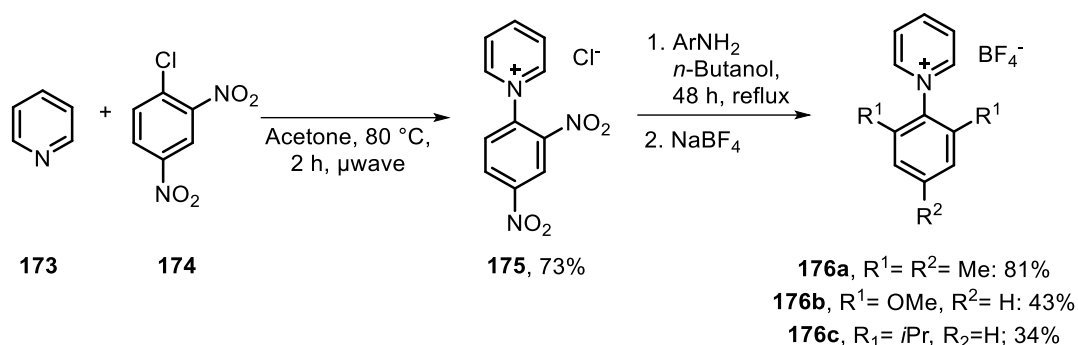
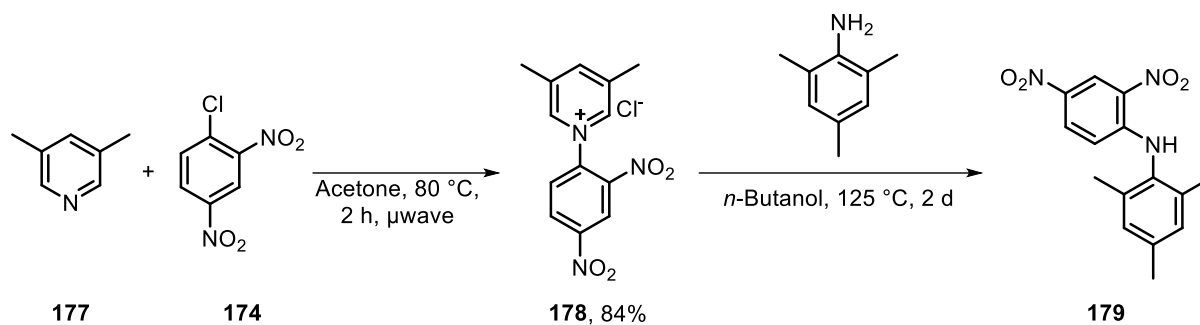


Scheme 66: attempts for the direct preparation of arene substituted pyridinium phosphines.

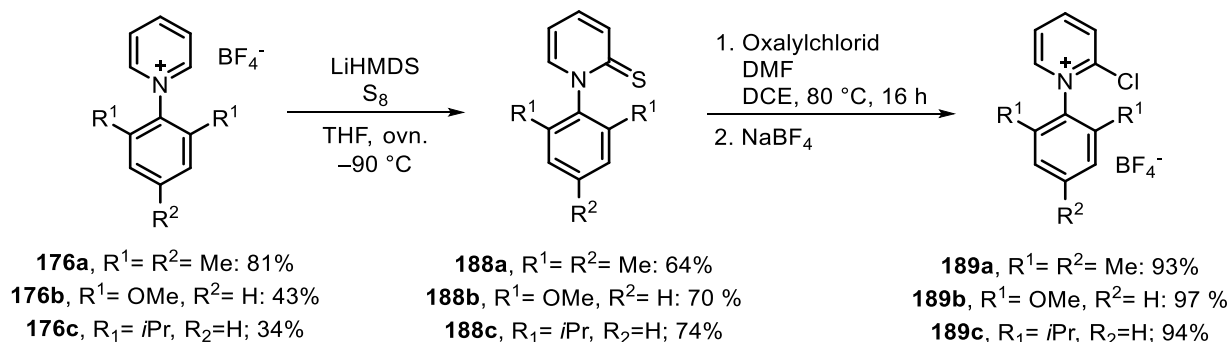
8.1.2 Pyridinium salt functionalization

Due to the limitations, an alternative synthetic strategy was considered. After preparation of the corresponding precursor **175** in 73% yield, using the well-established Zincke reaction,¹¹⁴ we could prepare the arene substituted pyridinium salts **176a-c** in moderate to good yields (34-81%). This reaction works with highly sterically encumbered amines like 2,6-diisopropylaniline or even 2,4,6-triisopropylaniline. However, further increasing the steric bulk at the pyridinium core (employing 3,5-lutidiniumsalt **178**) precludes the Zincke reaction to take place; the nucleophilic substitution of the chloride with the corresponding amine was observed. This side reaction can easily be understood considering the high steric bulk at the α -position of the pyridinium ring. Hence, the nucleophilic attack occurs at the α -position of the pyridinium ring (at the ipso position of the lower ring).

¹¹⁴ a) W. Moller, G.Heuser, T. Zincke, *Liebigs Ann.* **1904**, 330, 361; b) W. Moller, G.Heuser, T. Zincke, *Liebigs Ann.* **1904**, 333, 296; c) G. Weisspfenning, T. Zincke, *Liebigs Ann.* **1913**, 396, 103.

Scheme 67: preparation of pyridiniumsalts **176a-c**.Scheme 68: attempts of the Zincke reaction of lutidinumsalt **178**.

After the preparation of the pyridinium salts **176a-c**, we next functionalized the compounds to be able to introduce the phosphine at the α -position. Thus, we first performed an ortho functionalization to the corresponding thiopyridone **188a-c** by deprotonation of **176a-c** with LiHMDS and in situ trapping of the formed carbene with S₈ (64-70%). Afterwards, we converted the thiopyridone into the chloro pyridinium salt that should easily undergo nucleophilic aromatic substitution reaction with different phosphines. Consecutive chlorination with oxalylchloride in the presence of dimethylformamide led to the formation of chloro pyridinium salts **189a-c** in excellent yields (93-97%). Scale up of the just mentioned sequence to gram scale (up to 5 g) was possible for all substitution patterns up to the chloro pyridinium salt stage.

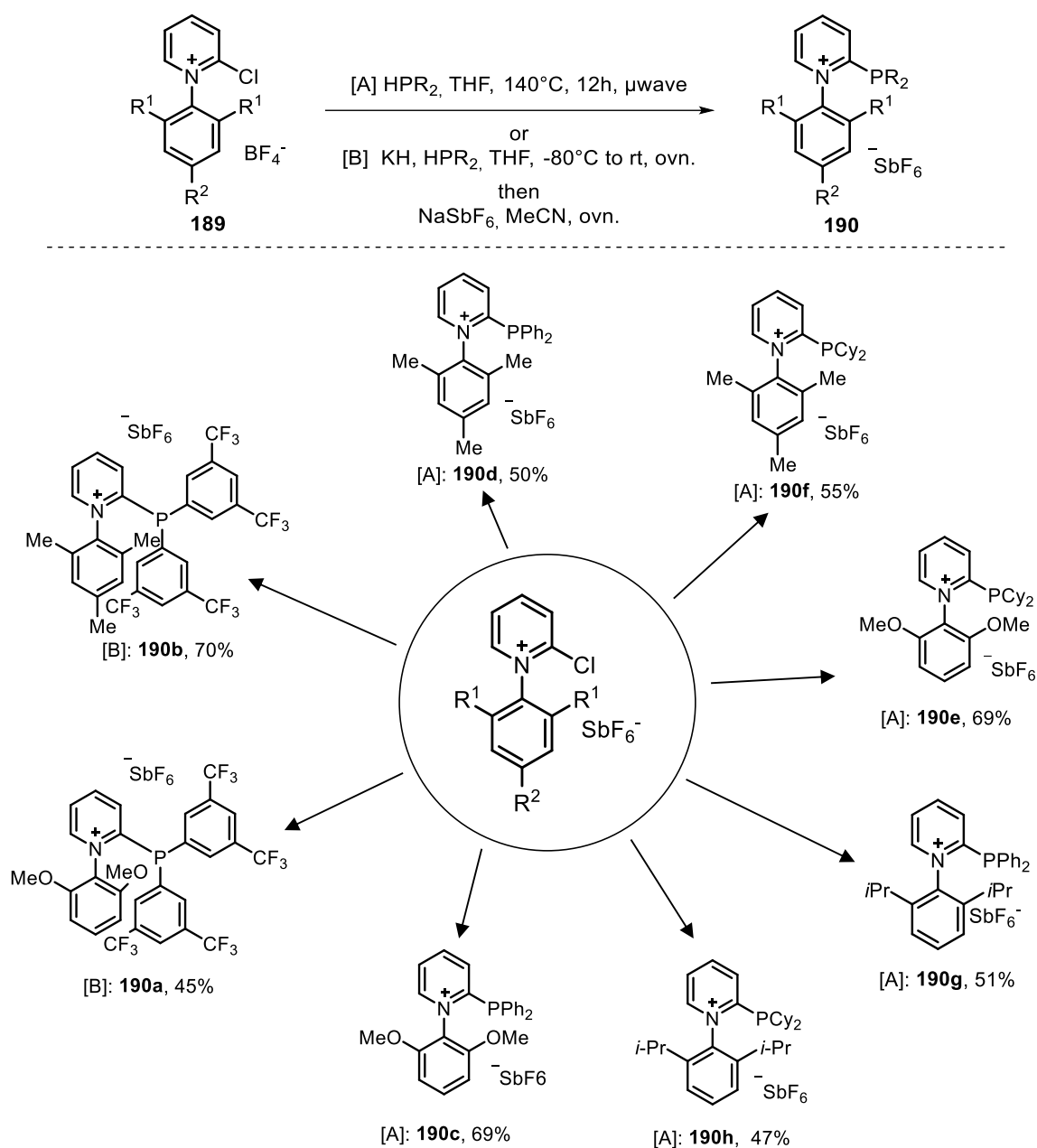


Scheme 69: Synthesis of the chloropyridinium salts.

With the chloro pyridinium salts in hand, we then commenced introducing different phosphines by direct phosphination with either diphenylphosphine (50-69%) or dicyclohexylphosphine (47-

69%) under microwave irradiation for 12 h at 140 °C in THF, or by deprotonation of the polyfluorinated phosphine and followed by direct condensation (**190a-h**, 45–70%). Unfortunately, the introduction of *t*Bu₂PH could not be achieved under the chosen reaction conditions.

Overall this reaction sequence allowed fast, scalable and direct access to the arene substituted pyridinium phosphines in a five step sequence with overall yields between 8.1% (**190a**) and 24.6% (**190b**).



Scheme 70: Synthesis of pyridinium phosphines.

After the successful preparation of the new pyridinium phosphines, we were able to crystallize a few examples to confirm the expected connectivity. This enabled us to check if the phosphorus lone pair, even in the sterically demanding environment, is available for coordination.

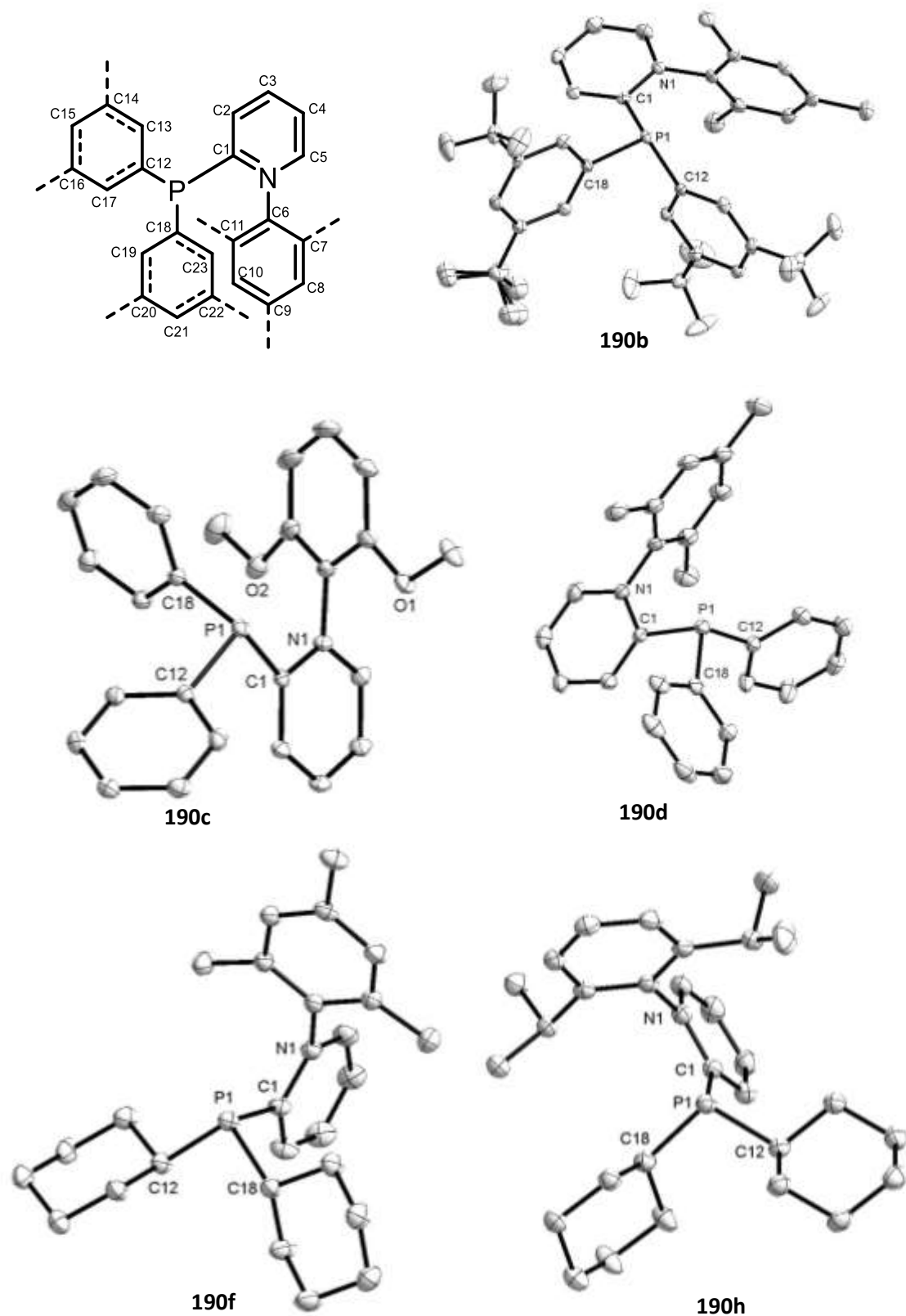


Figure 28: schematic representation and numbering of cationic arene substituted phosphine gold complexes. Solid state structures of phosphines **190 b**, **c**, **d**, **f** and **h**. Hydrogen atoms and anions are omitted for clarity. Anisotropic displacement parameter are shown at 50% probability level.

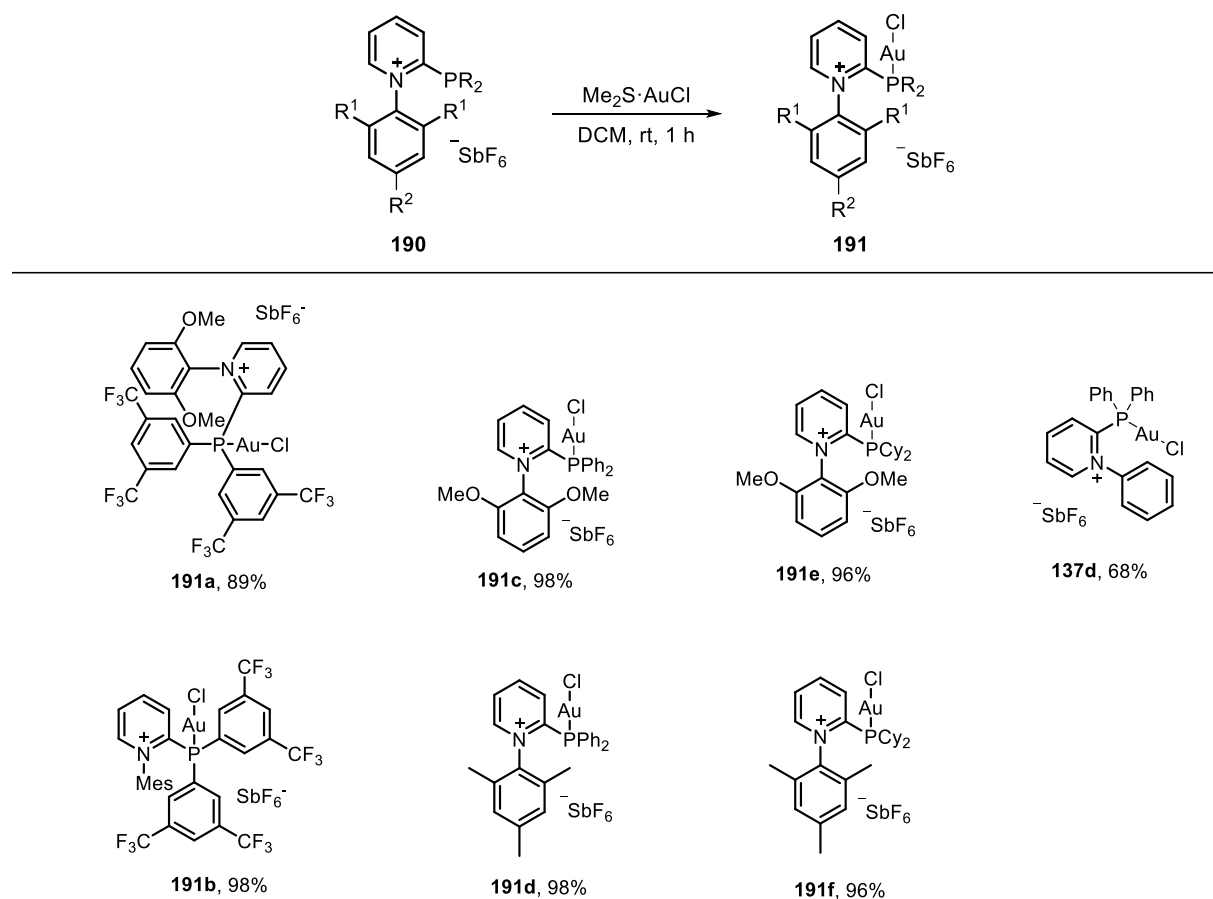
Compound	Phosphine	d(P-C1) [Å]	d(P-C12) [Å]	d(P-C18) [Å]	pyramidalization [°]
190b	MesPolyCF ₃	1.849	1.831	1.829	308.02
190c	DiOMePyPPh ₂	1.850	1.836	1.821	305.71
190d	MesPyPPh ₂	1.850	1.828	1.821	304.91
190f	MesPyCy ₂	1.863	1.867	1.865	303.57
190h	<i>i</i> Pr ₂ PyPCy ₂	1.860	1.877	1.855	303.96
124a	MePyPPh ₂	1.855	1.826	1.824	304.87
124e	MePyCy ₂	1.858	1.873	1.849	303.79
46a	CyclopropPPh ₂	1.814	1.834	1.831	303.67

Table 5: important distances and angles in the solid state structure of phosphines.

Despite the vastly increased steric bulk comparing for example the methyl substituted pyridinium phosphine **124a** and the mesityl substituted phosphine **190d**, only minor differences in bond angles and bond distances are observed (1.855 Å for **124a** vs. 1.850 Å for **190d** and 304.91° vs. 304.87°). Furthermore, the high degree of pyramidalization (303.57 -308.02°) present in all phosphines indicates its availability to coordination.

8.2 Synthesis of gold complexes

Next the coordination chemistry of phosphines **124j** and **190a-f** was examined. Hence, we prepared the corresponding gold complexes by simple ligand exchange reaction with $\text{Me}_2\text{S}\cdot\text{AuCl}$. In all cases the gold complexes were obtained in moderate (**137d**, 68%) to excellent yields (**191a-f**, 89-99%).



Scheme 71: synthesis of gold complexes **137d** and **191a-f**.

Compound **137d** was crystallized and its structure was in agreement with our expectations. The solid state structure shows a secondary interaction between the gold atom and the C11 atom of the arene ring (3.14 Å), which is different to the neutral equivalent $\text{Cy}_2\text{JohnPhos}$, which also shows a secondary gold interaction, but to the carbon in ipso position of the arene ring (3.136 Å)¹¹⁵. The differences arise from the presence of the cationic charge next to carbon C7, which lowers the electron density of this carbon and therefore is less prone to coordination.

¹¹⁵ D. V. Partyka, T. J. Robilotto, M. Zeller, A. D. Hunter, T. G. Gray, *Organometallics* **2008**, 27, 28.

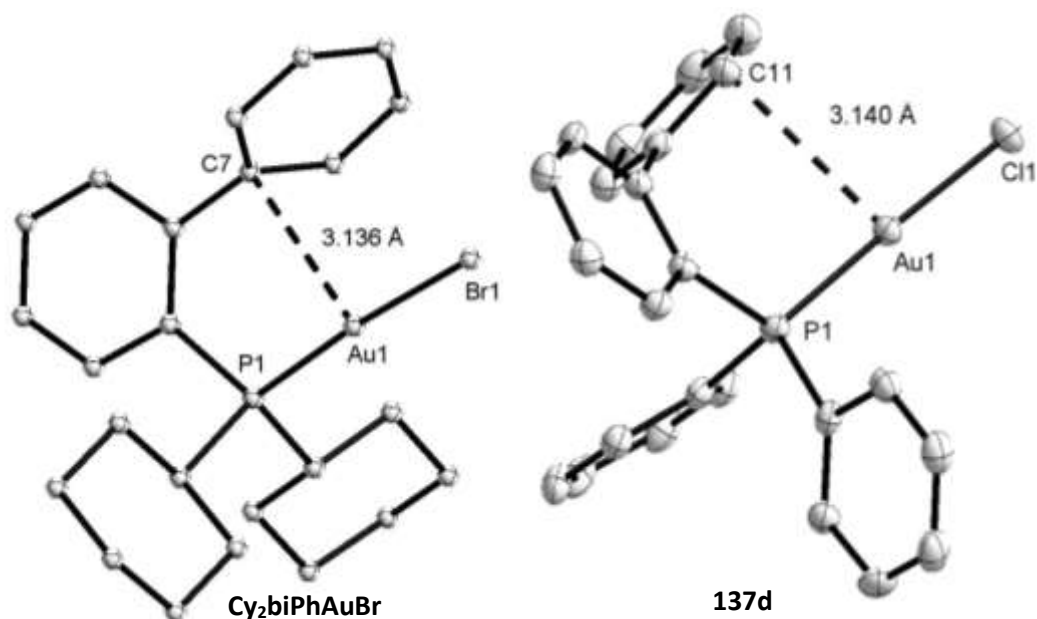


Figure 29: molecular structure of **Cy₂biPhAuBr** and **137d** in the solid state. Hydrogen atoms and anions are omitted for clarity. Anisotropic displacement parameters are shown at 50% probability level.

To be able to compare the electronic and steric influence and the secondary interaction with the gold atom of the additional arene ring, we crystallised and analysed the five gold complexes (**191a**, **b**, **d** and **191f**) by x-ray diffraction techniques. This allowed us to compare the influence of the additional cationic charge in comparison to their neutral congeners and, furthermore, to assess the effect of the additional steric bulk on the structure of the Au-precatalyst.

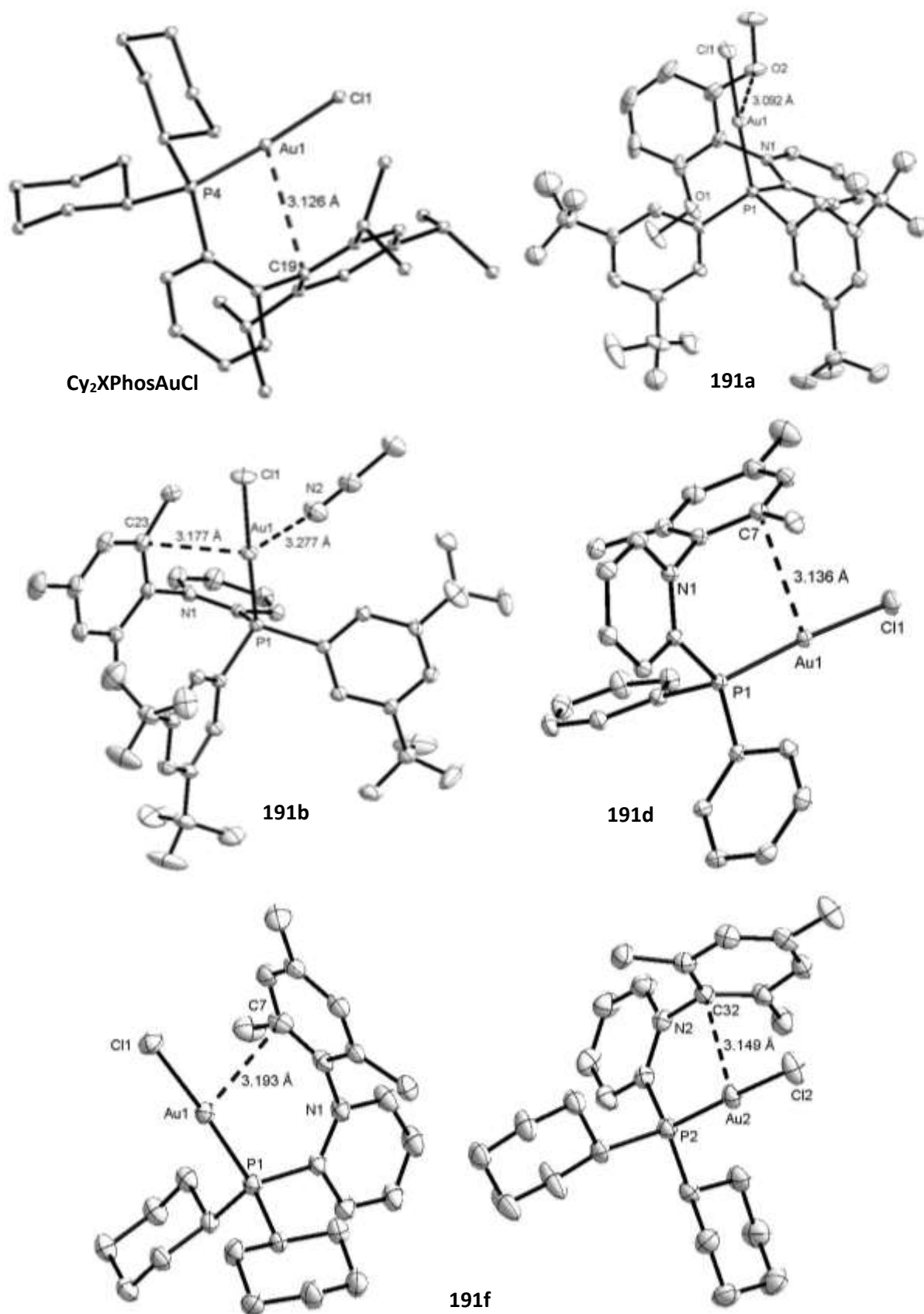
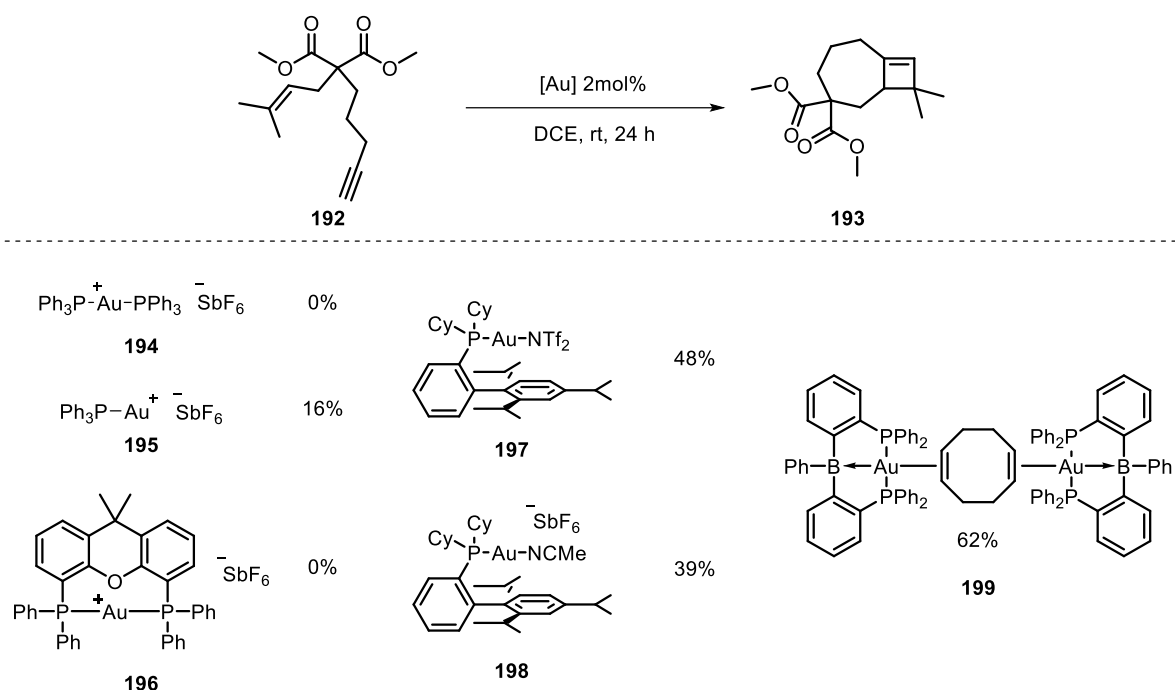


Figure 30: solid state structures of Cy₂XPhos¹¹⁵ and pyridinium phosphine gold complexes **191a**, **b**, **d** and **191f**. Hydrogen atoms, disorder and cations are omitted for clarity. Anisotropic displacement parameter are shown at 50% probability level.

In all crystallised complexes a secondary interaction between the pyridinium arene unit and the gold atom is present. Although the bond distances in these complexes are slightly different (3.092-3.193 Å), they all are shorter than the corresponding sum of the van-der-Waals radii (3.360 Å). The nature of the interaction differs depending on the substitution pattern. While usually the main interaction occurs towards the ortho carbon of the pyridinium arene substituent, in gold complex **191a** and **191f** the nature of the interaction differs. In complex **191a** the interaction occurs between the oxygen and the gold atom and in gold complex **191 f** the closest arene gold contact aligns at the ipso carbon of the pyridinium arene (3.149 Å). All bond distances are comparable to literature known interactions between gold atoms and biphenyl units (XPhos: 3.126 Å, CyJohnPhos: 3.136 Å; compare Gray *et al.*¹¹⁵) and therefore, during catalysis the pyridinium complexes might show improved catalyst stabilities as well.

8.3 Applications in gold catalysis

We next examined the effect of the newly prepared ligand system in a gold catalysed reaction. We chose a gold catalysed [2+2] cycloaddition reported by Mukai¹¹⁶ in 2015. This transformation is accelerated by the use of very bulky catalytic systems like XPhos and as well by the use of the Z-type, electron poor gold complex as described by Mukai (**199**). However none of the reported ligand could reach full conversion even in a timeframe of 24 hours. Therefore, we decided to test our ligand system, which combines the bulk and reactivity needed in this cycloaddition.



Scheme 72: effect of the catalytic mixtures toward to the [2+2] cycloaddition reported by Mukai et al.

¹¹⁶ F. Inagaki, C. Matsumoto, Y. Okada, N. Maruyama, C. Mukai, *Angew. Chem. Int. Ed.* **2015**, 3, 818.

First we performed studies under the same reaction conditions as Mukai reported and checked them by NMR (Figure 31). However, in all the performed NMR experiments no proper of the reaction mixtures could be ensured during the measurement. Despite these problems already by NMR studies a clear trend can be observed. The commercial ligand gold complexes of SPhos, PPh₃ and XPhos already reached low conversions (2%, 7% and 15%) within 80 minutes, while our pyridinium system converted already 40% within the same timeframe, illustrating the enhanced reactivity introduced by the additional positive charge already at this stage.

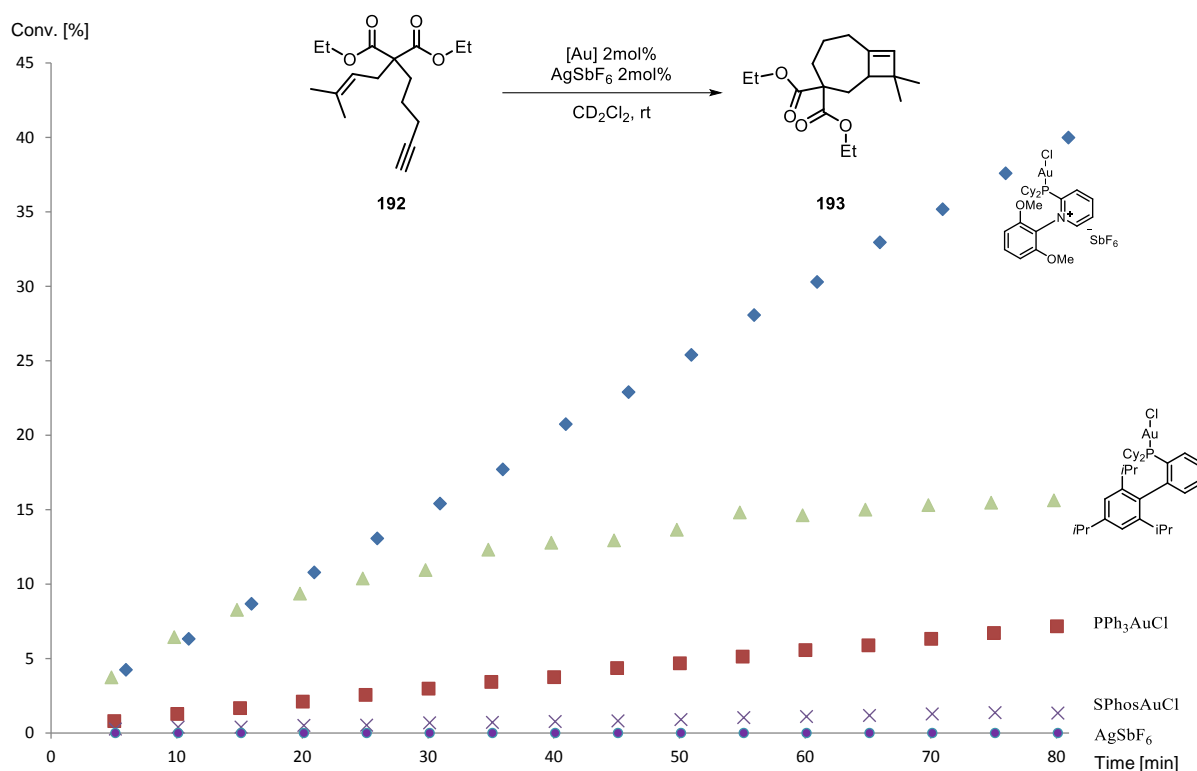


Figure 31: ligand effect in the gold catalyzed cycloaddition of enine **192** to cyclobutene **193**, conversion determined by ¹H NMR, 2 mol% [Au], 2 mol% AgSbF₆, 0.1M in CD₂Cl₂ at rt.

Not only the π -acceptor properties of the applied ligand are important, the bond strength between the used ligand and the gold atom and the before mentioned steric protection of the gold atom needs to be considered as well.

Figure 32 shows performing the reaction in a classical laboratory setup, that increasing the steric bulk from a methyl to a mesityl group heads to an improved reactivity (10% higher conversion, **137a** vs. **191d**). This additional reactivity stems from the increased stability of gold complex **191d**, caused by the aforementioned arene gold interaction. The stability of the gold phosphine complex can be further increased employing more σ -donating phosphines. Cyclohexyl substituted phosphines **191f** led to full conversion, while phenyl substituted phosphine **191d** and polyfluorinated phosphine **191b** led to 25% and 50% conversion.

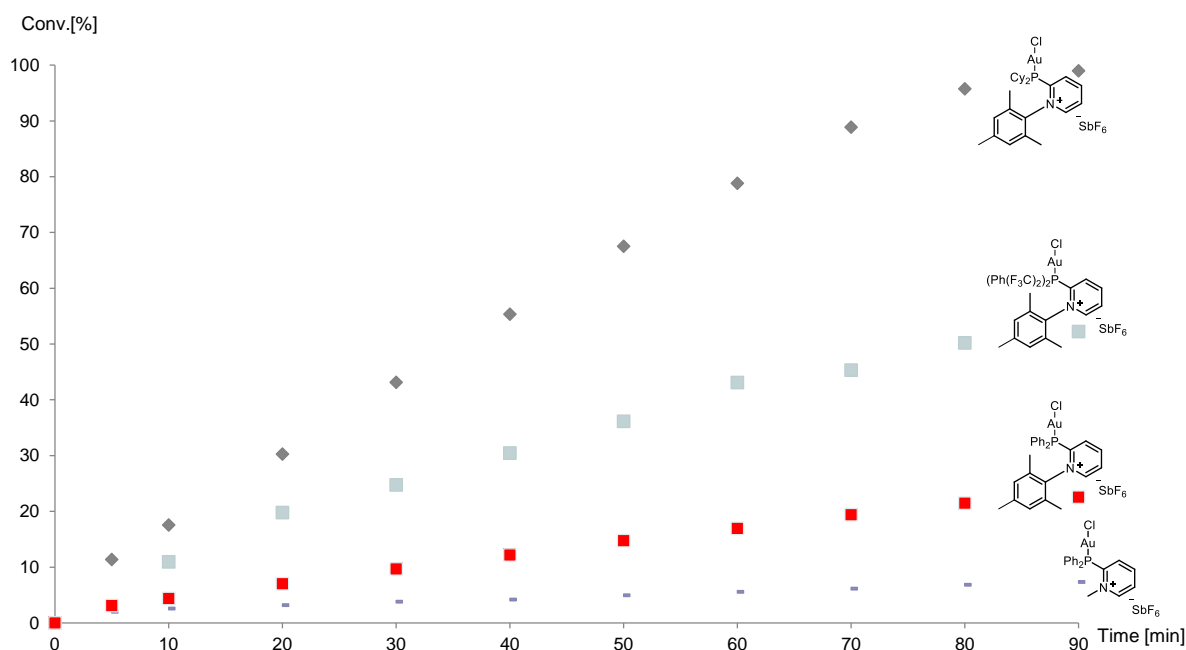


Figure 32: ligand effect in the gold catalysed cycloaddition of enine **192** to cyclobutene **193**, 2 mol% [Au], 2 mol% AgSbF₆, 0.1M in CH₂Cl₂ at rt; conversion determined by gas chromatography versus an internal standard

While the silver salt alone did not convert enine **192** to cyclobutene **193**, well established ligands for gold catalysis like PPh₃, SPhos and XPhos performed poorly within the examined timeframe (up to 25% within 90 min.), compare Figure 33. However, the different steric and electronic interacting effects can easily explain the observed behaviour. While more π -acidic ligand like triphenylphosphite perform at a significantly higher rate in the first 20 min of the transformation their reactivity ceases due to their lower stability with prolonged reaction times. Therefore on the other hand also good result can be obtained employing more stable gold complexes SPhosAuCl and XPhosAuCl with arene gold interactions, which show an almost linear correlation of the observed reactivity with time only offset by a low reaction rate. Combining the enhanced reactivity of good π -acceptor ligands and at the same time enhancing the steric protection of the gold atom and therefore the stability of the catalytically active species, the reaction rate could greatly be improved – pyridinium phosphine complexes **191e** and **191f** led to full conversion towards the cyclobutene **193** within 90 min.

It should be noted, that further prolonged reaction times lead to decomposition of the product and starting material in all examined cases and after 24 h of reaction time, only traces of the desired product could be found.

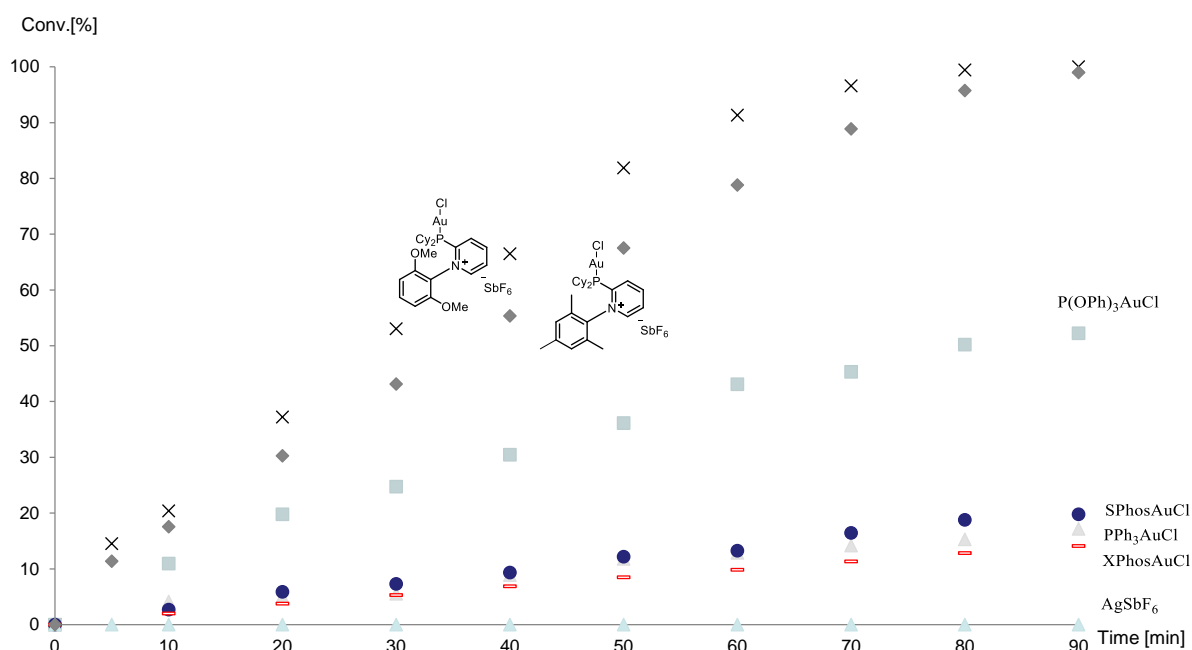
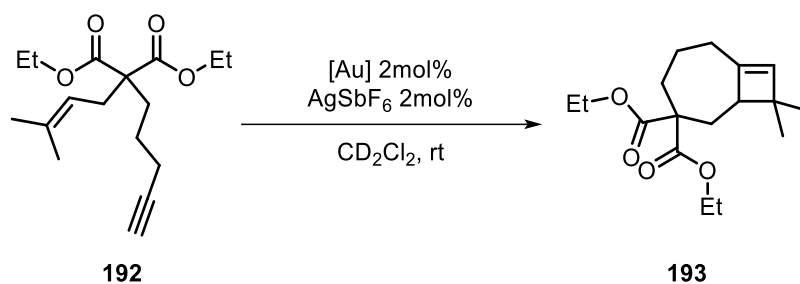
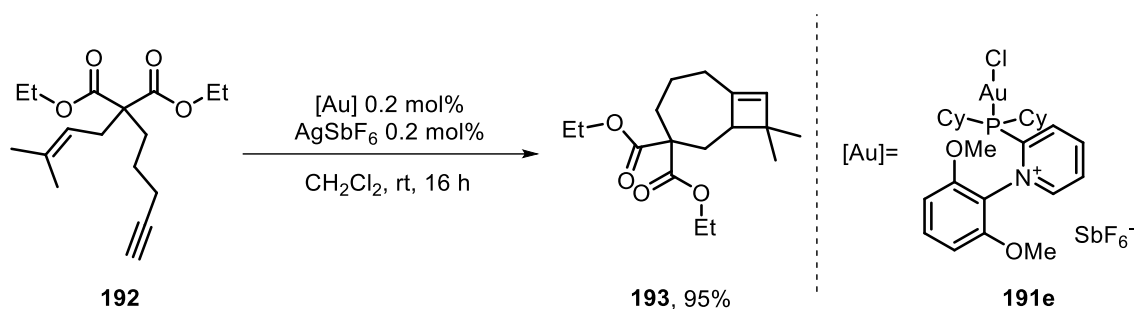


Figure 33: ligand effect in the gold catalysed cycloaddition of enine **192** to cyclobutene **193**, 2 mol% [Au], 2 mol% $AgSbF_6$, 0.1M in CH_2Cl_2 at rt; conversion determined by gas chromatography versus an internal standard

After this promising results, we then lowered the catalyst loading to 0.2 mol% and still achieved full conversion within 16 hours (95% isolated yield), once again demonstrating the high reactivity, as well as stability of the newly developed cationic arene substituted pyridinium phosphine **191e**.

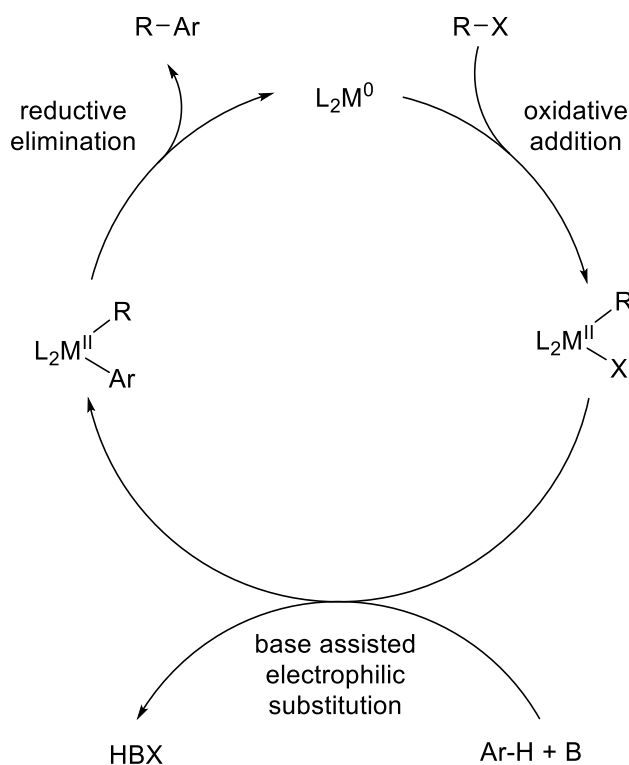


Scheme 73: Cycloaddition of enine **192** to cyclobutene **193** under optimized conditions using 0.2mol% X, 0.2mol% $AgSbF_6$ in DCM for 16 hours at rt.

8.4 Applications in palladium chemistry

After these highly encouraging results we aimed to find other catalytic applications in areas different to π -acid catalysis. Hence, we decided to examine the use of our developed ligand in palladium chemistry.

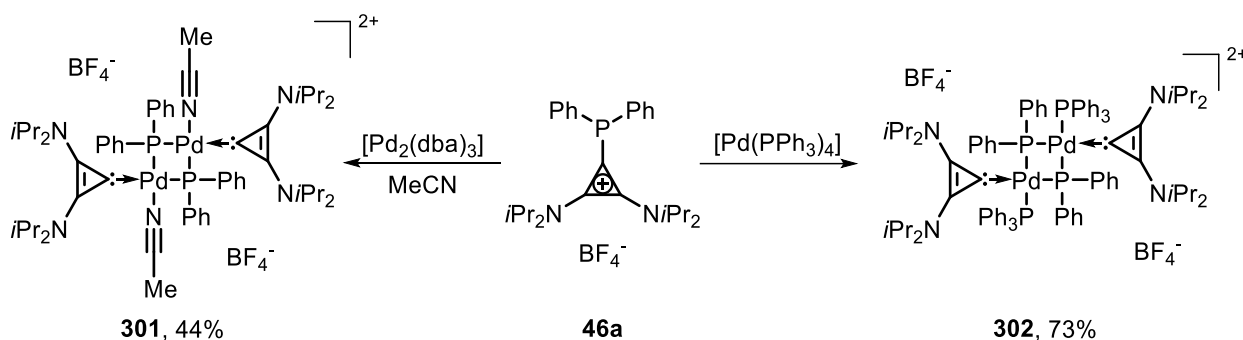
In general in palladium chemistry highly π -accepting ligands are rarely used, however they should be able to facilitate a number of steps of a general catalytic cycle. For example palladium catalysed C-H activations might be an interesting area to test our ligands. The catalytic cycle for a C-H activation can consist of oxidative addition, precoordination, electrophilic reaction, base promoted deprotonation and reductive elimination. The oxidative addition to palladium systems bearing one of our cationic ligands is going to be more difficult, because a palladium(II) state has to be generated starting from an already cationic palladium(0) centre. On the other hand the electrophilic substitution occurs at a faster rate, because for the described C-H activation sequence the generated palladium(II) centre is stabilized by two organic residues, instead of like in case of cross coupling reactions by one and a halogen atom. Our ligand influence the base assisted deprotonation also to our benefit. The deprotonation from a highly cationic intermediate is faster and easier, therefore less basic bases can most likely be employed. Last the reductive elimination (for a number of palladium catalysed reaction rate determining) occurs at a higher rate, regenerating the palladium(0) centre and minimizing partial charges.



Scheme 74: mechanism of a C-H activation based on an electrophilic substitution.

To compensate the more difficult oxidative addition, when cationic ligands are employed, we decided to use aryl iodides instead of the classically employed aryl bromides and chlorides. Due to the weaker aryl halide bond these undergo oxidative addition with relative ease.

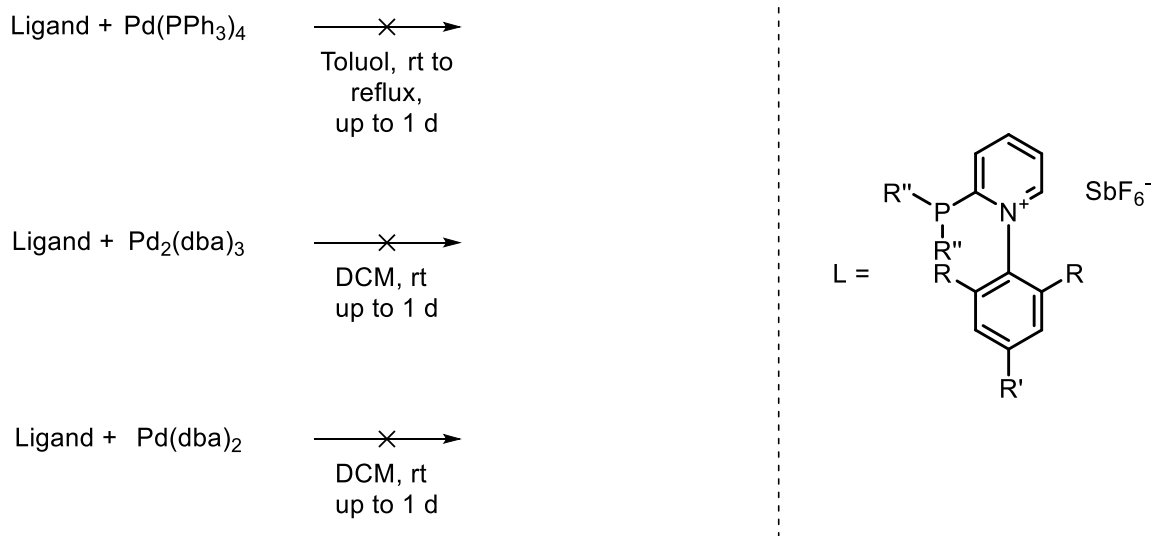
This promising assessment of cationic phosphines promoted our group to test our ligands in palladium chemistry. However, for the cyclopropenium substituted phosphines instead of the coordination product the insertion of palladium between the phosphorus atom and the cyclopropenium moiety was observed.⁷⁶



Scheme 75: synthesis of palladium complexes **301** and **302**.

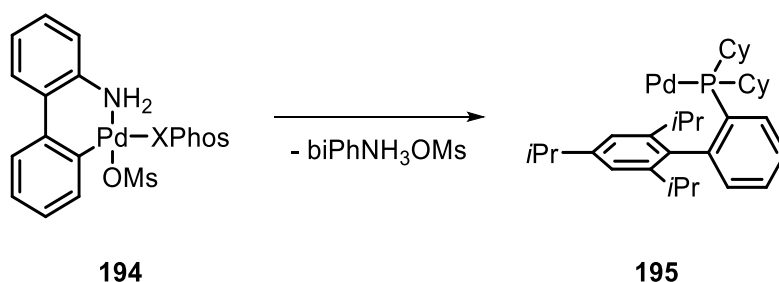
Nevertheless, we tried to prepare the corresponding palladium complexes of the newly prepared pyridinium phosphines **190a**, **b** and **c**. Unfortunately no coordination product was obtained for pyridinium phosphines **190a**, **b** and **c** and different palladium sources. Luckily no

insertion product was obtained, showing that in general pyridinium phosphines might find applications in palladium catalysed reactions.



Scheme 76: coordination attempts of different Pd(0) sources.

Therefore, we decided to deliver the palladium(0) species *in situ* during catalysis, starting from a palladium(II) source as described by Buchwald *et al.*¹¹⁷ Beginning from the corresponding palladium(II) amino biphenyl system **194**, the palladium(0) phosphine complexes **195** is formed under catalytic conditions either by thermal or base promoted reductive elimination of the ammonium biphenyl mesylate.



Scheme 77: reductive elimination leading to catalytic active palladium(0) species as reported by Buchwald.

Analogously to Buchwald's report, we prepared the corresponding palladium(II) complexes in THF, however, due to fast thermal reductive elimination of the amino biphenyl unit we had to perform this reaction at -20°C yielding the corresponding pyridinium phosphine palladium complex **196** after an anion exchange with NaSbF_6 in only moderate yield (54% over two steps). The same system was prepared for the SPhos ligand (51% over two steps).

¹¹⁷ P. Ruiz-Castillo, D. G. Blackmond, S. L. Buchwald, *J. Am. Chem. Soc.* **2015**, *137*, 3085.

With these complexes in hand, after several attempts, we were able to crystallize complex **196** from THF and *n*-pentane by diffusion at -20°C. The solid state structure shows two independent units both possessing a strong interaction between the arene (C1-Pd_(averaged): 2.357 Å) and the palladium centre, resulting in a distorting of the aryl pyridinium plane ($\phi_{(N-Aryl)_{averaged}} = 151^\circ$). Because the analogue complexes derived from SPhos were not crystallised and no direct comparison was possible, we compared the solid state structure of our complex **196** with the closest relative, complex **200**.⁶⁸ In our newly prepared palladium complex **196** the bond distance (2.357 Å) is already shorter than in complex **200** (C1-Pd: 2.447 Å), while in our palladium complex a stronger bending away from the ideal 180° is present ($\phi_{(N-Aryl)} = 151^\circ$ to Buchwald's $\phi_{(C-Aryl)} = 163^\circ$). This interaction should stabilise the palladium intermediates of a catalytic cycle for our cationic phosphines even more than for the SPhos derivatives. Therefore our catalytic system should outperform in catalysis, in which catalyst decomposition is an issue.

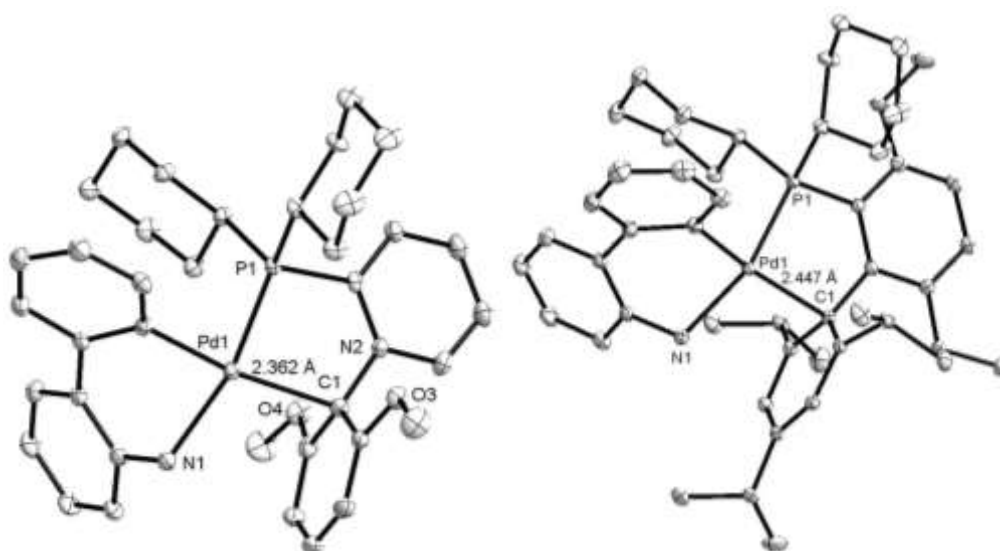


Figure 34: solid state structure of palladium complex **196** (one molecule of the two units in the unit cell shown) and the by Buchwald reported palladium complex **200**. Hydrogen atoms and anions are omitted for clarity. Anisotropic displacement parameter are shown at 50% probability level.

With these palladium complexes we then tested their applications in catalysis. We first performed the already mentioned direct arylation of thiophene reported by Itami *et al.*¹⁰⁶

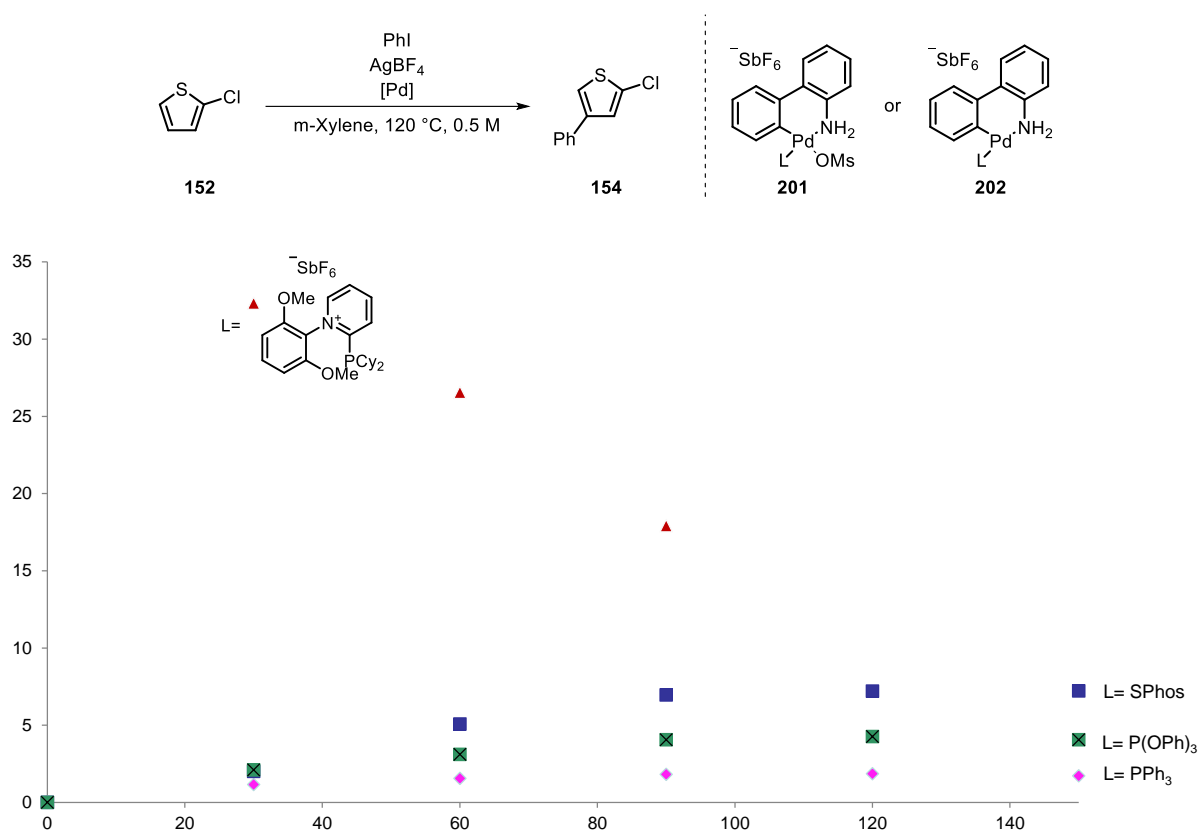
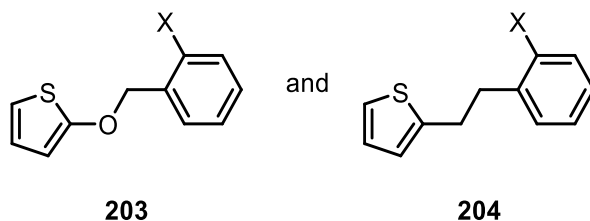


Figure 35: ligand effect in the phenylation of chloro thiophene **152** (1.5 eq) with phenyl iodide (1 eq) in m-xylene (0.5 M) at 120 °C with 1.5 eq AgBF₄ and 5 mol% of the corresponding palladium complexes. Conversion to phenyl chloro thiophene shown. Conversion were determined by GC versus an internal standard (eicosane).

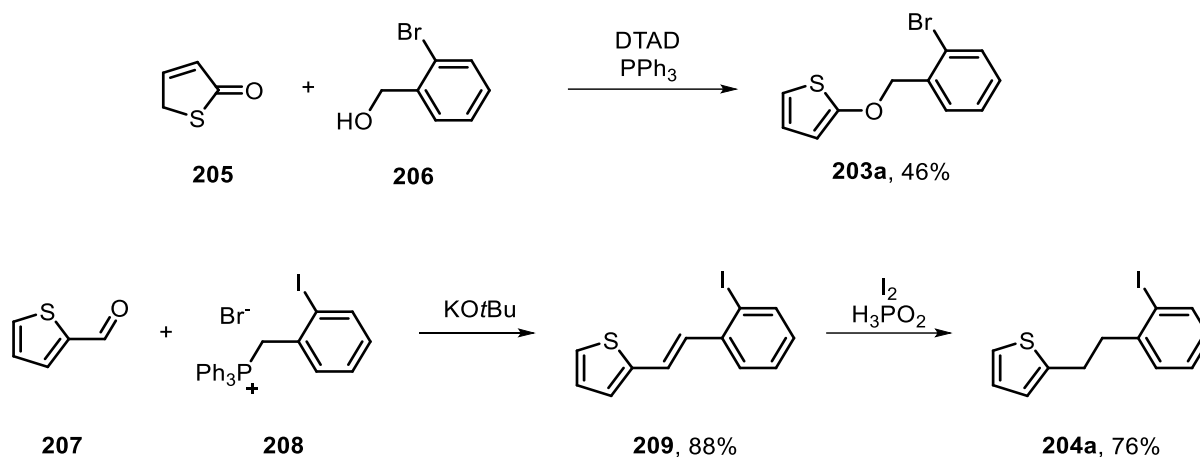
While more electron poor ligand slightly promoted the reaction – triphenylphosphite instead of triphenylphosphine led to 3% conversion instead of 1% - sterically hindered and therefore kinetically more stable phosphines like SPhos **22** enhanced the reaction rate even further (7%). Combining both effects in the pyridinium phosphines **126c** led to a high conversion of 33% after 30 min. to the desired product. However, under the reaction conditions this product further reacted with prolonged reaction times to deliver the diphenylated thiophene. This wanes the reaction of limited use.

To avoid the additional phenylation we decided to design intermolecular systems, which should possess similar reactivity.



Scheme 80: designed intermolecular system for C-H activation with palladium.

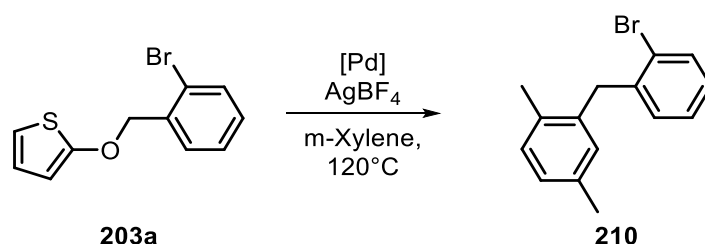
After several optimizations we were able to prepare both system in a short and reliable synthesis. Compound **203** was obtained by Mitsunobu etherification of 2(5H)-thiophenone (**205**) with bromo benzyl alcohol (**206**) in the presence of DTAD and PPh₃ (46%),¹¹⁸ while compound **204a** was prepared through Wittig reaction of 2-thiophenecarboxaldehyde (**207**) and the corresponding phosphonium salt (**208**; 88%) followed by reduction with iodine and phosphinic acid (76%)¹¹⁹.



Scheme 81: synthesis of substrates for the intermolecular C-H activation.

With these substrates in hand, we tested them in the palladium catalysis. However, none of the desired products was formed.

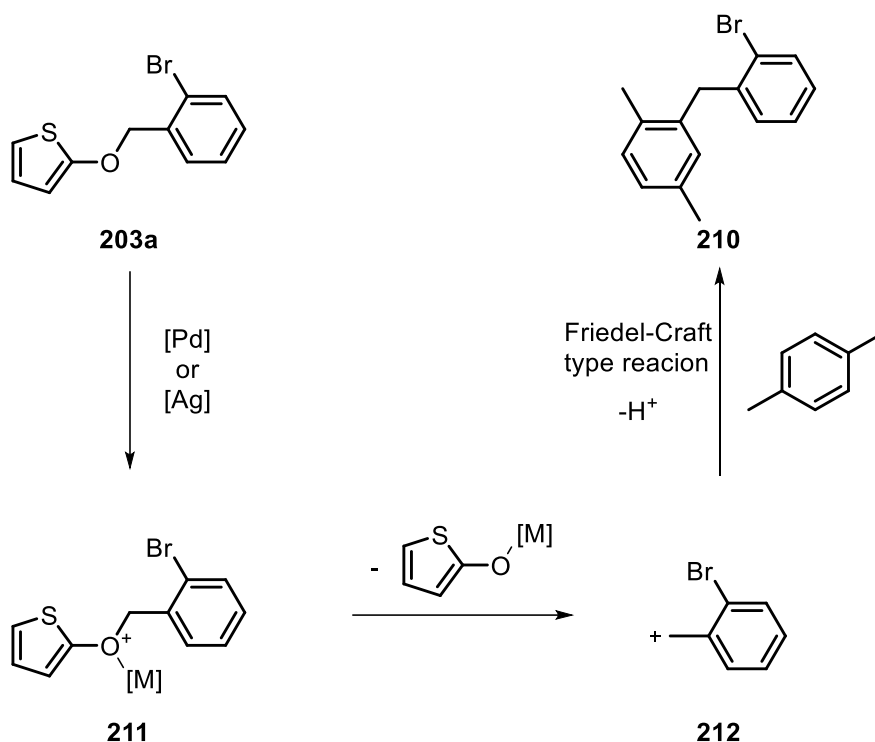
The first substrate **203a** reacted in a Friedel-Crafts type reaction, resulting in nucleophilic substitution of the thienone fragment and formation of 2-benzyl-1,4-dimethylbenzene (**210**). This reaction is believed to be promoted by the high Lewis acidity of the monoligated palladium sources or the silver salt, which activates the oxygen atom of the ether bridge, to promote its nucleophilic substitution by mesitylene.



Scheme 82: reaction of substrate **203a** to benzyldimethylbenzene **210**.

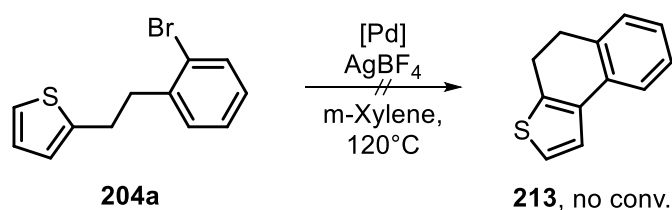
¹¹⁸ C. S. Harris, H. Germain, G. Pasquet, *Tetrahedron Lett.* **2008**, 49, 5946.

¹¹⁹ J. Esquivias, A. Lafuente, L. Rubio, J. G. Rodriguez, *Tetrahedron* **2006**, 62, 3112.



Scheme 83: proposed reaction mechanism for the transformation of ether **203a** to arene **210**.

Due to the absence of the ether bridge the second substrate should not undergo a Friedel-Crafts type reaction, we hoped to transform the substrate to the desired tricyclic system **213**. However, with all the different catalytic systems employed, only starting material was reisolated. This might be caused by the inefficient orbital overlap between the π -system and the bromo arene during the oxidative addition step as this occurs from within the plane, while the aromatic system points above or below the plane of the molecule.



Scheme 84: attempted C-H activation and oxidative, intermolecular coupling of thiophene **204a** to tricyclic system **213**.

To be able to assess whether or not the lack of reactivity of the before mentioned transformation is caused by inefficient orbital overlap or due to the slow rate of the oxidative addition step, we decided to test an palladium catalysed amination described by Buchwald *et al.* in which the substrate is known to easily undergo the oxidative insertion elemental step.

Buchwald *et al.*¹²⁰ reported that the SPhosPd complex **214** undergoes - after activation with a strong base generating the reactive Pd⁰ metal - oxidative addition even at -40°C in THF with aryl chlorides generating aryl chloro palladium complex **215**.

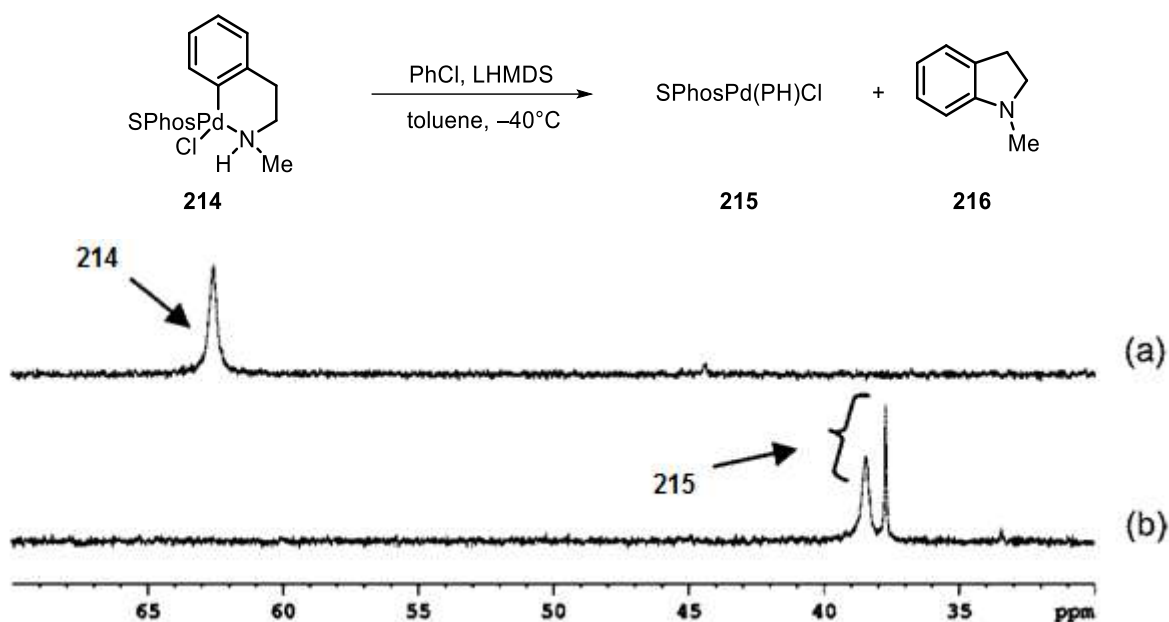
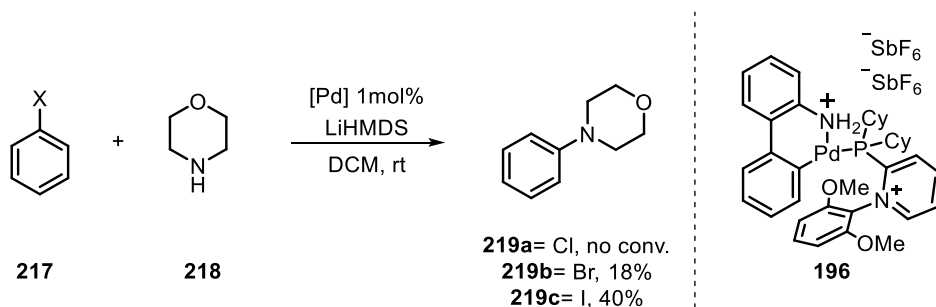


Figure 36: ³¹P{¹H} NMR spectra of (a) **214** in toluene/PhCl at -40 °C and (b) **214** in toluene/PhCl w/LHMDS (1 equiv) after 110 min at -40 °C.¹²⁰

We then employed our ligand system **191e** as well as different phenyl halides and tested, whether or not higher conversion than the catalyst loading (1 mol%) could be achieved to confirm a full catalytic cycle undergoing. First, we tested phenyl chloride and morpholine at room temperature; however, no conversion was obtained even employing different bases (LiHMDS, K₂CO₃ and NaOtBu) to achieve activation of the catalyst. Luckily, employing phenyl bromide or phenyl iodide, conversions to some extent could be achieved (18% for bromide and 40% for iodide within 2 h), confirming the reactivity of the developed catalytic system, however it should be noted, that the reactivity drastically depletes, probable due to catalyst degradation processes. With these results we could confirm, that the catalytic mixture undergoes all elemental reaction steps for the palladium catalysed direct arylation including the difficult oxidative addition. Even at -20°C for aryl iodides higher conversions than the catalyst loading could be achieved (up to 10%), confirming once again several catalytic cycle undergoing.

¹²⁰ M. R. Biscoe, B. P. Fors, S. L. Buchwald *J. Am. Chem. Soc.* **2008**, *130*, 6686.



Scheme 85: Buchwald-Hartwig-coupling of morpholine with aryl halides

In the before mentioned reaction we applied LiHMDS as a base, which seems to be compatible to some extent with the newly developed palladium complex **196**. To test whether or not the catalytic mixture is compatible with other bases or if higher conversion could be obtained with different bases employed, we then tested other sterically hindered bases for the activation process and the deprotonation of morpholine. We found, that neither K_2CO_3 nor NaOtBu are compatible with the catalytic system **196** yielding no conversion at all.

Despite the low reactivity of the applied palladium catalyst, at least to some extent the reactivity of cationic phosphines in palladium catalysed reactions could be confirmed. The newly developed palladium complexes undergo every elemental step necessary for a Pd catalysed reaction. However, due to the low stability of the developed system or the degradation processes observed further development is necessary. Furthermore, it could be shown, that these cationic palladium complexes tolerate to some extent the employment of strong, hindered bases such as LiHMDS. Further development of the employed catalytic systems is necessary to avoid catalyst decomposition and reach full conversions.

9. Summary and Outlook

In summary we were able to develop new cationic phosphines and successfully apply them in transition metal catalyses. In π -acid catalysis they proved their superiority in comparison with state of the art ligand systems described in literature. The pyridinium phosphines were prepared through a concise two step sequence (methylation and phosphination) from commercially available starting materials in excellent yields. We evaluated their electronic structure by CO-stretching frequency analysis of the corresponding Vaska-type complexes and by cyclic voltammetry. Furthermore, we have examined the solid state structure of the phosphine themselves and the corresponding metal complexes through x-ray analysis.

The coordination behaviour to Au(I), Pt(II), Rh(I) and Pd(II) sources was also evaluated and the obtained complexes were applied in catalyses.

The newly developed pyridinium phosphines show tremendous effects in the described reactions. For example in hydroarylations reaction times as short as a few minutes can be achieved, while classical ligands like triphenylphosphine need several hours to achieve similar conversions. This beneficial effect was shown in two platinum, one gold and one palladium catalysed reaction.

After this promising results we then further improved the pyridinium phosphines through introduction of an aryl unit towards the nitrogen of the pyridinium moiety allowing secondary stabilizing interactions to the coordinated metal centre.

The benefits of this additional stabilisation was shown along a [2+2] cycloaddition. In comparison to the previously described methyl substituted pyridinium phosphines the aryl substituted pyridinium phosphine gave even better results. For example, the catalyst loading could be vastly reduced performing complex reaction at only 0.2 mol% catalyst loading.

Overall, we could prepare new pyridinium substituted phosphines, confirm their solid state structure, assess their electronic nature, exploit their coordination chemistry and apply the corresponding complexes in catalysis with excellent results.

10. Experimental part

10.1 General procedures

All manipulations were carried out under argon atmosphere either in flame-dried glassware on a Schlenk line or in an MBraun Labmaster 130 Glove box, unless stated otherwise. The solvents employed for the reactions were purified by distillation over the drying agents indicated and were stored and handled under argon atmosphere: THF, Et₂O (Mg/anthracene), CH₂Cl₂, CHCl₃, fluorobenzene, chlorobenzene, 1,2-dichlorobenzene, pyridine, NEt₃ (CaH₂, stored over 4°A molecular sieves), n-pentane, toluene (Na/K), MeOH (Mg, stored over 3 Å molecular sieves). DMF, 1,4-dioxane and CH₃CN were dried by an adsorption solvent purification system based on molecular sieves. Benzene was dried by treatment of a freshly opened bottle with activated 4°A molecular sieves and then stored under inert atmosphere. Flash chromatography separations were performed using Merck 60 silica gel (40-63 μm), whereas preparative thin-layer chromatography (TLC) was performed on Merck 25-DC-Plastic sheets (20 x 20 cm) coated with 60 silica gel. Reactions were controlled by TLC analysis, performed using Merck silica gel 60 F254 TLC plates and visualised by UV irradiation and/or ceric ammonium molybdate or potassium permanganate dip. When it was possible, the reactions were additionally followed by GC/MS measurements performed on Agilent Technology GC 6890 Series and MSD 5973 (carrier gas: helium) with HP6890 Series Injector, employing a MN 121 III.1.

All commercially available compounds (Acros, Fluka, Lancaster, Alfa Aesar and Aldrich) were used as received unless stated otherwise. Compounds **134**¹¹³, **138**¹²¹, **140**¹⁰⁴ and **220**¹¹⁷ were prepared accordingly to the procedure described in the literature

10.2 Experimental procedures and characterizations

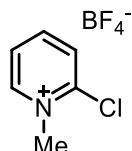
NMR spectra were recorded on a Bruker AV500, AV400 or DPX300 as stated for each case, using dry deuterated solvents. ¹H and ¹³C chemical shifts are given in ppm relative to TMS, using the solvent signals as references and converting the chemical shifts to the TMS scale. ³¹P and ¹⁹F chemical shifts are given in ppm relative to H₃PO₄ and CFCI₃ respectively (external standard). Mass spectrometry analysis was performed by the department for mass spectrometry at the Max-Planck-Institut für Kohlenforschung, using the following equipment: Finnigan MAT 8200 (70 eV, EI), Finnigan MAT 95 (ESI) and Bruker APEX III FT-MS (7 T magnet, HRMS). Infrared spectra were recorded on Nicolet FT-7199 or Bruker ALPHA FT-IR Platinum ATR spectrometers at room temperature. X-Ray diffraction analysis was performed by the department of chemical at the Max-Planck-Institut für Kohlenforschung. The X-ray

¹²¹ S. J. Pastine, S. W. Youn, D. Sames, *Org. Lett.* **2003**, *5*, 1055.

intensity data were measured on a Bruker AXS Proteum X8, Bruker AXS KappaCCD and Bruker AXS Apex II diffractometers. The crystal structures were solved by direct methods using SHELXS-97 and refined with SHELXL-2014. The crystals suitable for X-ray analysis were grown by slow diffusion of different solvent mixtures of the metal complexes or by slow solvent evaporation/cooling of saturated solutions of the corresponding compounds.

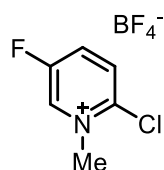
General procedure for the Alkylation of 2-Chloropyridines.

A solution of the corresponding 2-chloropyridine (1 equiv.) in DCM (0.05 M) was added to solid Me_3OBF_4 or Et_3OBF_4 (1 equiv.) and the suspension stirred overnight. Then, the solvent was filtered off and the remaining white solid washed twice with dichloromethane and dried in vacuum.



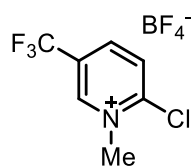
Compound 127a: Prepared from 2-chloropyridine (2.0 g, 17.6 mmol) and Me_3OBF_4 (2.6 g, 17.6 mmol) following the general procedure. After washing with DCM (2 x 20 ml), **127a** was obtained as a white solid (3.47 g, 91%).

^1H NMR (300 MHz, CD_3CN) δ = 8.75 (d, J = 6.2 Hz, 1H), 8.47 (td, J = 8.2, 1.5 Hz, 1H), 8.12 (d, J = 8.3 Hz, 1H), 7.94 (t, 3J = 6.8 Hz, 1H), 4.30 (s, 3H); ^{13}C NMR (75 MHz, CD_3CN) δ = 149.0, 148.9, 148.4, 131.0, 127.4, 48.6; IR (neat) $\bar{\nu}$ = 712, 735, 778, 805, 1024, 1123, 1177, 1274, 1286, 1314, 1446, 1499, 1574, 1623, 3059, 3094, 3115, 3138 cm^{-1} HRMS *calcd.* for $\text{C}_{12}\text{H}_{14}\text{BCl}_2\text{F}_4\text{N}_2$: 343.056684; *found*: 343.056646.



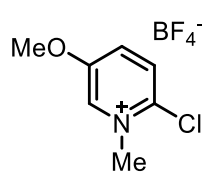
Compound 127b: Prepared from 2-chloro-5-fluoropyridine (1.0 g, 7.6 mmol) and Me_3OBF_4 (1.12 g, 7.6 mmol) following the general procedure. After washing with DCM (2 x 20 ml), **127b** was obtained as a white solid (1.75 g, 99%).

^1H NMR (300 MHz, CD_3CN) δ = 8.88 (t, J = 3.1 Hz, 1H), 8.36 (ddd, J = 9.4, 6.7, 2.9 Hz, 1H), 8.16 (dd, J = 9.3, 4.9 Hz, 1H), 4.31 (s, 3H); ^{13}C NMR (75 MHz, CD_3CN) δ = 159.9 (d, $J_{\text{C-F}}$ = 255.1 Hz), 145.6, 138.7 (d, $J_{\text{C-F}}$ = 40.0 Hz), 136.2 (d, $J_{\text{C-F}}$ = 19.8 Hz), 132.2 (d, $J_{\text{C-F}}$ = 7.9 Hz), 49.5; ^{19}F NMR (282 MHz, CD_3CN) δ = -120.22, -151.77, -151.82; IR (neat) $\bar{\nu}$ = 655, 698, 743, 767, 854, 901, 1022, 1126, 1165, 1282, 1392, 1439, 1509, 1593, 1641, 3084, 3104 cm^{-1} ; HRMS *calcd.* for $\text{C}_{12}\text{H}_{12}\text{N}_2\text{BCl}_2\text{F}_6$: 379.036928; *found*: 379.037035.



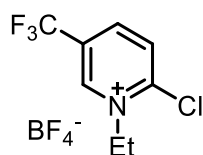
Compound 127c: Prepared from 2-chloro-5-(trifluoromethyl)pyridine (400 mg, 2.2 mmol) and Me_3OBF_4 (325 mg, 2.2 mmol) following the general procedure. After washing with DCM (2 x 2 ml), **127c** was obtained as a white solid (620 mg, 99%).

^1H NMR (300 MHz, CD_3CN) δ = 9.23 (s, 1H), 8.75 (dd, J = 8.7, 2.0 Hz, 1H), 8.34 (d, J = 8.7 Hz, 1H), 4.39 (s, 3H); ^{13}C NMR (75 MHz, CD_3CN) δ = 153.3, 147.4 (m), 145.0 (q, $J_{\text{C-F}}$ = 3.0 Hz), 132.1, 129.4 (q, $J_{\text{C-F}}$ = 37.0 Hz), 122.3 (q, $J_{\text{C-F}}$ = 272.7 Hz), 49.5; ^{19}F NMR (282 MHz, CD_3CN) δ = -63.45, -151.99, -152.04; IR (neat) $\bar{\nu}$ = 663, 690, 722, 804, 861, 888, 916, 944, 998, 1025, 1125, 1192, 1268, 1331, 1435, 1479, 1590, 1639, 2296, 2342, 2383, 3055 cm^{-1} ; HRMS *calcd.* for $\text{C}_7\text{H}_6\text{NCIF}_3$: 196.013540; *found*: 196.013563.



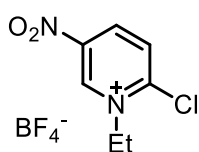
Compound 127d: Prepared from 2-chloro-5-methoxypyridine (965 mg, 6.72 mmol) and Me_3OBF_4 (994 mg, 6.72 mmol) in DCM (20 ml) following the general procedure. After washing with DCM (2 x 20 ml), **127d** was obtained as a white solid (1.47 g, 89%).

^1H NMR (300 MHz, CD_3CN) δ = 8.47 (d, J = 2.7 Hz, 1H), 8.10 – 7.93 (m, 2H), 4.27 (s, 3H), 4.00 (s, 3H); ^{13}C NMR (75 MHz, CD_3CN) δ = 158.3, 140.0, 136.0, 134.1, 130.9, 58.8, 49.0; ^{19}F NMR (282 MHz, CD_3CN) δ = -151.67, -151.72; IR (neat) $\bar{\nu}$ = 697, 739, 847, 875, 936, 1013, 1037, 1099, 1159, 1177, 1197, 1271, 1308, 1391, 1425, 1445, 1469, 1513, 1590, 1622, 3101, 3156 cm^{-1} ; HRMS *calcd.* for $\text{C}_{14}\text{H}_{18}\text{N}_2\text{BCl}_2\text{F}_4\text{O}_2$: 403.077864; *found*: 403.078070.



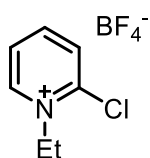
Compound 129a: Prepared from 2-chloro-5-(trifluoromethyl)pyridine (1 g, 5.5 mmol) and Et_3OBF_4 (1.05 g, 5.5 mmol) in DCM (20 ml) following the general procedure and purified by filtration and washing with DCM (2 x 10 ml) to afford **129a** as a white solid (1.6 g, 5.4 mmol, 99%).

^1H NMR (300 MHz, CD_3CN) δ = 9.24 (d, J = 0.7 Hz, 1H), 8.74 (dd, J = 8.7, 2.1 Hz, 1H), 8.34 (d, J = 8.7 Hz, 1H), 4.82 (q, J = 7.3 Hz, 2H), 1.62 (t, J = 7.3 Hz, 3H); ^{13}C NMR (75 MHz, CD_3CN) = 152.3, 146.3, 144.9 (q, $J_{\text{C-F}}$ = 3.0 Hz), 132.8, 129.9 (q, $J_{\text{C-F}}$ = 36.9 Hz), 122.2 (q, $J_{\text{C-F}}$ = 273.7 Hz); ^{19}F NMR (282 MHz, CD_3CN) δ = -63.46, -151.88, -151.94; IR (neat) $\bar{\nu}$ = 727, 740, 767, 809, 858, 939, 1023, 1056, 1095, 1110, 1146, 1183, 1193, 1233, 1299, 1328, 1395, 1413, 1453, 1473, 1509, 1586, 1639, 3089 cm^{-1} ; HRMS *calcd.* for $\text{C}_8\text{H}_8\text{NCIF}_3$: 210.029185; *found*: 210.028857.



Compound 129b: Prepared from 2-chloro-5-nitropyridine (500 mg, 3.15 mmol) and Me_3OBF_4 (466 mg, 3.15 mmol) in DCM (20 ml) following the general procedure. After washing with DCM (2 x 20 ml), **129b** was obtained as a white solid (855 mg, 99%).

^1H NMR (300 MHz, CD_3CN) δ = 9.70 (d, J = 2.5 Hz, 1H), 9.11 (dd, J = 9.1, 2.6 Hz, 1H), 8.37 (d, J = 9.1 Hz, 1H), 4.88 (q, J = 7.3 Hz, 2H), 1.64 (t, J = 7.3 Hz, 3H); ^{13}C NMR (75 MHz, CD_3CN) δ = 153.6, 146.3, 145.1, 141.8, 132.6, 59.3, 14.5; IR (neat) $\bar{\nu}$ = 714, 738, 766, 792, 809, 863, 903, 934, 979, 1031, 1094, 1139, 1148, 1166, 1177, 1212, 1281, 1363, 1391, 1449, 1465, 1498, 1543, 1586, 1636, 3090 cm^{-1} ; HRMS *calcd.* for $\text{C}_{14}\text{H}_{16}\text{N}_4\text{BCl}_2\text{F}_4\text{O}_4$: 461.057231; *found*: 461.057551.

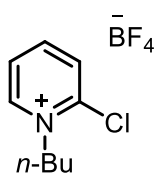


Compound 129c: Prepared from 2-chloropyridine (2 g, 17.6 mmol) and triethyloxoniumtetrafluoroborate (3.3 g, 17.6 mmol) in DCM (80 ml) following the general procedure and purified by filtration and washing with DCM (2x 20 ml) to afford **129c** as a white solid (4 g, 99%).

^1H NMR (300 MHz, CD_3CN) δ = 8.82 (d, $J=6.0$, 1H), 8.47 (t, $J=8.0$, 1H), 8.12 (d, $J=8.3$, 1H), 7.98 (t, $J=6.8$, 1H), 4.72 (q, $J=7.2$, 2H), 1.57 (t, $J=7.2$, 3H); ^{13}C NMR (75 MHz, CD_3CN) δ = 148.2, 147.93, 147.91, 131.5, 127.8, 57.3, 14.9; ^{19}F NMR (282 MHz, CD_3CN) δ = -151.59, -151.66; IR (neat) $\bar{\nu}$ = 706, 723, 785, 897, 1023, 1131, 1158, 1185, 1228, 1292, 1395, 1441, 1455, 1467, 1500, 1574, 1617, 3110, 3138 cm^{-1} ; HRMS *calcd.* for $\text{C}_{14}\text{H}_{18}\text{N}_2\text{BCl}_2\text{F}_4$: 371.087087; *found*: 371.087072.

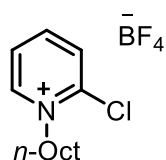
General procedure for the Chlorination of 2-Pyridones 131

To a solution of **131** (1 eq) in dichloroethane (10 ml/mmol) was added oxalylchlorid (3 eq) and dimethylformamid (0.1 ml). The resulting mixture was heated overnight to 80 °C. After cooling to rt the reaction mixture was quenched with H_2O and diluted with ethylacetate. After addition of sat. aq. NaBF_4 solution, the aqueous phase was extracted with dichloromethane (3 x 50 ml). The combined organic phases were dried over MgSO_4 , filtered and concentrated. The solid obtained was washed with a small amount of THF (1 ml/mmol) or crystallized from DCM/*n*-Pentane if necessary and dried in vacuum.



Compound 132a: Prepared from **131a** (500 mg, 3.3 mmol), oxalylchlorid (0.85 ml, 10 mmol) and dimethylformamid (0.1 ml) in dichloroethane following the general procedure. Brownish solid (660 mg, 78%).

^1H NMR (300 MHz, CDCl_3) δ = 8.93 (dd, J = 6.2, 1.5 Hz, 1H), 8.50 (td, J = 8.1, 1.7 Hz, 1H), 8.07 (dd, J = 8.3, 1.2 Hz, 1H), 8.00 (ddd, J = 7.6, 6.3, 1.3 Hz, 1H), 4.79 – 4.67 (m, 2H), 2.02 – 1.82 (m, 2H), 1.53 – 1.34 (m, 2H), 0.96 (t, J = 7.3 Hz, 3H); ^{13}C NMR (75 MHz, CDCl_3) δ = 147.84, 147.80, 146.3, 130.6, 127.3, 60.8, 31.7, 19.4, 13.4; ^{19}F NMR (282 MHz, CDCl_3) δ = -152.01, -152.06; IR (neat) $\bar{\nu}$ = 711, 722, 745, 776, 894, 1027, 1158, 1286, 1297, 1337, 1385, 1460, 1464, 1498, 1572, 1618, 2877, 2936, 2964, 3106 cm^{-1} ; HRMS *calcd.* for 2 **132a** + BF_4 $\text{C}_{18}\text{H}_{26}\text{N}_2\text{BCl}_2\text{F}_4$: 427.149670; *found*: 427.149845.

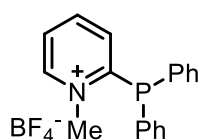


Compound **132b**: Prepared from **131b** (500 mg, 2.25 mmol), oxalylchlorid (0.58 ml, 6.78 mmol) and dimethylformamid (0.1 ml) in dichloroethane following the general procedure. Brownish solid (600 mg, 81%).

^1H NMR (400 MHz, CDCl_3) δ = 8.99 (dd, J = 6.0, 1.1 Hz, 1H), 8.50 (td, J = 8.0, 1.6 Hz, 1H), 8.08 – 8.01 (m, 2H), 4.78 – 4.71 (m, 2H), 1.96 (dt, J = 9.9, 7.8 Hz, 2H), 1.47 – 1.17 (m, 10H), 0.87 (t, J = 6.9 Hz, 3H); ^{13}C NMR (101 MHz, CDCl_3) δ = 148.2, 147.6, 146.2, 130.3, 127.5, 61.2, 31.8, 30.1, 29.1, 29.0, 26.2, 22.7, 14.2; IR (neat) $\bar{\nu}$ = 462, 482, 521, 712, 723, 779, 895, 1046, 1048, 1154, 1188, 1291, 1378, 1442, 1466, 1498, 1572, 1617, 2856, 2926, 2955, 3090, 3107, 3135 cm^{-1} ; HRMS *calcd.* for $\text{C}_{13}\text{H}_{21}\text{NCl}$: 226.135702; *found*: 226.135680.

General procedure for the Preparation of Pyridiniophosphines.

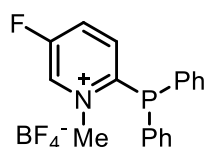
To a solution of the corresponding 1-alkyl/aryl-2-chloropyridinium tetrafluoroborate (1 equiv.) in THF (2 ml) was added the desired secondary phosphine (2.5-3.0 equiv.) and the resulting suspension heated for 1 to 3 days. After cooling to rt, the solvents were evaporated and the crude reaction mixture washed with *n*-Pentan (2 x 2 ml), solved in DCM and washed with sat. NaBF_4 aqueous solution. The organic phase was dried over NaSO_4 and the solvent evaporated. If necessary, the resulting solid could be further purified by an additional wash with THF (1-2 ml).



Compound **124a**: Prepared by heating a THF suspension of **127a** (400 mg, 1.8 mmol) and diphenylphosphine (1.1 ml, 5.6 mmol) at 65°C for 3 days.

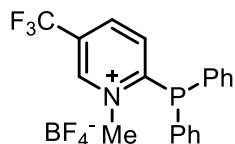
White solid (477 mg, 70%).

^1H NMR (300 MHz, CDCl_3) δ = 9.04 (d, J = 5.7 Hz, 1H), 8.25 (td, J = 7.9, 0.9 Hz, 1H), 8.03 – 7.95 (m, 1H), 7.57 – 7.43 (m, 6H), 7.39 – 7.27 (m, 5H), 4.30 (d, J = 1.1 Hz, 3H); ^{13}C NMR (75 MHz, CDCl_3) δ = 161.0 (d, $J_{\text{C-P}}$ = 33.4 Hz), 149.5, 144.0, 134.7 (d, $J_{\text{C-P}}$ = 21.7 Hz), 132.6, 131.6, 130.2 (d, $J_{\text{C-P}}$ = 8.4 Hz), 129.0 (d, J = 6.7 Hz), 128.0, 47.6 (d, $J_{\text{C-P}}$ = 21.0 Hz); ^{31}P NMR (121 MHz, CDCl_3) δ = -8.61; IR (neat) $\bar{\nu}$ = 696, 724, 748, 798, 954, 1000, 1038, 1051, 1161, 1181, 1265, 1310, 1436, 1492, 1571, 1610, 3055, 3103, 3134 cm^{-1} ; HRMS *calcd.* for $\text{C}_{18}\text{H}_{17}\text{NP}$: 278.109315; *found*: 278.109239.



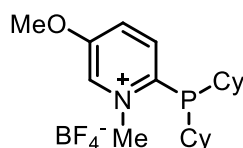
Compound 124b: Prepared by heating a THF suspension of **127b** (500 mg, 2.14 mmol) and diphenylphosphine (0.92 ml, 5.35 mmol) at 65°C for 3 days. White solid (351 mg, 43%).

^1H NMR (300 MHz, CD_3CN) δ = 8.94 – 8.82 (m, 1H), 8.18 – 8.07 (m, 1H), 7.58 (m, 6H), 7.42 (m, 5H), 4.23 (d, J = 1.4 Hz, 3H); ^{13}C NMR (75 MHz, CD_3CN) δ = 160.9 (d, $J_{\text{C-F}}$ = 255.7 Hz), 139.8 (d, $J_{\text{C-P}}$ = 38.2 Hz), 135.7 (d, $J_{\text{C-P}}$ = 0.9 Hz), 135.6 (d, $J_{\text{C-P}}$ = 21.9 Hz), 132.8 (d, $J_{\text{C-P}}$ = 17.4 Hz), 132.4 (d, $J_{\text{C-P}}$ = 0.6 Hz), 130.9 (d, $J_{\text{C-P}}$ = 8.3 Hz), 130.3 (d, $J_{\text{C-P}}$ = 6.7 Hz), 49.1 (d, $J_{\text{C-P}}$ = 21.5 Hz); ^{31}P NMR (121 MHz, CDCl_3) δ = -9.34; IR (neat) $\bar{\nu}$ = 699, 715, 738, 753, 760, 858, 895, 931, 958, 998, 1024, 1143, 1165, 1181, 1273, 1314, 1384, 1436, 1479, 1500, 1583, 1623 cm^{-1} ; HRMS *calcd.* for $\text{C}_{18}\text{H}_{16}\text{NFP}$: 296.099965; *found*: 296.099889.



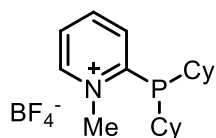
Compound 124c: Prepared by heating a THF suspension of **127c** (500 mg, 1.8 mmol) and diphenylphosphine (0.62 ml, 4.4 mmol) at 65°C for 1 day. White solid (451 mg, 60%).

^1H NMR (300 MHz, CD_3CN) δ = 9.18 (s, 1H), 8.51 (dd, J = 8.4, 1.3 Hz, 1H), 7.72 – 7.50 (m, 7H), 7.50 – 7.38 (m, 4H), 4.25 (d, J = 1.0 Hz, 3H); ^{13}C NMR (75 MHz, CD_3CN) δ = 167.4 (d, $J_{\text{C-P}}$ = 35.6 Hz), 147.7, 141.7 (q, $J_{\text{C-F}}$ = 3.0 Hz), 135.9 (d, $J_{\text{C-P}}$ = 22.0 Hz), 134.8 (d, $J_{\text{C-P}}$ = 1.2 Hz), 132.7, 131.1 (d, $J_{\text{C-P}}$ = 8.6 Hz), 129.9 (q, $J_{\text{C-F}}$ = 36.1), 129.4 (d, $J_{\text{C-P}}$ = 6.0 Hz), 122.5 (q, $J_{\text{C-F}}$ = 272.6 Hz), 49.2 (d, $J_{\text{C-P}}$ = 20.7); ^{19}F NMR (282 MHz, CD_3CN) δ = -63.67, -151.79, -151.84; ^{31}P NMR (121 MHz, CD_3CN) δ = -6.00; IR (neat) $\bar{\nu}$ = 693, 702, 727, 743, 752, 862, 892, 913, 996, 1048, 1090, 1115, 1148, 1174, 1267, 1342, 1435, 1504, 1579, 1639, 3103 cm^{-1} ; HRMS *calcd.* for $\text{C}_{19}\text{H}_{16}\text{NF}_3\text{P}$: 346.09727; *found*: 346.097027.



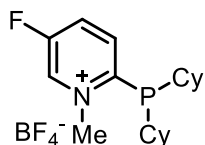
Compound 124d: Prepared by heating a THF suspension of **127d** (500 mg, 2.05 mmol) and dicyclohexylphosphine (1.25 ml, 6.16 mmol) at 65°C during 12 hours. White solid (744 mg, 89%).

^1H NMR (300 MHz, CDCl_3) δ = 8.48 (d, J = 2.1 Hz, 1H), 8.04 (d, J = 9.0 Hz, 1H), 7.94 (dd, J = 9.0, 2.6 Hz, 1H), 4.43 (s, 3H), 4.01 (s, 3H), 2.21 – 2.08 (m, 2H), 1.85 – 0.96 (m, 20H); ^{13}C NMR (75 MHz, CD_3CN) δ = 159.2, 138.1, 135.4, 135.3, 58.4, 49.9 (d, $J_{\text{C-P}}$ = 27.5 Hz), 34.8 (d, $J_{\text{C-P}}$ = 13.5 Hz), 30.8 (d, $J_{\text{C-P}}$ = 16.9 Hz), 30.0 (d, $J_{\text{C-P}}$ = 8.1 Hz), 27.5 (d, J = 13.2 Hz), 27.3 (d, $J_{\text{C-P}}$ = 8.8 Hz), 26.7 (d, $J_{\text{C-P}}$ = 1.1 Hz); ^{19}F NMR (282 MHz, CDCl_3) δ = -151.83, -151.88; ^{31}P NMR (121 MHz, CD_3CN) δ = -7.27; IR (neat) $\bar{\nu}$ = 704, 741, 816, 842, 884, 916, 1000, 1015, 1035, 1046, 1163, 1187, 1196, 1286, 1317, 1434, 1447, 1507, 1574, 1615, 2845, 2920 cm^{-1} ; HRMS *calcd.* for $\text{C}_{19}\text{H}_{31}\text{NOP}$: 320.213778; *found*: 320.213335.



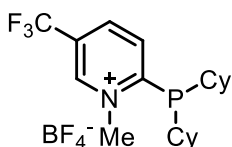
Compound 124e: Prepared by heating a THF suspension of **127a** (500 mg, 2.3 mmol) and dicyclohexylphosphine (0.75 ml, 5.8 mmol) at 65°C for 3 days. White solid (699 mg, 80%).

^1H NMR (400 MHz, CDCl_3) δ = 9.11 (d, J = 5.2 Hz, 1H), 8.48 (t, J = 7.8 Hz, 1H), 8.05 (dd, J = 14.3, 7.5 Hz, 2H), 4.59 (s, 3H), 2.11 (t, J = 11.8 Hz, 2H), 1.91 (d, J = 12.0 Hz, 2H), 1.81 (d, J = 12.8 Hz, 2H), 1.69 (t, J = 11.9 Hz, 4H), 1.51 (d, J = 12.5 Hz, 2H), 1.41 – 1.01 (m, 10H); ^{13}C NMR (101 MHz, CDCl_3) δ = 160.3 (d, $J_{\text{C-P}}$ = 42.5 Hz), 149.7, 143.6, 133.4 (d, $J_{\text{C-P}}$ = 3.2 Hz), 128.2, 48.8 (d, $J_{\text{C-P}}$ = 26.1 Hz), 34.4 (d, $J_{\text{C-P}}$ = 15.1 Hz), 30.0 (d, $J_{\text{C-P}}$ = 15.9 Hz), 29.4 (d, $J_{\text{C-P}}$ = 8.6 Hz), 26.8 (d, $J_{\text{C-P}}$ = 12.5 Hz), 26.7 (d, $J_{\text{C-P}}$ = 8.8 Hz), 25.9; ^{31}P NMR (162 MHz, CDCl_3) δ = -3.52; IR (neat) $\bar{\nu}$ = 728, 779, 851, 915, 1053, 1179, 1262, 1448, 1497, 1571, 1610, 2851, 2925 cm^{-1} ; HRMS *calcd.* for $\text{C}_{18}\text{H}_{29}\text{NP}$: 290.203217; *found*: 290.203415.



Compound 124f: Prepared by heating a THF suspension of **127b** (500 mg, 2.14 mmol) and dicyclohexylphosphine (1.08 ml, 5.35 mmol) at 65°C during 12 hours. White solid (648 mg, 77%).

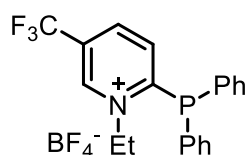
^1H NMR (300 MHz, CDCl_3) δ = 9.06 (d, J = 2.3 Hz, 1H), 8.34 – 8.21 (m, 1H), 8.21 – 8.08 (m, 1H), 4.64 (s, 3H), 2.12 (t, J = 11.5 Hz, 2H), 1.98 – 1.61 (m, 8H), 1.52 (d, J = 11.7 Hz, 2H), 1.44 – 1.02 (m, 10H); ^{13}C NMR (75 MHz, CD_3CN) δ = 160.9 (d, $J_{\text{C-F}}$ = 255.9 Hz), 158.2 (dd, $J_{\text{C-P}}$ = 43.7, $J_{\text{C-F}}$ = 4.2 Hz), 140.1 (d, $J_{\text{C-P}}$ = 36.1 Hz), 136.3 (dd, $J_{\text{C-P}}$ = 7.4 Hz, $J_{\text{C-F}}$ = 3.4 Hz), 131.9 (d, $J_{\text{C-P}}$ = 17.2 Hz), 50.1 (d, $J_{\text{C-P}}$ = 26.4 Hz), 34.7 (d, $J_{\text{C-P}}$ = 14.3 Hz), 30.4 (d, $J_{\text{C-P}}$ = 16.2 Hz), 30.0 (d, $J_{\text{C-P}}$ = 8.7 Hz), 27.4 (d, $J_{\text{C-P}}$ = 10.9 Hz), 27.2 (d, $J_{\text{C-P}}$ = 10.9 Hz), 26.6; ^{19}F NMR (282 MHz, CDCl_3) δ = -118.61, -151.62, -151.67; ^{31}P NMR (121 MHz, CD_3CN) δ = -4.49; IR (neat) $\bar{\nu}$ = 704, 738, 765, 817, 851, 889, 920, 958, 1004, 1025, 1040, 1057, 1112, 1170, 1182, 1202, 1269, 1279, 1433, 1450, 1504, 1582, 1626, 2852, 2925, 3077 cm^{-1} ; HRMS *calcd.* for $\text{C}_{18}\text{H}_{17}\text{NP}$: 308.193442; *found*: 308.193793.



Compound 124g: Prepared from **129c** (500 mg, 1.76 mmol) and dicyclohexylphosphine (1.07 ml, 5.3 mmol) at 65°C for 1 d to yield **124g** as a white solid (619 mg, 79%).

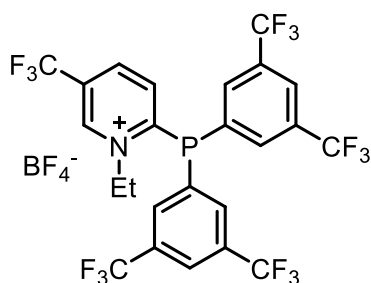
^1H NMR (300 MHz, CDCl_3) δ = 9.28 (s, 1H), 8.63 (d, J = 8.0, 1H), 8.35 (d, J = 8.2 Hz, 1H), 4.67 (s, 3H), 2.19 (t, J = 10.5 Hz, 2H), 1.91 (d, J = 7.6 Hz, 2H), 1.80 (d, J = 10.3 Hz, 2H), 1.68 (s, 4H), 1.56 (d, J = 11.1 Hz, 2H), 1.45 – 0.92 (m, 10H); ^{13}C NMR (75 MHz, CDCl_3) δ = 166.4 (dd, J = 106.5, 58.7 Hz), 147.1 (d, J = 4.0 Hz), 139.6, 134.5 (d, J = 3.3 Hz), 130.3 (q, J = 37.1 Hz), 121.2 (q, J = 273.8 Hz), 49.6 (d, J = 25.7 Hz), 34.4 (d, J = 15.6 Hz), 29.9 (d, J = 7.1 Hz), 29.7

(d, $J = 1.5$ Hz), 26.7 (t, $J = 10.4$ Hz), 25.9 (d, $J = 0.6$ Hz); ^{19}F NMR (282 MHz, CDCl_3) $\delta = -63.20, -152.05, -152.09$; ^{31}P NMR (121 MHz, CDCl_3) $\delta = -1.15$; IR (neat) $\bar{\nu} = 845, 887, 929, 1052, 1098, 1106, 1144, 1169, 1175, 1266, 1345, 1397, 1450, 1510, 1583, 1637, 2849, 2917$ cm^{-1} ; HRMS *calcd.* for $\text{C}_{19}\text{H}_{28}\text{NF}_3\text{P}$: 358.190595; *found*: 358.190641.



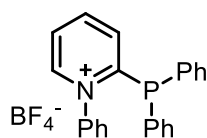
Compound 124h: Prepared from **129c** (500 mg, 1.68 mmol) and diphenylphosphine (0.88 ml, 5.04 mmol) at 65°C for 1 d to yield **124h** as a white solid (590 mg, 79%).

^1H NMR (300 MHz, CD_3CN) $\delta = 9.19$ (s, 1H), 8.50 (dd, $J = 8.4, 1.7$ Hz, 1H), 7.67 – 7.51 (m, 7H), 7.49 – 7.39 (m, 4H), 4.79 (qd, $J = 7.3, 2.5$ Hz, 2H), 1.41 (t, $J = 7.3$ Hz, 3H); ^{13}C NMR (75 MHz, CD_3CN) $\delta = 166.9$ (d, $J = 37.0$ Hz), 146.3, 142.0, 136.1, 135.8, 132.7, 131.1, 130.9, 130.2 (d, $J = 6.7$ Hz), 123.0 (q, $J = 338.1$ Hz), 57.6 (d, $J = 22.2$ Hz), 15.7; ^{19}F NMR (282 Hz, CD_3CN) = -63.66, -151.84, -151.90; ^{31}P NMR (121 MHz, CD_3CN) $\delta = -8.47$; IR (neat) $\bar{\nu} = 698, 740, 753, 803, 862, 929, 974, 995, 1031, 1110, 1150, 1189, 1229, 1284, 1333, 1405, 1438, 1501, 1578, 1633, 3075$ cm^{-1} ; HRMS *calcd.* for $\text{C}_{20}\text{H}_{18}\text{NF}_3\text{P}$: 360.112345; *found*: 360.111819.



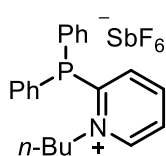
Compound 124i: To a suspension of KH (8.75 mg, 0.22 mmol) in THF (2 ml) was added bis(3,5-bis(trifluoromethyl)phenyl) phosphine (100 mg, 0.22 mmol) at -78°C and the resulting deep red suspension stirred for 1 hour. Then, the suspension was transferred at the same temperature to a precooled suspension (-78°C) of **129a** (64.9 mg, 0.22 mmol) in THF (2 ml) and the

mixture allowed to warm up to rt and stirred for 3 days. After evaporation of the solvent and washing with DCM (2x 2ml), compound **124i** was obtained as an off white solid (48 mg, 30%). ^1H NMR (300 MHz, CDCl_3) $\delta = 9.32$ (s, 1H), 8.62 (d, $J = 7.7$ Hz, 1H), 8.25 (s, 2H), 8.02 (d, $J = 7.2$ Hz, 4H), 7.92 (d, $J = 7.9$ Hz, 1H), 4.88 (m, 2H), 1.56 (t, $J = 7.3$ Hz, 3H); ^{13}C NMR (75 MHz, CD_3CN) $\delta = 162.0$ (d, $J_{\text{C-P}} = 33.4$ Hz), 147.9 – 146.4 (m), 144.0 – 142.4 (m), 137.4, 136.9 – 136.0 (m), 133.6 (qd, $J_{\text{C-F}} = 33.9$ Hz, $J_{\text{C-P}} = 7.7$ Hz), 133.2 (d, $J_{\text{C-P}} = 13.5$ Hz), 132.2 (d, $J_{\text{C-P}} = 36.9$ Hz), 124.1 (q, $J_{\text{C-F}} = 272.4$ Hz), 121.5 (q, $J_{\text{C-F}} = 273.0$ Hz), 58.6 (d, $J_{\text{C-P}} = 23.4$ Hz), 16.3 (d, $J_{\text{C-P}} = 3.5$ Hz); ^{19}F NMR (282 MHz, CDCl_3) $\delta = -63.52, -63.68, -151.80, -151.85$; ^{31}P NMR (121 MHz, CDCl_3) $\delta = -10.52$; IR (neat) $\bar{\nu} = 682, 700, 741, 767, 846, 862, 900, 913, 1051, 1095, 1120, 1279, 1331, 1356, 1405, 1459, 1502, 1588, 1634, 2001, 3090$ cm^{-1} ; HRMS *calcd.* for $\text{C}_{24}\text{H}_{14}\text{F}_{15}\text{NP}$: 632.062949; *found*: 632.061889.



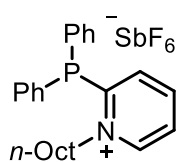
Compound 124j: Prepared by heating a THF suspension of **134** (650 mg, 2.3 mmol) and diphenylphosphine (1.2 ml, 6.9 mmol) at 130°C for 12 h in a μ wave oven. White solid (715 mg, 71%).

^1H NMR (300 MHz, CDCl_3) δ = 8.76 (d, J = 5.1 Hz, 1H), 8.46 (td, J = 8.0 Hz, 1.3, 1H), 8.06 (t, J = 6.9 Hz, 1H), 7.66 – 7.50 (m, 4H), 7.50 – 7.37 (m, 6H), 7.32 – 7.21 (m, 6H); ^{13}C NMR (75 MHz, CD_3CN) δ = 149.5, 146.7, 135.8 (d, $J_{\text{C-P}}$ = 22.5 Hz), 134.4, 132.5, 132.1, 131.4 (d, $J_{\text{C-P}}$ = 8.2 Hz), 130.6 (d, $J_{\text{C-P}}$ = 7.6 Hz), 128.3, 127.4 (d, $J_{\text{C-P}}$ = 3.8 Hz); ^{19}F NMR (282 MHz, CDCl_3) δ = -151.82, -151.87; ^{31}P NMR (121 MHz, CDCl_3) δ = -7.74; IR (neat) $\bar{\nu}$ = 692, 699, 734, 748, 757, 786, 841, 863, 901, 931, 979, 997, 1011, 1035, 1047, 1079, 1163, 1178, 1254, 1288, 1315, 1438, 1455, 1475, 1492, 1563, 1589, 1607, 3070, 3117 cm^{-1} ; HRMS *calcd.* for $\text{C}_{23}\text{H}_{19}\text{NP}$: 340.124626; *found*: 360.124961.



Compound 124k: Prepared from diphenylphosphine (1.01 ml, 1.94 mmol), **132a** (500 mg, 1.94 mmol) and NaSbF_6 (1500 mg, 5.8 mmol) in THF following the general procedure **A**. Drying at high vacuum for 3 days afforded **124k** as a black solid (690 mg, 64%).

^1H NMR (400 MHz, CDCl_3) δ = 8.78 (ddd, J = 6.1, 2.5, 1.2 Hz, 1H), 8.23 (td, J = 7.9, 1.4 Hz, 1H), 7.95 (ddd, J = 7.7, 6.4, 1.4 Hz, 1H), 7.57 – 7.46 (m, 6H), 7.42 – 7.32 (m, 5H), 4.72 – 4.59 (m, 2H), 1.74 – 1.62 (m, 2H), 1.30 (td, J = 14.7, 7.3 Hz, 3H), 0.81 (t, J = 7.4 Hz, 3H); ^{13}C NMR (101 MHz, CDCl_3) δ = 160.7 (d, J = 34.3 Hz), 147.3, 144.2, 134.7 (d, J = 21.9 Hz), 133.7, 131.7, 130.2 (d, J = 8.3 Hz), 129.4 (d, J = 6.7 Hz), 128.2, 60.0 (d, J = 21.3 Hz), 32.9 (d, J = 1.9 Hz), 19.6, 13.3; ^{31}P NMR (162 MHz, CDCl_3) δ = -10.79; IR (neat) $\bar{\nu}$ = 435, 484, 510, 568, 652, 698, 733, 748, 777, 809, 1000, 1027, 1091, 1177, 1278, 1329, 1433, 1470, 1489, 1568, 1611, 2856, 2927, 2956 cm^{-1} ; HRMS *calcd.* for $\text{C}_{21}\text{H}_{23}\text{NP}$: 320.156263; *found*: 320.156090.



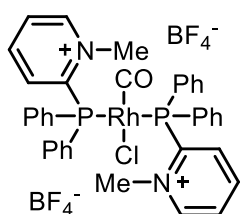
Compound 124l: Prepared from diphenylphosphine (0.79 ml, 4.56 mmol), **132b** (500 mg, 1.52 mmol), and NaSbF_6 (1180 mg, 4.57 mmol) in THF following the general procedure **A**. Drying at high vacuum for 3 days afforded **124l** as a black solid (561 mg, 59%).

^1H NMR (400 MHz, CDCl_3) δ = 8.81 (ddd, J = 6.1, 2.6, 1.2 Hz, 1H), 8.23 (td, J = 7.9, 1.4 Hz, 1H), 8.00 (ddd, J = 7.7, 6.3, 1.4 Hz, 1H), 7.59 – 7.47 (m, 6H), 7.41 – 7.32 (m, 5H), 4.71 – 4.62 (m, 2H), 1.72 (ddd, J = 12.3, 10.3, 6.6 Hz, 2H), 1.33 – 1.11 (m, 10H), 0.87 (t, J = 7.1 Hz, 3H); ^{13}C NMR (101 MHz, CDCl_3) δ = 159.8 (d, J = 34.2 Hz), 146.7, 143.3, 133.8 (d, J = 21.8 Hz), 132.9, 130.9, 129.4 (d, J = 8.4 Hz), 128.6 (d, J = 6.8 Hz), 127.5, 59.5 (d, J = 21.2 Hz), 30.9, 30.4 (d, J = 2.5 Hz), 28.1, 28.0, 25.5, 21.8, 13.3; ^{31}P NMR (162 MHz, CDCl_3) δ = -10.70; IR

(neat) $\bar{\nu}$ = 435, 484, 510, 568, 652, 698, 733, 748, 777, 809, 1000, 1027, 1091, 1177, 1278, 1329, 1434, 1469, 1489, 1568, 1611, 2856, 2927, 2954 cm^{-1} ; HRMS *calcd.* for $\text{C}_{25}\text{H}_{31}\text{NP}$: 376.218863; *found*: 376.218630.

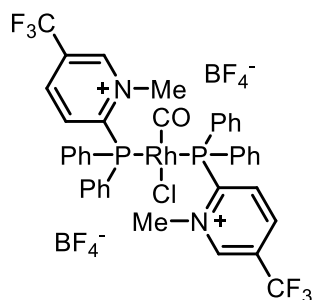
General procedure for the preparation of pyridiniophosphine rhodium complexes.

$[\text{Rh}(\text{CO})_2\text{Cl}]_2$ (0.25 equiv.) was added to a solution of the corresponding pyridiniophosphine ligand (1 equiv.) in DCM (2 ml). The resulting suspension was stirred for 1 hour at rt and after evaporation of the solvent, the solid was washed with *n*-pentan (2 x 2 ml) and dried in vacuum. These compounds can be crystalized from acetonitrile/ether mixtures.



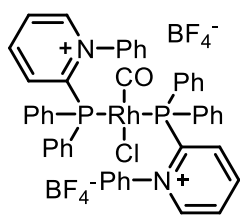
Compound 135a: Prepared from **127a** (100 mg, 0.274 mmol) and $[\text{Rh}(\text{CO})\text{Cl}_2]_2$ (26.6 mg, 0.063 mmol) following the general procedure. Yellow solid (121 mg, 99%).

^1H NMR (300 MHz, CDCl_3) δ = 8.84 (d, J = 5.9 Hz, 2H), 8.38 (t, J = 7.7 Hz, 2H), 8.11 – 8.02 (m, 2H), 7.84 (s, 8H), 7.79 – 7.72 (m, 4H), 7.72 – 7.58 (m, 10H), 4.50 (s, 6H); ^{13}C NMR (75 MHz, CDCl_3) δ = 186.1 (dt, $J_{\text{C-Rh}}$ = 31.9 Hz, $J_{\text{C-P}}$ = 15.6 Hz), 153.6 (t, $J_{\text{C-P}}$ = 18.1 Hz), 151.1, 145.6, 136.2, 135.0, 134.2, 131.1, 130.1, 126.6 (t, $J_{\text{C-P}}$ = 24.3 Hz), 50.8; ^{31}P NMR (121 MHz, CDCl_3) δ = 37.82 (d, $J_{\text{P-Rh}}$ = 130.7 Hz); IR (neat) $\bar{\nu}$ = 692, 707, 752, 773, 799, 900, 931, 998, 1056, 1165, 1182, 1274, 1314, 1411, 1438, 1481, 1499, 1576, 1610, 1996, 3093, 3138 cm^{-1} ; HRMS *calcd.* for $\text{C}_{37}\text{H}_{34}\text{BClF}_4\text{N}_2\text{OP}_2\text{Rh}$: 809.092884; *found*: 809.093025.



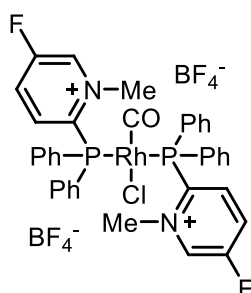
Compound 135b: Prepared from **127c** (100 mg, 0.231 mmol) and $[\text{Rh}(\text{CO})_2\text{Cl}]_2$ (22.5 mg, 0.058 mmol) following the general procedure. Yellow solid (68 mg, 57%).

^1H NMR (300 MHz, CDCl_3) δ = 9.28 (s, 2H), 8.65 (d, J = 8.2 Hz, 2H), 7.95 – 7.63 (m, 22H), 4.56 (s, 6H); ^{13}C NMR (75 MHz, CDCl_3) δ = 167.5 (d, $J_{\text{C-P}}$ = 36.8 Hz), 147.8, 141.7, 136.5 (d, $J_{\text{C-P}}$ = 22.1 Hz), 134.8, 132.8, 131.1 (d, $J_{\text{C-P}}$ = 8.5 Hz), 129.8 (d, $J_{\text{C-P}}$ = 36.7 Hz), 129.4 (d, $J_{\text{C-P}}$ = 5.4 Hz), 122.5 (q, $J_{\text{C-F}}$ = 272.8 Hz), 47.3 (d, $J_{\text{C-P}}$ = 20.6 Hz); ^{31}P NMR (121 MHz, CDCl_3) δ = 40.44 (d, $J_{\text{Rh-P}}$ = 131.0 Hz); IR (neat) $\bar{\nu}$ = 691, 705, 752, 858, 890, 932, 998, 1052, 1090, 1118, 1159, 1177, 1243, 1275, 1334, 1392, 1438, 1482, 1509, 1586, 1634, 1741, 2004, 3092 cm^{-1} ; HRMS *calcd.* for $\text{C}_{39}\text{H}_{32}\text{BClF}_{10}\text{N}_2\text{OP}_2\text{Rh}$: 945.067689; *found*: 945.067581.



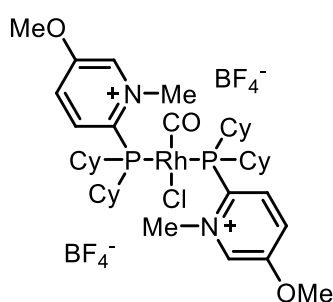
Compound 135c: Prepared from **134** (100 mg, 0.253 mmol) and $[\text{Rh}(\text{CO})_2\text{Cl}]_2$ (24.6mg, 0.063 mmol) following the general procedure. Yellow solid (94 mg, 78%).

^1H NMR (300 MHz, CDCl_3) δ = 8.62 (d, J = 5.6 Hz, 2H), 8.49 (t, J = 7.9 Hz, 2H), 8.17 – 8.07 (m, 4H), 7.78 (dd, J = 12.7, 6.3 Hz, 8H), 7.54 (ddd, J = 22.9, 14.9, 7.8 Hz, 16H), 7.33 (t, J = 7.5 Hz, 2H), 6.91 (t, J = 8.0 Hz, 4H); ^{13}C NMR (101 MHz, CDCl_3) δ = 155.0, 151.7, 146.2, 142.3, 136.5 (t, $J_{\text{C-P}}$ = 7.2 Hz), 136.1 – 135.3 (m), 133.7, 132.6, 130.7 (t, $J_{\text{C-P}}$ = 5.5 Hz), 130.5, 130.0, 128.2, 127.9, 127.7; ^{31}P NMR (121 MHz, CDCl_3) δ = 42.09 (d, $J_{\text{Rh-P}}$ = 134.4 Hz); IR (neat) $\bar{\nu}$ = 692, 749, 925, 998, 1034, 1048, 1182, 1254, 1286, 1318, 1437, 1457, 1479, 1587, 1603, 1981, 2350, 3060 cm^{-1} ; HRMS *calcd.* for $\text{C}_{47}\text{H}_{38}\text{BClF}_4\text{N}_2\text{OP}_2\text{Rh}$: 933.124354; *found*: 933.123835.



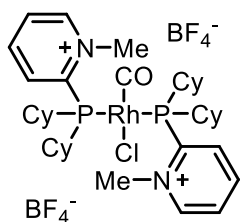
Compound 135d: Prepared from **127b** (75 mg, 0.2 mmol) and $[\text{Rh}(\text{CO})_2\text{Cl}]_2$ (19.3 mg, 0.05 mmol) following the general procedure. Yellow solid (121 mg, 69%).

^1H NMR (300 MHz, CDCl_3) δ = 8.98 (s, 2H), 8.27 – 8.16 (m, 2H), 7.84 (s, 8H), 7.76 (t, J = 7.4 Hz, 4H), 7.68 (t, J = 7.6 Hz, 10H), 4.54 (s, 6H); ^{13}C NMR (75 MHz, CDCl_3) δ = 161.6 (d, $J_{\text{C-F}}$ = 259.3 Hz), 150.7, 141.7 (d, $J_{\text{C-F}}$ = 38.2 Hz), 136.7 (d, $J_{\text{C-P}}$ = 8.5 Hz), 136.2, 134.4, 132.8 (d, $J_{\text{C-F}}$ = 17.3 Hz), 131.2, 126.5, 51.5 (d, $J_{\text{C-P}}$ = 1.6 Hz); ^{31}P NMR (121 MHz, CDCl_3) δ = 39.02 (d, $J_{\text{Rh-P}}$ = 130.7 Hz); IR (neat) $\bar{\nu}$ = 694, 738, 754, 850, 962, 998, 1054, 1169, 1282, 1437, 1482, 1505, 1590, 1624, 1994, 3087 cm^{-1} ; HRMS *calcd.* for $\text{C}_{37}\text{H}_{32}\text{BClF}_6\text{N}_2\text{OP}_2\text{Rh}$: 845.074040; *found*: 845.073864.



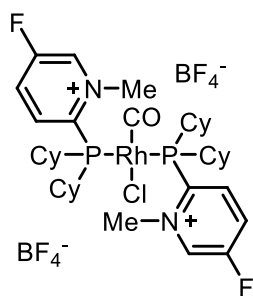
Compound 135e: Prepared from **127d** (75 mg, 0.184 mmol) and $[\text{Rh}(\text{CO})_2\text{Cl}]_2$ (17.9 mg, 0.046 mmol) following the general procedure. Yellow solid (67 mg, 74%).

^1H NMR (300 MHz, DMSO) δ = 9.11 (s, 2H), 8.38 (d, J = 9.1 Hz, 2H), 8.20 (dd, J = 9.0, 2.3 Hz, 2H), 4.90 (s, 6H), 4.08 (s, 6H), 2.17 (s, 4H), 2.02 – 0.94 (m, 40H); ^{13}C NMR (101 MHz, DMSO) δ = 185.1 (dt, $J_{\text{C-Rh}}$ = 33.4 Hz, $J_{\text{C-P}}$ = 16.4 Hz), 158.1, 140.4, 138.3 (t, $J_{\text{C-P}}$ = 12.9 Hz), 134.9, 127.4, 57.6, 51.1 (t, $J_{\text{C-P}}$ = 4.2 Hz), 36.0, 33.3, 29.4, 28.4, 27.6, 26.6, 25.8, 25.5; ^{31}P NMR (121 MHz, DMSO) δ = 40.26 (d, $J_{\text{Rh-P}}$ = 123.0 Hz); IR (neat) $\bar{\nu}$ = 706, 739, 765, 815, 854, 888, 918, 940, 1018, 1050, 1098, 1172, 1180, 1207, 1269, 1317, 1415, 1450, 1475, 1515, 1614, 1974, 2850, 2928 cm^{-1} ; HRMS *calcd.* for $\text{C}_{39}\text{H}_{62}\text{BClF}_4\text{N}_2\text{O}_3\text{P}_2\text{Rh}$: 893.301860; *found*: 893.302947.



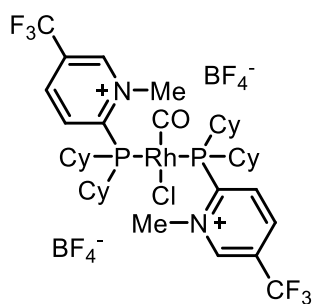
Compound 135f: Prepared from 2-(dicyclohexylphosphanyl)-1-methylpyridin-1-iumtetrafluoroborat (**124e**, 75 mg, 0.2 mmol) and $[\text{Rh}(\text{CO})\text{Cl}_2]_2$ (19.3 mg, 0.05 mmol) to yield **135f** as a white solid (121 mg, 69%).

^1H NMR (300 MHz, CDCN) δ = 8.85 (d, J = 6.1 Hz, 2H), 8.52 (t, J = 7.5 Hz, 2H), 8.26 (dd, J = 8.1 Hz, $J_{\text{H-P}}$ = 1.2 Hz, 2H), 8.10 (t, J = 6.9 Hz, 2H), 4.92 (s, 6H), 2.66 (t, J = 9.4 Hz, 4H), 2.23 (d, J = 11.8 Hz, 4H), 2.02 – 1.87 (m, 8H), 1.77 (t, J = 13.4 Hz, 8H), 1.69 – 1.33 (m, 16H), 1.31 – 1.15 (m, 4H); ^{13}C NMR (75 MHz, CDCN) δ = 186.0 (dt, $J_{\text{C-Rh}}$ = 72.0 Hz, $J_{\text{C-P}}$ = 16.4 Hz), 151.7, 150.9 (t, $J_{\text{C-P}}$ = 9.7 Hz), 145.0, 135.7, 130.0, 52.3 (t, $J_{\text{C-P}}$ = 4.6 Hz), 36.6 (m), 30.9, 29.8, 27.8 (t, $J_{\text{C-P}}$ = 6.9 Hz), 27.2 (t, $J_{\text{C-P}}$ = 5.4 Hz), 26.6; ^{31}P NMR (121 MHz, CDCN) δ = 44.98 (d, $J_{\text{P-Rh}}$ = 123.4 Hz); IR (neat) $\bar{\nu}$ = 736, 772, 850, 891, 1004, 1032, 1048, 1181, 1267, 1447, 1499, 1577, 1611, 1965, 2851, 2928 cm^{-1} ; HRMS *calcd.* for $\text{C}_{37}\text{H}_{58}\text{BClF}_4\text{N}_2\text{OP}_2\text{Rh}$: 833.280694; *found*: 833.280727.



Compound 135g: Prepared from 2-(dicyclohexylphosphanyl)-5-fluoro-1-methylpyridin-1-iumtetrafluoroborat (**124f**, 100 mg, 0.253 mmol) and $[\text{Rh}(\text{CO})\text{Cl}_2]_2$ (24.6mg, 0.063 mmol) to yield **135g** as a white solid (94 mg, 78%).

^1H NMR (300 MHz, CDCN) δ = 8.98 (s, 2H), 8.36 (ddd, J = 22.0, 11.5, 7.7 Hz, 4H), 4.96 (s, 6H), 2.67 (s, 4H), 2.24 (d, J = 10.2 Hz, 4H), 1.94 (dd, J = 4.6, 2.2 Hz, 6H), 1.78 (t, J = 12.7 Hz, 8H), 1.69 – 1.08 (m, 22H); ^{13}C NMR (75 MHz, CDCN) δ = 185.8 (dt, $J_{\text{C-Rh}}$ = 33.9 Hz, $J_{\text{C-P}}$ = 16.3 Hz), 161.6 (d, $J_{\text{C-F}}$ = 259.5 Hz), 148.1 – 147.3 (m), 53.0 (t, $J_{\text{C-P}}$ = 4.5 Hz), 37.4 – 36.3 (m), 30.9, 29.7, 27.8 (t, $J_{\text{C-P}}$ = 7.0 Hz), 27.1 (t, $J_{\text{C-P}}$ = 5.4 Hz), 26.6; ^{19}F NMR (282 MHz, CD_3CN) δ = -115.07, -151.30, -151.35; ^{31}P NMR (121 MHz, CDCN) δ = 45.03 (d, $J_{\text{Rh-P}}$ = 124.0 Hz); IR (neat) $\bar{\nu}$ = 740, 764, 815, 851, 892, 966, 1027, 1050, 1148, 1173, 1210, 1281, 1329, 1382, 1447, 1505, 1592, 1626, 1982, 2856, 2935, 3093 cm^{-1} ; HRMS *calcd.* for $\text{C}_{37}\text{H}_{56}\text{BClF}_6\text{N}_2\text{OP}_2\text{Rh}$: 869.261772; *found*: 869.261849.



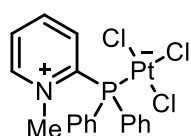
Compound 135h: Prepared from 2-(dicyclohexylphosphanyl)-5-(trifluoromethyl)-1-methylpyridin-1-iumtetrafluoroborat (**124g**, 100 mg, 0.231 mmol) and $[\text{Rh}(\text{CO})\text{Cl}_2]_2$ (22.5 mg, 0.058 mmol) to yield **135h** as a white solid (68 mg, 57%).

^1H NMR (300 MHz, CDCl_3) δ = 9.35 (s, 1H), 8.87 (d, J = 8.4 Hz, 1H), 8.53 (dd, J = 8.4, 4.1 Hz, 1H), 4.86 (s, 3H), 2.79 – 2.60 (m, 2H), 2.19 – 2.03 (m, 2H), 1.92 – 1.63 (m, 8H), 1.63 – 1.18 (m, 10H); ^{13}C NMR

(75 MHz, CDCl_3) δ = 153.1 (d, $J_{\text{C-P}}$ = 22.5 Hz), 150.6 (d, $J_{\text{C-P}}$ = 4.0 Hz), 143.7 – 142.7 (m), 136.9 (d, $J_{\text{C-P}}$ = 5.6 Hz), 132.2 (q, $J_{\text{C-F}}$ = 37.5), 122.2 (q, $J_{\text{C-F}}$ = 273.4 Hz), 52.2 (d, $J_{\text{C-P}}$ = 10.8 Hz), 36.1 (d, $J_{\text{C-P}}$ = 24.8 Hz), 30.9 (d, $J_{\text{C-P}}$ = 0.5 Hz), 30.7 (d, $J_{\text{C-P}}$ = 4.2 Hz), 27.0 (d, $J_{\text{C-P}}$ = 7.4 Hz), 26.8 (d, $J_{\text{C-P}}$ = 6.0 Hz), 26.1 (d, $J_{\text{C-P}}$ = 1.8 Hz); ^{19}F NMR (282 MHz, CD_3CN) δ = -63.84, -151.55, -151.59; ^{31}P NMR (121 MHz, CDCl_3) δ = 43.96 (br. s); IR (neat) $\bar{\nu}$ = 697, 730, 741, 748, 763, 816, 850, 863, 891, 922, 1003, 1051, 1093, 1116, 1149, 1174, 1269, 1295, 1337, 1393, 1449, 1508, 1585, 1634, 1987, 2858, 2932, 3083 cm^{-1} ; HRMS *calcd.* for $\text{C}_{39}\text{H}_{56}\text{BClF}_{10}\text{N}_2\text{OP}_2\text{Rh}$: 969,255498; *found*: 969.256209.

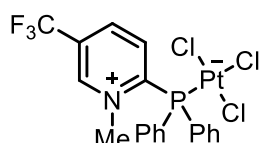
General procedure for the preparation of the phosphine platinum complexes.

Finely ground K_2PtCl_4 (1 equiv) was added to a solution of the pyridiniophosphine salt (1 equiv.) in MeCN (2 ml) and the resulting suspension stirred overnight at rt. After evaporation of the solvent, the solid was washed with *n*-Pentan (2 x 2 ml), crystallized from DMSO/DCM and dried in vacuum to yield the desired platinum complexes.



Compound 136a: Prepared from **124a** (100 mg, 0.274 mmol) and K_2PtCl_4 (114 mg, 0.274 mmol) following the general procedure. White solid (127 mg, 80%).

^1H NMR (300 MHz, DMSO) δ = 9.18 (d, J = 5.7 Hz, 1H), 8.53 (t, J = 7.9 Hz, 1H), 8.20 (t, J = 6.9 Hz, 1H), 8.02 (dd, J = 12.3 Hz, J = 7.2 Hz, 4H), 7.79 – 7.57 (m, 6H), 7.39 (t, J = 7.0 Hz, 1H), 4.35 (s, 3H); ^{13}C NMR (75 MHz, CD_3CN) δ = 150.1, 144.5 (d, $J_{\text{C-P}}$ = 5.7 Hz), 135.3 (d, $J_{\text{C-P}}$ = 11.6 Hz), 132.8 (d, $J_{\text{C-P}}$ = 7.5 Hz), 132.6 (d, $J_{\text{C-P}}$ = 2.5 Hz), 129.3 (d, $J_{\text{C-P}}$ = 11.6 Hz), 128.8, 124.6, 123.7, 48.3 (d, $J_{\text{C-P}}$ = 7.3 Hz); ^{31}P NMR (121 MHz, DMSO) δ = 8.49 (J = 3908 Hz); IR (neat) $\bar{\nu}$ = 673, 822, 1003, 1023, 1051, 1659, 2126, 2253, 2342, 2383 cm^{-1} ; HRMS for DMSO adduct *calcd.* for $\text{C}_{20}\text{H}_{23}\text{Cl}_2\text{NOPPtS}$: 621.024487; *found*: 621.024734.

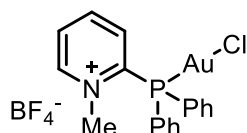


Compound 136b: Prepared from **124c** (100 mg, 0.231 mmol) and K_2PtCl_4 (96 mg, 0.231 mmol) following the general procedure. White solid (59 mg, 40%).

^1H NMR (300 MHz, DMSO) δ = 9.85 (s, 1H), 8.98 (d, J = 8.2 Hz, 1H), 8.05 (dd, J = 12.4 Hz, J = 7.4 Hz, 4H), 7.81 – 7.60 (m, 6H), 7.55 (dd, J = 7.5 Hz, J = 7.1 Hz, 1H), 4.42 (s, 3H); ^{13}C NMR (75 MHz, CD_3CN) δ = 155.1 (d, $J_{\text{C-P}}$ = 46.9 Hz), 148.5, 141.6, 135.5 (d, $J_{\text{C-P}}$ = 11.7 Hz), 133.5 (d, $J_{\text{C-P}}$ = 7.7 Hz), 133.0, 129.5 (d, $J_{\text{C-P}}$ = 11.6 Hz), 128.8 (d, $J_{\text{C-P}}$ = 36.1 Hz), 123.5 (d, $J_{\text{C-P}}$ = 64.0 Hz), 121.2 (q, $J_{\text{C-P}}$ = 273.6 Hz), 49.2 (d, $J_{\text{C-P}}$ = 6.8 Hz); ^{31}P NMR (121 MHz, DMSO) δ = 10.63 (J = 3906 Hz); IR (neat) $\bar{\nu}$ = 692, 704, 725, 755, 872, 890, 1036, 1114, 1148, 1179, 1192, 1270, 1332, 1388, 1438, 1481, 1508, 1631, 3001, 3044 cm^{-1} ; HRMS for DMSO adduct *calcd.* for $\text{C}_{21}\text{H}_{22}\text{Cl}_2\text{F}_3\text{NOPtS}$: 689.013152; *found*: 689.014029.

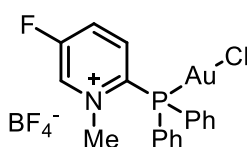
General procedure for the preparation of the phosphine gold complexes.

$\text{AuCl}\cdot\text{SMe}_2$ (1 equiv.) was added to a solution of the desired pyridiniophosphine salt (1 equiv.) in DCM (2 ml) and the resulting suspension stirred for 1 hour at rt. After evaporation of the solvent, the resulting solid washed with *n*-Pentan (2 x 2 ml) and dried in vacuum to yield the desired gold complexes.



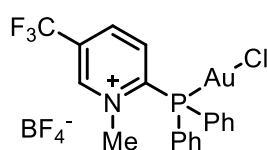
Compound 137a: Prepared from **124a** (100 mg, 0.274 mmol) and $\text{AuCl}\cdot\text{SMe}_2$ (80.7 mg, 0.274 mmol) following the general procedure. White solid (159 mg, 99%).

^1H NMR (300 MHz, CDCl_3) δ = 9.06 (d, J = 0.5 Hz, 1H), 8.44 (t, J = 7.7 Hz, 1H), 8.20 (t, J = 6.4 Hz, 1H), 7.86 – 7.53 (m, 10H), 7.38 (t, J = 7.5 Hz, 1H), 4.45 (s, 3H); ^{13}C NMR (75 MHz, CDCl_3) δ = 151.7, 147.1 (d, $J_{\text{C-P}}$ = 52.2 Hz), 145.4 (d, J = 5.6 Hz), 134.8 (d, $J_{\text{C-P}}$ = 15.6 Hz), 134.1 (d, $J_{\text{C-P}}$ = 2.0 Hz), 133.8 (d, $J_{\text{C-P}}$ = 9.3 Hz), 130.5 (d, $J_{\text{C-P}}$ = 12.8 Hz), 122.6, 121.9, 48.6 (d, $J_{\text{C-P}}$ = 11.4 Hz); ^{31}P NMR (121 MHz, CDCl_3) δ = 30.88; IR (neat) $\bar{\nu}$ = 692, 729, 913, 998, 1055, 1097, 1162, 1185, 1278, 1438, 1482, 1500, 1609, 3061, 3138 cm^{-1} ; HRMS *calcd.* for $\text{C}_{18}\text{H}_{17}\text{NAuClP}$: 510.044722; *found*: 510.044585.



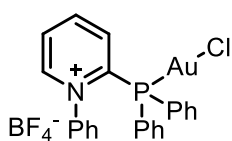
Compound 137b: Prepared from **124f** (100 mg, 0.26 mmol) and $\text{AuCl}\cdot\text{SMe}_2$ (76.6 mg, 0.26 mmol) following the general procedure. White solid (166 mg, 97%).

^1H NMR (400 MHz, CD_3CN) δ = 9.02 (dd, J = 6.0 Hz, 2.7, 1H), 8.27 (ddd, J = 9.1, 6.6, 2.6 Hz, 1H), 7.88 – 7.63 (m, 10H), 7.58 – 7.48 (m, 1H), 4.40 (s, 3H); ^{13}C NMR (101MHz, CD_3CN) δ = 162.2 (d, $J_{\text{C-F}}$ = 260.5 Hz), 143.0 (d, $J_{\text{C-P}}$ = 37.3 Hz), 137.5 (dd, $J_{\text{C-F}}$ = 10.0 Hz, $J_{\text{C-P}}$ = 8.4 Hz), 136.2 (d, $J_{\text{C-P}}$ = 15.9 Hz), 135.4 (d, $J_{\text{C-P}}$ = 2.6 Hz), 133.8 (d, $J_{\text{C-P}}$ = 6.2 Hz), 133.6 (d, $J_{\text{C-P}}$ = 6.3 Hz), 131.7 (d, $J_{\text{C-P}}$ = 12.8 Hz), 124.0 (d, $J_{\text{C-P}}$ = 62.6 Hz), 50.7 (d, $J_{\text{C-P}}$ = 11.9 Hz); ^{31}P NMR (162 MHz, CD_3CN) δ = 28.68; IR (neat) $\bar{\nu}$ = 690, 717, 737, 751, 852, 964, 996, 1034, 1048, 1170, 1279, 1437, 1478, 1505, 1594, 1615, 3055, 3079 cm^{-1} ; HRMS *calcd.* for $\text{C}_{18}\text{H}_{16}\text{NAuClFP}$: 528.035295; *found*: 528.035127.



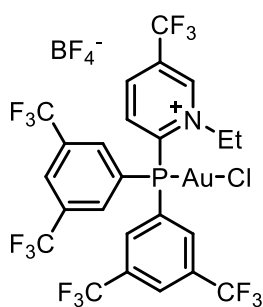
Compound 137c: Prepared from **124c** (100 mg, 0.23 mmol) and $\text{AuCl}\cdot\text{SMe}_2$ (68 mg, 0.23 mmol) following the general procedure. White solid (151 mg, 99%).

^1H NMR (300 MHz, CD_3CN) δ = 9.38 (s, 1H), 8.80 – 8.71 (m, 1H), 7.90 – 7.67 (m, 11H), 4.47 (s, 3H); ^{13}C NMR (75 MHz, CD_3CN) δ = 153.8 (d, $J_{\text{C-P}}$ = 46.8 Hz), 150.4 (d, $J_{\text{C-P}}$ = 2.5 Hz), 143.9 (td, $J_{\text{C-P}}$ = 6.1, $J_{\text{C-F}}$ = 3.0 Hz), 136.4 (d, $J_{\text{C-P}}$ = 15.7 Hz), 136.4, 135.6 (d, $J_{\text{C-P}}$ = 2.7 Hz), 133.4 – 132.0 (dq, $J_{\text{C-P}}$ = 37.1 Hz, $J_{\text{C-F}}$ = 1.6 Hz), 131.7 (d, $J_{\text{C-P}}$ = 13.0 Hz), 123.2 (d, $J_{\text{C-P}}$ = 64.7 Hz), 122.1 (q, $J_{\text{C-F}}$ = 273.3 Hz), 50.8 (d, $J_{\text{C-P}}$ = 11.3 Hz); ^{19}F NMR (282 MHz, CDCl_3) δ = -63.71, -151.49, -151.54; ^{31}P NMR (121 MHz, CD_3CN) δ = 31.54; IR (neat) $\bar{\nu}$ = 691, 705, 715, 752, 873, 892, 996, 1053, 1118, 1162, 1200, 1280, 1334, 1393, 1440, 1481, 1510, 1590, 1634, 3092 cm^{-1} ; HRMS *calcd.* for $\text{C}_{20}\text{H}_{18}\text{F}_3\text{NP}$: 578.032104; *found*: 578.032257.



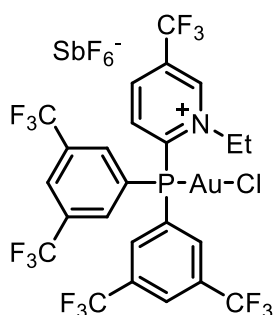
Compound 137d: Prepared from **124j** (50 mg, 0.12 mmol) and $\text{AuCl}\cdot\text{SMe}_2$ (34.5 mg, 0.12 mmol) following the general procedure. White solid (53 mg, 68%).

^1H NMR (400 MHz, CD_3CN) δ = 8.94 (s, 1H), 8.63 (t, J = 8.0 Hz, 1H), 8.29 (t, J = 6.7 Hz, 1H), 7.83 – 7.59 (m, 12H), 7.43 (t, J = 8.0 Hz, 2H), 7.23 (d, J = 7.9 Hz, 2H); ^{13}C NMR (101MHz, CD_3CN) δ = 152.2, 148.3 (d, $J_{\text{C-P}}$ = 5.2 Hz), 141.6 (d, $J_{\text{C-P}}$ = 4.5 Hz), 136.3 (d, $J_{\text{C-P}}$ = 15.9 Hz), 136.1 (d, $J_{\text{C-P}}$ = 8.2 Hz), 134.9 (d, $J_{\text{C-P}}$ = 2.5 Hz), 133.3, 131.3 (d, $J_{\text{C-P}}$ = 3.2 Hz), 131.2, 131.0, 127.9, 125.8, 125.2; ^{31}P NMR (162 MHz, CD_3CN) δ = 31.36; IR (neat) $\bar{\nu}$ = 668, 689, 712, 735, 753, 765, 786, 853, 926, 980, 997, 1030, 1044, 1099, 1144, 1162, 1189, 1256, 1283, 1433, 1442, 1458, 1483, 1587, 1603, 3060 cm^{-1} ; HRMS *calcd.* for $\text{C}_{23}\text{H}_{19}\text{NAuClP}$: 572.060365; *found*: 572.060083.



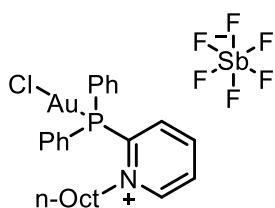
Compound 137e: Prepared from **124i** (73 mg, 0.1 mmol) and AuCl·SMe₂ (30 mg, 0.1 mmol) following the general procedure. White solid (37 mg, 38%).

¹H NMR (400 MHz, CD₃CN) δ = 9.44 (s, 1H), 8.78 (d, *J* = 8.4 Hz, 1H), 8.45 (s, 2H), 8.30 (d, *J* = 13.7 Hz, 4H), 7.92 (t, *J* = 7.7 Hz, 1H), 4.83 (qd, *J* = 7.0, 0.9 Hz, 2H), 1.64 (t, *J* = 7.2 Hz, 3H); ¹³C NMR (101 MHz, CD₃CN) δ = 149.2, 144.4 (dd, *J*_{C-P} = 5.9 Hz, *J*_{C-F} = 3.0 Hz), 138.5 (d, *J*_{C-P} = 9.6 Hz), 137.1 (d, *J*_{C-P} = 3.1 Hz), 137.0 (d, *J*_{C-P} = 3.1 Hz), 134.1 (qd, *J*_{C-F} = 34.5 Hz, *J*_{C-P} = 13.2 Hz), 134.0 (d, *J*_{C-P} = 37.3 Hz), 130.0 (d, *J*_{C-P} = 2.4 Hz), 126.6 (d, *J*_{C-P} = 60.9 Hz), 123.7 (q, *J*_{C-F} = 273.1 Hz), 122.0 (q, *J*_{C-F} = 273.6 Hz), 59.0 (d, *J*_{C-P} = 12.7 Hz), 16.5; ¹⁹F NMR (282 MHz, CDCl₃) δ = -63.49, -63.59, -151.86, -151.90; ³¹P NMR (162 MHz, CD₃CN) δ = 32.38; IR (neat) $\bar{\nu}$ = 681, 699, 718, 731, 742, 764, 847, 866, 899, 927, 997, 1032, 1058, 1097, 1123, 1186, 1280, 1337, 1358, 1405, 1447, 1505, 1630, 3093 cm⁻¹; HRMS *calcd.* for C₂₄H₁₄NAuClF₁₅P: 863.997295; *found*: 863.997181.



Compound 137e(SbF₆): Prepared from **124j**(SbF₆) (160 mg, 0.18 mmol) and AuCl·SMe₂ (54.3 mg, 0.18 mmol) following the general procedure to yield **137e(SbF₆)** as a white solid (104 mg, 51%).

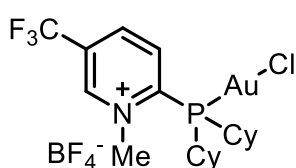
¹H NMR (400 MHz, CD₃CN) δ = 9.42 (s, 1H), 8.77 (d, *J* = 8.4 Hz, 1H), 8.47 (s, 2H), 8.29 (d, *J* = 13.8 Hz, 4H), 7.89 (t, *J* = 7.8 Hz, 1H), 4.80 (qd, *J* = 7.1, 1.0 Hz, 2H), 1.64 (t, *J* = 7.2 Hz, 3H); ¹³C NMR (101 MHz, CD₃CN) δ = 149.2, 144.4 (dd, *J*_{C-P} = 6.0 Hz, *J*_{C-F} = 3.1 Hz), 138.5 (d, *J*_{C-P} = 9.8), 137.1 (d, *J*_{C-P} = 3.1), 137.0 (d, *J*_{C-P} = 3.0), 134.1 (qd, *J*_{C-F} = 34.5 Hz, *J*_{C-P} = 13.3 Hz), 134.0 (d, *J*_{C-P} = 37.6 Hz), 130.1 (d, *J*_{C-P} = 2.9 Hz), 126.3 (d, *J*_{C-P} = 64.9), 123.6 (q, *J*_{C-F} = 272.5), 121.9 (q, *J*_{C-F} = 268.7 Hz), 59.0 (d, *J*_{C-P} = 12.4), 16.5; ¹⁹F NMR (282 MHz, CD₃CN) δ = -63.49, -63.59, -124.01 (sex, *J*_{F-121Sb} = 1940 Hz), -124.01 (oct, *J*_{F-123Sb} = 1060 Hz); ³¹P NMR (121 MHz, CD₃CN) δ = 32.21; IR (neat) $\bar{\nu}$ = 681, 699, 718, 731, 742, 764, 847, 866, 899, 927, 997, 1032, 1058, 1097, 1123, 1186, 1280, 1337, 1358, 1405, 1447, 1505, 1630, 3093 cm⁻¹; HRMS *calcd.* for C₂₄H₁₄NAuClF₁₅P: 863.997295; *found*: 863.997181.



Compound 137f: Prepared from phosphine **124i** (100 mg, 0.20 mmol) and Me₂S·AuCl (59.0 mg, 0.20 mmol) following the general procedure. White solid (142 mg, 97%).

¹H NMR (400 MHz, CD₃CN) δ = 8.93 (dd, *J* = 4.7, 3.0 Hz, 1H), 8.42 (t, *J* = 7.9 Hz, 1H), 8.19 (t, *J* = 6.9 Hz, 1H), 7.85 – 7.61 (m, 10H), 7.50

(t, $J = 7.4$ Hz, 1H), 4.76 – 4.61 (m, 2H), 1.85 (dd, $J = 9.7, 6.3$ Hz, 2H), 1.32 – 1.12 (m, 10H), 0.87 (t, $J = 7.0$ Hz, 3H); ^{13}C NMR (126 MHz, CD_3CN) $\delta = 150.4, 149.4$ (d, $J = 48.0$ Hz), 146.8 (d, $J = 5.5$ Hz), 136.2 (d, $J = 15.9$ Hz), 135.9 (d, $J = 9.0$ Hz), 135.1 (d, $J = 2.1$ Hz), 131.4 (d, $J = 12.5$ Hz), 131.3, 124.5 (d, $J = 60.6$ Hz), 61.1 (d, $J = 12.0$ Hz), 32.4, 32.2, 29.5, 29.5, 26.8, 23.2, 14.3; ^{31}P NMR (162 MHz, CD_3CN) $\delta = 27.21$; IR (neat) $\bar{\nu} = 423, 447, 488, 503, 523, 539, 563, 571, 600, 652, 679, 711, 725, 735, 754, 775, 801, 817, 851, 890, 905, 1004, 1022, 1041, 1112, 1140, 1182, 1211, 1234, 1245, 1266, 1300, 1345, 1426, 1441, 1486, 1601, 2847, 2930, 3057, 3092, 3127$ cm^{-1} ; HRMS *calcd.* for $\text{C}_{25}\text{H}_{31}\text{NAuClP}$: 608.154269; *found*: 608.153960.

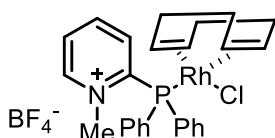


Compound 137g: Prepared from 2-(dicyclohexylphosphanyl)-5-(trifluoromethyl)-1-methylpyridin-1-iumtetrafluoroborat (**124g**, 50 mg, 0.11 mmol) and $\text{AuCl}\cdot\text{SMe}_2$ (33 mg, 0.11 mmol) to yield **137g** as a white solid (57 mg, 99%).

^1H NMR (300 MHz, CDCl_3) $\delta = 9.35$ (s, 1H), 8.87 (d, $J = 8.4$ Hz, 1H), 8.53 (dd, $J = 8.4, 4.1$ Hz, 1H), 4.86 (s, 3H), 2.78 – 2.61 (m, 2H), 2.16 – 2.05 (m, 2H), 1.92 – 1.66 (m, 8H), 1.63 – 1.17 (m, 10H); ^{13}C NMR (75 MHz, CD_3CN) $\delta = 153.1$ (d, $J_{\text{C-P}} = 22.5$ Hz), 150.6 (d, $J_{\text{C-P}} = 4.0$ Hz), 143.2 (td, $J_{\text{C-P}} = 6.4$ Hz, $J_{\text{C-F}} = 3.0$ Hz), 136.9 (d, $J_{\text{C-P}} = 5.6$ Hz), 132.2 (qd, $J_{\text{C-F}} = 36.9$, $J_{\text{C-P}} = 0.8$ Hz), 122.2 (q, $J_{\text{C-F}} = 273.4$ Hz), 52.2 (d, $J_{\text{C-P}} = 10.8$ Hz), 36.1 (d, $J_{\text{C-P}} = 24.8$ Hz), 30.9 (d, $J_{\text{C-P}} = 0.5$ Hz), 30.7 (d, $J_{\text{C-P}} = 4.2$ Hz), 27.0 (d, $J_{\text{C-P}} = 7.4$ Hz), 26.8 (d, $J_{\text{C-P}} = 6.0$ Hz), 26.1 (d, $J_{\text{C-P}} = 1.8$ Hz); ^{19}F NMR (282 MHz, CDCl_3) $\delta = -63.83, -151.54, -151.59$; ^{31}P NMR (121 MHz, CDCl_3) $\delta = 43.96$; IR (neat) $\bar{\nu} = 699, 733, 749, 850, 891, 1036, 1055, 1119, 1149, 1176, 1269, 1337, 1450, 1514, 1586, 1636, 2856, 2932$ cm^{-1} ; HRMS *calcd.* for $\text{C}_{19}\text{H}_{28}\text{NAuClF}_3\text{P}$: 590.126008; *found*: 590.126122.

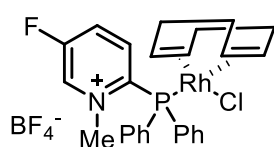
General procedure for the synthesis of Rh(cod) complexes.

$[\text{RhCl}(\text{cod})_2]$ (0.5 equiv.) was added to a solution of the corresponding pyridiniophosphine ligand (1 equiv.) in DCM (2 ml). The resulting suspension was stirred for 1 hour at rt and after evaporation of the solvent, the solid was washed with *n*-pentane (2 x 2 ml) and dried in vacuum.



Compound 150a: Prepared from **124a** (100 mg, 0.27 mmol) and $[\text{RhCl}(\text{cod})_2]$ (67.5 mg, 0.14 mmol) following the general procedure. Yellow solid (59.5 mg, 91%).

^1H NMR (300 MHz, CDCl_3) δ = 9.11 (d, J = 4.3 Hz, 1H), 8.21 (t, J = 7.8 Hz, 1H), 8.02 (t, J = 6.9 Hz, 1H), 7.67 – 7.41 (m, 10H), 7.26 – 7.20 (m, 1H), 5.65 (s, 2H), 5.26 (s, 3H), 3.94 (s, 2H), 2.44 (s, 4H), 2.15 (s, 4H); ^{13}C NMR (101 MHz, CDCl_3) δ = 154.6 (d, J = 34.3 Hz), 150.4, 143.4 (d, J = 3.7 Hz), 134.5 (d, J = 12.5 Hz), 133.1 (d, J = 4.0 Hz), 132.8 (d, J = 2.0 Hz), 130.3 (d, J = 10.2 Hz), 128.7, 126.5 (d, J = 41.2 Hz), 107.2 (dd, J = 11.9, 7.3 Hz), 73.0 (d, J = 13.2 Hz), 50.6 (d, J = 11.7 Hz), 33.1 (d, J = 2.4 Hz), 29.0 (d, J = 1.0 Hz); ^{31}P NMR (121 MHz, CDCl_3) δ = 31.90 (d, J = 149.1 Hz); IR (neat) $\bar{\nu}$ = 693, 722, 905, 996, 1055, 1092, 1165, 1184, 1270, 1320, 1339, 1436, 1496, 1575, 1609, 1698, 2261, 2841, 286, 3059 cm^{-1} ; HRMS *calcd.* for $\text{C}_{26}\text{H}_{29}\text{ClINPRh}$: 524.077570; *found*: 524.077655.

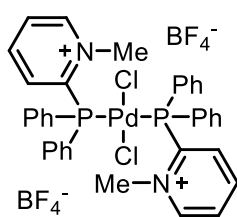


Compound 150b: Prepared from **124b** (100 mg, 0.26 mmol) and $[\text{RhCl}(\text{cod})]_2$ (64.3 mg, 0.13 mmol) following the general procedure. Yellow solid (74.8 mg, 91%).

^1H NMR (300 MHz, CD_3CN) δ = 9.03 (dd, J = 6.0, 2.5 Hz, 1H), 8.13 (ddd, J = 9.3, 6.8, 2.6 Hz, 1H), 7.71 – 7.62 (m, 2H), 7.60 – 7.49 (m, 8H), 7.43 (ddd, J = 9.3, 5.6, 3.9 Hz, 1H), 5.14 – 4.90 (m, overlapping, 3H), 4.71 (br. s, overlapping, 4H); ^{13}C NMR (101 MHz, CD_3CN) δ = 162.4 (d, J = 23.9 Hz), 159.9, 140.8 (d, J = 39.8 Hz), 136.1 (dd, J = 7.8, 4.5 Hz), 135.5 (d, J = 13.7 Hz), 133.5 (d, J = 1.7 Hz), 132.2 (dd, J = 18.2, 4.5 Hz), 130.8 (d, J = 10.0 Hz), 127.9 (d, J = 36.3 Hz), 51.6 (d, J = 12.3 Hz), 31.2 (br. s); ^{31}P NMR (121 MHz, CD_3CN) δ = 26.98 (br. s); IR (neat) $\bar{\nu}$ = 691, 737, 749, 856, 962, 996, 1032, 1050, 1278, 1434, 1480, 1503, 1587, 1625, 2833, 2880, 3055, 3079 cm^{-1} ; HRMS *calcd.* for $\text{C}_{26}\text{H}_{28}\text{ClFNPtRh}$: 542.068148; *found*: 542.068597.

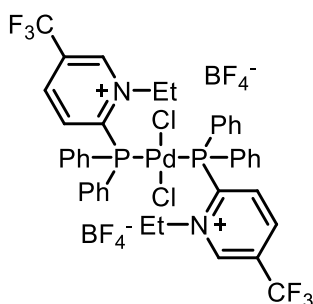
General procedure for the synthesis of palladium complexes.

(MeCN)₂PdCl₂ (0.5 equiv.) was added to a solution of the corresponding pyridiniophosphine ligand (1 equiv.) in DCM (2 ml). The resulting suspension was stirred for 1 hour at rt and after evaporation of the solvent, the solid was washed with *n*-pentane (2 x 2 ml) and dried in vacuum. These compounds can be crystallized from acetonitrile/ether mixtures.



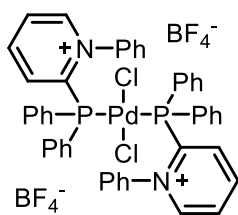
Compound 151a: Prepared from **124a** (100 mg, 0.27 mmol) and (MeCN)₂PdCl₂ (35.5 mg, 0.14 mmol) following the general procedure. Yellow solid (123 mg, 74%).

¹H NMR (400 MHz, CD₃CN) δ = 8.84 (d, *J* = 5.9 Hz, 2H), 8.40 (t, *J* = 7.9 Hz, 2H), 8.12 – 8.04 (m, 2H), 7.98 (dd, *J* = 12.8, 6.3 Hz, 8H), 7.80 (t, *J* = 7.4 Hz, 4H), 7.69 (t, *J* = 7.6 Hz, 10H), 4.38 (s, 6H); ¹³C NMR (101 MHz, CD₃CN) δ = 151.8 (t, *J* = 22.1 Hz), 151.1, 146.0, 136.8 (t, *J* = 6.7 Hz), 135.0, 134.7, 131.0 (t, *J* = 5.6 Hz), 130.4, 123.0 (t, *J* = 26.3 Hz), 50.7 (t, *J* = 4.3 Hz); ³¹P NMR (121 MHz, CD₃CN) δ = 25.40; IR (neat) $\bar{\nu}$ = 691, 702, 713, 749, 763, 800, 898, 973, 997, 1022, 1060, 1093, 1161, 1191, 1271, 1312, 1410, 1438, 1481, 1499, 1576, 1610, 3065, 3107, 3134 cm⁻¹; HRMS *calcd.* for C₃₆H₃₄BCl₂F₄N₂P₂Pd: 819.063198; *found*: 819.062550.



Compound 151b: Prepared from **124h** (100 mg, 0.22 mmol) and (MeCN)₂PdCl₂ (29 mg, 0.11 mmol) following the general procedure. Yellow solid (115 mg, 98%).

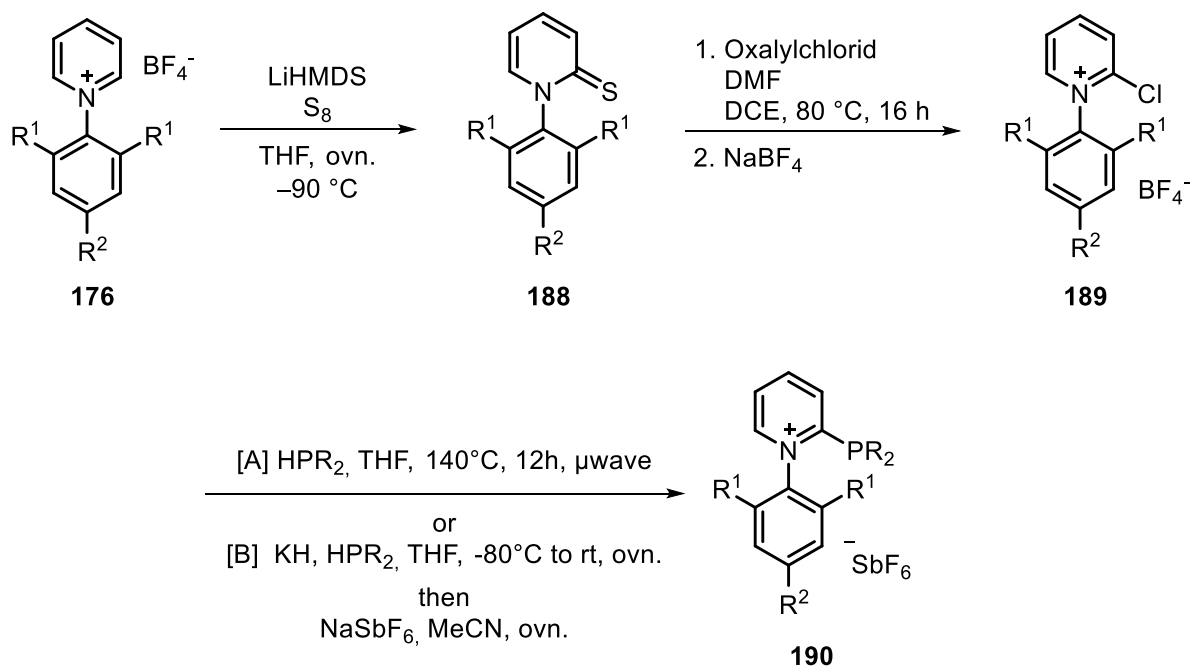
¹H NMR (300 MHz, CD₃CN) δ = 9.25 (s, 1H), 8.66 (d, *J* = 8.3 Hz, 1H), 8.03 (dd, *J* = 12.8, 6.2 Hz, 4H), 7.90 (d, *J* = 8.3 Hz, 1H), 7.83 (m, 2H), 7.72 (m, 4H), 5.02 (q, *J* = 6.9 Hz, 2H), 0.95 (t, *J* = 7.1 Hz, 3H); ¹³C NMR (101 MHz, CD₃CN) δ = 155.5, 145.9, 141.9, 134.4 (t, *J* = 3.6 Hz), 133.8, 131.3 (d, *J* = 36.7 Hz), 130.0 (t, *J* = 5.8 Hz), 121.1 (t, *J* = 26.1 Hz), 120.1 (q, *J* = 137.0 Hz), 58.7 (t, *J* = 5.5 Hz), 13.7; ³¹P NMR (121 MHz, CD₃CN) δ = 27.27; IR (neat) $\bar{\nu}$ = 689, 697, 713, 745, 765, 786, 905, 925, 977, 997, 1028, 1049, 1137, 1167, 191, 1231, 1250, 1288, 1322, 1426, 1438, 1457, 1475, 1561, 1574, 1585, 1599, 3059, 3080, 3118 cm⁻¹; HRMS *calcd.* for C₄₀H₃₆BCl₂F₁₀N₂P₂Pd: 983.069271; *found*: 983.070690.



Compound 151c: Prepared from **124j** (100 mg, 0.27 mmol) and $(\text{MeCN})_2\text{PdCl}_2$ (35.5 mg, 0.14 mmol) following the general procedure. Yellow solid (118 mg, 98%).

^1H NMR (400 MHz, CD_3CN) δ = 8.74 (d, J = 5.4 Hz, 1H), 8.59 (t, J = 7.9 Hz, 1H), 8.24 – 7.98 (m, 2H), 7.89 – 7.26 (m, 15H); ^{31}P NMR (162 MHz, CD_3CN) δ = 28.50; elemental analysis (%) calcd. for $\text{C}_{46}\text{H}_{38}\text{B}_2\text{Cl}_2\text{F}_8\text{N}_2\text{P}_2\text{Pd}$: C, 53.55; H, 3.71; N, 2.72; found: C: 53.51; H: 3.73; N: 2.71; IR (neat) $\bar{\nu}$ = 689, 704, 729, 741, 752, 798, 864, 973, 998, 1039, 1042, 1086, 1118, 1157, 1202, 1238, 1292, 1337, 1405, 1463, 1482, 1502, 1632, 3074.

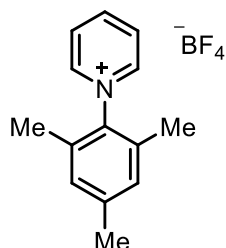
General scheme for the synthesis of pyridinium phosphines 190



General procedure for the synthesis pyridinium tetrafluoroborates 176

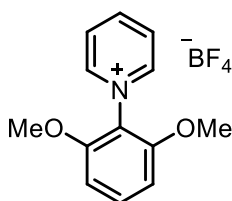
To a solution of **175** (1 eq) in *n*-Butanol (3 ml/mmol) was added the corresponding amine (1 eq). The resulting mixture was stirred for 3 days at 125 °C. After cooling to rt the solvent was evaporated and H_2O (100 ml) was added to the crude reaction mixture. After filtration the aqueous solution was washed with dichloromethane (3 x 50 ml), then NaBF_4 was added to the aqueous phase and the solution extracted with dichloromethane (3 x 100 ml). The combined

organic phases were dried over MgSO_4 , filtered and concentrated. The solid thus obtained was dried in vacuum.



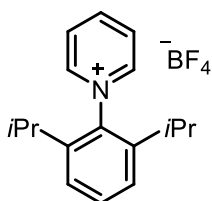
Compound 176a: Prepared from **175** (900 mg, 3.2 mmol) and mesitylamine (0.45 ml, 3.2 mmol) following the general procedure. White solid (545 mg, 73%).

^1H NMR (400 MHz, CDCl_3) δ = 8.76 (tt, J = 8.0, 1.3 Hz, 1H), 8.66 (dd, J = 6.7, 1.3 Hz, 2H), 8.40 (dd, J = 7.8, 6.7 Hz, 2H), 7.06 (s, 2H), 2.36 (s, 3H), 1.95 (s, 6H); ^{13}C NMR (100 MHz, CDCl_3) δ = 147.4, 145.9, 142.0, 139.3, 132.4, 130.3, 130.0, 21.2, 17.1; IR (neat) $\bar{\nu}$ = 434, 458, 520, 554, 576, 690, 713, 733, 784, 852, 955, 1026, 1046, 1208, 1237, 1268, 1286, 1392, 1471, 1627, 3075, 3129 cm^{-1} ; HRMS *calcd.* for $\text{C}_{14}\text{H}_{16}\text{N}$: 198.127724; *found*: 198.127690.



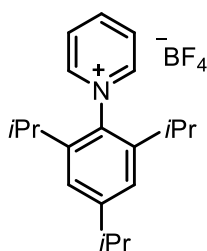
Compound 176b: Prepared from **175** (1 g, 3.6 mmol) and 2,6-dimethoxyaniline (550 mg, 3.6 mmol) following the general procedure. White solid (460 mg, 43%).

^1H NMR (400 MHz, DMSO) δ = 9.23 – 9.10 (m, 2H), 8.81 (tt, J = 7.9, 1.4 Hz, 1H), 8.38 – 8.29 (m, 2H), 7.66 (t, J = 8.6 Hz, 1H), 7.04 (d, J = 8.6 Hz, 2H), 3.81 (s, 6H); ^{13}C NMR (101 MHz, DMSO) δ = 153.3, 147.8, 147.7, 133.1, 128.3, 120.0, 105.3, 56.8; IR (neat) $\bar{\nu}$ = 455, 520, 533, 552, 590, 619, 687, 731, 776, 872, 903, 986, 1023, 1064, 1112, 1174, 1190, 1208, 1259, 1274, 1305, 1348, 1443, 1470, 1485, 1593, 1606, 1627, 2843, 2942, 3036, 3081, 3129 cm^{-1} ; HRMS *calcd.* for $\text{C}_{13}\text{H}_{14}\text{NO}_2$: 216.101904; *found*: 216.101890.



Compound 176c: Prepared from **175** (1 g, 3.6 mmol) and 2,6-diisopropylaniline (0.68 ml, 3.6 mmol) following the general procedure. White solid (400 mg, 34%).

^1H NMR (400 MHz, CD_3CN) δ = 8.82 – 8.75 (m, 1H), 8.31 – 8.23 (m, 1H), 7.71 – 7.64 (m, 1H), 7.49 (d, J = 7.9 Hz, 1H), 2.06 (sep, J = 6.8 Hz, 1H), 1.14 (d, J = 6.8 Hz, 4H); ^{13}C NMR (101 MHz, CD_3CN) δ = 148.6, 147.0, 144.4, 139.5, 133.2, 130.1, 126.0, 29.3, 24.0; IR (neat) $\bar{\nu}$ = 458, 521, 561, 59, 693, 743, 764, 772, 783, 821, 938, 1020, 1035, 1168, 1213, 1282, 1332, 1345, 1370, 1390, 1474, 1538, 1597, 1627, 2876, 2954, 3079, 3121 cm^{-1} ; HRMS *calcd.* for $\text{C}_{17}\text{H}_{22}\text{N}$: 240.174674; *found*: 240.174640.



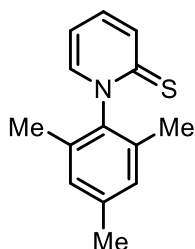
Compound 176d: Prepared from **175** (1 g, 3.6 mmol) and 2,4,6-triisopropylaniline (790 mg, 3.6 mmol) following the general procedure. White solid (570 mg, 43%).

$^1\text{H NMR}$ (400 MHz, CD_2Cl_2) δ = 8.83 (tt, J = 7.9, 1.4 Hz, 1H), 8.70 – 8.60 (m, 2H), 8.41 (dd, J = 7.8, 6.7 Hz, 2H), 7.25 (s, 2H), 3.02 (sep, J = 6.9 Hz, 1H), 2.03 (sep, J = 6.8 Hz, 2H), 1.31 (d, J = 6.9 Hz, 6H), 1.16 (d, J = 6.8 Hz, 12H);

$^{13}\text{C NMR}$ (101 MHz, CD_2Cl_2) δ = 154.0, 148.0, 146.4, 143.3, 136.9, 129.9, 123.5, 34.9, 29.1, 24.2, 23.9; IR (neat) $\bar{\nu}$ = 424, 445, 473, 520, 593, 656, 696, 787, 883, 956, 1048, 1172, 1208, 1227, 1283, 1324, 1343, 1369, 1390, 1471, 1538, 1600, 1626, 2874, 2932, 2965, 3080, 3124 cm^{-1} ; HRMS *calcd.* for $\text{C}_{20}\text{H}_{28}\text{N}$: 282.221624; *found*: 282.221840.

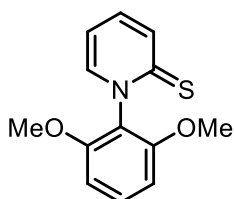
General procedure for the synthesis of pyridinthiones **188**

To a solution of **176** (1 eq) and S_8 (0.25 eq) in THF (10 ml/mmol) at $-100\text{ }^\circ\text{C}$ was added a solution of LiHMDS (1 eq) in THF (5 ml/mmol). The resulting mixture was stirred overnight letting it warm up to rt. After evaporation of the solvent the resulting crude mixture was purified by column chromatography (EtOAc/*n*-Pentan 1/1) and dried under vacuum.



Compound 188a: Prepared from **176a** (1 g, 3.5 mmol), S_8 (225 mg, 0.875 mmol) and LiHMDS (587 mg, 3.5 mmol) following the general procedure. White solid (515 mg, 64%).

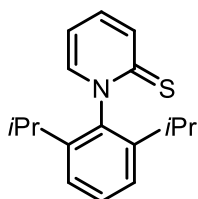
$^1\text{H NMR}$ (300 MHz, CD_2Cl_2) δ = 7.68 (dq, J = 8.8, 0.7 Hz, 1H), 7.40 (ddd, J = 6.6, 1.5, 0.6 Hz, 1H), 7.27 (ddd, J = 8.7, 6.8, 1.7 Hz, 1H), 7.01 (s, 2H), 6.72 (td, J = 6.7, 1.4 Hz, 1H), 2.35 (s, 3H), 1.99 (s, 6H); $^{13}\text{C NMR}$ (75 MHz, CD_2Cl_2) δ = 181.8, 141.5, 140.9, 139.4, 137.2, 134.8, 134.1, 129.9, 113.7, 21.4, 18.1; IR (neat) $\bar{\nu}$ = 426, 439, 494, 561, 645, 684, 718, 730, 749, 758, 857, 900, 952, 994, 1033, 1056, 1086, 1131, 1149, 1170, 1181, 1214, 1252, 1268, 1311, 1375, 1403, 1446, 1484, 1523, 1591, 1616, 2854, 2919, 2952, 3026, 3092 cm^{-1} ; HRMS *calcd.* for $\text{C}_{14}\text{H}_{15}\text{NSNa}$: 252.081740; *found*: 252.081940.



Compound 188b: Prepared from **176b** (1 g, 3.3 mmol), S_8 (211 mg, 0.825 mmol) and LiHMDS (552 mg, 3.3 mmol) following the general procedure. White solid (570 mg, 70%).

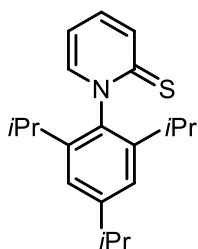
$^1\text{H NMR}$ (400 MHz, CDCl_3) δ = 7.75 (ddd, J = 8.8, 1.4, 0.8 Hz, 1H), 7.45 – 7.35 (m, 2H), 7.23 (ddd, J = 8.7, 6.8, 1.7 Hz, 1H), 6.70 (d, J = 8.5 Hz,

2H), 6.65 (td, $J = 6.7, 1.5$ Hz, 1H), 3.81 (s, 6H); ^{13}C NMR (101 MHz, CDCl_3) $\delta = 183.2, 155.7, 143.7, 136.3, 135.9, 131.3, 123.4, 113.4, 105.8, 56.8$; IR (neat) $\bar{\nu} = 443, 468, 496, 532, 569, 598, 619, 684, 702, 725, 735, 762, 776, 861, 902, 940, 957, 997, 1026, 1118, 1121, 1141, 1177, 1194, 1218, 1258, 1276, 1299, 1350, 1406, 1440, 1452, 1479, 1524, 1601, 1616, 1661, 2841, 2942, 3024, 3062, 3087, 3143$ cm^{-1} ; HRMS *calcd.* for $\text{C}_{14}\text{H}_{15}\text{NSNa}$: 270.055920; *found*: 270.055820.



Compound **188c**: Prepared from **176c** (1 g, 1.53 mmol), S_8 (98 mg, 3.06 mmol) and LiHMDS (256 mg, 1.53 mmol) following the general procedure. White solid (307 mg, 74%).

^1H NMR (400 MHz, CDCl_3) $\delta = 7.64 - 7.57$ (m, 2H), 7.48 – 7.41 (m, 1H), 7.38 (ddd, $J = 8.8, 4.3, 1.3$ Hz, 1H), 7.33 (s, 1H), 7.31 (s, 1H), 6.78 (td, $J = 6.8, 1.4$ Hz, 1H), 2.36 (sep, $J = 6.9$ Hz, 2H), 1.19 (d, $J = 6.8$ Hz, 6H), 1.07 (d, $J = 6.9$ Hz, 6H); ^{13}C NMR (101 MHz, CDCl_3) $\delta = 183.1, 144.9, 142.6, 141.5, 136.7, 136.1, 130.5, 125.4, 113.6, 29.3, 24.2, 23.4$; IR (neat) $\bar{\nu} = 419, 446, 463, 478, 573, 594, 724, 759, 769, 802, 833, 856, 937, 998, 1027, 1057, 1085, 1107, 1131, 1143, 1159, 1203, 1259, 1302, 1332, 1361, 1382, 1403, 1441, 1521, 1613, 2867, 2925, 2959, 3018, 3073$ cm^{-1} ; HRMS *calcd.* for $\text{C}_{17}\text{H}_{21}\text{NSNa}$: 294.128690; *found*: 294.128410.

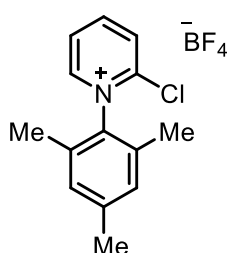


Compound **188d**: Prepared from **176d** (1 g, 2.70 mmol), S_8 (173 mg, 5.42 mmol) and LiHMDS (451 mg, 2.70 mmol) following the general procedure. White solid (288 mg, 34%).

^1H NMR (400 MHz, CDCl_3) $\delta = 7.67$ (ddd, $J = 8.8, 1.3, 0.8$ Hz, 1H), 7.42 (ddd, $J = 6.6, 1.7, 0.7$ Hz, 1H), 7.27 (ddd, $J = 8.7, 6.8, 1.7$ Hz, 1H), 7.14 (s, 2H), 6.67 (td, $J = 6.7, 1.4$ Hz, 1H), 2.97 (sep, $J = 6.9$ Hz, 1H), 2.42 (sep, $J = 6.9$ Hz, 2H), 1.30 (d, $J = 6.2$ Hz, 6H), 1.22 (d, $J = 6.8$ Hz, 6H), 1.09 (d, $J = 6.9$ Hz, 6H); ^{13}C NMR (101 MHz, CDCl_3) $\delta = 183.3, 150.6, 144.3, 141.7, 139.2, 137.0, 134.7, 123.0, 112.8, 34.7, 29.2, 24.6, 24.2, 23.7$; IR (neat) $\bar{\nu} = 448, 463, 496, 538, 575, 595, 652, 690, 722, 749, 770, 820, 843, 862, 877, 893, 946, 999, 1028, 1057, 1085, 1120, 1137, 1145, 1163, 1186, 1210, 1260, 1320, 1340, 1361, 1382, 1406, 1441, 1522, 1614, 2867, 2926, 2959, 3018, 3051, 3071$ cm^{-1} ; HRMS *calcd.* for $\text{C}_{20}\text{H}_{28}\text{NSNa}$: 314.193696; *found*: 314.193780.

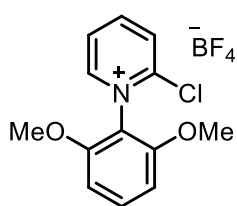
General procedure for the synthesis of chloropyridinium tetrafluoroborates 189:

To a solution of **188** (1 eq) in dichloroethane (10 ml/mmol) was added oxalylchlorid (3 eq) and dimethylformamid (0.1 ml). The resulting mixture was heated overnight to 80 °C. After cooling to rt the reaction mixture was quenched with H₂O and diluted with ethylacetate. After addition of sat. aq. NaBF₄ solution, the aqueous phase was extracted with dichloromethane (3 x 50 ml). The combined organic phases were dried over MgSO₄, filtered and concentrated. The solid obtained was washed with a small amount of THF (1 ml/mmol) or crystallized from DCM/*n*-pentane and dried in vacuum.



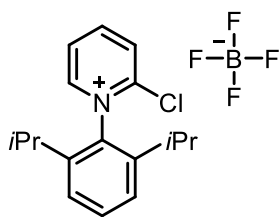
Compound **189a**: Prepared from **188a** (229 mg, 1.0 mmol), oxalylchlorid (0.26 ml, 3.0 mmol) and dimethylformamid (0.1 ml) in dichloroethane following the general procedure. Brownish solid (181 mg, 57%).

¹H NMR (400 MHz, CDCl₃) δ = 8.90 (td, *J* = 7.9, 1.3 Hz, 1H), 8.79 (dd, *J* = 6.1, 1.7 Hz, 1H), 8.49 – 8.42 (m, 1H), 8.41 – 8.34 (m, 1H), 7.11 (s, 2H), 2.39 (s, 3H), 1.96 (s, 6H); ¹³C NMR (101 MHz, CDCl₃) δ = 150.3, 148.8, 147.4, 142.8, 137.4, 132.6, 130.7, 130.6, 129.2, 21.3, 17.3; IR (neat) $\bar{\nu}$ = 427, 451, 479, 517, 550, 572, 587, 636, 691, 726, 749, 763, 783, 822, 860, 914, 1029, 1056, 1100, 1134, 1224, 1258, 1348, 1378, 1439, 1472, 1565, 1612, 1672, 1897, 2927, 2979, 3058, 3119 cm⁻¹; HRMS *calcd.* for C₁₄H₁₅NCl: 232.088752; *found*: 232.088680.



Compound **189b**: Prepared from **188b** (500 mg, 2.0 mmol), oxalylchlorid (0.52 ml, 6.0 mmol) and dimethylformamid (0.1 ml) in dichloroethane following the general procedure. Brownish solid (625 mg, 93%).

¹H NMR (400 MHz, CDCl₃) δ = 8.81 (td, *J* = 8.2, 1.4 Hz, 1H), 8.75 (dd, *J* = 6.1, 1.3 Hz, 1H), 8.39 (t, *J* = 6.5 Hz, 1H), 8.28 (d, *J* = 8.2 Hz, 1H), 7.59 (t, *J* = 8.6 Hz, 1H), 6.79 (d, *J* = 8.6 Hz, 2H), 3.84 (s, 6H); ¹³C NMR (101 MHz, CD₃CN) δ = 154.9, 150.8, 150.5, 150.3, 135.1, 131.2, 127.8, 119.0, 106.1, 57.6; IR (neat) $\bar{\nu}$ = 416, 449, 461, 485, 521, 566, 618, 688, 701, 729, 781, 902, 1050, 1111, 1173, 1266, 1307, 1394, 1438, 1474, 1486, 1562, 1592, 1607, 1688, 1738, 1773, 2850, 2925, 2950, 3028, 3059, 3117 cm⁻¹; HRMS *calcd.* for C₁₃H₁₃NO₂Cl: 250.062932; *found*: 250.063000.



Compound **189c**: Prepared from **188c** (500 mg, 1.84 mmol), oxalylchlorid (0.47 ml, 5.52 mmol) and dimethylformamid (0.1 ml) in dichloroethane following the general procedure. Brownish solid (665 mg, 94%).

^1H NMR (400 MHz, CDCl_3) δ = 8.99 (td, J = 8.1, 1.7 Hz, 1H), 8.85 (dd, J = 6.1, 1.6 Hz, 1H), 8.52 (ddd, J = 7.6, 6.1, 1.3 Hz, 1H), 8.45 (dd, J = 8.3, 1.0 Hz, 1H), 7.65 (t, J = 7.9 Hz, 1H), 7.41 (d, J = 7.9 Hz, 2H), 1.98 (sep, J = 6.8 Hz, 2H), 1.21 (d, J = 6.8 Hz, 6H), 1.15 (d, J = 6.8 Hz, 6H); ^{13}C NMR (101 MHz, CDCl_3) δ = 150.1, 147.7, 147.1, 142.5, 135.8, 132.1, 130.1, 127.9, 124.9, 28.2, 23.7, 22.5; IR (neat) $\bar{\nu}$ = 434, 475, 486, 520, 571, 597, 672, 725, 761, 793, 805, 812, 938, 1022, 1051, 1172, 1204, 1284, 1294, 1331, 1371, 1391, 1435, 1472, 1561, 1606, 1692, 2931, 2968, 3110 cm^{-1} ; HRMS *calcd.* for $\text{C}_{17}\text{H}_{21}\text{NCl}$: 274.135702; *found*: 274.135510.

General Procedure for the synthesis of pyridiniumphosphine salts **190**:

Method A:

The corresponding phosphine (3 equiv.) was added to a solution of **189** (1 equiv.) in THF (3 ml/mmol) inside a microwave. The resulting mixture was heated to 120-140 °C for 12 h. After evaporation of the solvent the residue was washed with *n*-pentane (2 x 5 ml), redissolved in acetonitrile and then NaSbF_6 (3 equiv) was added. After evaporation of the solvents dichloromethane was added and filtered. Evaporation of the solvents and recrystallization from dichloromethane/*n*-pentane gave the desired compounds.

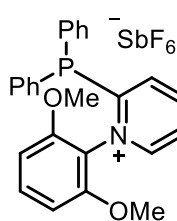
Method B:

A suspension of potassium hydride (8 equiv.) in THF (3 ml/mmol) was cooled to -78°C and then the desired phosphine (1 equiv) was added. The resulting mixture was stirring for 1 h, letting it warm up to -50°C. The excess of potassium hydrid was filtered off and the resulting solution was transferred at -78 °C to a precooled solution (-78 °C) of the chloropyridinium salt **189** in THF (3 ml/mmol). The resulting mixture was stirred overnight, while it was allowed to warm up to rt. After evaporation of the solvent the residue was washed with *n*-pentane (2 x 5 ml), redissolved in acetonitrile and NaSbF_6 (3 eq) was added. The obtained mixture was stirred for 3 h and after evaporation of solvents, DCM was added and the resulting salts filtered off. Evaporation of the filtrate and recrystallization from dichloromethane/*n*-pentane gave the desired compound.

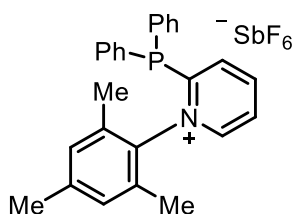
Compound **190a**: Prepared from potassium hydride (474 mg, 11.8 mmol), bis(3,5-bis(trifluoromethyl)phenyl)phosphine (678 mg, 1.48 mmol), **189b** (500 mg, 1.48 mmol), and NaSbF₆ (1150 mg, 4.45 mmol) following the general procedure. Brownish solid (592 mg, 45%).
¹H NMR (400 MHz, CDCl₃) δ = 8.69 – 8.63 (m, 1H), 8.56 (td, *J* = 8.0, 1.5 Hz, 1H), 8.21 (s, 2H), 8.17 (ddd, *J* = 7.7, 6.1, 1.4 Hz, 1H), 7.84 (dd, *J* = 8.1, 0.9 Hz, 1H), 7.80 (d, *J* = 7.7 Hz, 4H), 7.58 (t, *J* = 8.6 Hz, 1H), 6.69 (d, *J* = 8.6 Hz, 2H), 3.56 (s, 6H); ¹³C NMR (101 MHz, CDCl₃) δ = 161.1 (d, *J* = 25.7 Hz), 154.5 (d, *J* = 1.5 Hz), 151.5, 148.1, 136.0 (dd, *J* = 23.7, 3.3 Hz), 135.4 (d, *J* = 14.8 Hz), 133.3 (d, *J* = 15.1 Hz), 132.9 (dq, *J* = 33.78, 8.01 Hz), 129.8, 126.5 (quin, *J* = 3.8 Hz), 123.9 (q, *J* = 272.5 Hz), 119.2 (d, *J* = 3.7 Hz), 105.9, 57.2; ³¹P NMR (121 MHz, CDCN) δ = -7.18; IR (neat) $\bar{\nu}$ = 436, 484, 509, 569, 655, 683, 699, 733, 748, 778, 898, 1000, 1027, 1094, 1116, 1132, 1180, 1278, 1310, 1330, 1354, 1434, 1469, 1489, 1568, 1609, 2856, 2870, 2927, 2954 cm⁻¹; HRMS *calcd.* for C₂₉H₁₉NF₁₂O₂P: 672.095635; *found*: 672.095340.

Compound **190b**: Prepared from potassium hydride (502 mg, 12.5 mmol), bis(3,5-bis(trifluoromethyl)phenyl)phosphine (717 mg, 1.56 mmol), **189a** (500 mg, 1.56 mmol), and NaSbF₆ (1214 mg, 4.7 mmol) following the general procedure. Brownish solid (974 mg, 70%).
¹H NMR (400 MHz, CDCl₃) δ = 8.78 – 8.68 (m, 1H), 8.61 (td, *J* = 8.0, 1.5 Hz, 1H), 8.27 – 8.15 (m, 3H), 8.02 (dd, *J* = 8.1, 1.0 Hz, 1H), 7.88 (d, *J* = 7.8 Hz, 4H), 7.00 (d, *J* = 0.4 Hz, 2H), 2.35 (s, 3H), 1.64 (s, 6H); ¹³C NMR (101 MHz, CDCl₃) δ = 159.4 (d, *J*_{C-P} = 28.7 Hz), 150.0, 148.2, 144.1, 137.7 (d, *J*_{C-P} = 3.4 Hz), 136.4 (d, *J*_{C-P} = 2.7 Hz), 136.2 (d, *J*_{C-P} = 2.8 Hz), 135.7 (d, *J*_{C-P} = 0.7 Hz), 134.5 (d, *J*_{C-P} = 2.4 Hz), 133.0 (dq, *J*_{C-F} = 25.1, *J*_{C-P} = 8.1 Hz), 131.1, 130.6, 126.8 (dq, *J* = 4.1, 4.1 Hz), 123.9 (q, *J* = 272.6 Hz), 21.0, 17.9, 17.9; ³¹P NMR (121 MHz, CDCN) δ = -6.89; IR (neat) $\bar{\nu}$ = 412, 433, 458, 471, 504, 518, 585, 612, 653, 682, 700, 706, 727, 740, 779, 845, 865, 897, 920, 1094, 1125, 1353, 1386, 1438, 1470, 1507, 1521, 1541, 1567, 1608, 2962, 3048, 3115 cm⁻¹; HRMS *calcd.* for C₃₀H₂₁NF₁₂P: 654.121455; *found*: 654.121220.

Compound **190c**: Prepared from diphenylphosphine (0.77 ml, 4.45 mmol), **189b** (500 mg, 1.48 mmol) and NaSbF₆ (1150 mg, 4.45 mmol) in THF following the general procedure **A**. Brownish solid (650 mg, 69%).
¹H NMR (400 MHz, CD₃CN) δ = 8.62 – 8.54 (m, 1H), 8.48 (td, *J* = 8.0, 1.5 Hz, 1H), 8.05 (ddd, *J* = 7.7, 6.1, 1.5 Hz, 1H), 7.70 – 7.65 (m, 1H), 7.59 – 7.51 (m, 3H), 7.49 – 7.41 (m, 4H), 7.27 – 7.18 (m, 4H), 6.69 (d, *J* = 8.6 Hz, 2H), 3.51 (s, 6H); ¹³C NMR

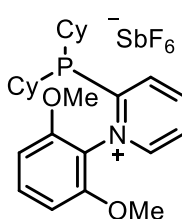


(101 MHz, CD₃CN) δ = 165.7 (d, J = 30.2 Hz), 154.7, 150.6, 147.3, 135.4 (d, J = 22.7 Hz), 134.8, 134.6, 131.9, 130.9 (d, J = 9.0 Hz), 130.4 (d, J = 8.1 Hz), 128.6, 119.8, 105.6, 57.0; ³¹P NMR (162 MHz, CD₃CN) δ = -7.23; IR (neat) $\bar{\nu}$ = 406, 449, 485, 501, 511, 531, 567, 599, 653, 697, 724, 736, 754, 760, 776, 850, 905, 977, 1000, 1007, 1024, 1058, 1111, 1177, 1242, 1264, 1304, 1338, 1436, 1468, 1486, 1559, 1590, 1602, 2846, 2946, 3018, 3067, 3106 cm⁻¹; HRMS *calcd.* for C₂₅H₂₃NO₂P: 400.146093; *found*: 400.146200.



Compound **190d**: Prepared from diphenylphosphine (0.81 ml, 4.69 mmol), **189a** (500 mg, 1.56 mmol), and NaSbF₆ (1214 mg, 4.69 mmol) in THF following the general procedure **A**. Brownish solid (482 mg, 50%).

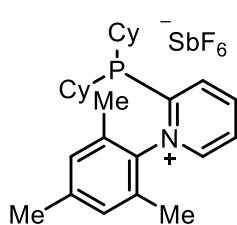
¹H NMR (400 MHz, CD₂Cl₂) δ = 8.52 (td, J = 7.9, 1.5 Hz, 1H), 8.46 (dddd, J = 6.1, 2.2, 1.5, 0.6 Hz, 1H), 8.15 (ddd, J = 7.7, 6.1, 1.5 Hz, 1H), 7.85 – 7.80 (m, 1H), 7.55 (ddt, J = 6.6, 2.4, 1.2 Hz, 2H), 7.51 – 7.44 (m, 4H), 7.32 – 7.24 (m, 4H), 7.00 (d, J = 0.6 Hz, 2H), 2.41 (s, 3H), 1.60 (s, 6H); ¹³C NMR (101 MHz, CD₂Cl₂) δ = 165.5 (d, J = 34.9 Hz), 147.9, 146.5, 143.2, 138.1, 135.4 (d, J = 22.7 Hz), 134.3, 133.5 (d, J = 2.9 Hz), 132.0, 130.7, 130.3 (d, J = 8.3 Hz), 128.99 (d, J = 3.3 Hz), 128.95 (d, J = 5.0 Hz), 21.5, 17.7, 17.7; ¹⁹F NMR (282 MHz, CD₂Cl₂) δ = -123.61 (sex, $J_{121\text{Sb-F}}$ = 1933.8, oct, $J_{123\text{Sb-F}}$ = 1065.3 Hz); ³¹P NMR (121 MHz, CD₂Cl₂) δ = -7.19; IR (neat) $\bar{\nu}$ = 414, 429, 451, 487, 510, 537, 562, 585, 651, 696, 741, 750, 780, 856, 977, 999, 1026, 1073, 1089, 1141, 1185, 1231, 1245, 1282, 1313, 1378, 1436, 1473, 1560, 1603, 2923, 2955, 3044, 3071, 3109 cm⁻¹; HRMS *calcd.* for C₂₆H₂₅NP: 382.171913; *found*: 382.172110.



Compound **190e**: Prepared from dicyclohexylphosphine (0.97 mg, 4.45 mmol), **189b** (500 mg, 1.48 mmol) and NaSbF₆ (1150 mg, 4.45 mmol) in THF following the general procedure **A**. Brownish solid (960 mg, 69%).

¹H NMR (400 MHz, CD₃CN) δ = 8.63 (dddd, J = 6.1, 2.2, 1.5, 0.6 Hz, 1H), 8.57 (td, J = 7.9, 1.6 Hz, 1H), 8.37 – 8.31 (m, 1H), 8.08 (ddt, J = 8.0, 6.1, 0.9 Hz, 1H), 7.62 (t, J = 8.6 Hz, 1H), 6.85 (d, J = 8.6 Hz, 2H), 3.76 (s, 6H), 2.04 – 1.96 (m, 2H), 1.77 – 1.61 (m, 8H), 1.51 – 1.43 (m, 2H), 1.34 – 0.98 (m, 10H); ¹³C NMR (101 MHz, CD₃CN) δ = 165.1 (d, J = 39.3 Hz), 154.5 (d, J = 2.3 Hz), 150.9, 146.0, 134.7 (d, J = 3.7 Hz), 134.1, 128.5, 120.9, 105.2, 56.8, 34.8 (d, J = 15.6 Hz), 30.4 (d, J = 11.2 Hz), 30.0 (d, J = 16.2 Hz), 27.5, 27.4 (d, J = 3.0 Hz), 26.5; ³¹P NMR (162 MHz, CD₃CN) δ = 0.00; IR (neat) $\bar{\nu}$ = 410, 452, 499, 522, 533, 568, 595, 652, 724, 733, 779, 852, 892, 903, 1005, 1025, 1110, 1139, 1174,

1205, 1262, 1306, 1445, 1485, 1560, 1604, 1660, 2850, 2927, 3123 cm^{-1} ; HRMS *calcd.* for $\text{C}_{25}\text{H}_{23}\text{NO}_2\text{P}$: 412.239993; *found*: 412.239700.

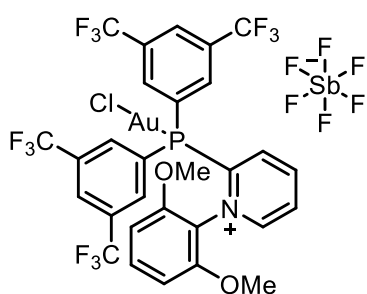


Compound **190f**: Prepared from dicyclohexylphosphine (1.03 ml, 4.69 mmol), **189a** (500 mg, 1.56 mmol) and NaSbF_6 (1214 mg, 4.69 mmol) in THF following the general procedure **A**. Brownish solid (540 mg, 55%).

^1H NMR (400 MHz, CDCl_3) δ = 8.70 (td, J = 7.9, 1.5 Hz, 1H), 8.58 – 8.54 (m, 1H), 8.29 – 8.22 (m, 2H), 7.12 – 7.05 (m, 2H), 2.41 (s, 3H), 1.95 (s, 6H), 1.92 – 1.84 (m, 2H), 1.75 (dt, J = 23.9, 11.4 Hz, 8H), 1.56 – 1.44 (m, 2H), 1.35 – 1.08 (m, 10H); ^{13}C NMR (101 MHz, CDCl_3) δ = 163.5 (d, J = 41.5 Hz), 138.5 (d, J = 3.1 Hz), 133.7 (d, J = 2.8 Hz), 132.6 (d, J = 3.0 Hz), 33.8 (d, J = 16.9 Hz), 31.4 (d, J = 17.7 Hz), 28.6 (d, J = 10.2 Hz), 27.3 (d, J = 12.8 Hz), 27.0 (d, J = 8.8 Hz), 18.3 (d, J = 4.6 Hz); ^{31}P NMR (121 MHz, CDCl_3) δ = 0.00; IR (neat) $\bar{\nu}$ = 452, 465, 521, 560, 585, 653, 712, 775, 852, 866, 887, 921, 954, 1005, 1091, 1135, 1173, 1203, 1232, 1265, 1307, 1331, 1383, 1448, 1471, 1562, 1607, 2853, 2925 cm^{-1} ; HRMS *calcd.* for $\text{C}_{26}\text{H}_{37}\text{NP}$: 394.265813; *found*: 394.266130.

General Procedure for the synthesis of pyridiniumphosphin gold complexes **191**:

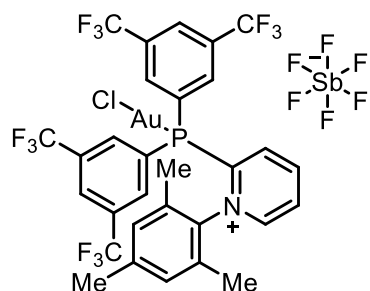
$\text{Me}_2\text{S}\cdot\text{AuCl}$ (1 equiv.) was added to the phosphine **190** (1 equiv.) in DCM (1ml/mmol) at rt. After stirring for 1 h the solvent was evaporated and the resulting solid washed with Et_2O (2x 2ml/mmol) and *n*-pentane (2x 2ml/mmol).



Compound **191a**: Prepared from phosphine **190a** (100 mg, 0.11 mmol) and $\text{Me}_2\text{S}\cdot\text{AuCl}$ (32.4 mg, 0.11 mmol) following the general procedure. White solid (111.6 mg, 89%).

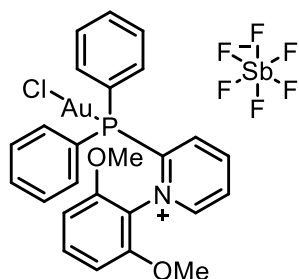
^1H NMR (400 MHz, CD_3CN) δ = 8.80 (ddd, J = 6.1, 3.3, 1.4 Hz, 1H), 8.75 (tt, J = 8.1, 1.5 Hz, 1H), 8.40 (s, 3H), 8.14 (d, J = 13.5 Hz, 4H), 8.06 (t, J = 7.3 Hz, 1H), 7.65 (t, J = 8.6 Hz, 1H), 6.67 (d, J = 8.6 Hz, 2H), 3.50 (s, 6H); ^{13}C NMR (101 MHz, CD_3CN) δ = 155.2, 154.5, 149.6 (d, J = 5.5 Hz), 137.6 (d, J = 9.1 Hz), 136.9 (d, J = 2.7 Hz), 136.7 (d, J = 2.7 Hz), 136.3, 133.6 (qd, J = 34.4, 13.1 Hz), 132.8, 129.3, 127.3 (d, J = 62.4 Hz), 125.0 (q, J = 272.2 Hz), 118.8 (d, J = 4.8 Hz), 106.4, 57.2; ^{31}P NMR (162 MHz, CD_3CN) δ = 30.90; IR (neat) $\bar{\nu}$ = 421, 439, 455, 467, 515, 525, 542, 563, 599, 616, 651, 658, 672, 681, 695, 706, 731, 778, 825, 848, 898, 911, 935,

956, 1005, 1021, 1097, 1111, 1141, 1153, 1186, 1205, 1277, 1308, 1328, 1355, 1435, 1466, 1487, 1588, 1602, 1621, 2955, 3057, 3108, 3128 cm^{-1} ; HRMS *calcd.* for $\text{C}_{29}\text{H}_{19}\text{NO}_2\text{AuClF}_{12}\text{P}$: 904.031041; *found*: 904.030620.



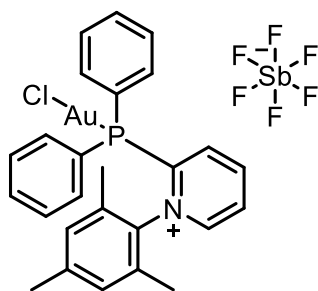
Compound **191b**: Prepared from phosphine **190b** (100 mg, 0.11 mmol) and $\text{Me}_2\text{S}\cdot\text{AuCl}$ (33 mg, 0.11 mmol) following the general procedure. White solid (124 mg, 98%).

^1H NMR (400 MHz, CDCl_3) δ = 8.93 (t, J = 4.6 Hz, 1H), 8.82 (t, J = 8.1 Hz, 1H), 8.50 – 8.44 (m, 1H), 8.41 (s, 2H), 8.27 (t, J = 7.2 Hz, 1H), 8.16 (d, J = 13.3 Hz, 4H), 7.05 (d, J = 1.1 Hz, 2H), 2.39 (s, 3H), 1.62 (s, 6H); ^{13}C NMR (101 MHz, CD_3CN) δ = 152.9, 149.8, 144.9, 138.0, 137.5 (d, J = 4.5 Hz), 136.9 (d, J = 2.9 Hz), 136.7 (d, J = 2.4 Hz), 135.0, 133.6 (qd, J = 34.3, 12.6 Hz), 133.6 (d, J = 2.9 Hz), 132.1, 129.4, 126.8 (d, J = 7.8 Hz), 123.6 (q, J = 272.8 Hz), 21.2, 18.7; ^{31}P NMR (121 MHz, CD_3CN) δ = 30.54; IR (neat) $\bar{\nu}$ = 435, 442, 467, 484, 515, 523, 539, 563, 582, 616, 655, 682, 696, 704, 718, 738, 780, 787, 846, 858, 896, 905, 931, 1001, 1028, 1062, 1098, 1113, 1126, 1144, 1178, 1198, 1229, 1279, 1357, 1386, 1435, 1476, 1606, 1620, 3036, 3093, 3118 cm^{-1} ; HRMS *calcd.* for $\text{C}_{30}\text{H}_{21}\text{NAuClF}_{12}\text{P}$: 886.056861; *found*: 886.057350.



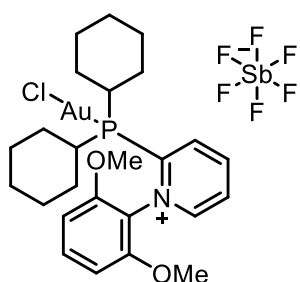
Compound **191c**: Prepared from phosphine **190c** (100 mg, 0.16 mmol) and $\text{Me}_2\text{S}\cdot\text{AuCl}$ (46.4 mg, 0.16 mmol) following the general procedure. White solid (134 mg, 98%).

^1H NMR (300 MHz, CD_3CN) δ = 8.79 – 8.56 (m, 2H), 8.34 – 8.21 (m, 1H), 7.89 – 7.78 (m, 1H), 7.76 – 7.65 (m, 2H), 7.68 – 7.41 (m, 9H), 6.68 (d, J = 8.6 Hz, 2H), 3.46 (s, 6H); ^{13}C NMR (101 MHz, CD_3CN) δ = 155.5, 154.0, 149.2, 136.6, 136.4, 136.3, 135.8, 134.9, 133.2 (d, J = 10.2 Hz), 131.3 (d, J = 11.9 Hz), 130.5 (d, J = 13.0 Hz), 120.0, 106.6, 57.3; ^{31}P NMR (162 MHz, CD_3CN) δ = 29.93; IR (neat) $\bar{\nu}$ = 542, 564, 601, 654, 692, 713, 735, 750, 776, 846, 905, 927, 998, 1025, 1112, 1140, 1178, 1266, 1308, 1438, 1486, 1602, 2846, 2945, 2974, 3052, 3115 cm^{-1} ; HRMS *calcd.* for $\text{C}_{25}\text{H}_{23}\text{NO}_2\text{AuClP}$: 632.0815; *found*: 632.0814.



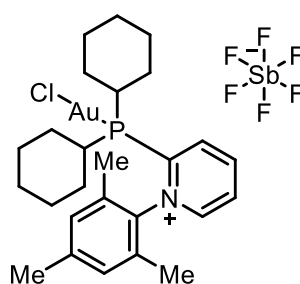
Compound **191d**: Prepared from phosphine **190d** (100 mg, 0.16 mmol) and $\text{Me}_2\text{S}\cdot\text{AuCl}$ (46.4 mg, 0.16 mmol) following the general procedure. White solid (134 mg, 98%).

^1H NMR (300 MHz, CD_3CN) δ = 8.86 – 8.79 (m, 1H), 8.64 (ddd, J = 5.9, 2.9, 1.4 Hz, 1H), 8.43 (ddt, J = 7.5, 6.0, 1.4 Hz, 1H), 8.03 – 7.96 (m, 1H), 7.78 – 7.72 (m, 2H), 7.69 – 7.58 (m, 8H), 7.11 (d, J = 0.5 Hz, 2H), 2.46 (s, 3H), 1.58 (s, 6H); ^{13}C NMR (101 MHz, CD_3CN) δ = 152.2, 149.4 (d, J = 4.9 Hz), 144.2, 137.2 (d, J = 7.9 Hz), 136.3 (d, J = 15.8 Hz), 135.0 (d, J = 2.6 Hz), 134.5, 132.5, 132.2, 131.2 (d, J = 12.6 Hz), 124.6, 124.0, 21.4, 18.1; ^{31}P NMR (162 MHz, CD_3CN) δ = 29.51; IR (neat) $\bar{\nu}$ = 510, 537, 564, 582, 653, 692, 717, 737, 750, 780, 853, 998, 1027, 1096, 1136, 1187, 1228, 1252, 1285, 1313, 1382, 1437, 1472, 1561, 1605, 2918, 3051, 3113 cm^{-1} ; HRMS *calcd.* for $\text{C}_{26}\text{H}_{25}\text{NAuClP}$: 614.107319; *found*: 614.107590.



Compound **191e**: Prepared from phosphine **190e** (100 mg, 0.15 mmol) and $\text{Me}_2\text{S}\cdot\text{AuCl}$ (45.5 mg, 0.15 mmol) following the general procedure. White solid (131 mg, 96%).

^1H NMR (300 MHz, CD_3CN) δ = 8.84 (tdd, J = 8.0, 1.6, 0.8 Hz, 1H), 8.80 – 8.70 (m, 1H), 8.55 (ddd, J = 8.1, 3.7, 1.2 Hz, 1H), 8.34 (ddt, J = 7.6, 6.1, 1.4 Hz, 1H), 7.75 (t, J = 8.6 Hz, 1H), 6.91 (d, J = 8.6 Hz, 2H), 3.82 (s, 6H), 2.68 – 2.50 (m, 2H), 2.12 – 1.99 (m, 2H), 1.91 – 1.76 (m, 4H), 1.74 – 1.56 (m, 4H), 1.52 – 1.18 (m, 10H); ^{13}C NMR (126 MHz, CD_3CN) δ = 154.9, 154.3, 151.2 (d, J = 37.8 Hz), 148.6 (d, J = 4.1 Hz), 135.5 (d, J = 4.7 Hz), 135.1, 131.4, 120.6 (d, J = 4.0 Hz), 106.5, 57.2, 37.9 (d, J = 29.1 Hz), 31.3 (d, J = 4.7 Hz), 30.7, 26.9 (d, J = 12.7 Hz), 26.8 (d, J = 14.6 Hz), 26.1 (d, J = 2.1 Hz); ^{31}P NMR (162 MHz, CD_3CN) δ = 48.93; IR (neat) $\bar{\nu}$ = 423, 447, 488, 503, 523, 539, 563, 571, 600, 652, 679, 711, 725, 735, 754, 775, 801, 817, 851, 890, 905, 1004, 1022, 1041, 1112, 1140, 1182, 1211, 1234, 1245, 1266, 1300, 1345, 1426, 1441, 1486, 1601, 2847, 2930, 3057, 3092, 3127 cm^{-1} ; HRMS *calcd.* for $\text{C}_{25}\text{H}_{35}\text{NO}_2\text{AuClP}$: 644.175399; *found*: 644.175860.



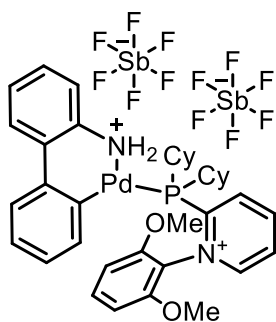
Compound **191f**: Prepared from phosphine **190f** (100 mg, 0.16 mmol) and $\text{Me}_2\text{S}\cdot\text{AuCl}$ (45.5 mg, 0.16 mmol) following the general procedure. White solid (131 mg, 96%).

^1H NMR (400 MHz, CDCl_3) δ = 8.97 (t, J = 7.2 Hz, 1H), 8.57 (d, J = 4.4 Hz, 1H), 8.53 (d, J = 3.5 Hz, 1H), 8.40 (t, J = 6.2 Hz, 1H), 7.13 (s, 2H), 2.49 – 2.33 (m, 5H), 1.95 (d, J = 11.0 Hz, 2H), 1.88 (s, 6H),

1.85 – 1.60 (m, 8H), 1.47 (ddd, $J = 10.5, 9.5, 5.8$ Hz, 2H), 1.39 – 1.26 (m, 6H), 1.21 (ddd, $J = 16.1, 10.6, 6.9$ Hz, 2H); ^{13}C NMR (126 MHz, CD_3CN) $\delta = 153.2, 148.73$ (d, $J = 35.4$ Hz), 148.71 (d, $J = 3.9$ Hz), 144.2, 139.1 (d, $J = 3.6$ Hz), 136.4 (d, $J = 4.4$ Hz), 134.0, 132.2 (d, $J = 0.9$ Hz), 132.1, 37.6 (d, $J = 28.8$ Hz), 32.1 (d, $J = 1.9$ Hz), 30.6 (d, $J = 3.0$ Hz), 27.1 (d, $J = 14.4$ Hz), 26.9 (d, $J = 14.5$ Hz), 25.9 (d, $J = 1.8$ Hz), 21.5, 18.5; ^{31}P NMR (162 MHz, CD_3CN) $\delta = 46.35$; IR (neat) $\bar{\nu} = 416, 438, 454, 484, 500, 513, 524, 562, 582, 655, 783, 862, 1003, 1138, 1228, 1432, 1449, 1477, 1601, 2858, 2935$ cm^{-1} ; HRMS *calcd.* for $\text{C}_{25}\text{H}_{37}\text{NAuClP}$: 626.201219; *found*: 626.202080.

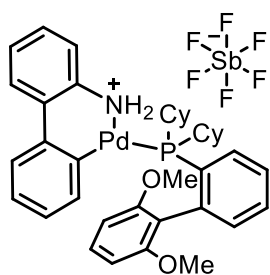
General Procedure for the synthesis of phosphine palladium complexes 196-197:

THF (2 ml/mmol) was added to a mixture of the carefully dried phosphine (1 equiv.), NaSbF_6 (3 equiv.) and the palladium precursor [1,1'-biphenyl]-2-amine-palladium-mesylate-dimer (**220**, 0.5 equiv.)¹¹⁷ at -20°C . After stirring for 2 hours the solvent was removed at -20°C in vacuo. DCM was added and the solution obtained filtered at -20°C . Removal of the solvent in vacuo at -20°C afforded the desired product.



Compound **196**: Prepared from phosphine **191e** (100 mg, 0.154 mmol) and palladium precursor **220**¹¹⁷ (57 mg, 0.077 mmol) following the general procedure. White solid (96.5 mg, 54%).

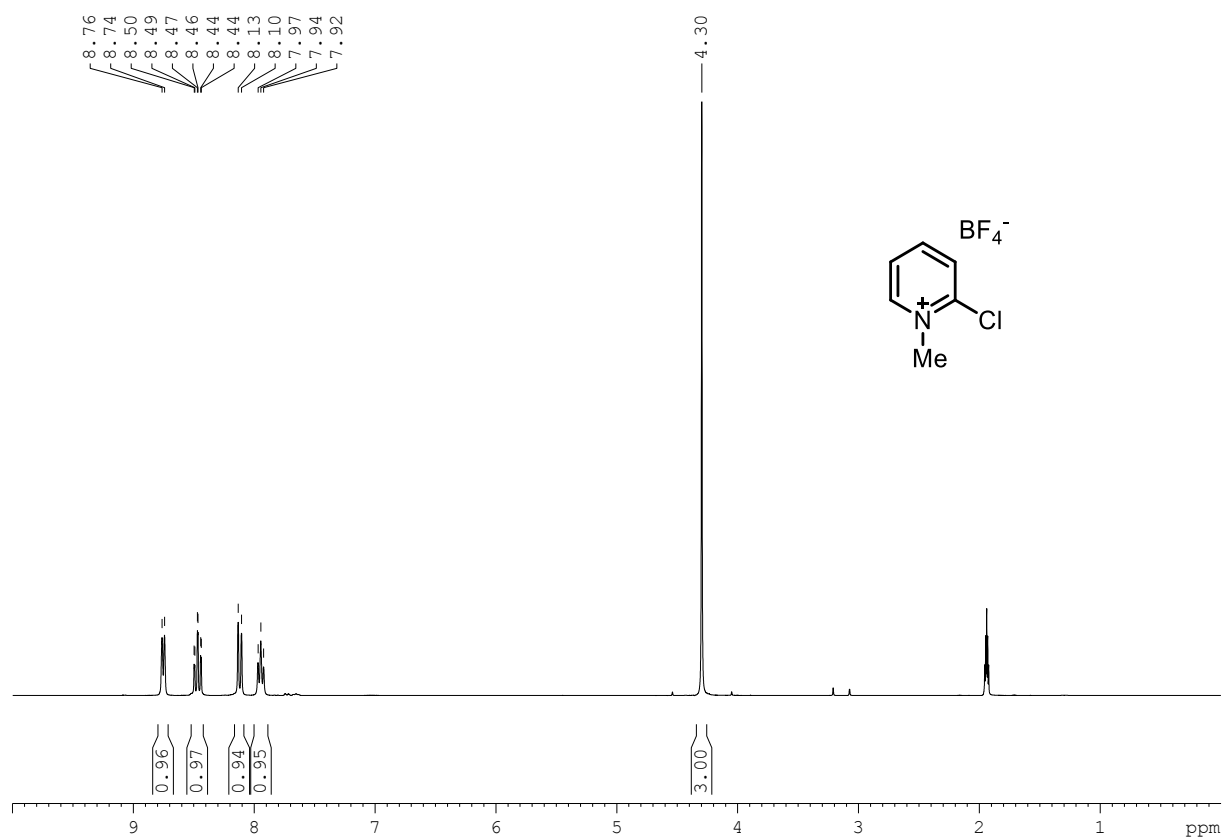
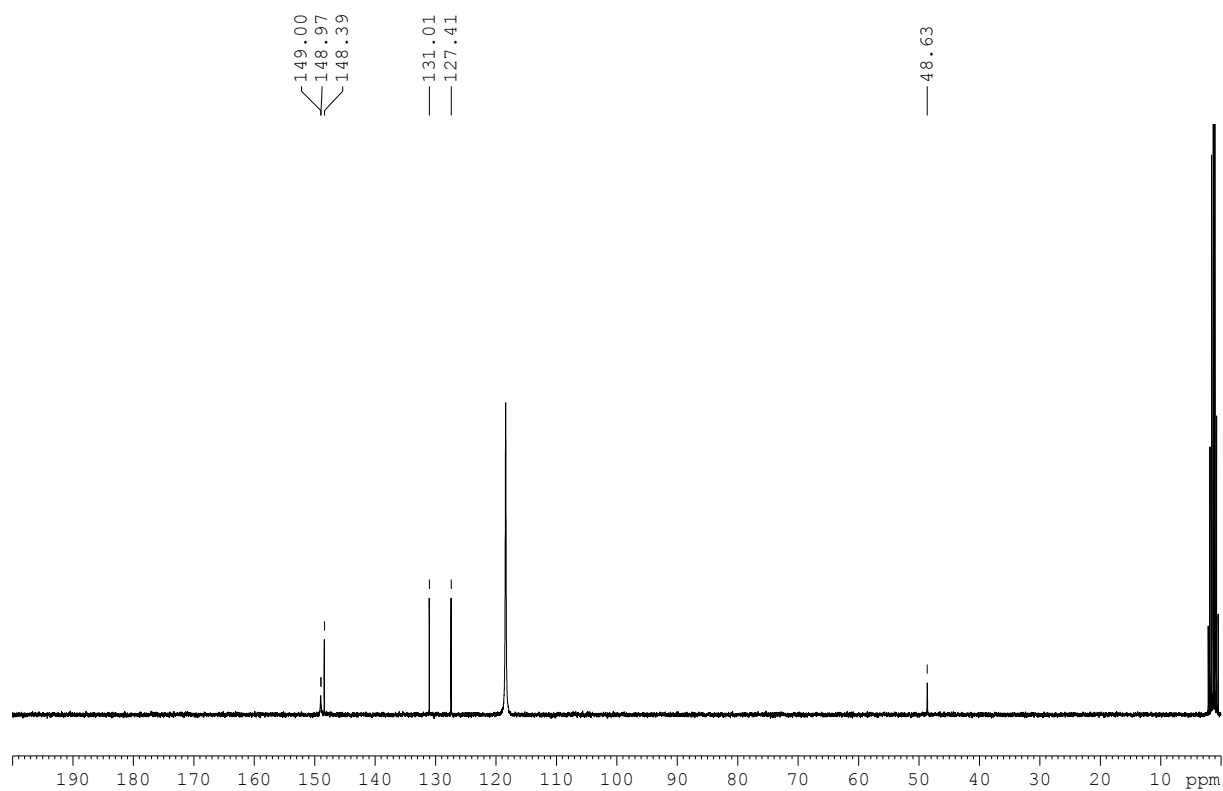
^1H NMR (400 MHz, CD_2Cl_2) $\delta = 8.84$ (dd, $J = 11.3, 4.1$ Hz, 1H), 8.54 (d, $J = 7.9$ Hz, 1H), 8.41 (t, $J = 8.5$ Hz, 1H), 8.35 – 8.27 (m, 2H), 7.60 (dd, $J = 7.0, 2.1$ Hz, 1H), 7.40 – 7.27 (m, 5H), 7.15 (dd, $J = 11.2, 7.8$ Hz, 2H), 7.06 (d, $J = 8.4$ Hz, 1H), 7.01 (dd, $J = 7.7, 4.0$ Hz, 1H), 5.17 (dd, $J = 10.2, 4.6$ Hz, 1H), 4.10 (s, 3H), 3.47 (s, 3H), 2.66 (t, $J = 11.7$ Hz, 1H), 2.42 – 2.24 (m, 2H), 2.17 – 1.97 (m, 3H), 1.83 (d, $J = 12.9$ Hz, 1H), 1.64 – 1.38 (m, 6H), 1.28 – 1.02 (m, 7H), 0.92 – 0.74 (m, 2H), -0.14 – -0.29 (m, 1H); ^{31}P NMR (162 MHz, CD_3CN) $\delta = 53.38$; IR (neat) $\bar{\nu} = 510, 520, 537, 565, 600, 651, 738, 761, 780, 819, 851, 892, 916, 938, 1001, 1018, 1045, 1111, 1152, 1182, 1215, 1268, 1302, 1433, 1449, 1484, 1570, 1581, 1603, 2855, 2930$ cm^{-1} ; HRMS *calcd.* for $\text{C}_{37}\text{H}_{45}\text{N}_2\text{O}_2\text{F}_6\text{SbPPd}$: 921.118882; *found*: 921.119940.

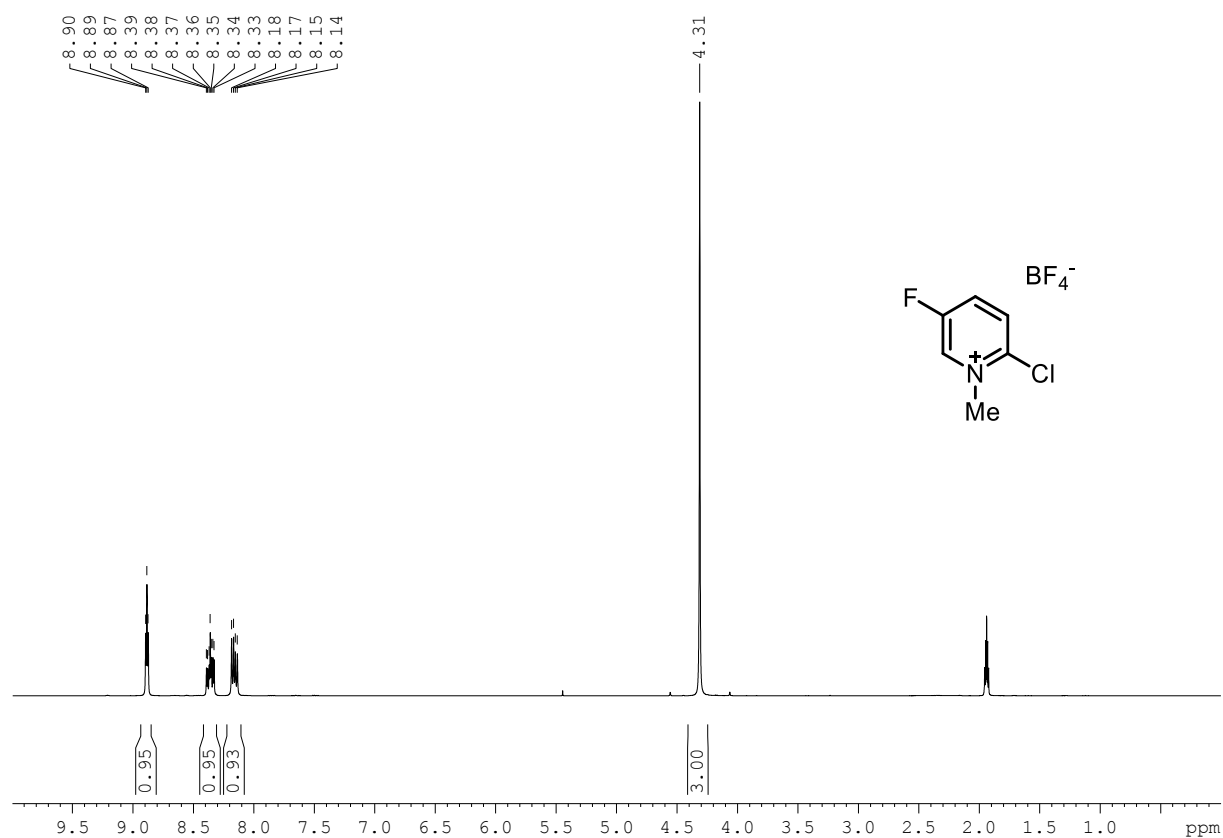
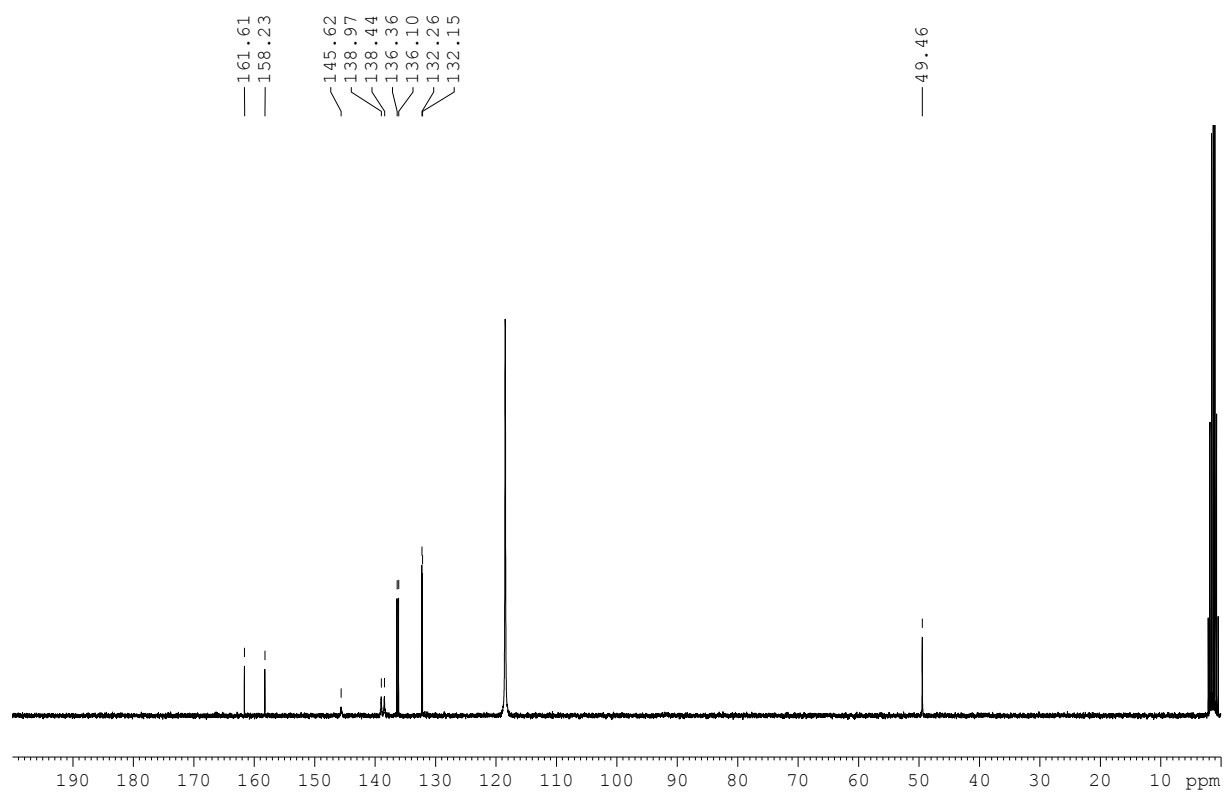


Compound **197**: Prepared from phosphine **22** (100 mg, 0.24 mmol) and palladium precursor **220**¹¹⁷ (89.9 mg, 0.12 mmol) following the general procedure. White solid (114 mg, 51%).

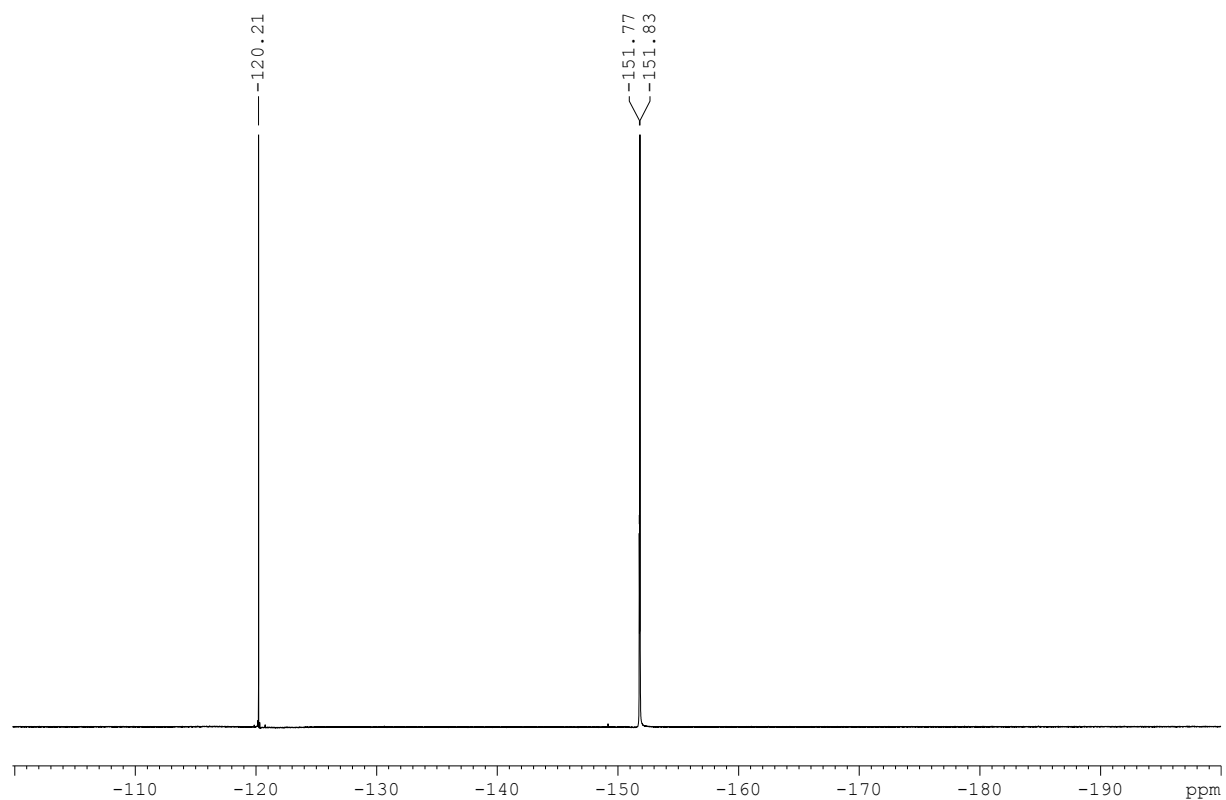
¹H NMR (400 MHz, CD₂Cl₂) δ = 8.08 (t, J = 8.4 Hz, 1H), 7.66 (td, J = 7.3, 1.2 Hz, 1H), 7.56 – 7.42 (m, 3H), 7.31 – 7.23 (m, 4H), 7.23 – 7.17 (m, 1H), 7.12 (dd, J = 7.0, 1.9 Hz, 1H), 7.05 (dt, J = 6.5, 2.1 Hz, 1H),

6.89 (ddd, J = 8.5, 3.6, 0.8 Hz, 2H), 6.86 – 6.82 (m, 1H), 4.70 – 4.56 (m, 1H), 3.91 (s, 3H), 3.35 (s, 3H), 2.42 (dd, J = 10.9, 8.3 Hz, 1H), 2.19 (t, J = 10.5 Hz, 1H), 2.07 – 1.87 (m, 4H), 1.85 – 1.48 (m, 5H), 1.46 – 1.32 (m, 3H), 1.28 – 1.07 (m, 4H), 1.01 (ddd, J = 17.2, 13.0, 3.7 Hz, 2H), 0.91 – 0.72 (m, 2H), -0.09 – -0.23 (m, 1H); ¹³C NMR (126 MHz, CD₂Cl₂) δ = 163.1 (d, J = 146.3 Hz), 143.0 (d, J = 18.1 Hz), 141.2, 140.3, 139.9, 136.2 (d, J = 3.3 Hz), 136.0 (d, J = 6.5 Hz), 135.7, 135.5, 135.4, 132.7 (d, J = 2.7 Hz), 132.3, 131.9 (d, J = 11.5 Hz), 129.1 (d, J = 3.7 Hz), 128.9, 128.2 (d, J = 6.0 Hz), 128.1, 127.9, 127.7, 126.8, 120.6, 106.2 (d, J = 4.1 Hz), 105.6, 105.3, 56.8, 56.1, 36.0 (d, J = 30.6 Hz), 31.1 (d, J = 25.4 Hz), 30.6 (d, J = 4.0 Hz), 29.4 (d, J = 5.0 Hz), 28.2 (d, J = 9.1 Hz), 28.1, 27.8 (d, J = 8.2 Hz), 27.0, 26.9 (d, J = 2.7 Hz), 26.5, 26.3, 25.9; ³¹P NMR (162 MHz, CD₃CN) δ = 44.83; IR (neat) $\bar{\nu}$ = 506, 521, 539, 565, 597, 615, 641, 656, 741, 759, 774, 782, 851, 893, 1001, 1018, 1044, 1104, 1255, 1296, 1427, 1447, 1469, 1493, 1458, 1583, 2852, 2928, 3261, 3319 cm⁻¹; HRMS *calcd.* for C₃₈H₄₅NO₂PPd: 684.221640; *found*: 684.221440.

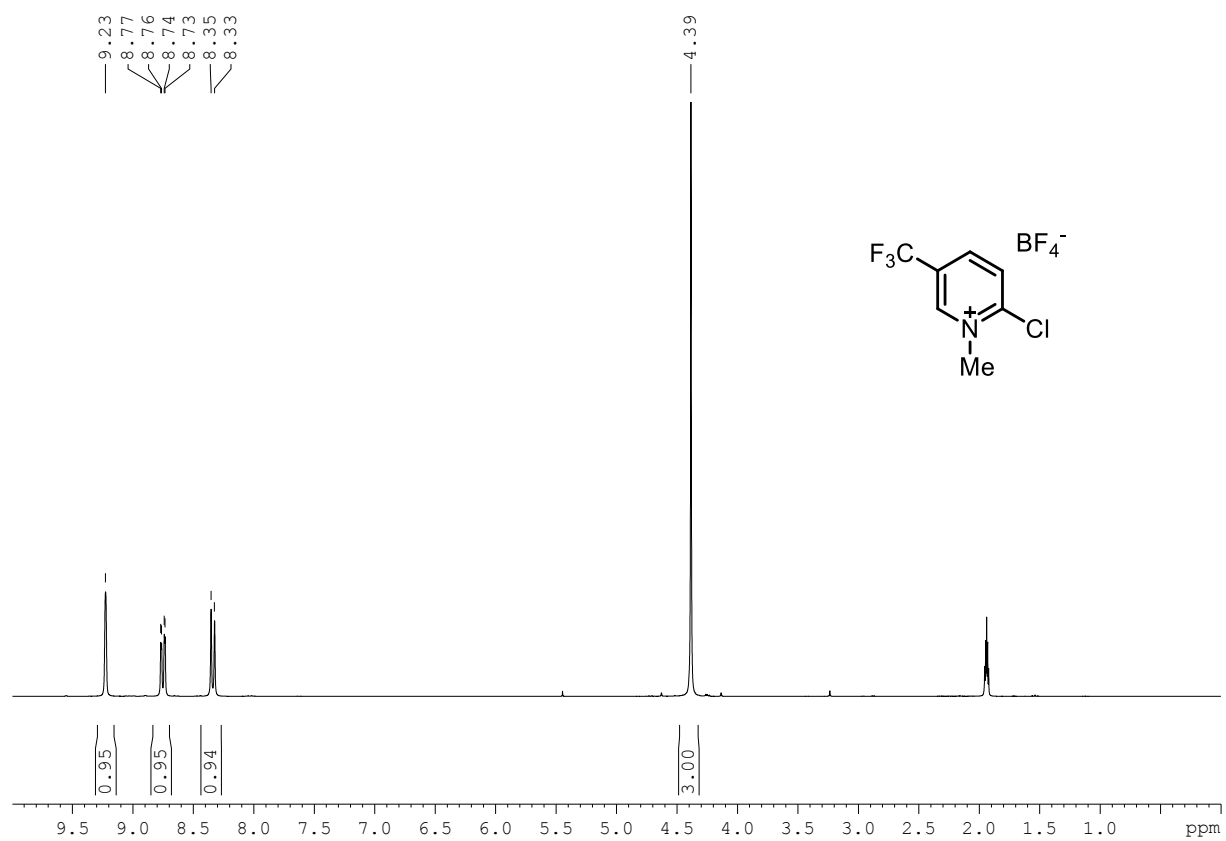
Compound 127a: $^1\text{H-NMR}$ (300 MHz, CD_3CN)**Compound 127a:** $^{13}\text{C-NMR}$ (75 MHz, CD_3CN)

Compound 127b: $^1\text{H-NMR}$ (300 MHz, CD_3CN)**Compound 127b:** $^{13}\text{C-NMR}$ (75 MHz, CD_3CN)

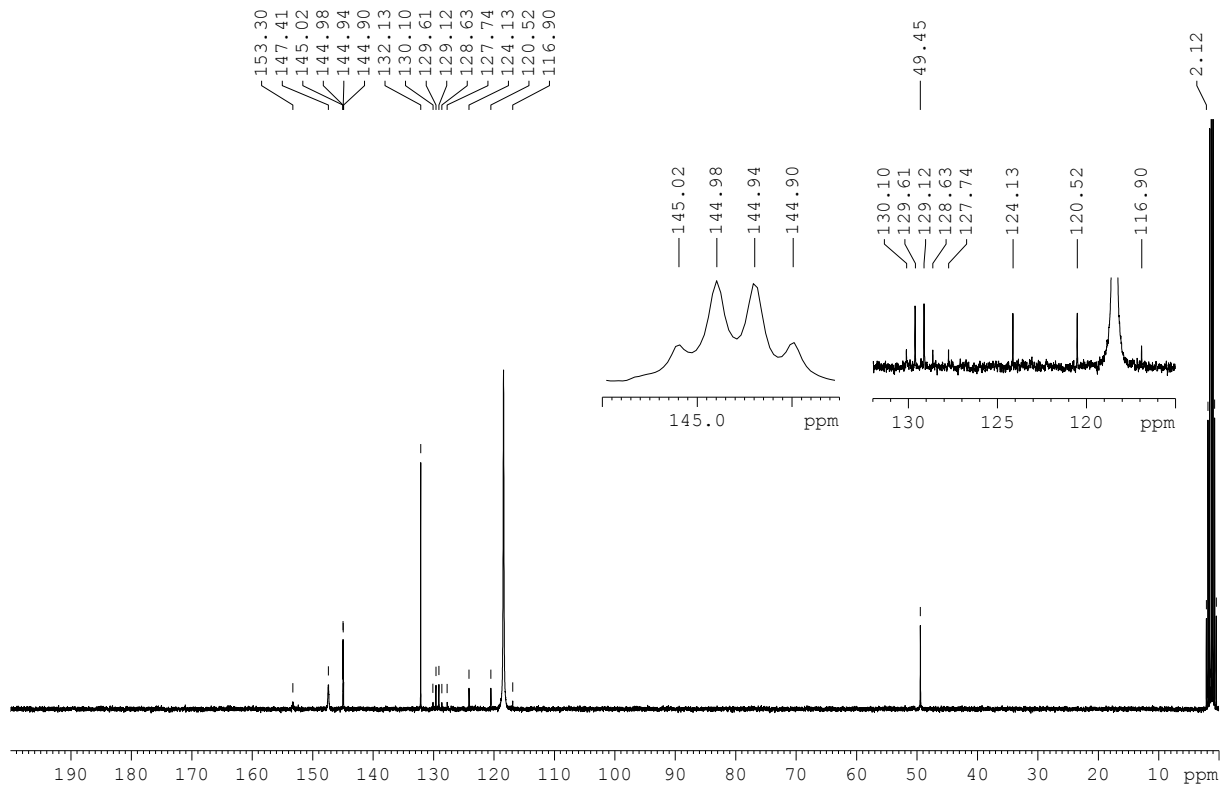
Compound 127b: ^{19}F NMR (282 MHz, CD_3CN)



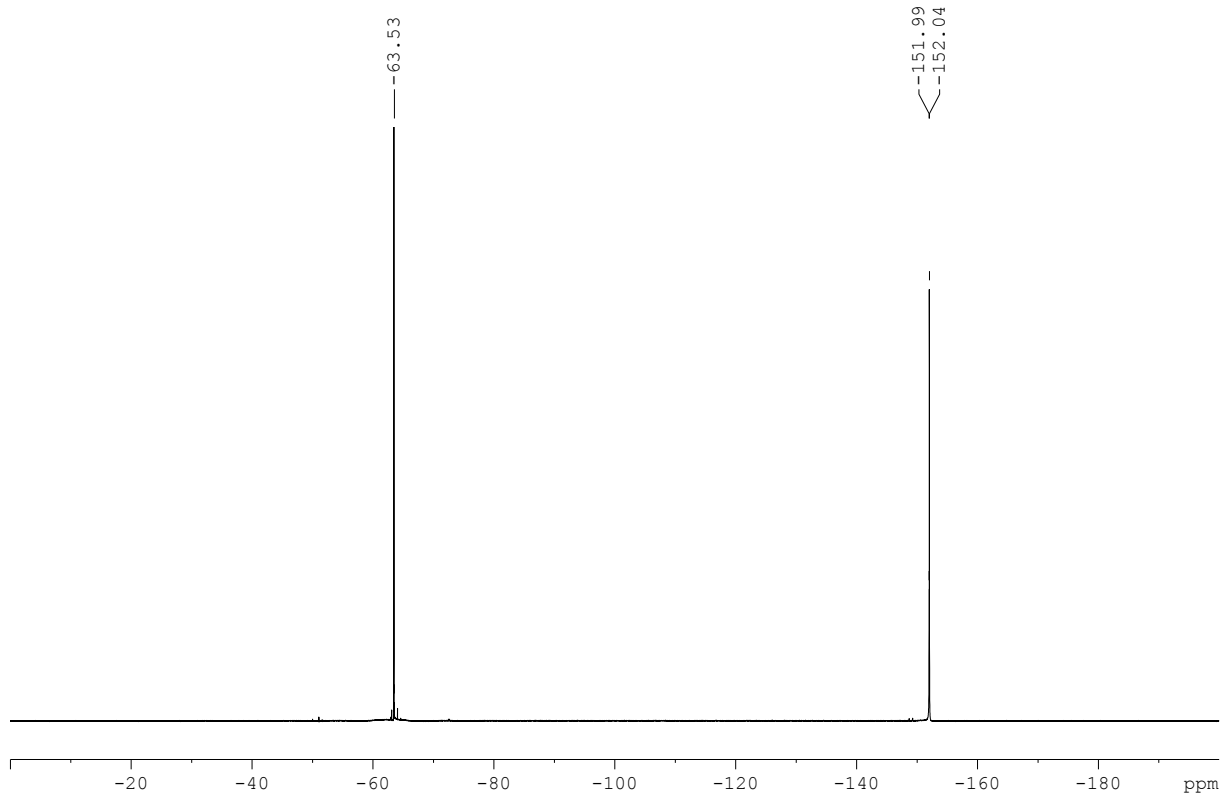
Compound 127c: ^1H -NMR (300 MHz, CD_3CN)



Compound 127c: ^{13}C NMR (75 MHz, CD_3CN)



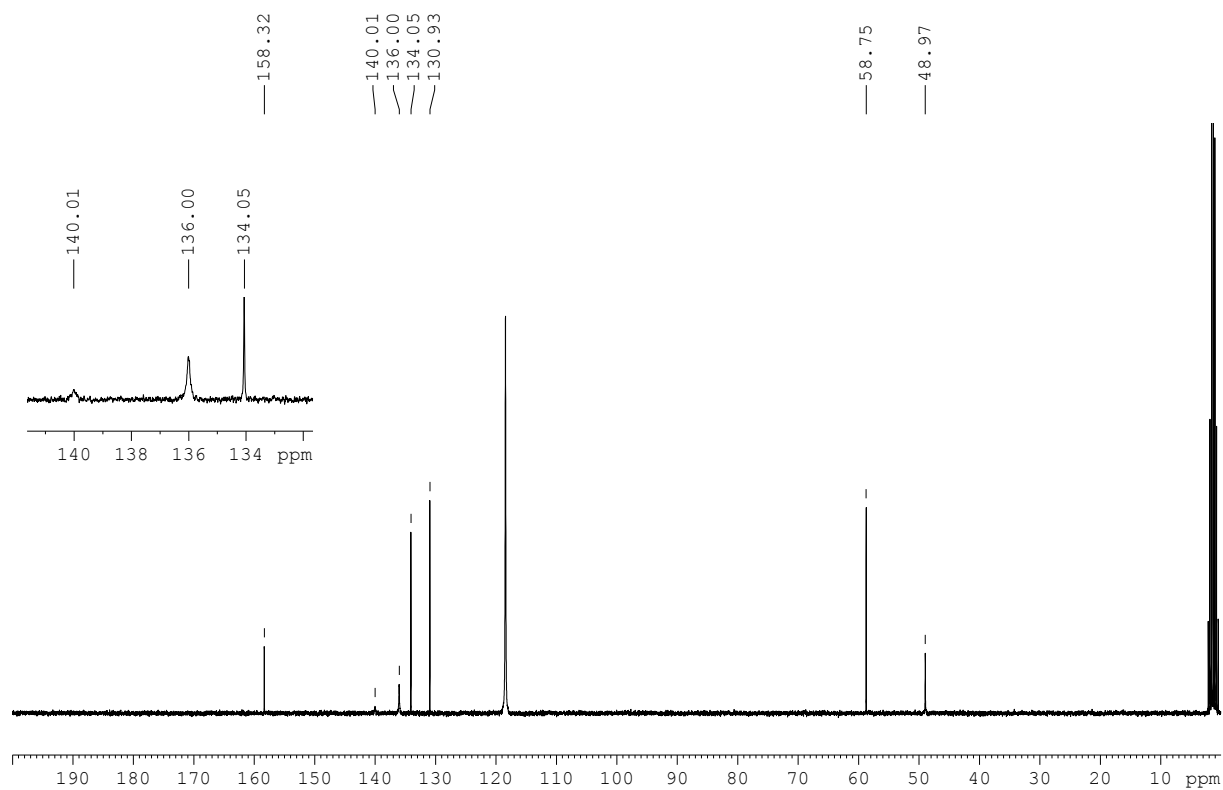
Compound 127c: ^{19}F NMR (282 MHz, CD_3CN)



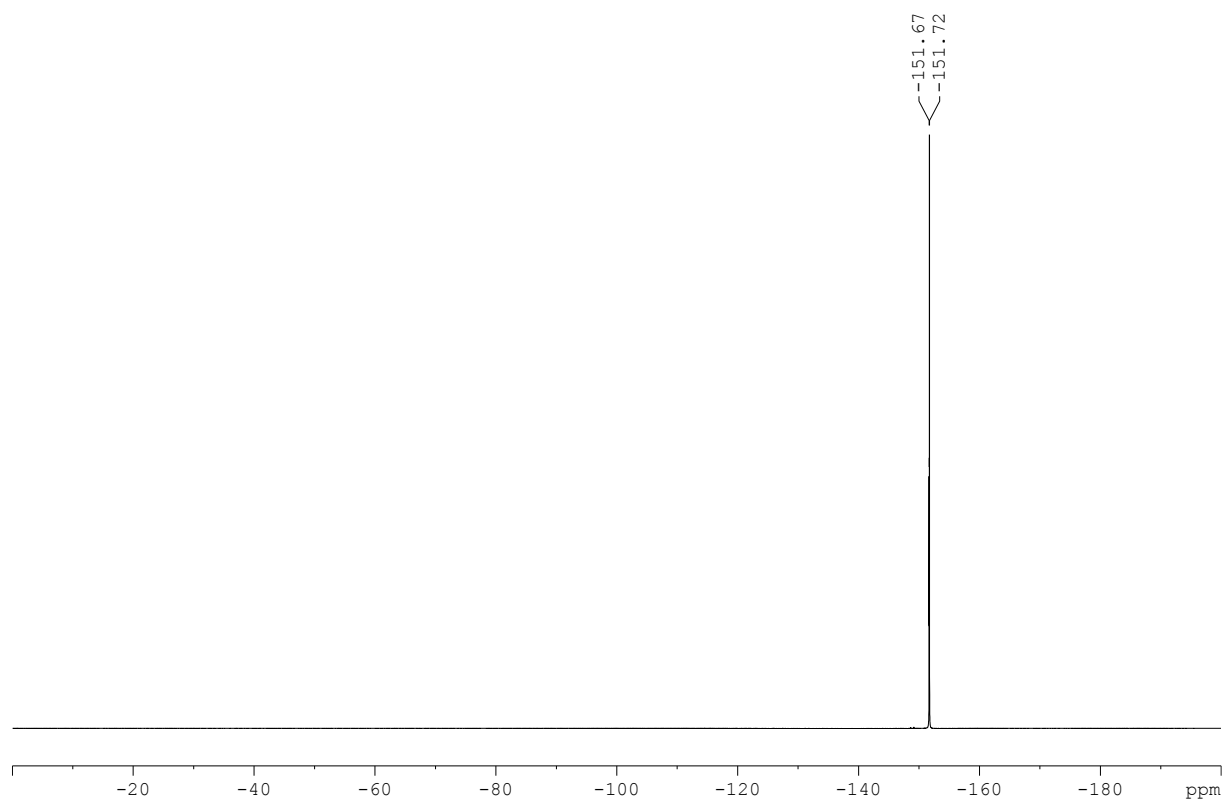
Compound 127d: $^1\text{H-NMR}$ (300 MHz, CD_3CN)



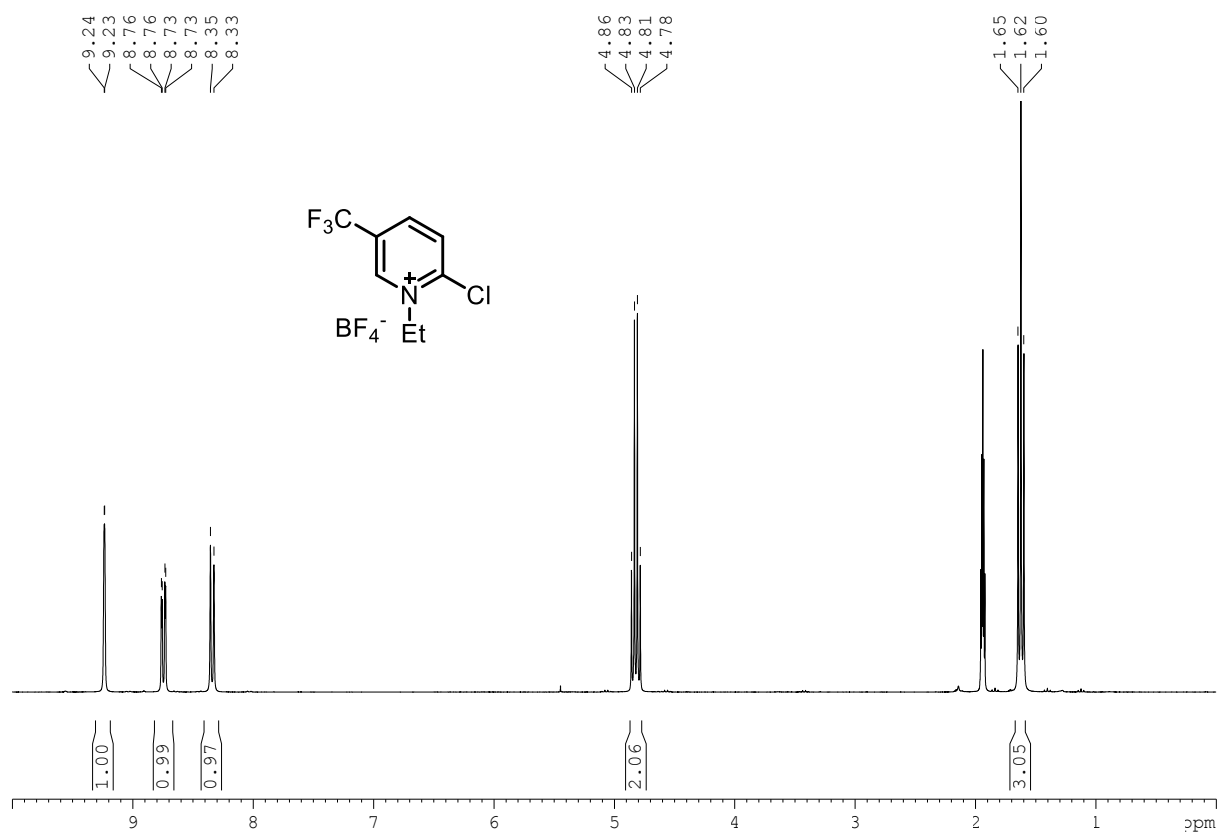
Compound 127d: $^{13}\text{C-NMR}$ (75 MHz, CD_3CN)



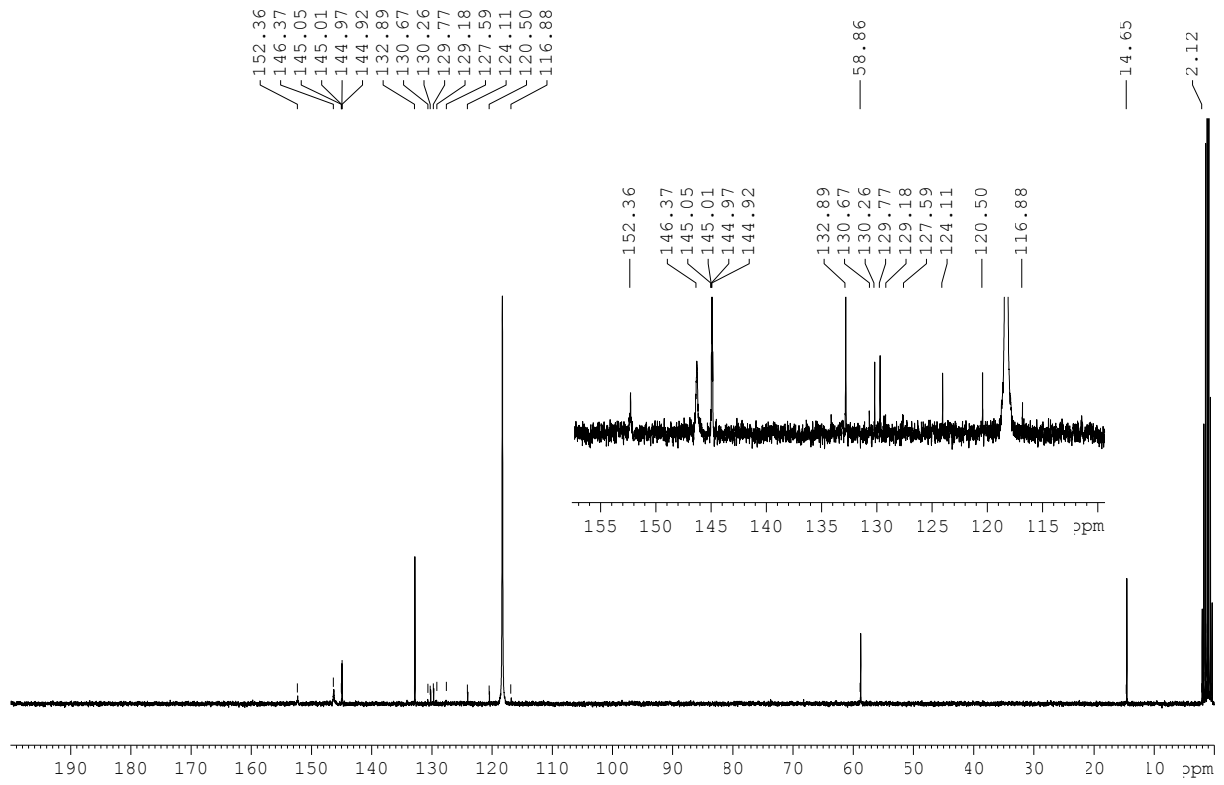
Compound 127d: ^{19}F NMR (282 MHz, CD_3CN)



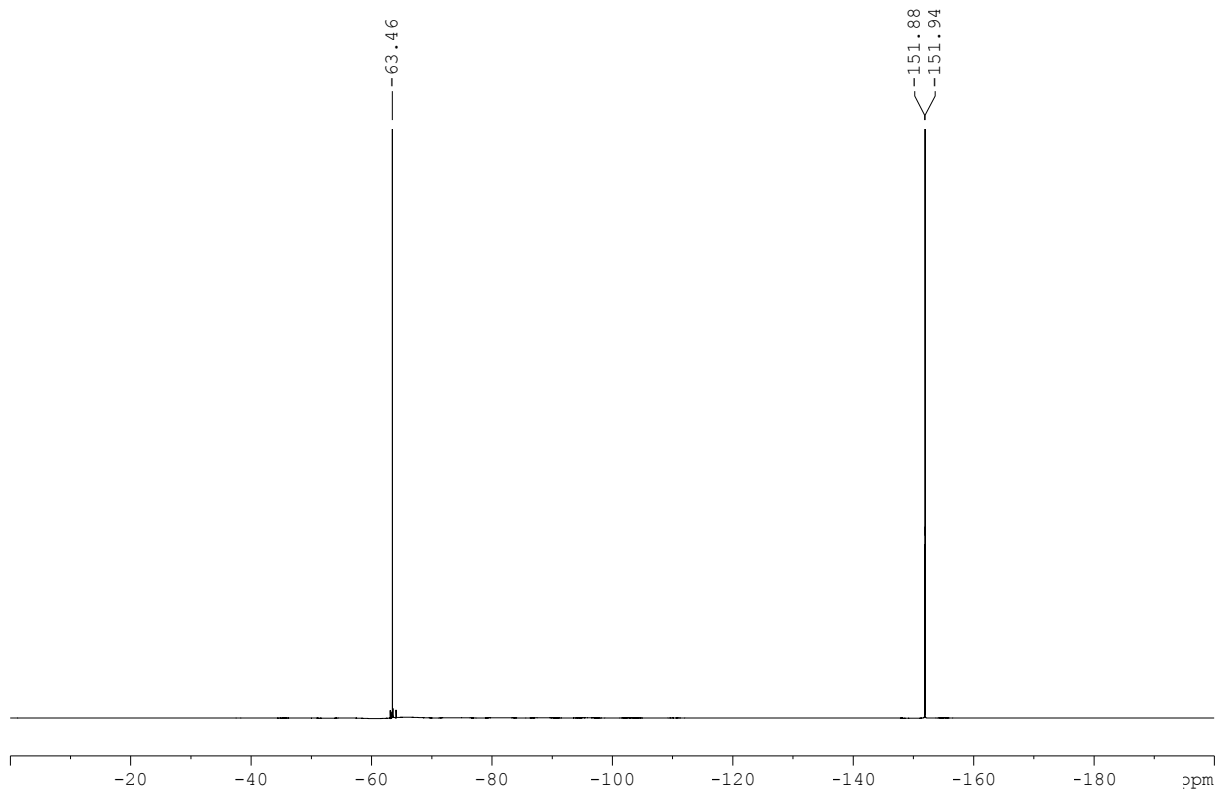
Compound 129a: ^1H NMR (300 MHz, CD_3CN)



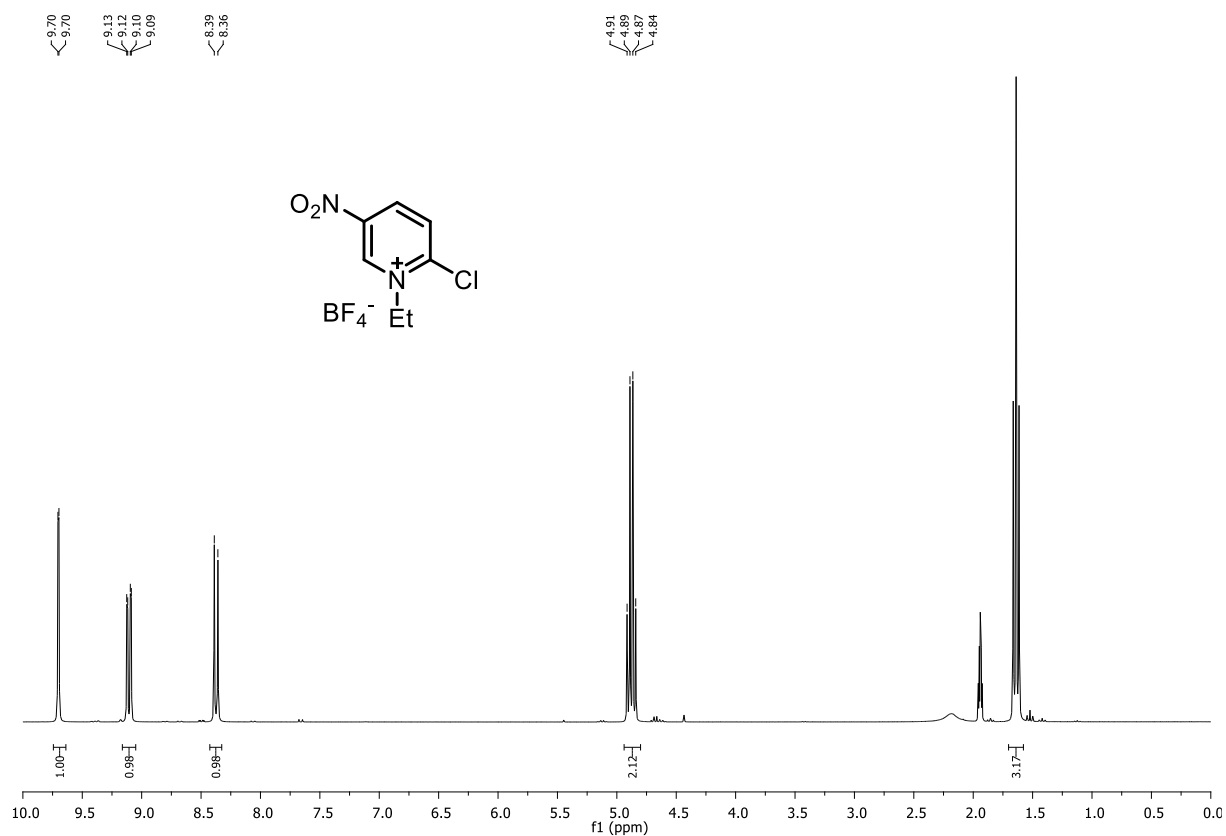
Compound 129a: ^{13}C NMR (75 MHz, CD_3CN)



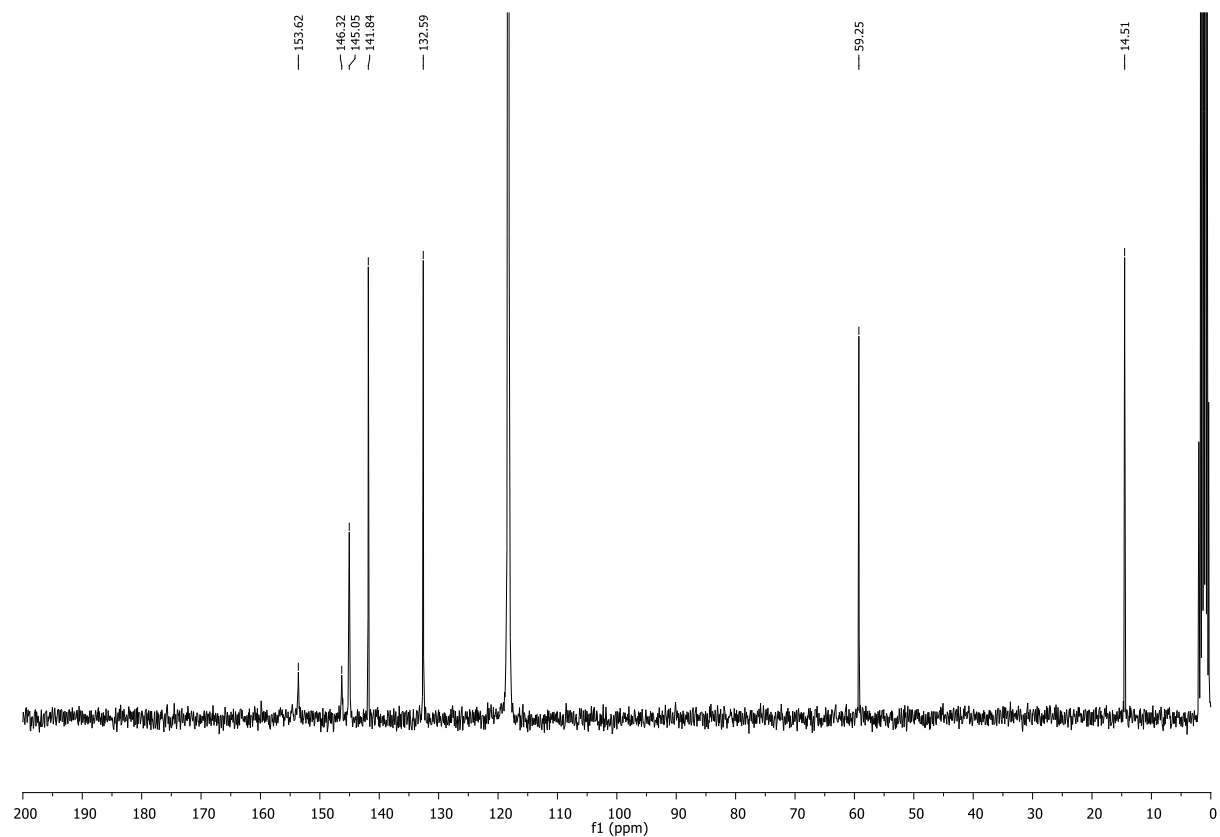
Compound 129a: ^{19}F NMR (282 MHz, CD_3CN)



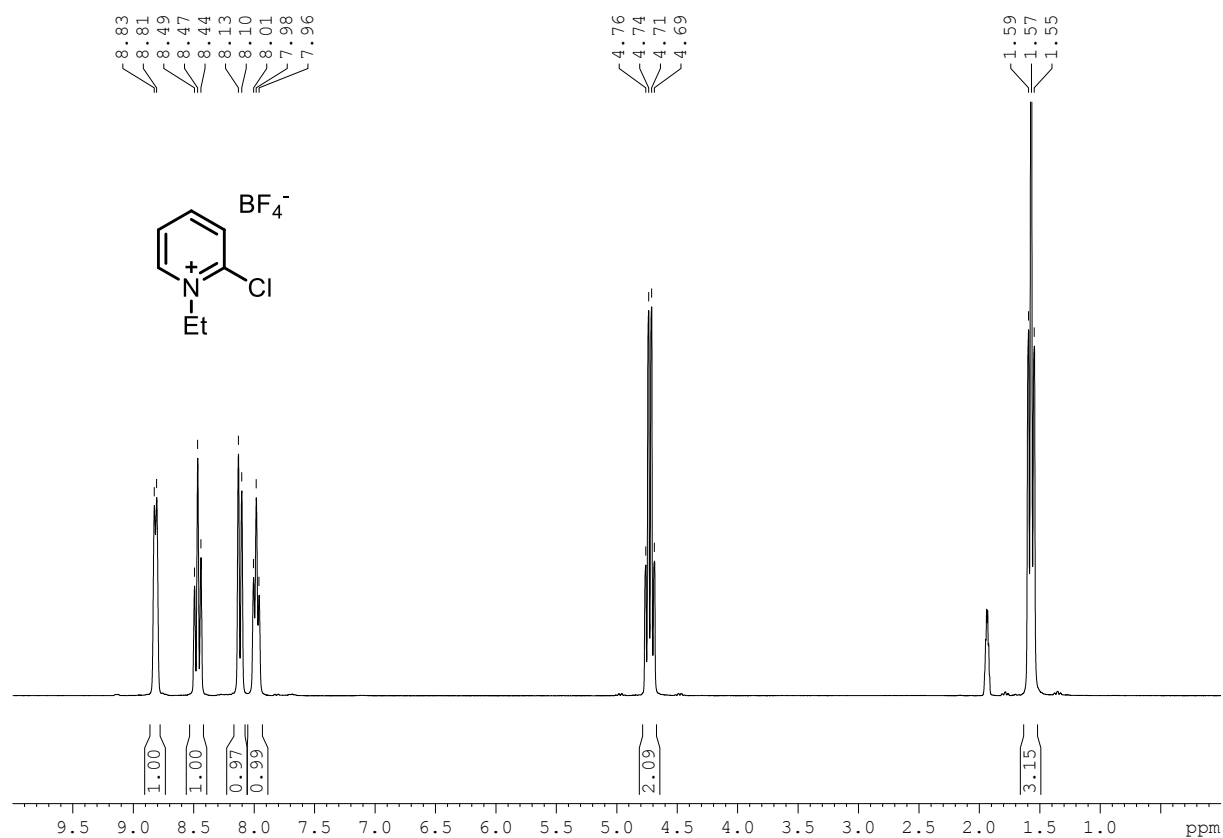
Compound 129b : ^1H NMR (300 MHz, CD_3CN)



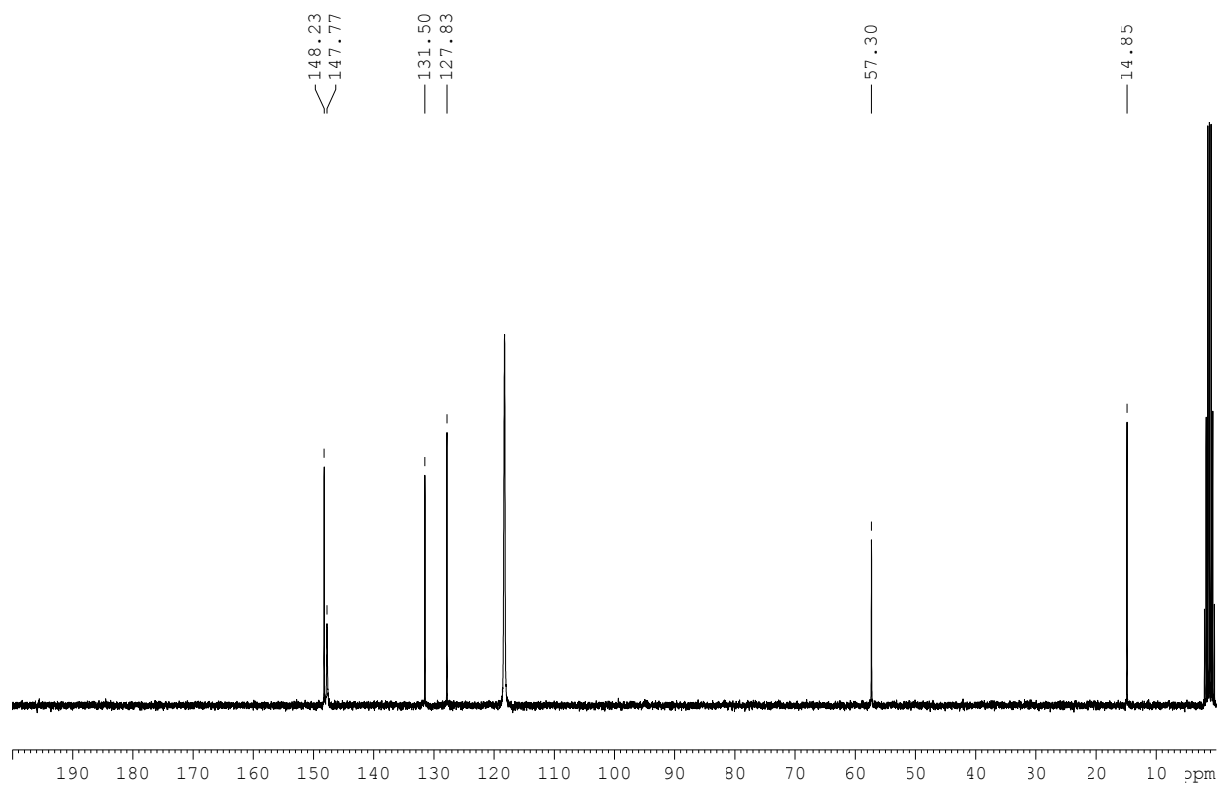
Compound 129b: ^1H NMR (300 MHz, CD_3CN)



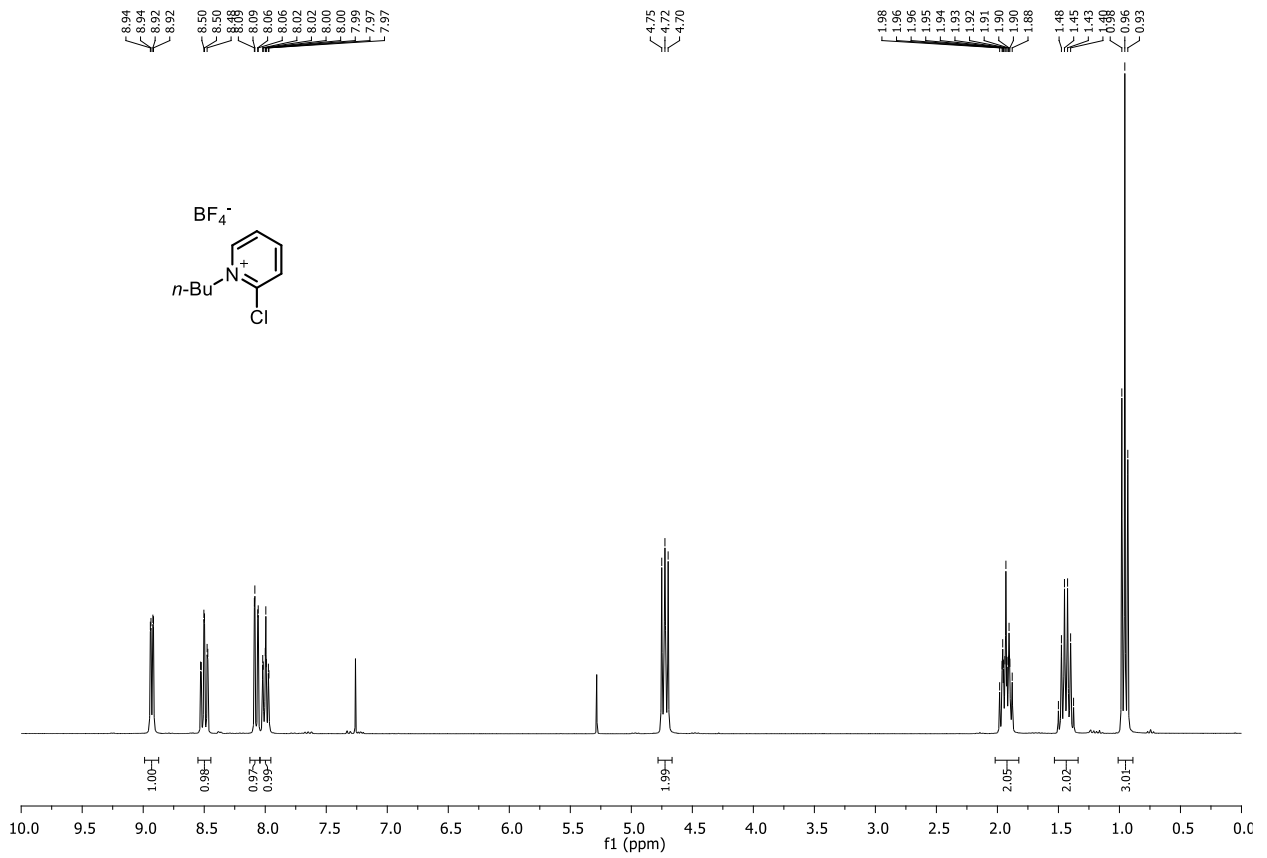
Compound 129c: ^1H NMR (300 MHz, CD_3CN)



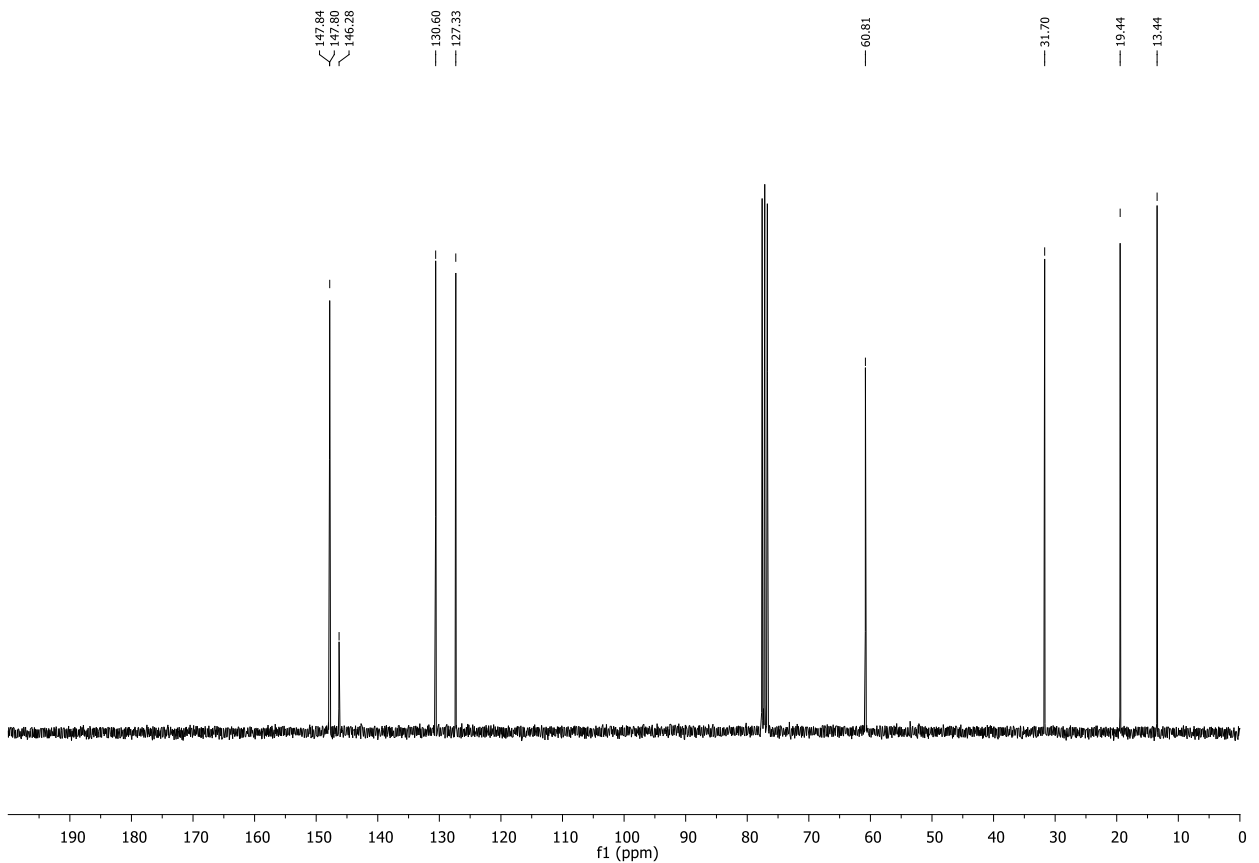
Compound 129c: ^{13}C NMR (75 MHz, CD_3CN)



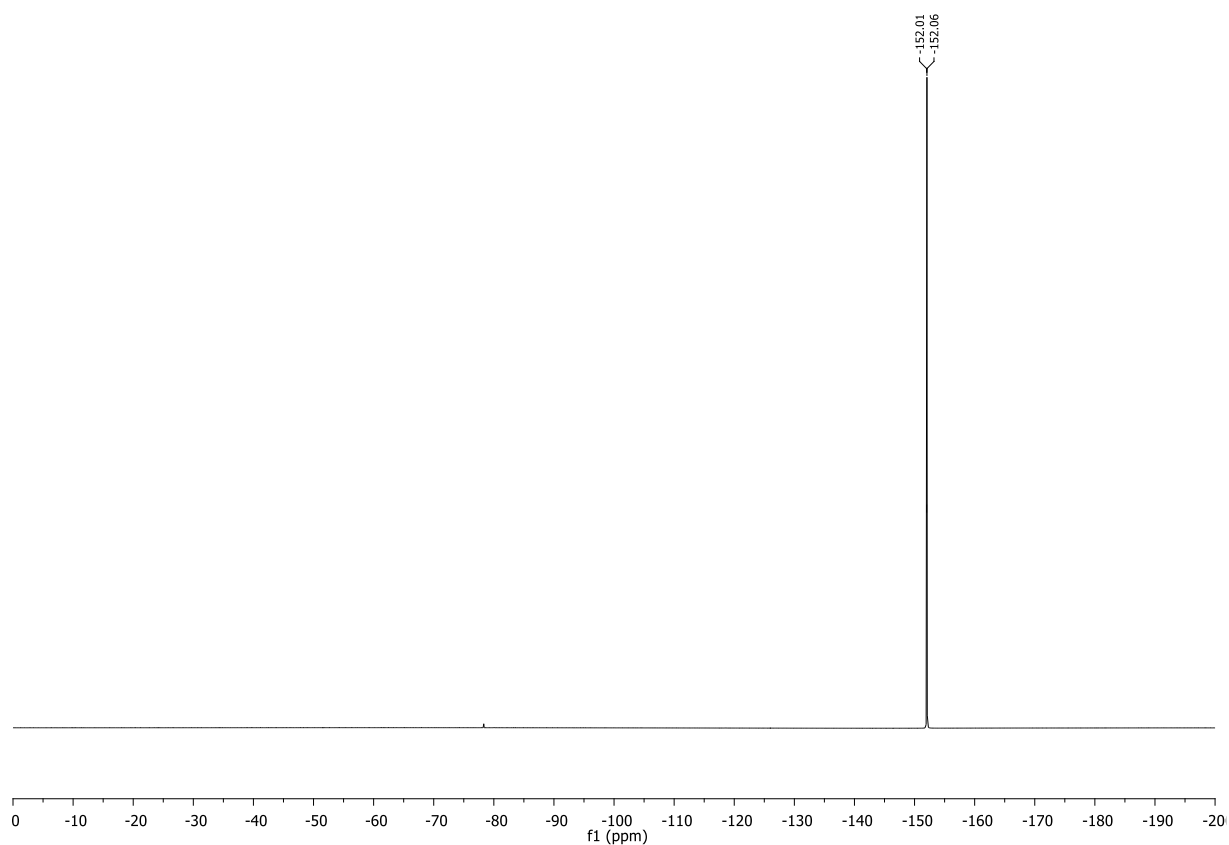
Compound 132a: ^1H NMR (300 MHz, CDCl_3)



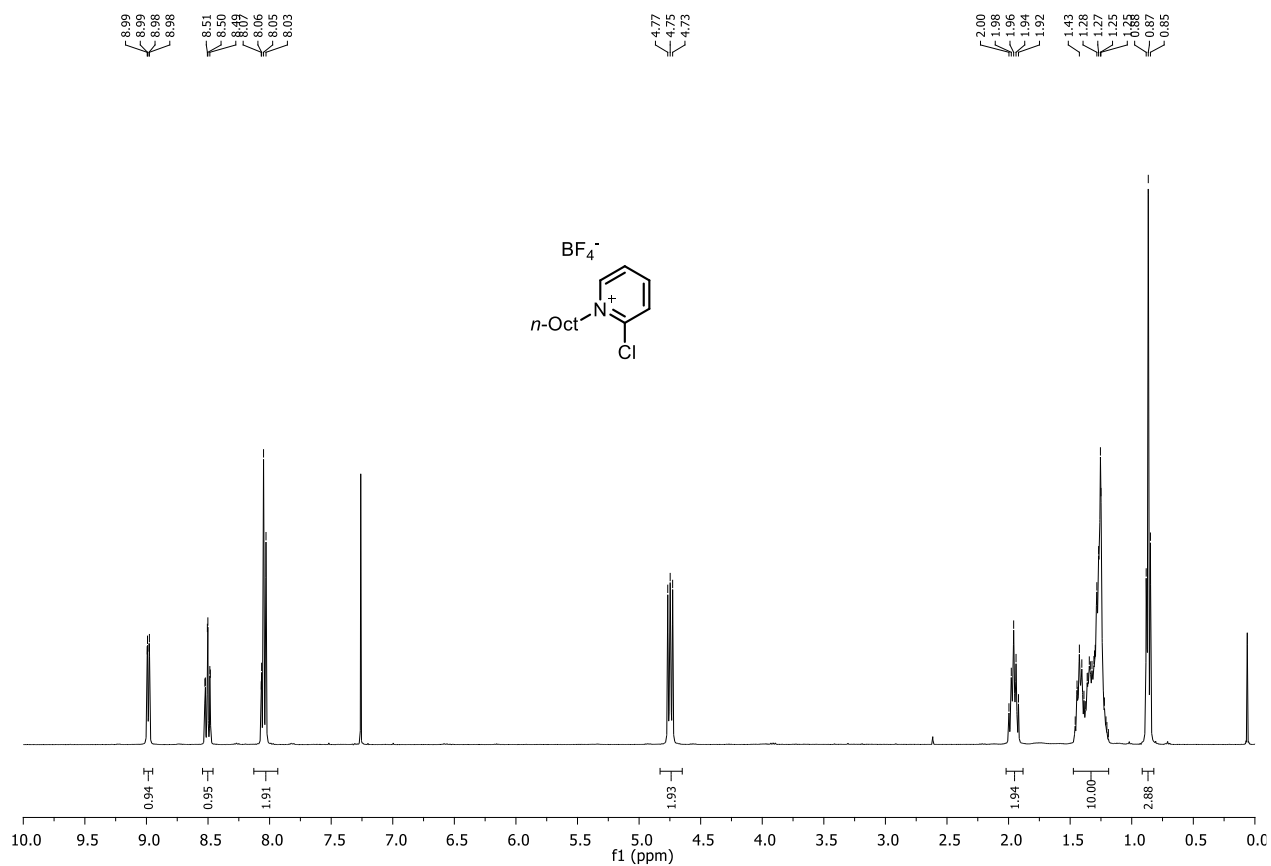
Compound 132a: ^{13}C NMR (75 MHz, CDCl_3)



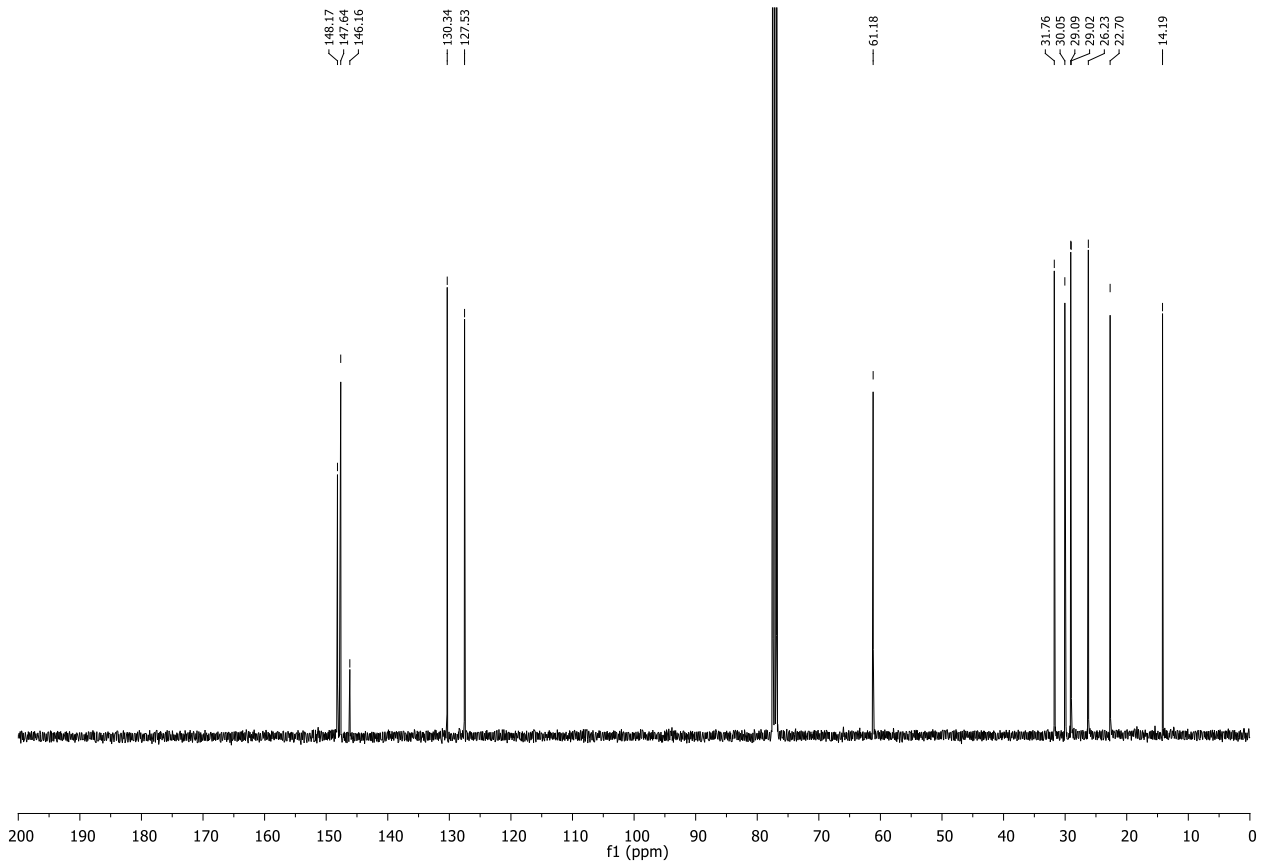
Compound 132a: ^{19}F NMR (282 MHz, CD_3CN)



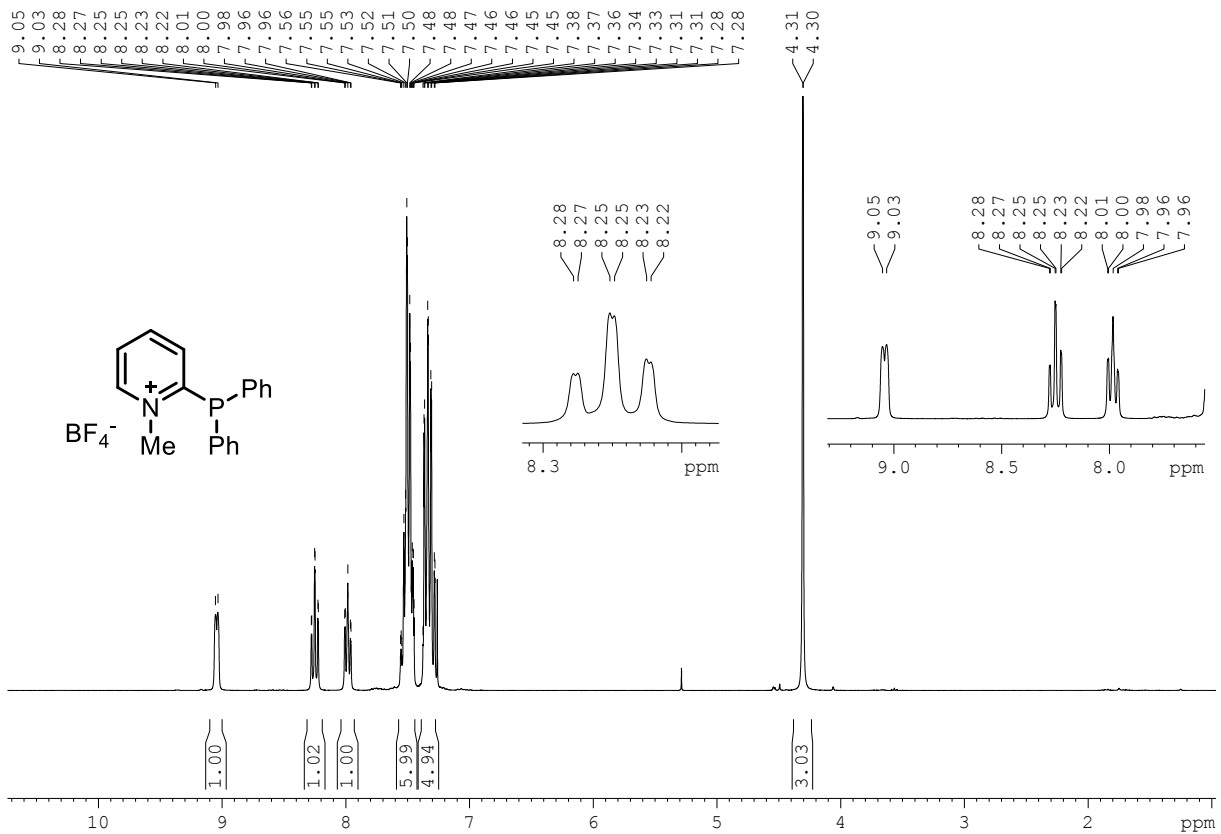
Compound 132b: ^1H NMR (300 MHz, CDCl_3)



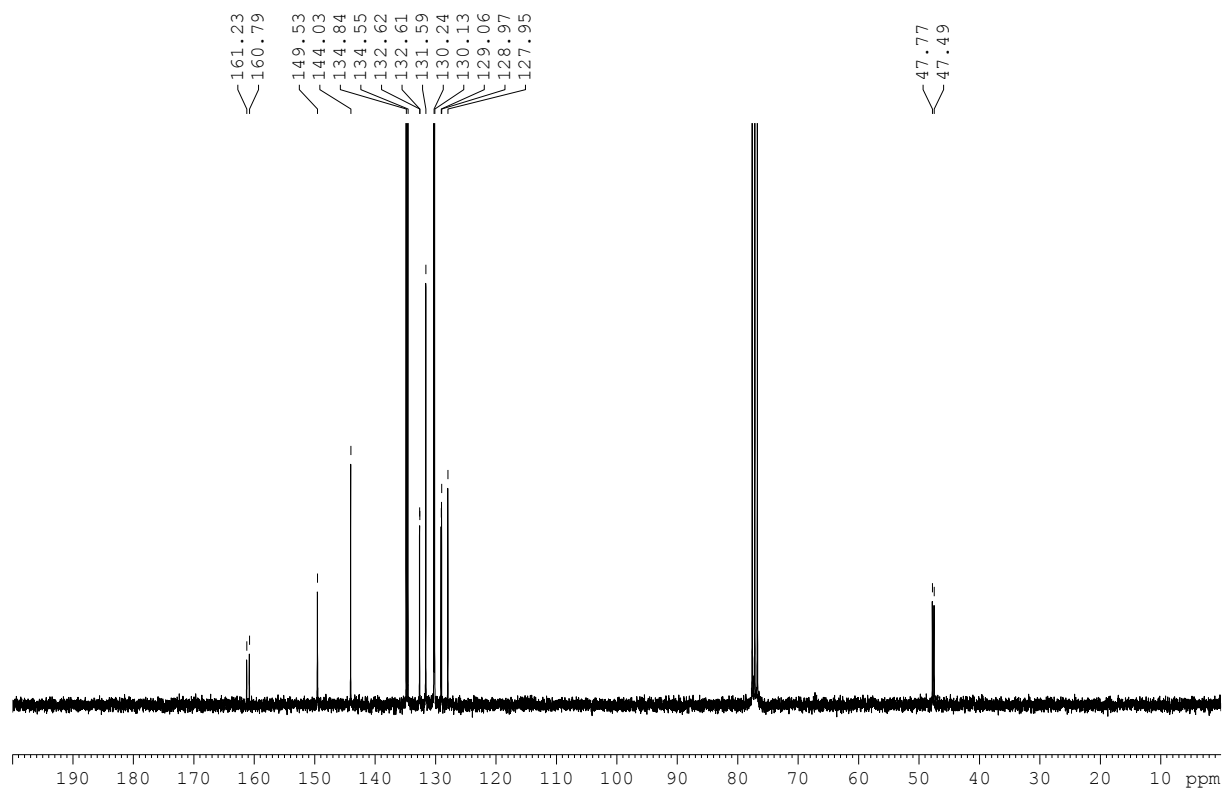
Compound 132b: ^{13}C NMR (75 MHz, CDCl_3)



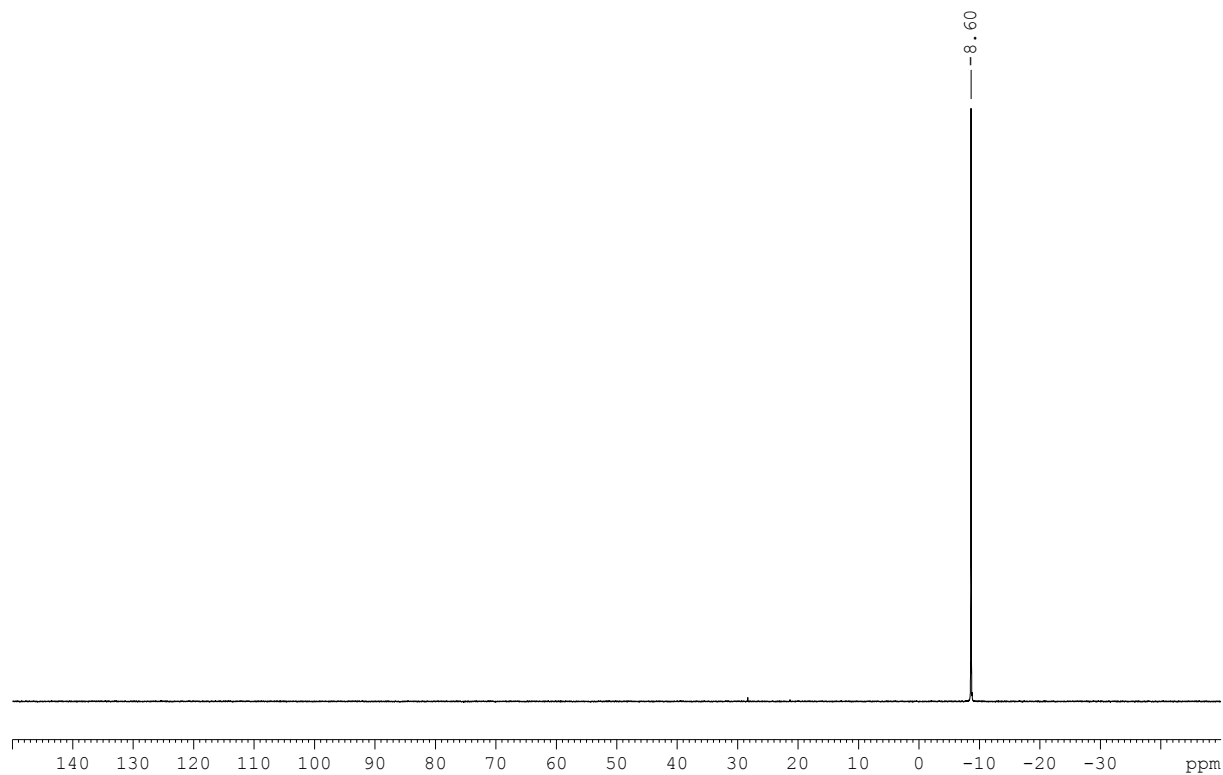
Compound 124a: ^1H NMR (300 MHz, CDCl_3)



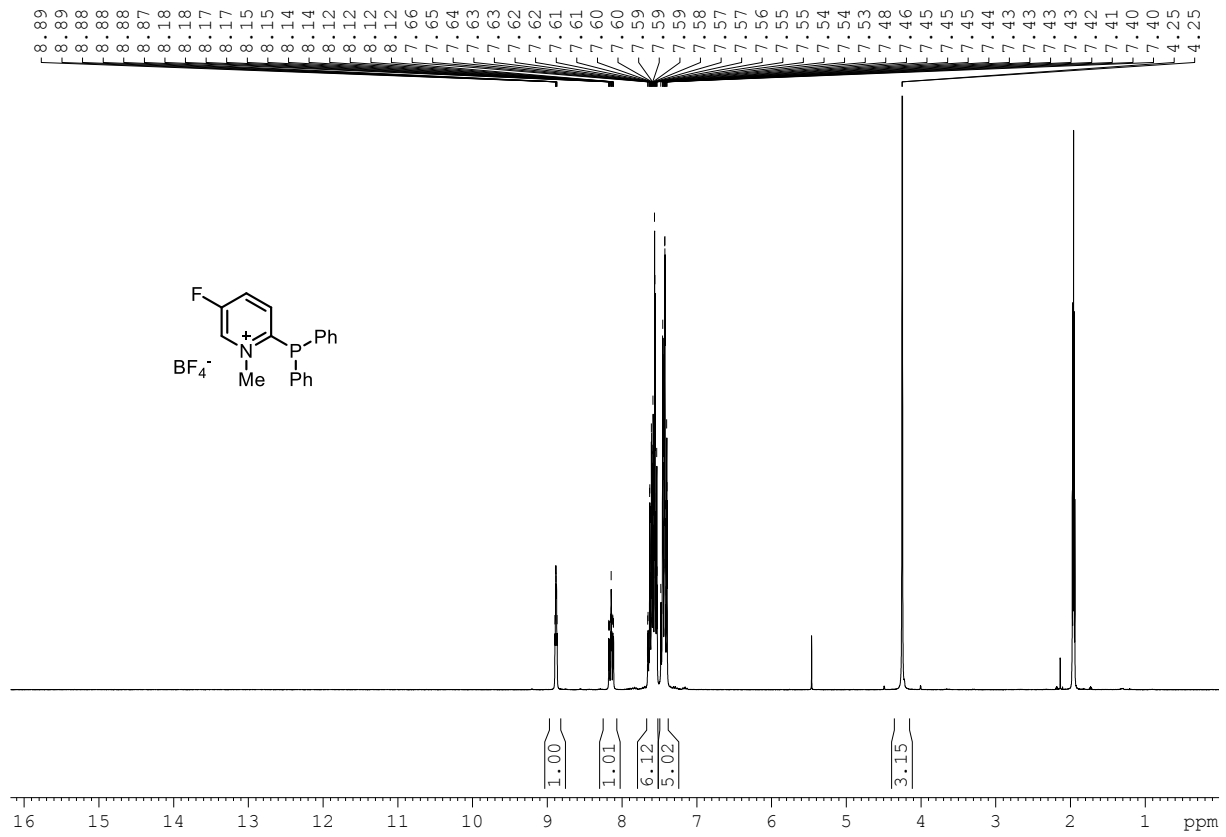
Compound 124a: ^{13}C NMR (75 MHz, CDCl_3)



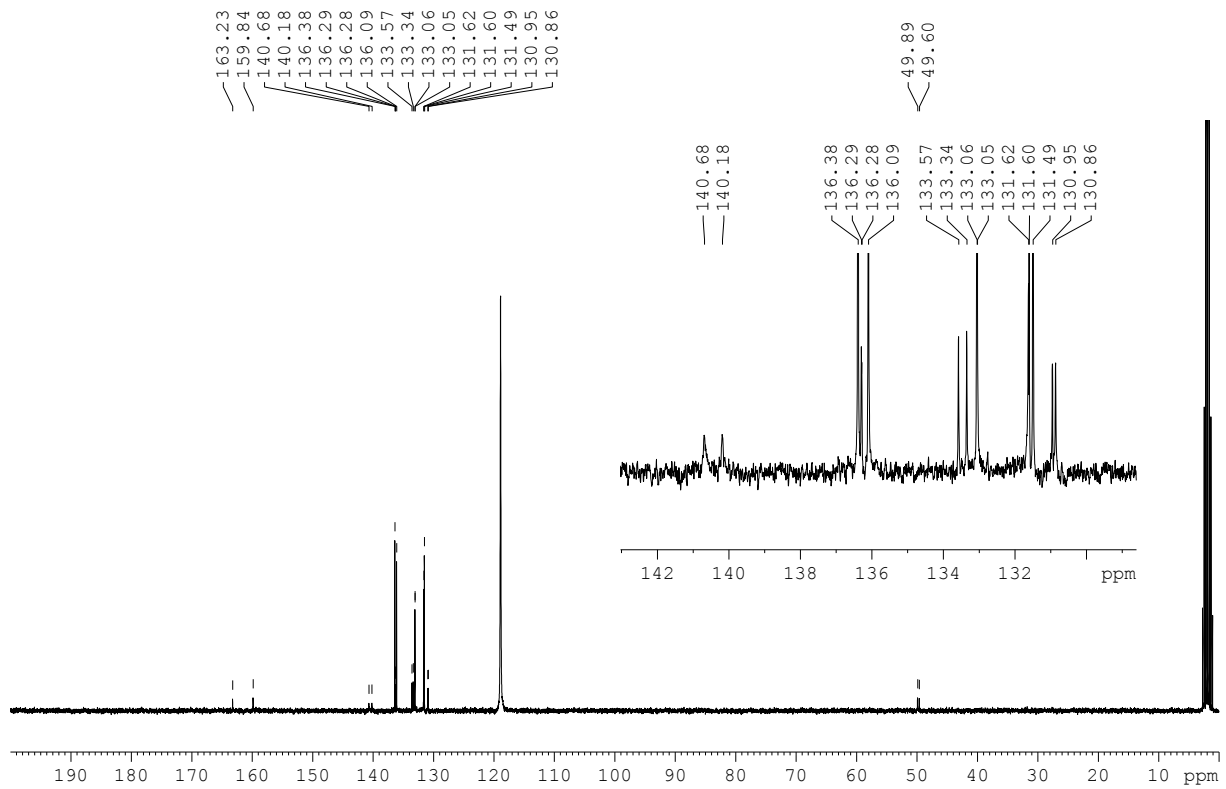
Compound 124a ^{31}P (121 MHz, CDCl_3):



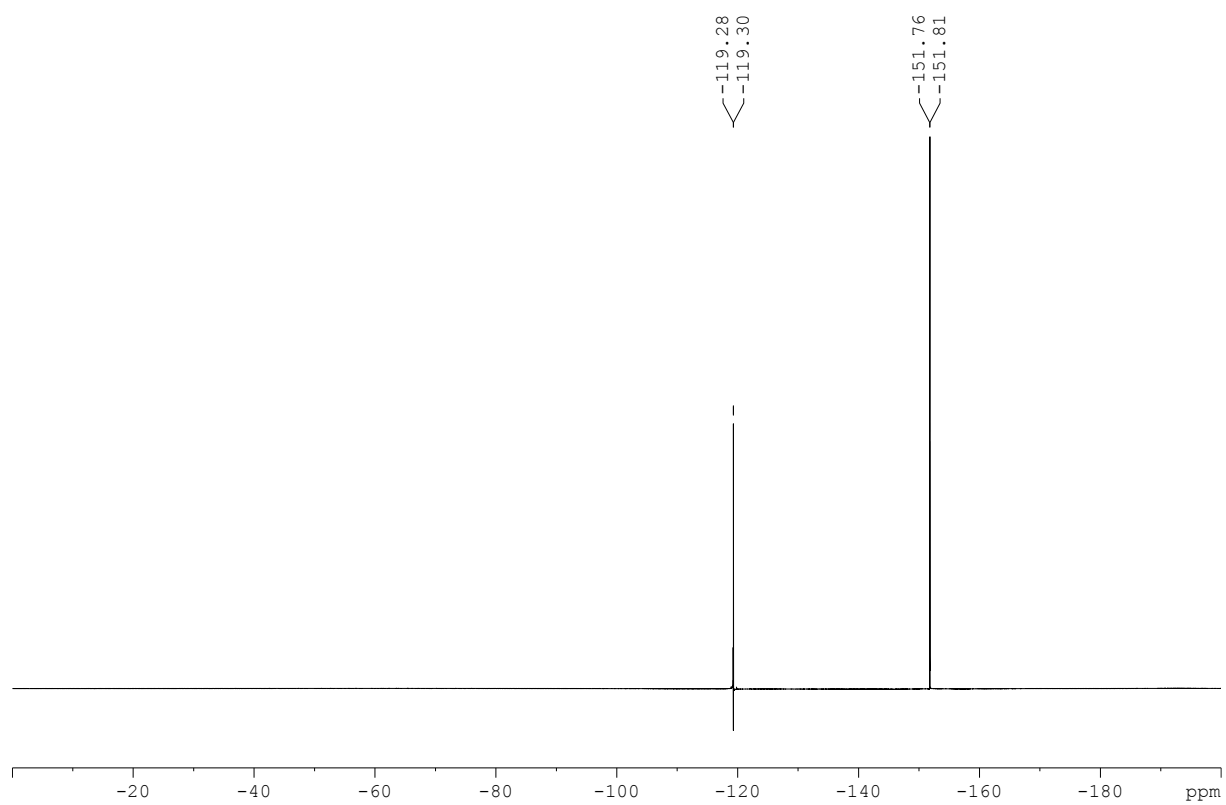
Compound 124b: ^1H NMR (300 MHz, CD_3CN)



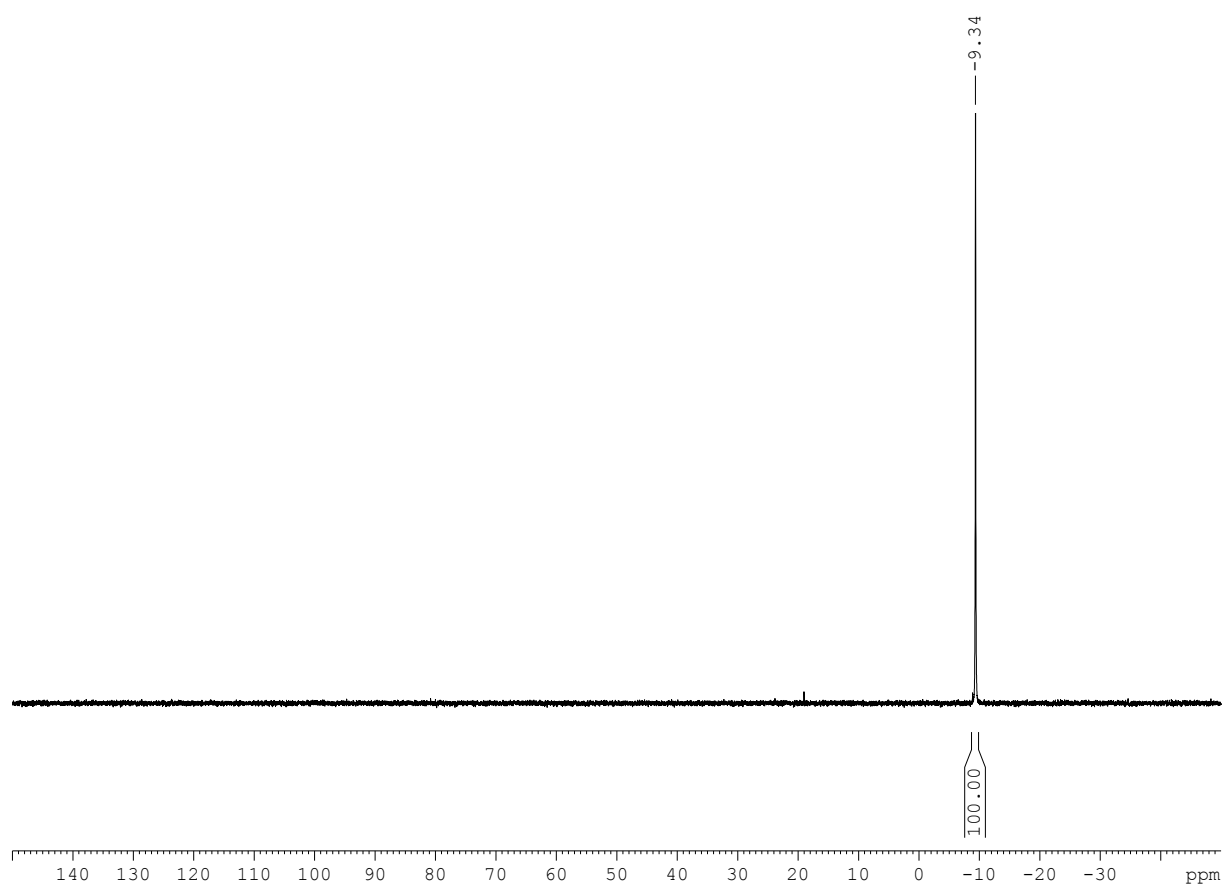
Compound 124b: ^{13}C NMR (282 MHz, CD_3CN)



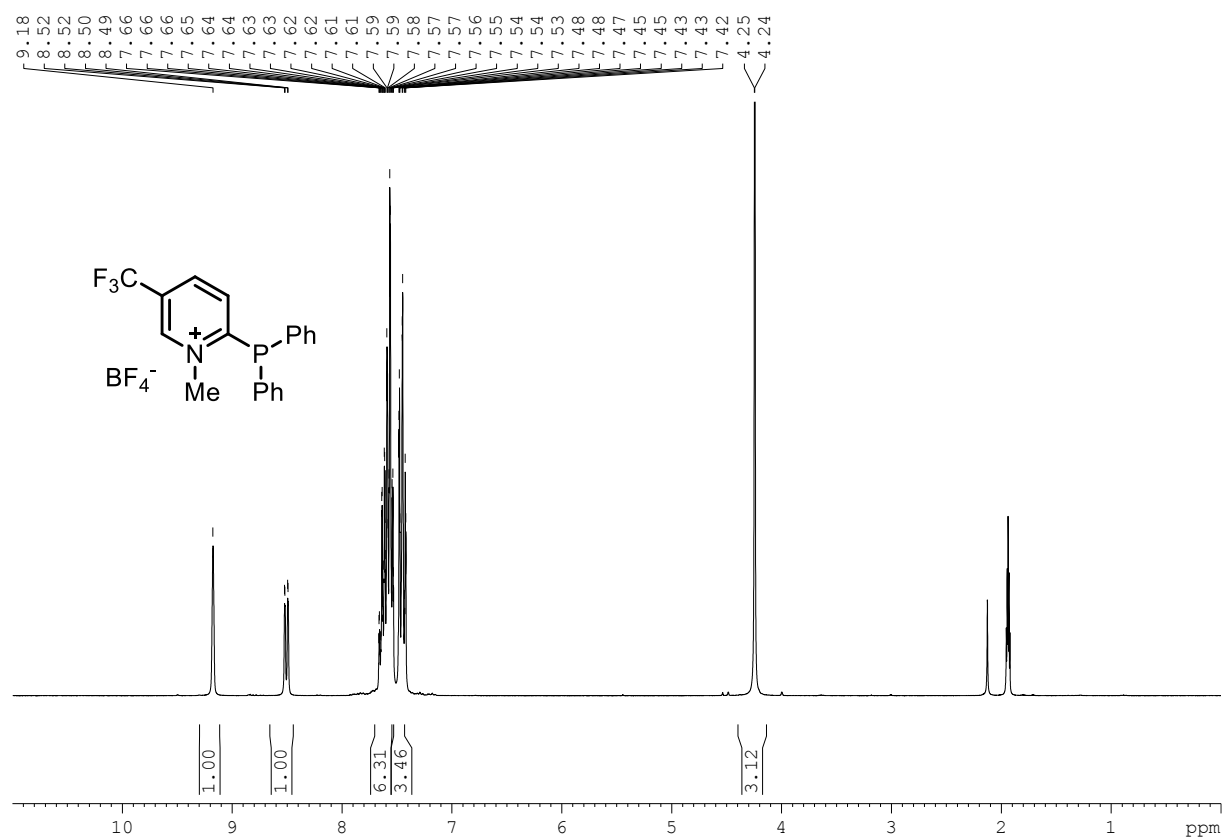
Compound 124b: ^{19}F NMR (282 MHz, CDCl_3)



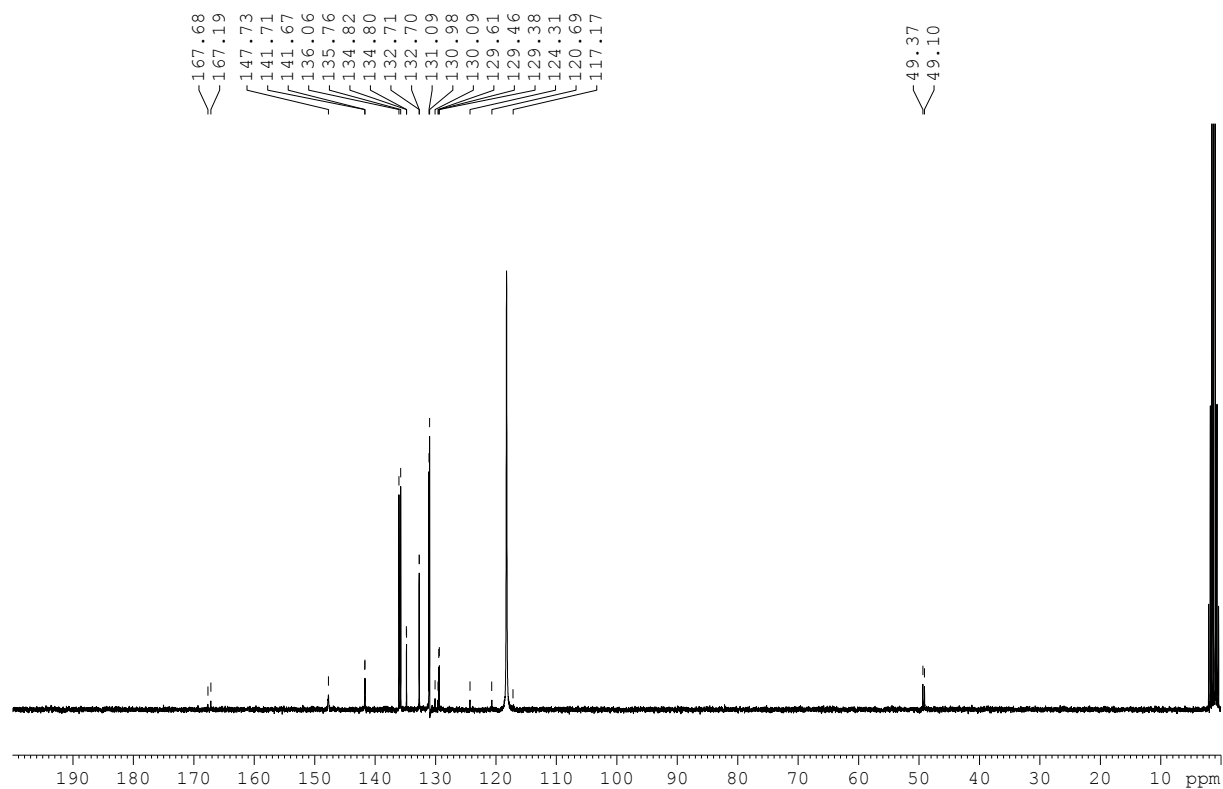
Compound 124b: ^{31}P NMR (75 MHz, CDCl_3)



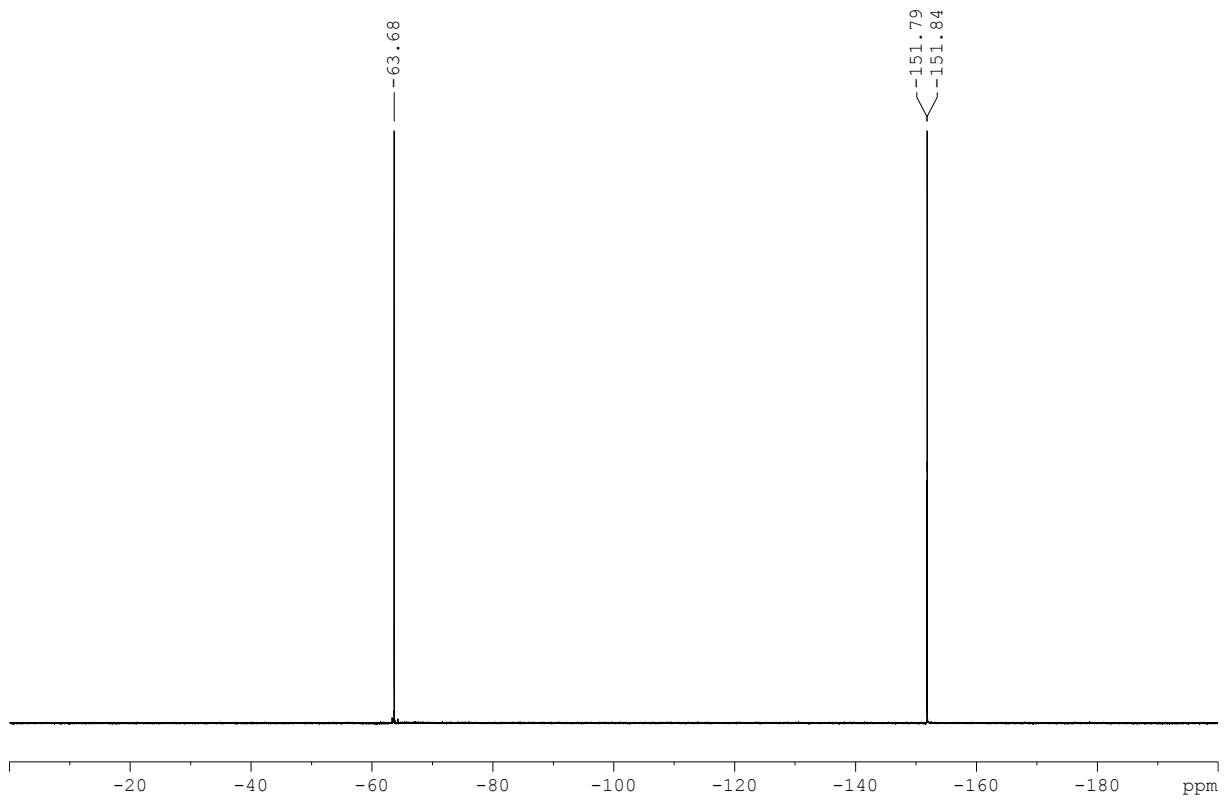
Compound 124c: ^1H NMR (300 MHz, CDCl_3)



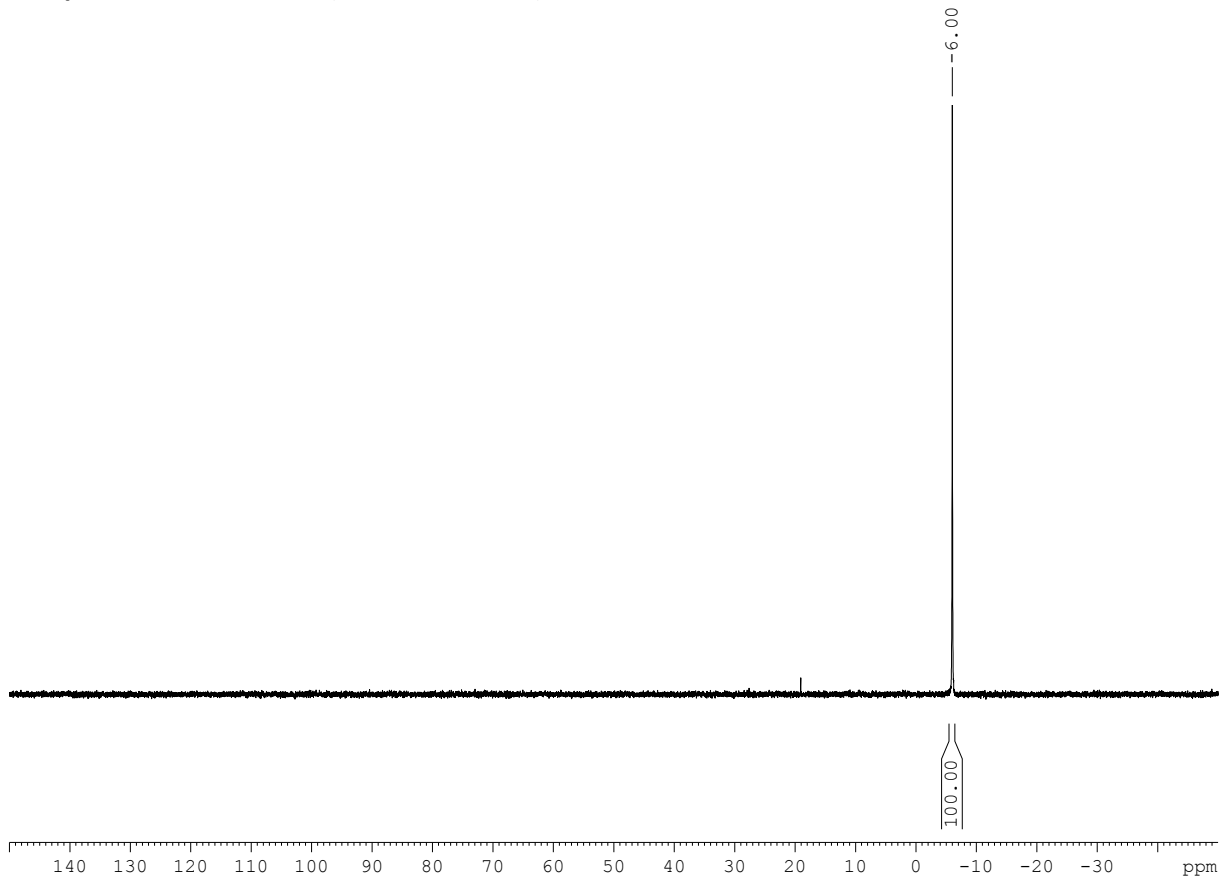
Compound 124c: ^{13}C NMR (101 MHz, CDCl_3)



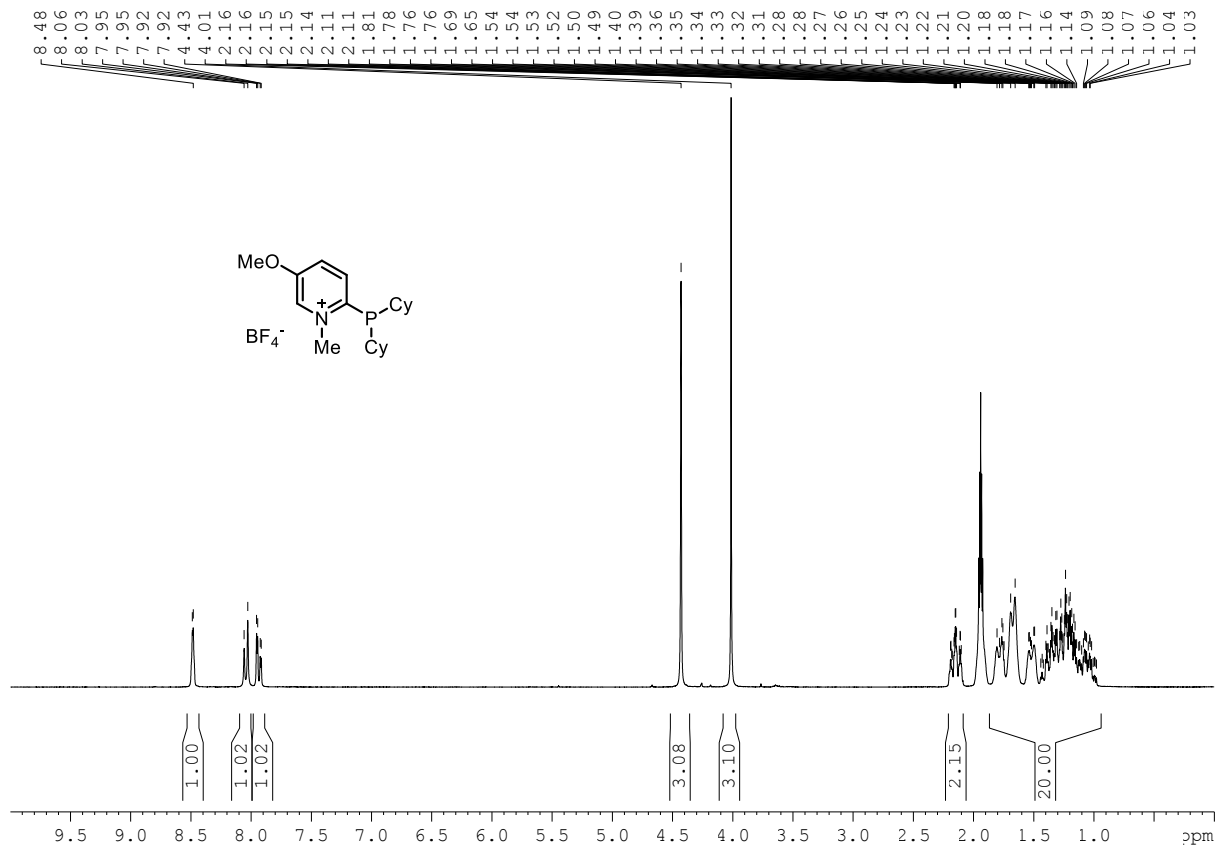
Compound 124c: ^{19}F NMR (282 MHz, CD_3CN)



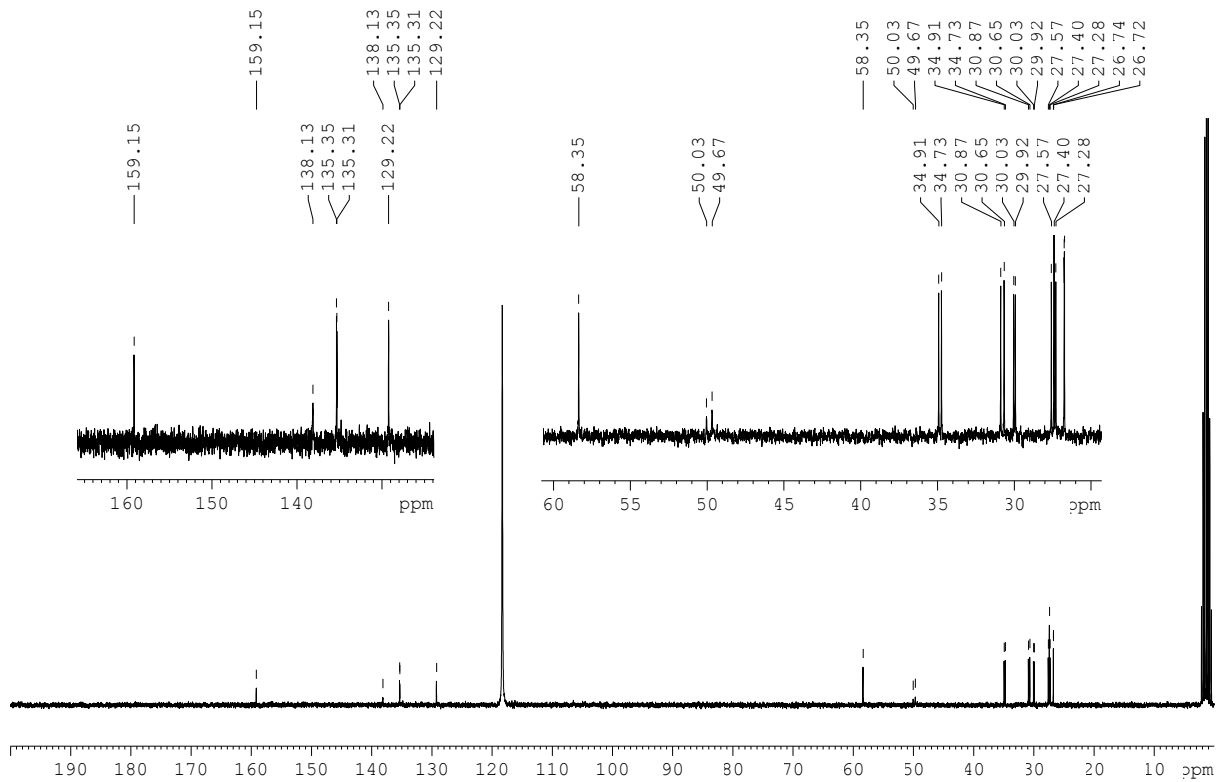
Compound 124c: ^{31}P NMR (121 MHz, CD_3CN)



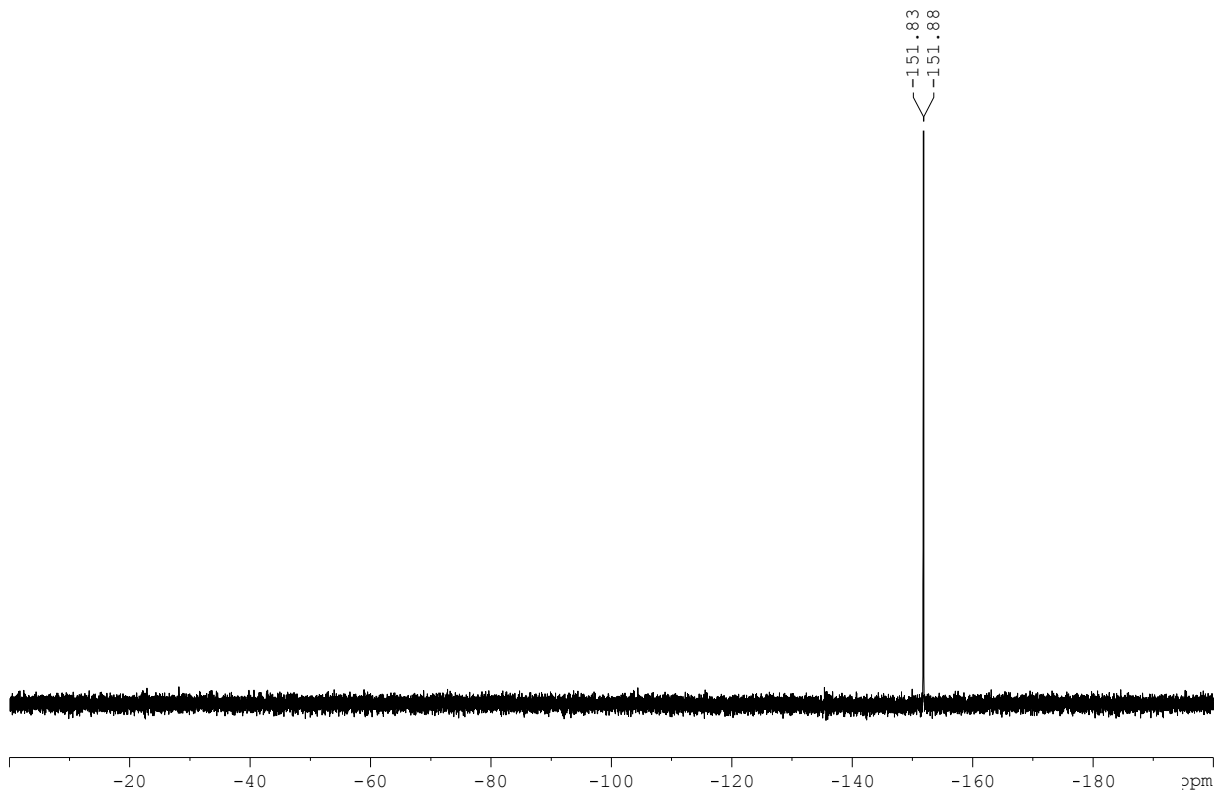
Compound 124d: ^1H NMR (300 MHz, CDCl_3)



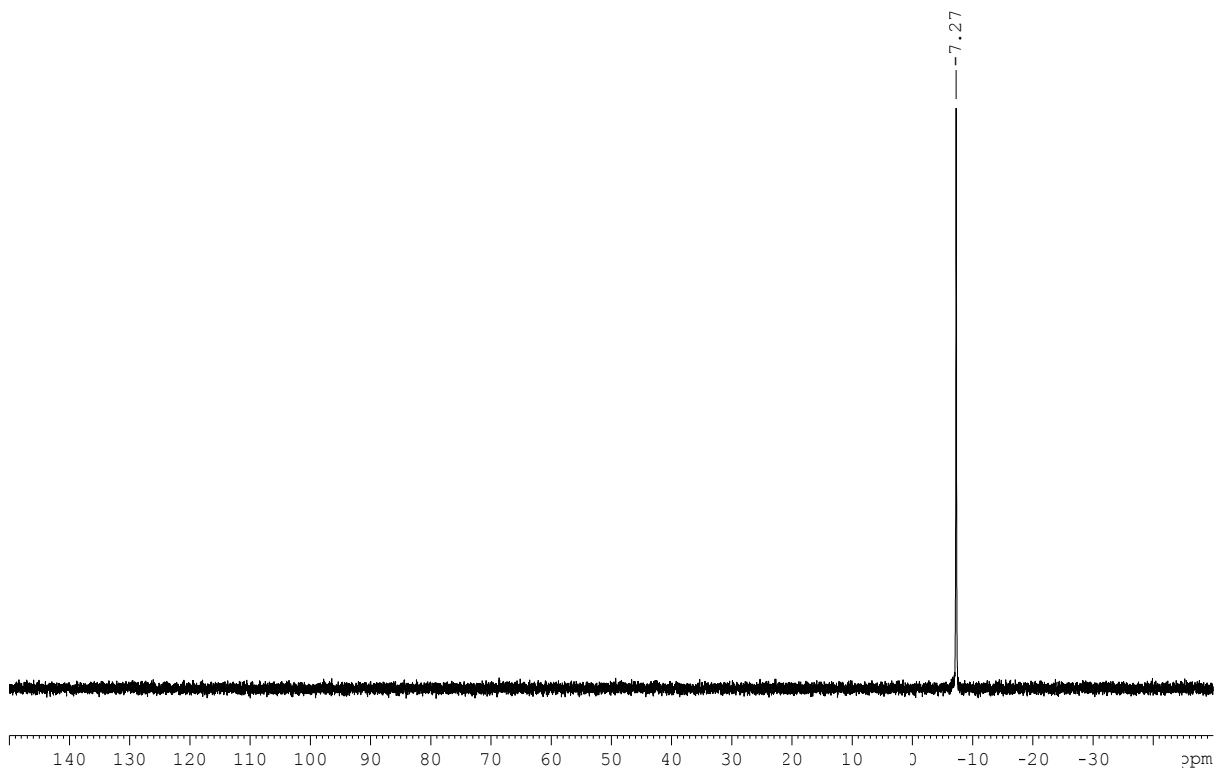
Compound 124d: ^{13}C NMR (75 MHz, CDCl_3)

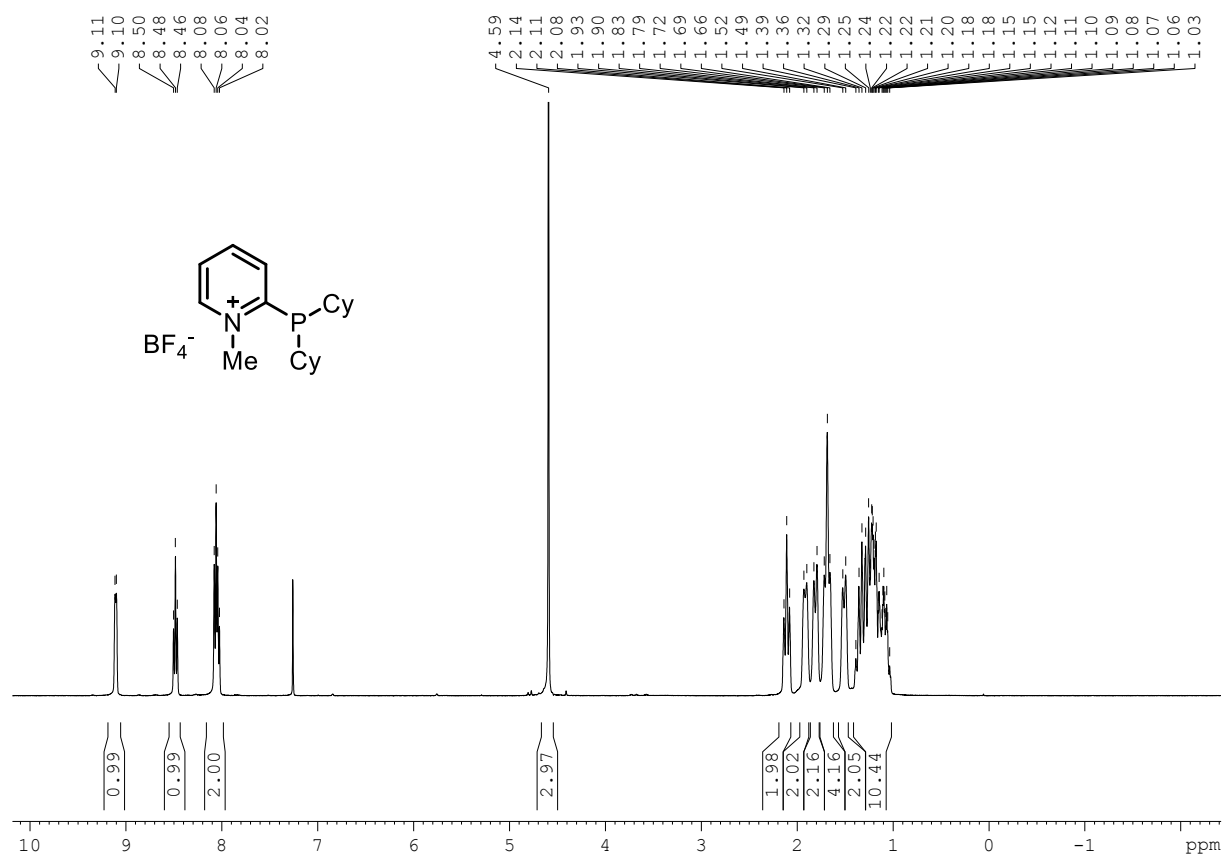
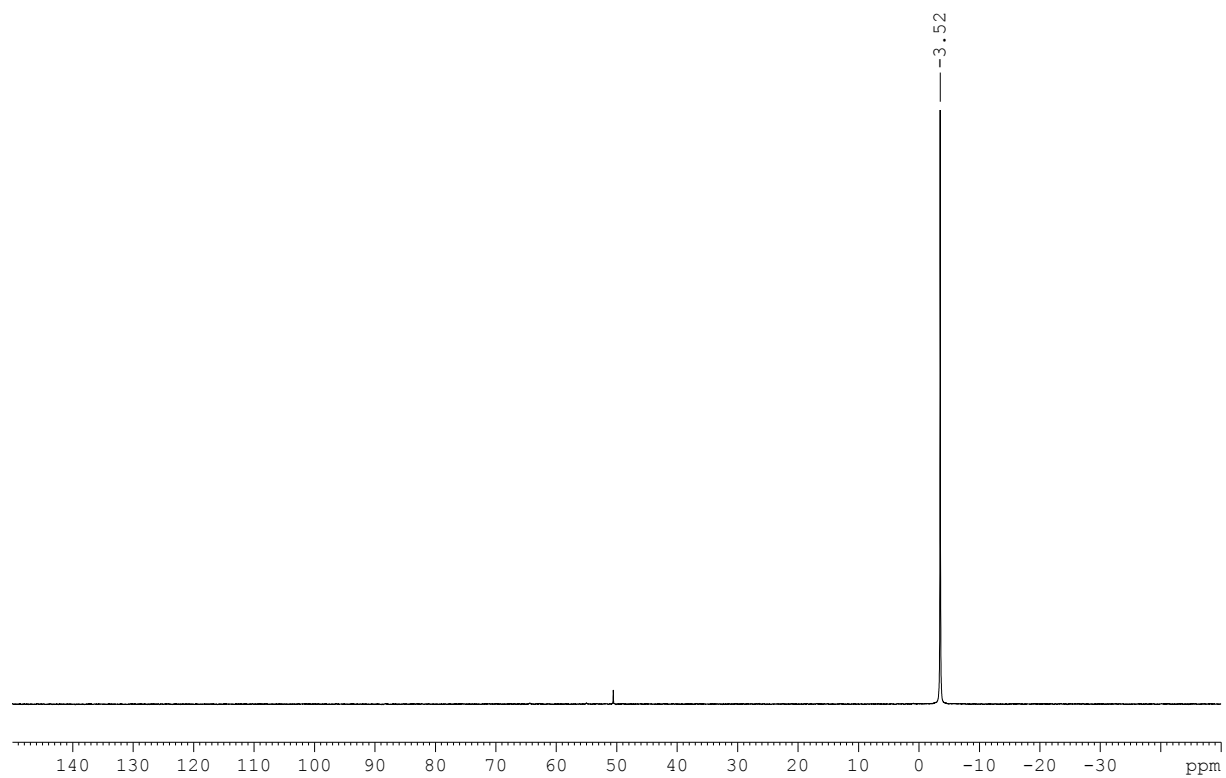


Compound 124d: ^{19}F NMR (282 MHz, CDCl_3)

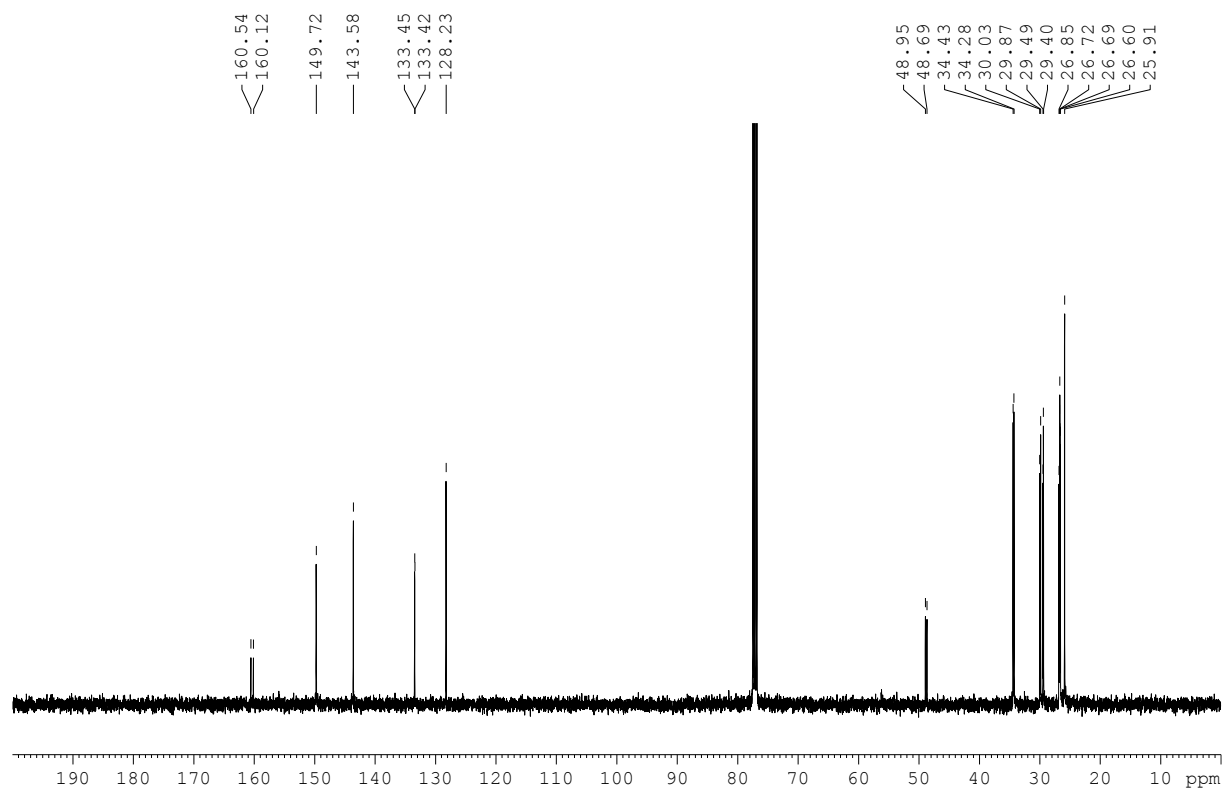


Compound 124d: ^{31}P NMR (121 MHz, CDCl_3)

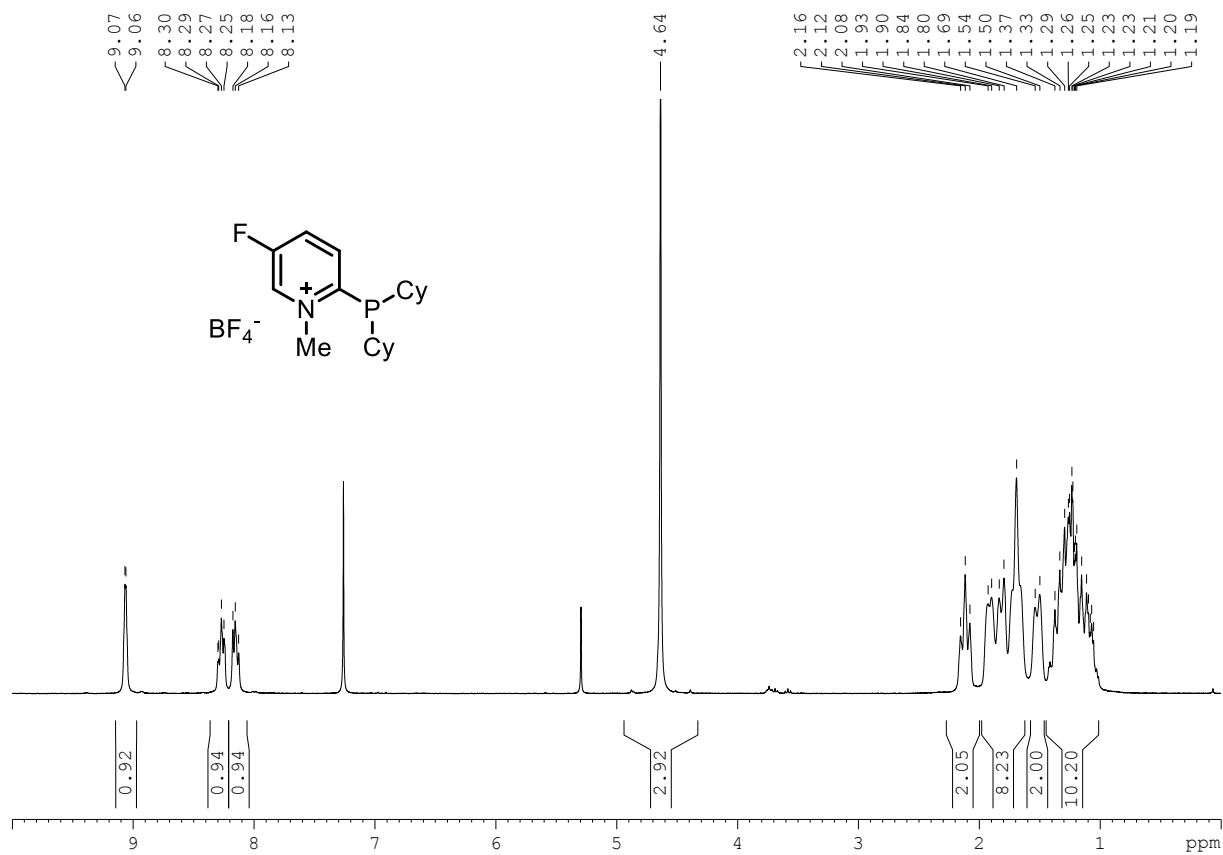


Compound 124e: ^1H NMR (400 MHz, CDCl_3)**Compound 124e:** ^{31}P NMR (162 MHz, CDCl_3)

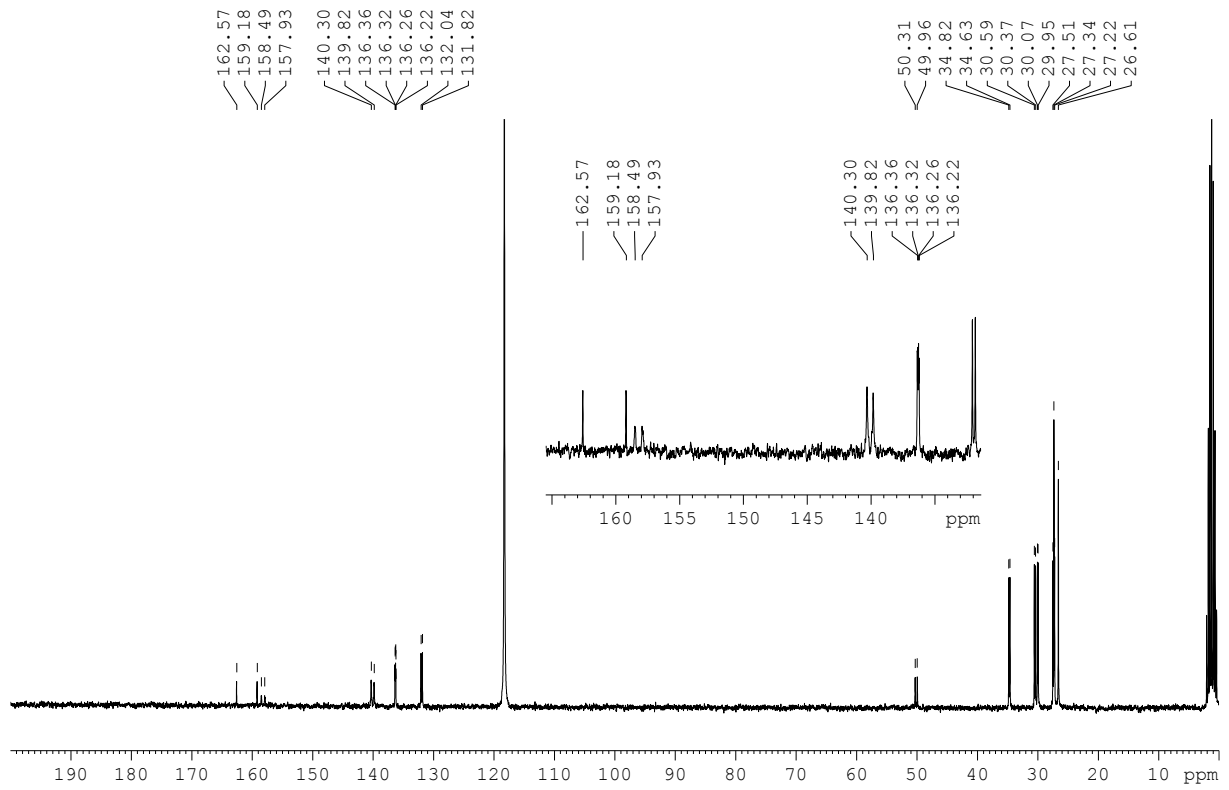
Compound 124e: ^{13}C NMR (101 MHz, CDCl_3)



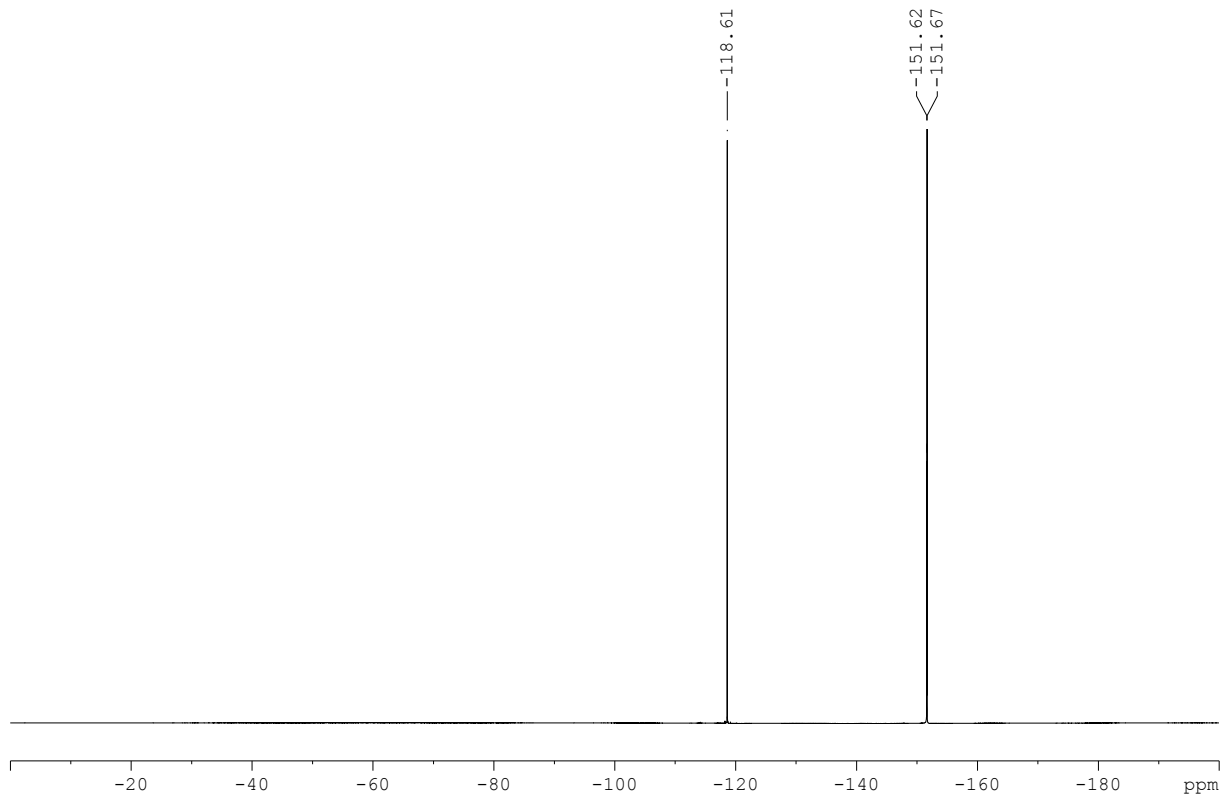
Compound 124f: ^1H NMR (300 MHz, CDCl_3)



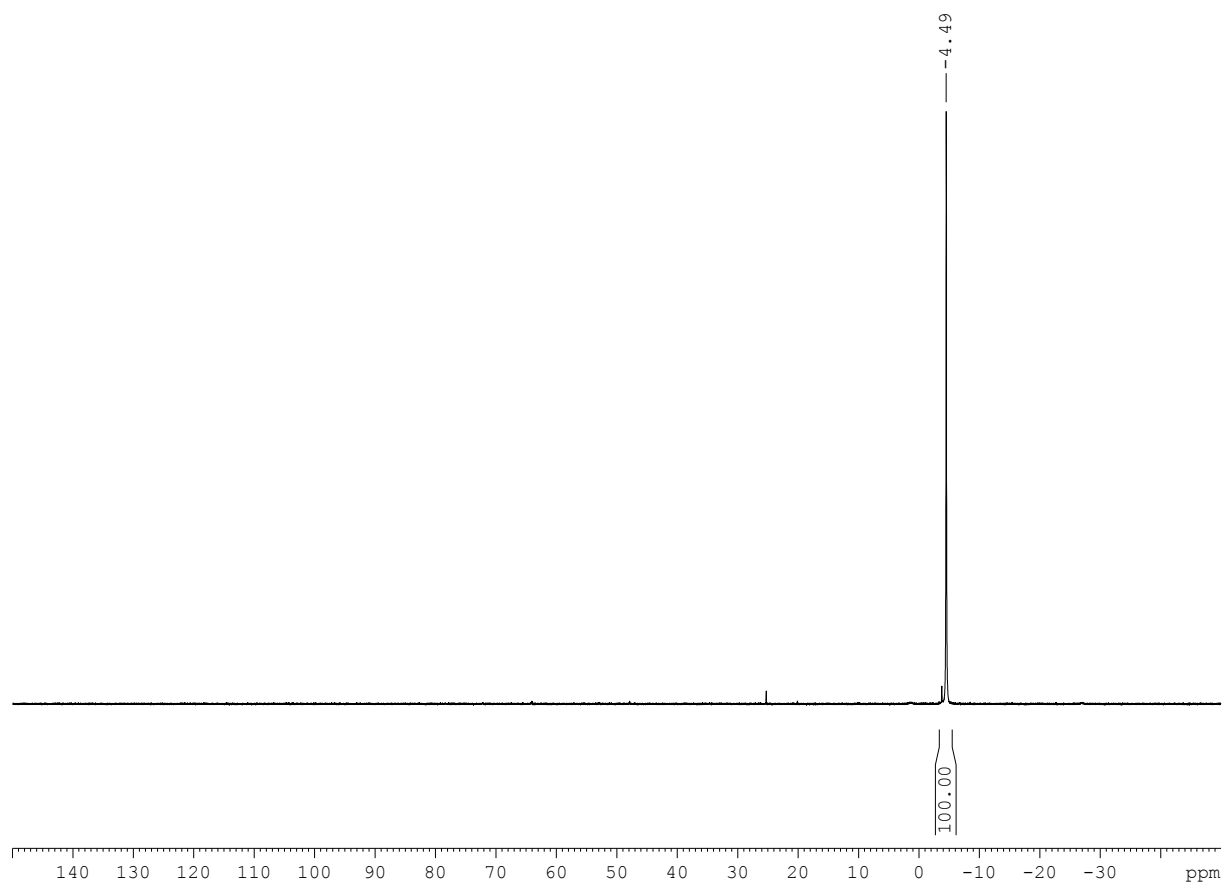
Compound 124f: ^{13}C NMR (282 MHz, CDCl_3)



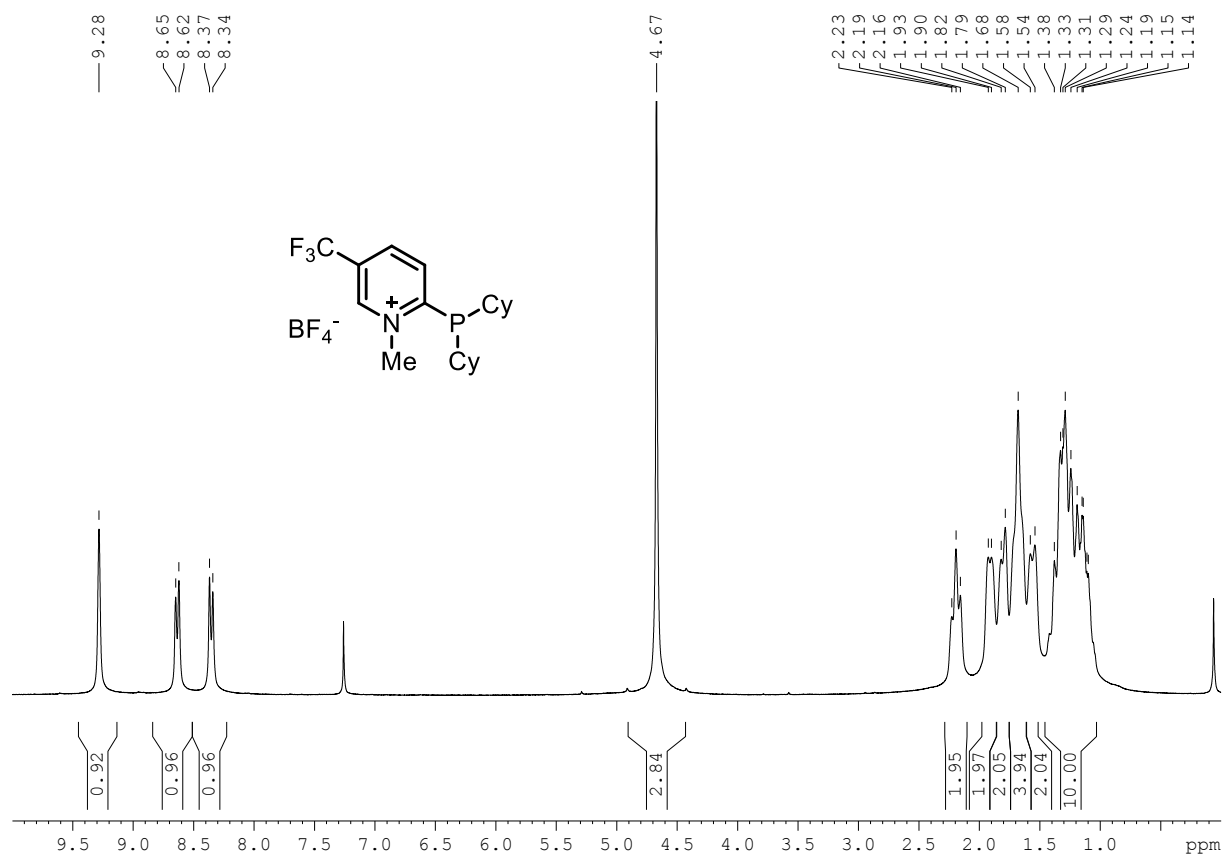
Compound 124f: ^{19}F NMR (282 MHz, CDCl_3)



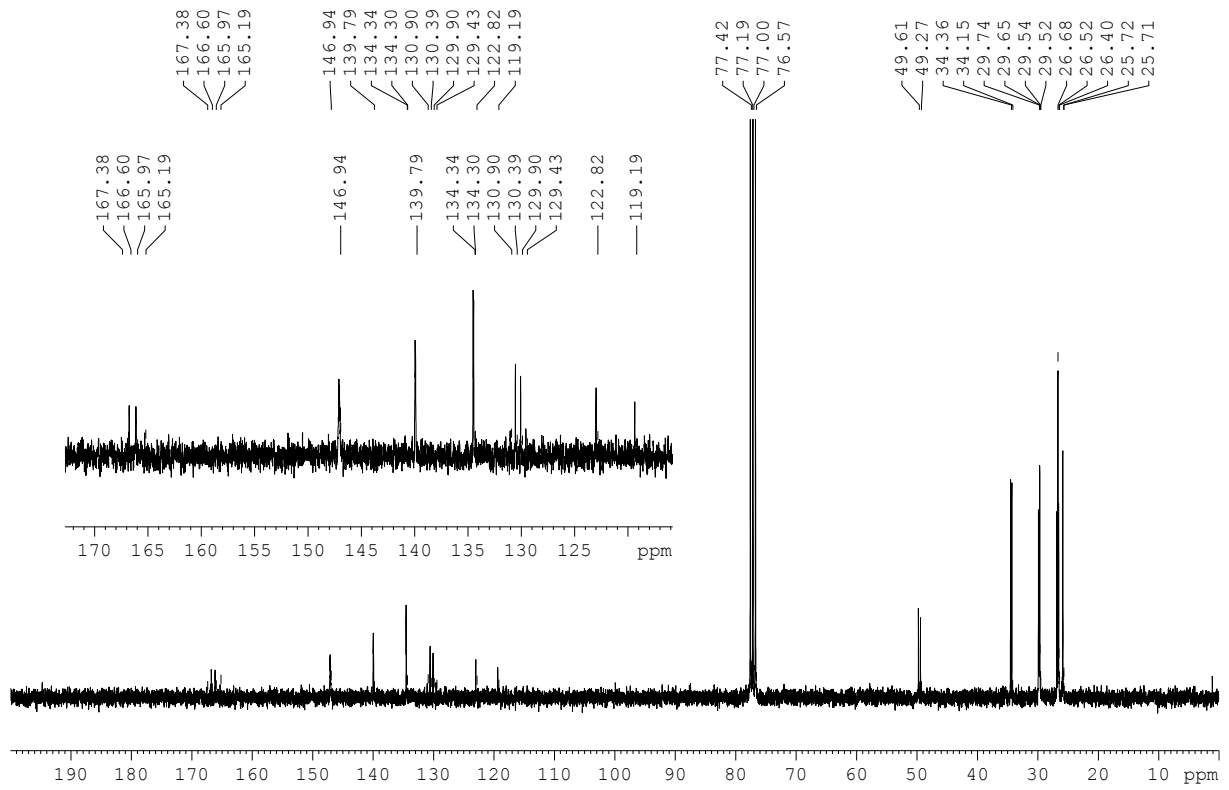
Compound 124f: ^{31}P NMR (121 MHz, CDCl_3)



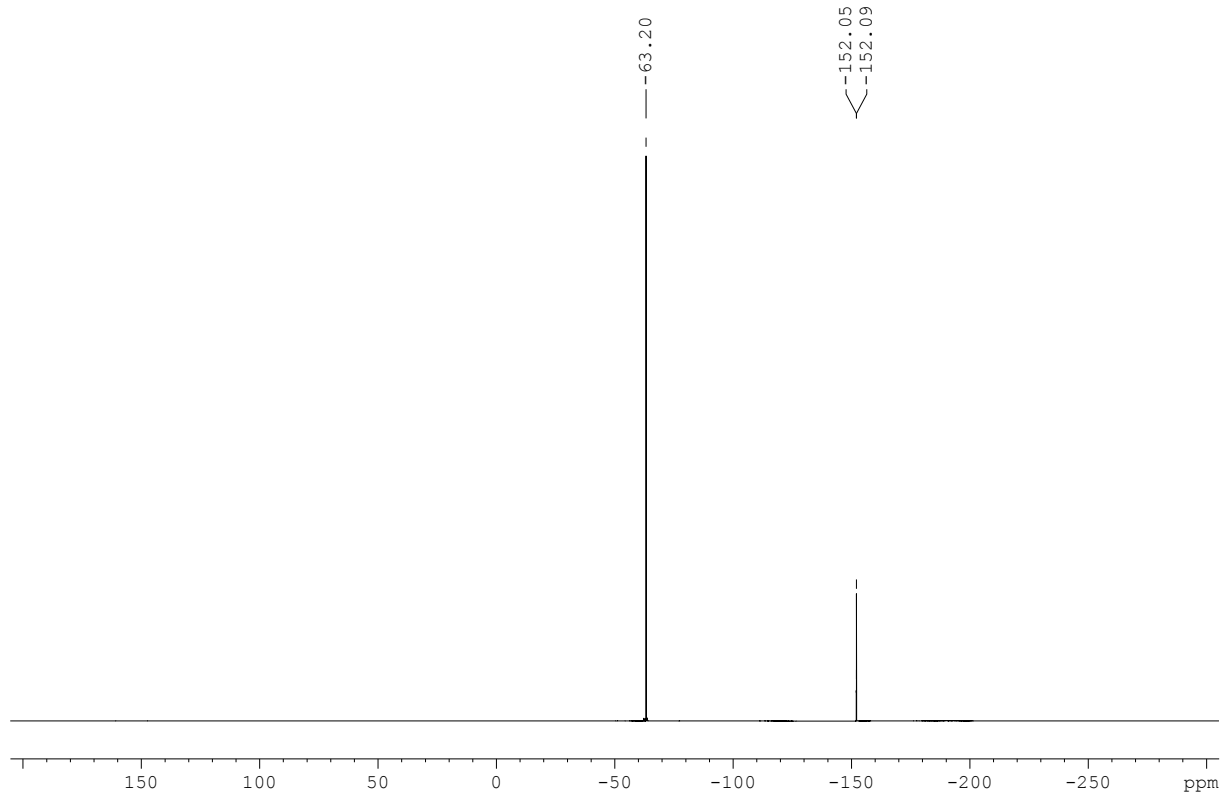
Compound 124g: ^1H NMR (300 MHz, CDCl_3)



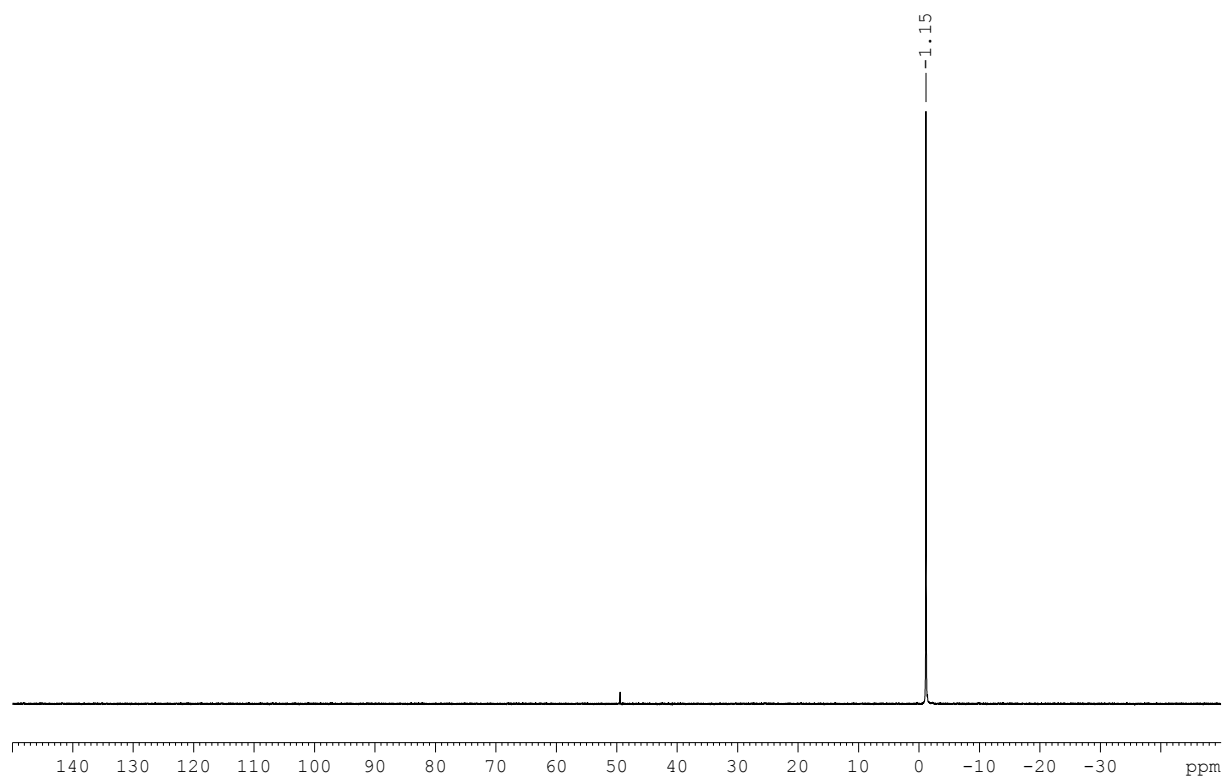
Compound 124g: ^{13}C NMR (75 MHz, CDCl_3)



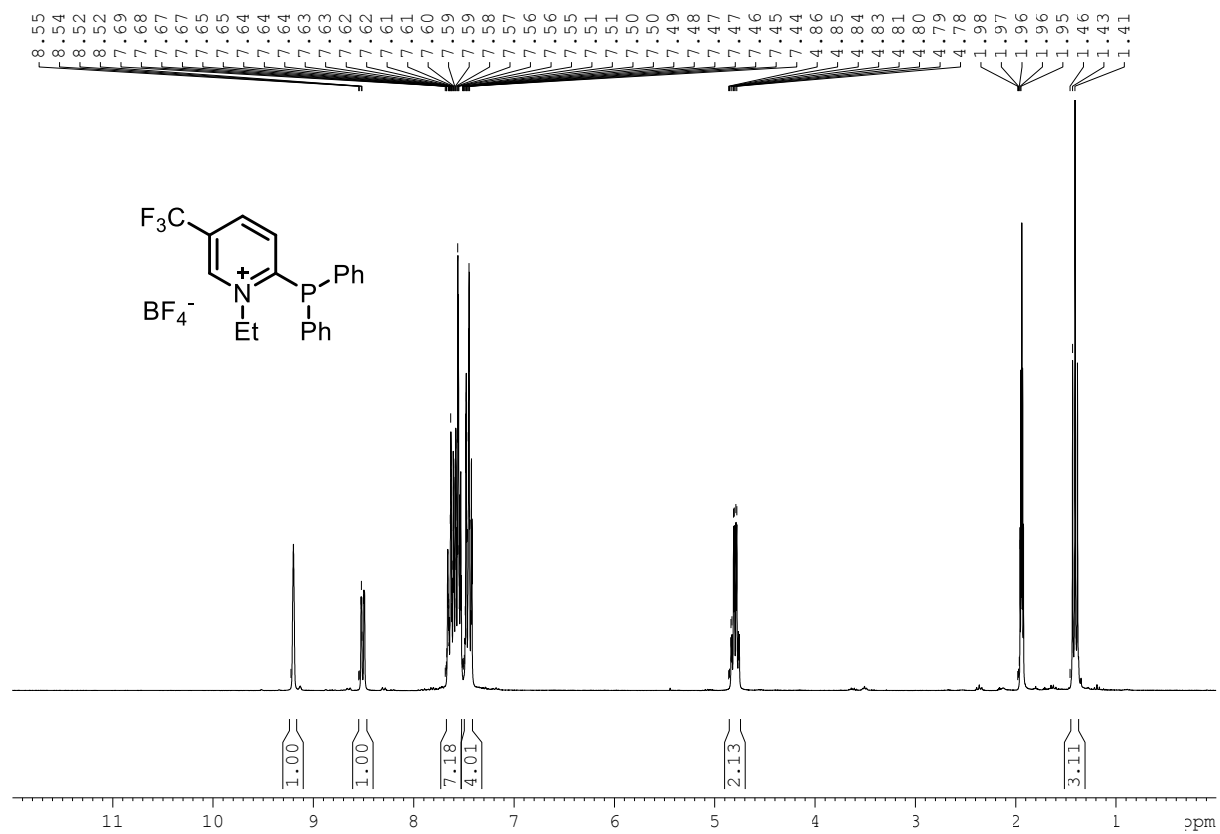
Compound 124g: ^{19}F NMR (282 MHz, CDCl_3)



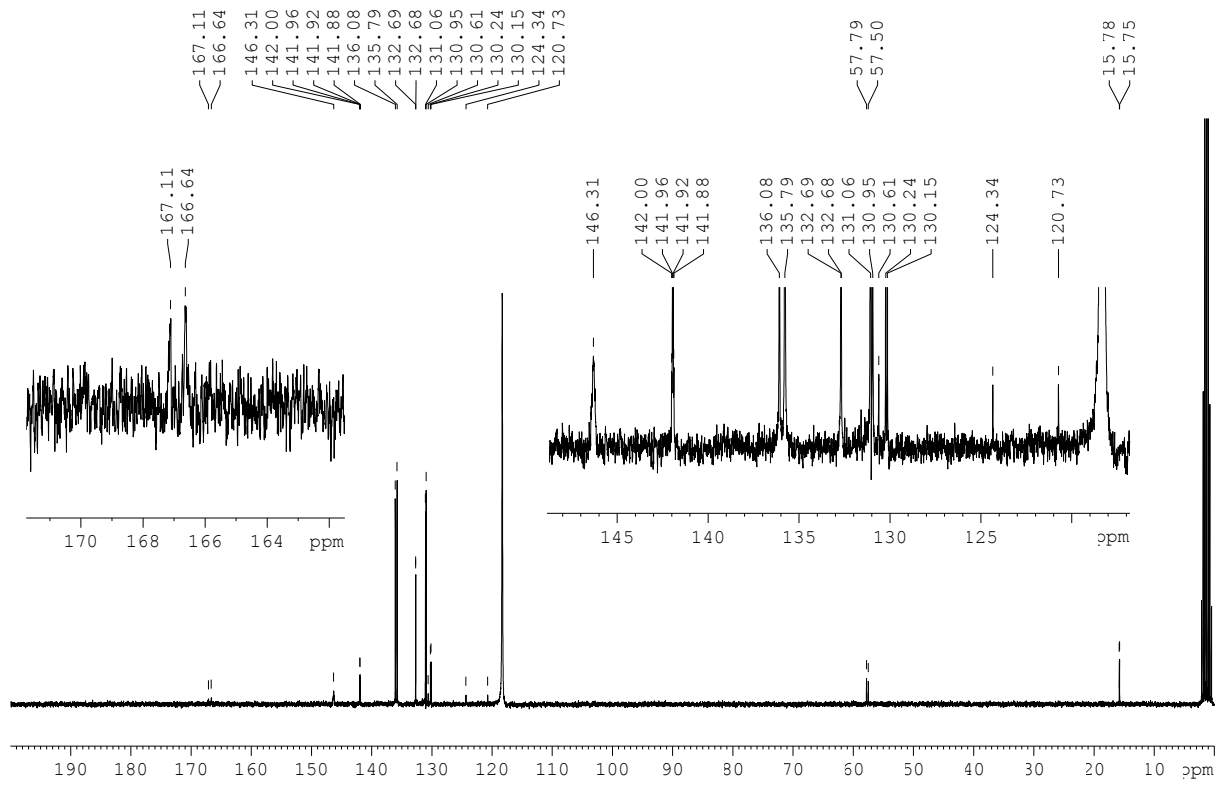
Compound 124g: ^{31}P NMR (121 MHz, CD_3CN)



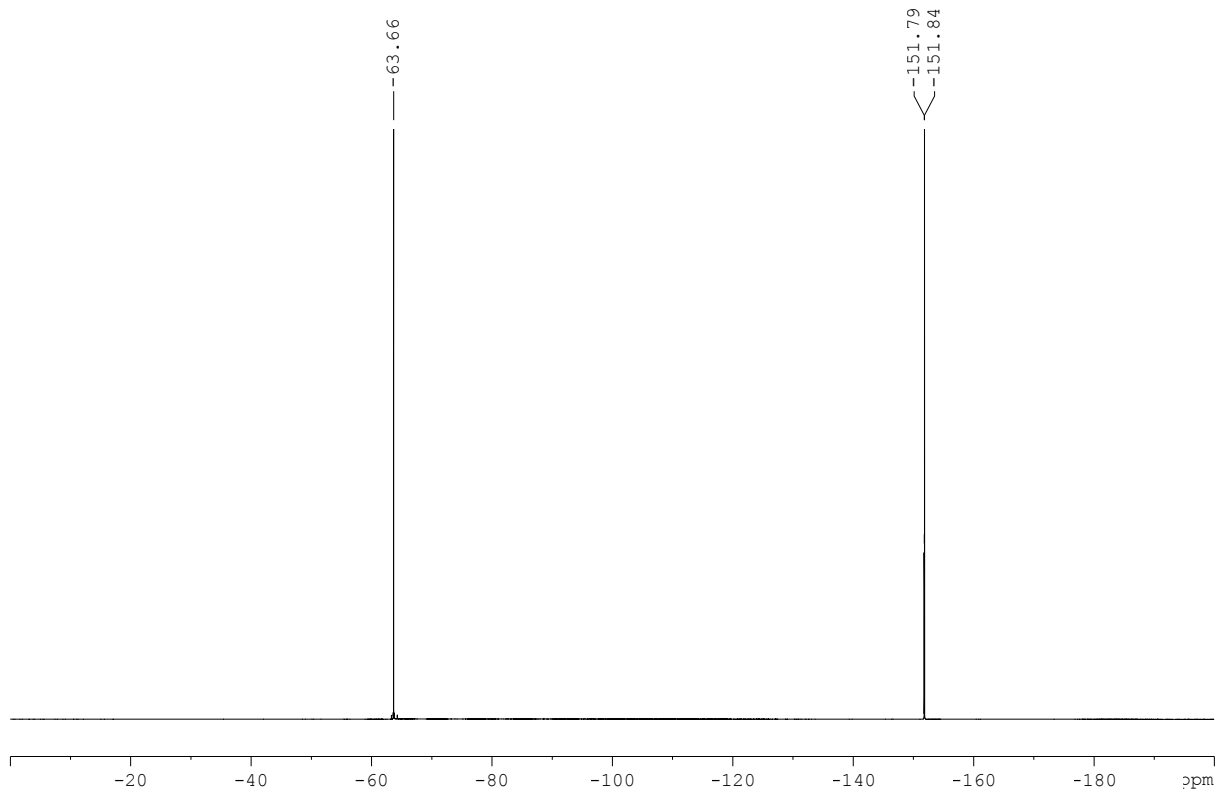
Compound 124h: ^1H NMR (300 MHz, CD_3CN)

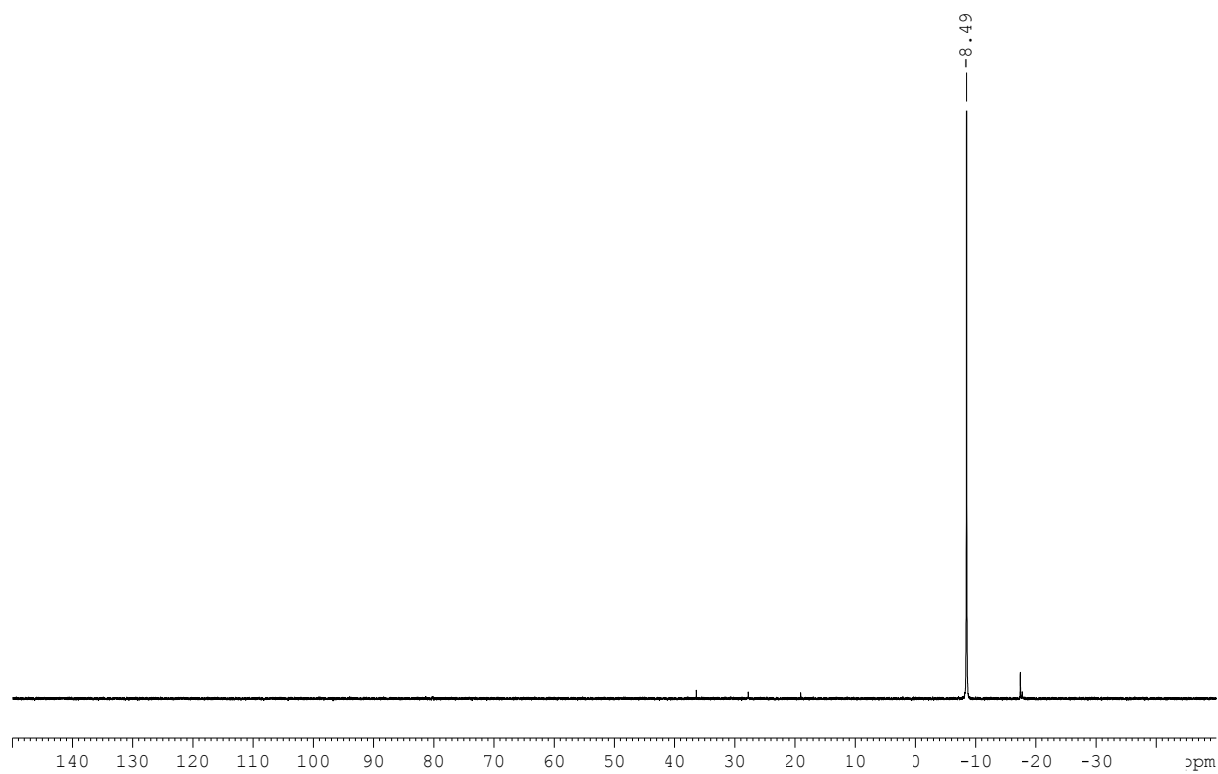


Compound 124h: ^{13}C NMR (75 MHz, CD_3CN)

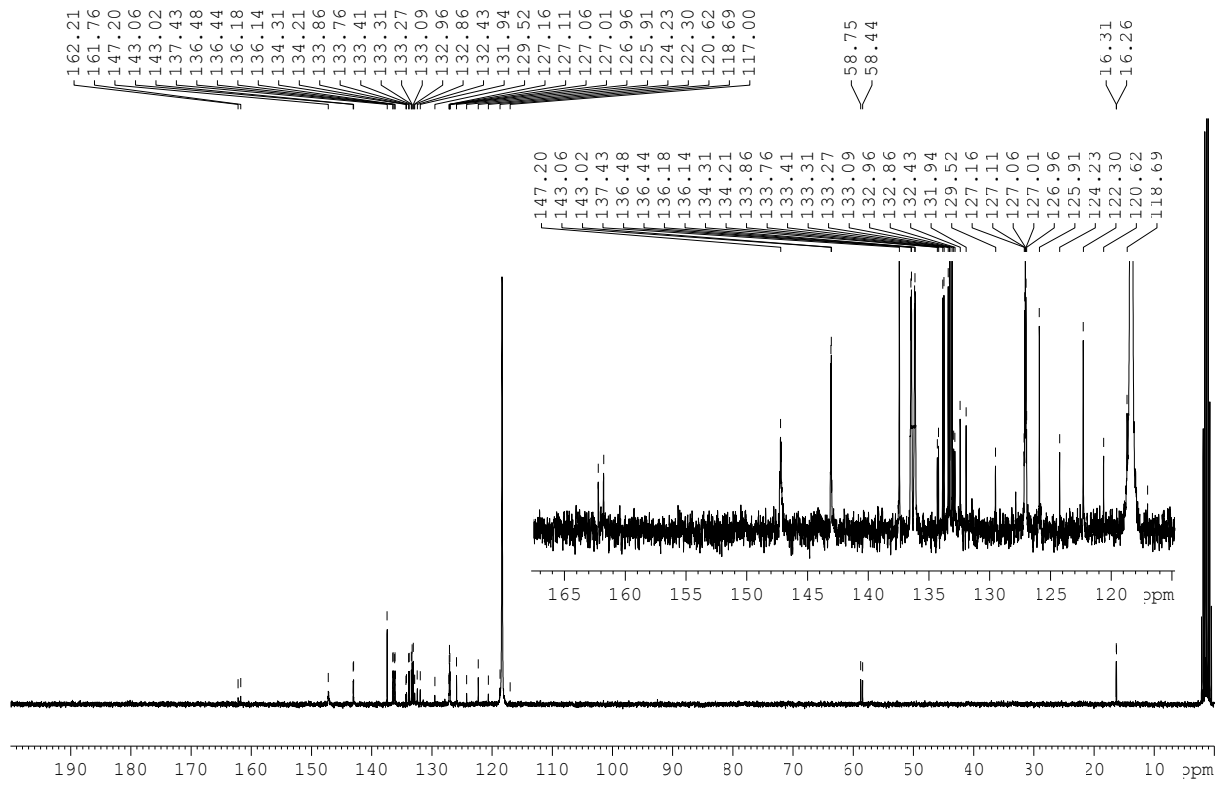


Compound 124h: ^{19}F NMR (282 MHz, CD_3CN)

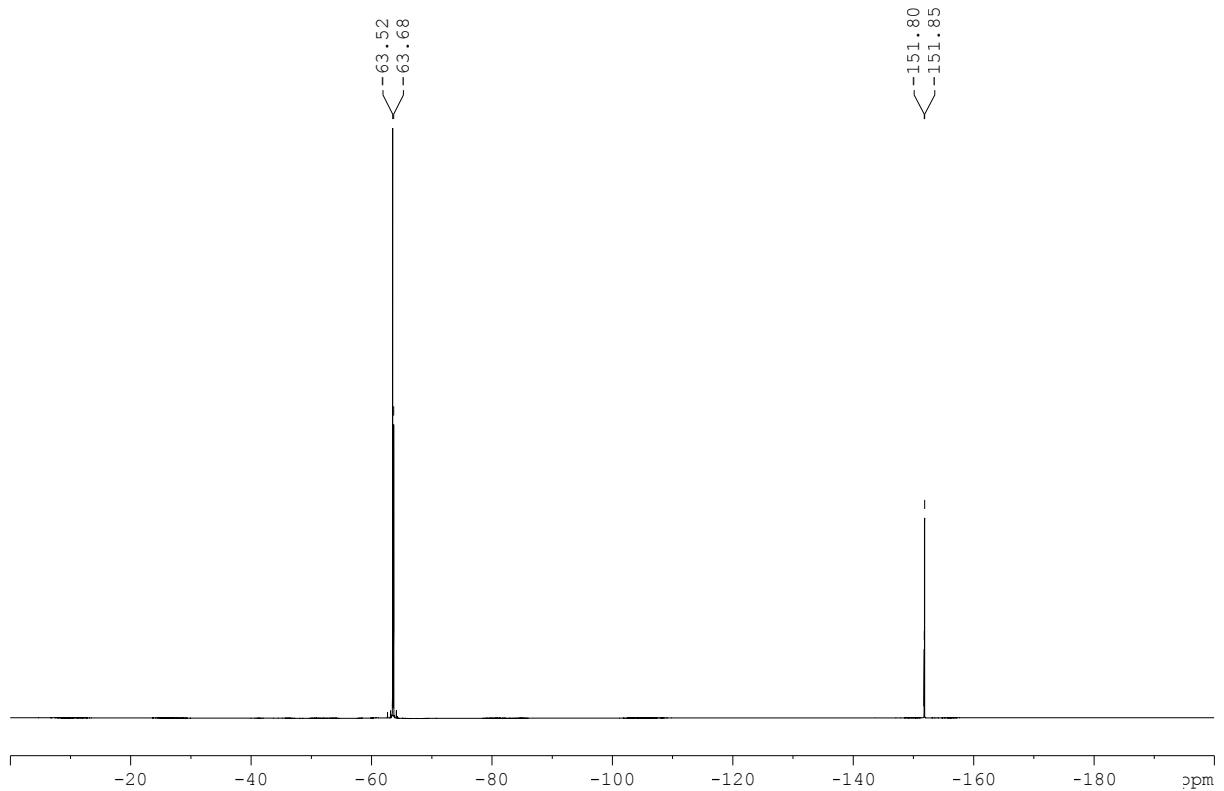


Compound 124h: ^{31}P NMR (121 MHz, CD_3CN)**Compound 124i:** ^1H NMR (300 MHz, CD_3CN)

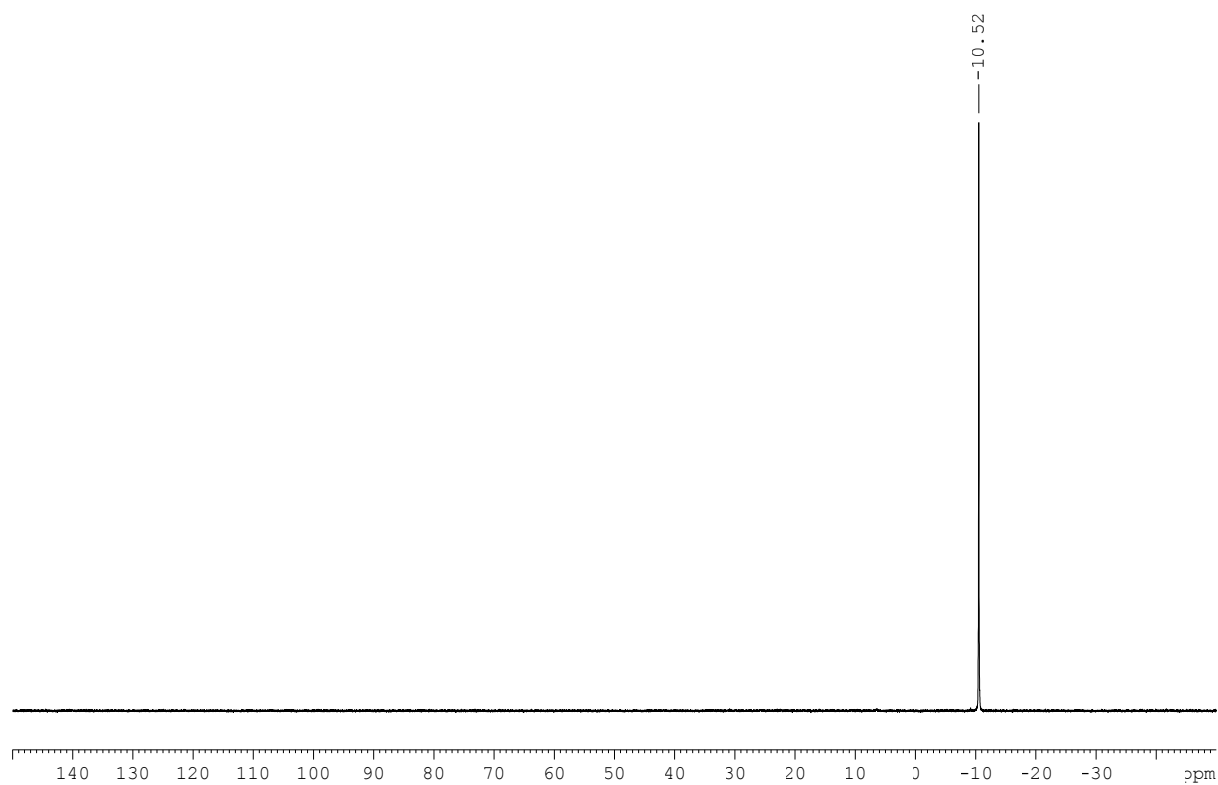
Compound 124i: ^{13}C NMR (75 MHz, CD_3CN)



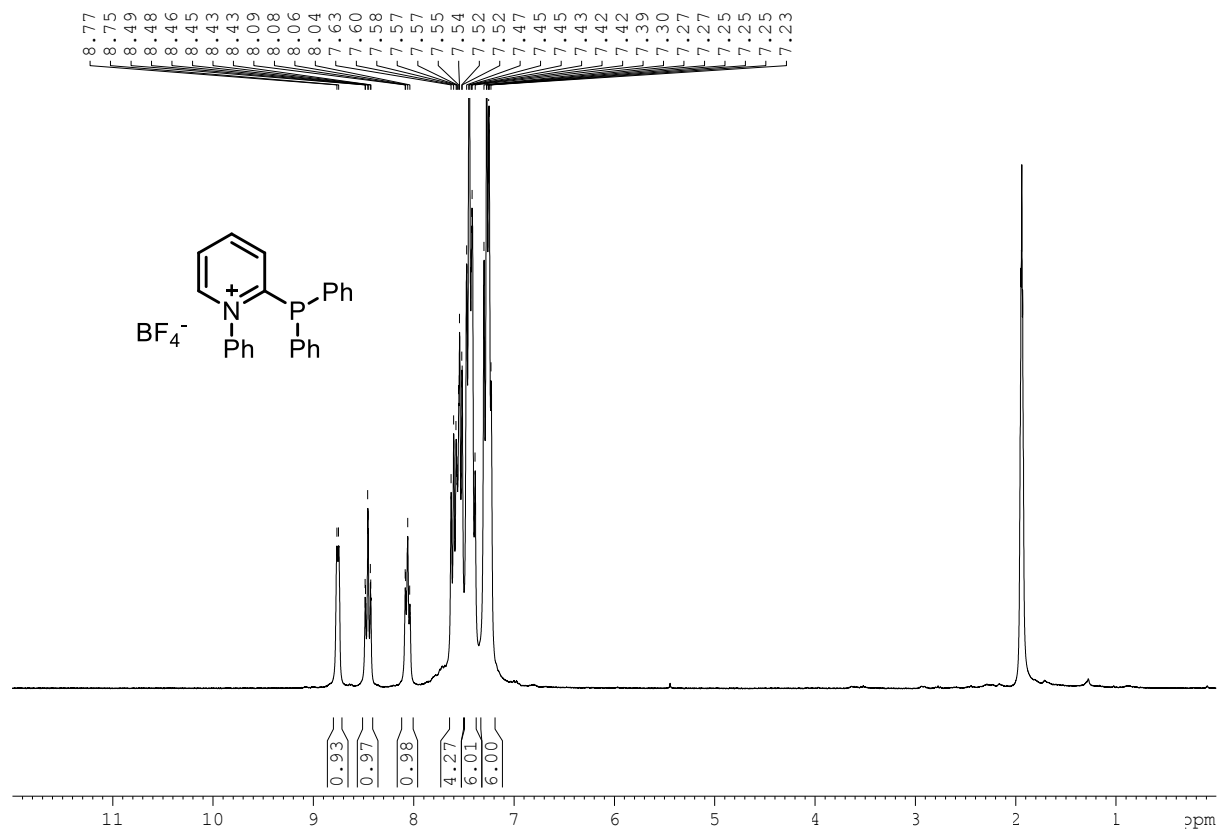
Compound 124i: ^{19}F NMR (282 MHz, CD_3CN)



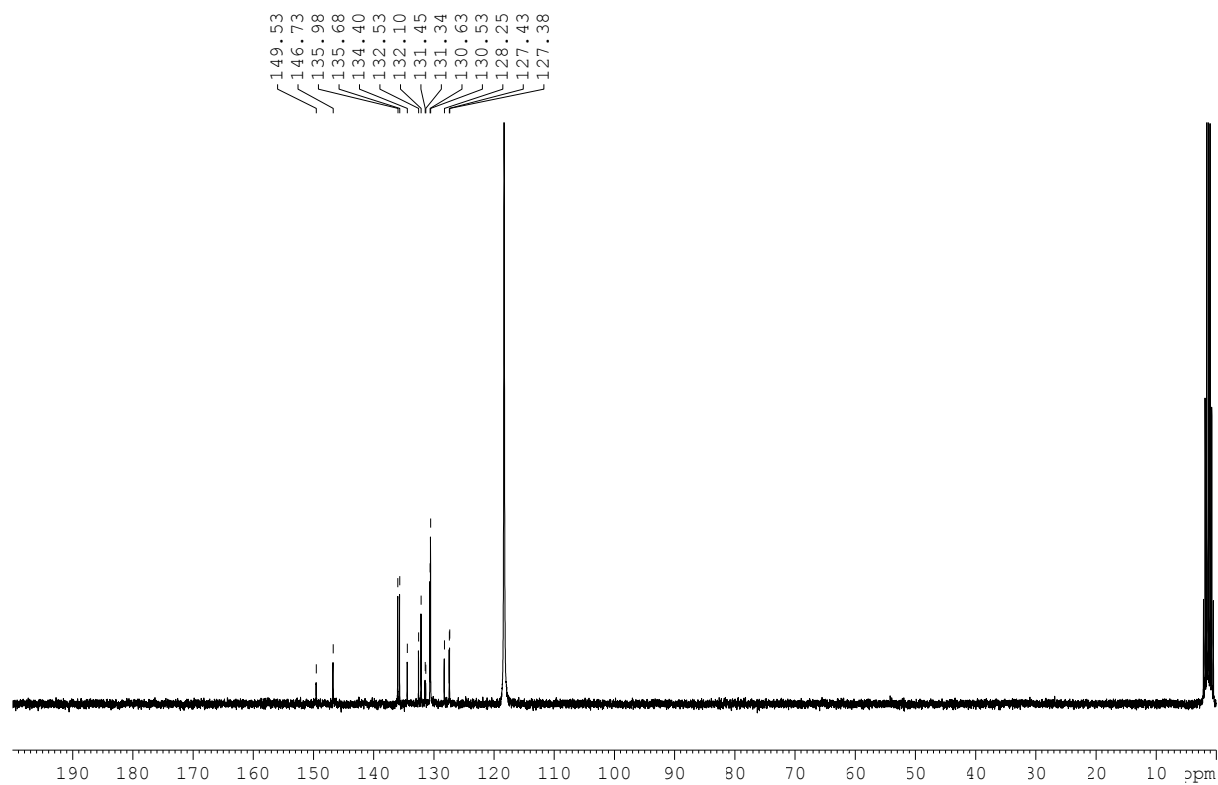
Compound 124i: ^{31}P NMR (121 MHz, CD_3CN)



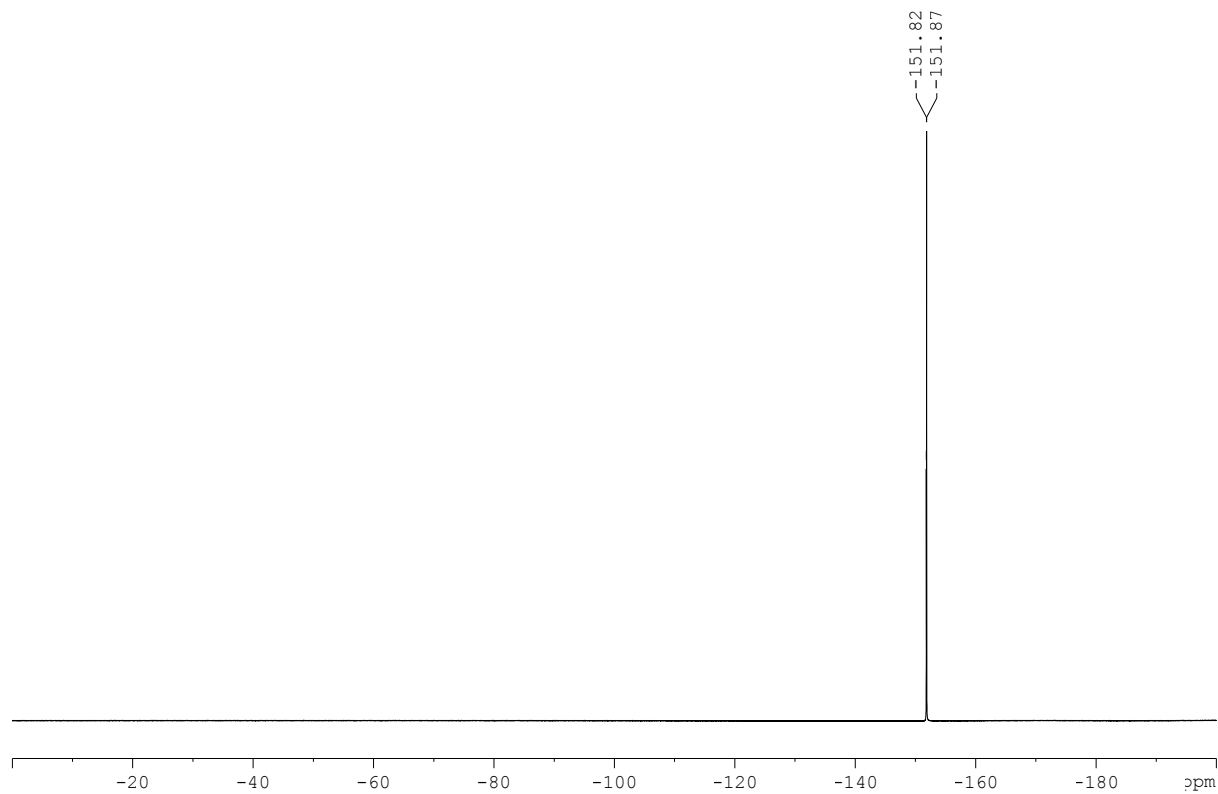
Compound 124j: ^1H NMR (300 MHz, CD_3CN)



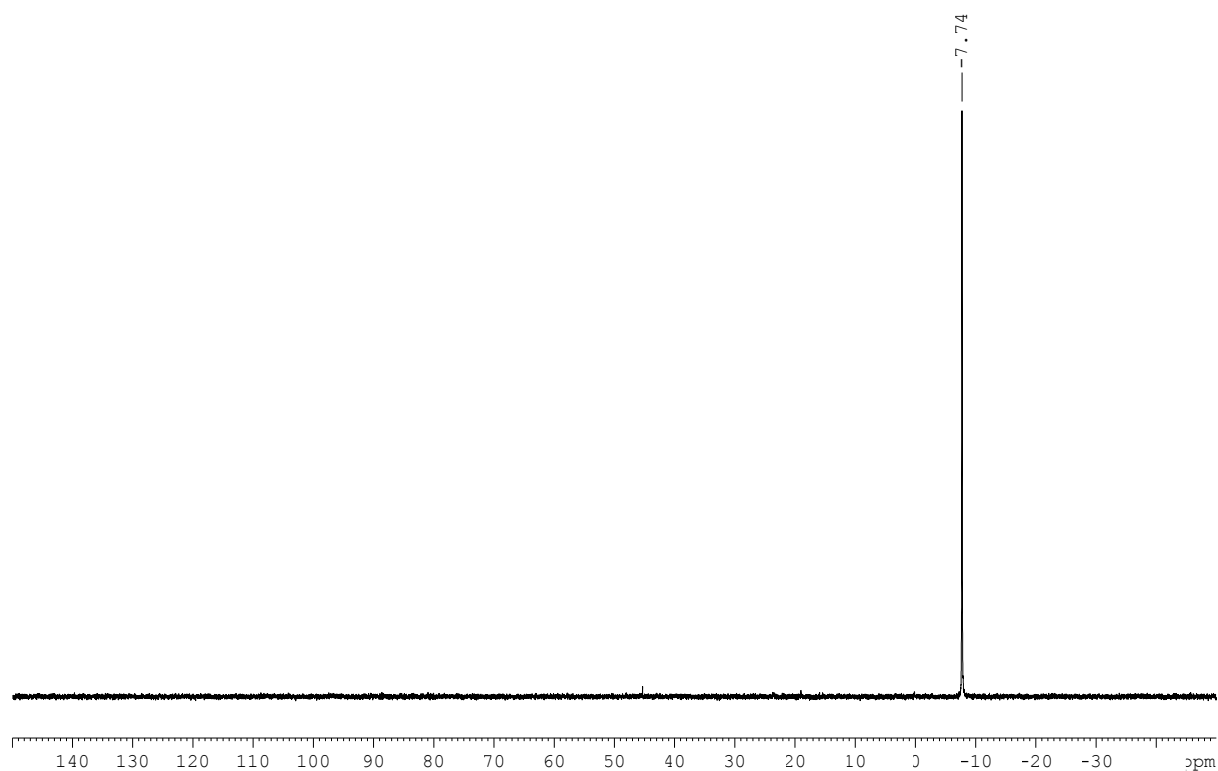
Compound 124j: ^{13}C NMR (75 MHz, CD_3CN)



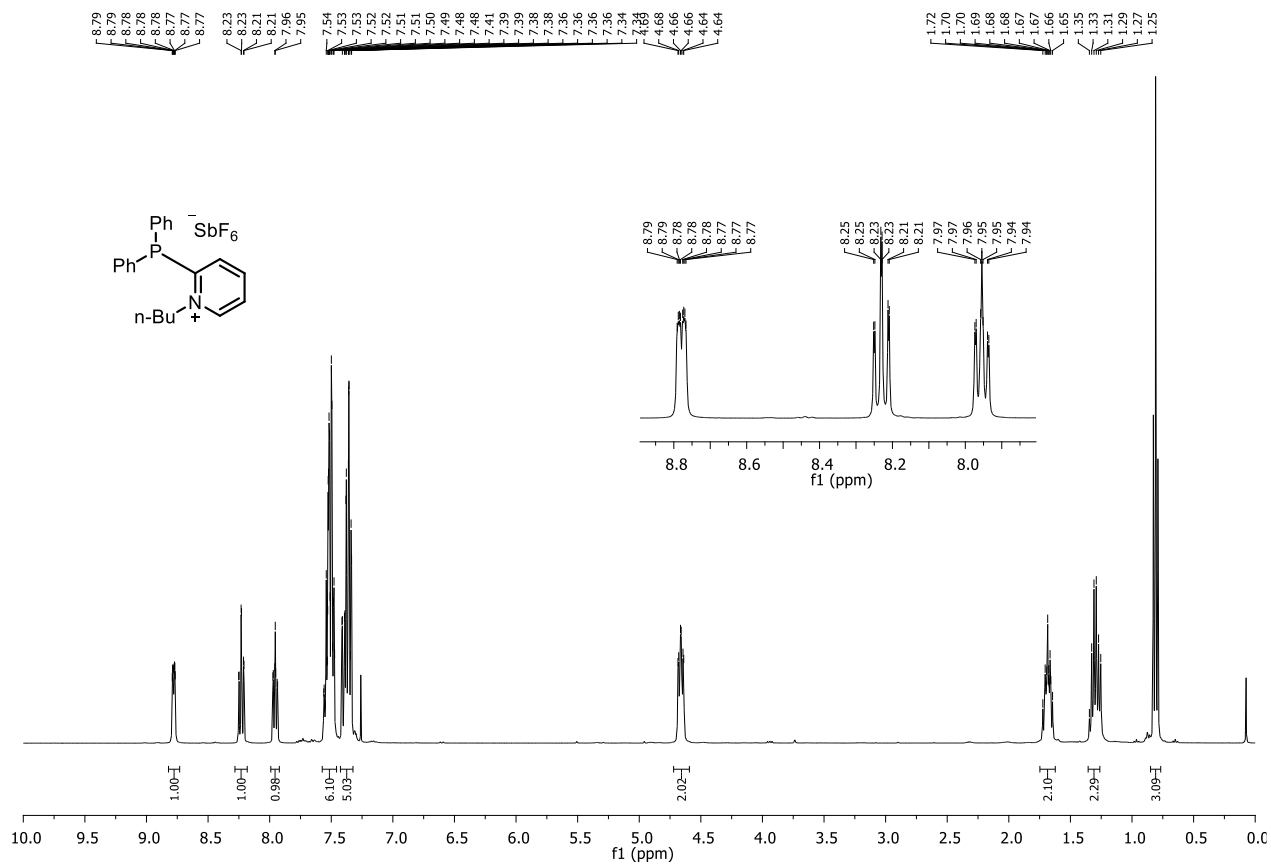
Compound 124j: ^{19}F NMR (282 MHz, CD_3CN)



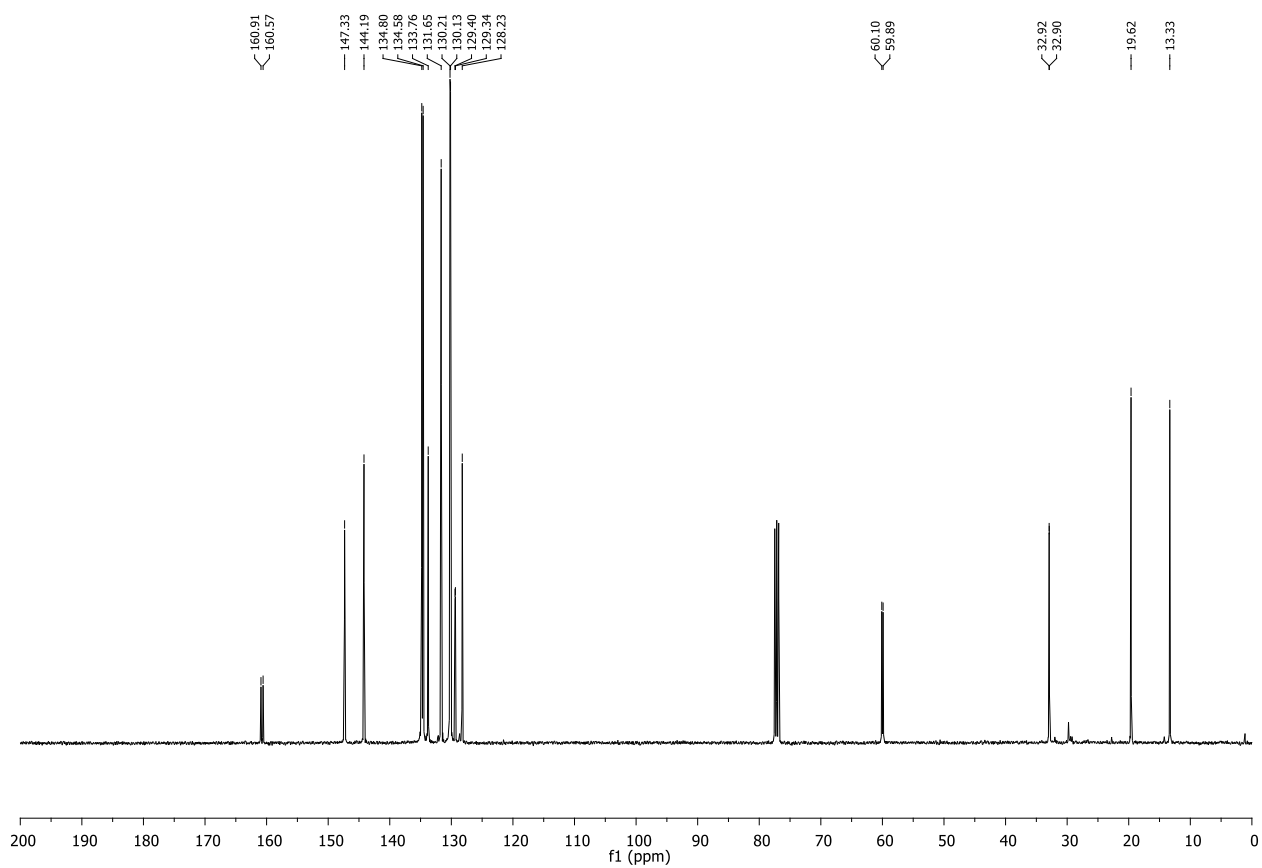
Compound 124j: ^{31}P NMR (121 MHz, CD_3CN)



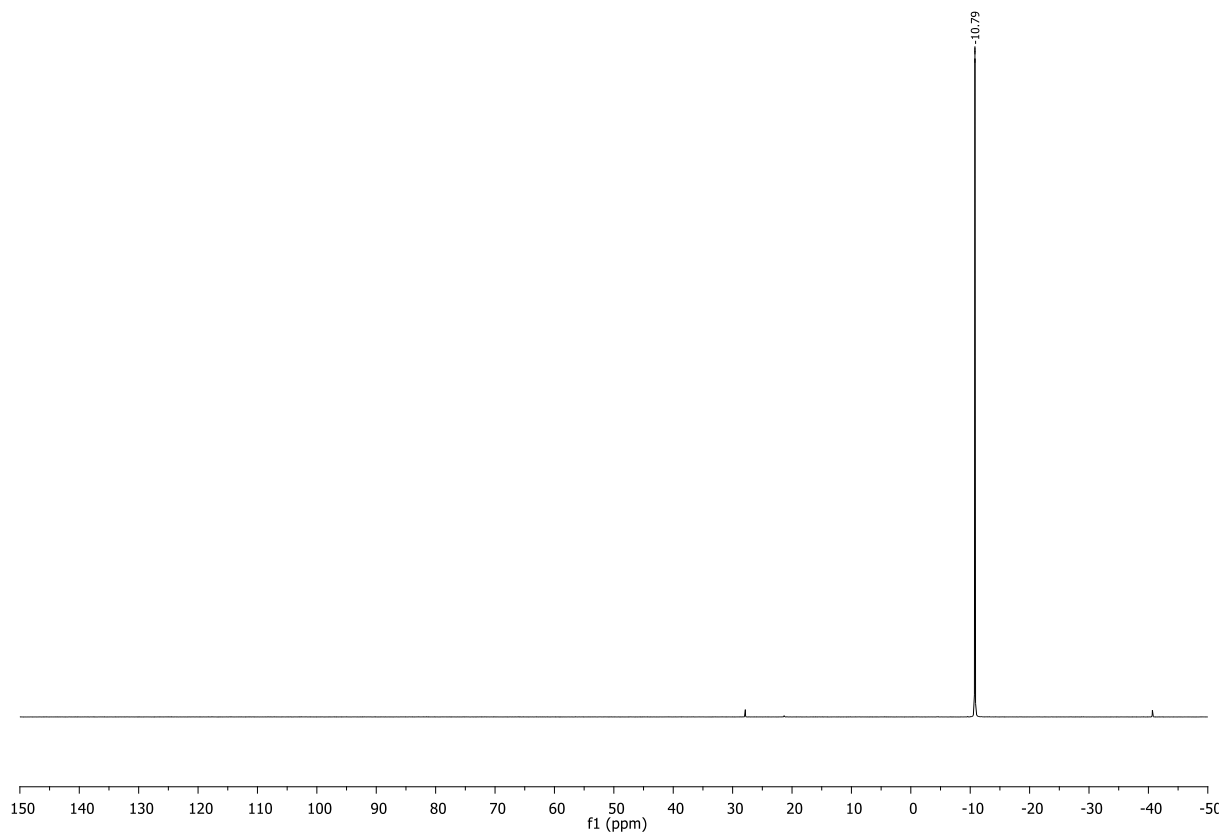
Compound 124k: ^1H NMR (300 MHz, CDCl_3)



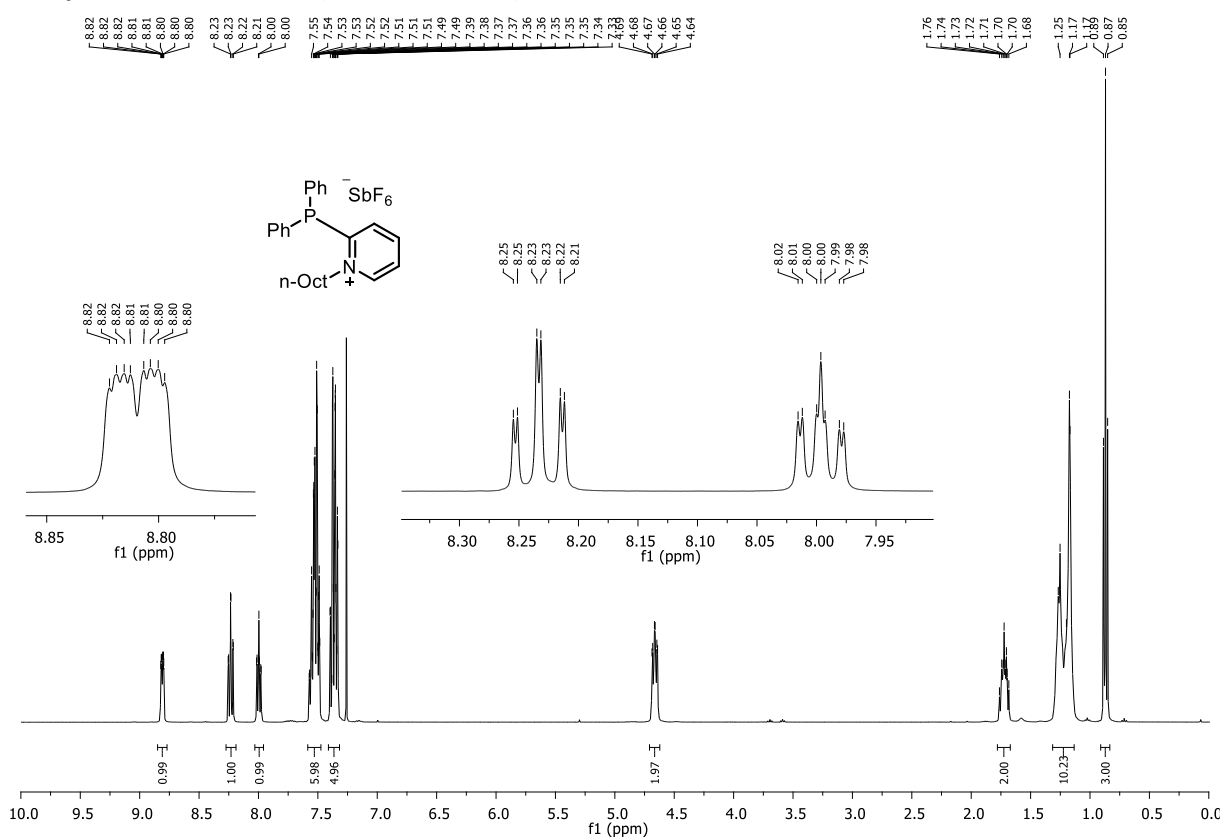
Compound 124k: ^{13}C NMR (75 MHz, CDCl_3)



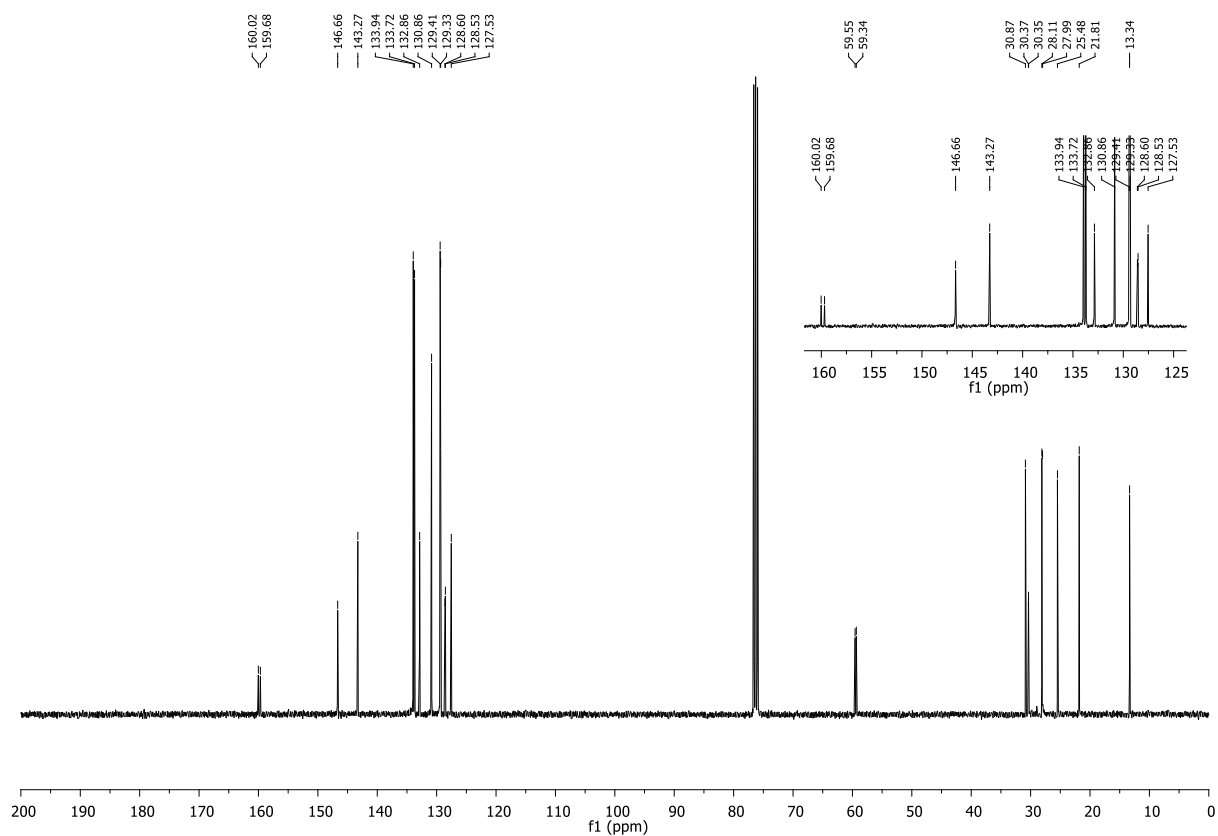
Compound 124k: ^{31}P NMR (121 MHz, CDCl_3)



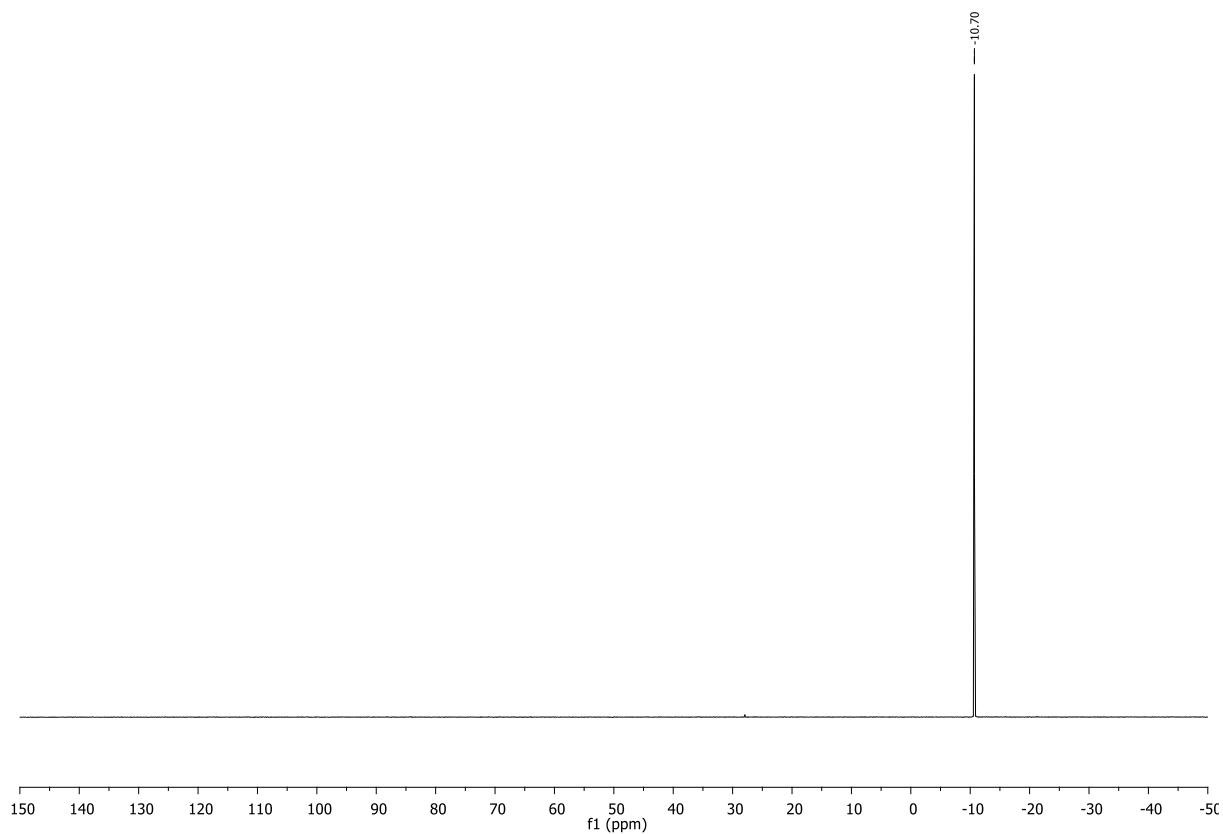
Compound 124i: ^1H NMR (300 MHz, CDCl_3)



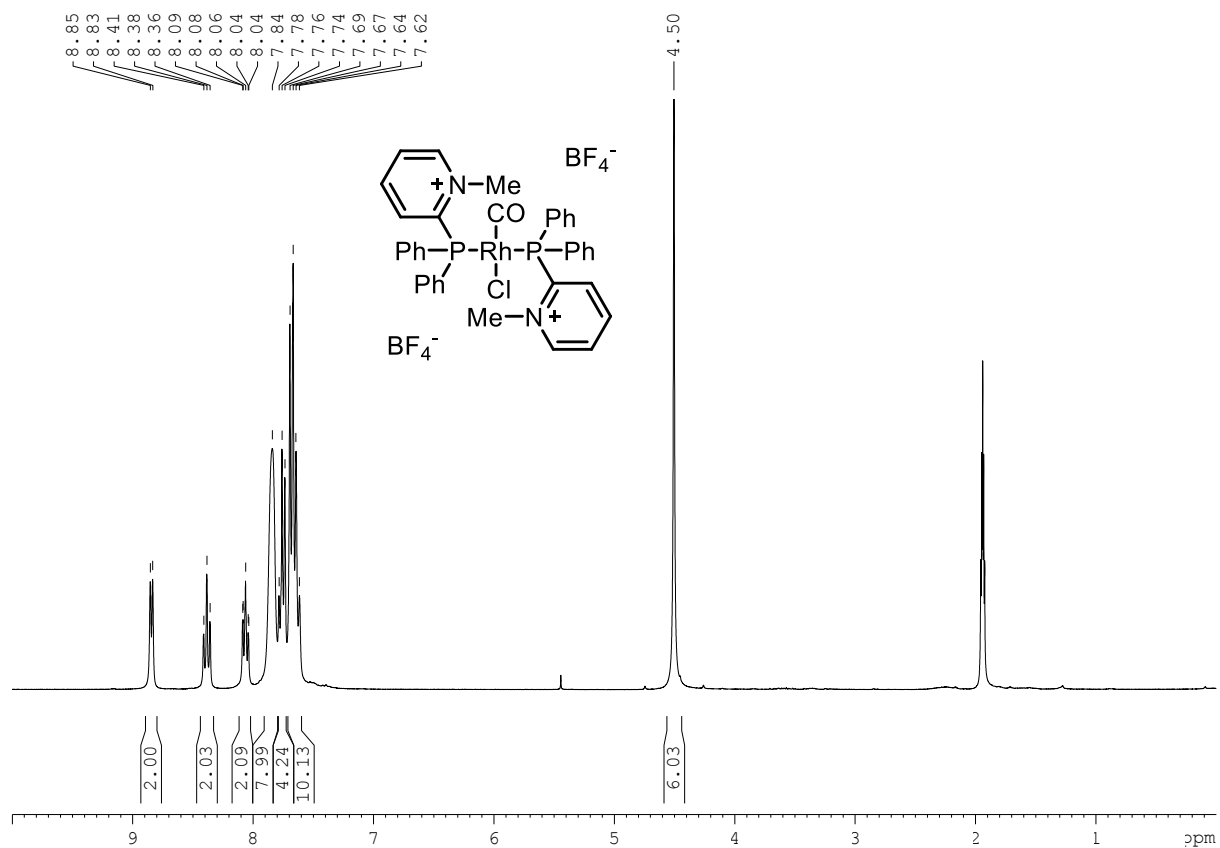
Compound 124i: ^{13}C NMR (75 MHz, CDCl_3)



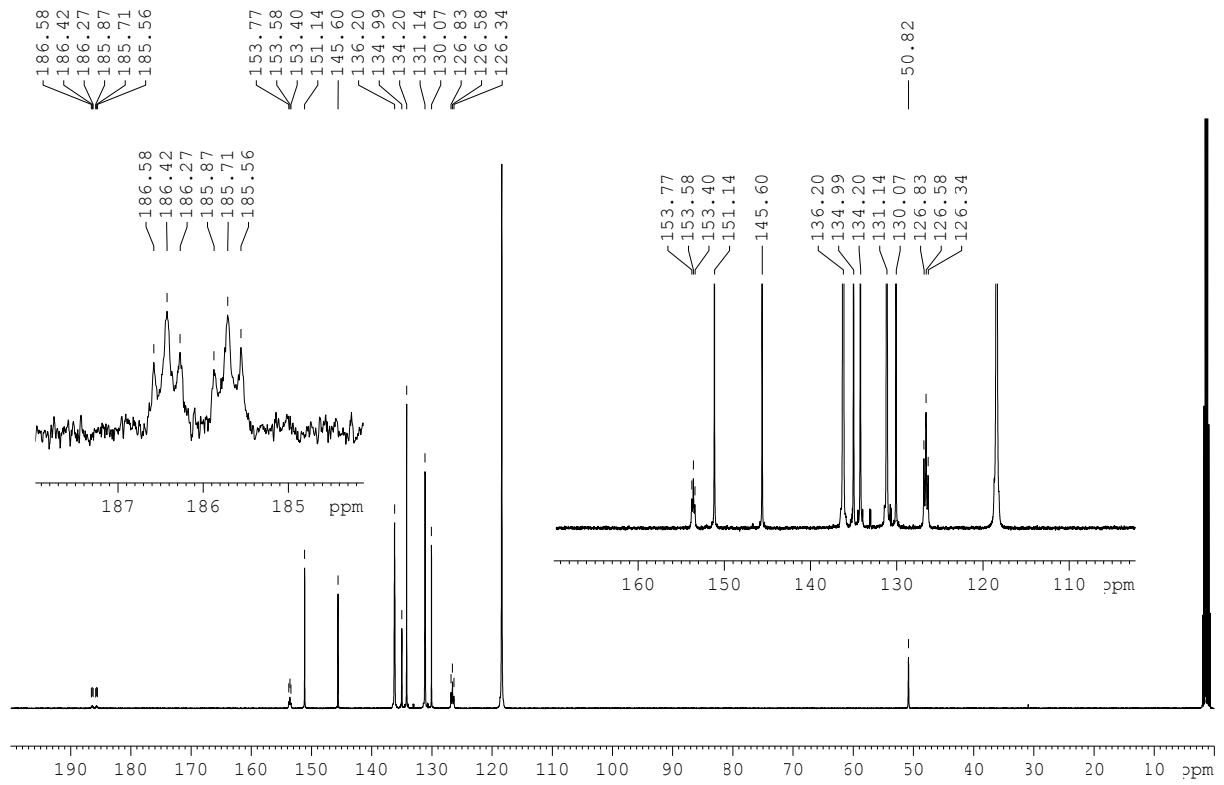
Compound 124i: ^{31}P NMR (121 MHz, CDCl_3)



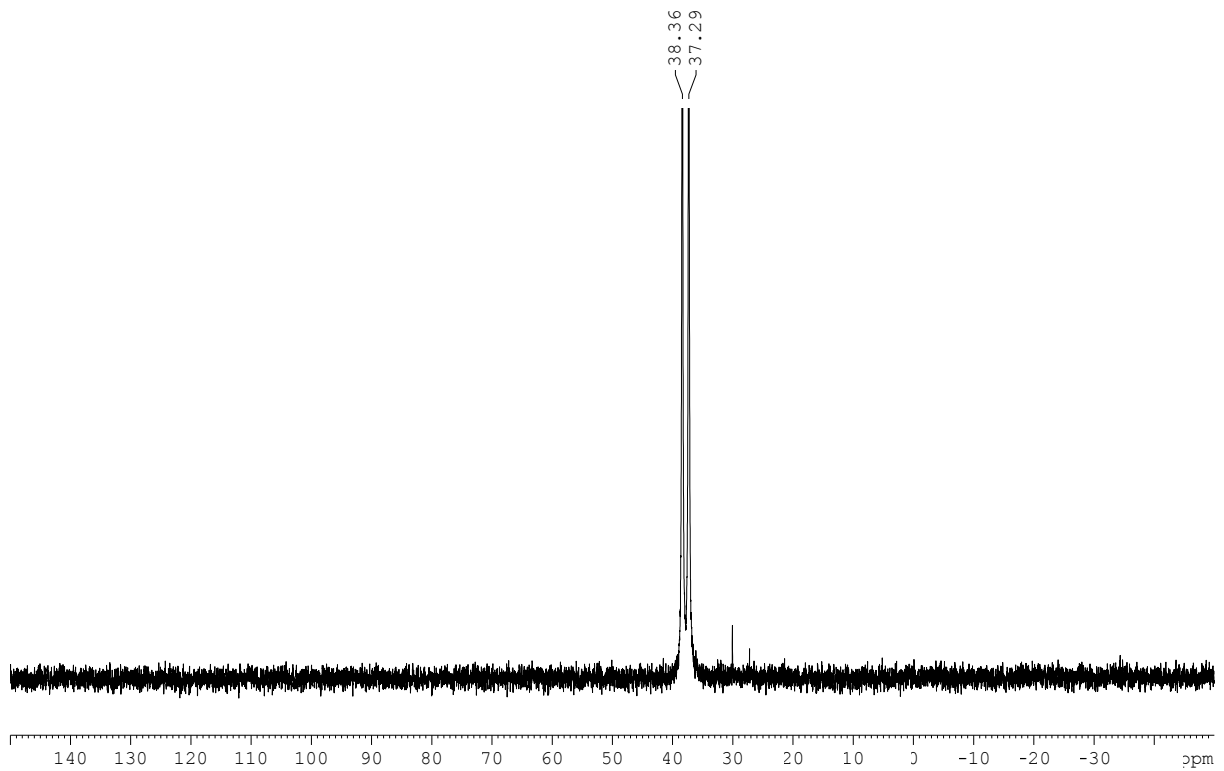
Compound 135a: ^1H NMR (300 MHz, CDCl_3)

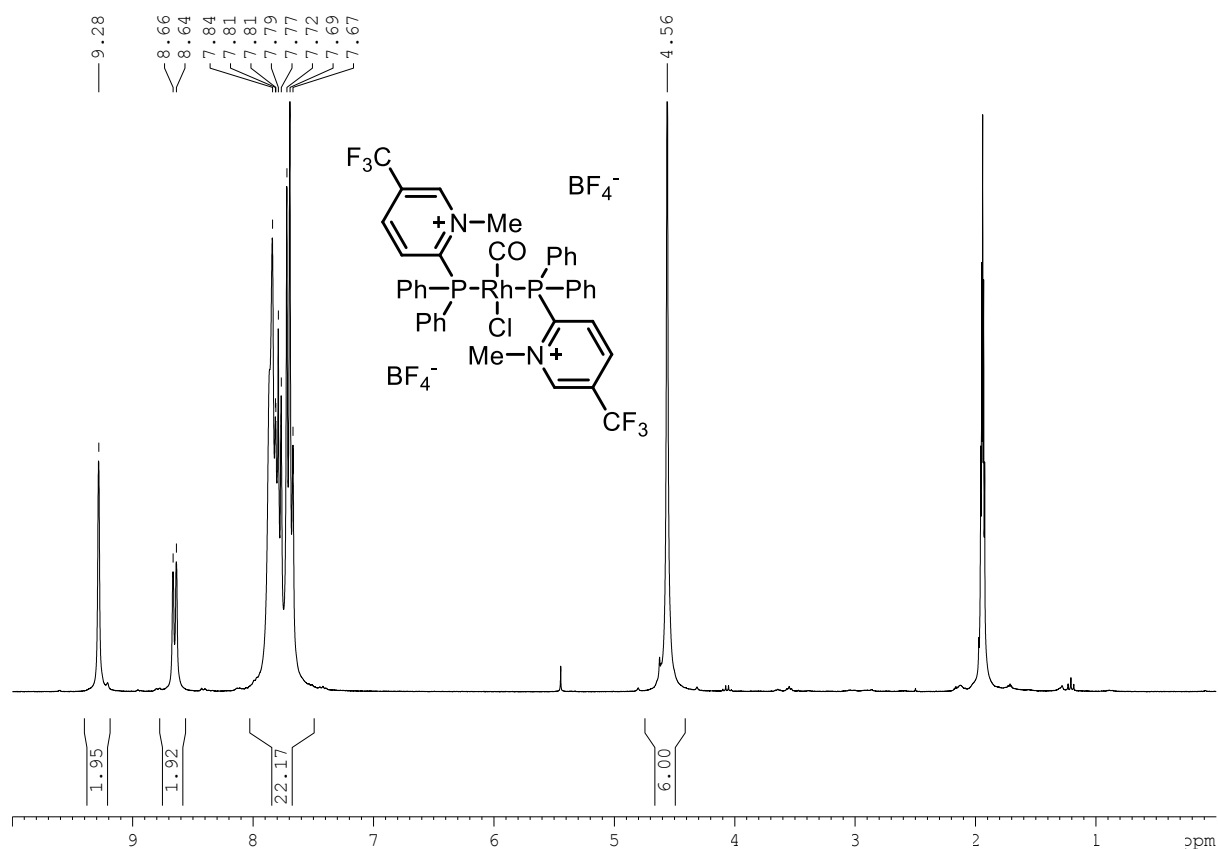
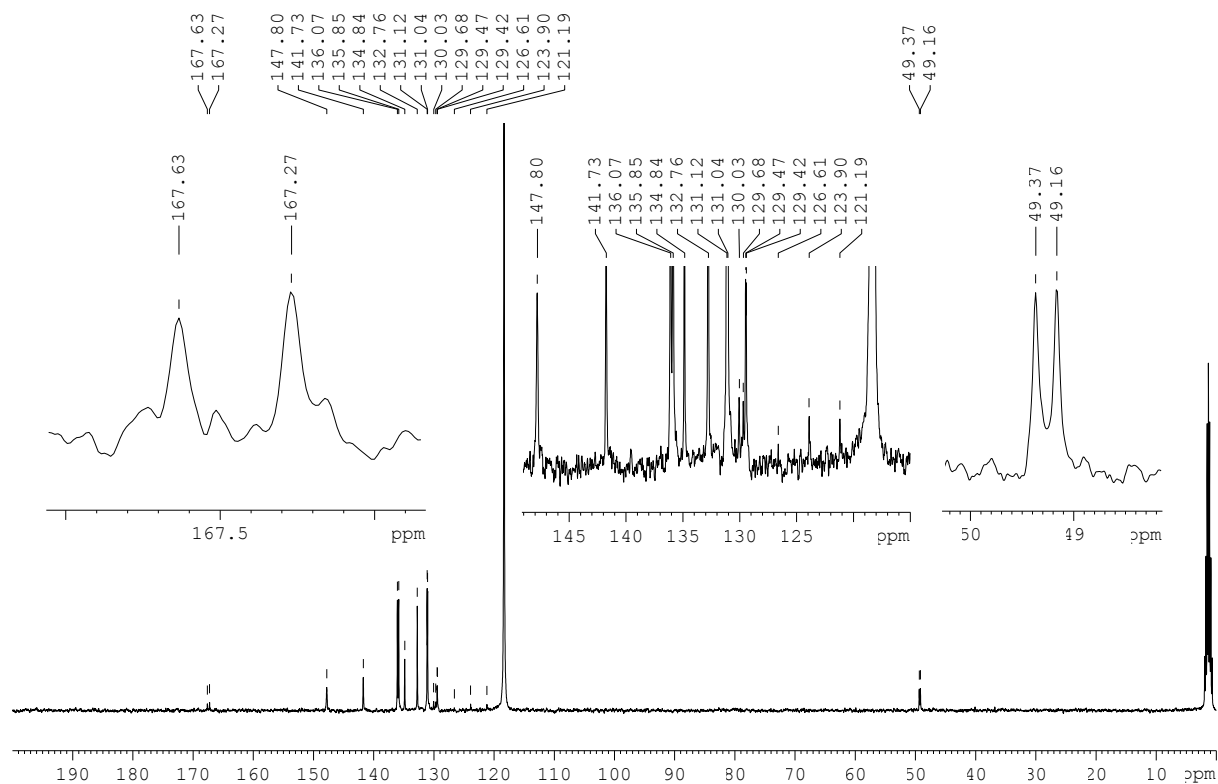


Compound 135a: ^{13}C NMR (75 MHz, CDCl_3)

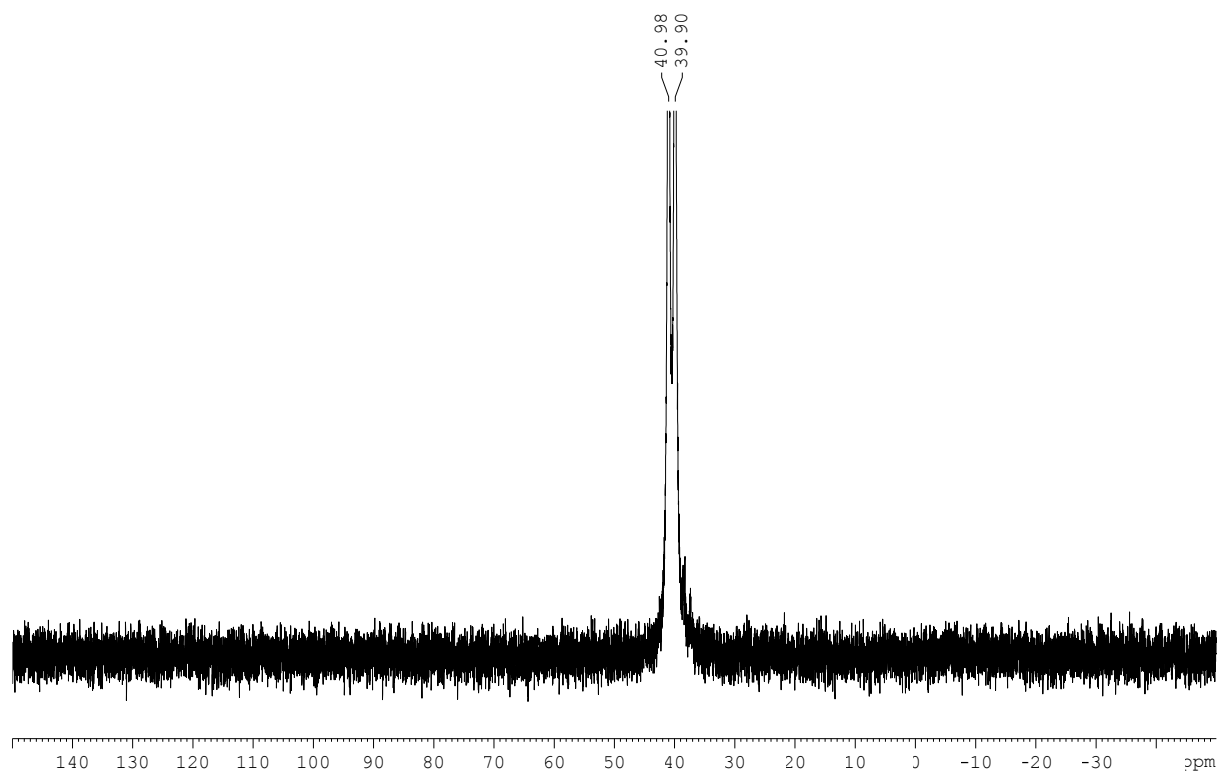


Compound 135a: ^{31}P NMR (121 MHz, CDCl_3)

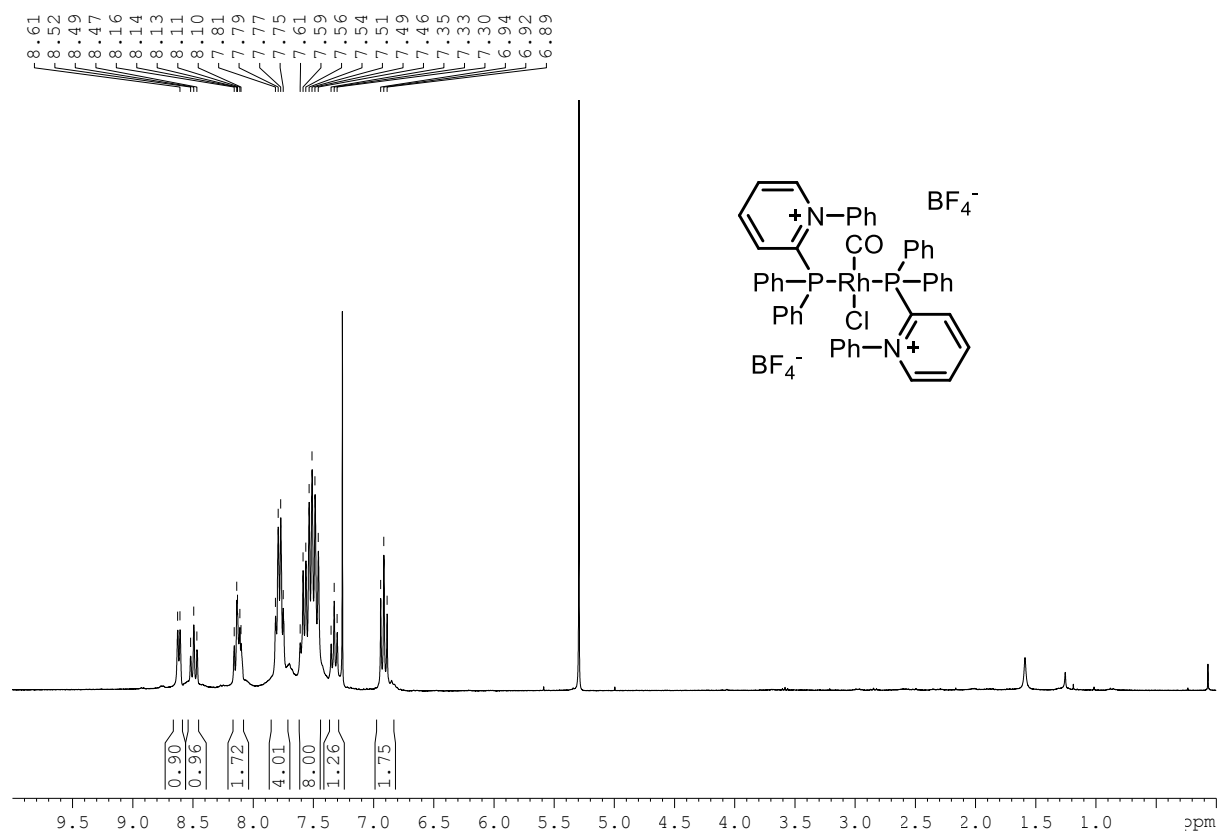


Compound 135b: ^1H NMR (300 MHz, CDCl_3)Compound 135b: ^{13}C NMR (75 MHz, CDCl_3)

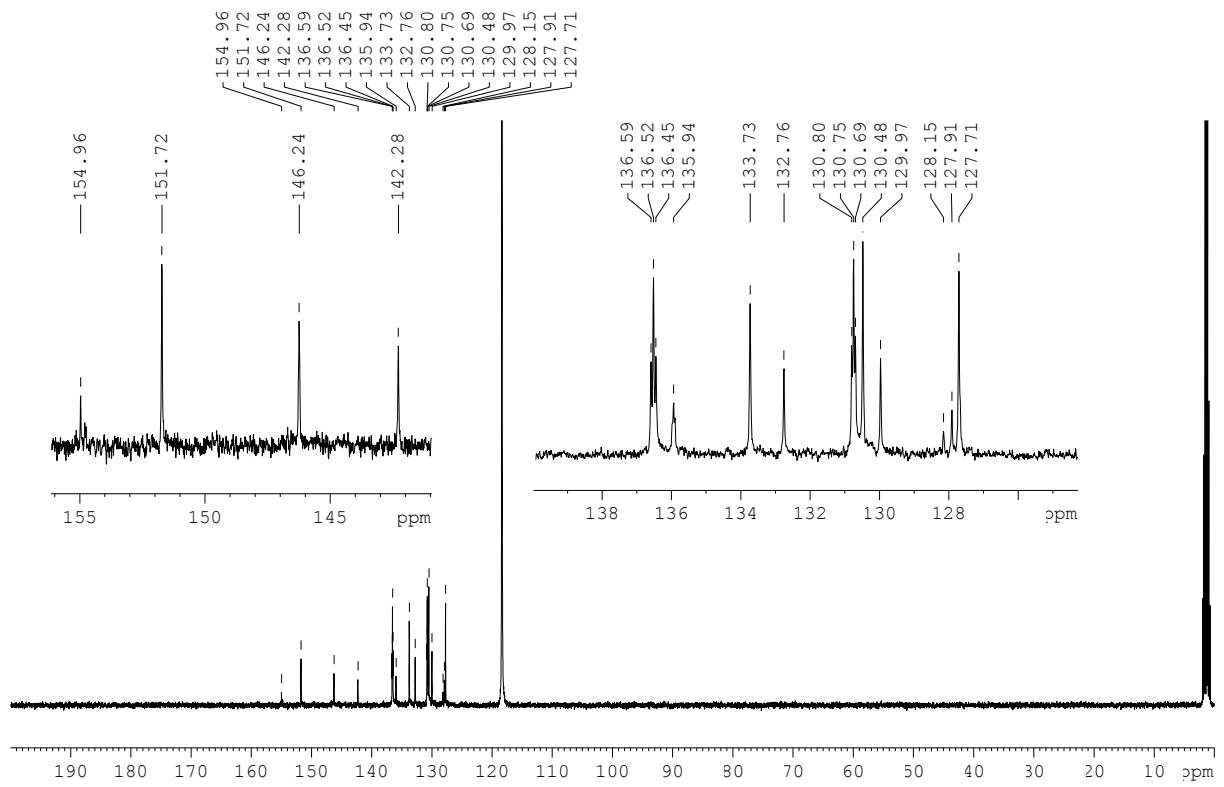
Compound 135b: ^{31}P NMR (121 MHz, CDCl_3)



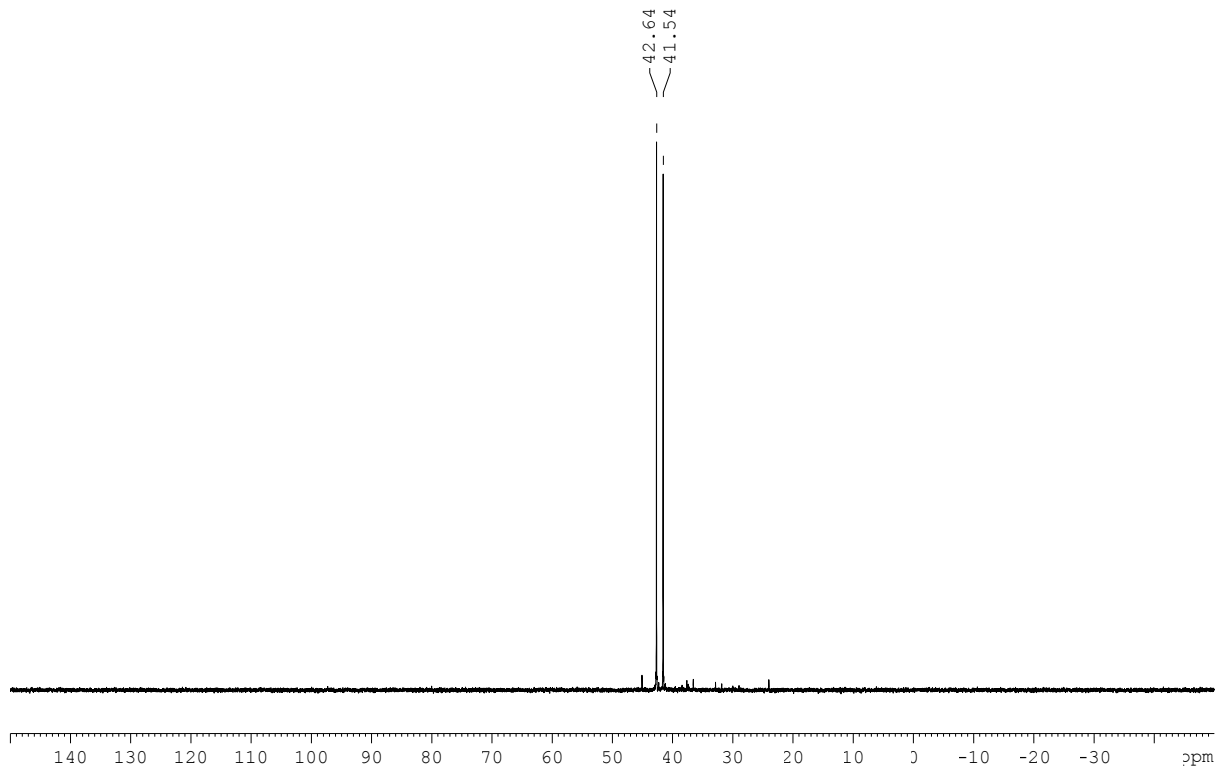
Compound 135c: ^1H NMR (300 MHz, CDCl_3)



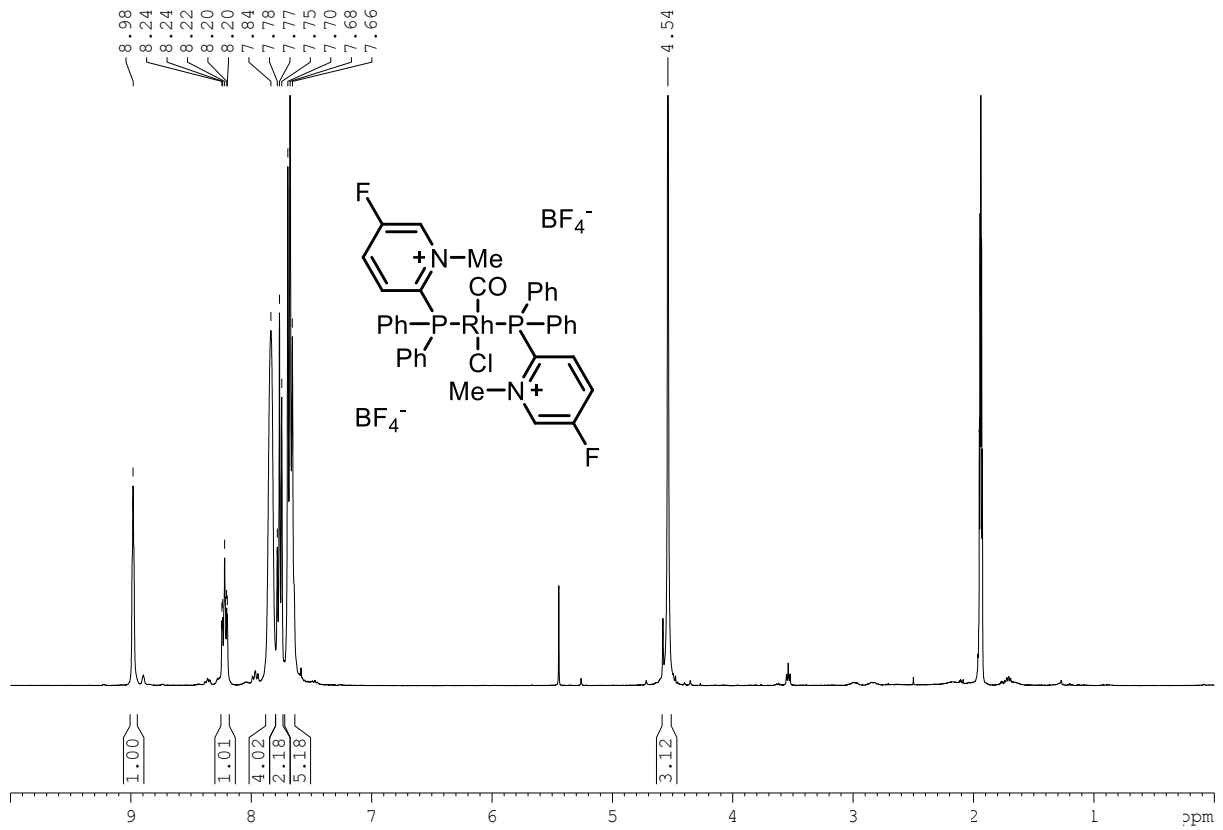
Compound 135c: ^{13}C NMR (75 MHz, CD_3CN)



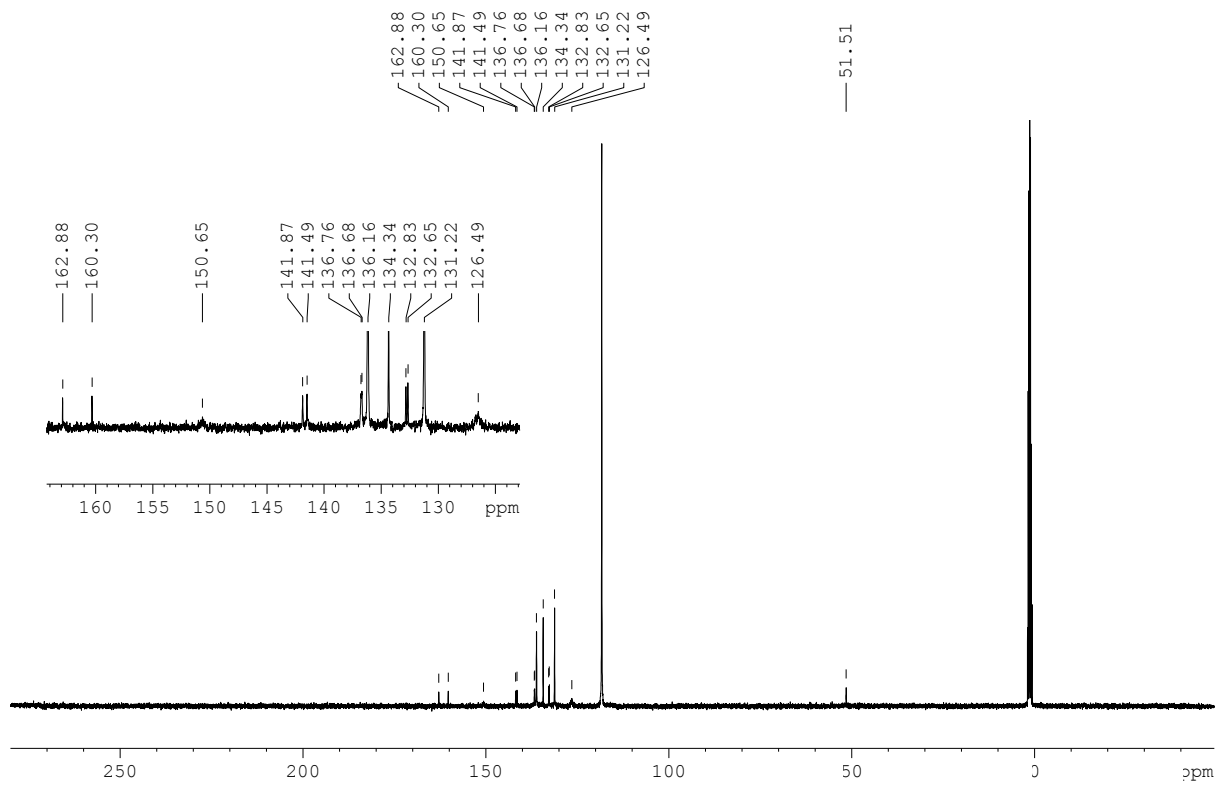
Compound 135c: ^{31}P NMR (121 MHz, CDCl_3)



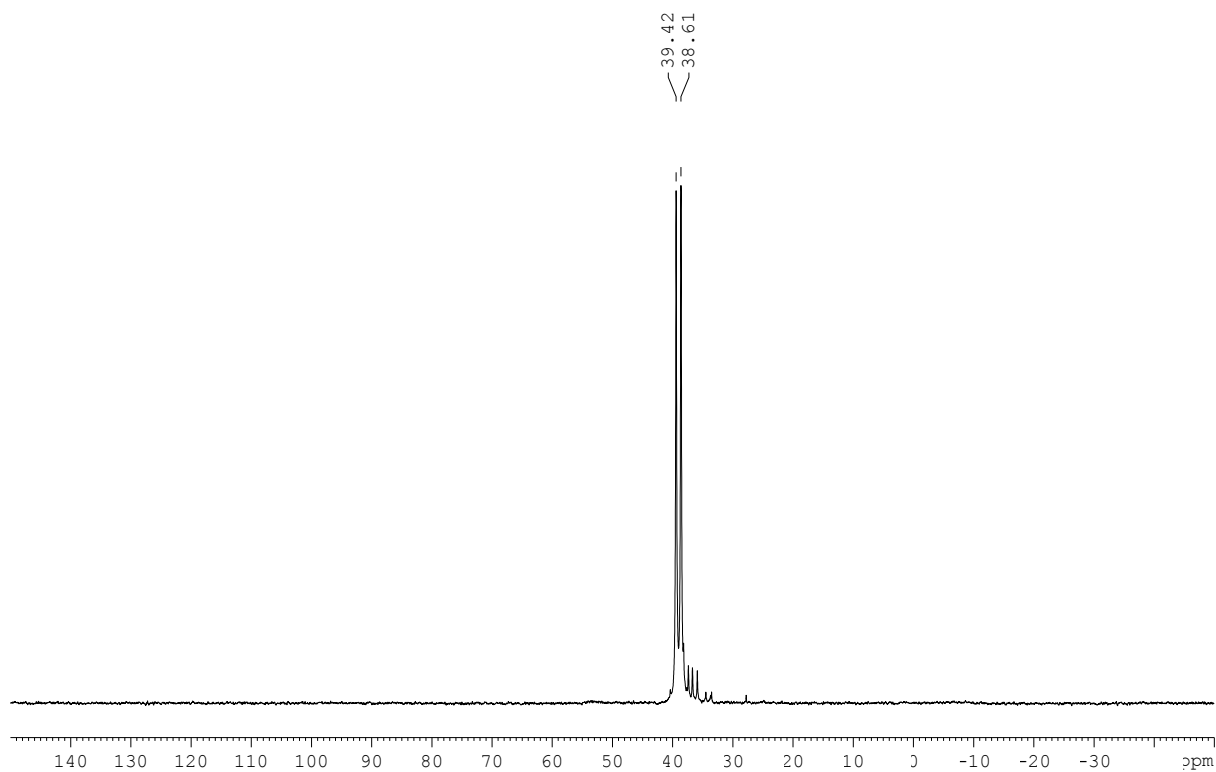
Compound 135d: ^1H NMR (300 MHz, CDCl_3)



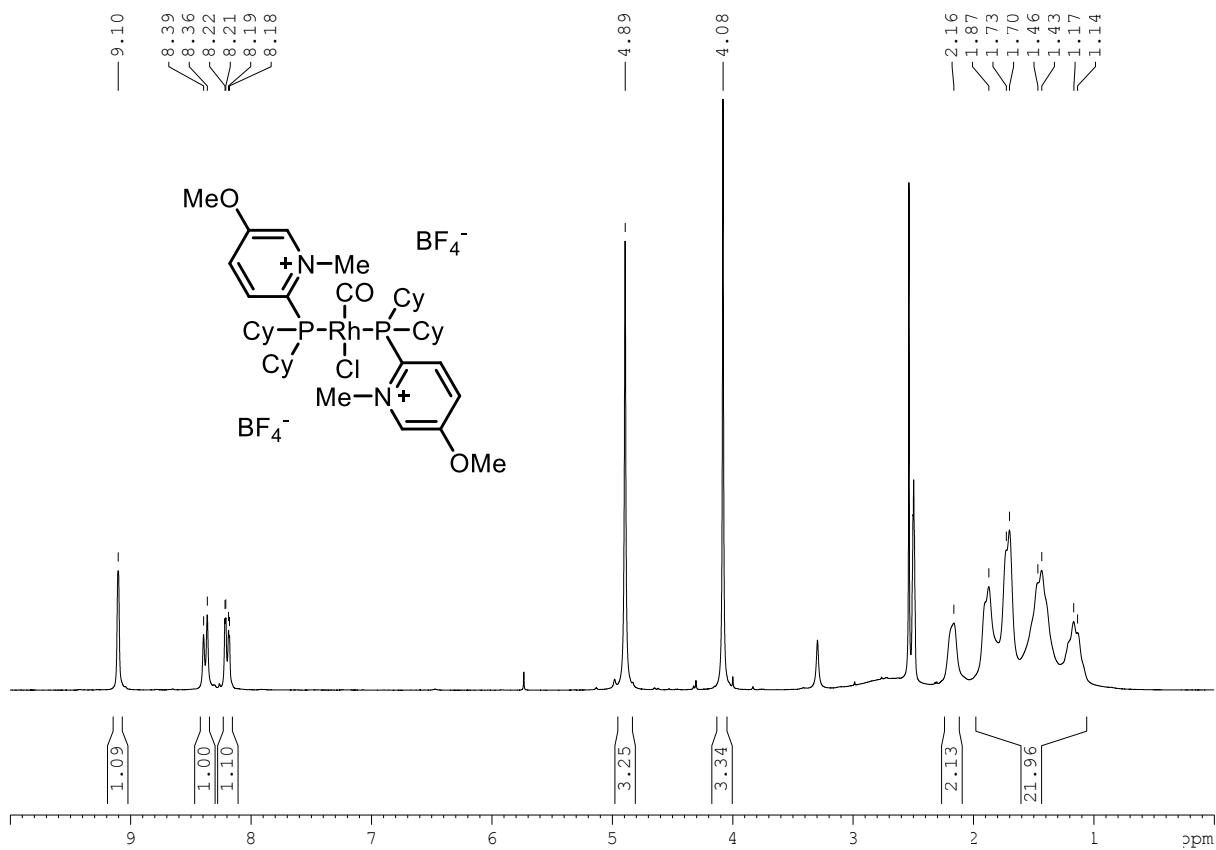
Compound 135d: ^{13}C NMR (75 MHz, CDCl_3)



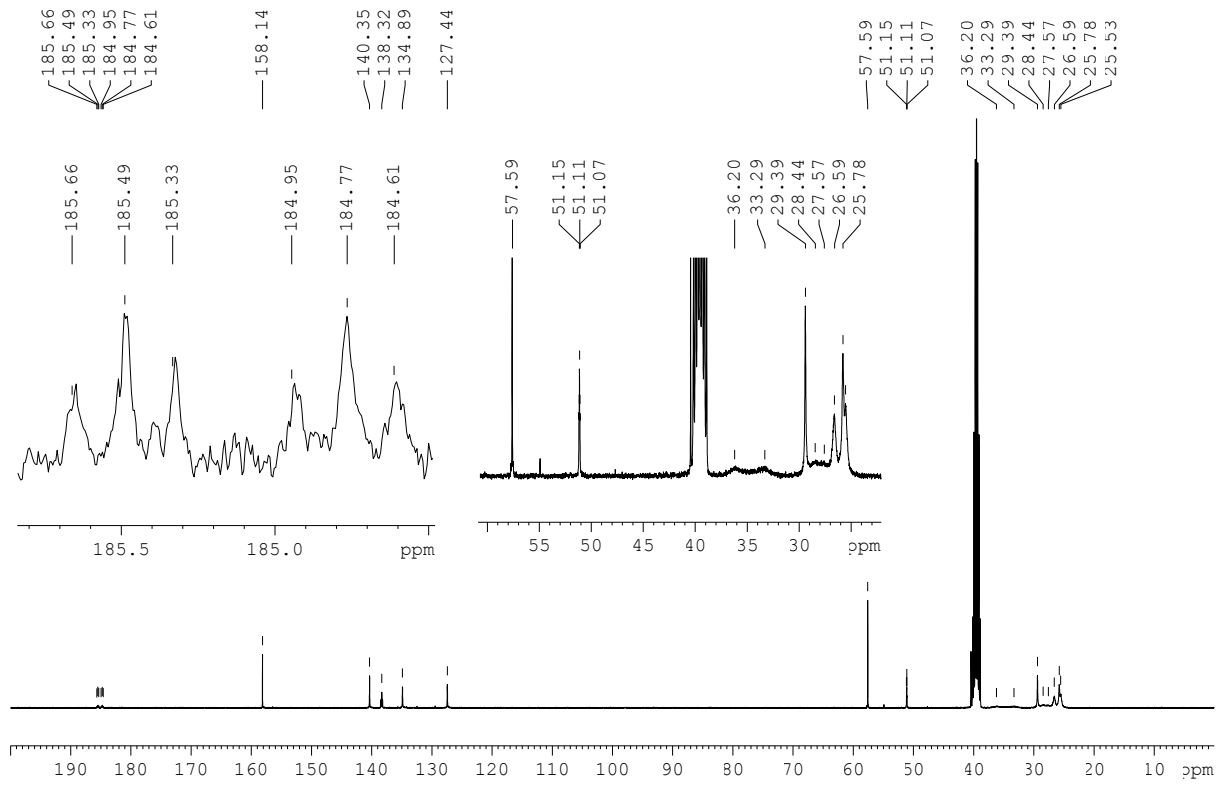
Compound 135d: ^{31}P NMR (121 MHz, CDCl_3)



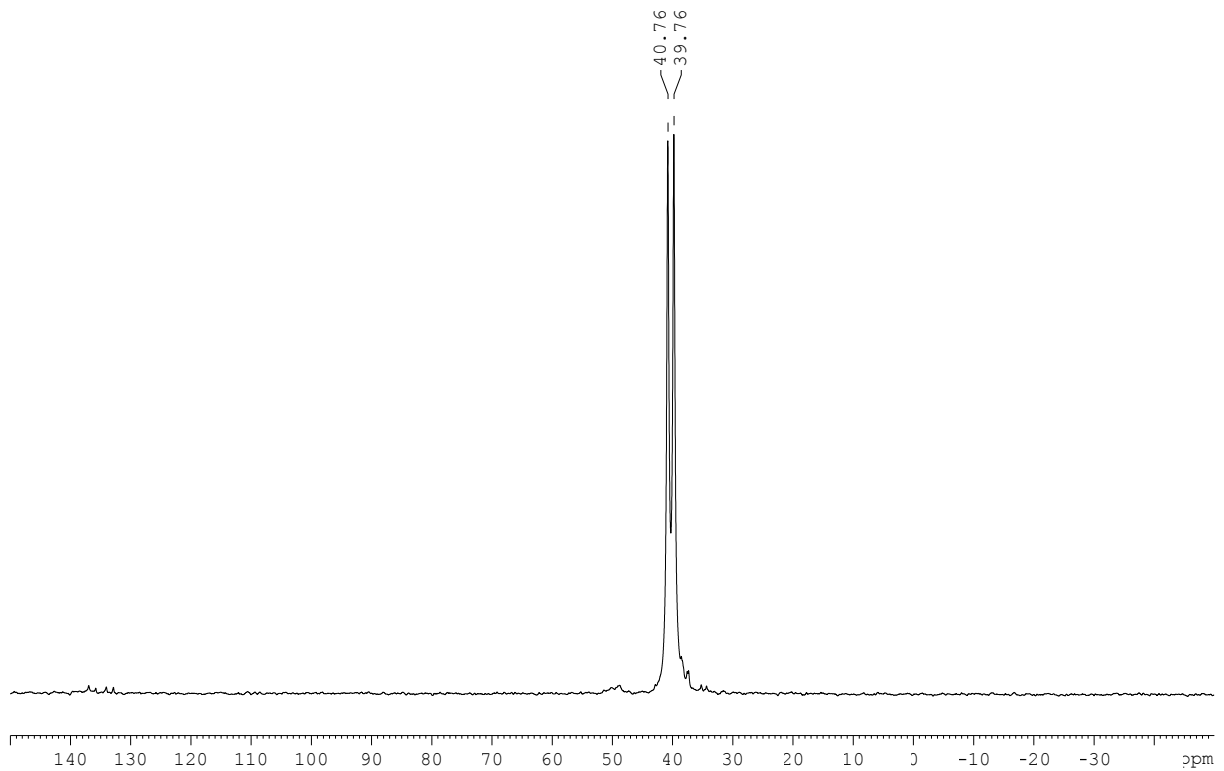
Compound 135e: ^1H NMR (300 MHz, DMSO)



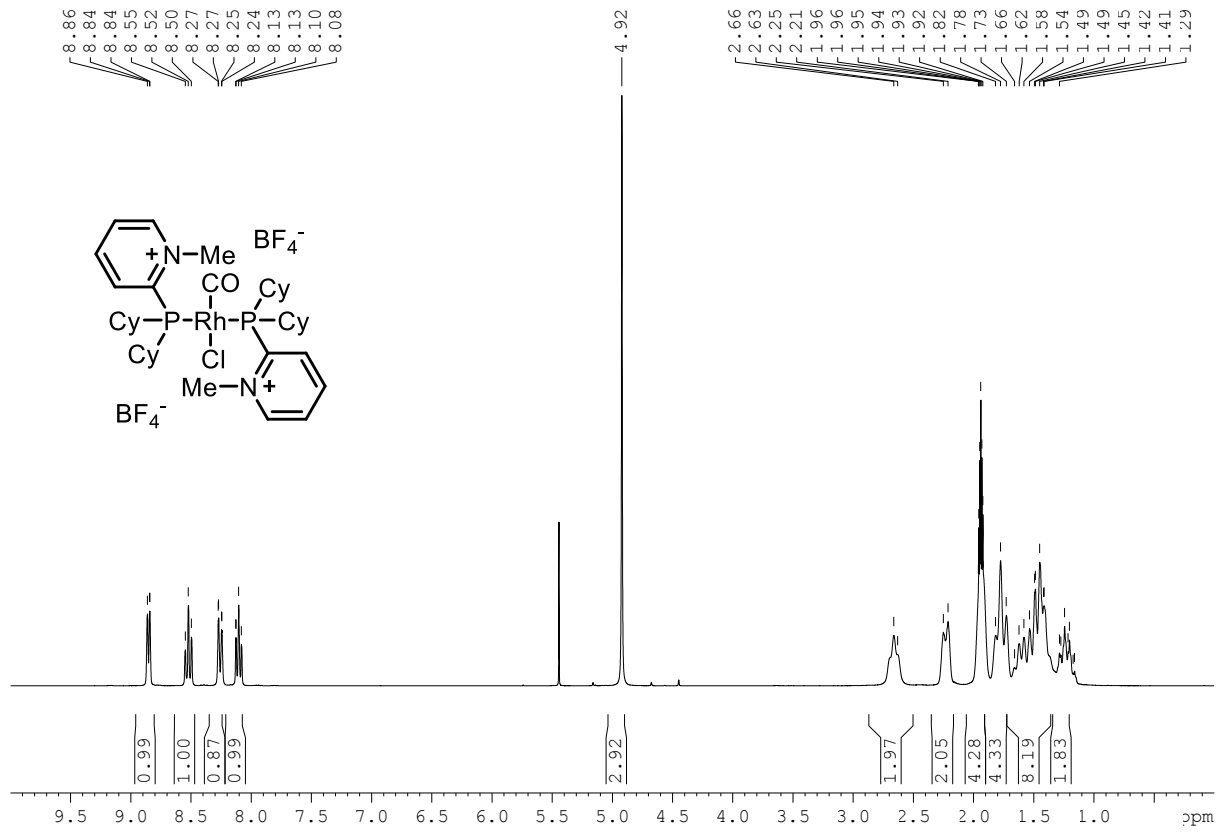
Compound 135e: ^{13}C NMR (75 MHz, CDCl_3)



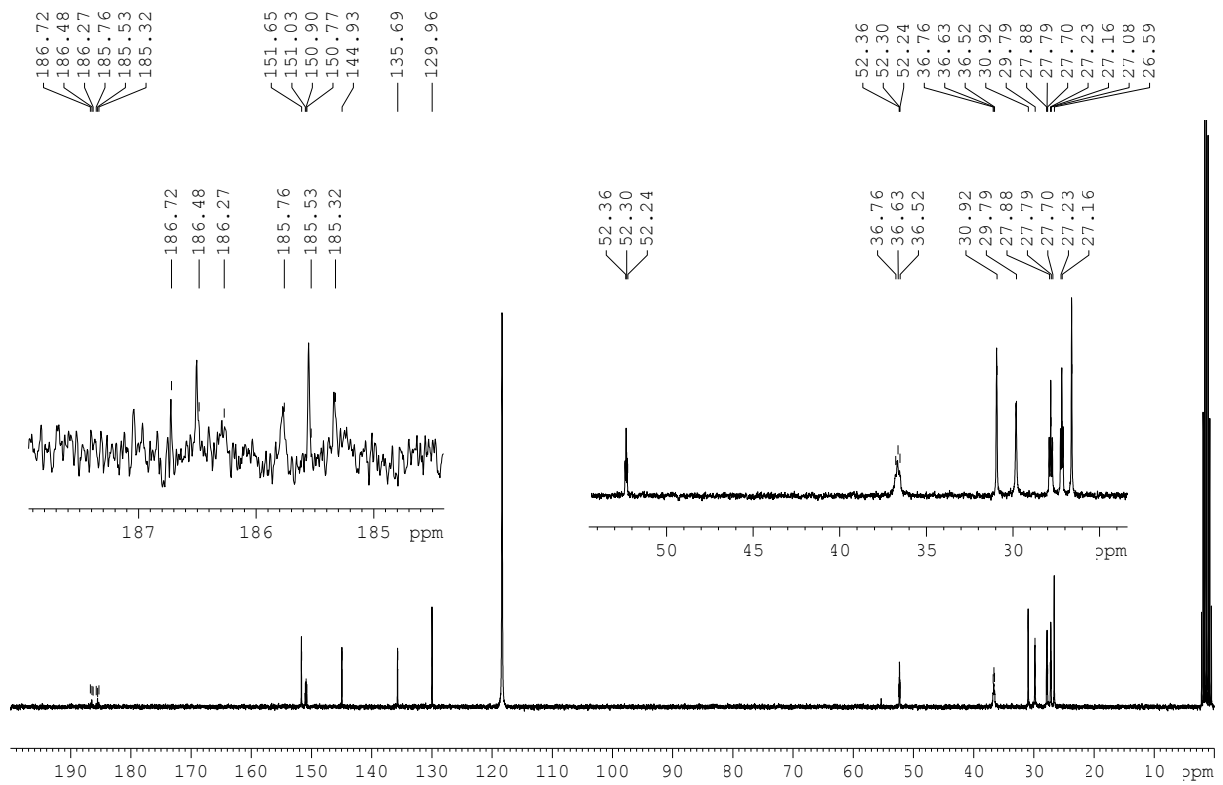
Compound 135e: ^{31}P NMR (121 MHz, DMSO)



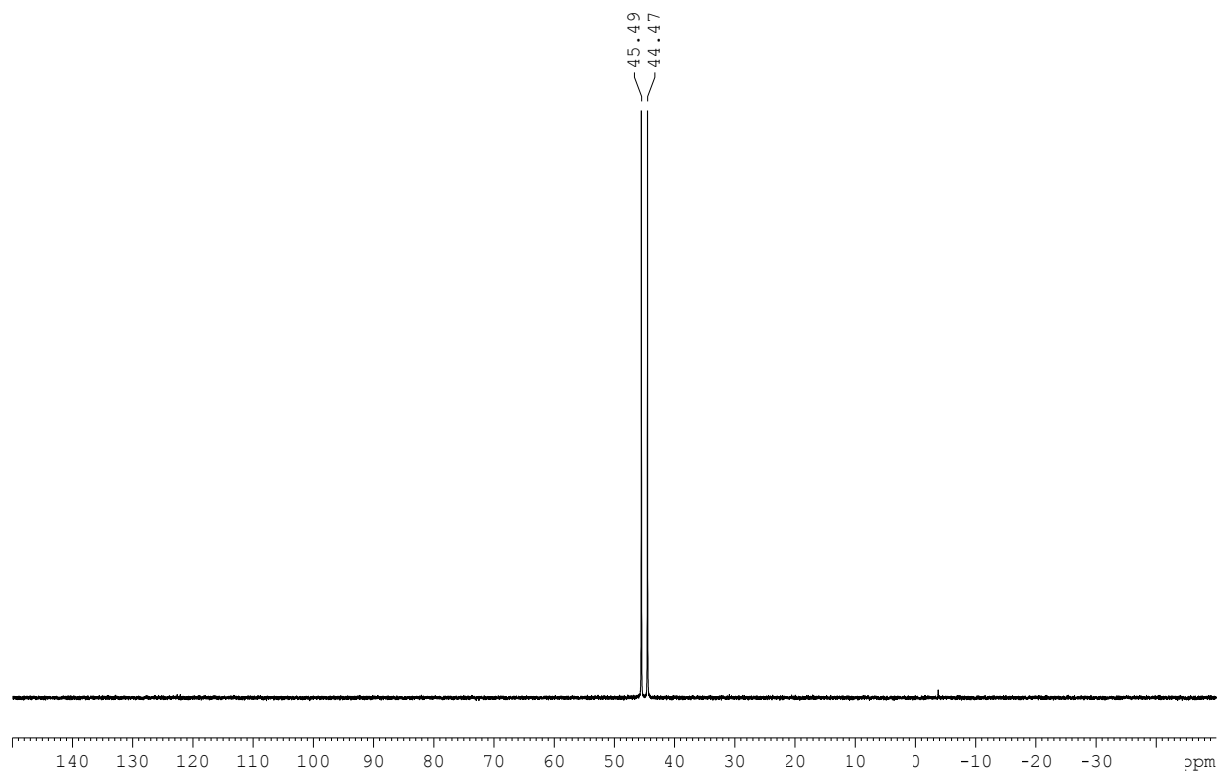
Compound 135f: ^1H NMR (300 MHz, CDCl_3)



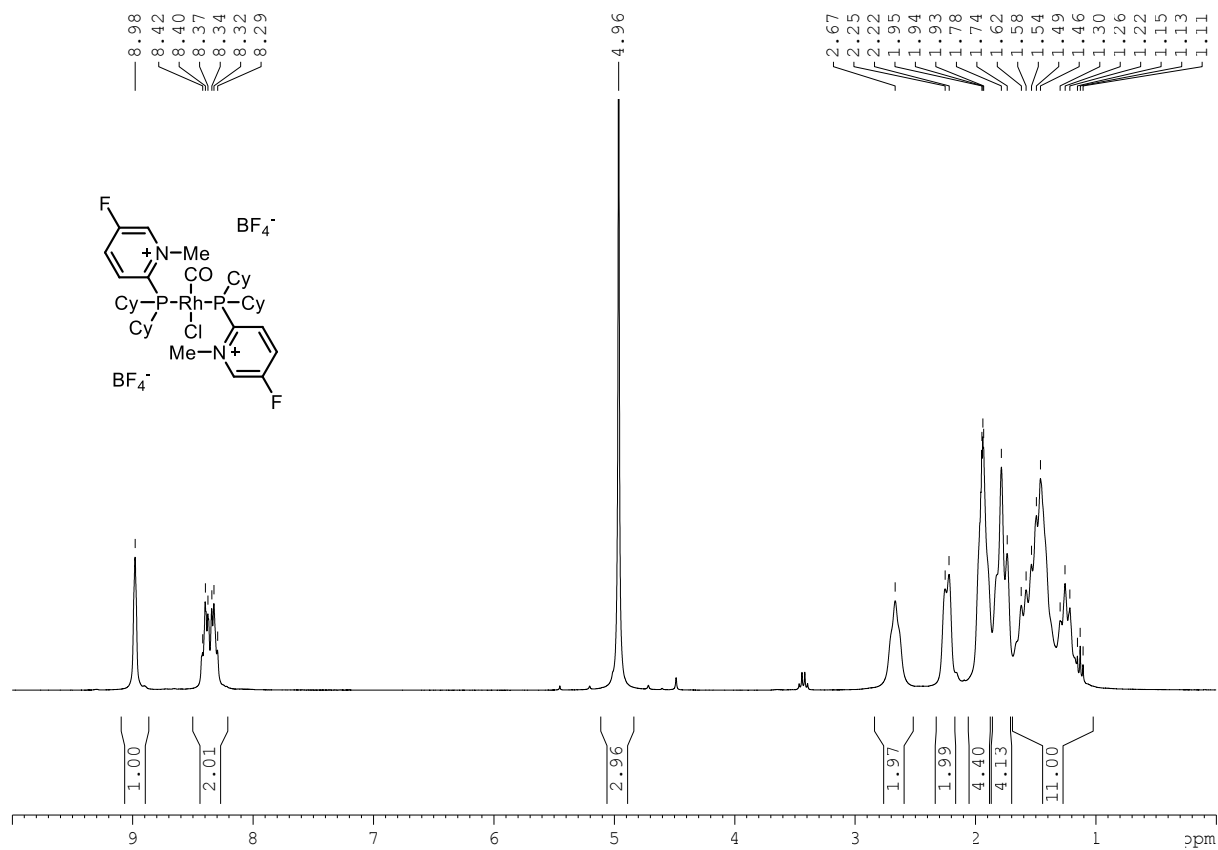
Compound 135f: ^{13}C NMR (75 MHz, CDCl_3)



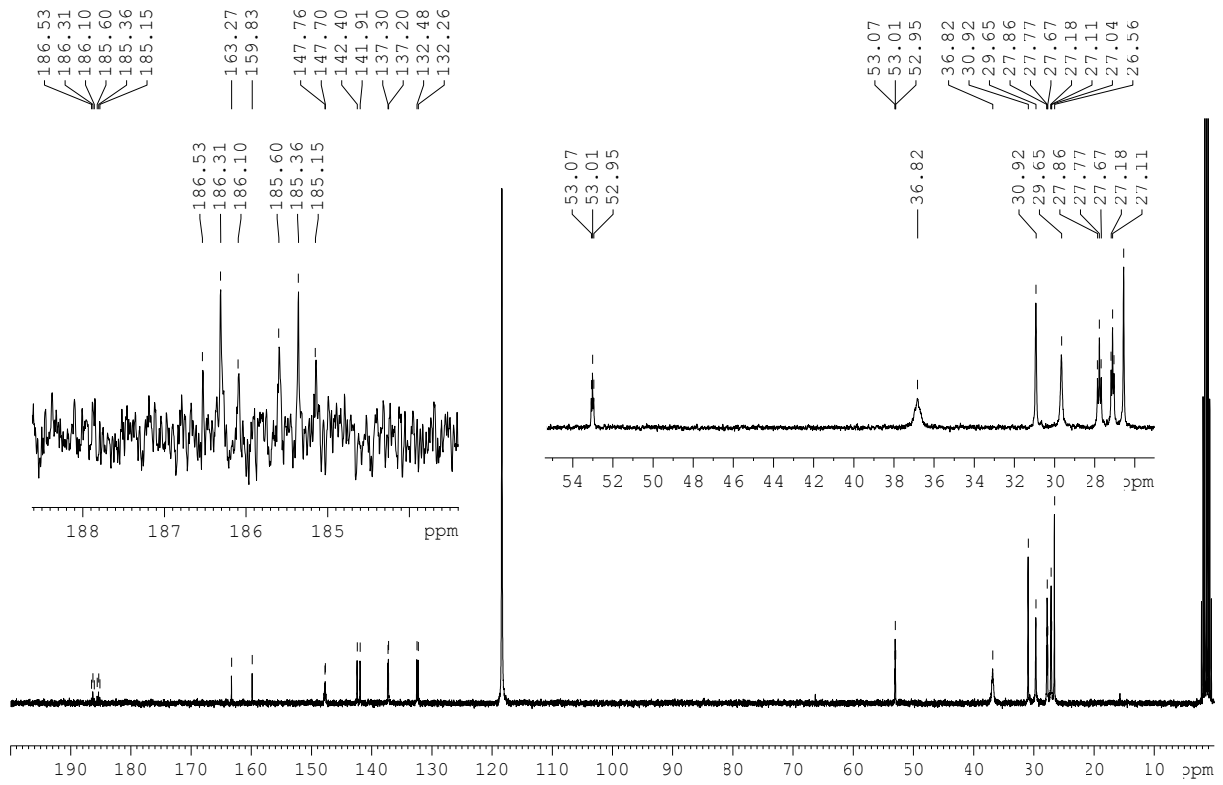
Compound 135f: ^{31}P NMR (121 MHz, CDCl_3)



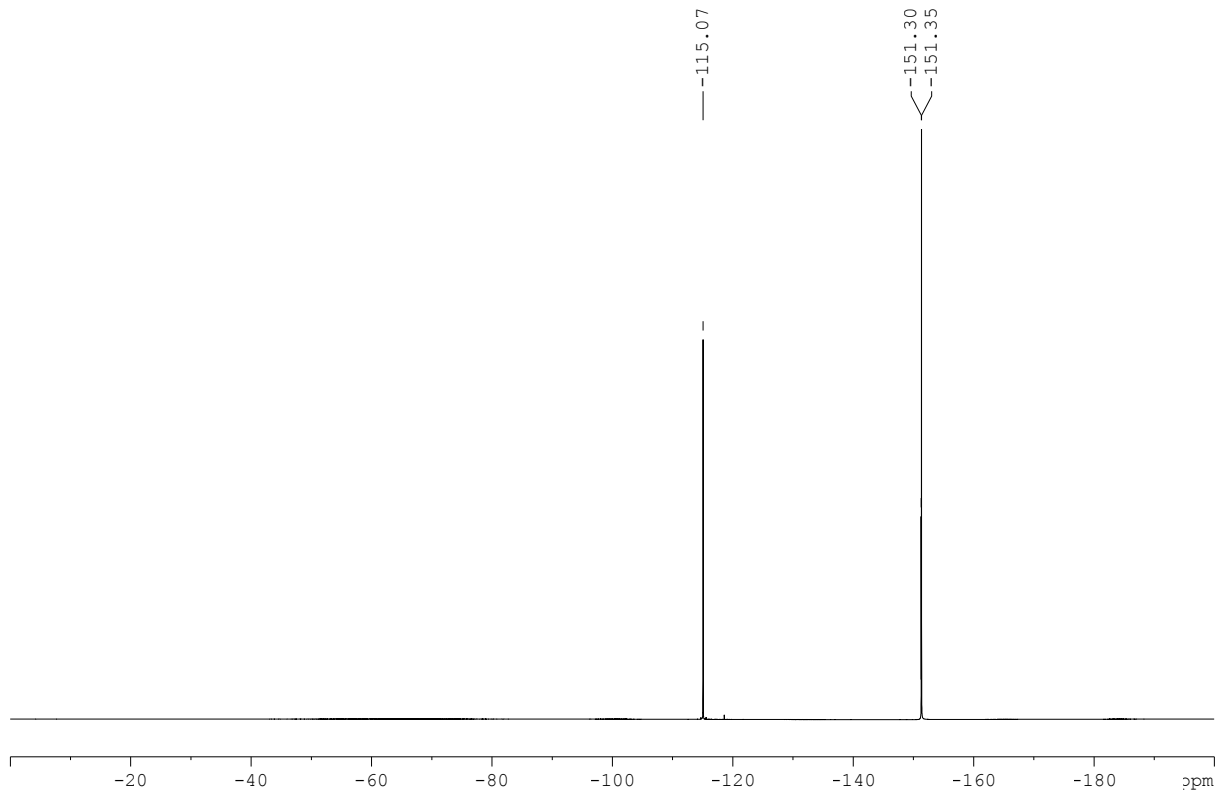
Compound 135g: ^1H NMR (300 MHz, CDCl_3)



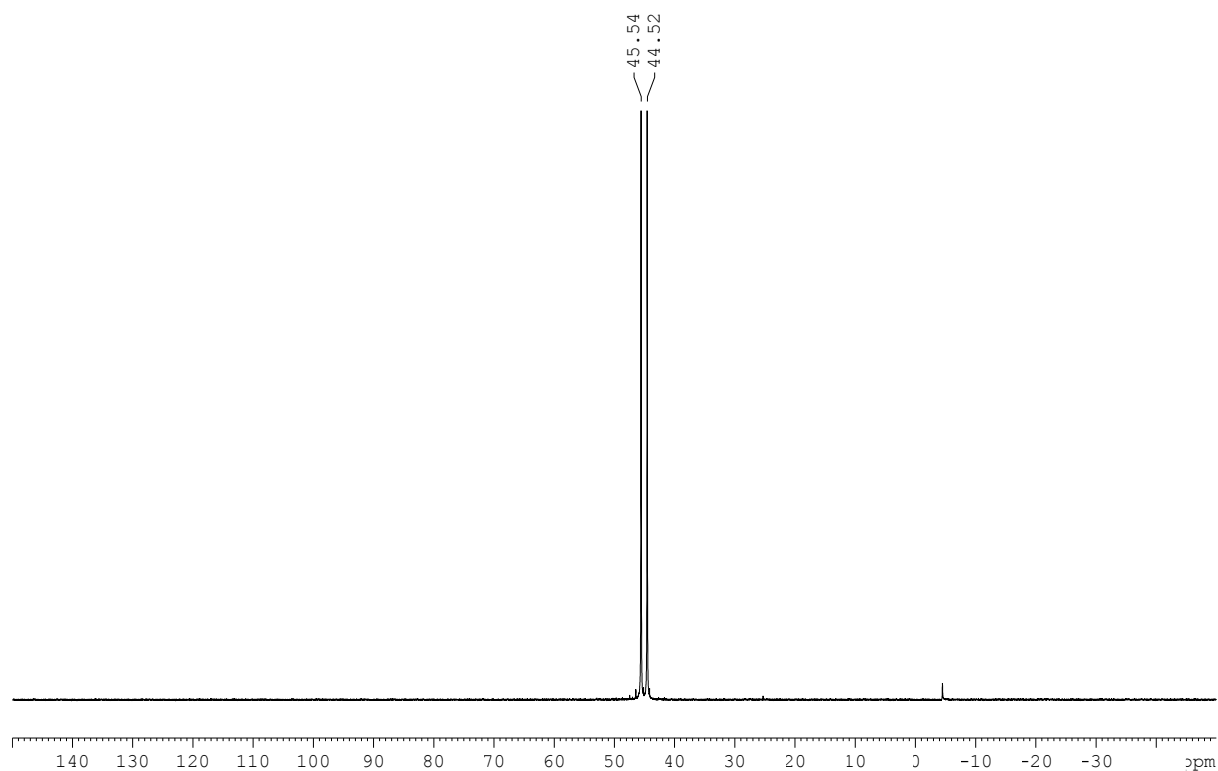
Compound 135g: ^{13}C NMR (75 MHz, CDCl_3)



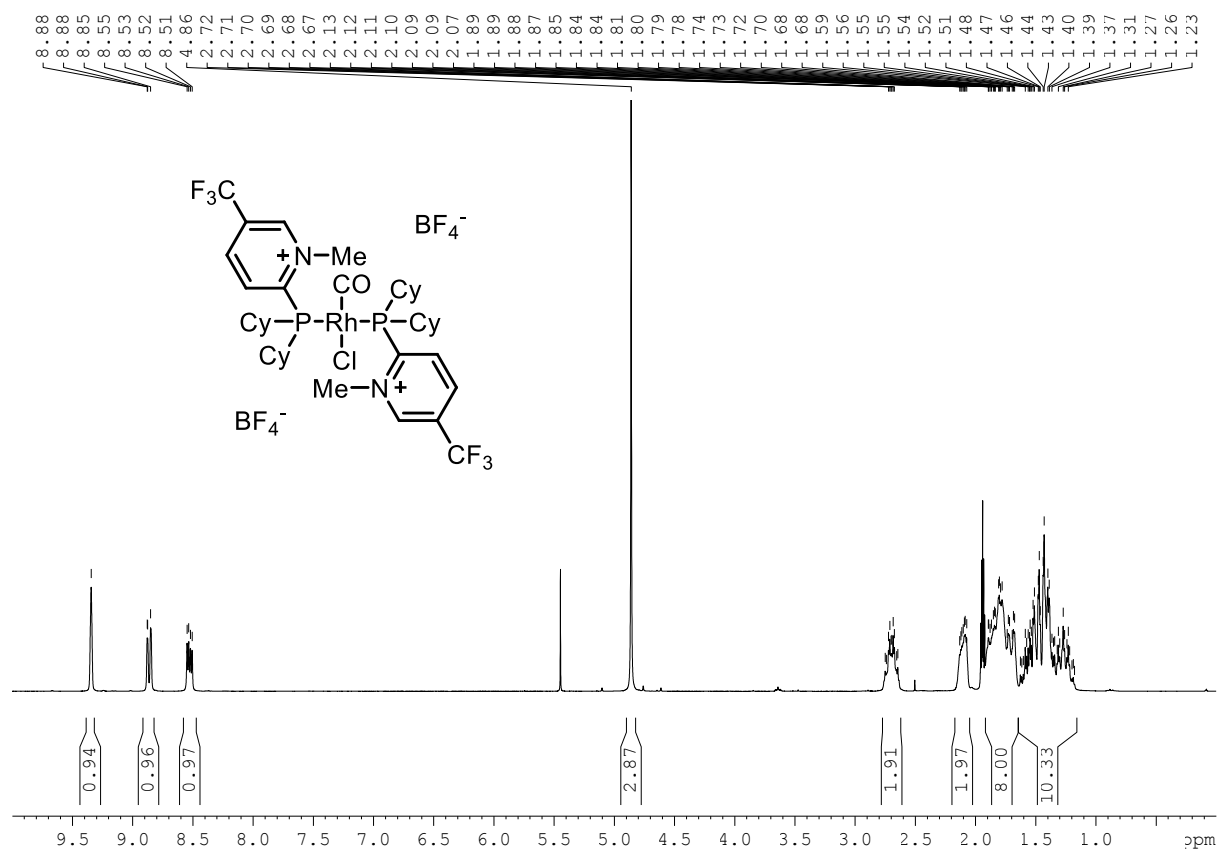
Compound 135g: ^{19}F NMR (282 MHz, CDCl_3)



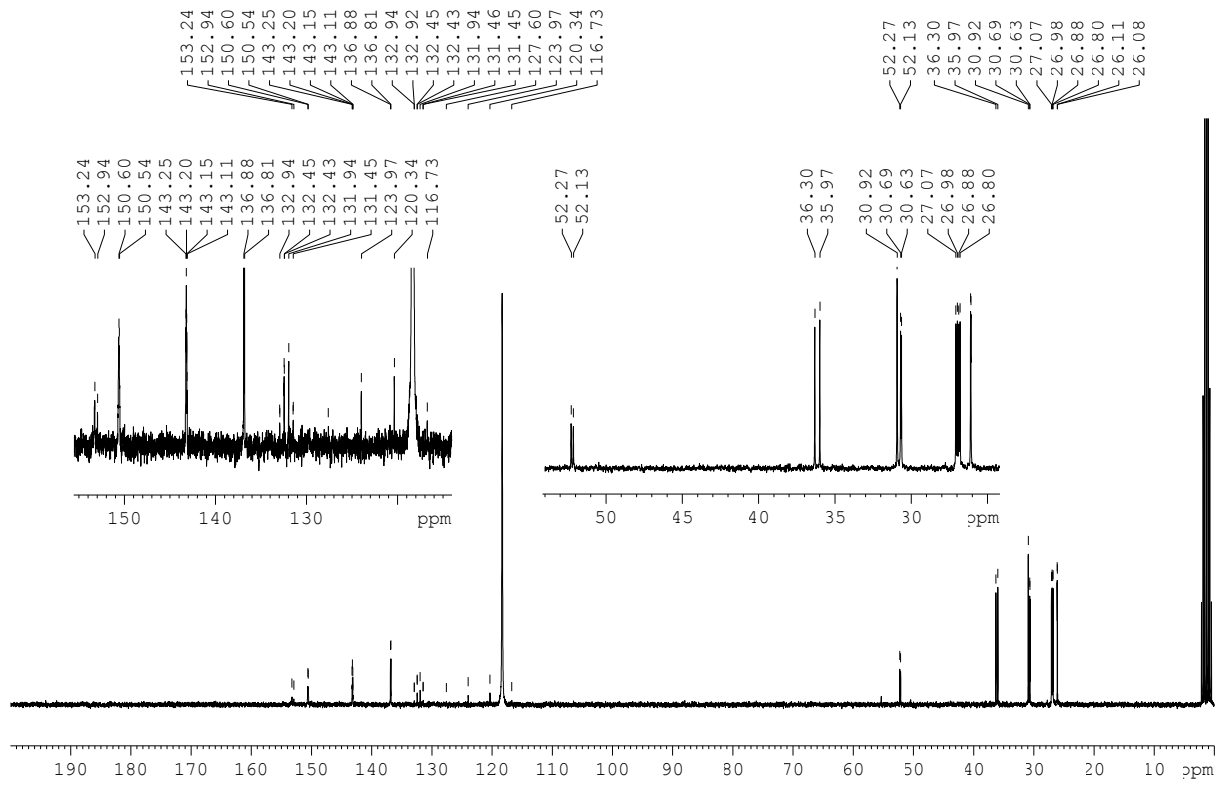
Compound 135g: ^{31}P NMR (121 MHz, CDCl_3)



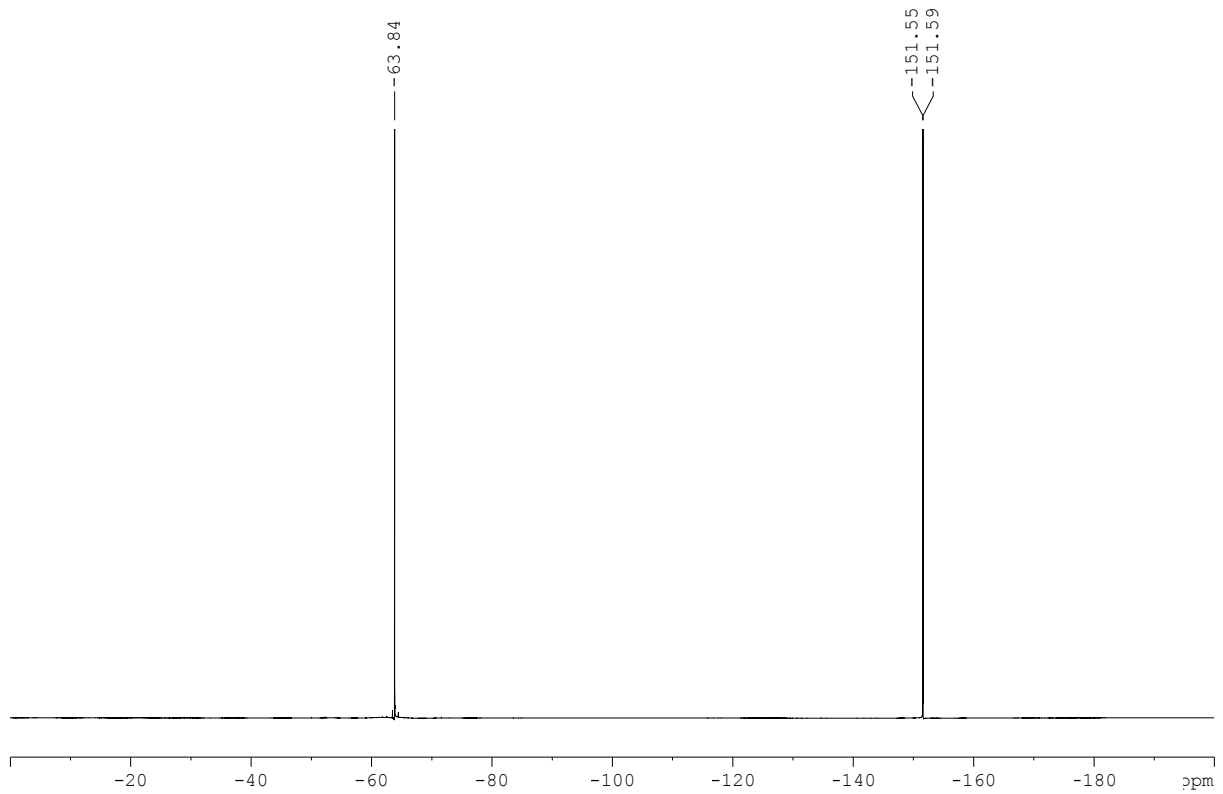
Compound 135h: ^1H NMR (300 MHz, CDCl_3)



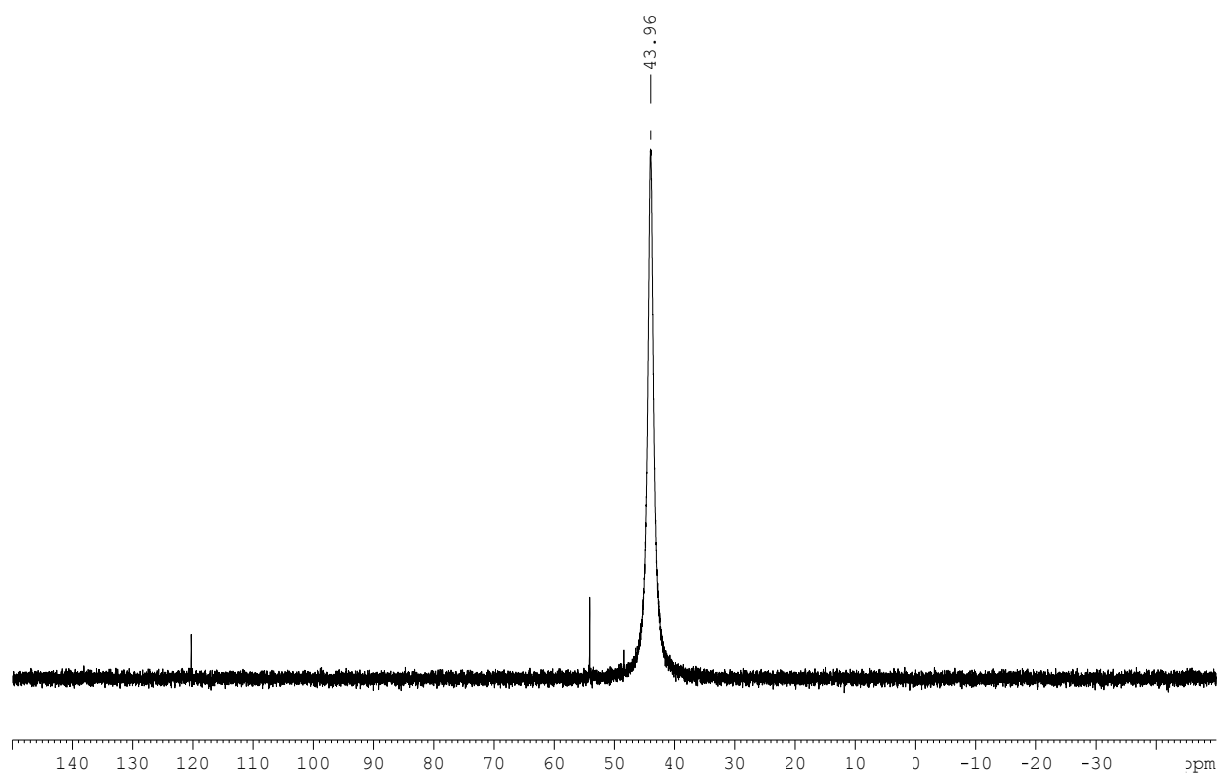
Compound 135h: ^{13}C NMR (75 MHz, CDCl_3)



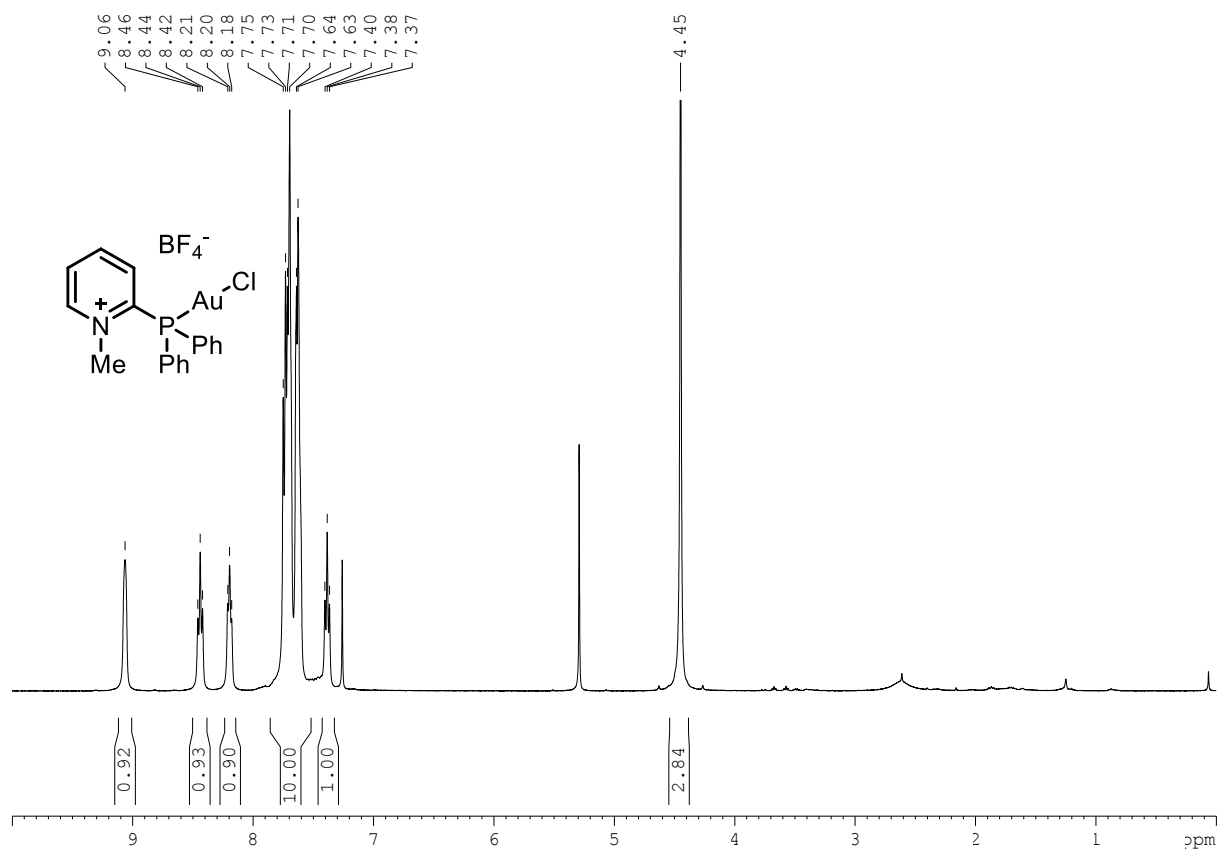
Compound 135h: ^{19}F NMR (282 MHz, CDCl_3)



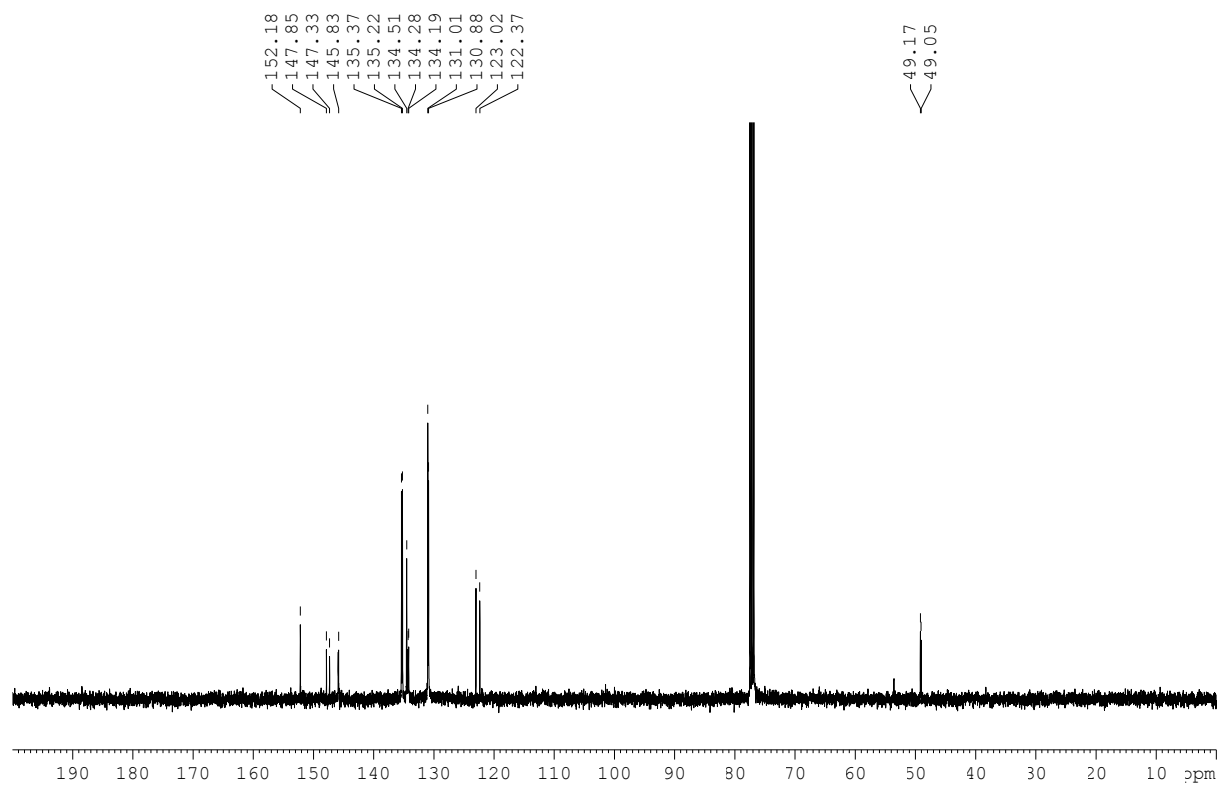
Compound 135h: ^{31}P NMR (121 MHz, CDCl_3)



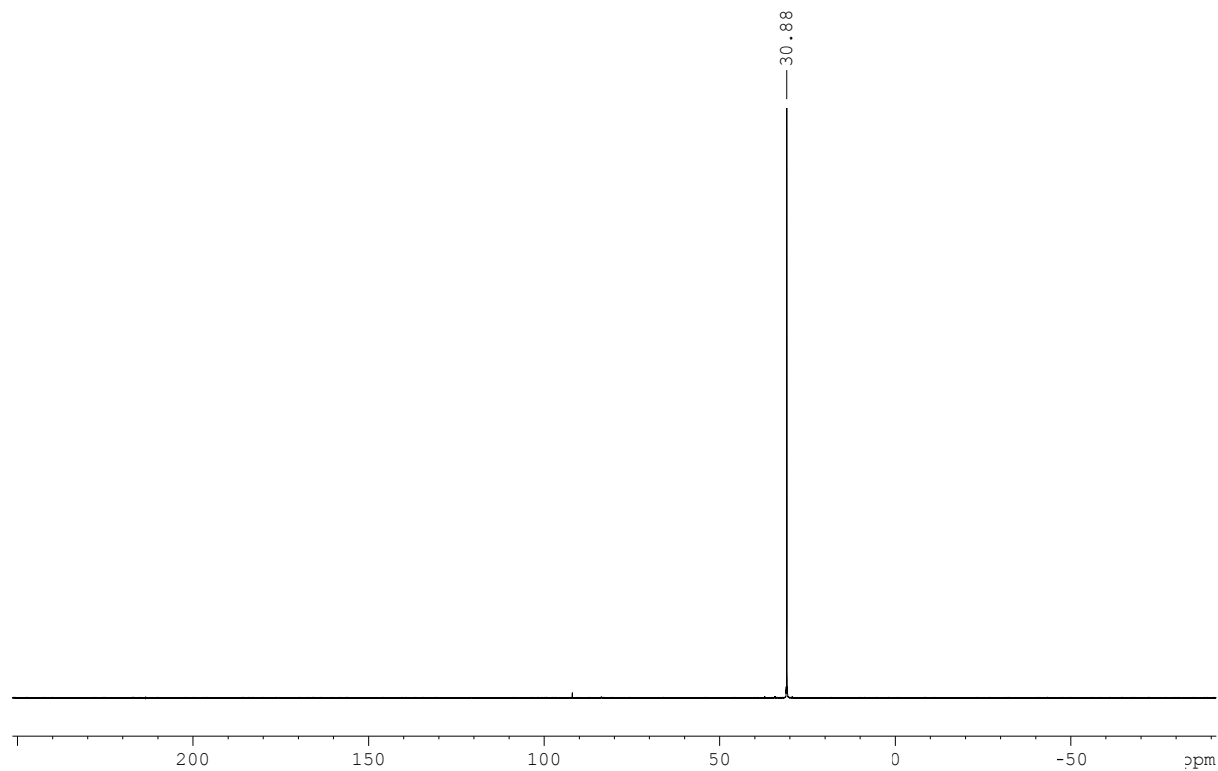
Compound 137a: ^1H NMR (300 MHz, CDCl_3)



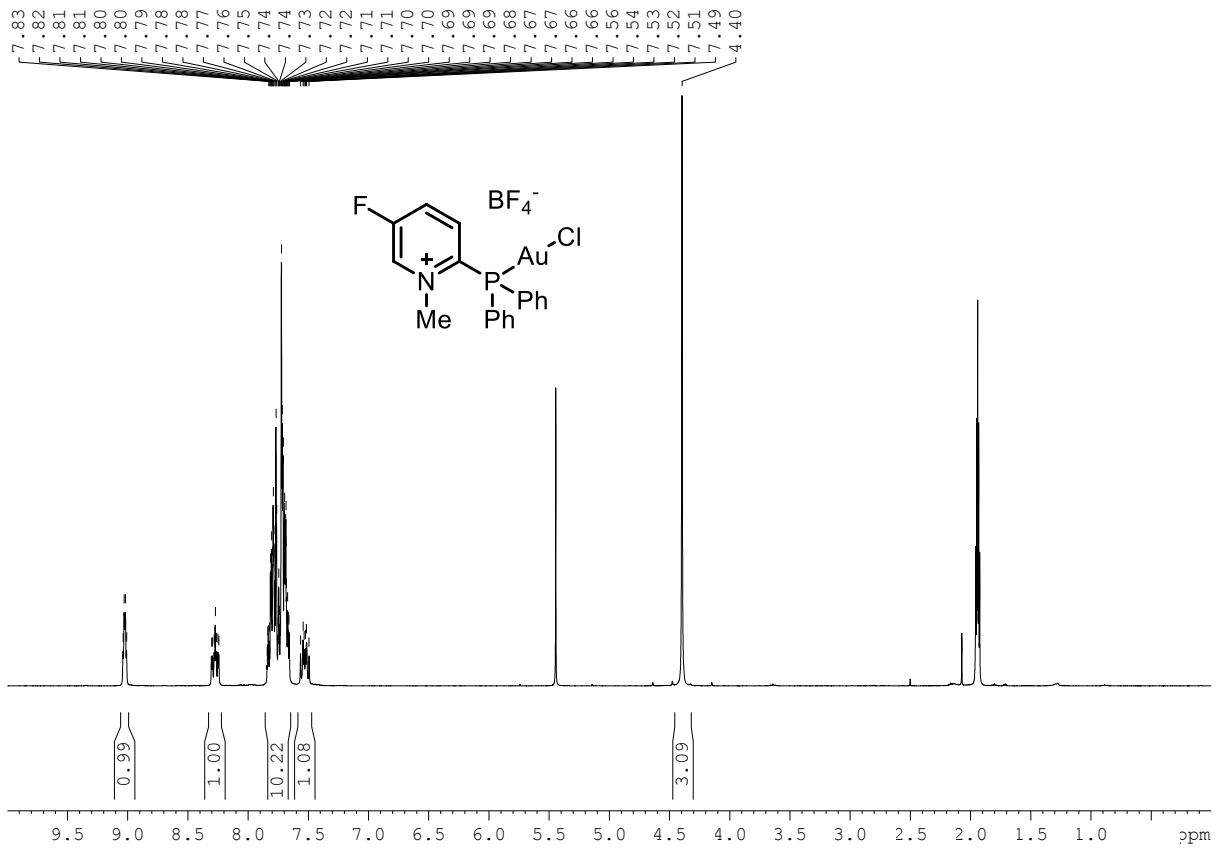
Compound 137a: ^{13}C NMR (75 MHz, CDCl_3)



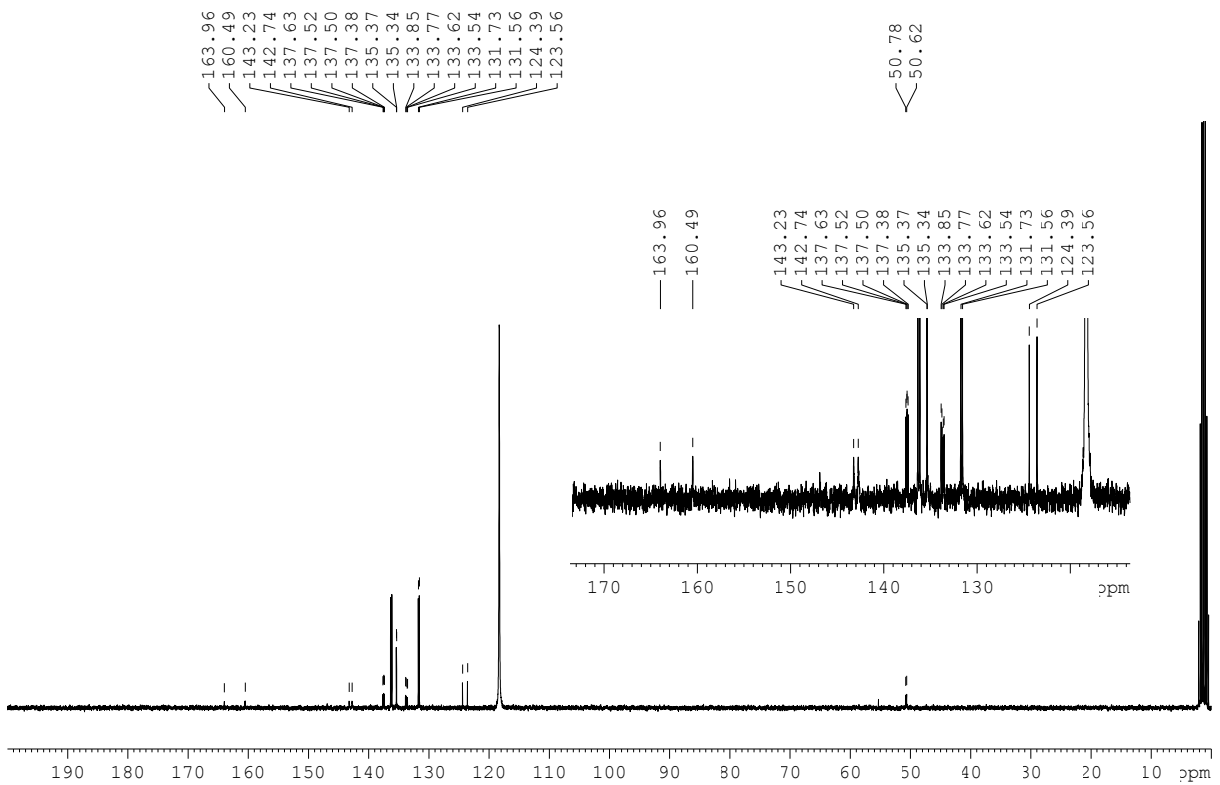
Compound 137a: ^{31}P NMR (162 MHz, CDCl_3)

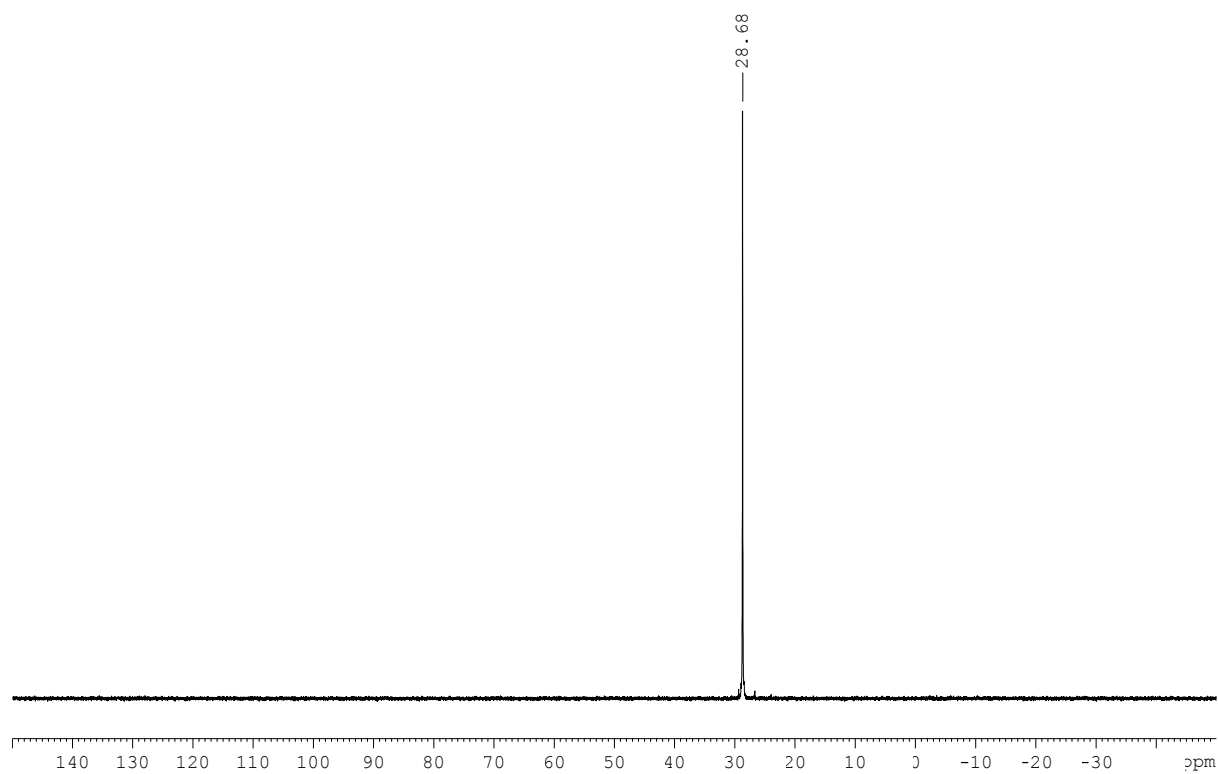
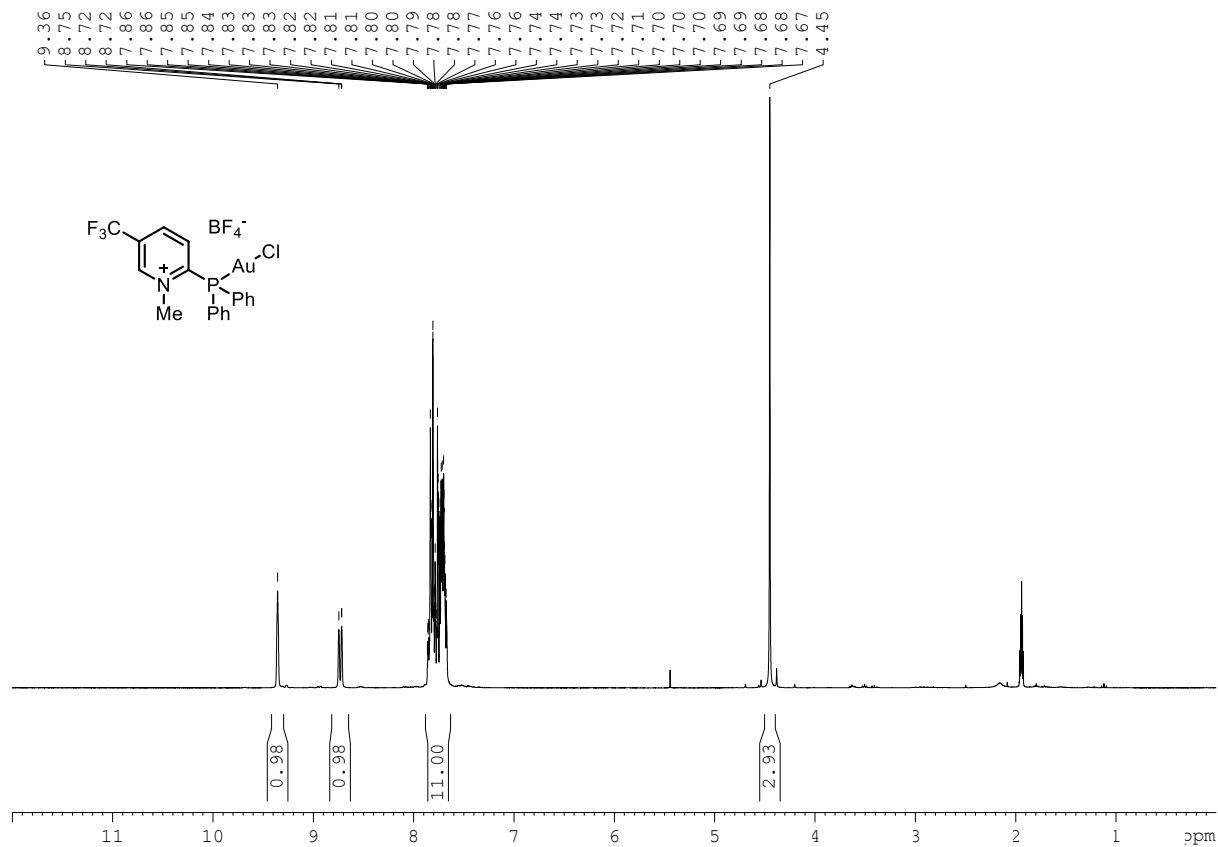


Compound 137b: ^1H NMR (300 MHz, CD_3CN)

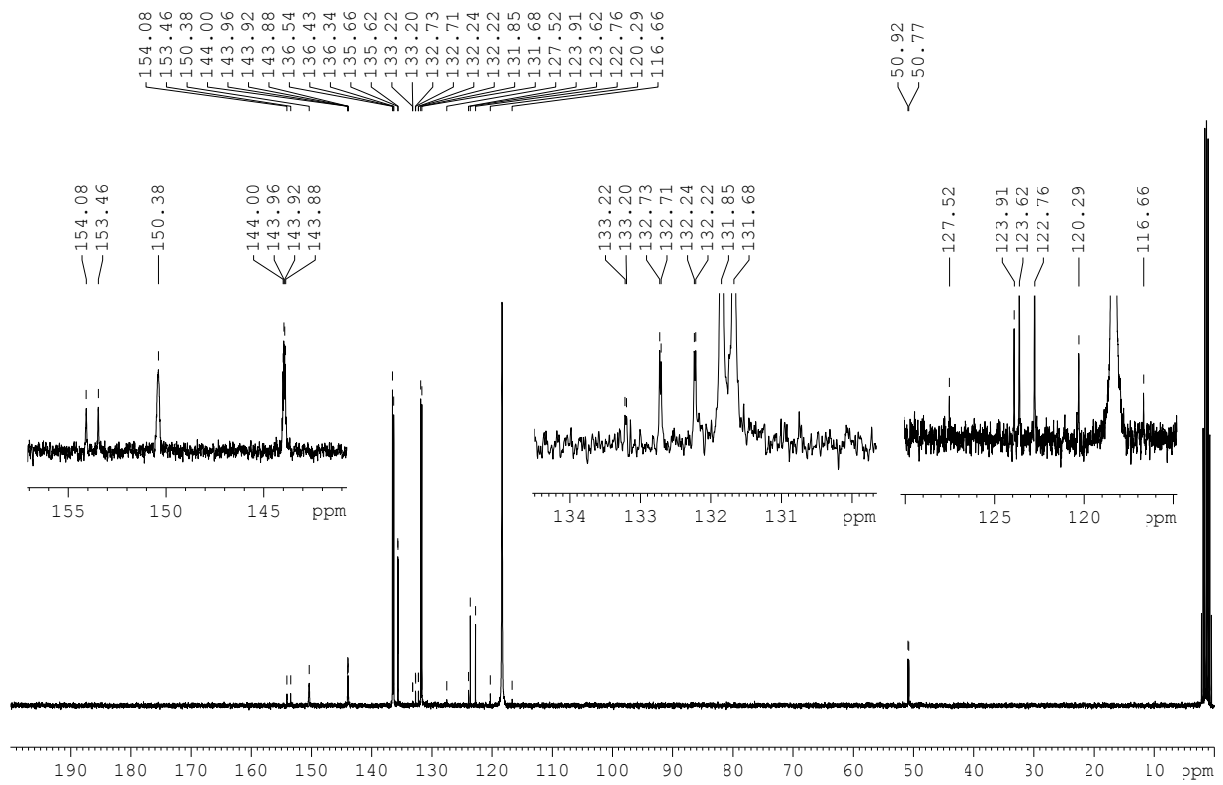


Compound 137b: ^{13}C NMR (75 MHz, CD_3CN)

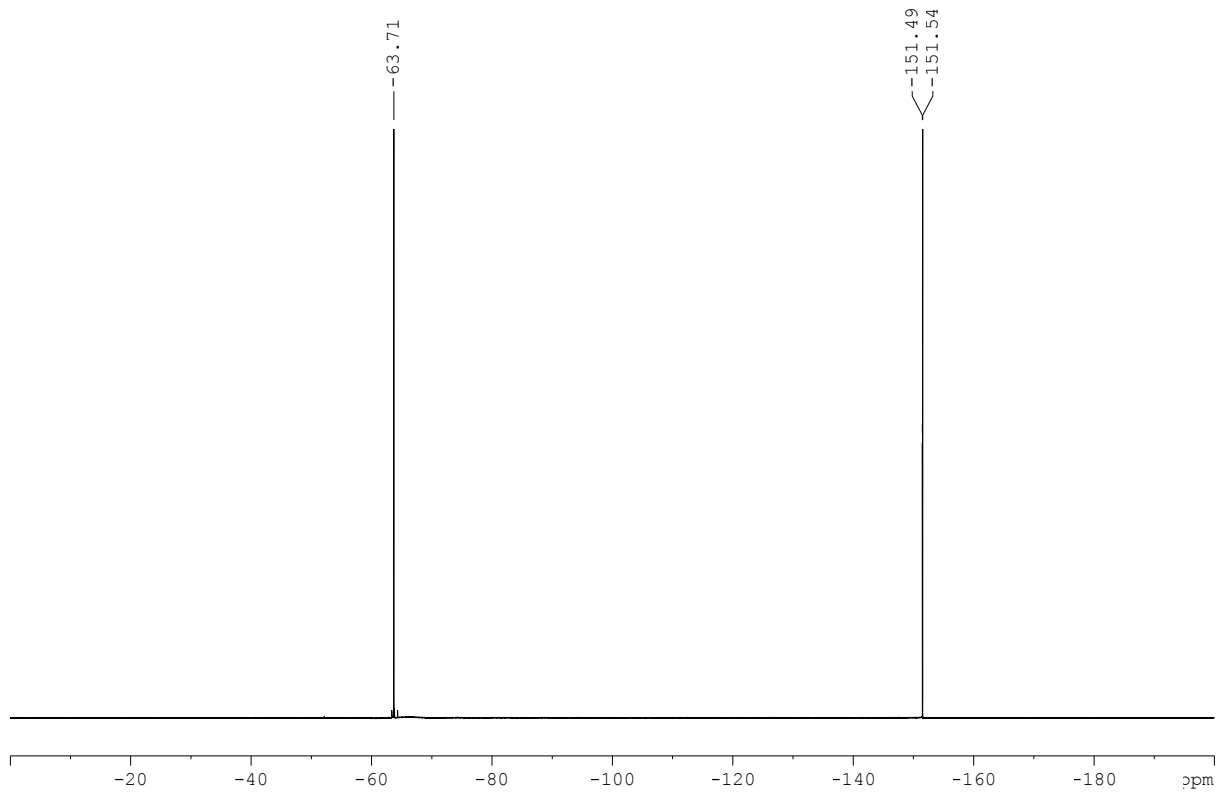


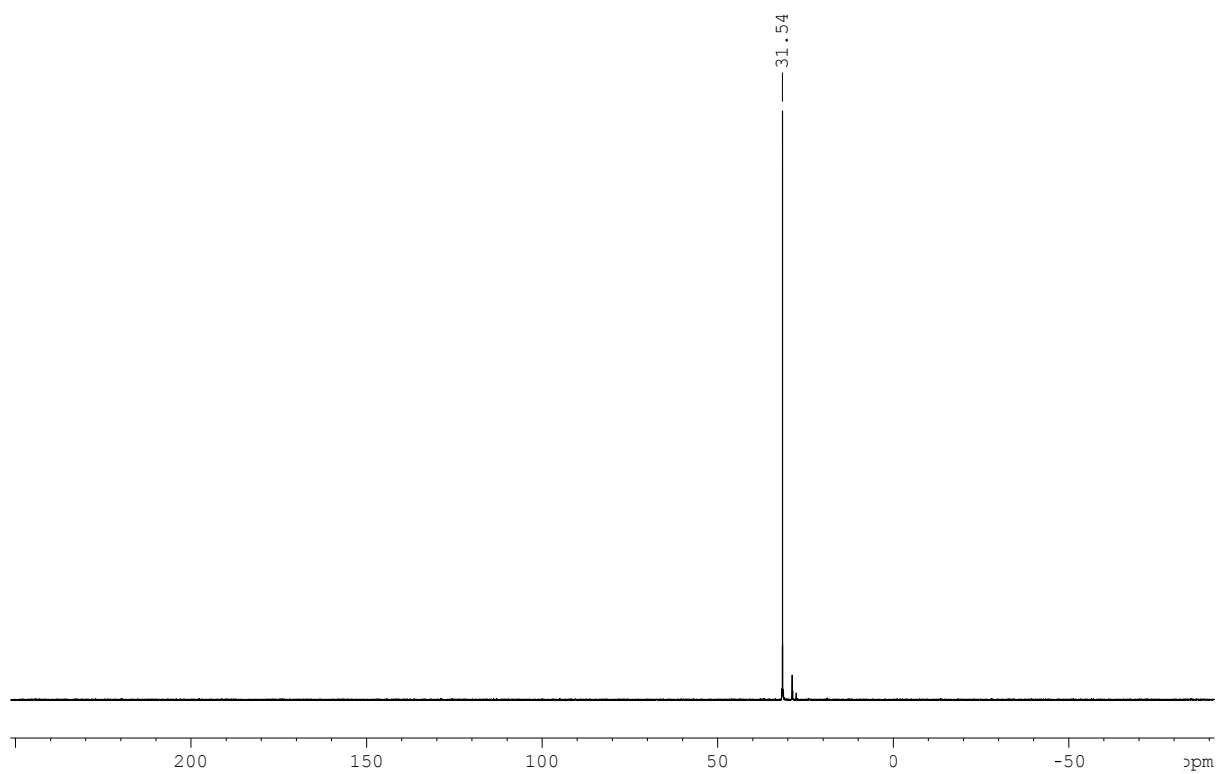
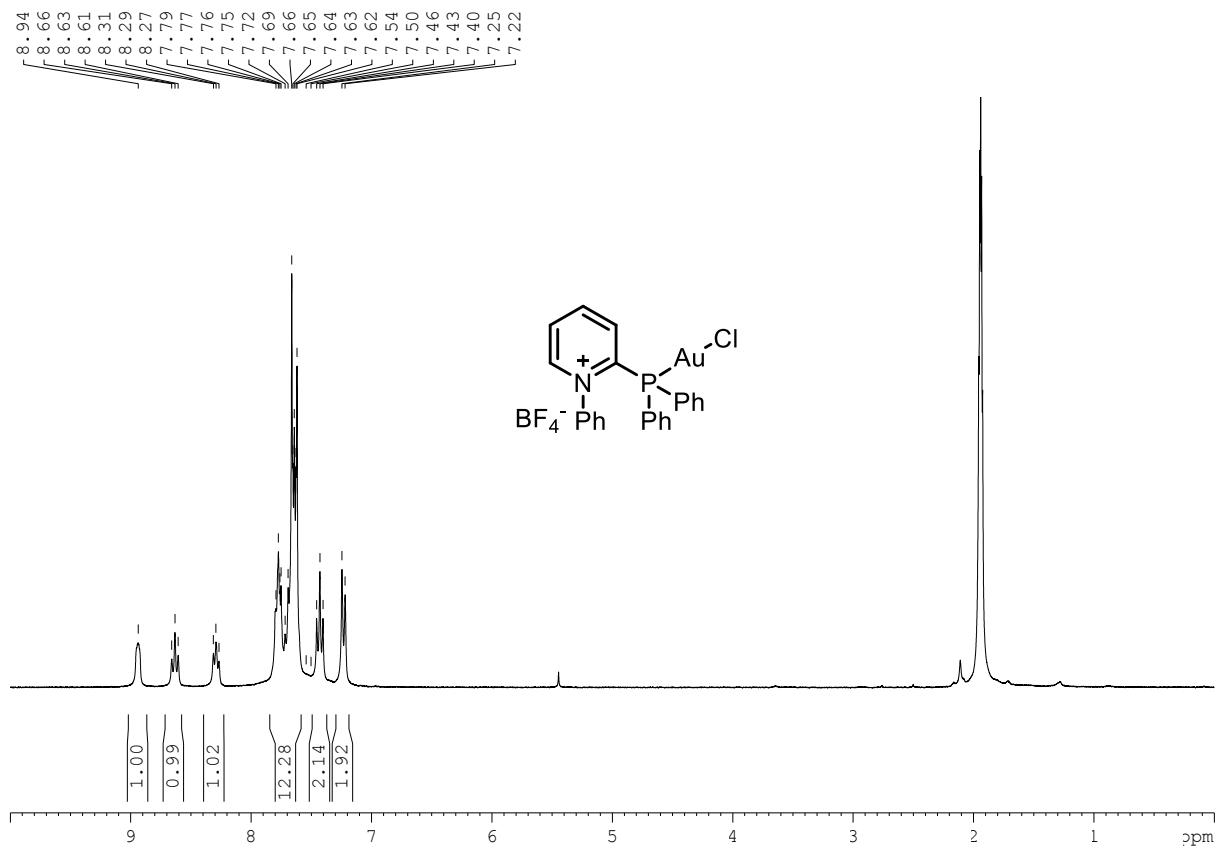
Compound 137b: ^{31}P NMR (162 MHz, CD_3CN)**Compound 137c:** ^1H NMR (300 MHz, CD_3CN)

Compound 137c: ^{13}C NMR (75 MHz, CD_3CN)

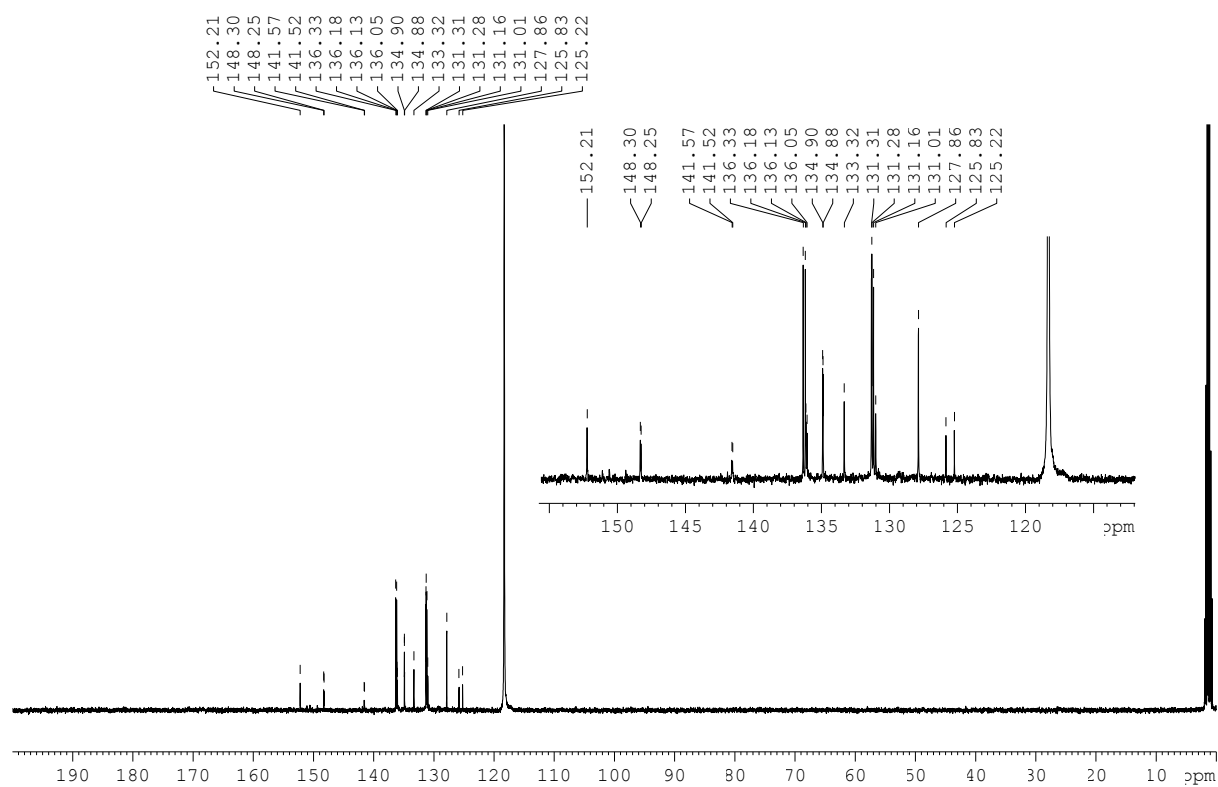


Compound 137c: ^{19}F NMR (282 MHz, CD_3CN)

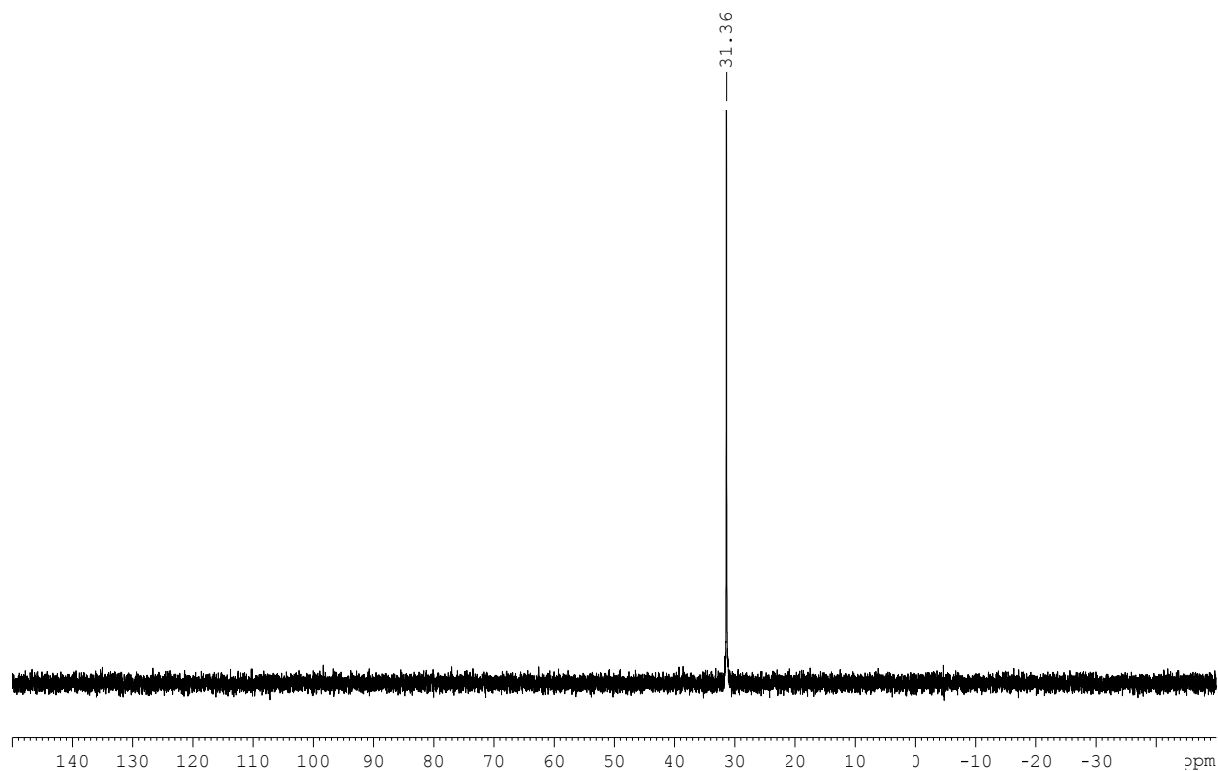


Compound 137c: ^{31}P NMR (162 MHz, CD_3CN)**Compound 137d:** ^1H NMR (400 MHz, CD_3CN)

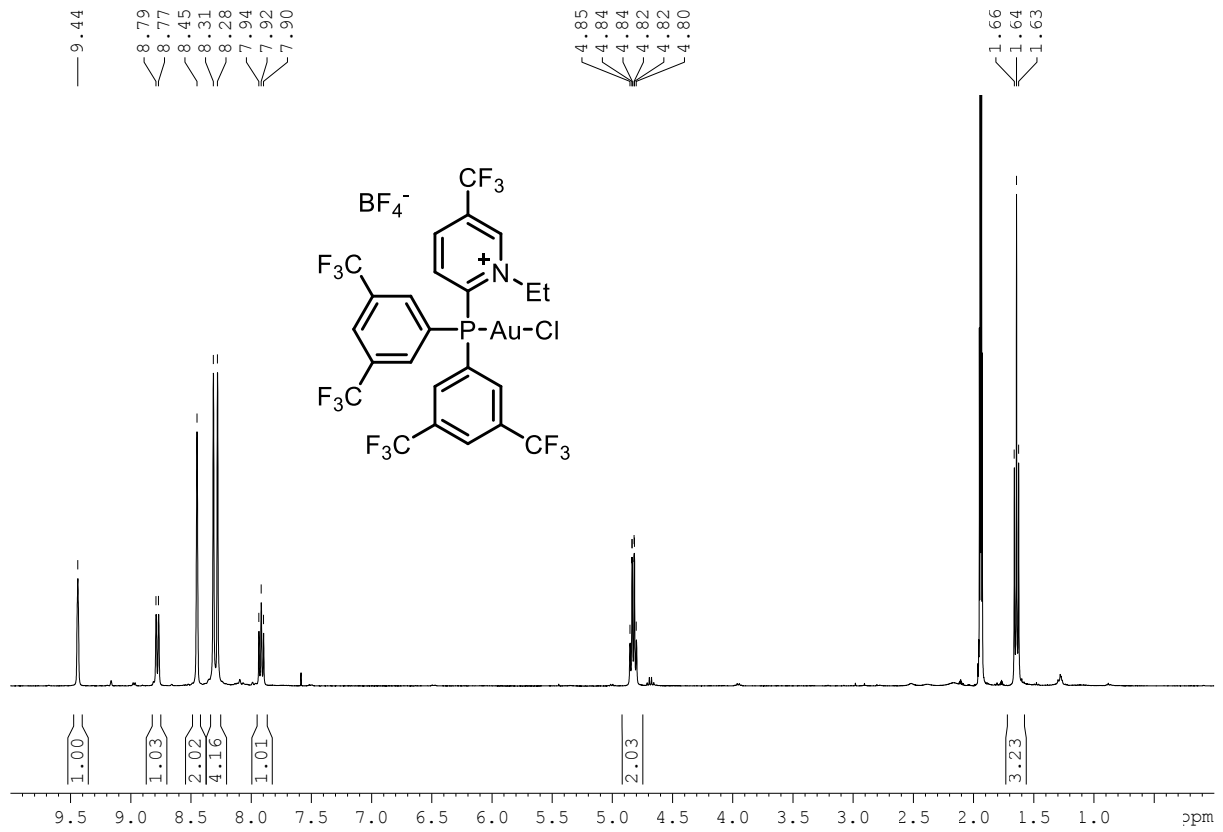
Compound 137d: ^{13}C NMR (102 MHz, CD_3CN)



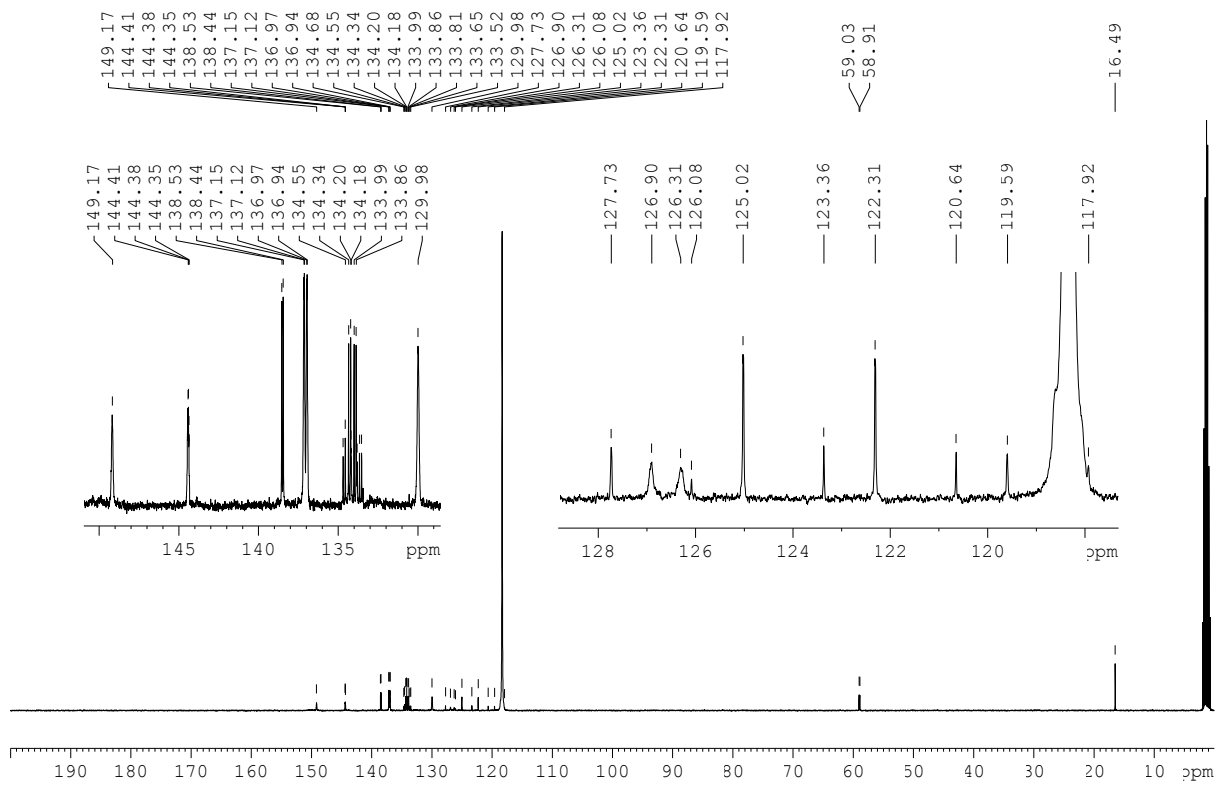
Compound 137d: ^{31}P NMR (162 MHz, CD_3CN)



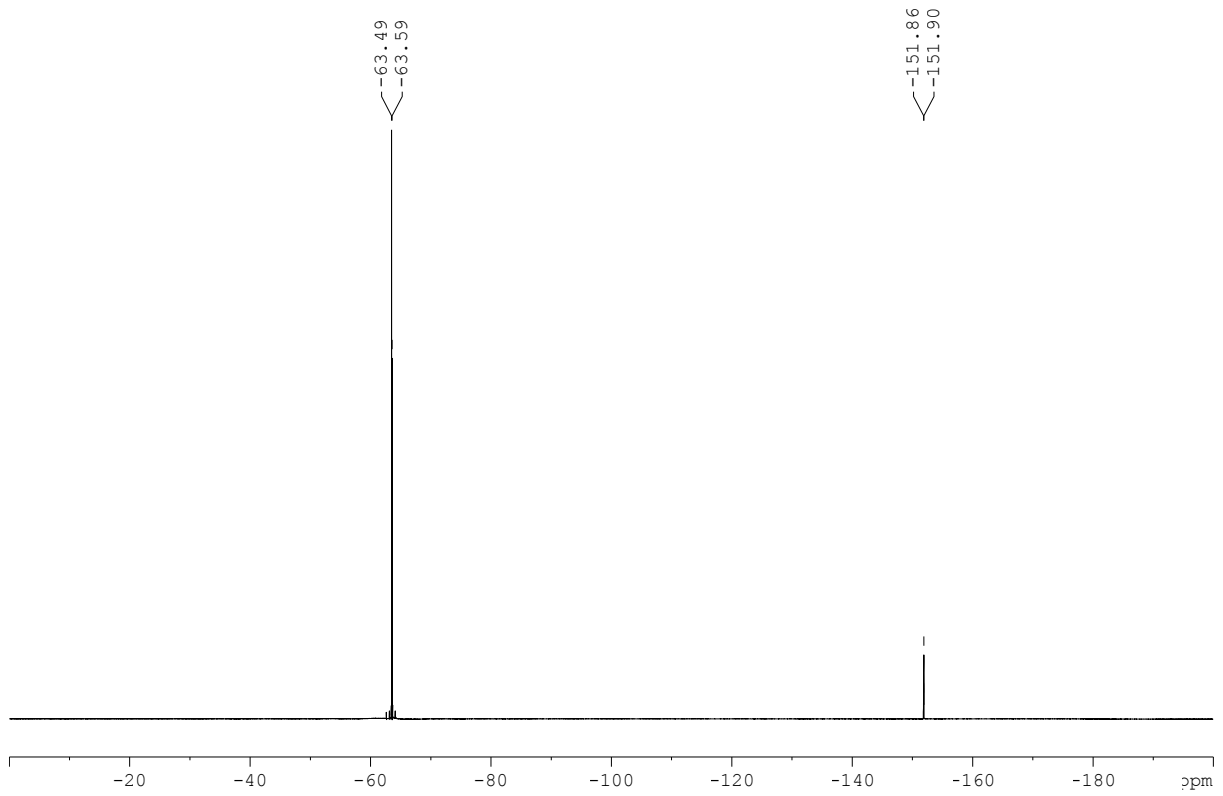
Compound 137e: ^1H NMR (400 MHz, CD_3CN)



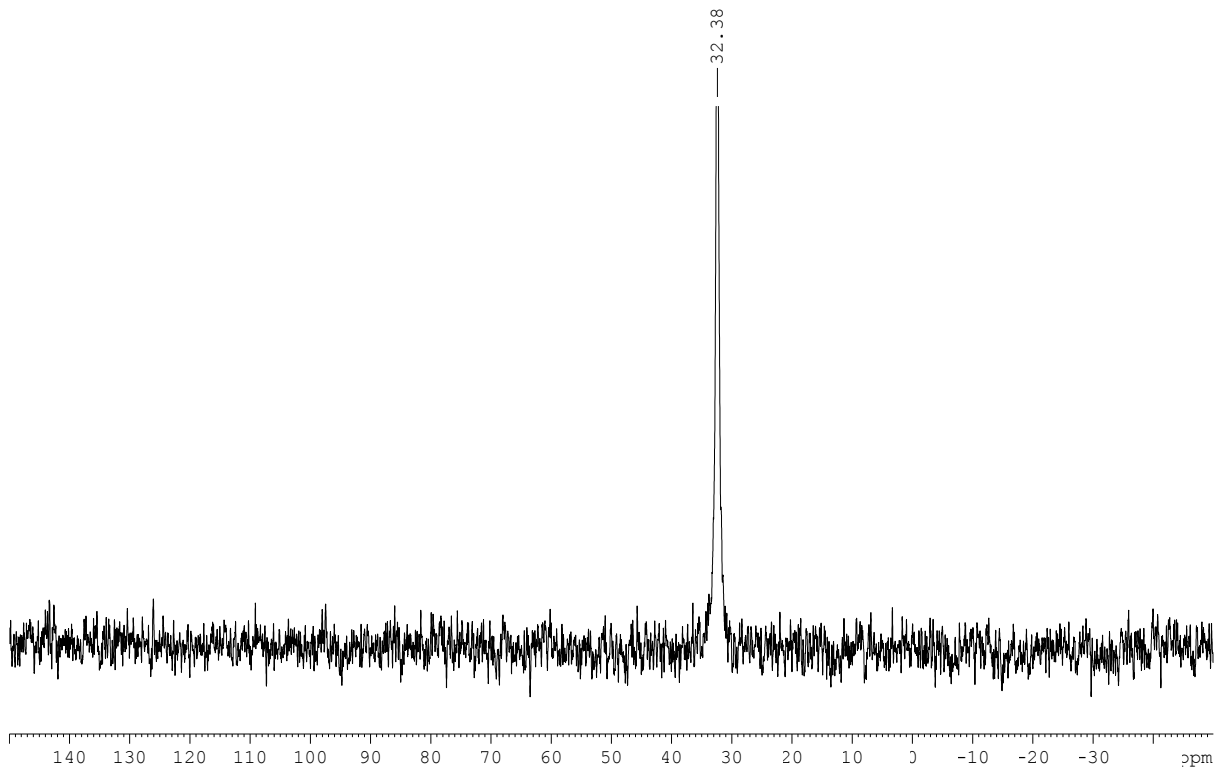
Compound 137e: ^{13}C NMR (102 MHz, CD_3CN)



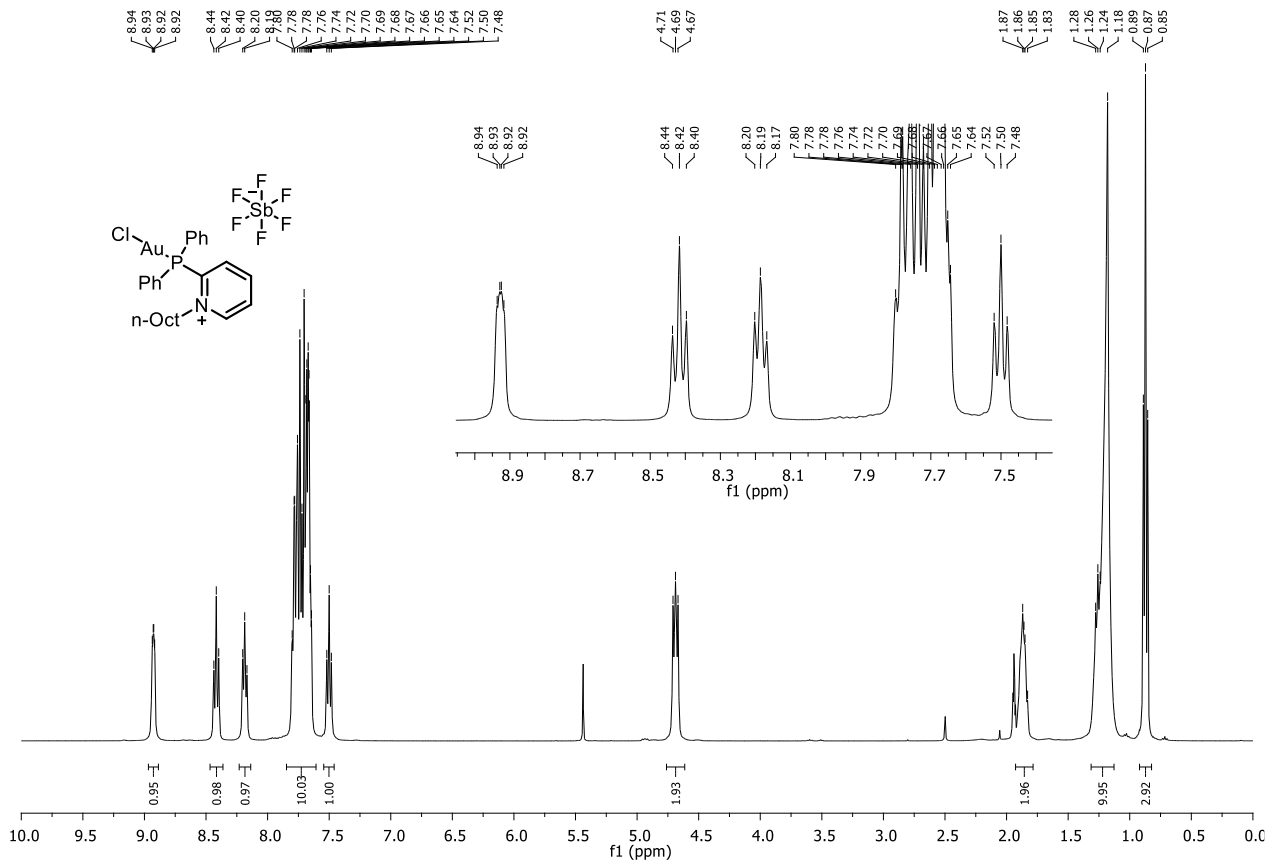
Compound 137e: ^{19}F NMR (282 MHz, CD_3CN)



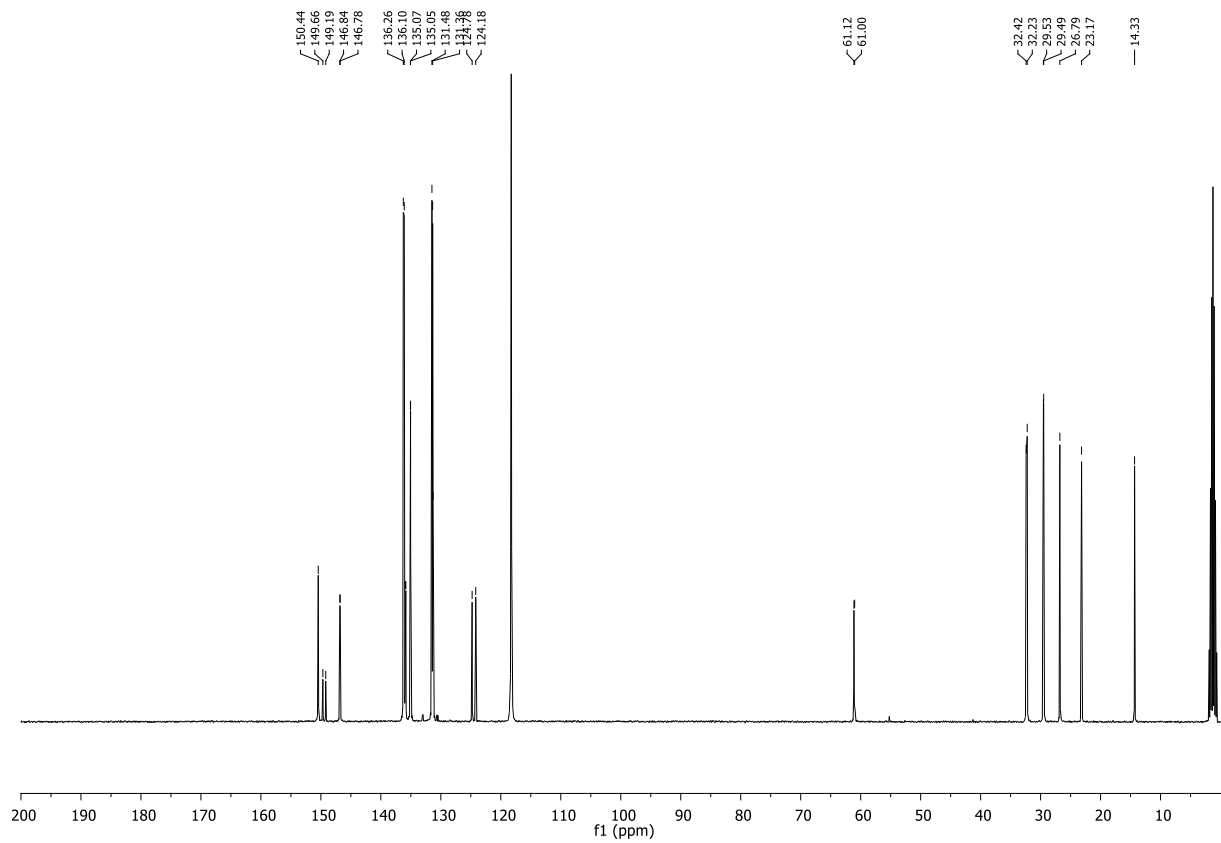
Compound 137e: ^{31}P NMR (162 MHz, CD_3CN)



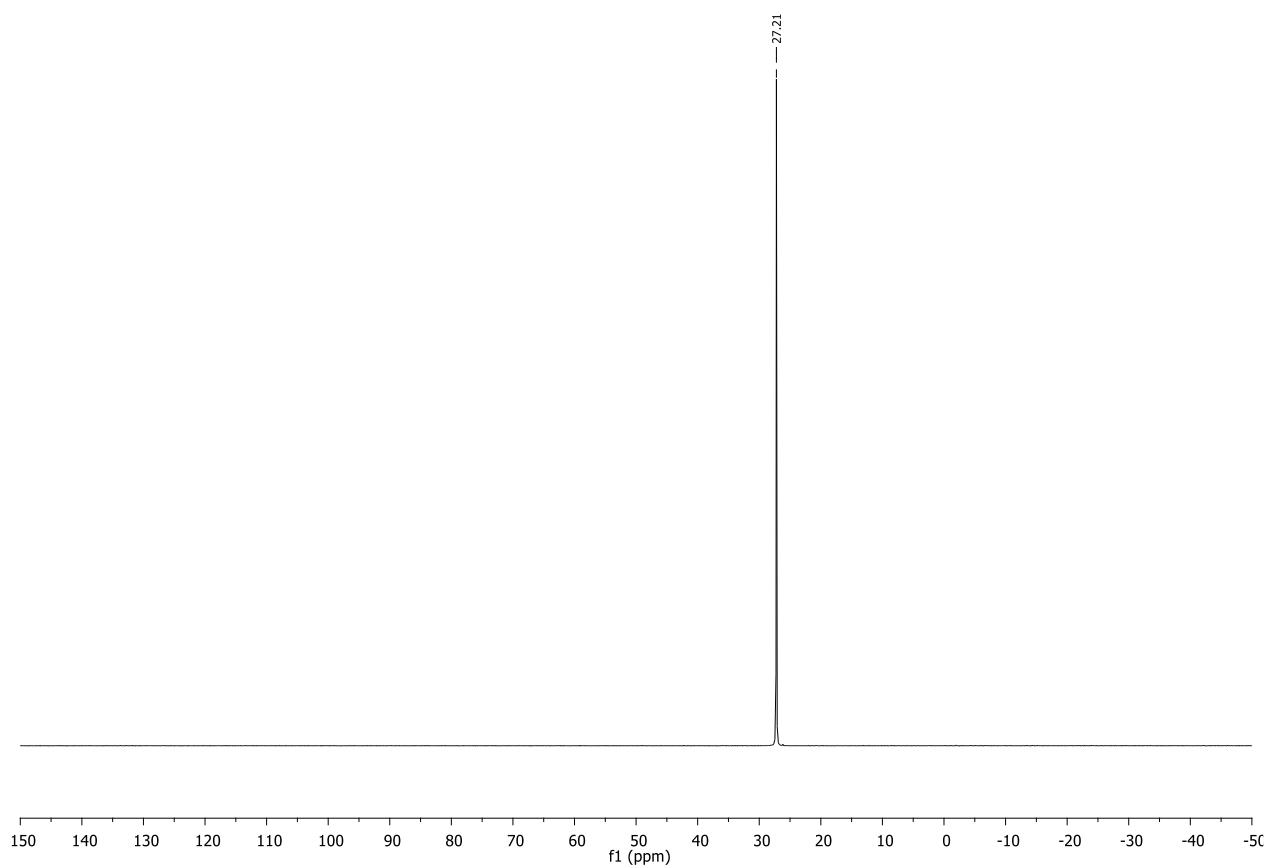
Compound 137f: ^1H NMR (400 MHz, CD_3CN)



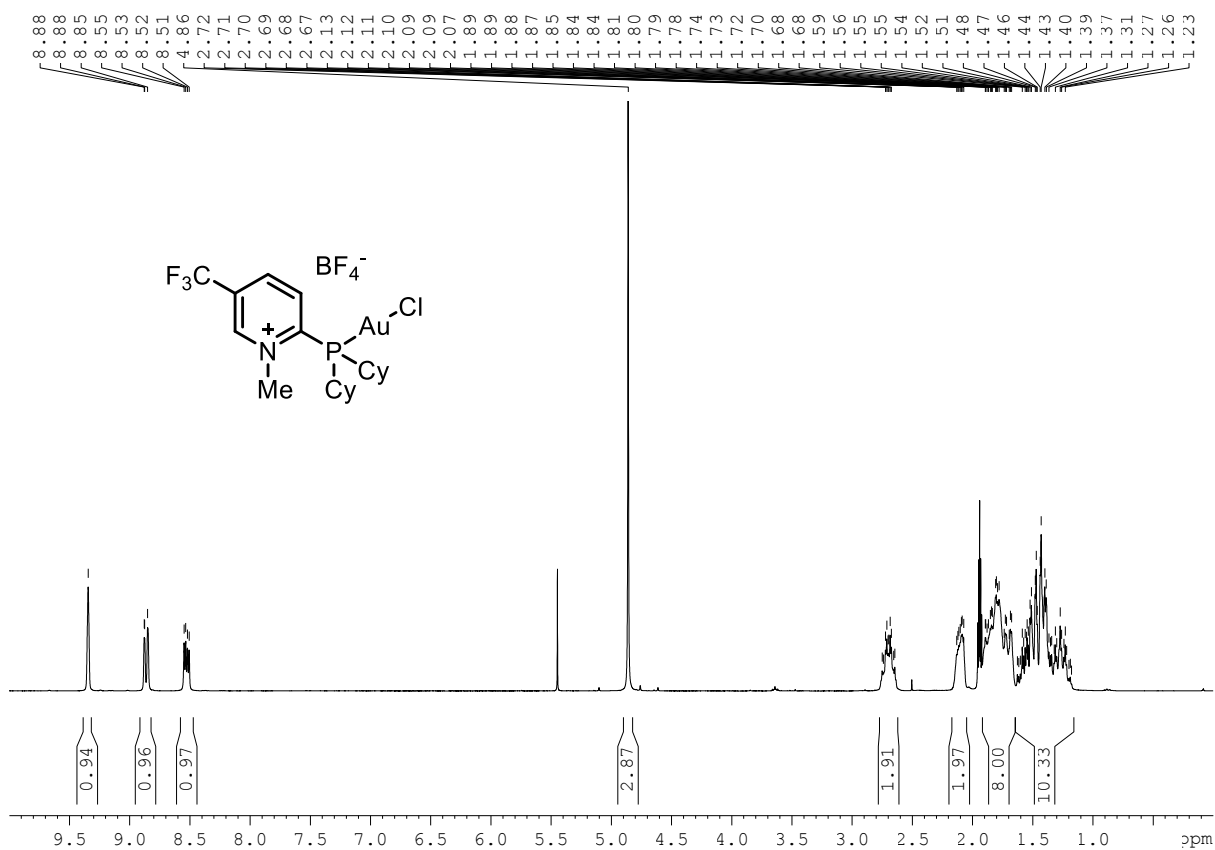
Compound 137f: ^{13}C NMR (102 MHz, CD_3CN)



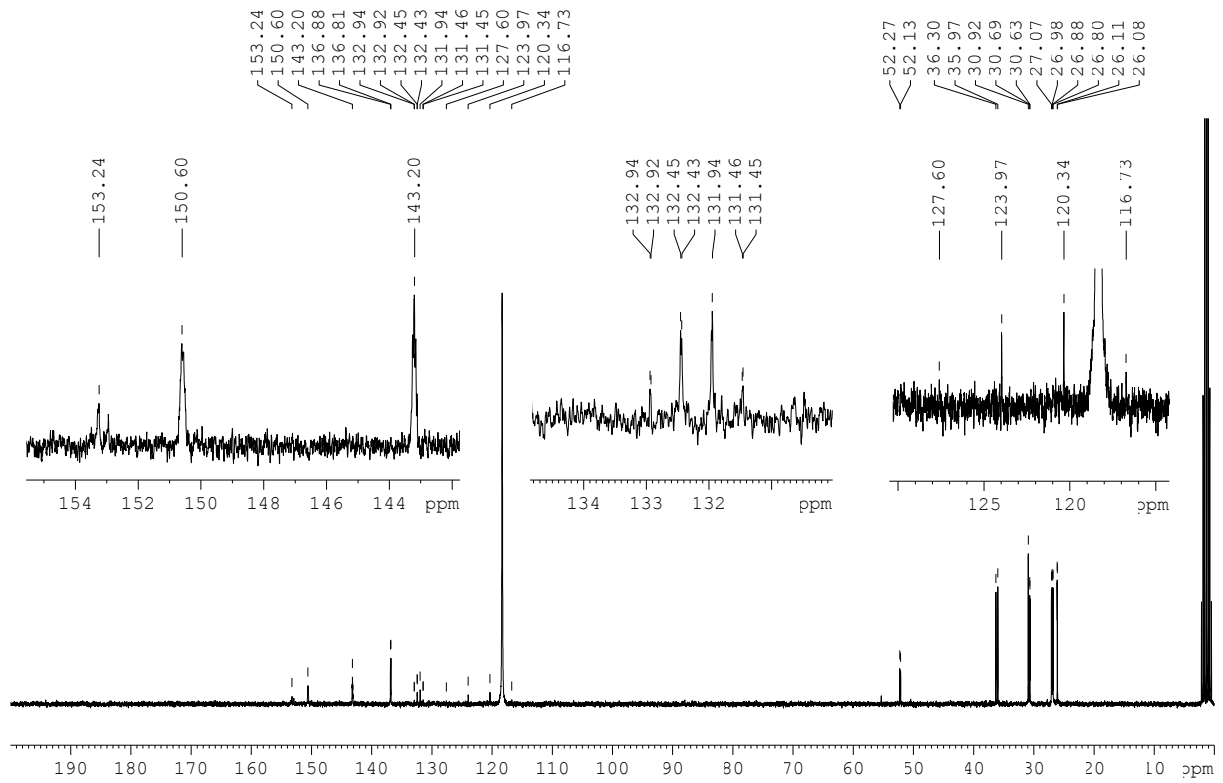
Compound 137f: ^{31}P NMR (162 MHz, CD_3CN)



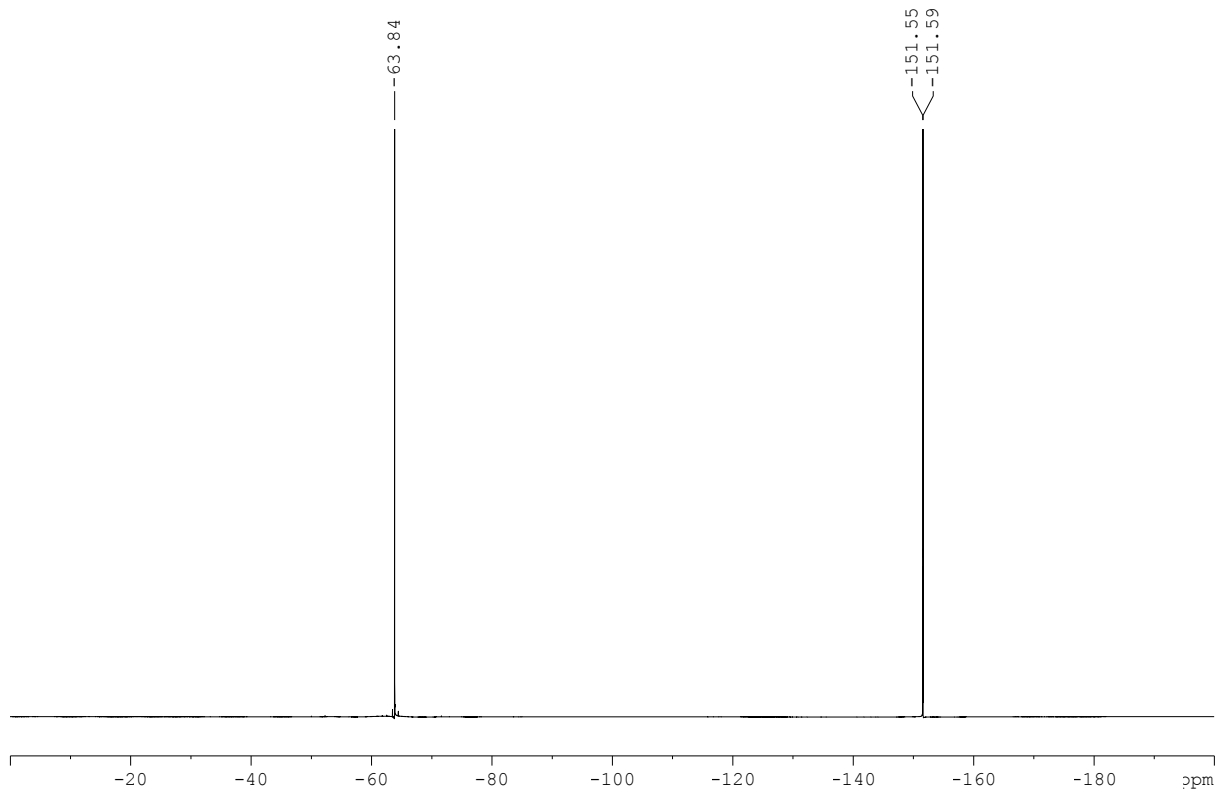
Compound 137g: ^1H NMR (300 MHz, CD_3CN)



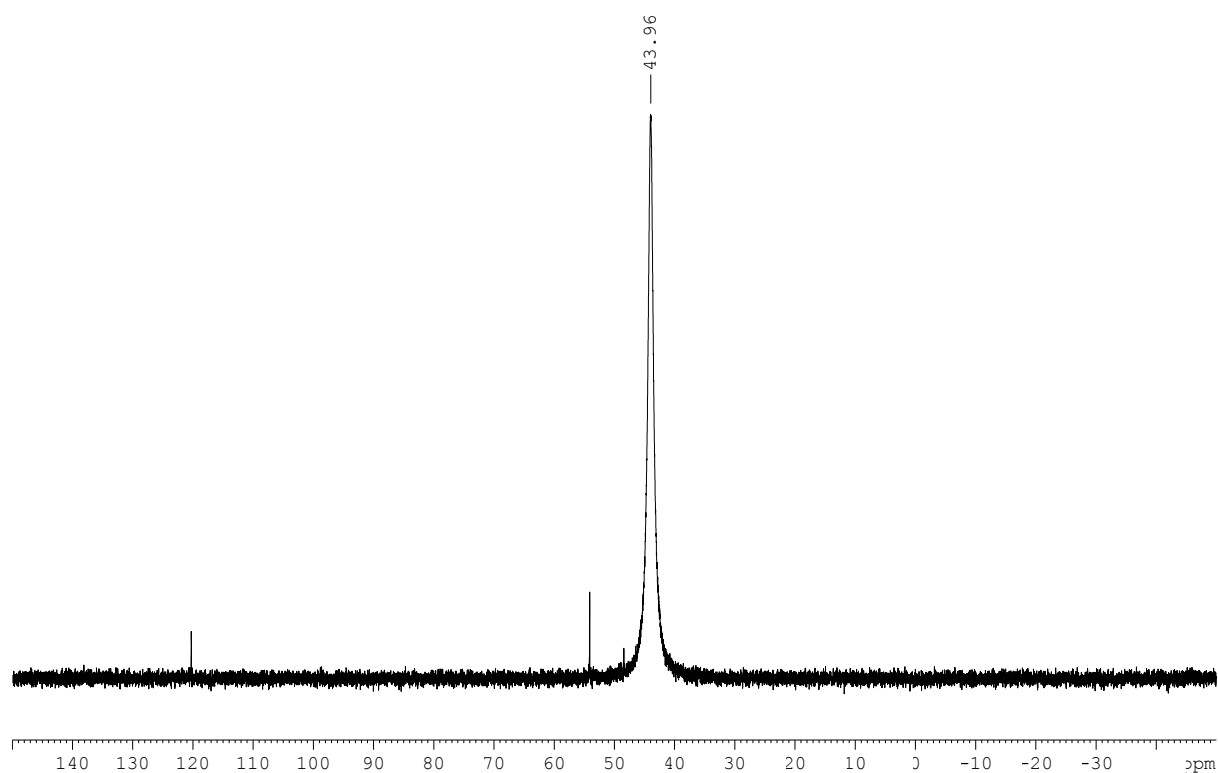
Compound 137g: ^{13}C NMR (75 MHz, CD_3CN)



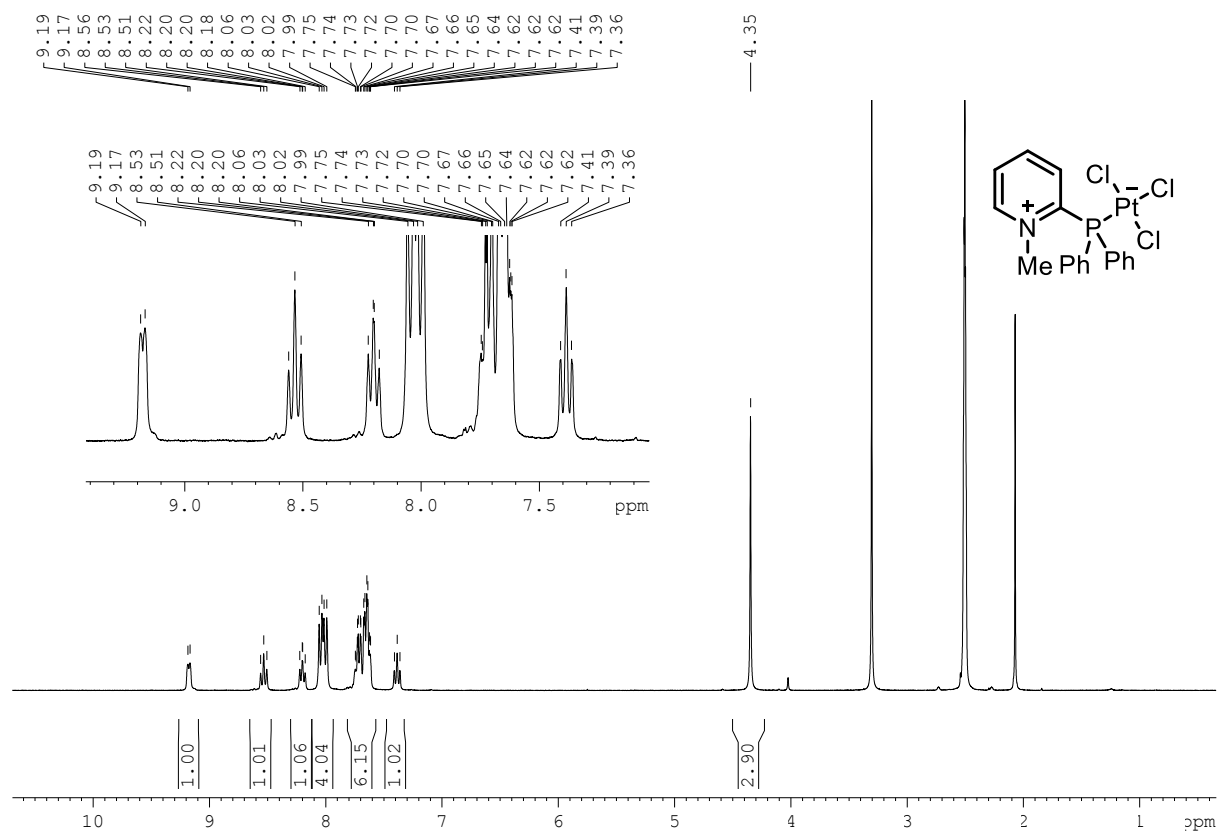
Compound 137g: ^{19}F NMR (282 MHz, CD_3CN)



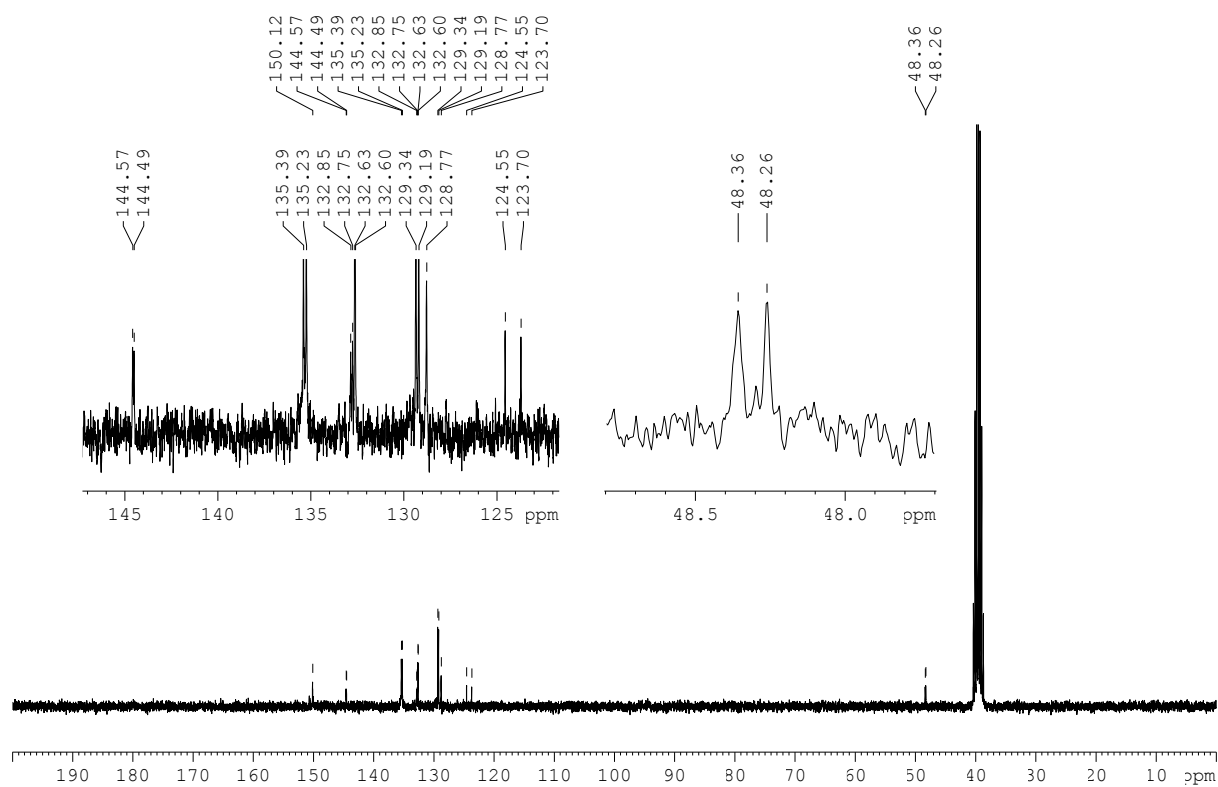
Compound 137g: ^{31}P NMR (162 MHz, CDCl_3)



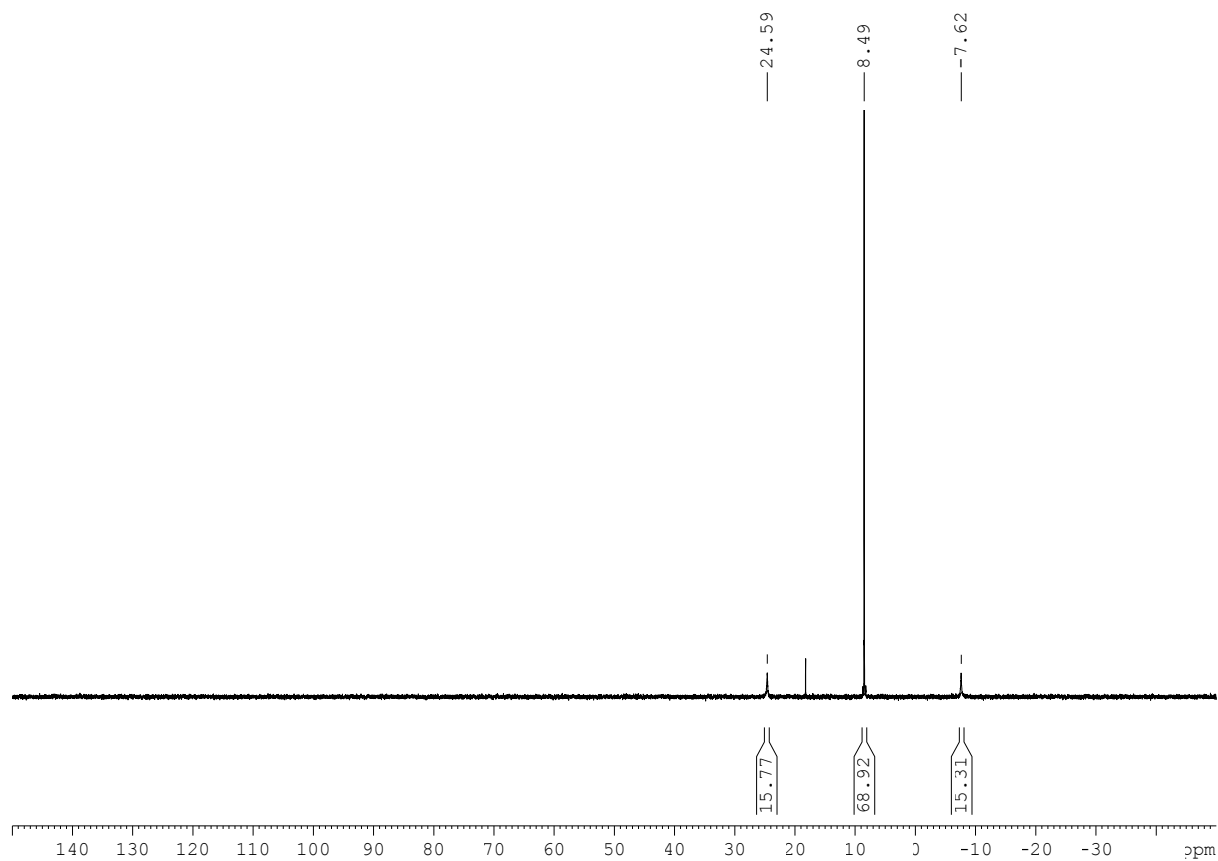
Compound 136a: ^1H NMR (300 MHz, d_6 -DMSO/ CD_3CN)



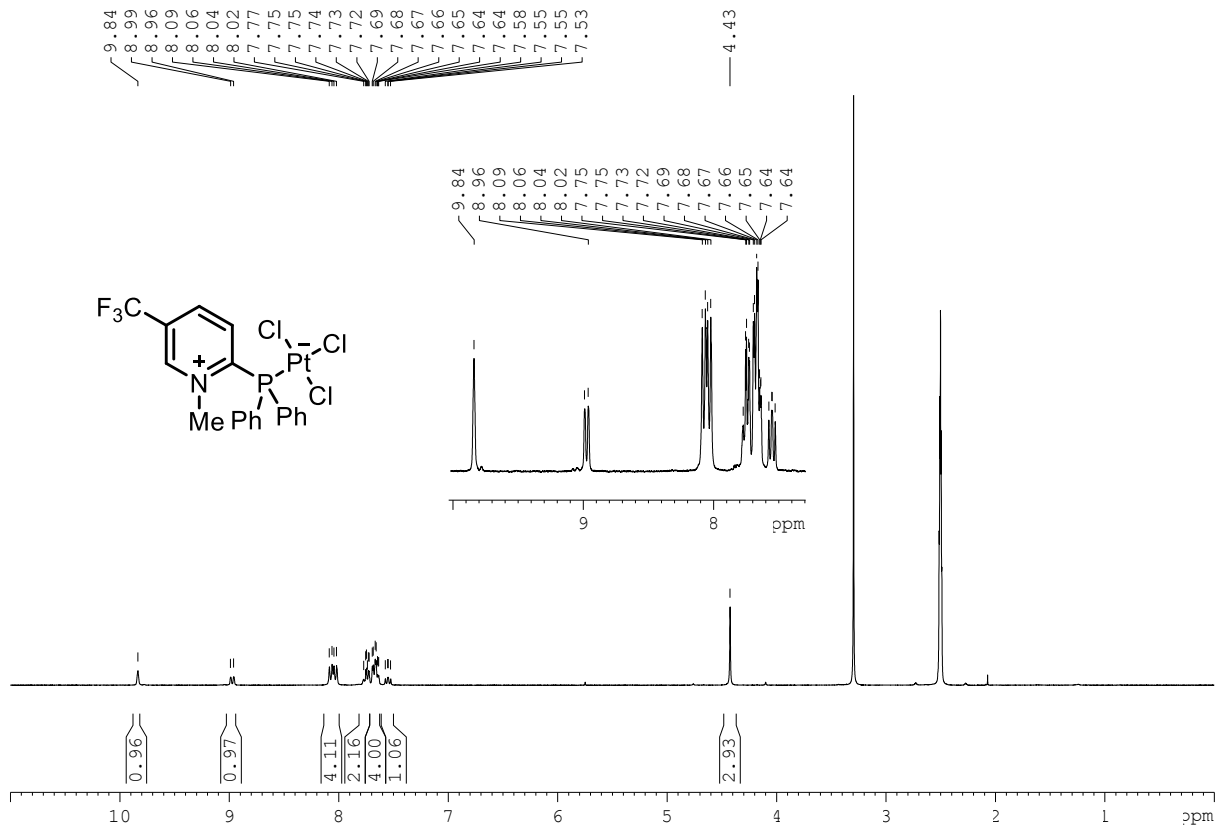
Compound 136a: ^{13}C NMR (75 MHz, DMSO)



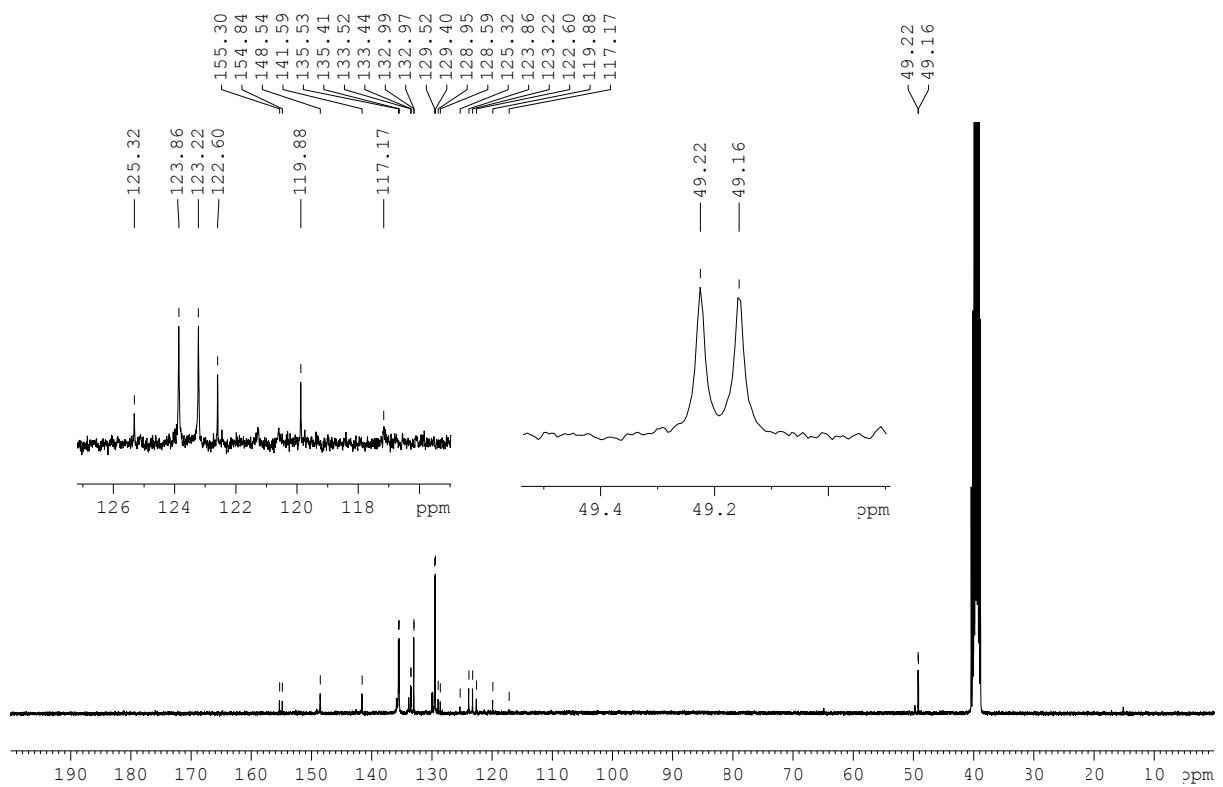
Compound 136a: ^{31}P NMR (162 MHz, d_6 -DMSO/ CD_3CN)



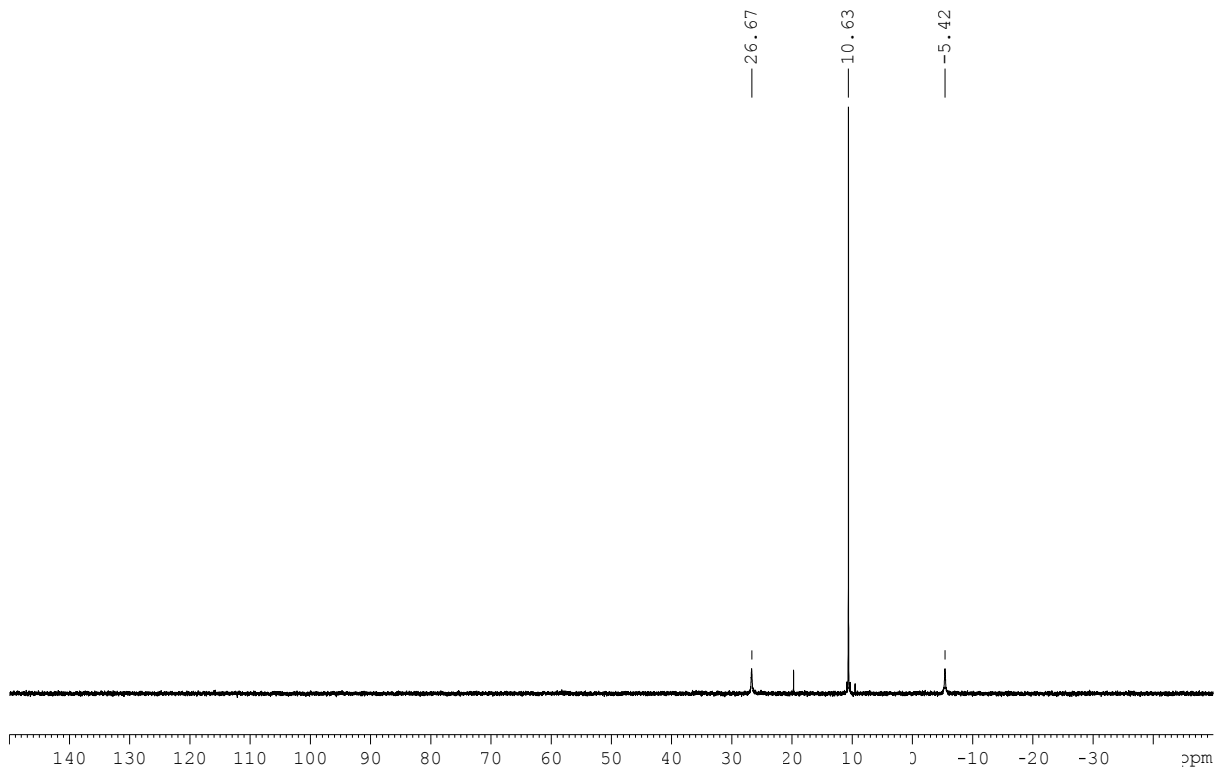
Compound 136b: ^1H NMR (300 MHz, d_6 -DMSO)



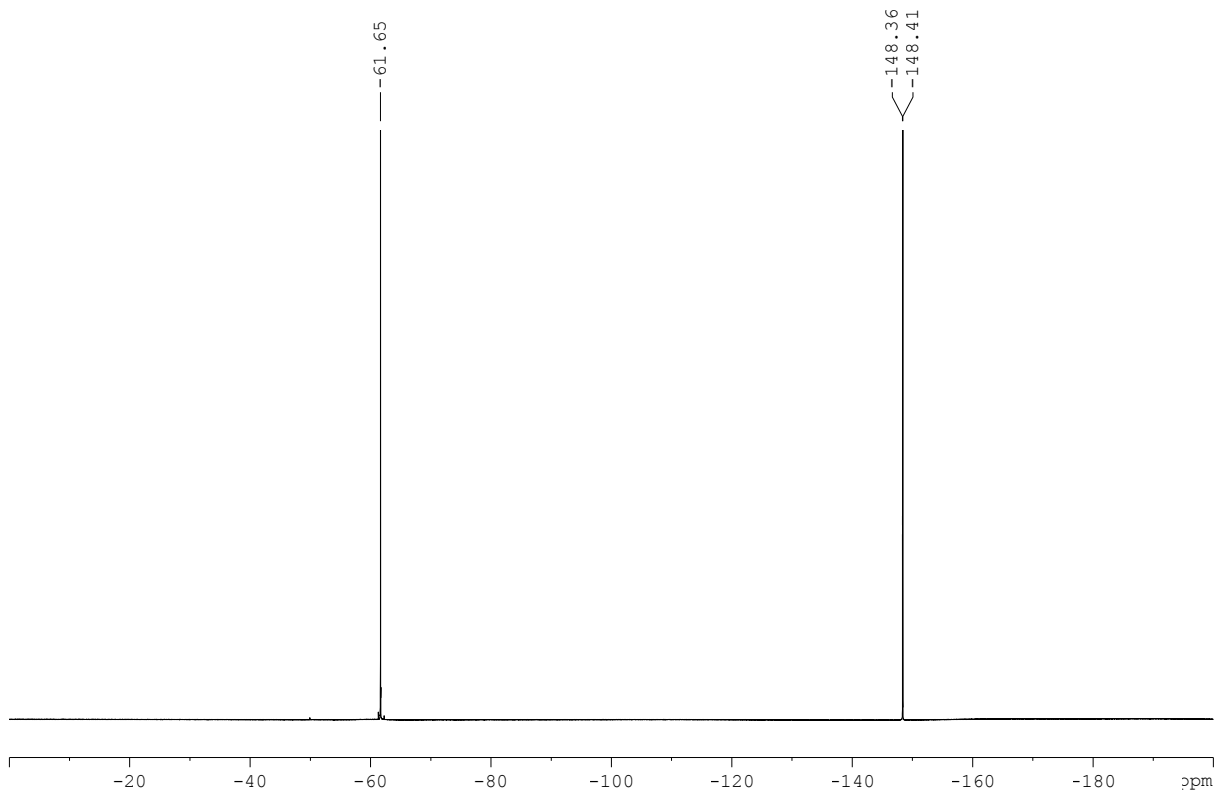
Compound 136b: ^{13}C NMR (75 MHz, DMSO)

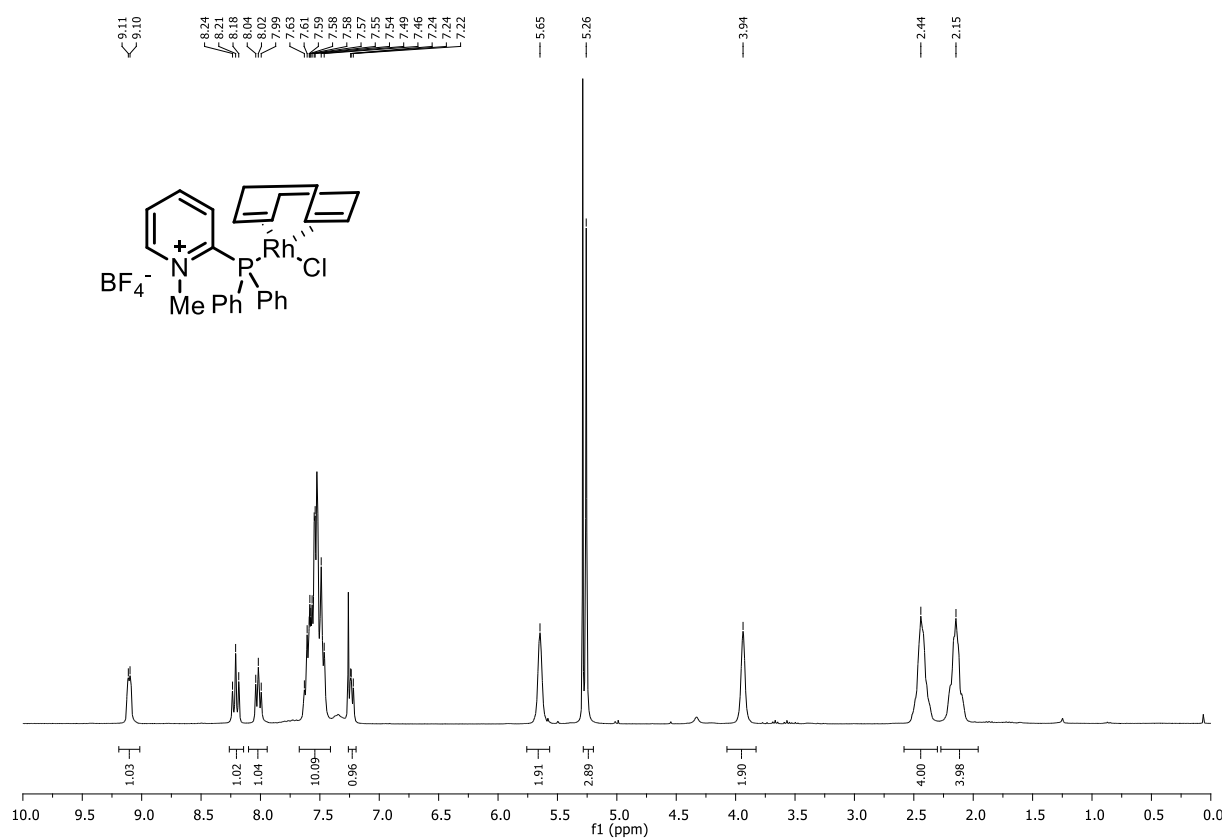
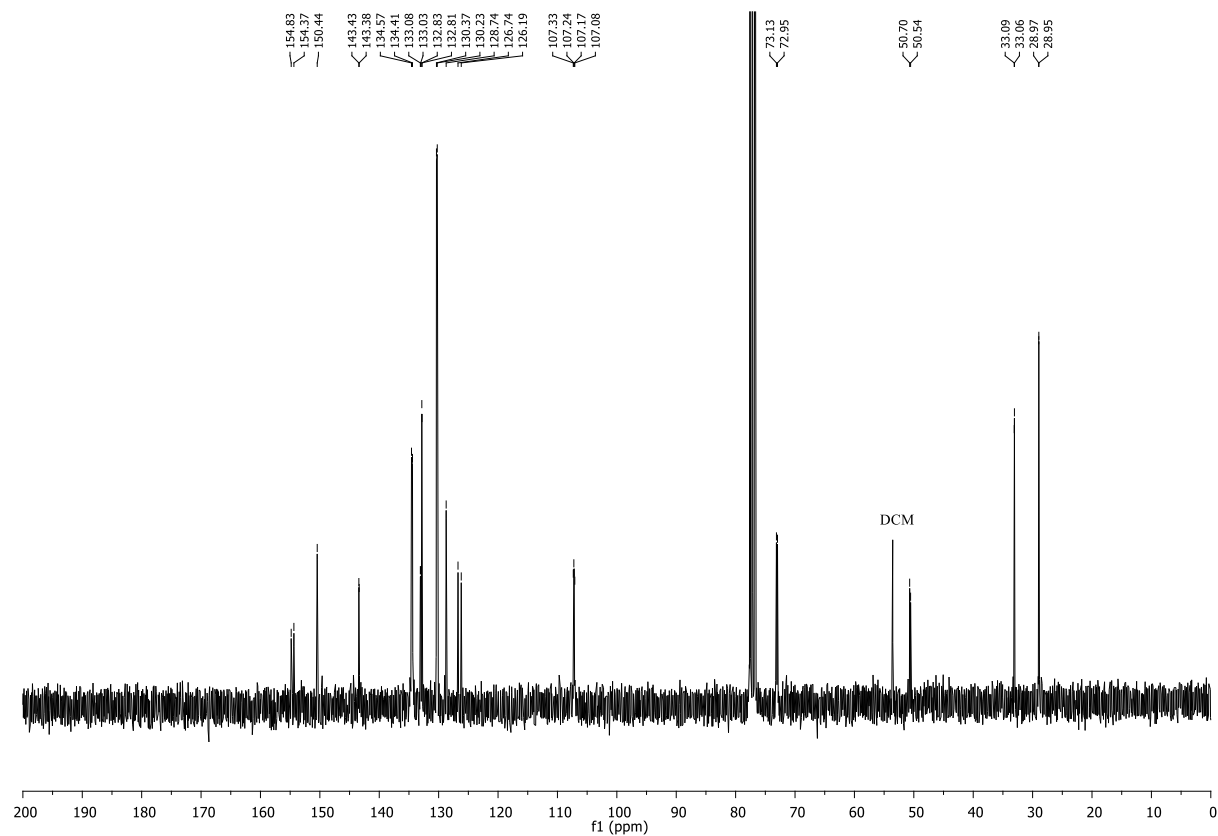


Compound 136b: ^{31}P NMR (162 MHz, $\text{d}_6\text{-DMSO}$)

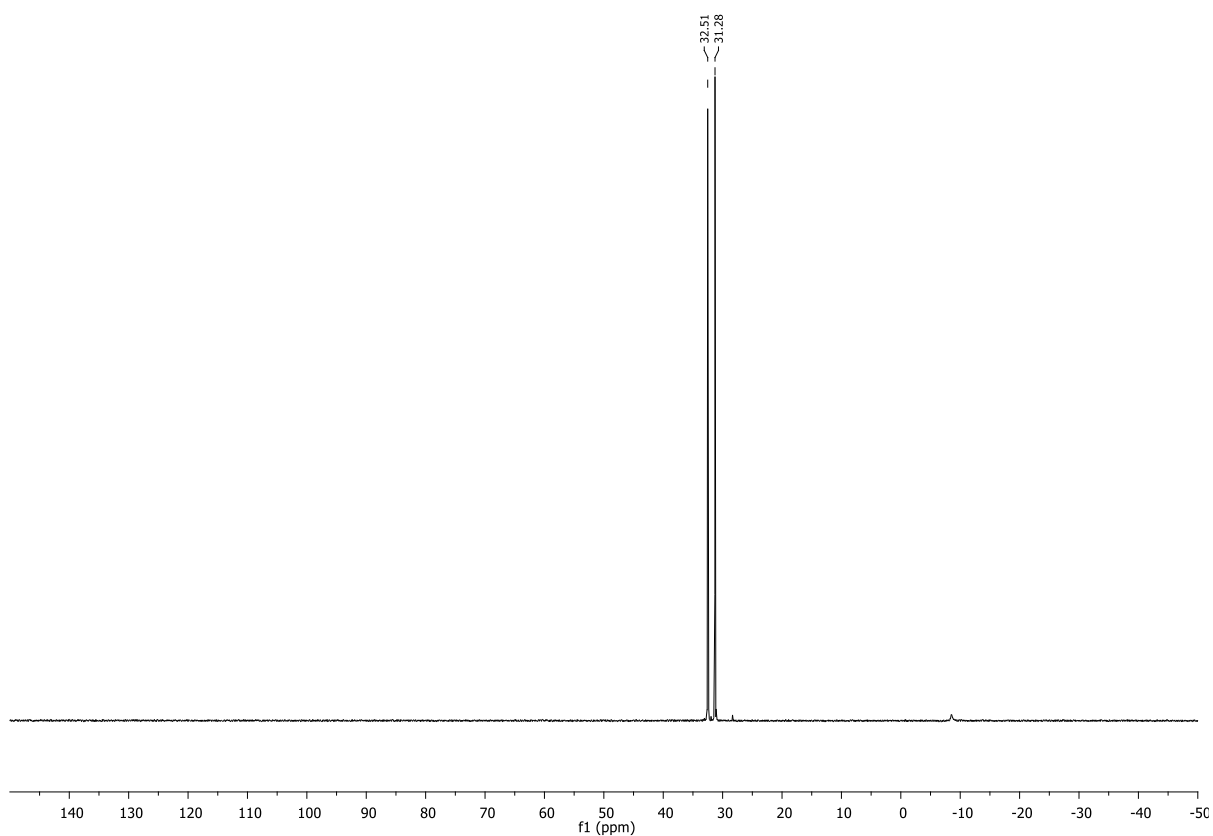


Compound 136b: ^{19}F NMR (282 MHz, CD_3CN)

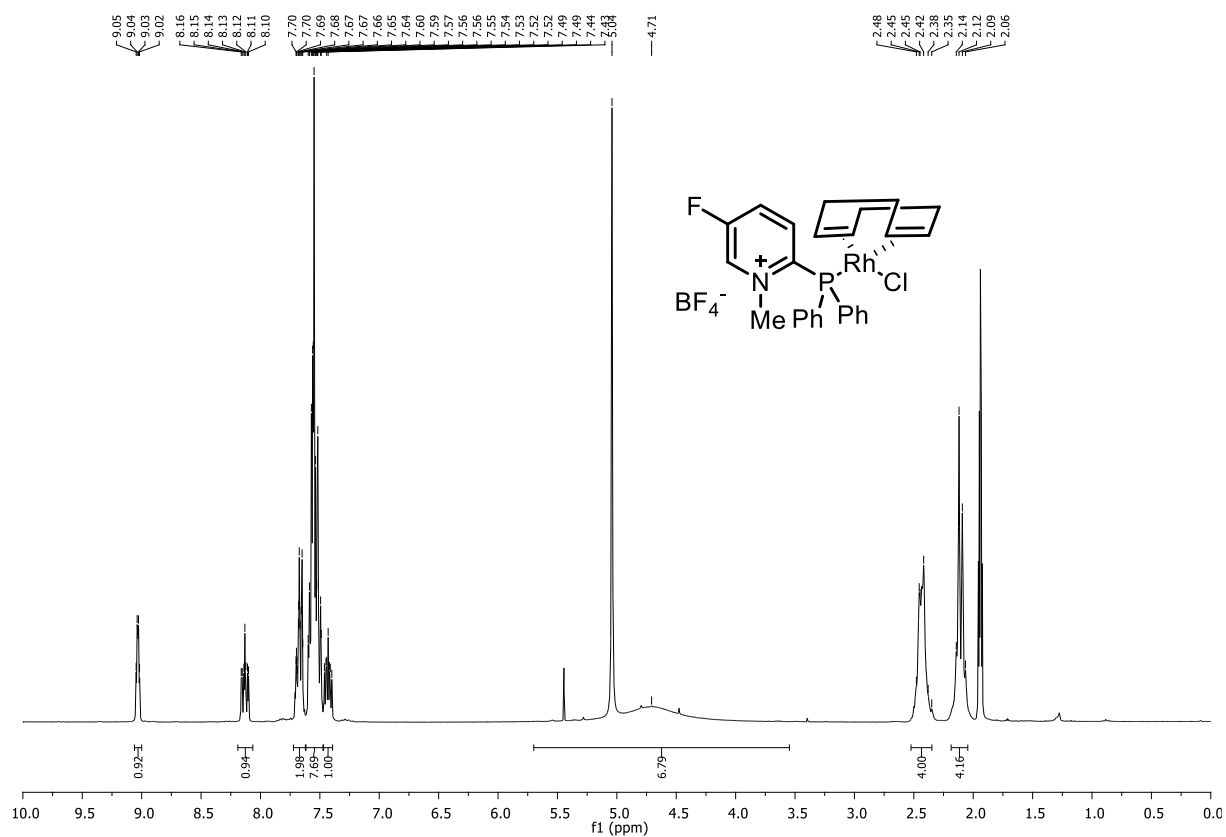


Compound 150a: ^1H NMR (300 MHz, CDCl_3)Compound 150a: ^{13}C NMR (101 MHz, CDCl_3)

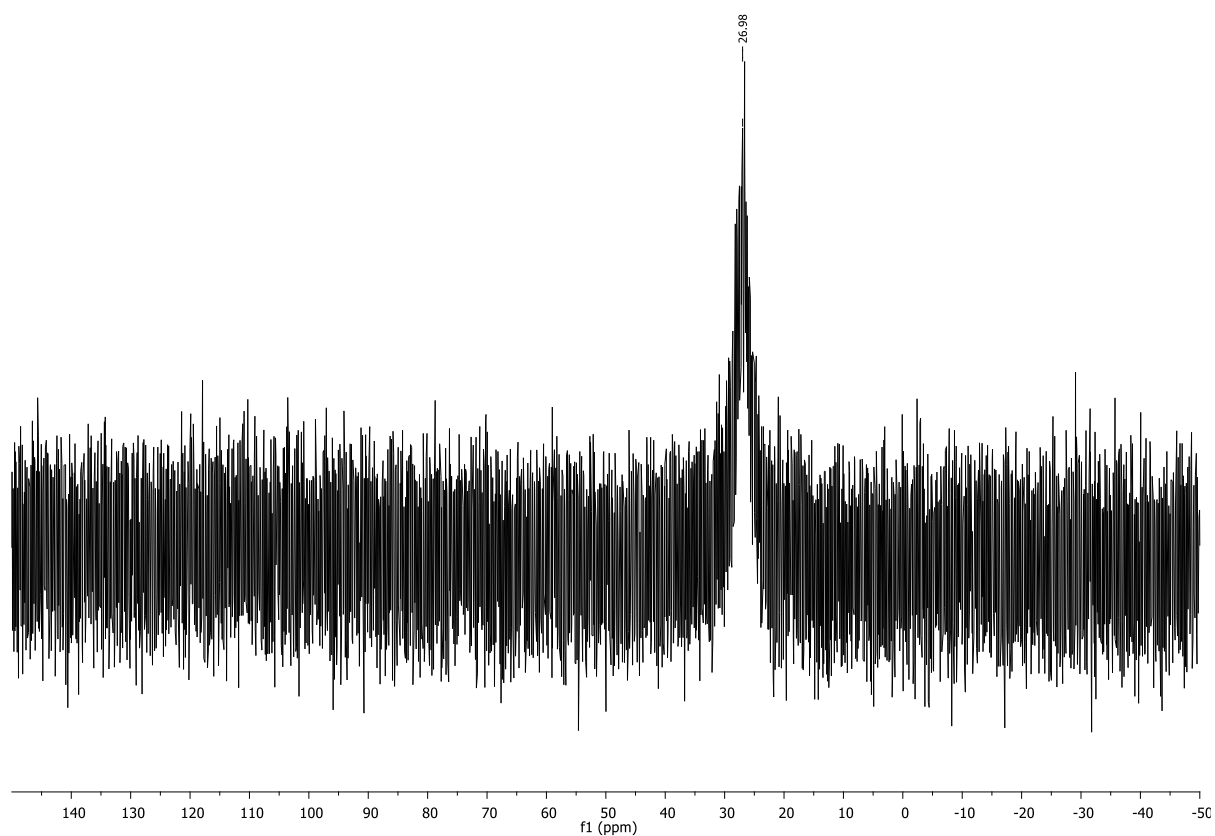
Compound 150a: ^{31}P NMR (121 MHz, CDCl_3)



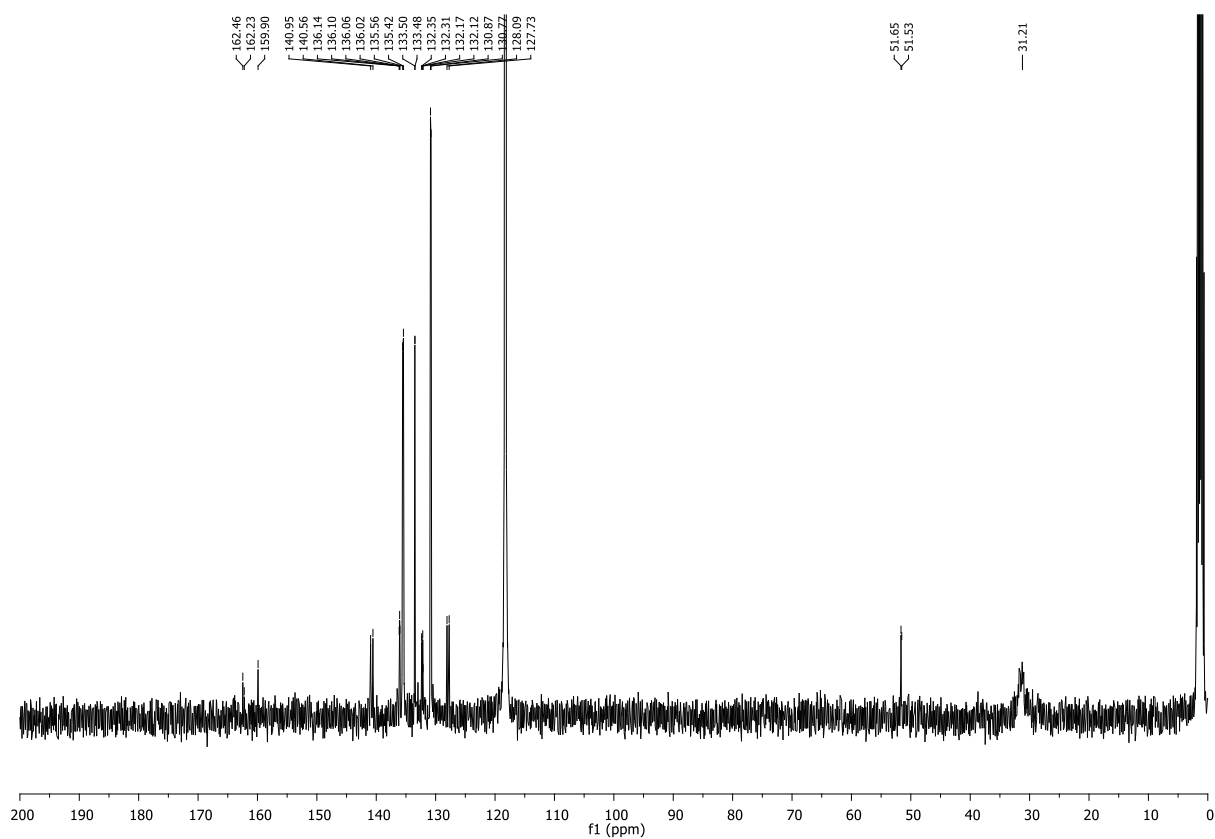
Compound 150b: ^1H NMR (300 MHz, CD_3CN)



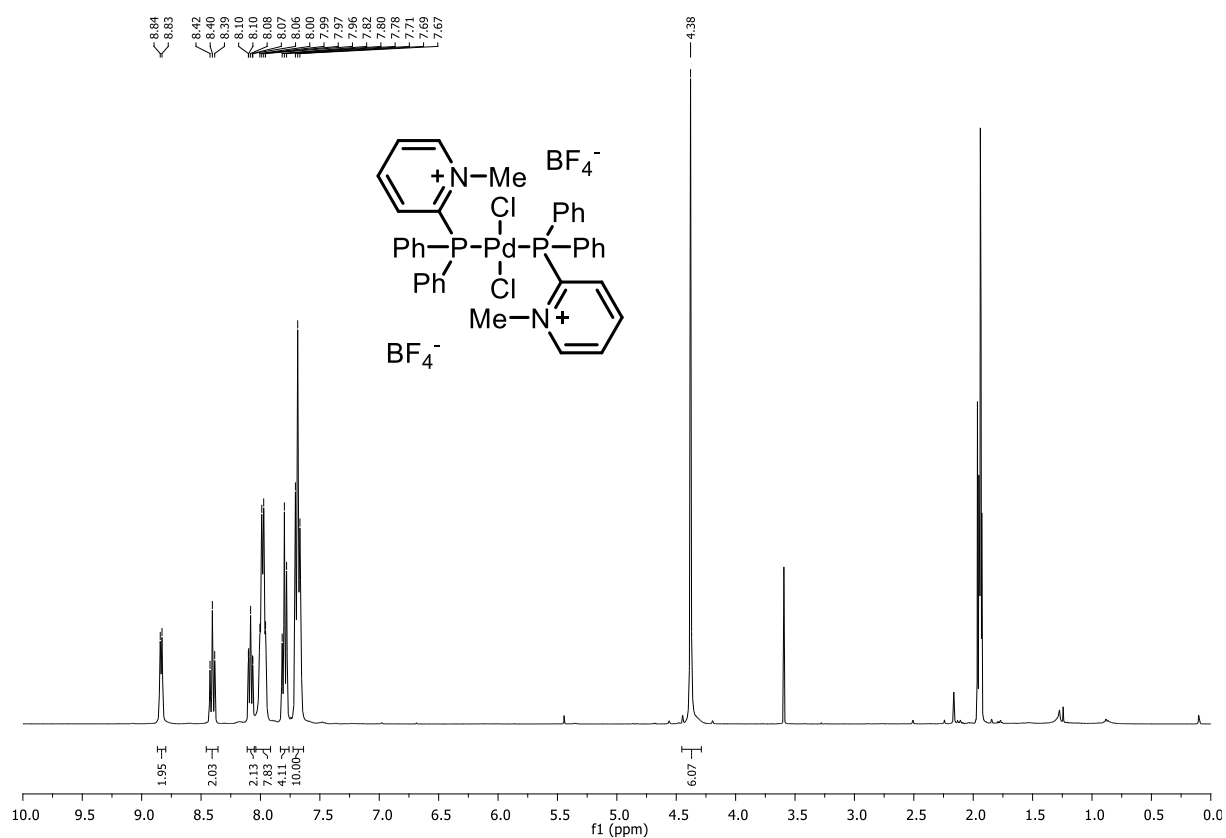
Compound 150b: ^{31}P NMR (121 MHz, CD_3CN)



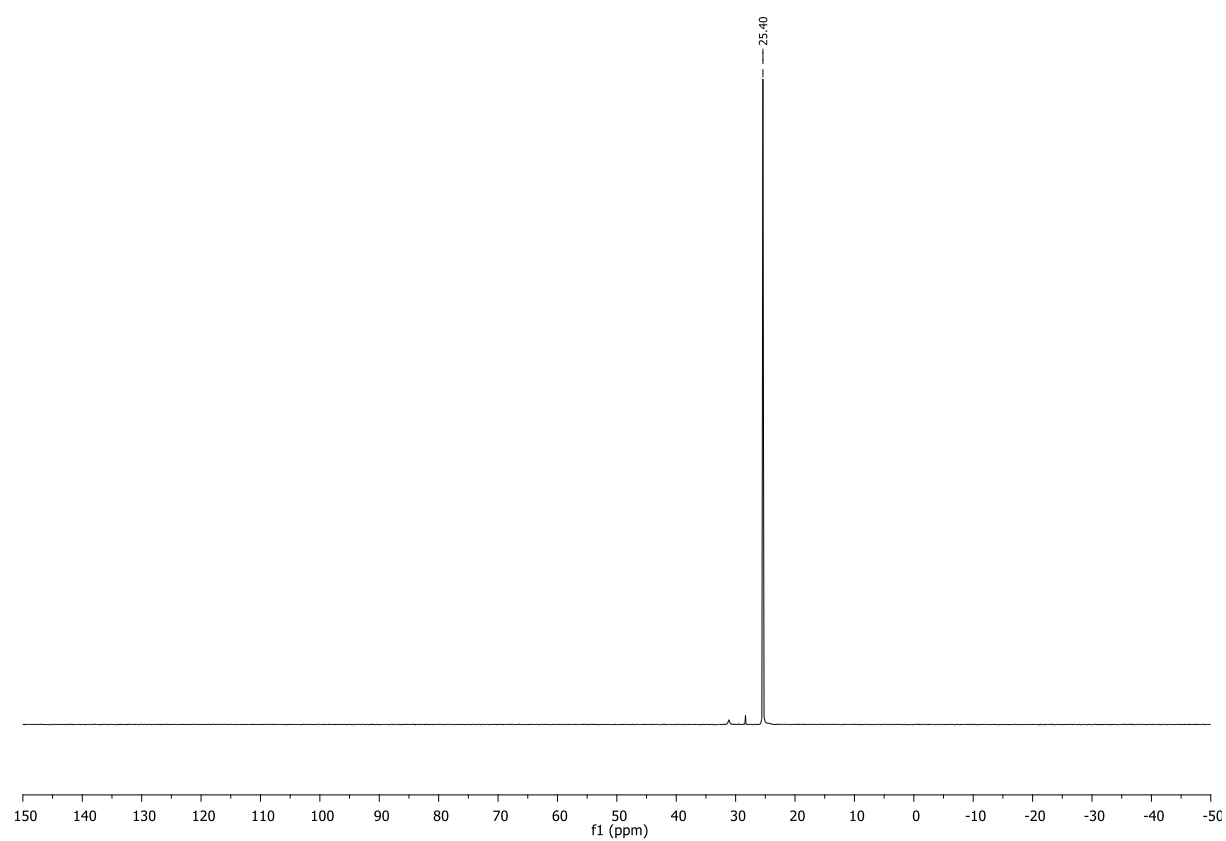
Compound 150b: ^{13}C NMR (101 MHz, CD_3CN)



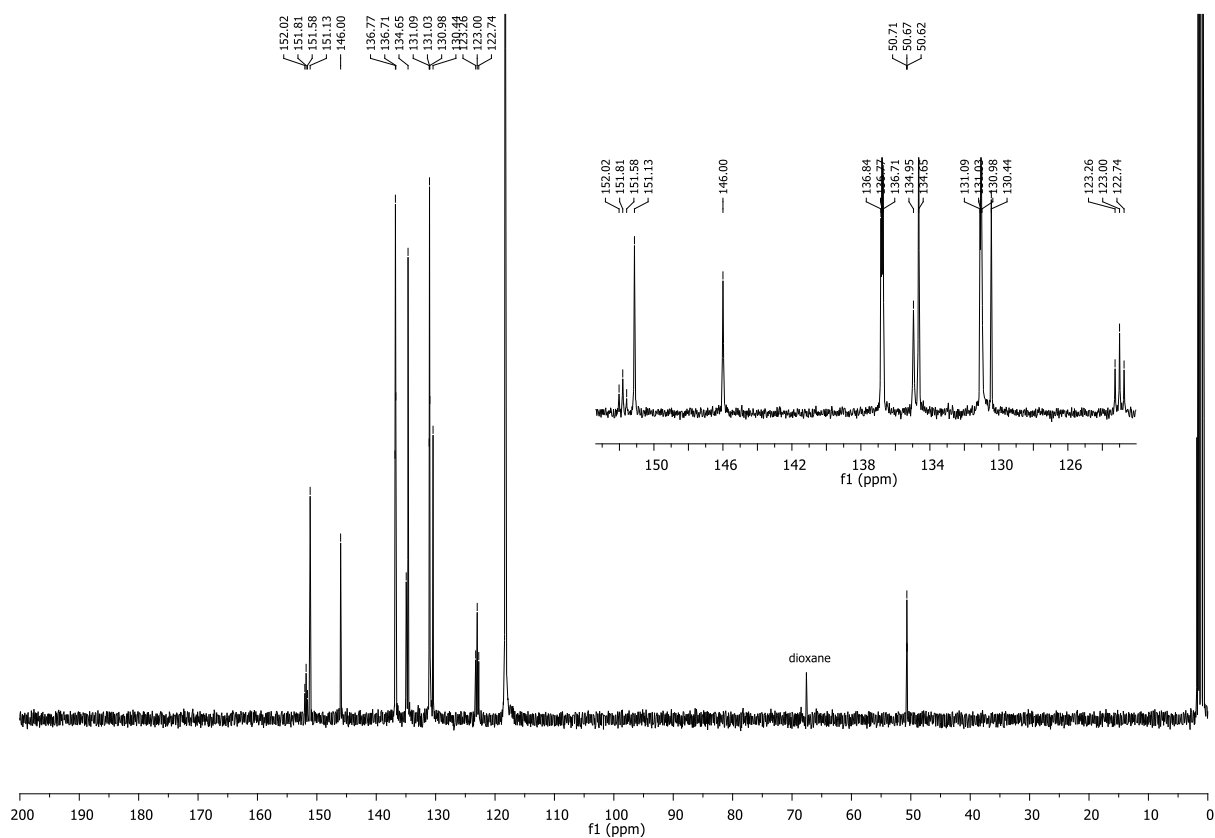
Compound 151a: ^1H NMR (400 MHz, CD_3CN)



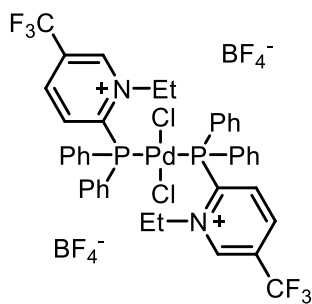
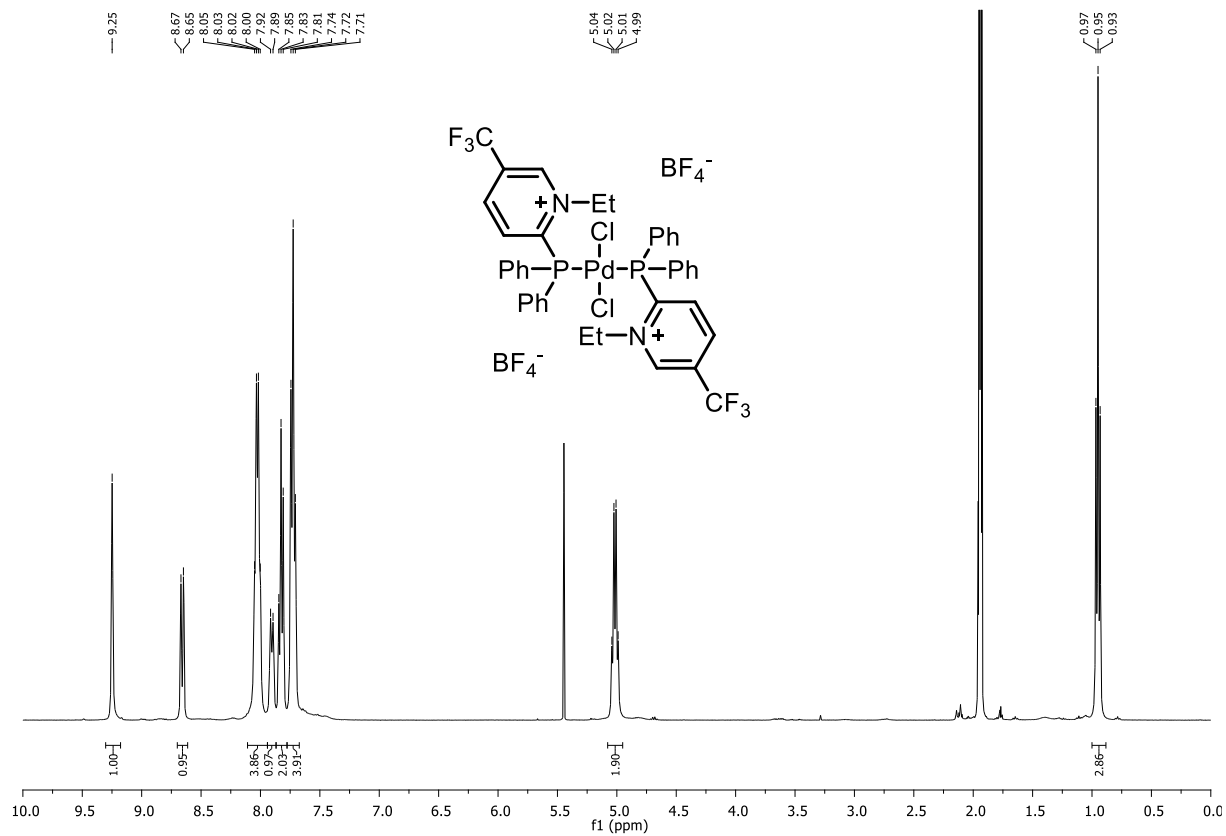
Compound 151a: ^{31}P NMR (162 MHz, CD_3CN)



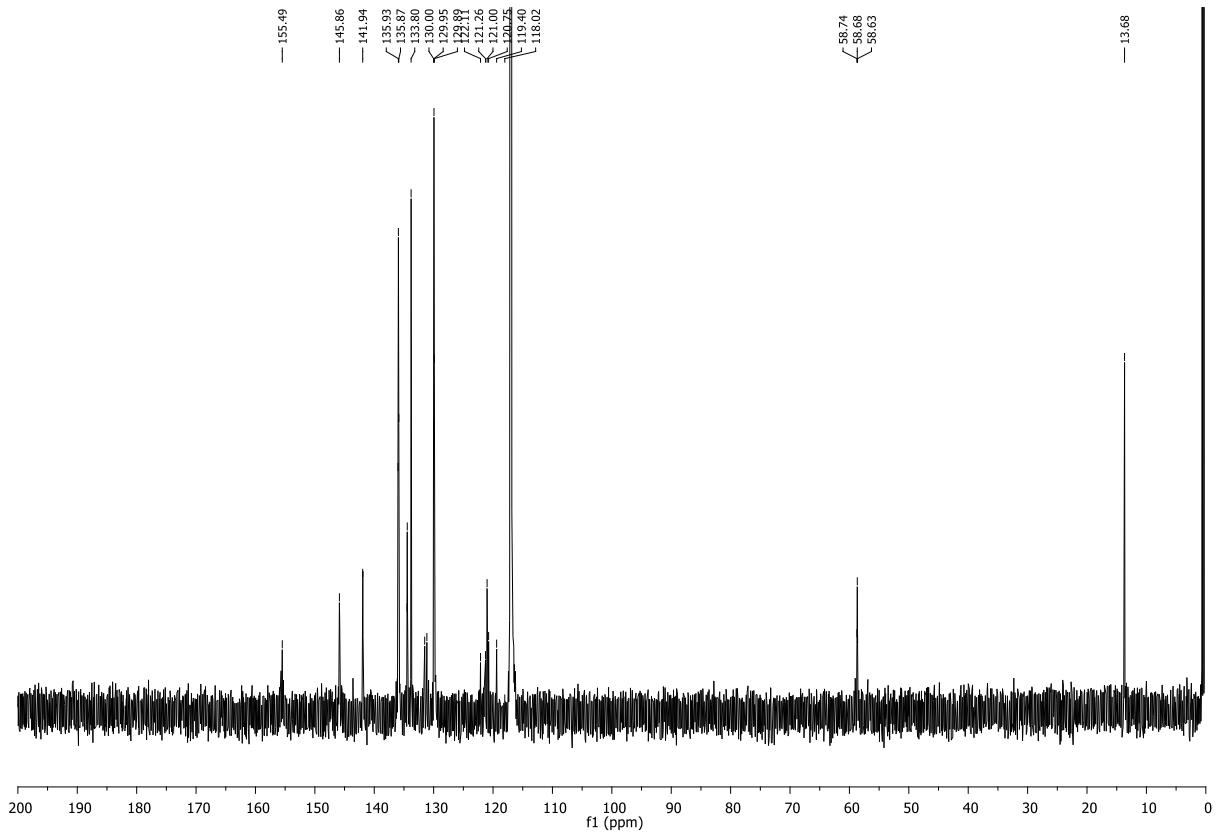
Compound 151a: ^{13}C NMR (101 MHz, CD_3CN)



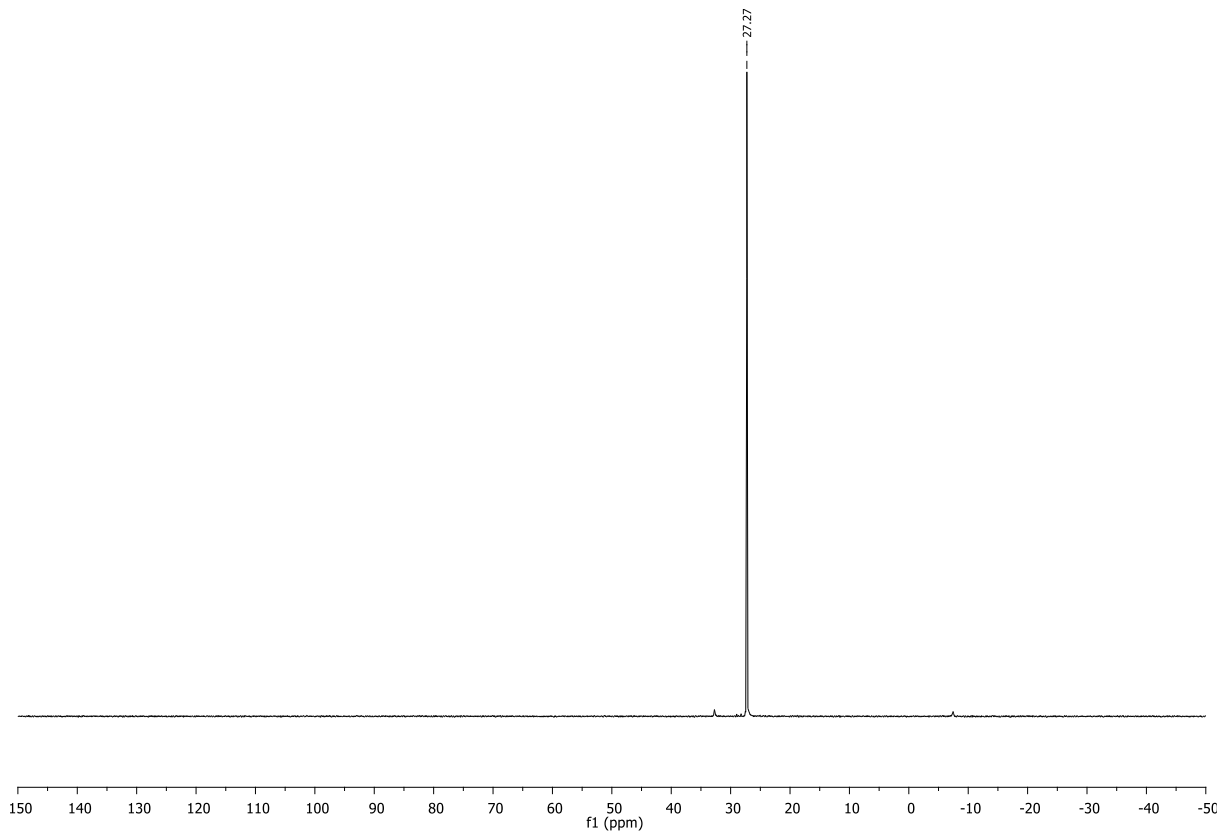
Compound 151b: ^1H NMR (300 MHz, CD_3CN)

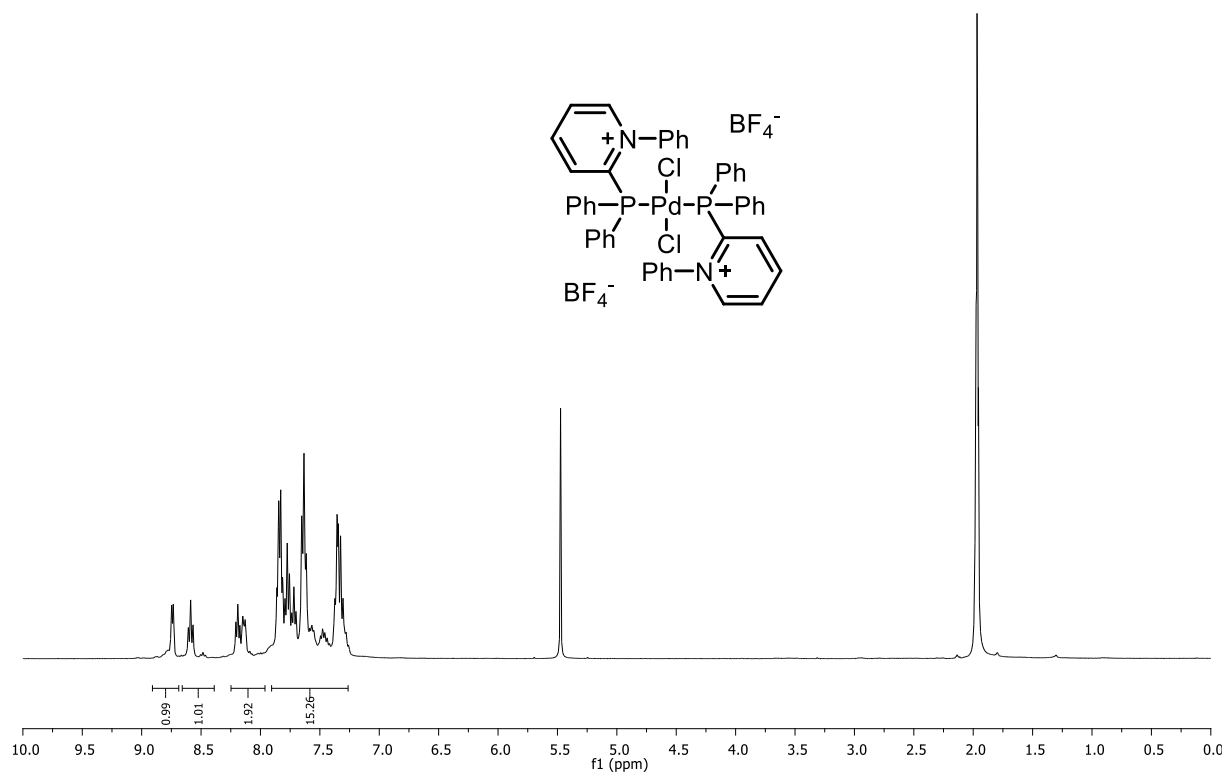
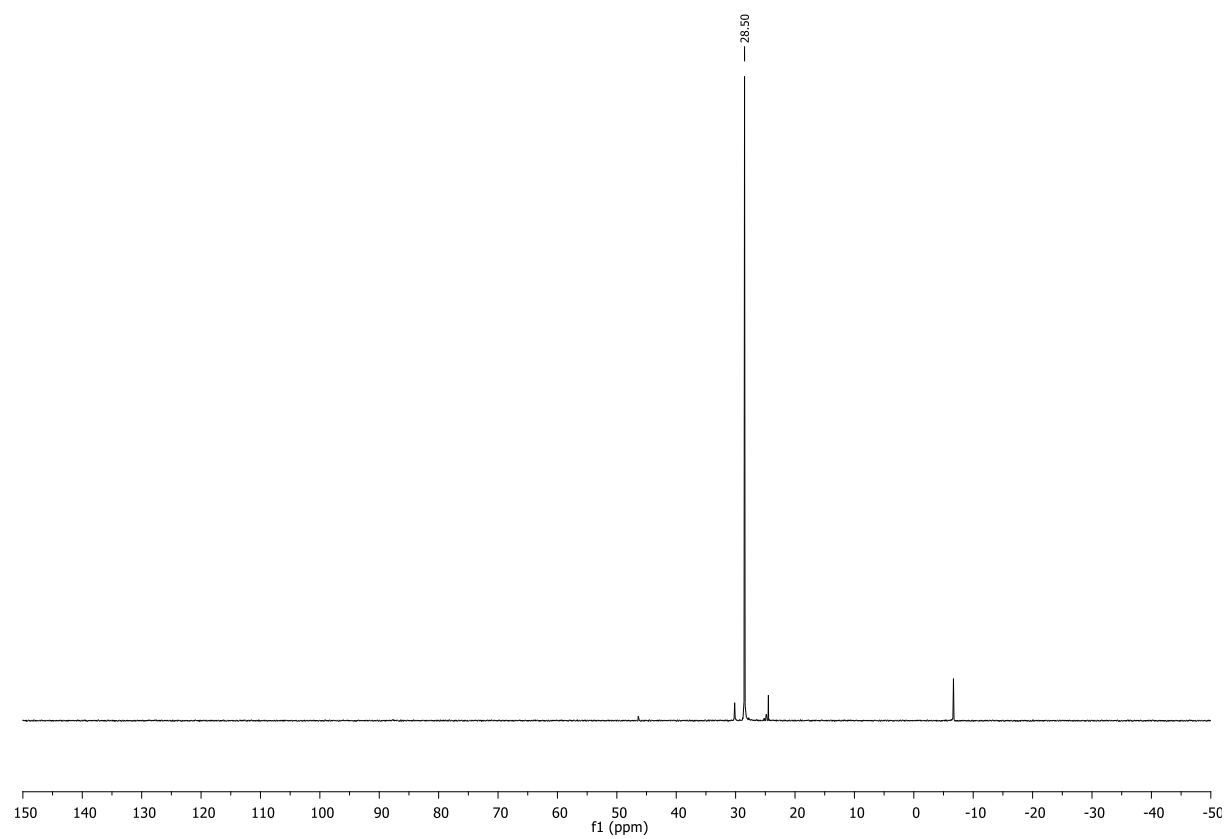


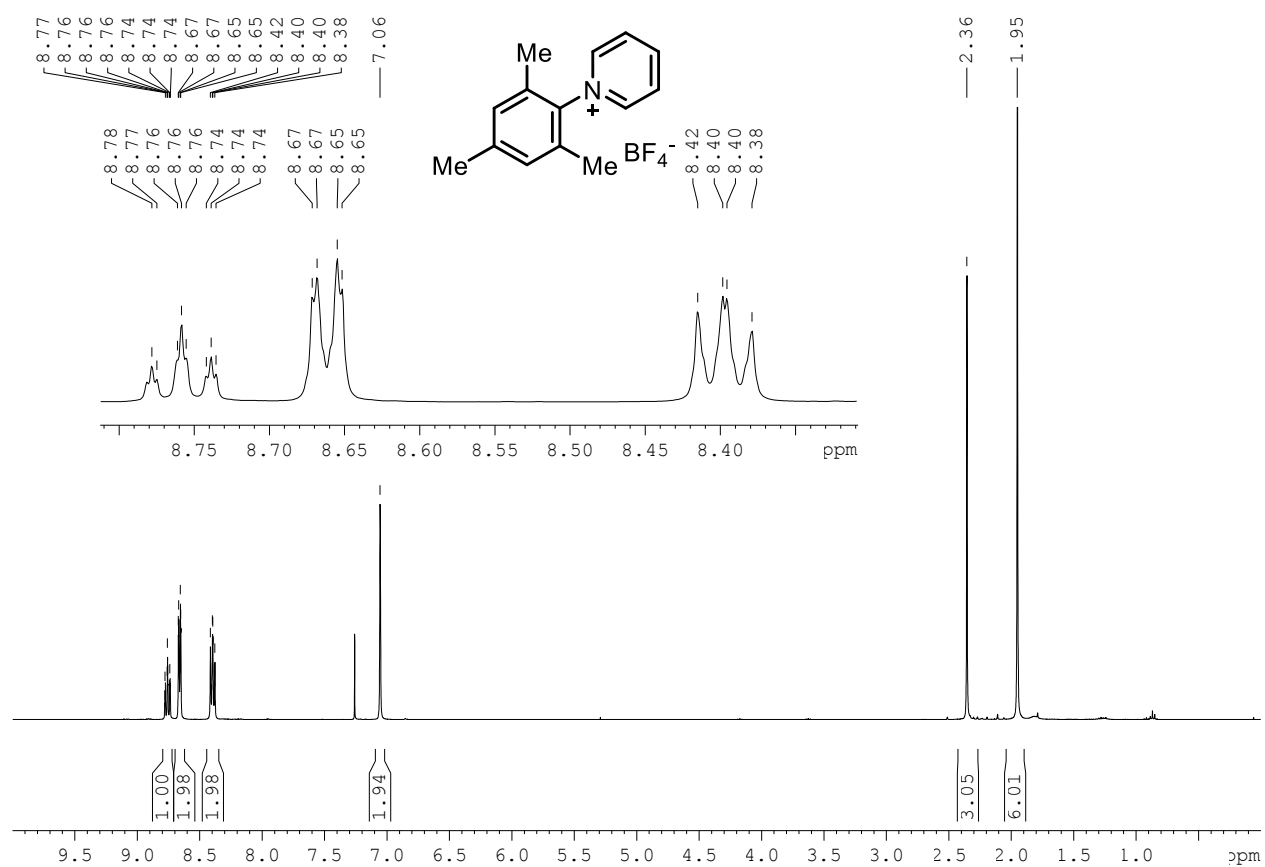
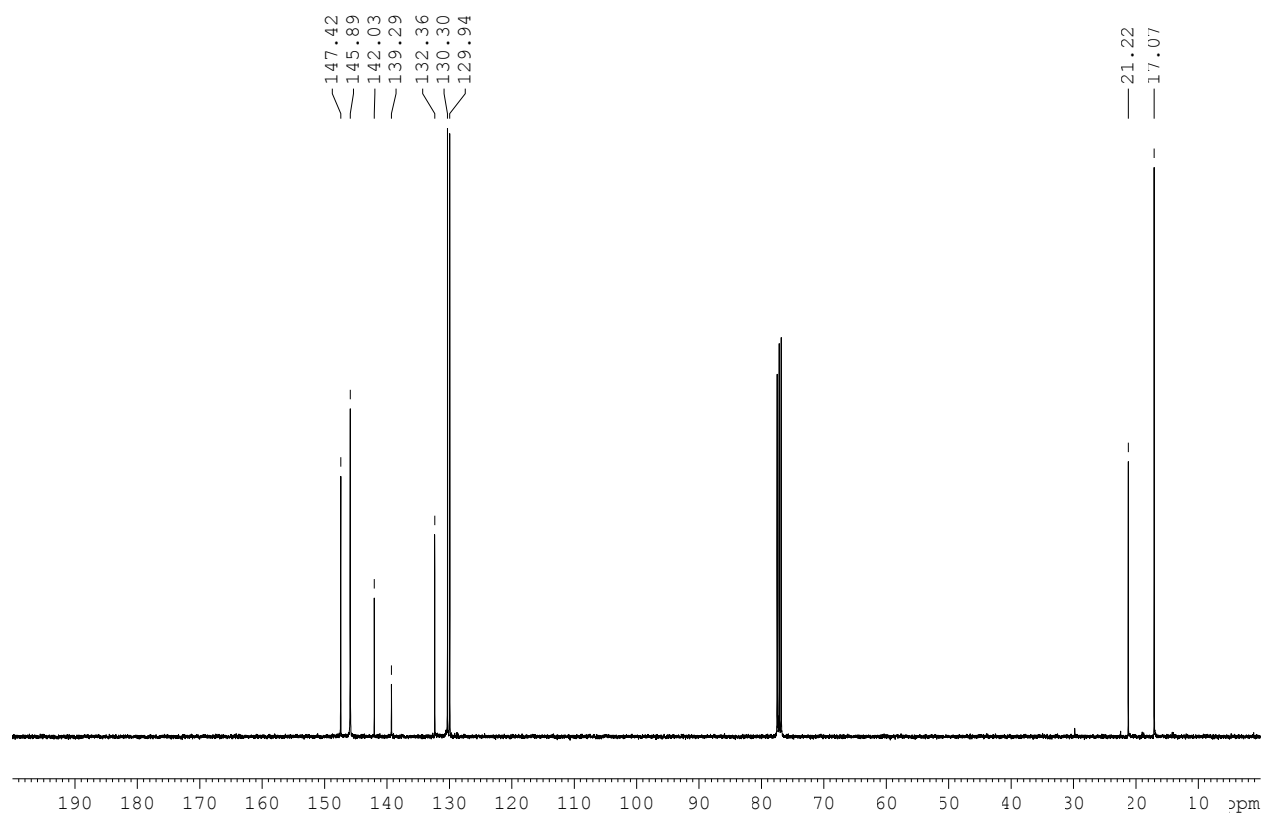
Compound 151b: ^{13}C NMR (101 MHz, CD_3CN)



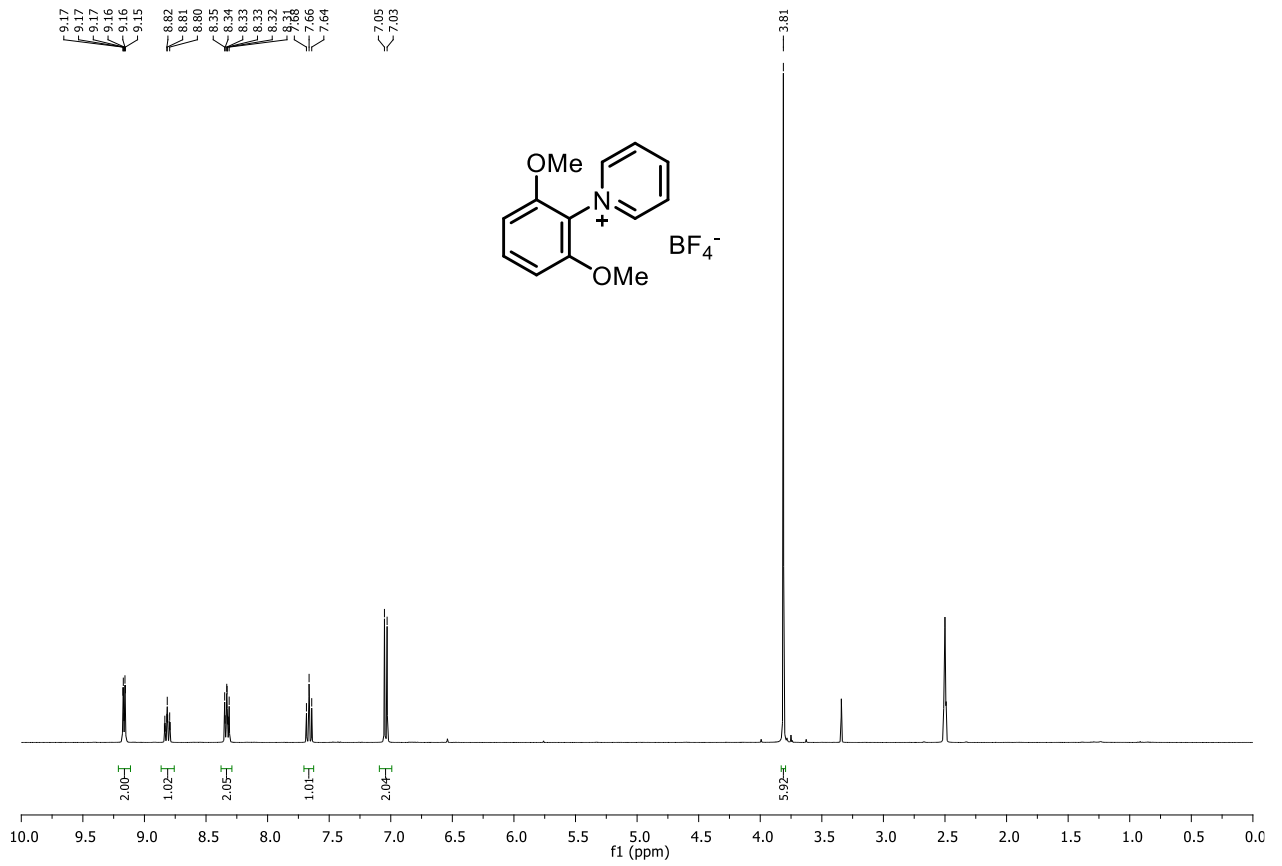
Compound 151b: ^{31}P NMR (162 MHz, CD_3CN)



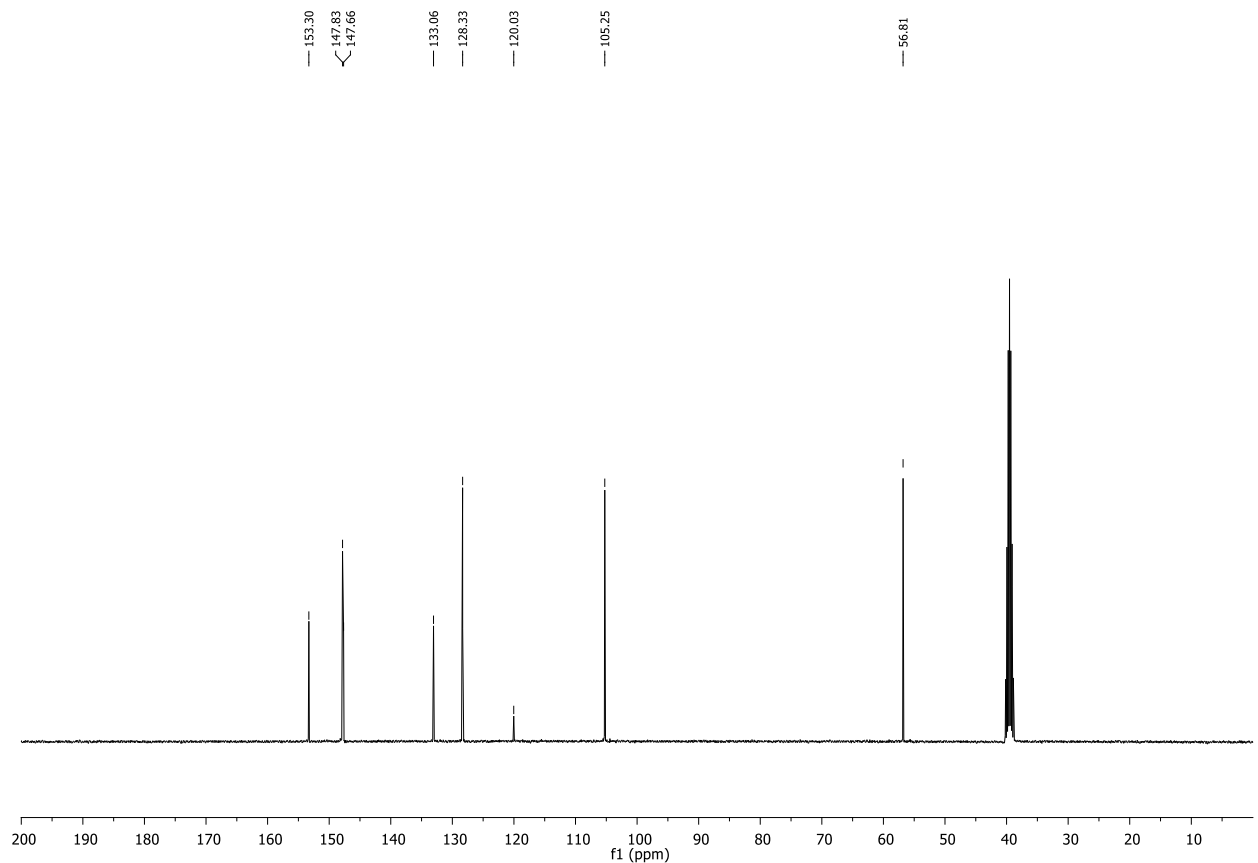
Compound 151c: ^1H NMR (400 MHz, CD_3CN)**Compound 151c:** ^{31}P NMR (162 MHz, CD_3CN)

Compound 176a: ^1H NMR (300 MHz, CDCl_3)**Compound 176a:** ^{13}C NMR (75 MHz, CDCl_3)

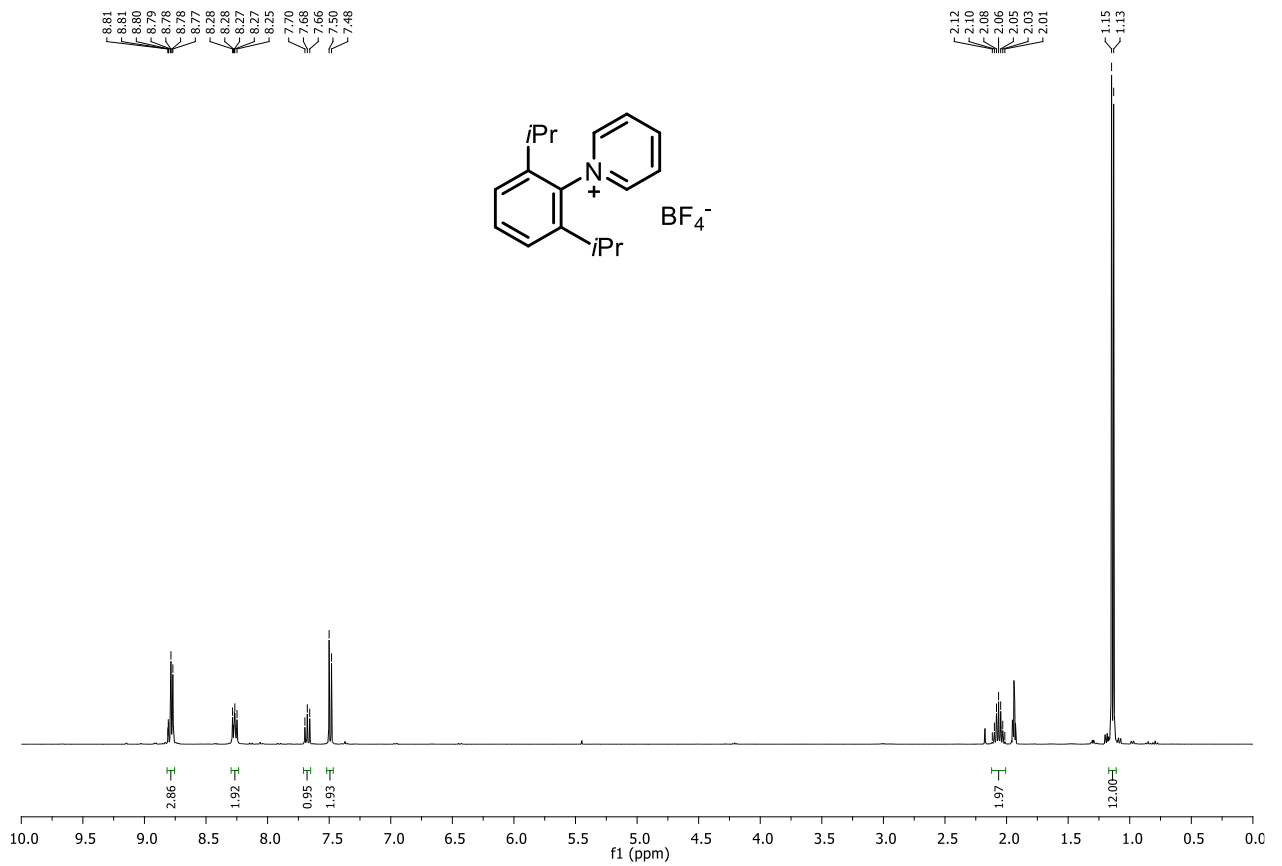
Compound 176b: ¹H NMR (300 MHz, DMSO)



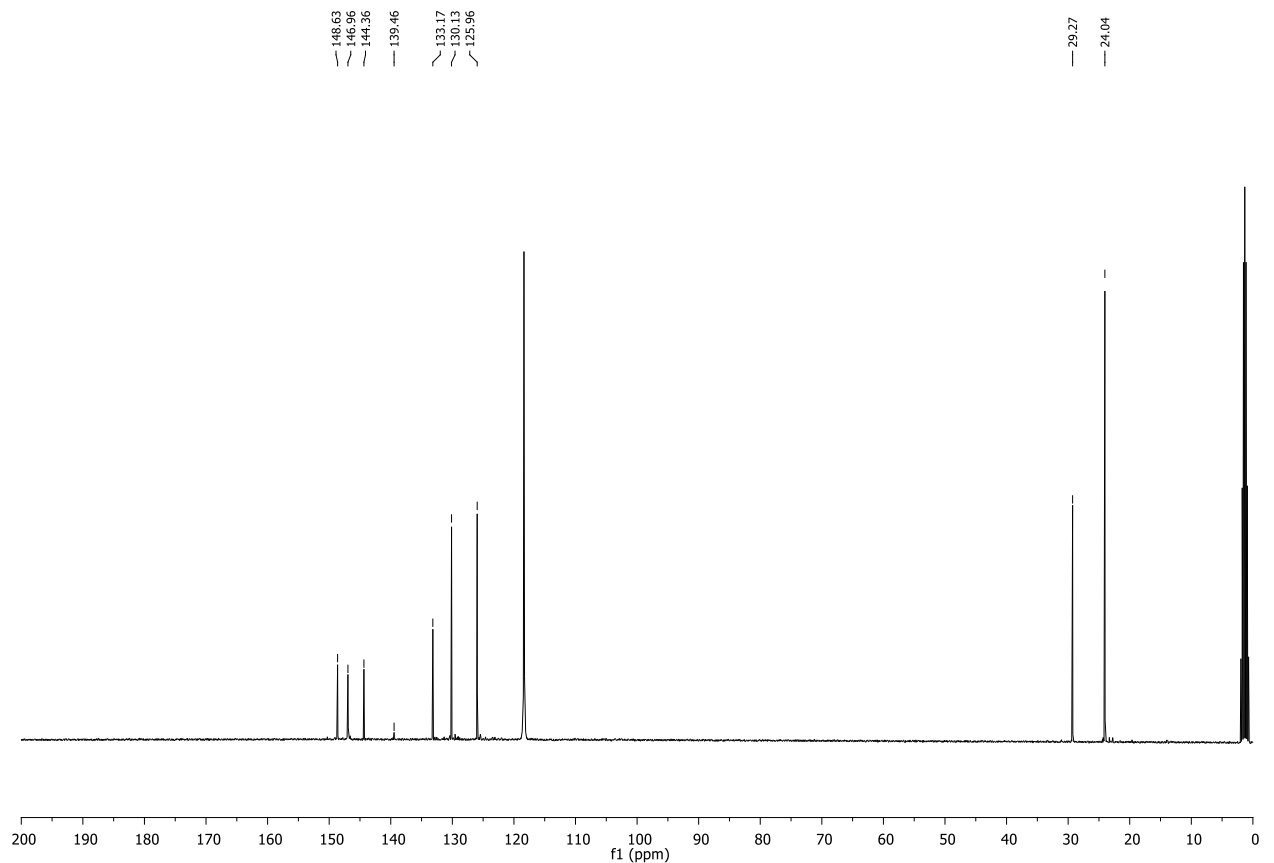
Compound 176b: ¹³C NMR (75 MHz, DMSO)



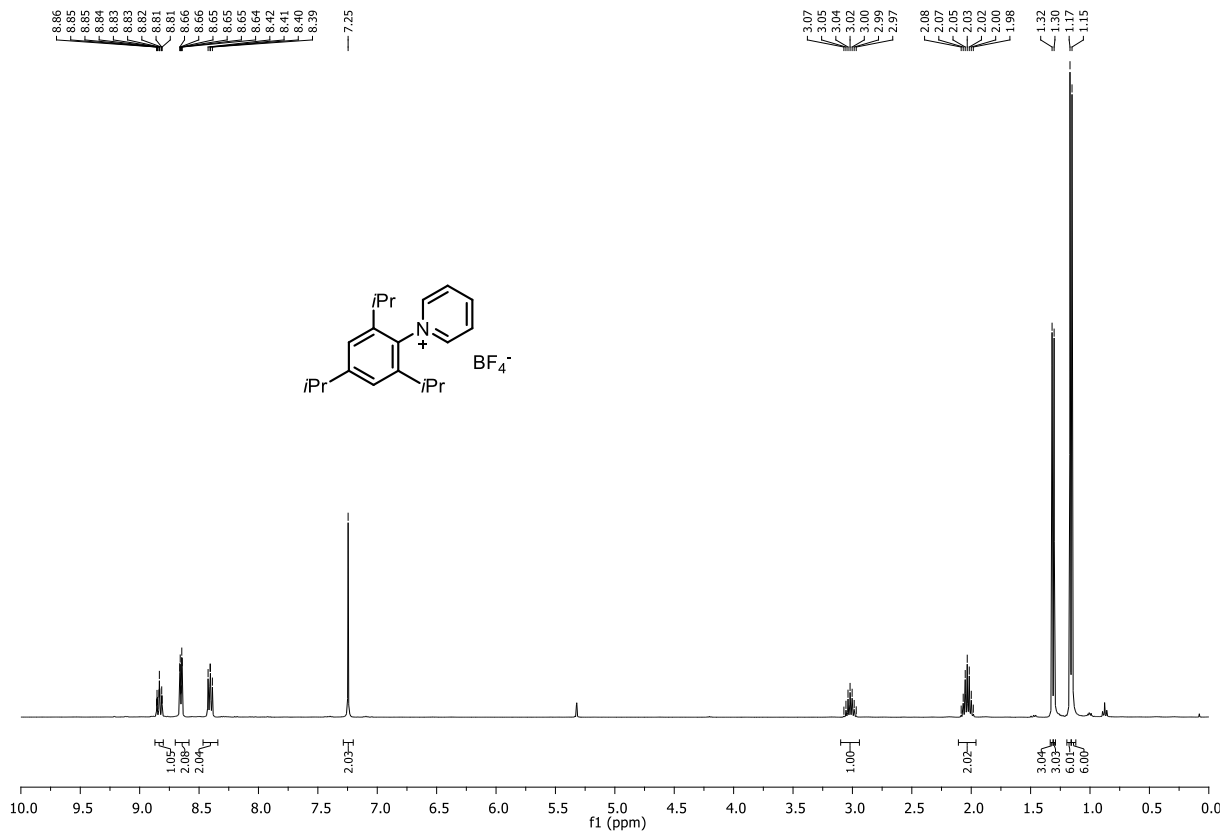
Compound 176c: ^1H NMR (300 MHz, CD_3CN)



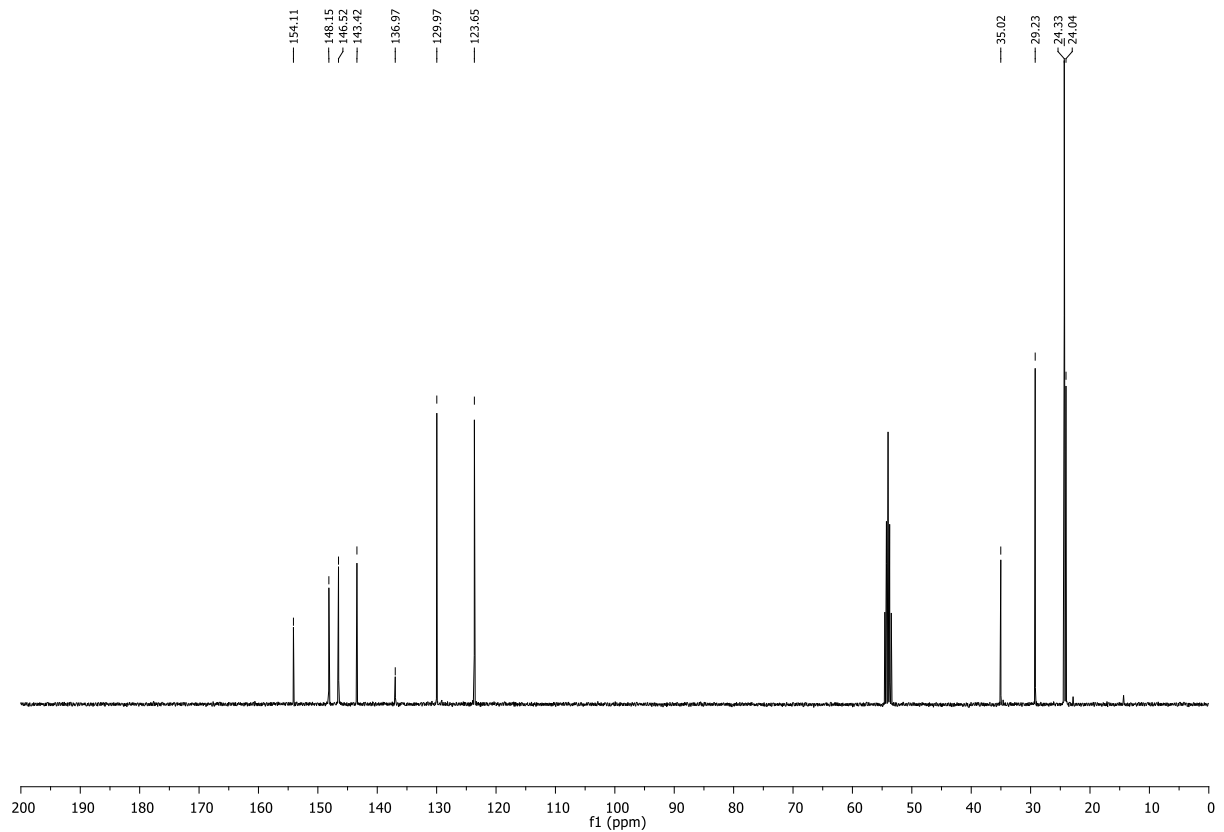
Compound 176c: ^{13}C NMR (75 MHz, CD_3CN)



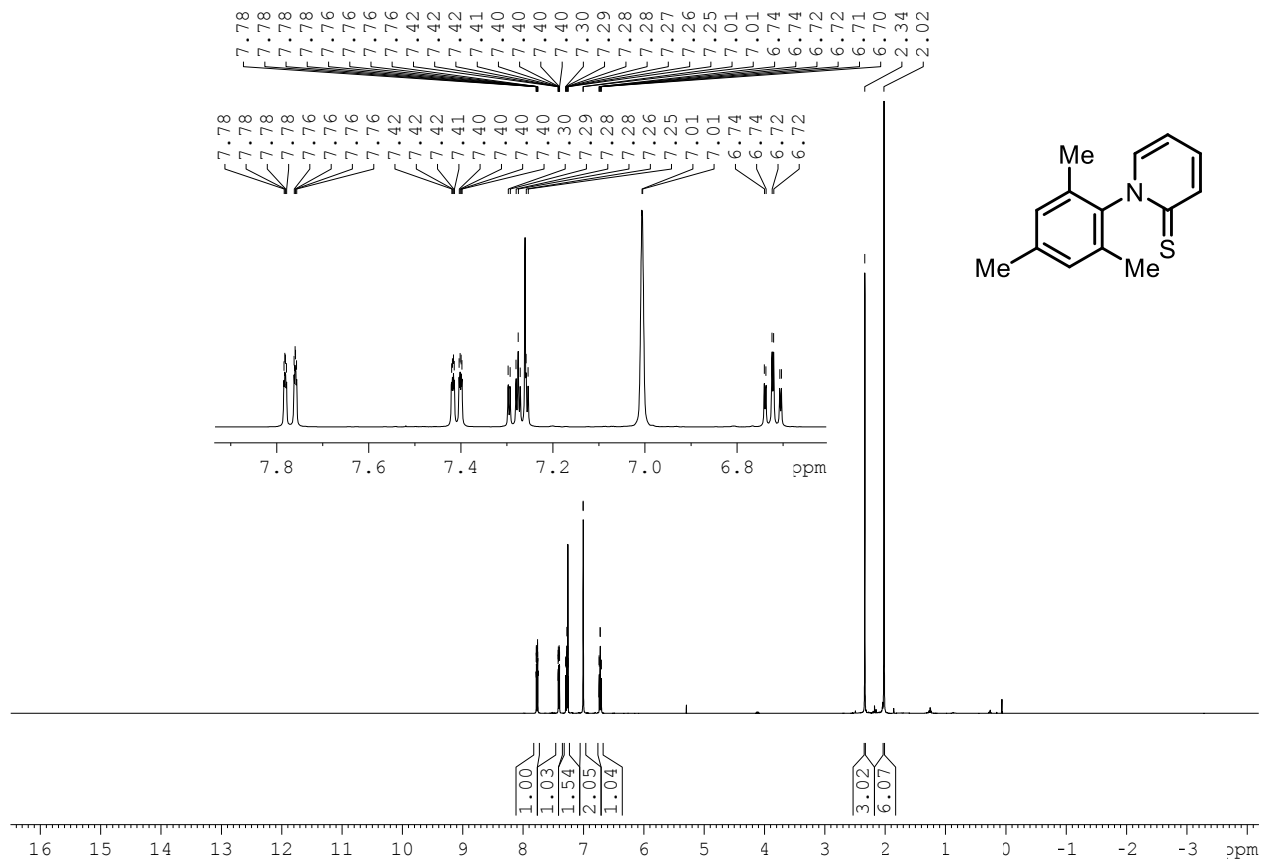
Compound 176d: ^1H NMR (300 MHz, CD_2Cl_2)



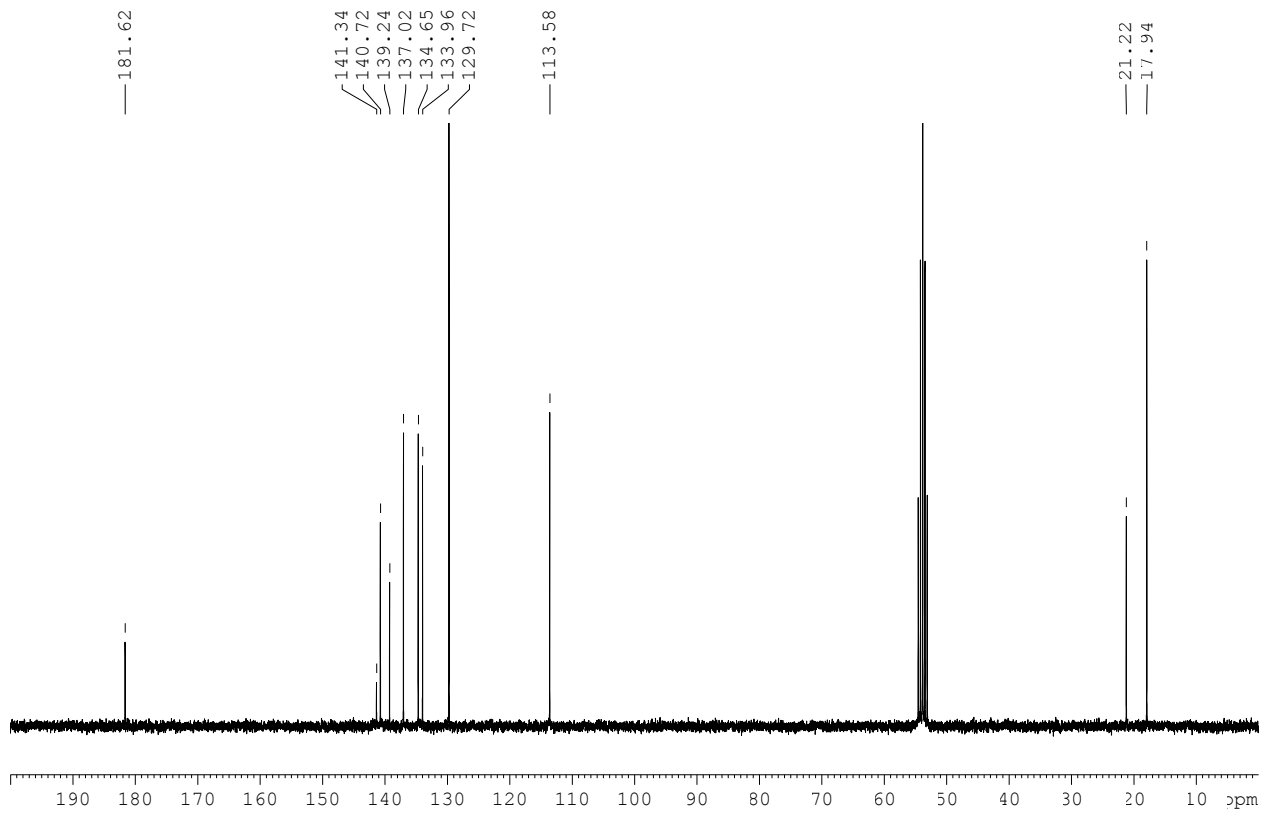
Compound 176d: ^{13}C NMR (75 MHz, CD_2Cl_2)

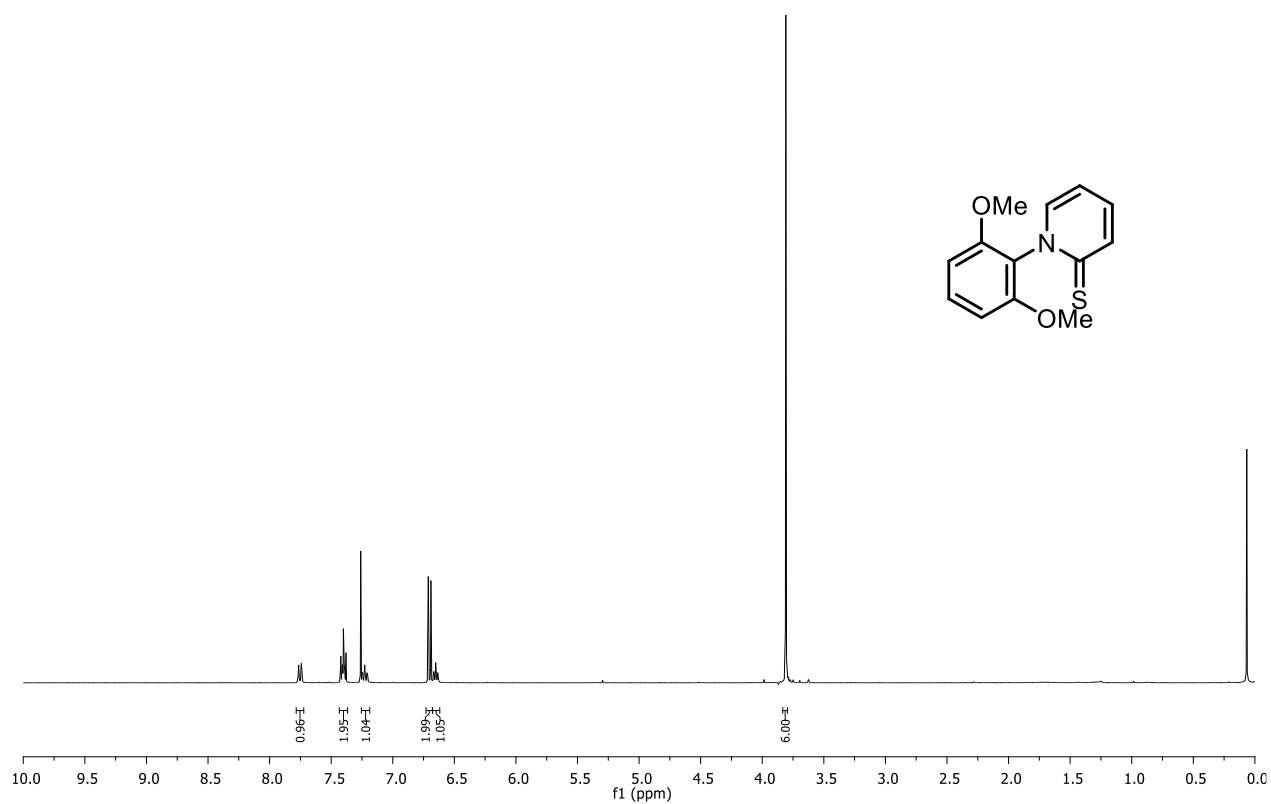
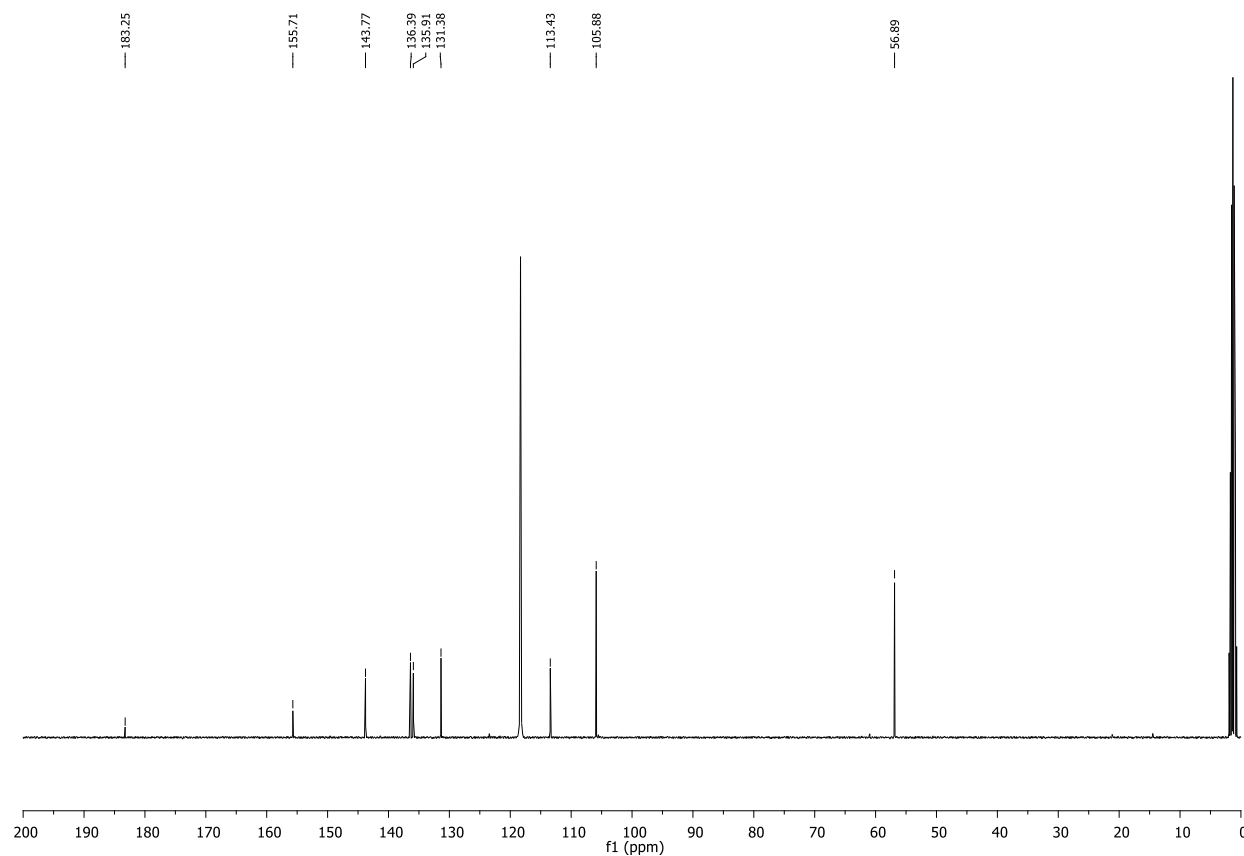


Compound 188a: ^1H NMR (300 MHz, CD_2Cl_2)

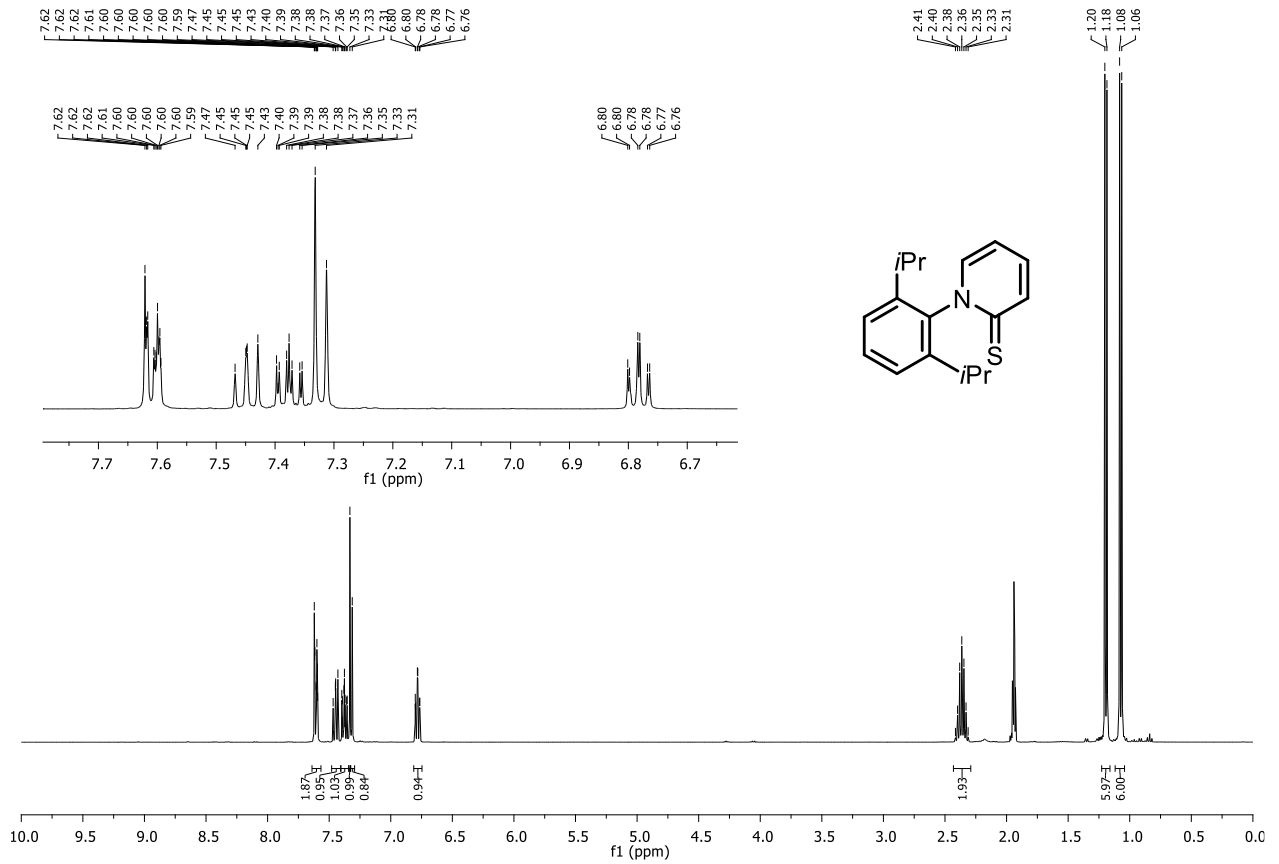


Compound 188a: ^{13}C NMR (75 MHz, CD_2Cl_2)

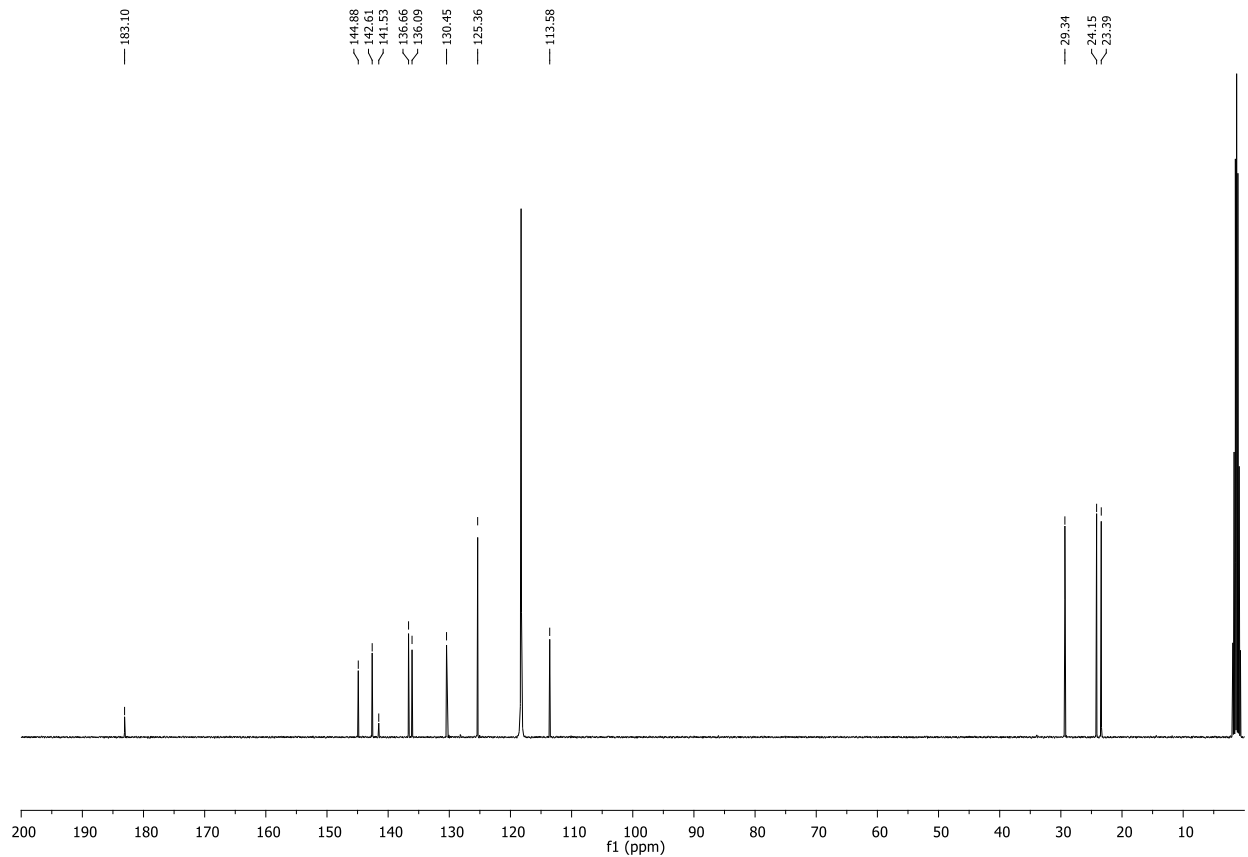


Compound 188b: ^1H NMR (300 MHz, CDCl_3)**Compound 188b:** ^{13}C NMR (75 MHz, CD_3CN)

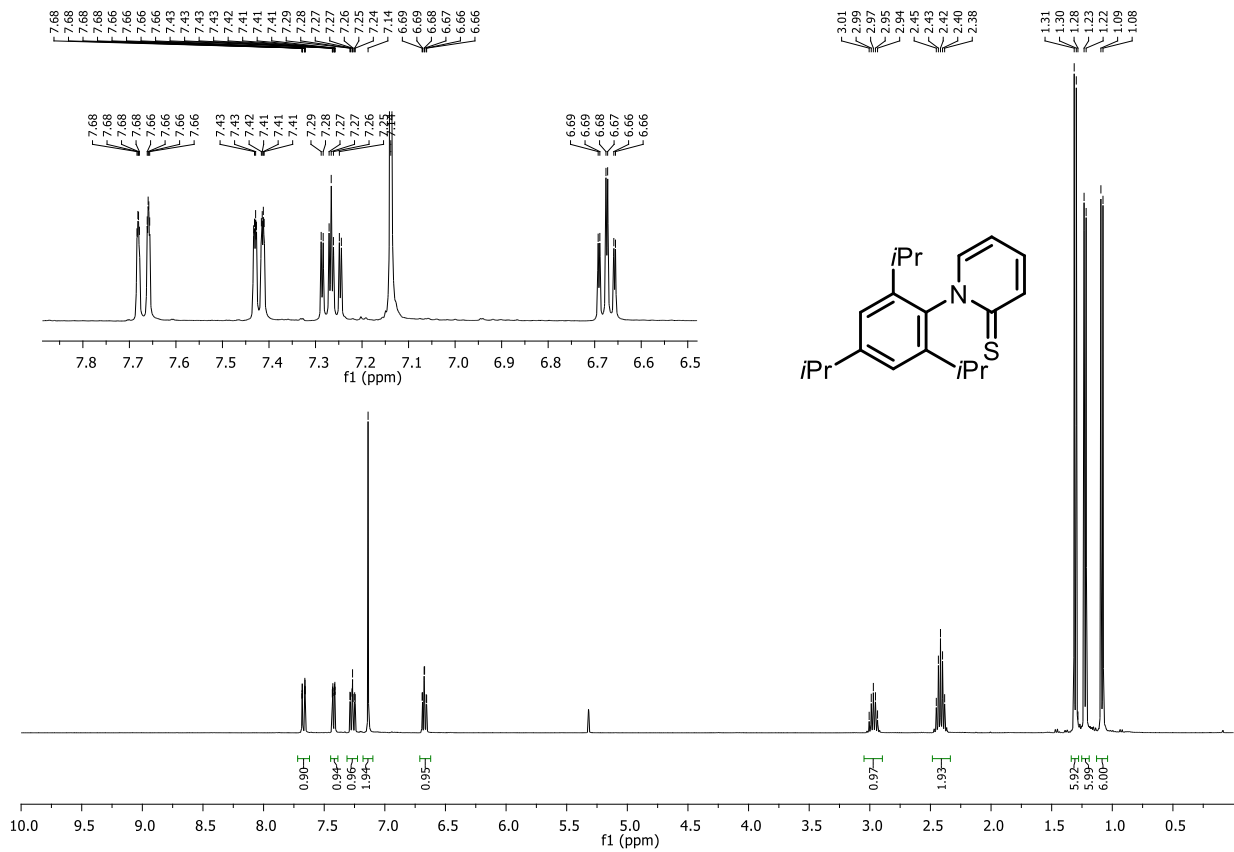
Compound 188c: ^1H NMR (300 MHz, CD_3CN)



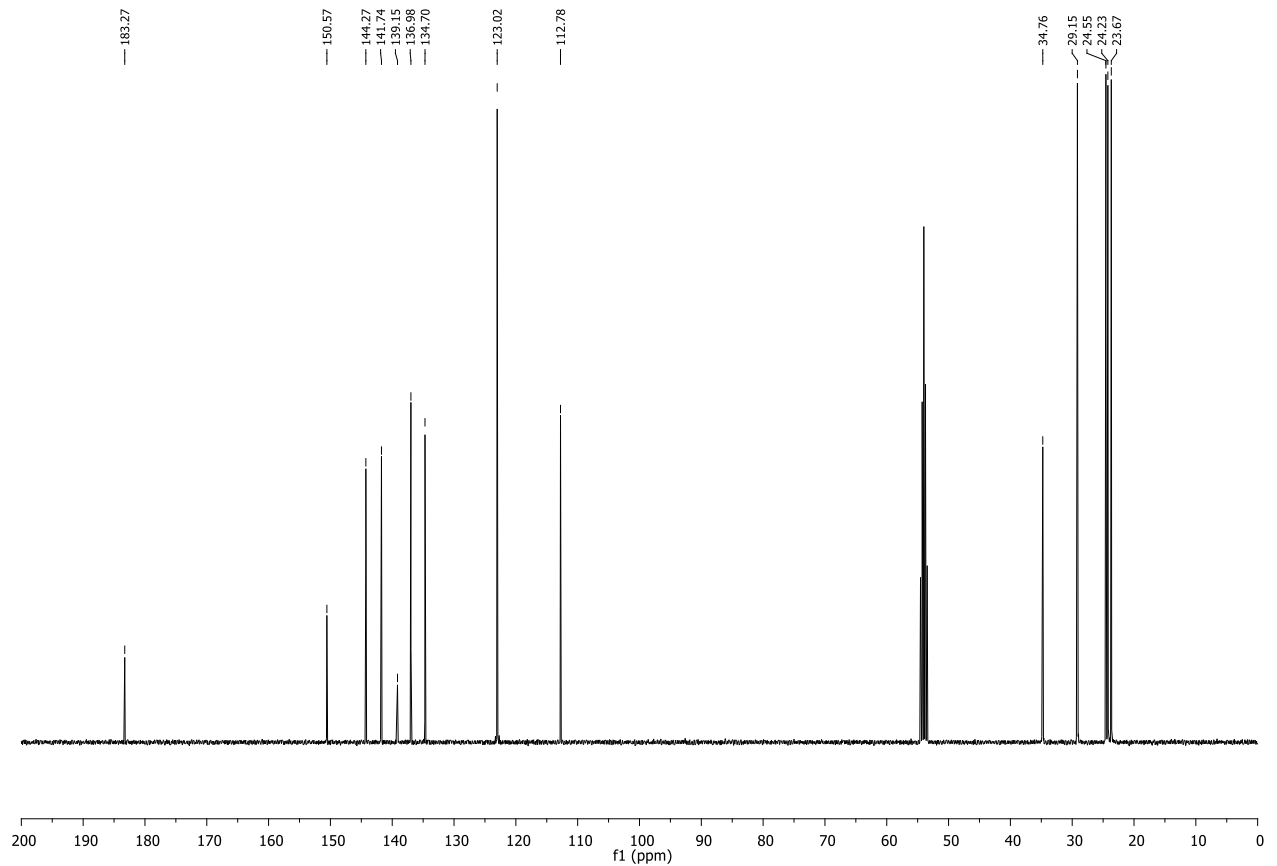
Compound 188c: ^{13}C NMR (75 MHz, CD_3CN)



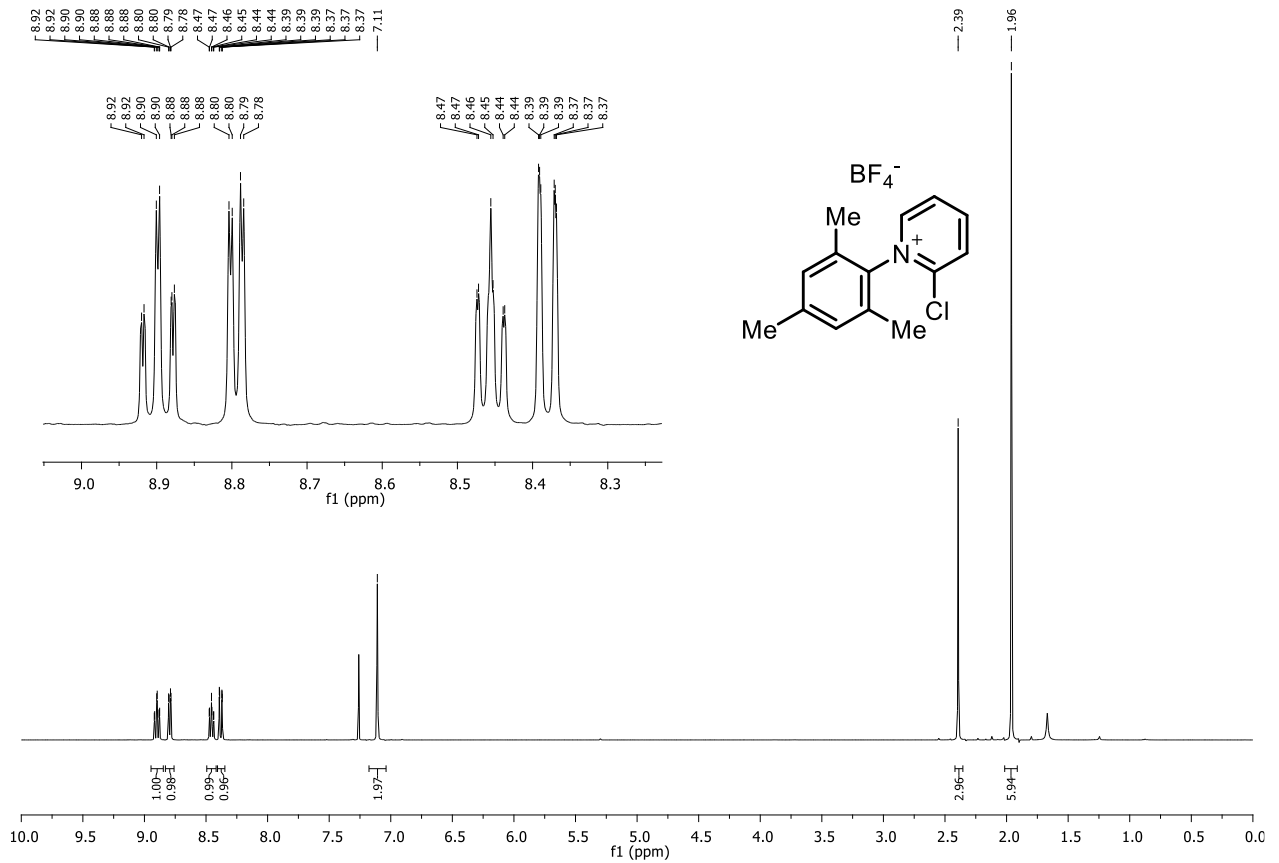
Compound 188d: ^1H NMR (300 MHz, CD_2Cl_2)



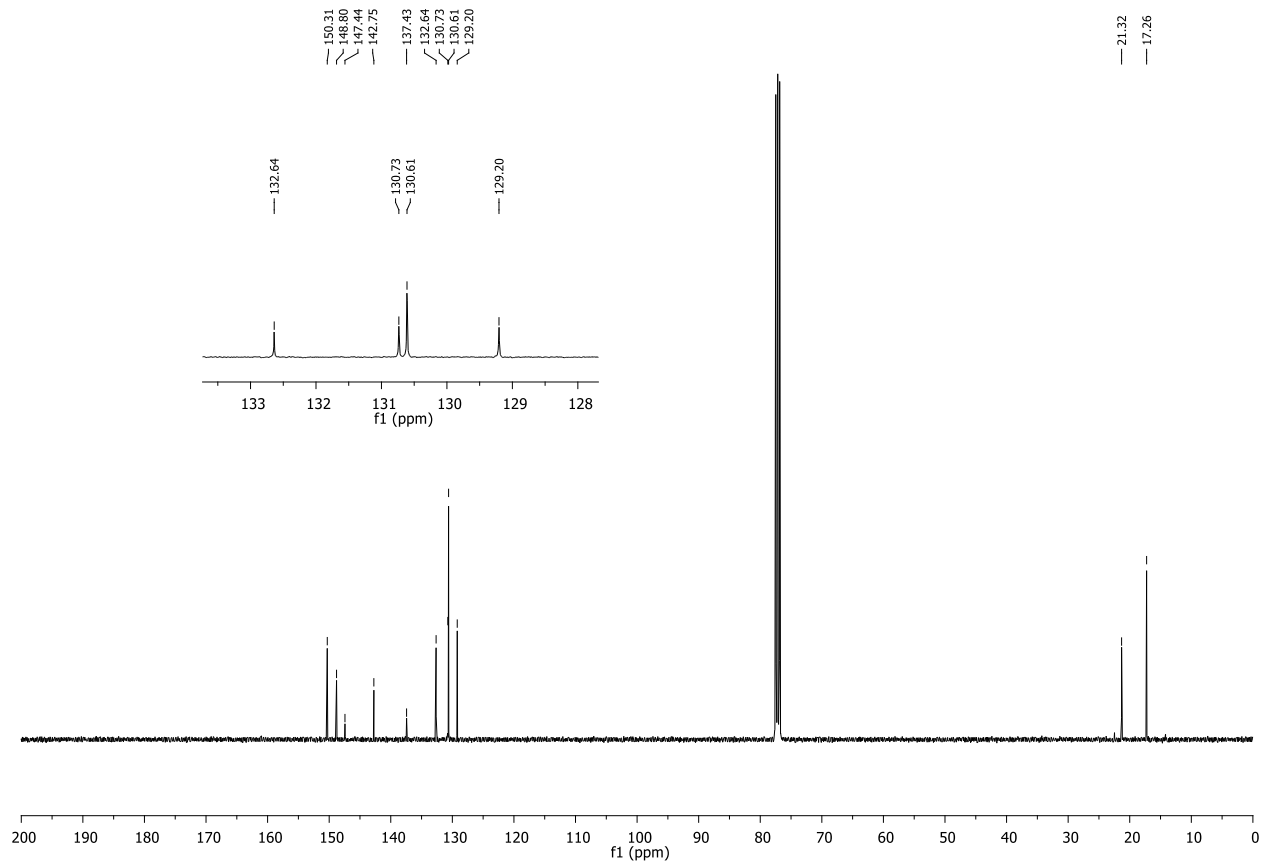
Compound 188d: ^{13}C NMR (75 MHz, CD_2Cl_2)



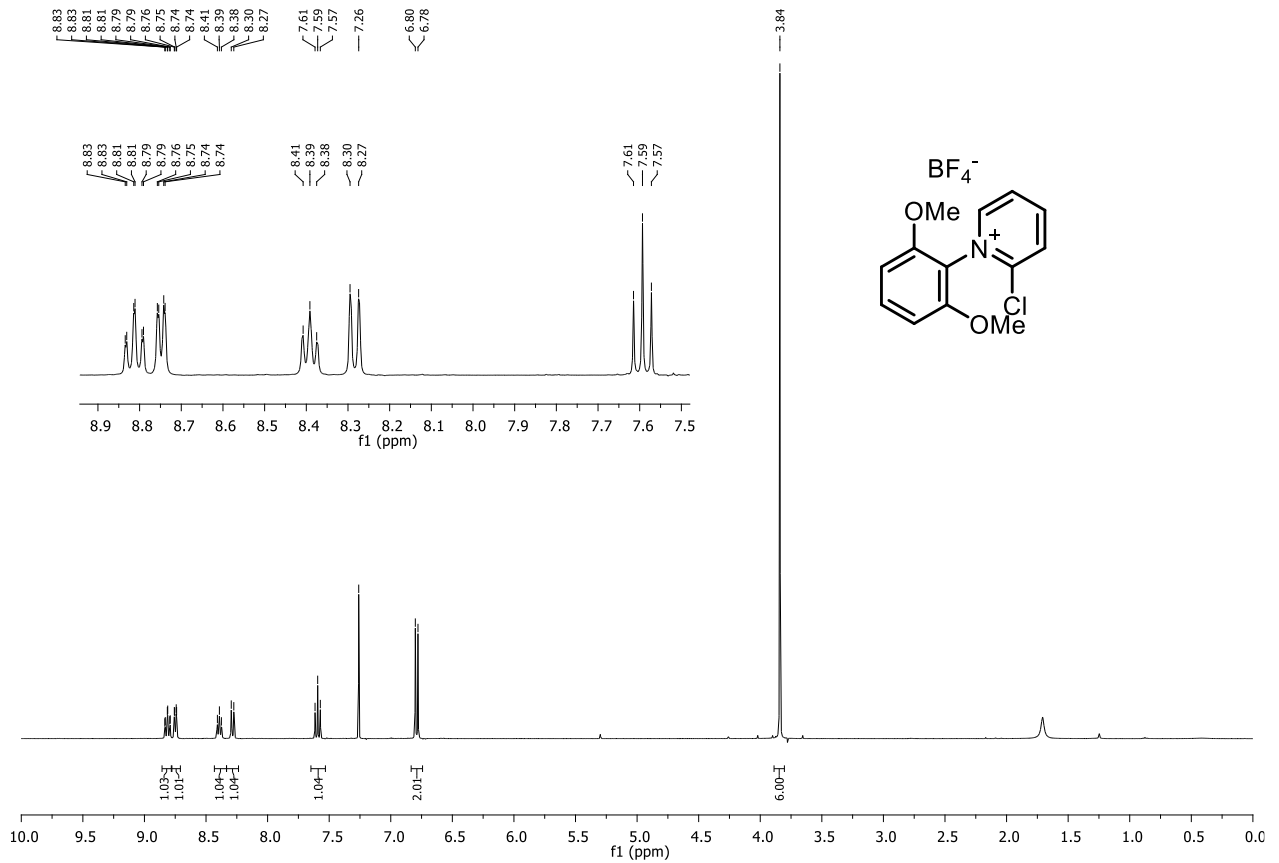
Compound 189a: ^1H NMR (300 MHz, CDCl_3)



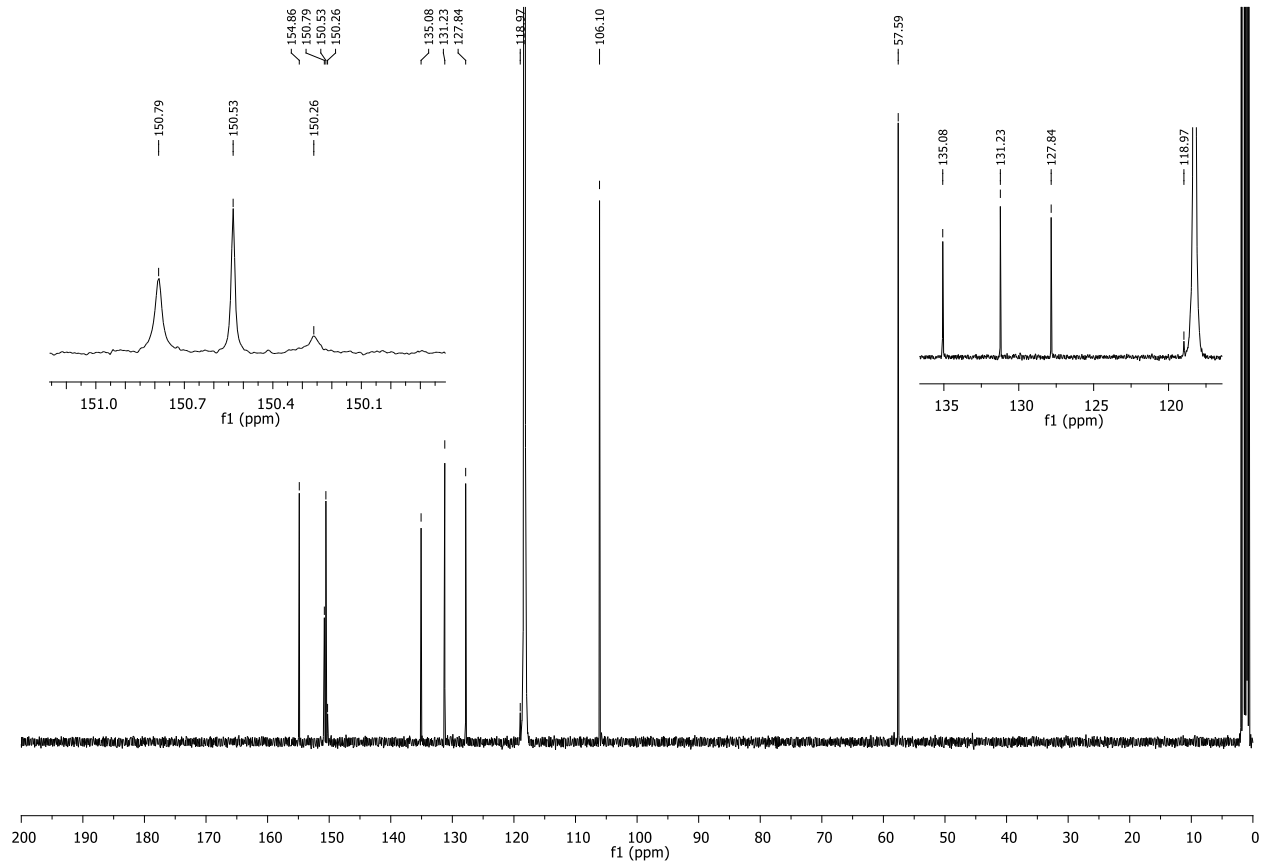
Compound 189a: ^{13}C NMR (75 MHz, CDCl_3)



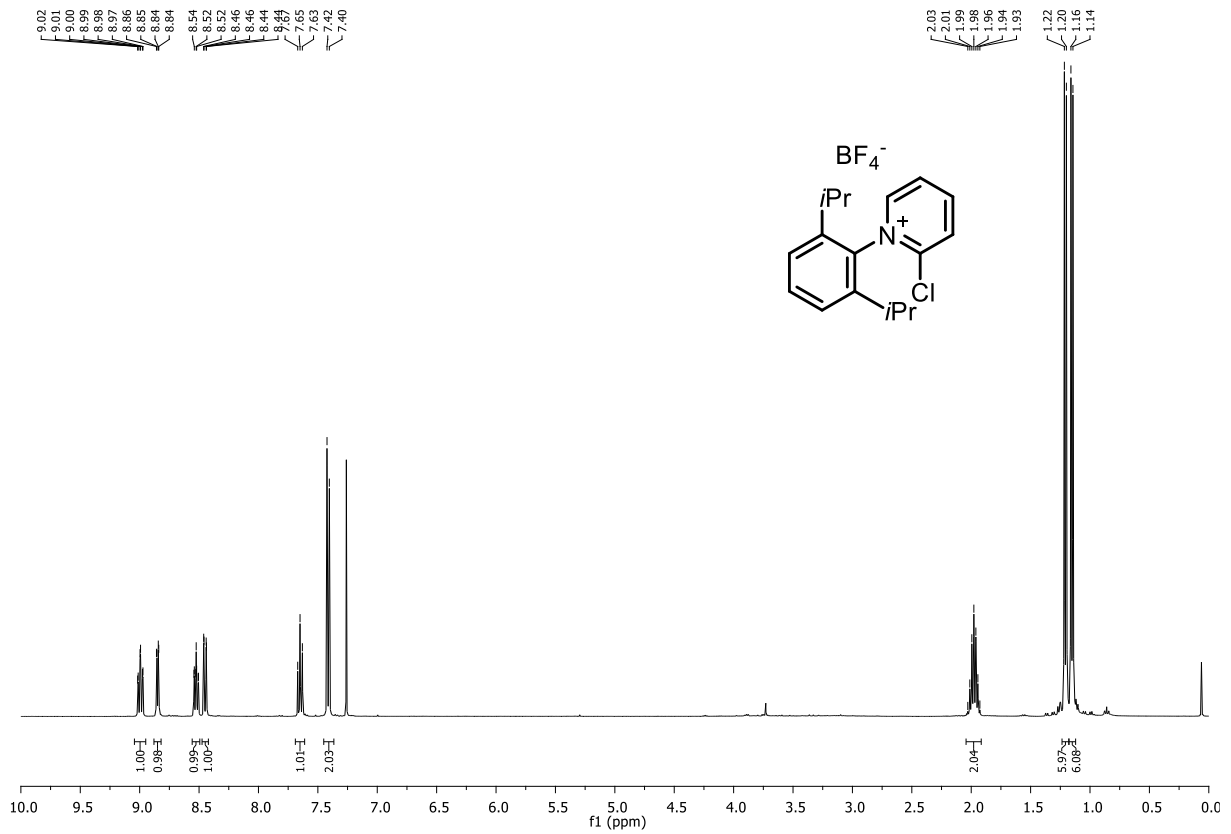
Compound 189b: ^1H NMR (300 MHz, CDCl_3)



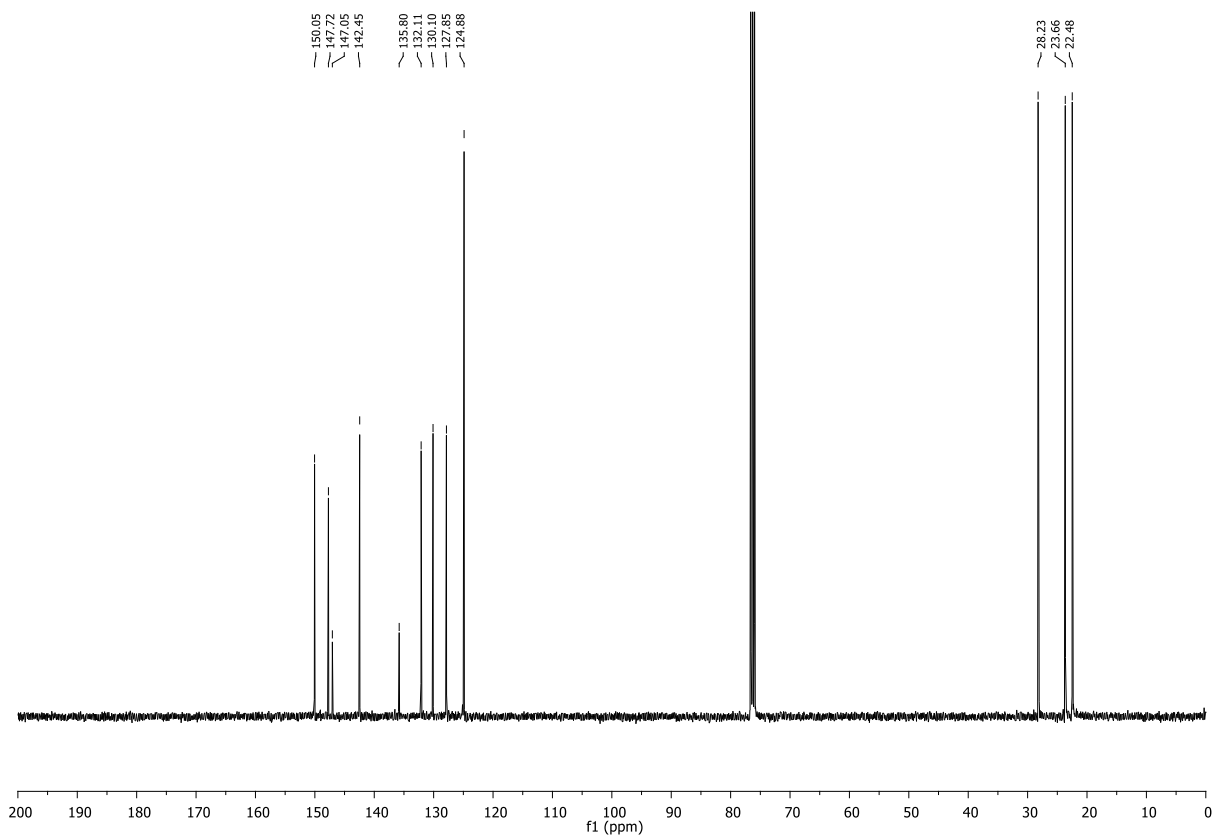
Compound 189b: ^{13}C NMR (75 MHz, CDCl_3)



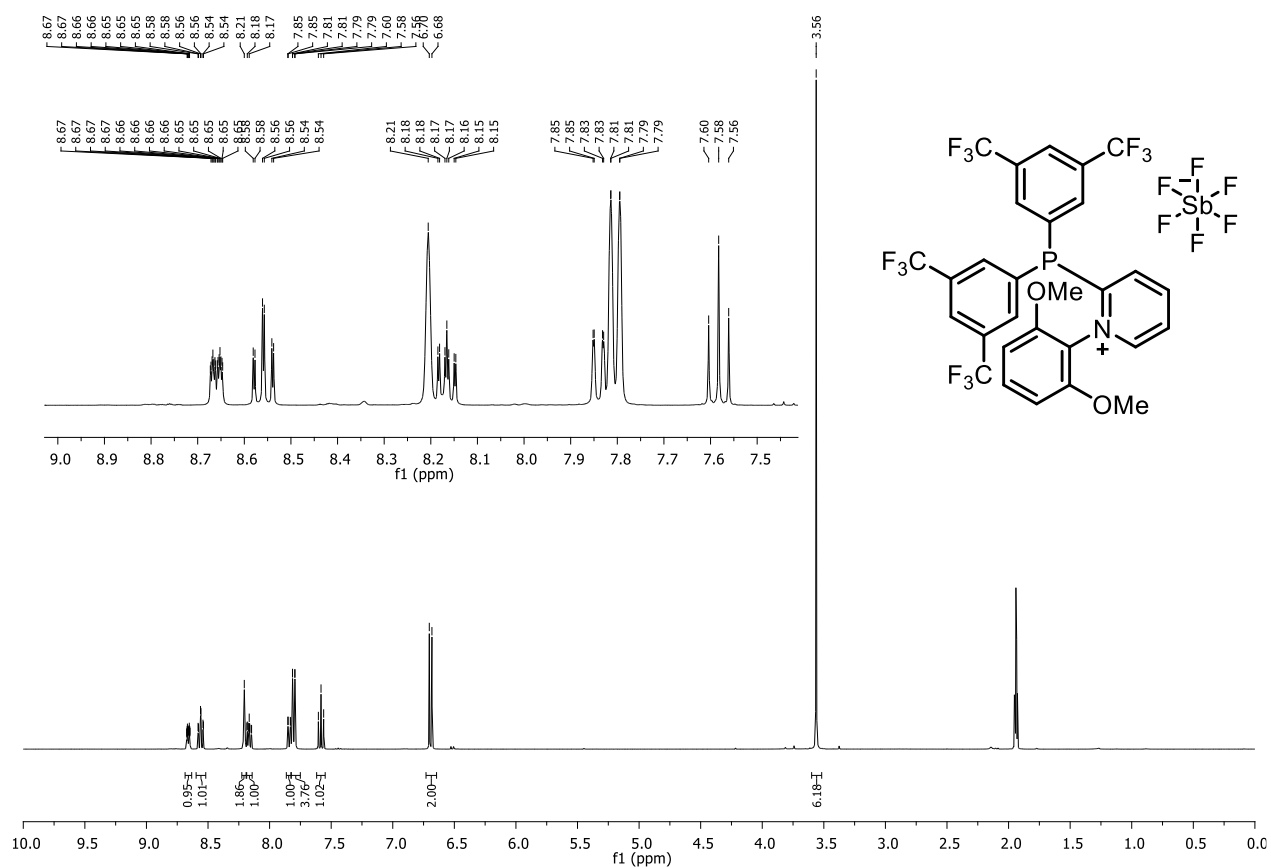
Compound 189c: ^1H NMR (300 MHz, CD_2Cl_2)



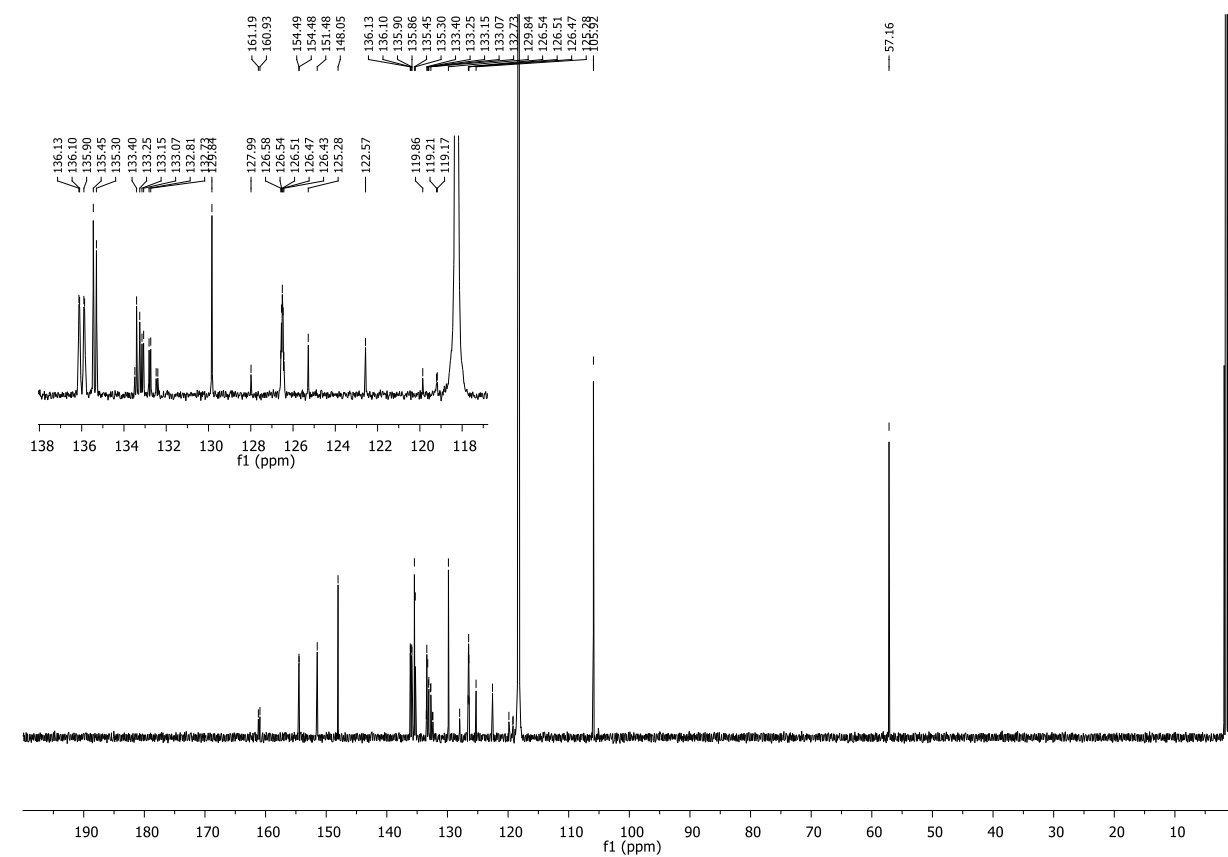
Compound 189c: ^{13}C NMR (75 MHz, CD_2Cl_2)



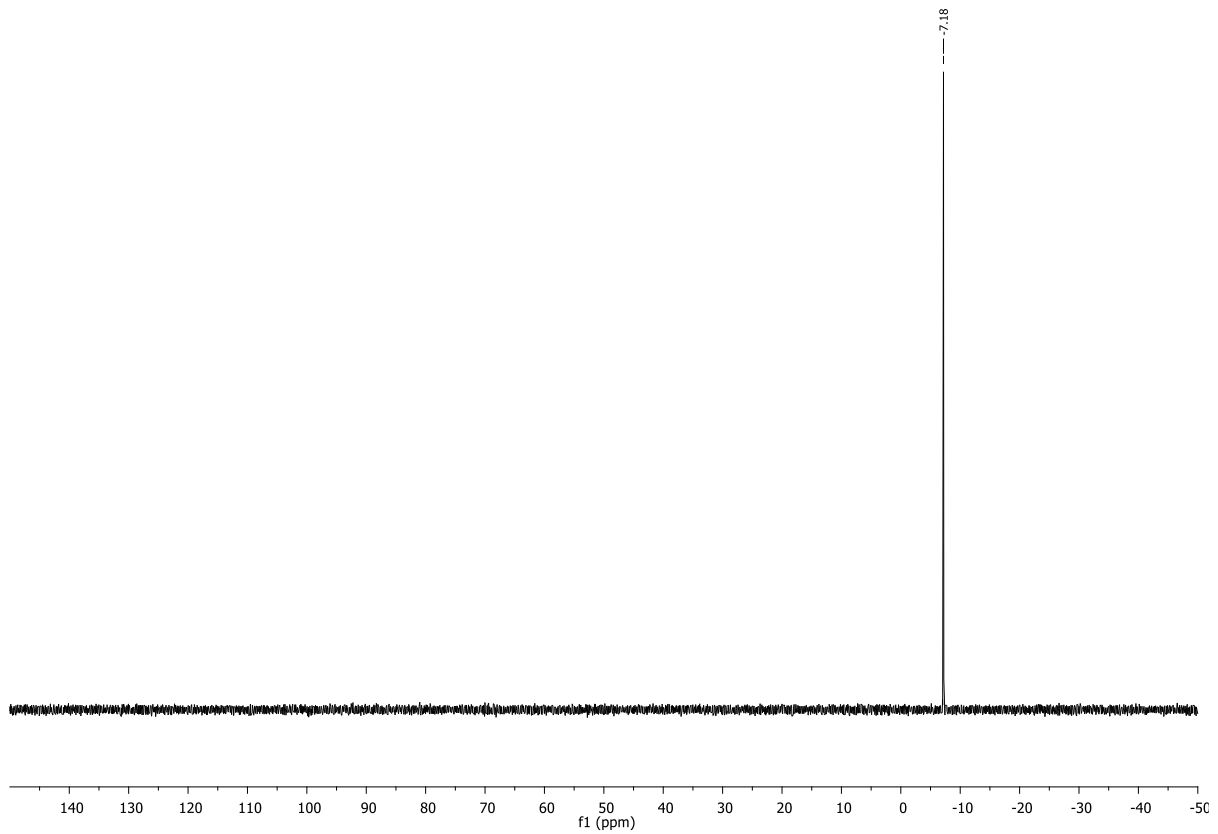
Compound 190a: ^1H NMR (400 MHz, CD_3CN)



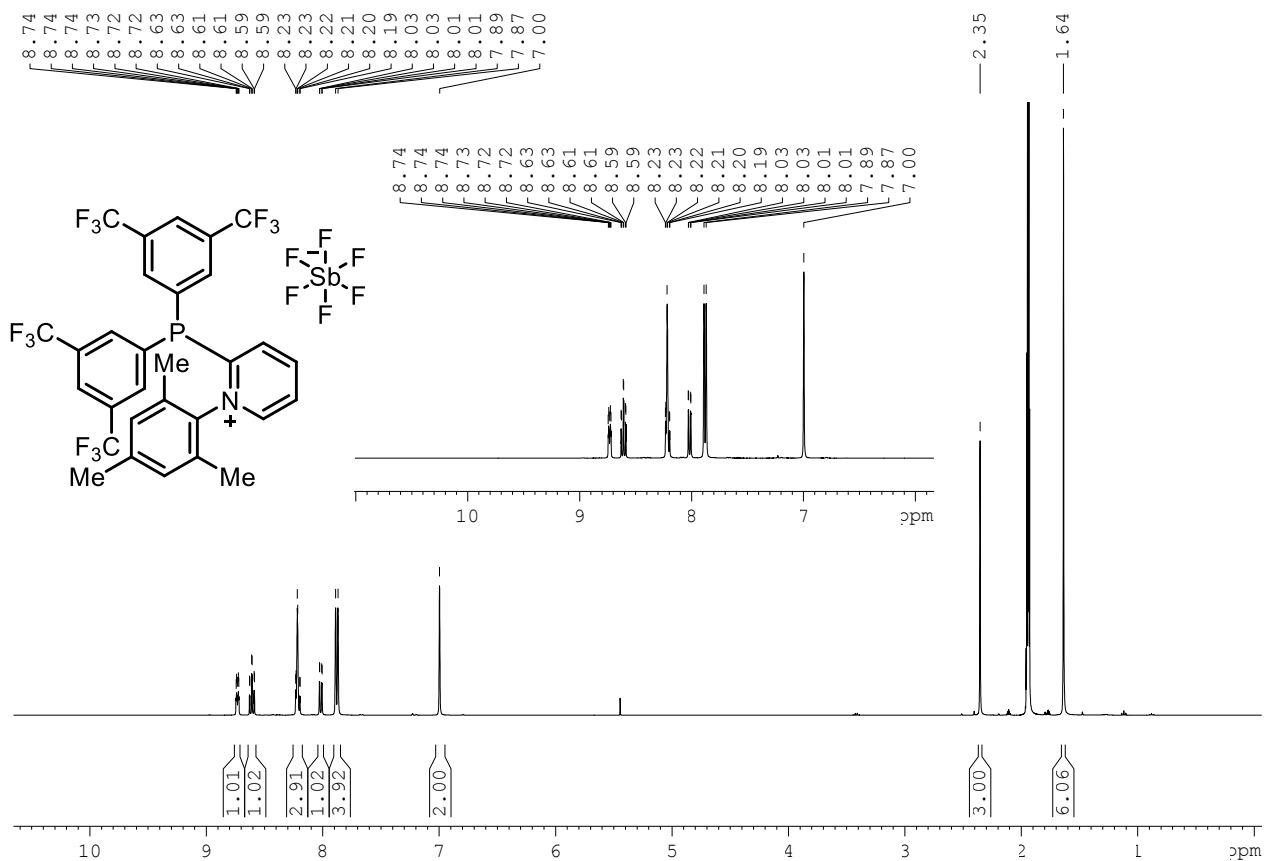
Compound 190a: ^{13}C NMR (101 MHz, CD_3CN)



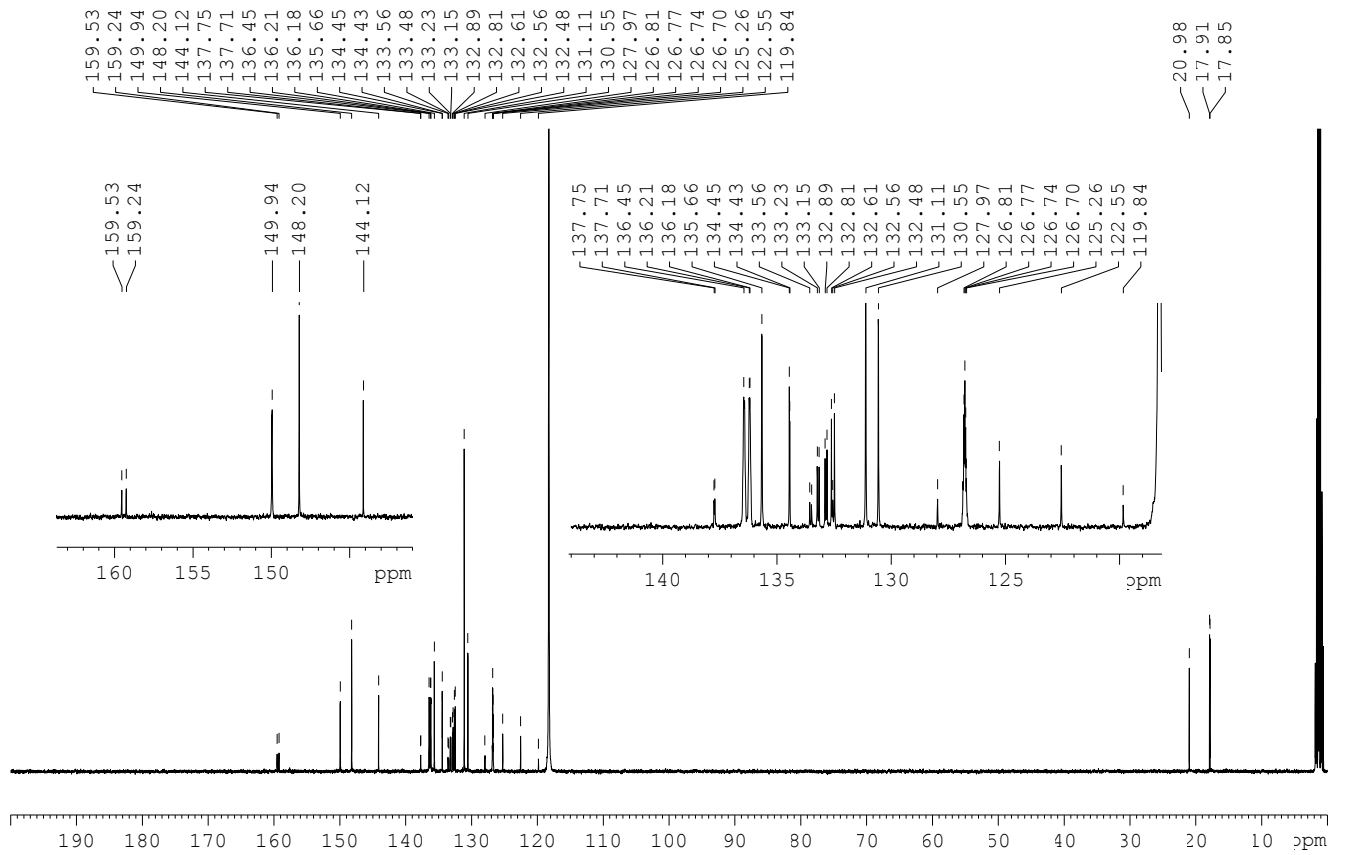
Compound 190a: ^{31}P NMR (121 MHz, CD_3CN_2)



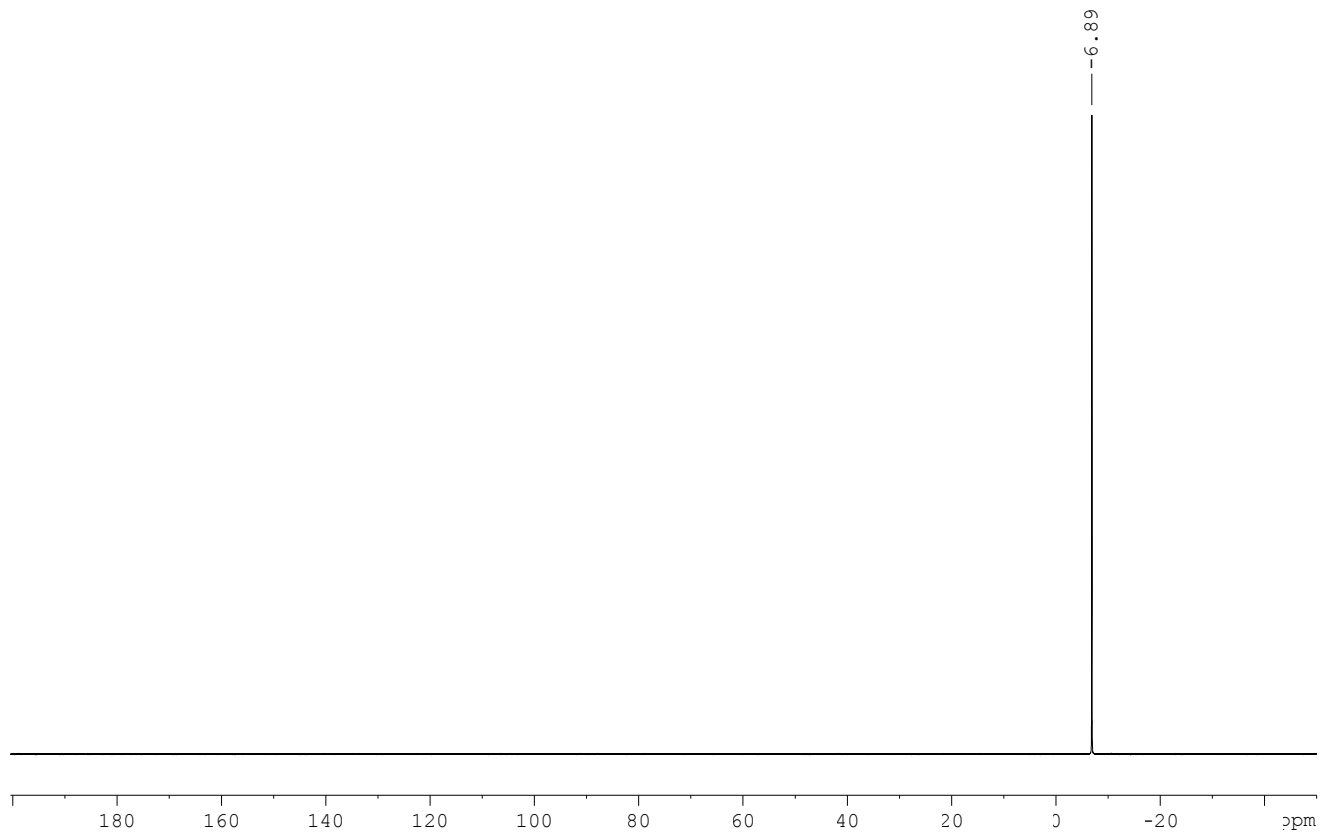
Compound 190b: ^1H NMR (400 MHz, CD_3CN)



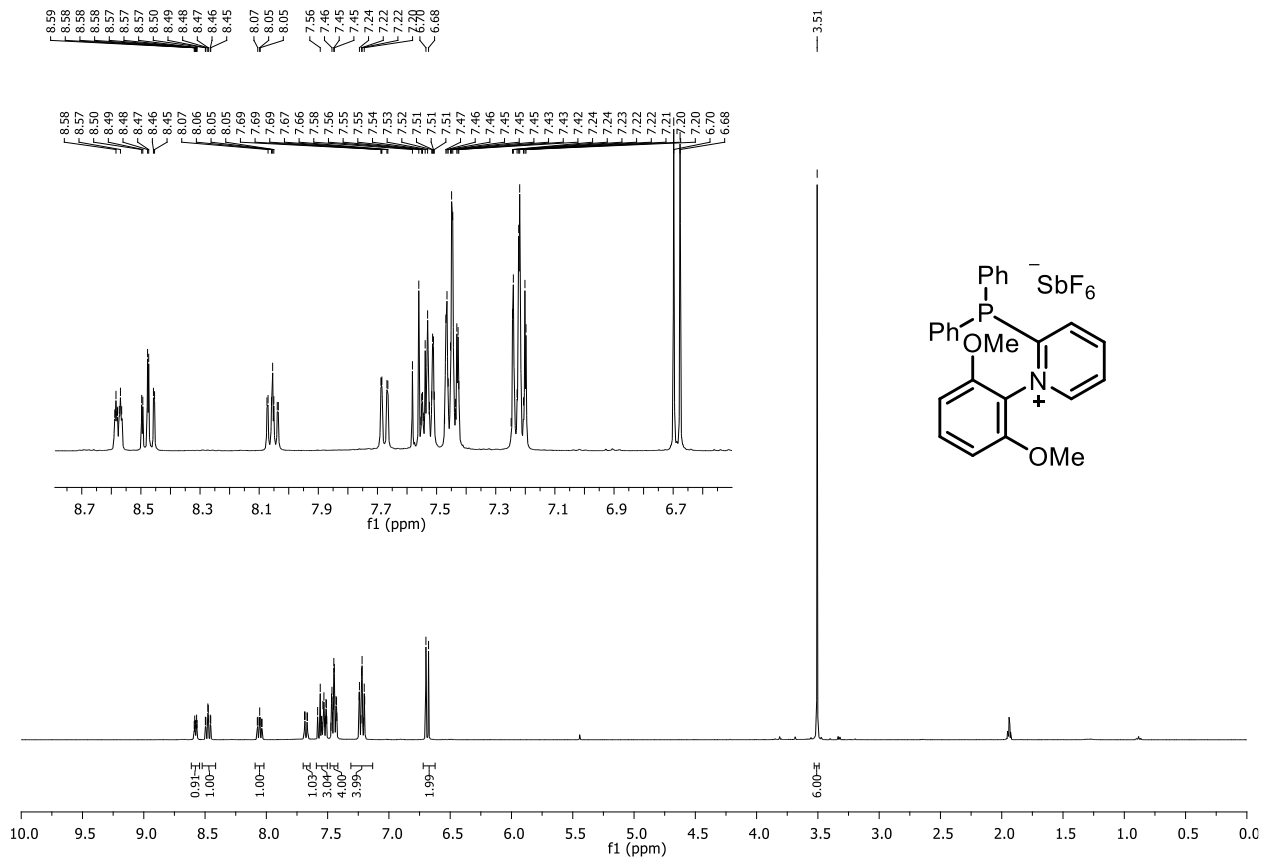
Compound 190b: ^{13}C NMR (101 MHz, CD_3CN)



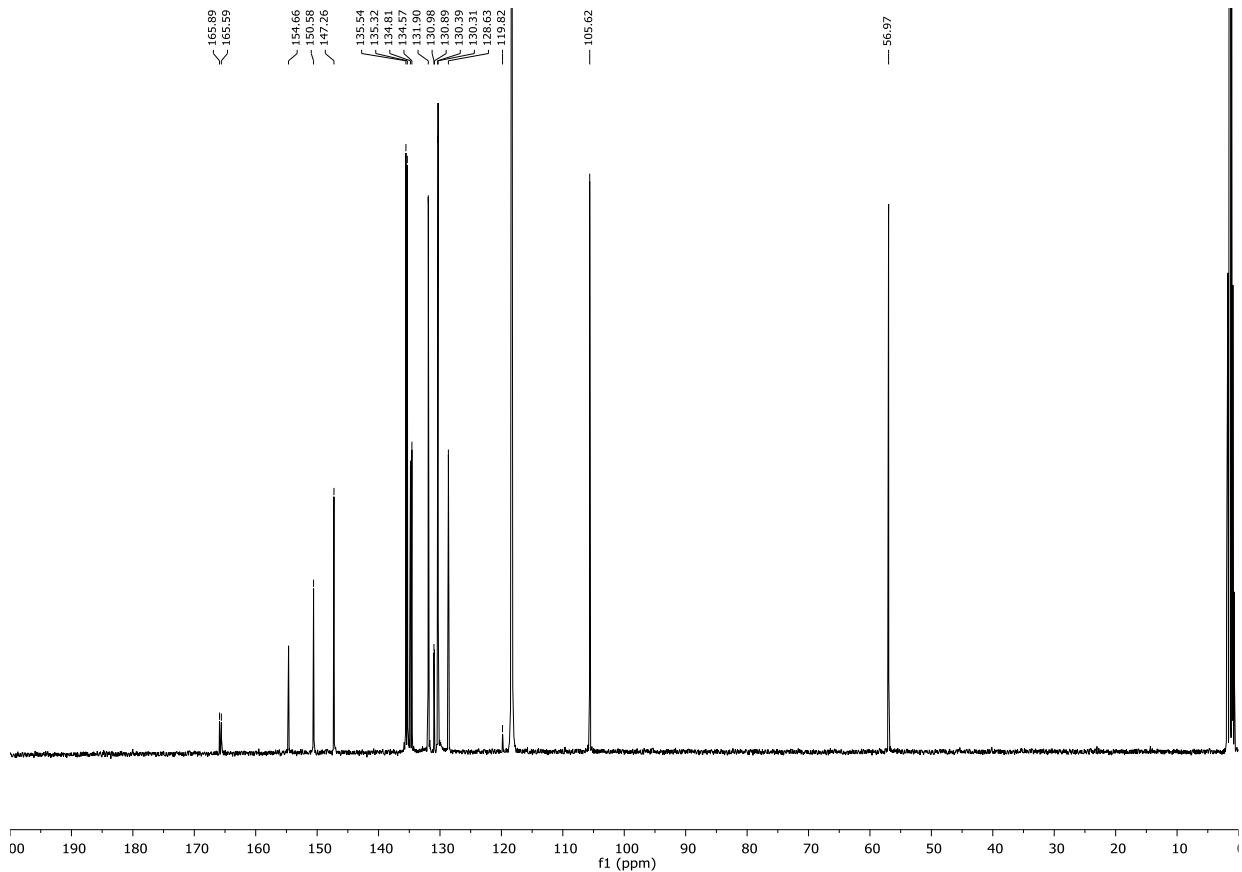
Compound 190b: ^{31}P NMR (121 MHz, CD_3CN_2)



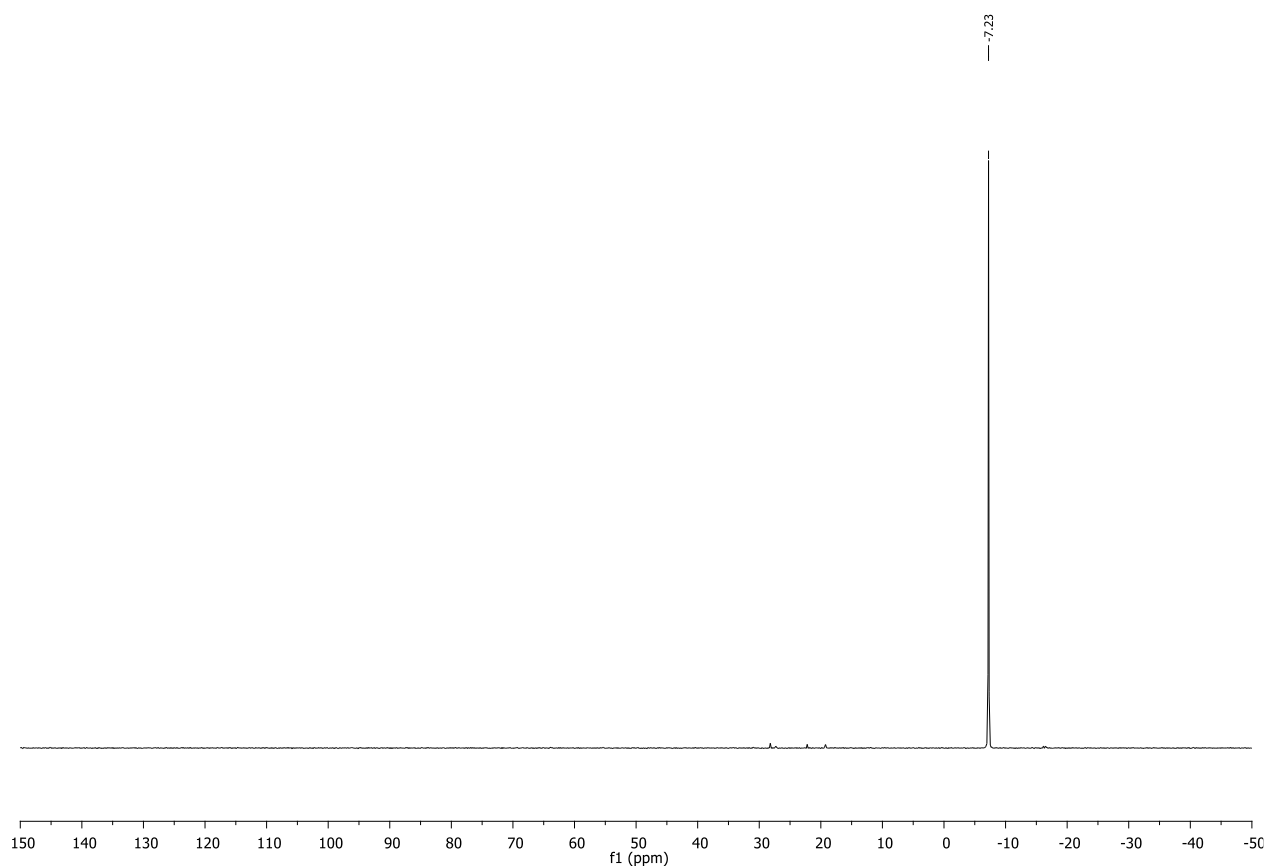
Compound 190c: ^1H NMR (400 MHz, CD_3CN)



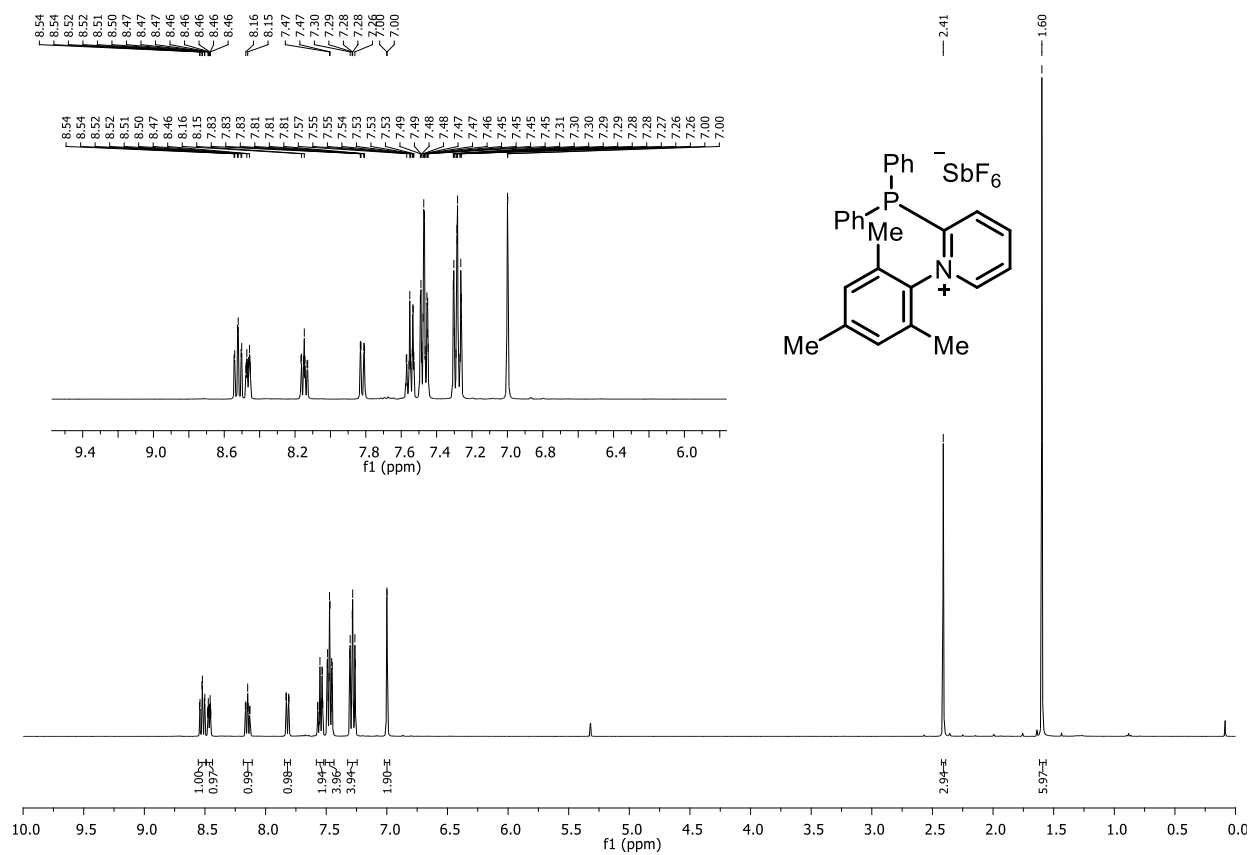
Compound 190c: ^{13}C NMR (101 MHz, CD_3CN)



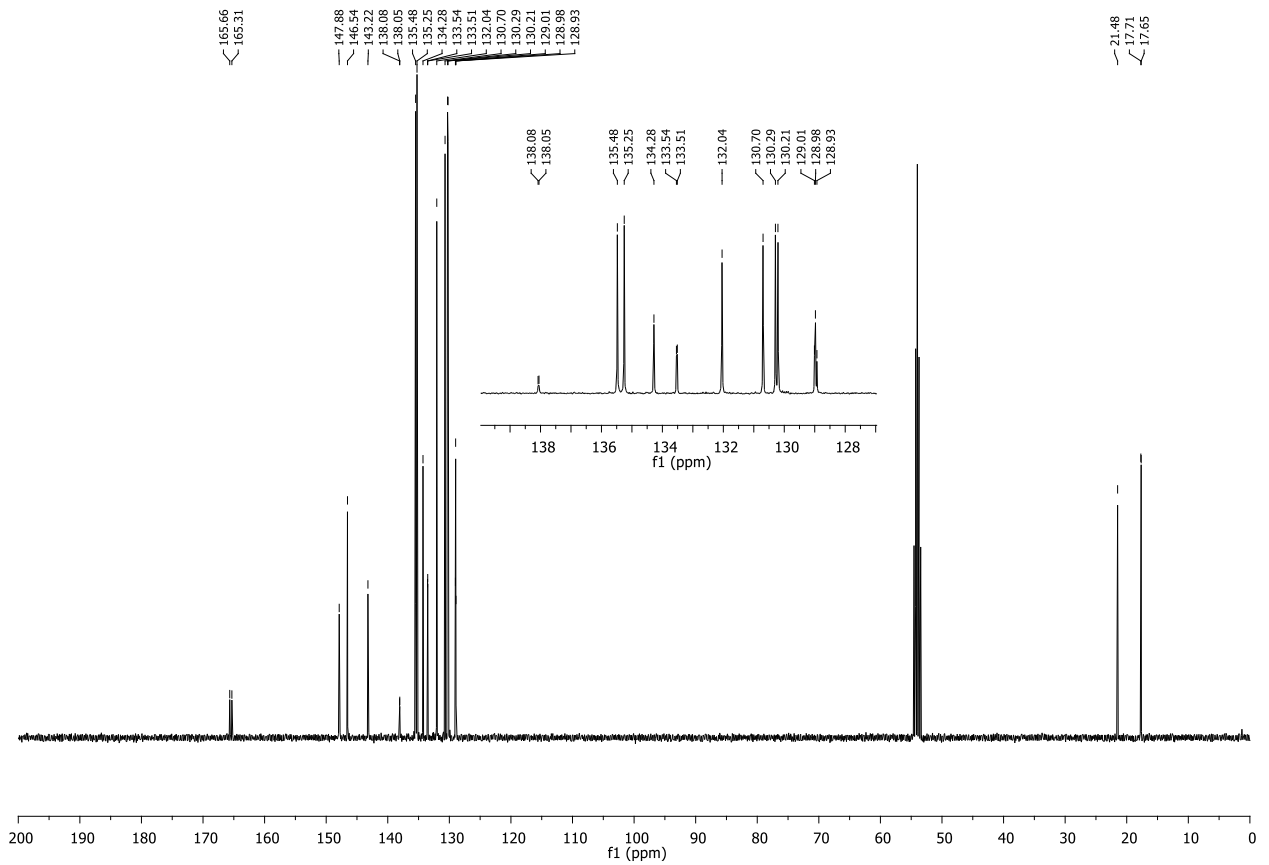
Compound 190c: ^{31}P NMR (121 MHz, CD_3CN)



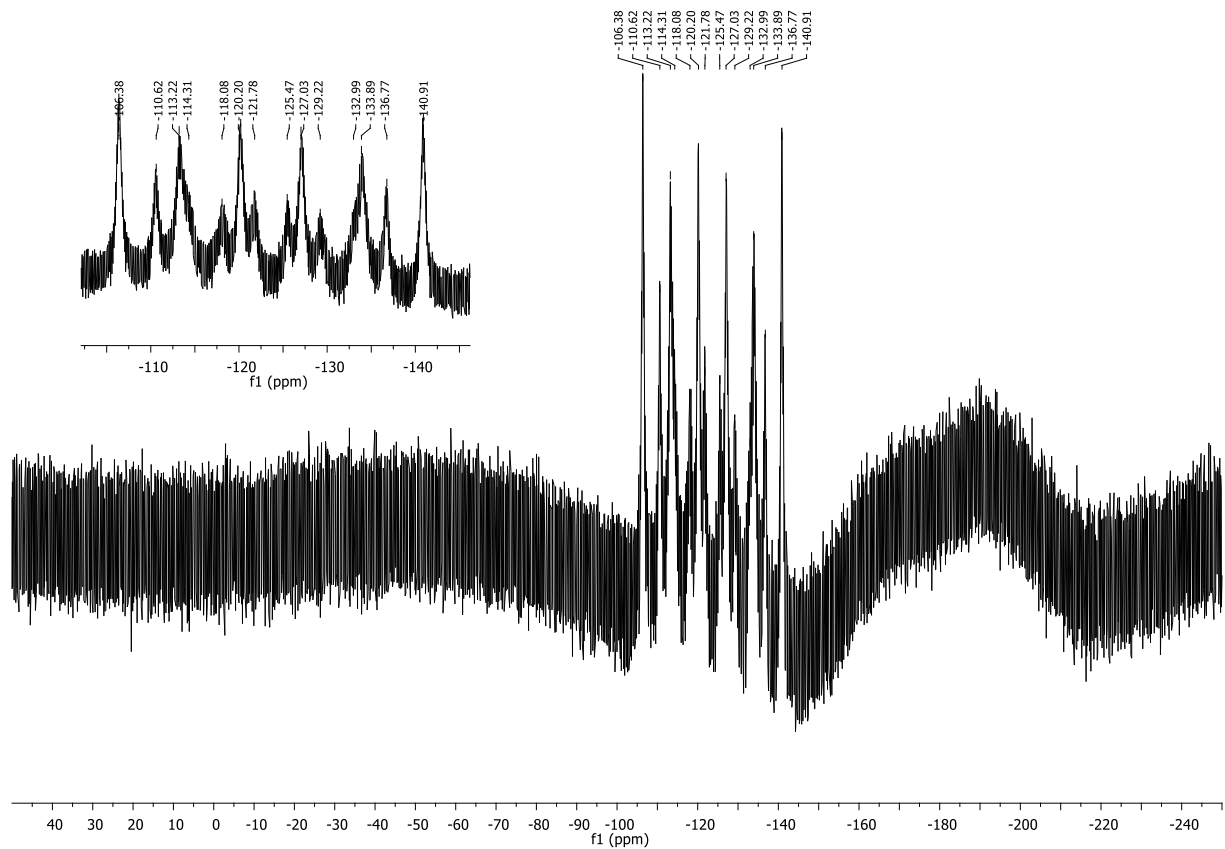
Compound 190d: ^1H NMR (400 MHz, CD_2Cl_2)



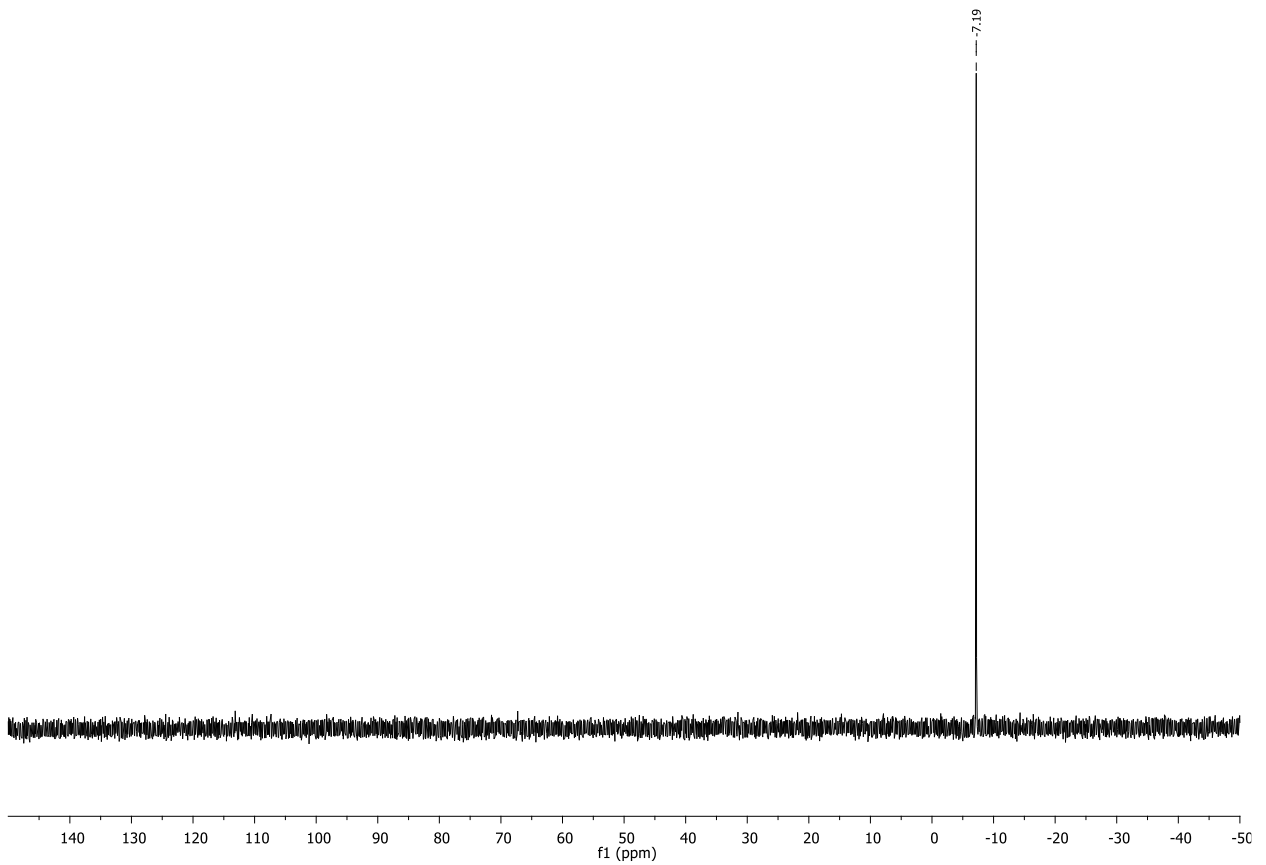
Compound 190d: ^{13}C NMR (101 MHz, CD_2Cl_2)



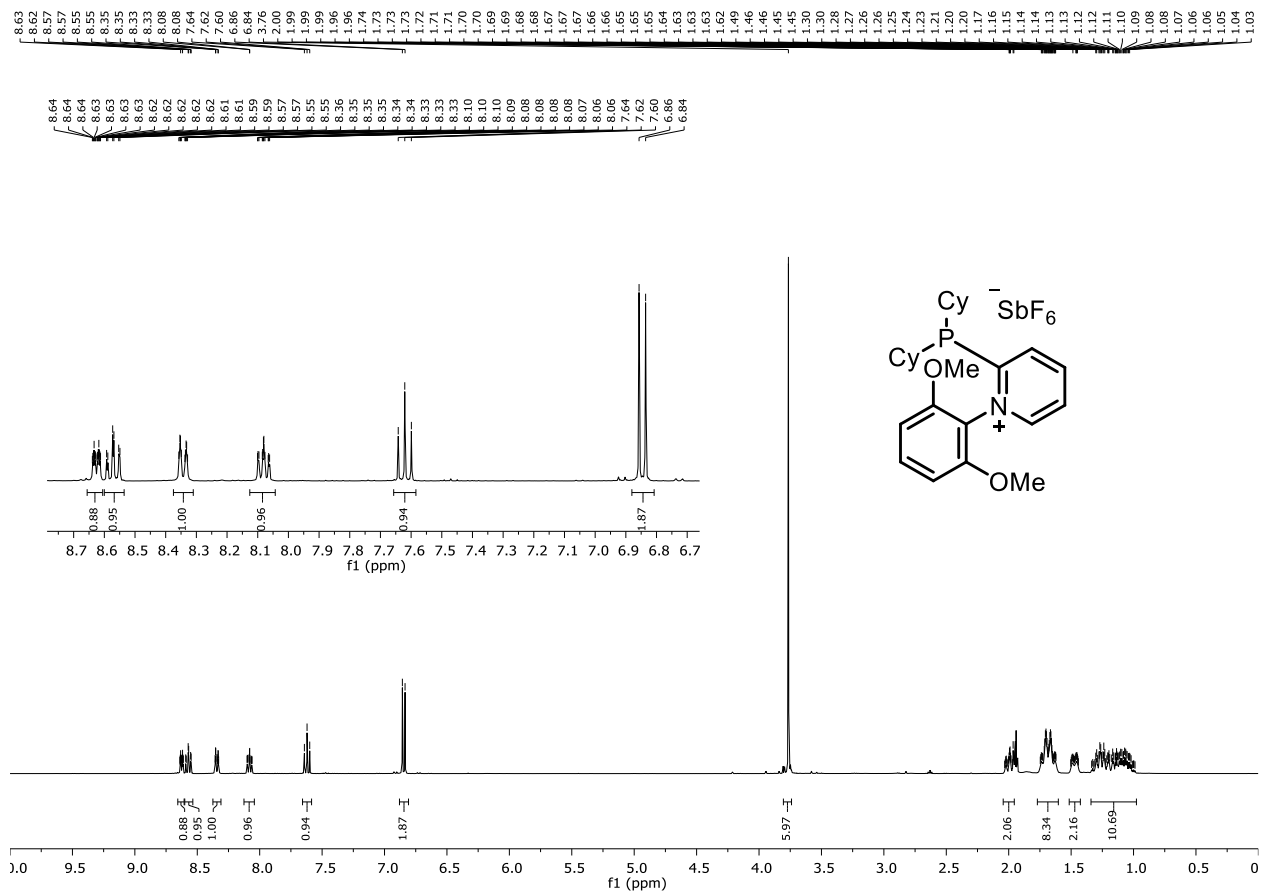
Compound 190d: ^{19}F NMR (282 MHz, CD_2Cl_2)



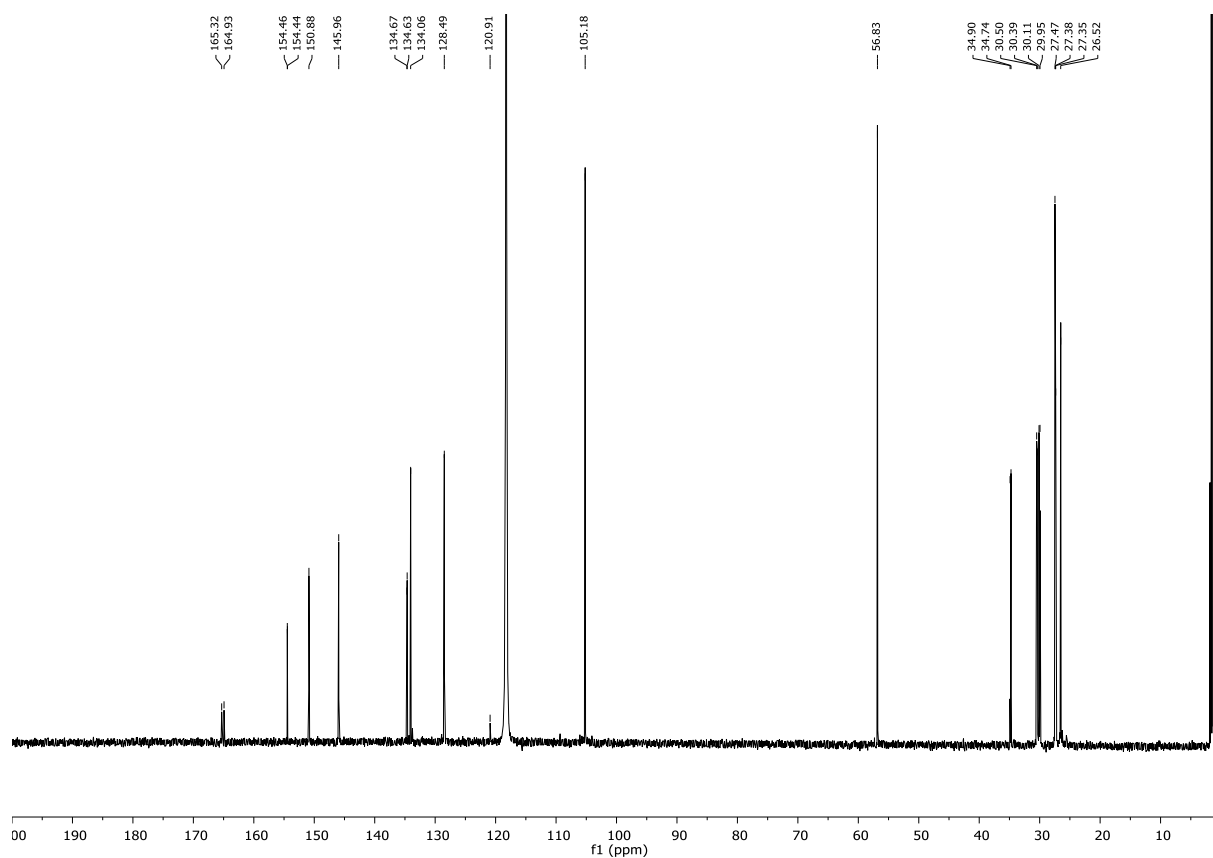
Compound 190d: ^{31}P NMR (121 MHz, CD_2Cl_2)



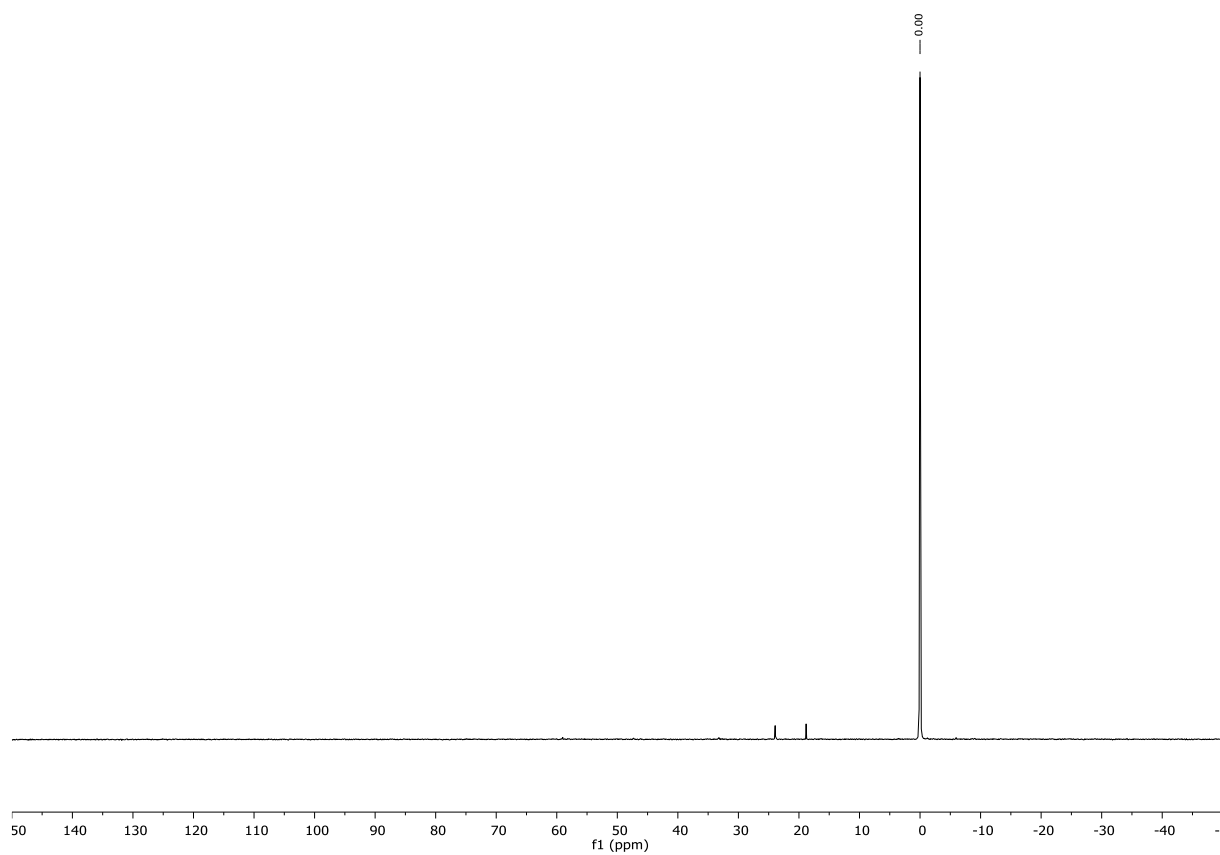
Compound 190e: ^1H NMR (400 MHz, CD_3CN)



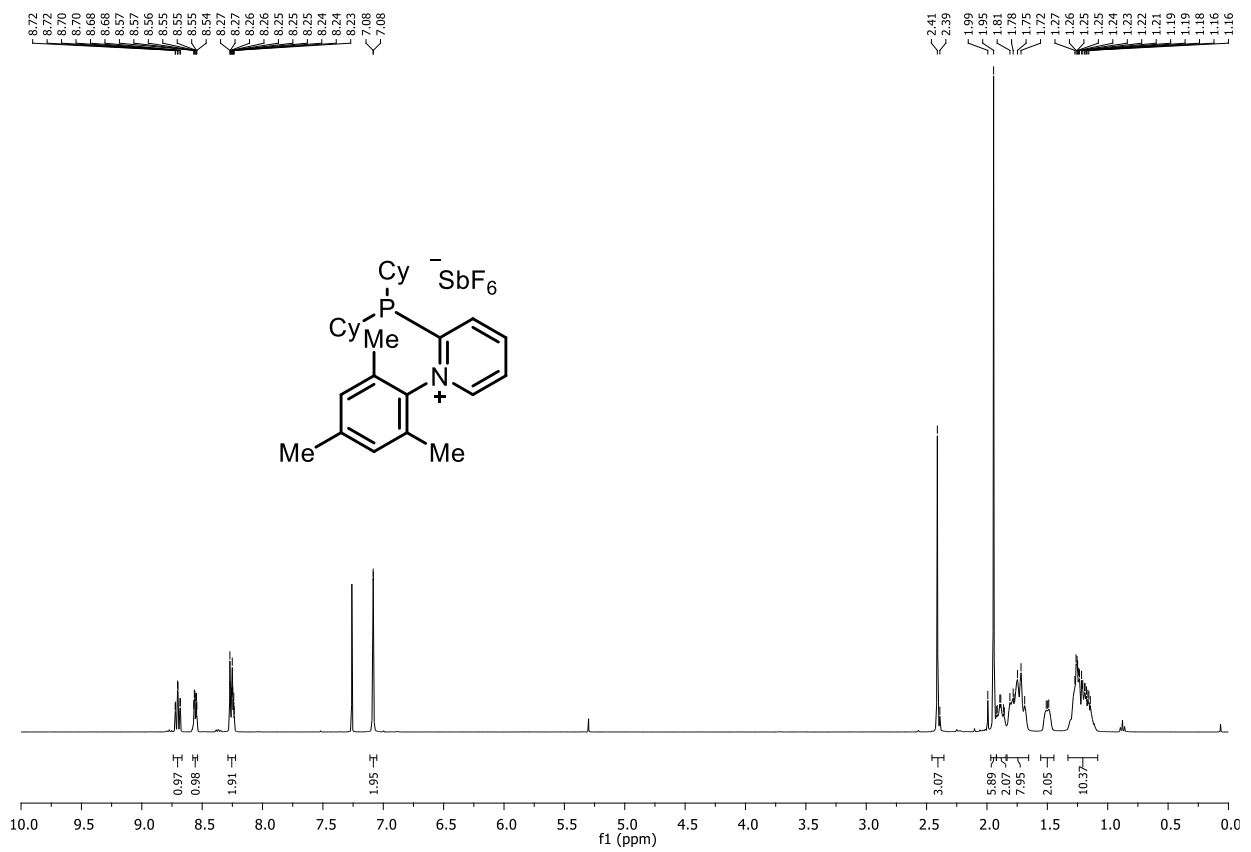
Compound 190e: ^{13}C NMR (101 MHz, CD_3CN)



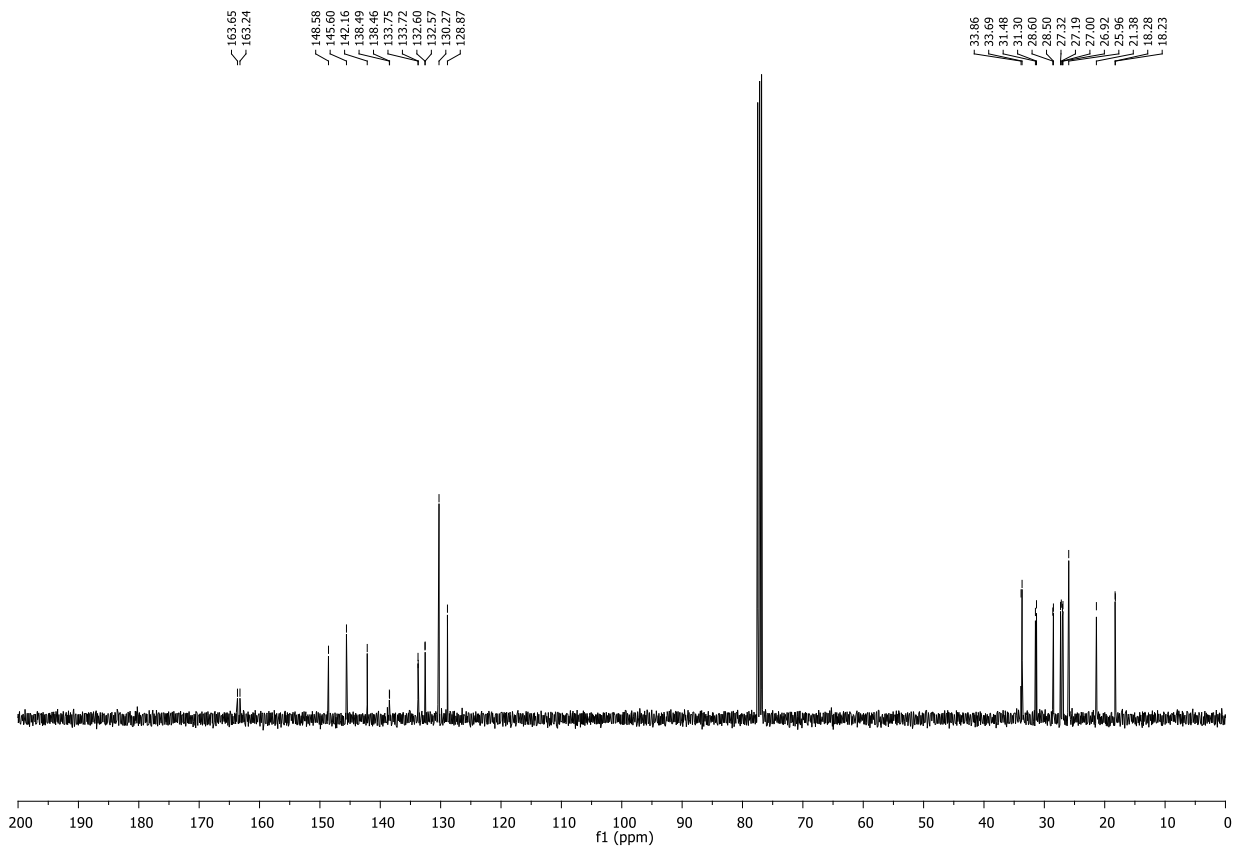
Compound 190e: ^{31}P NMR (121 MHz, CD_3CN)



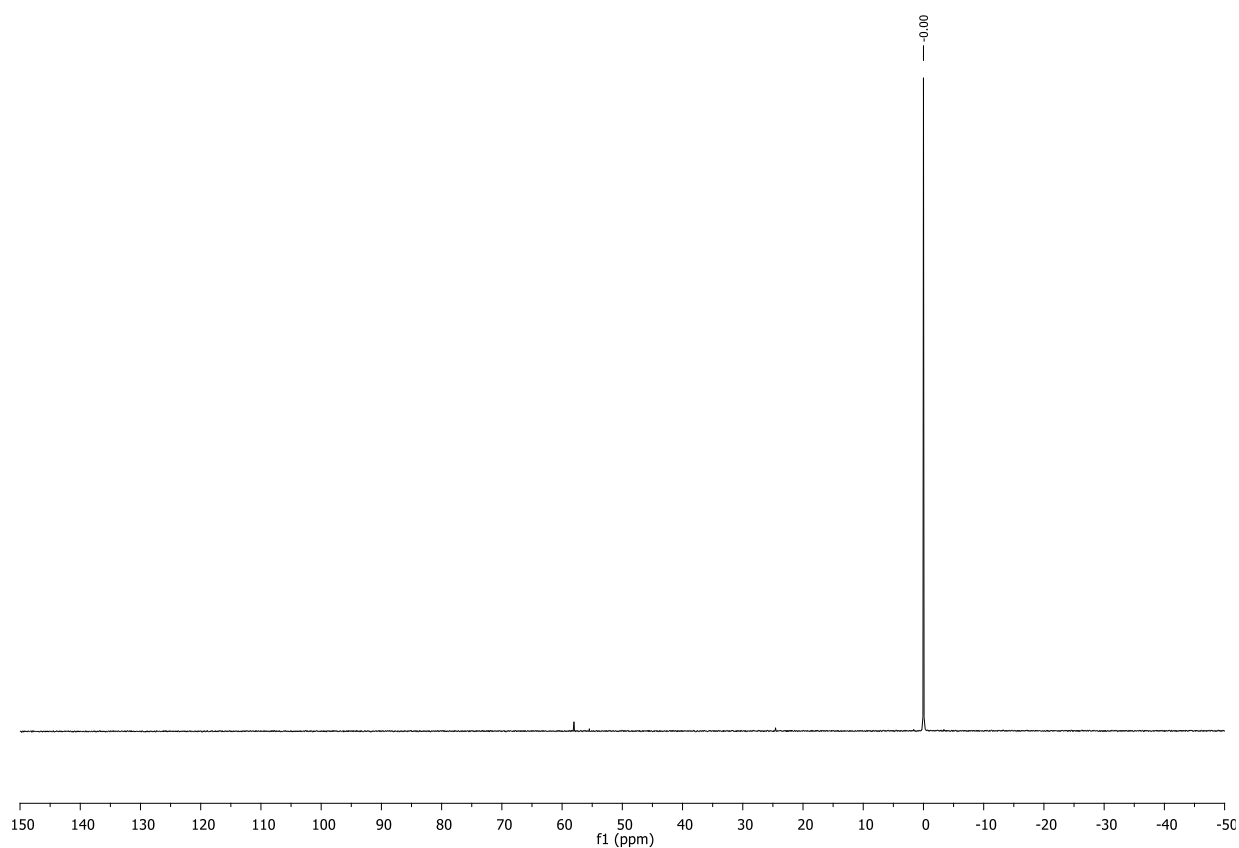
Compound 190f: ^1H NMR (400 MHz, CDCl_3)



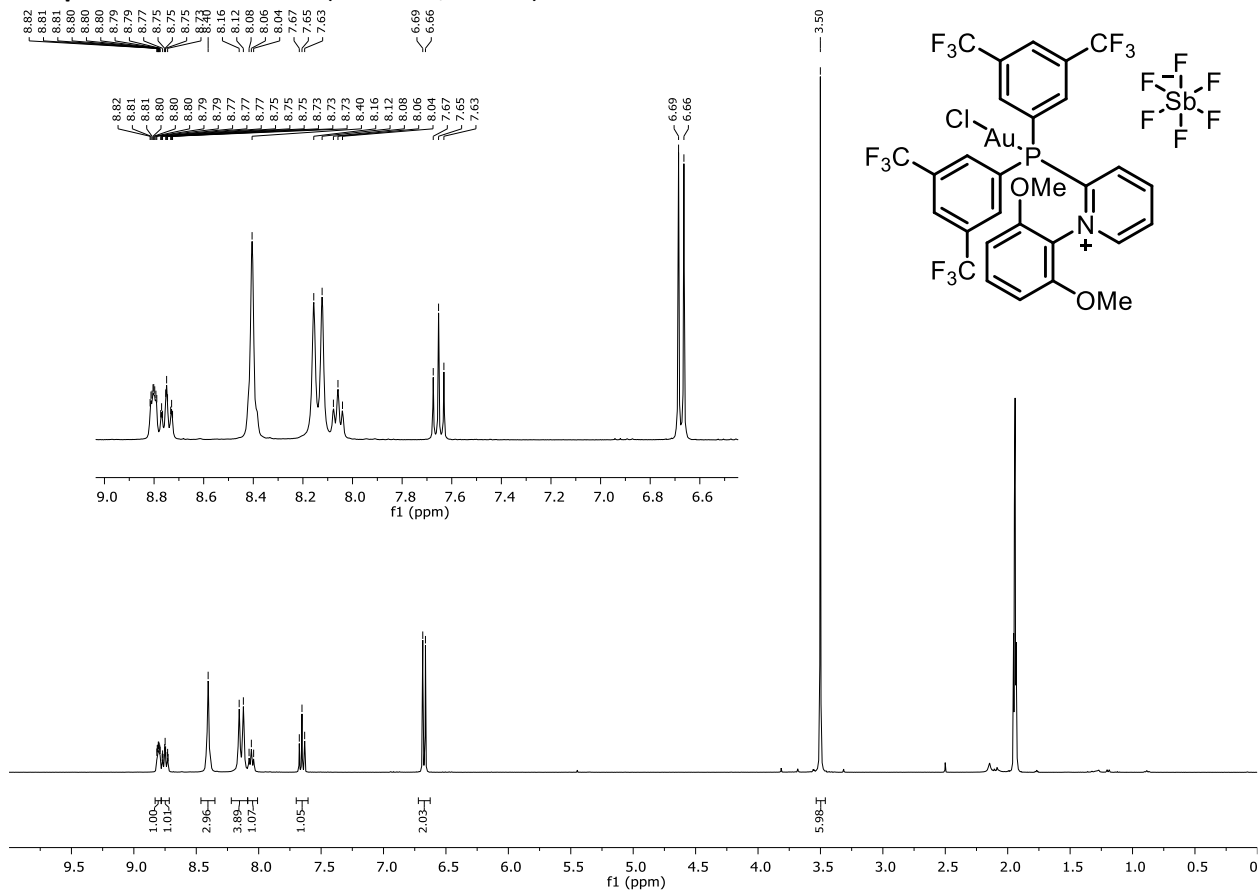
Compound 190f: ^{13}C NMR (101 MHz, CDCl_3)



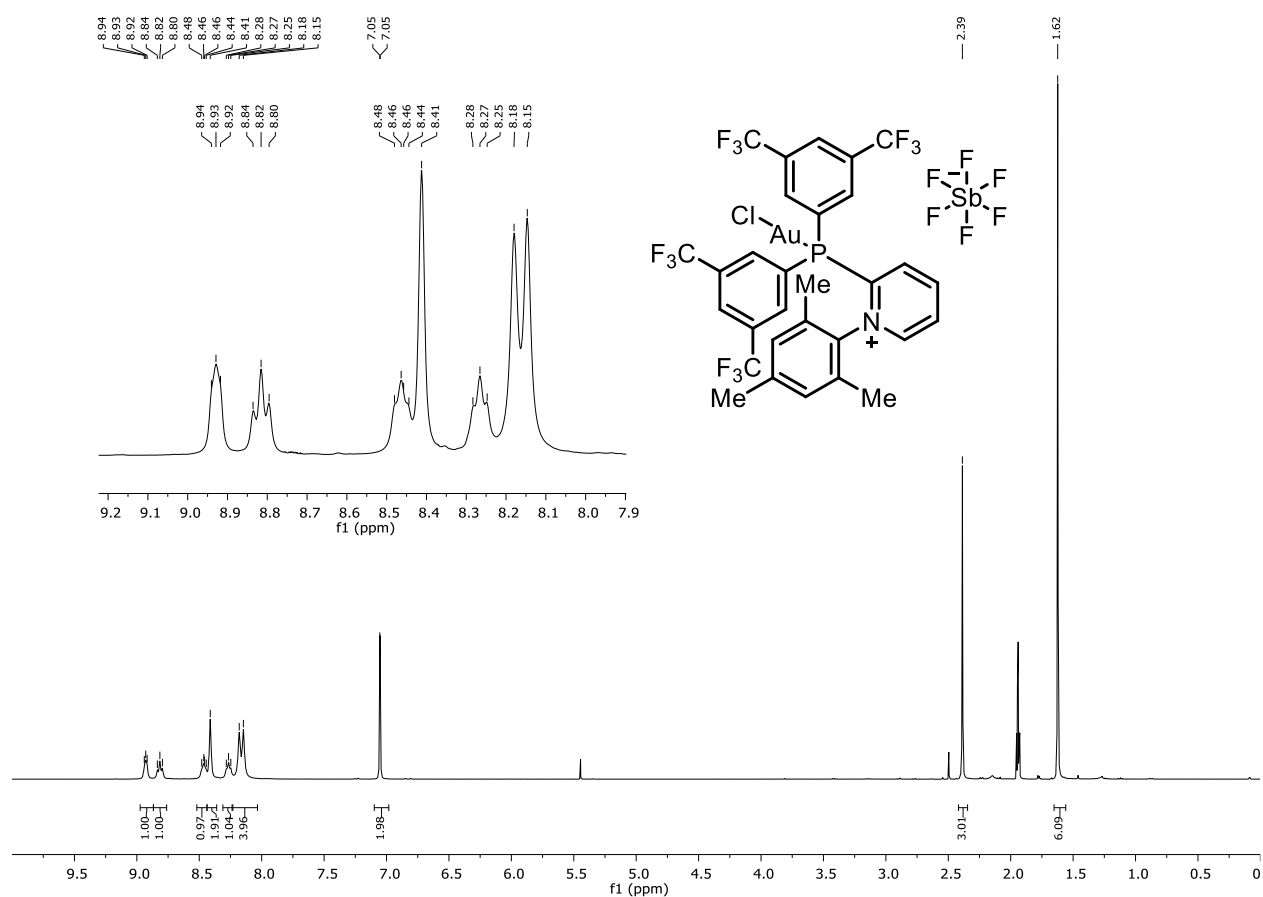
Compound 190f: ^{31}P NMR (121 MHz, CD_3CN)



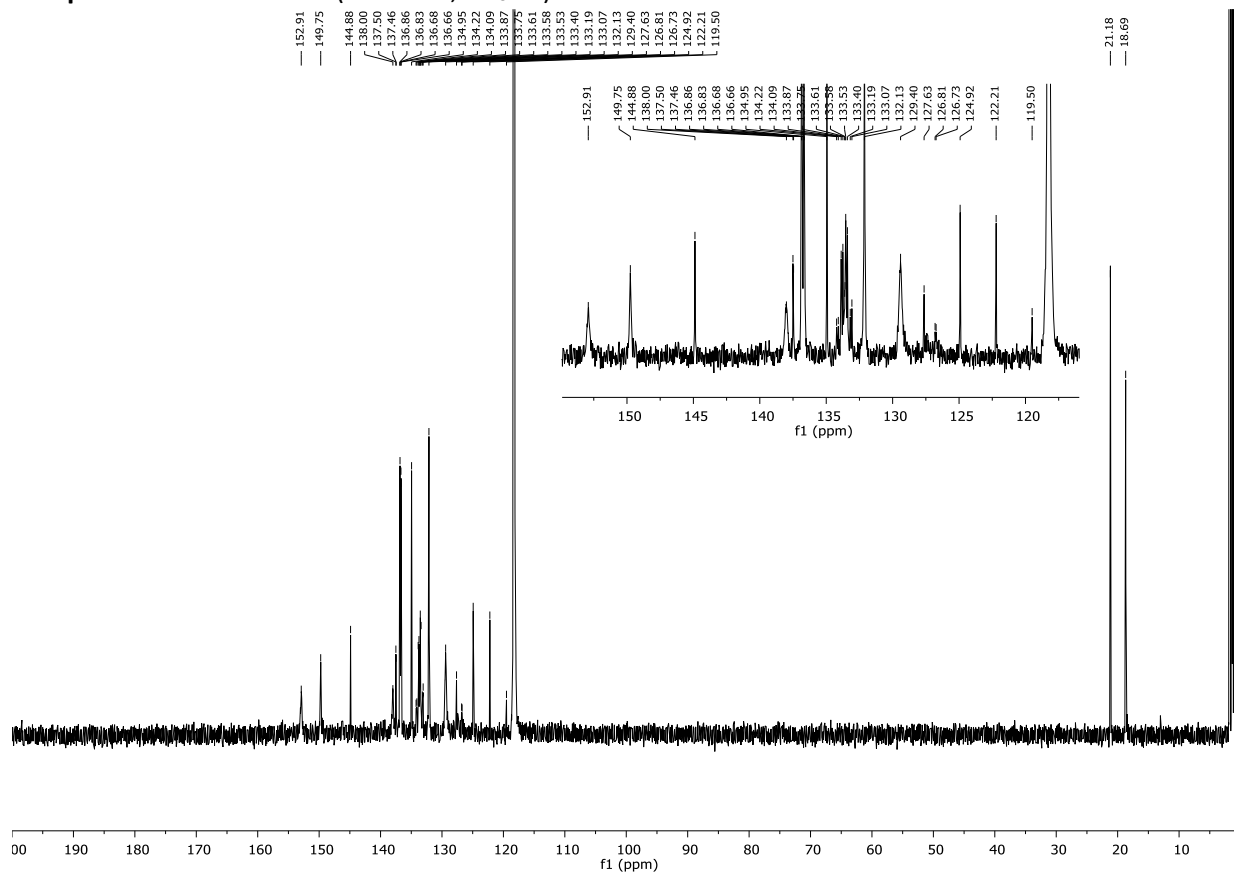
Compound 191a: ^1H NMR (400 MHz, CD_3CN)



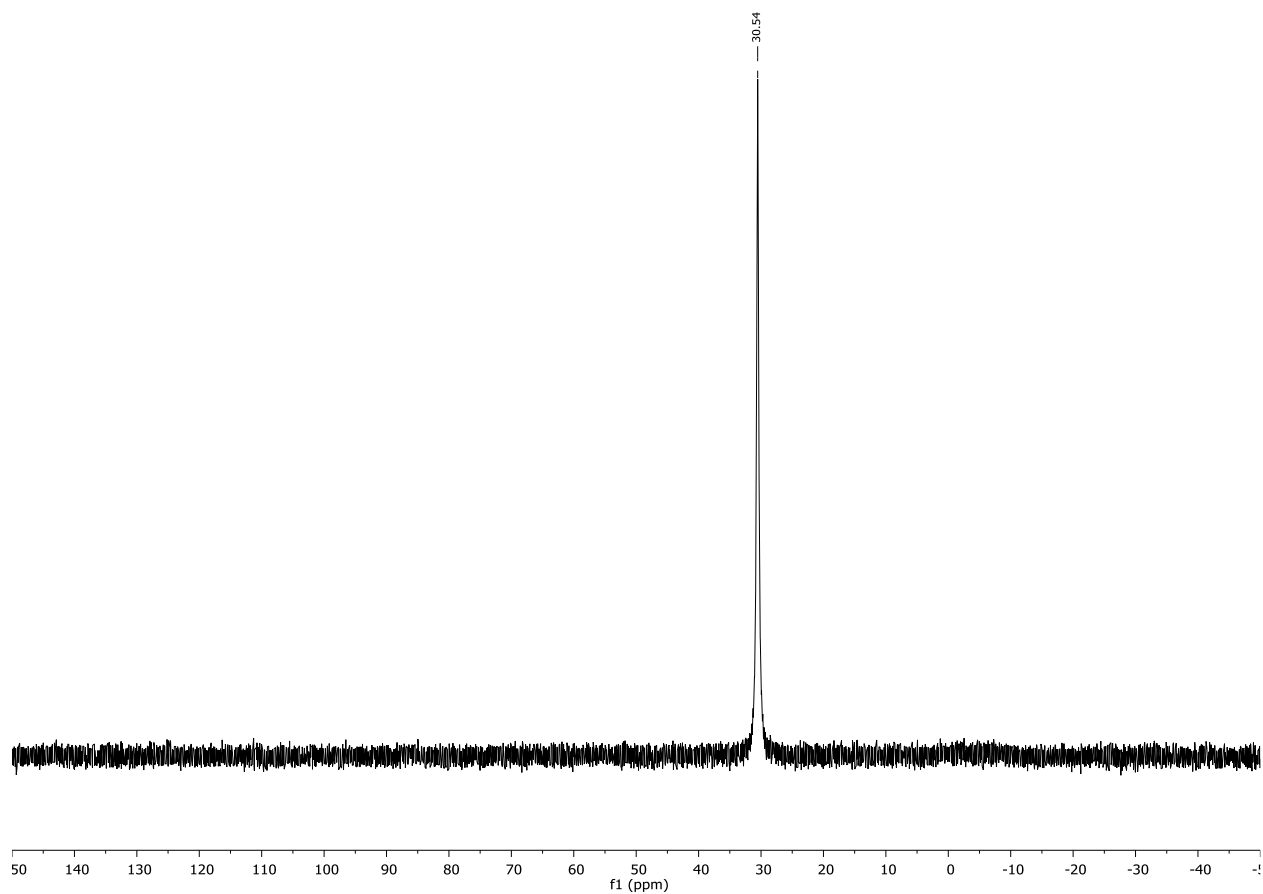
Compound 191b: ^1H NMR (400 MHz, CD_3CN)



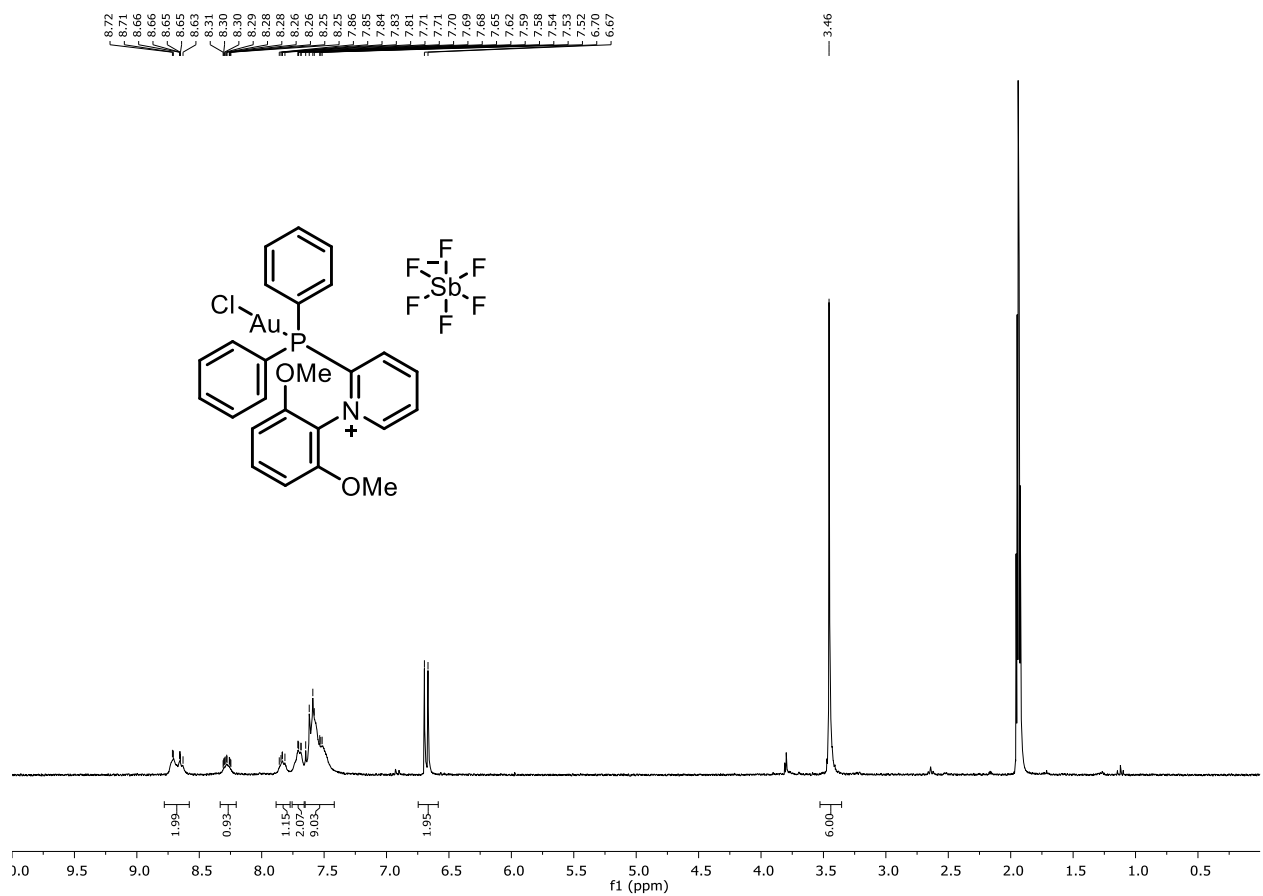
Compound 191b: ^{13}C NMR (101 MHz, CD_3CN)



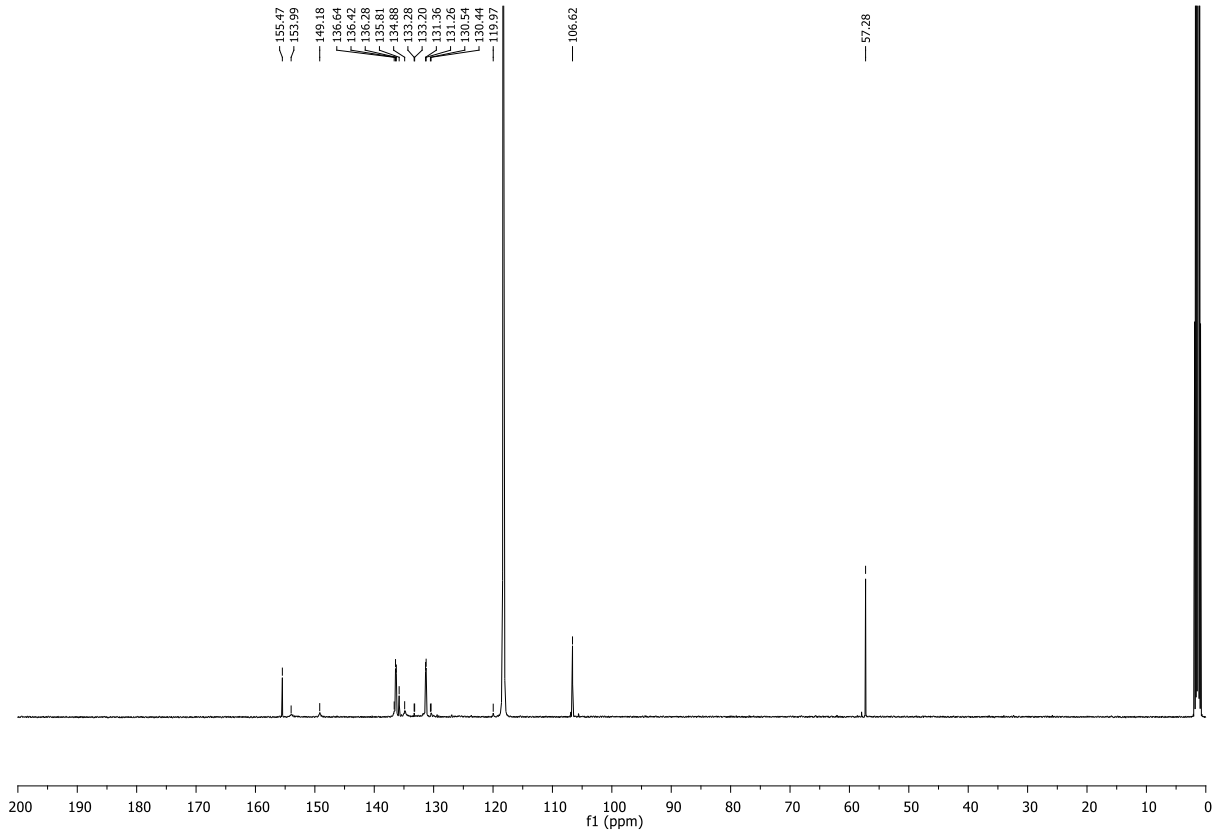
Compound 191b: ^{31}P NMR (121 MHz, CD_3CN)



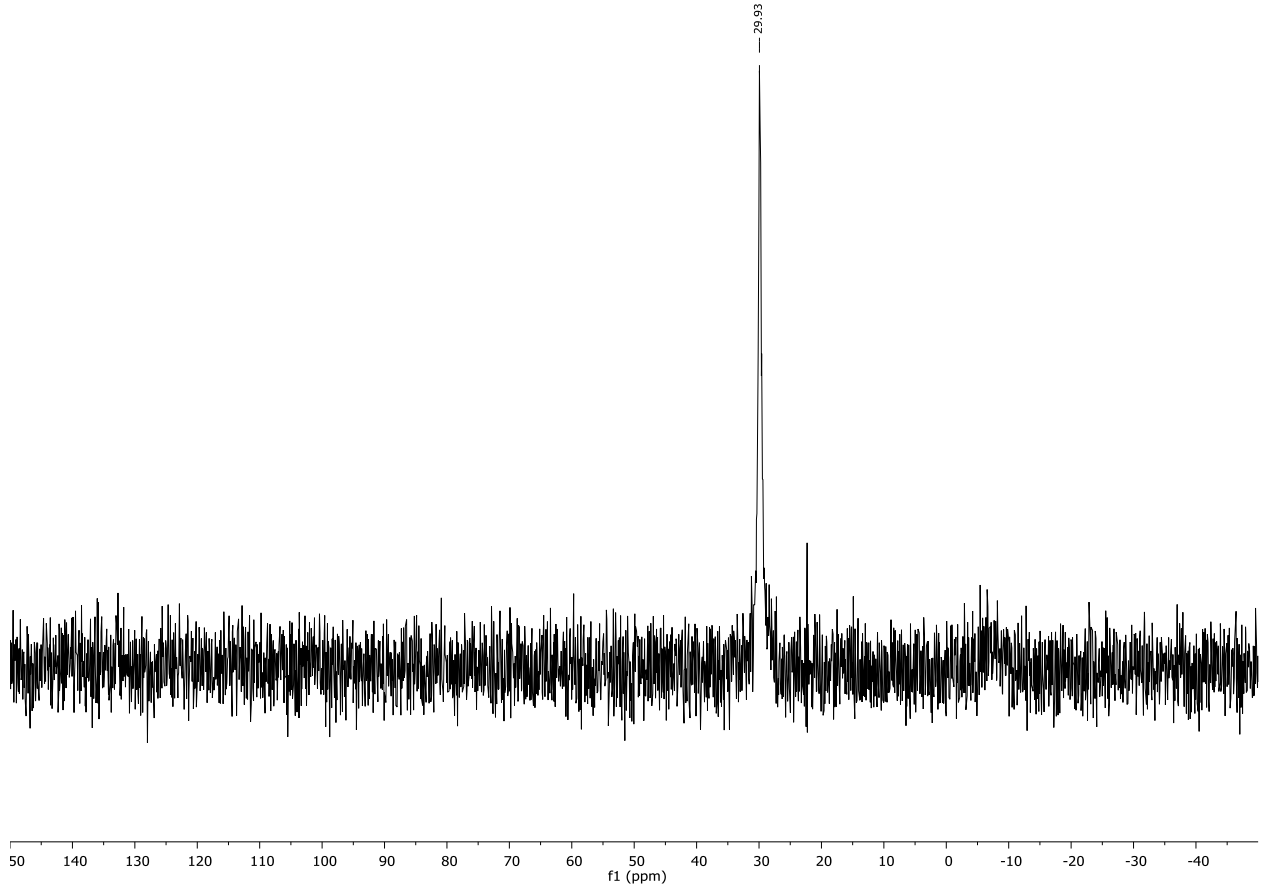
Compound 191c: ¹H NMR (400 MHz, CD₃CN)



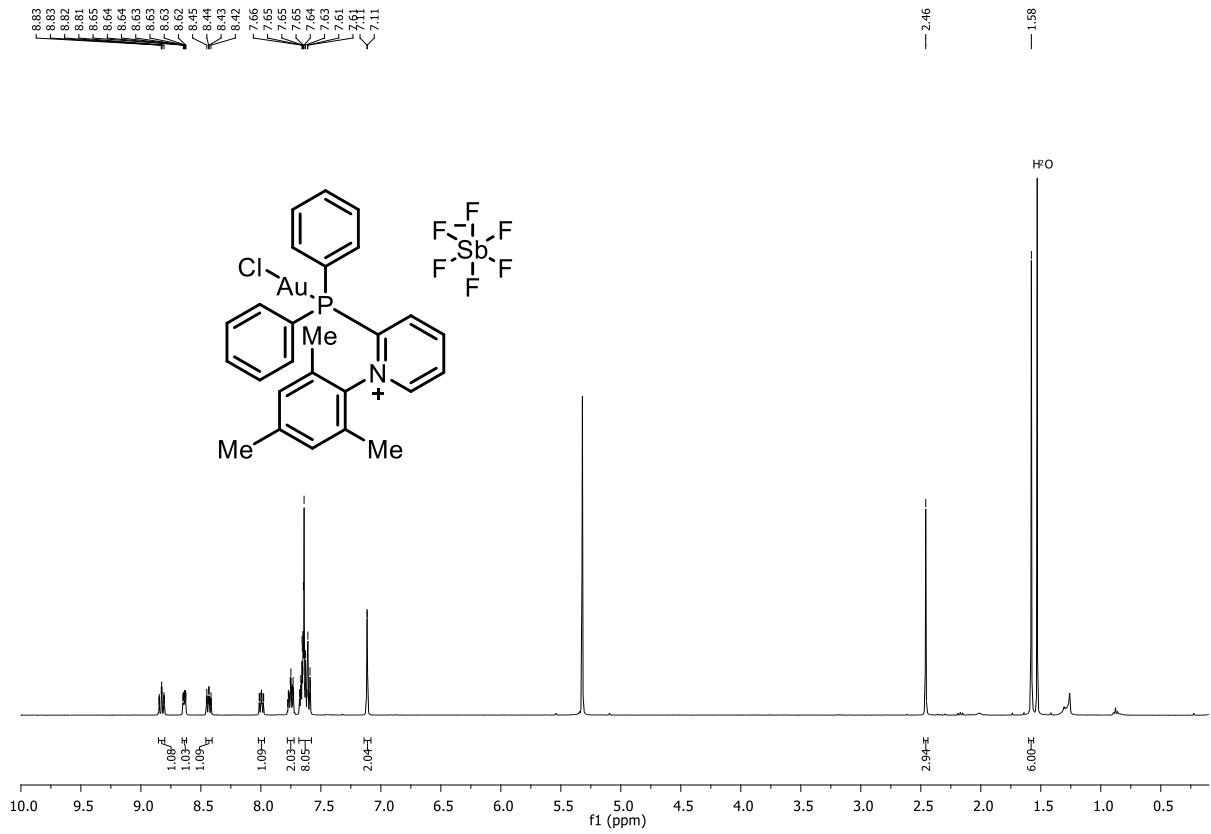
Compound 191c: ^{13}C NMR (101 MHz, CD_3CN)



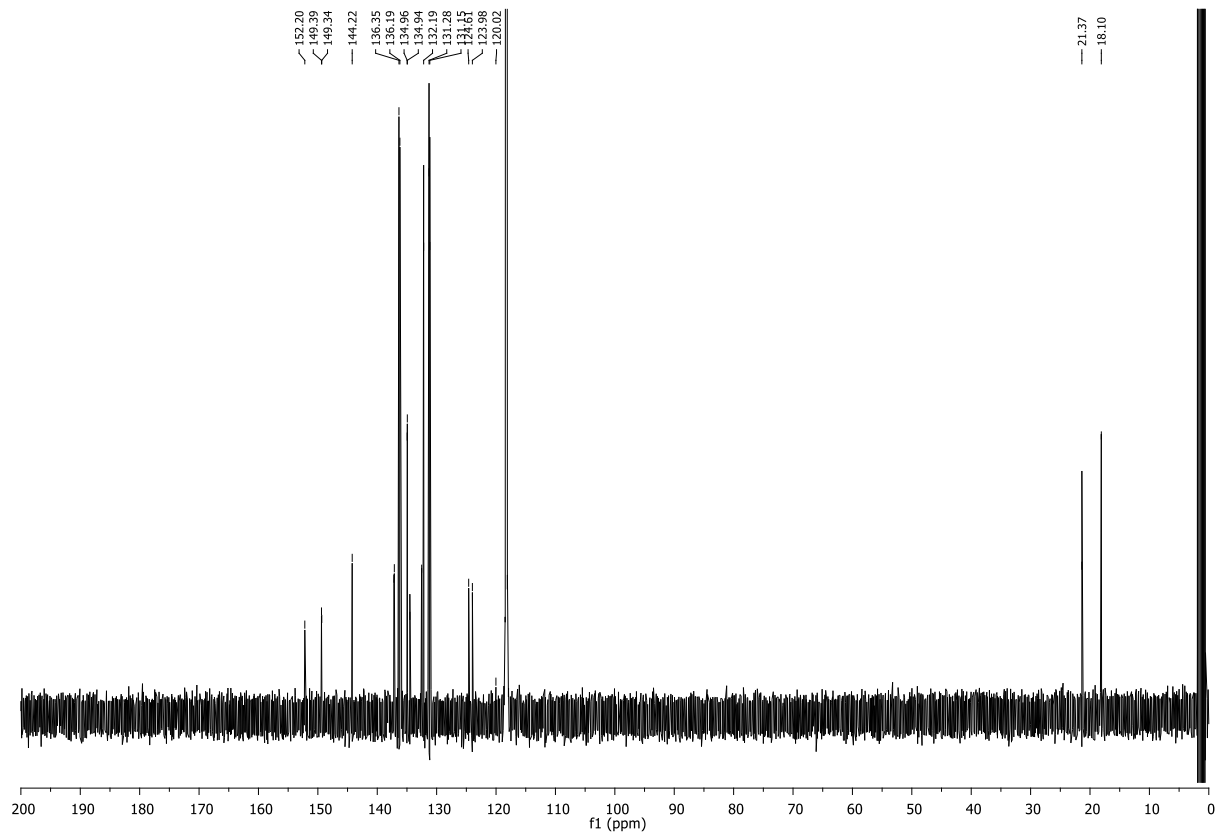
Compound 191c: ^{31}P NMR (121 MHz, CD_3CN)



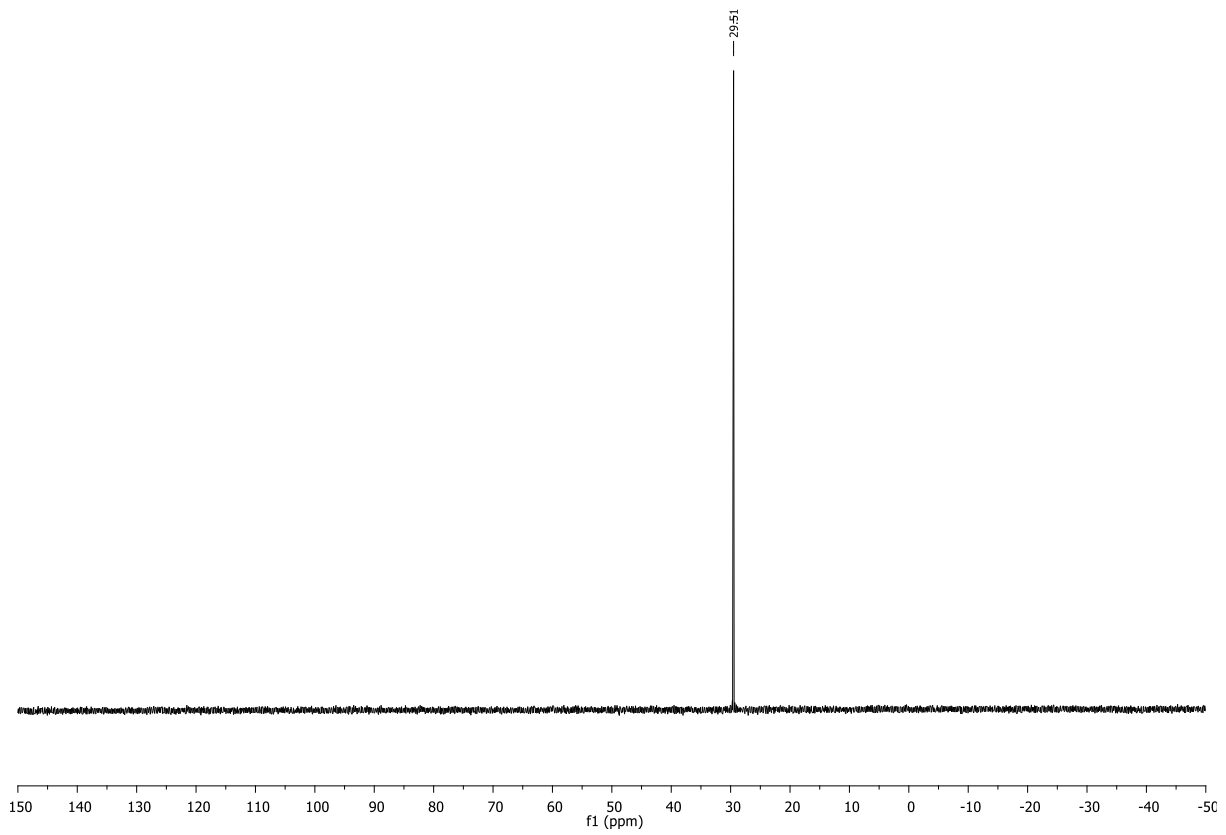
Compound 191d: ^1H NMR (400 MHz, CD_3CN)



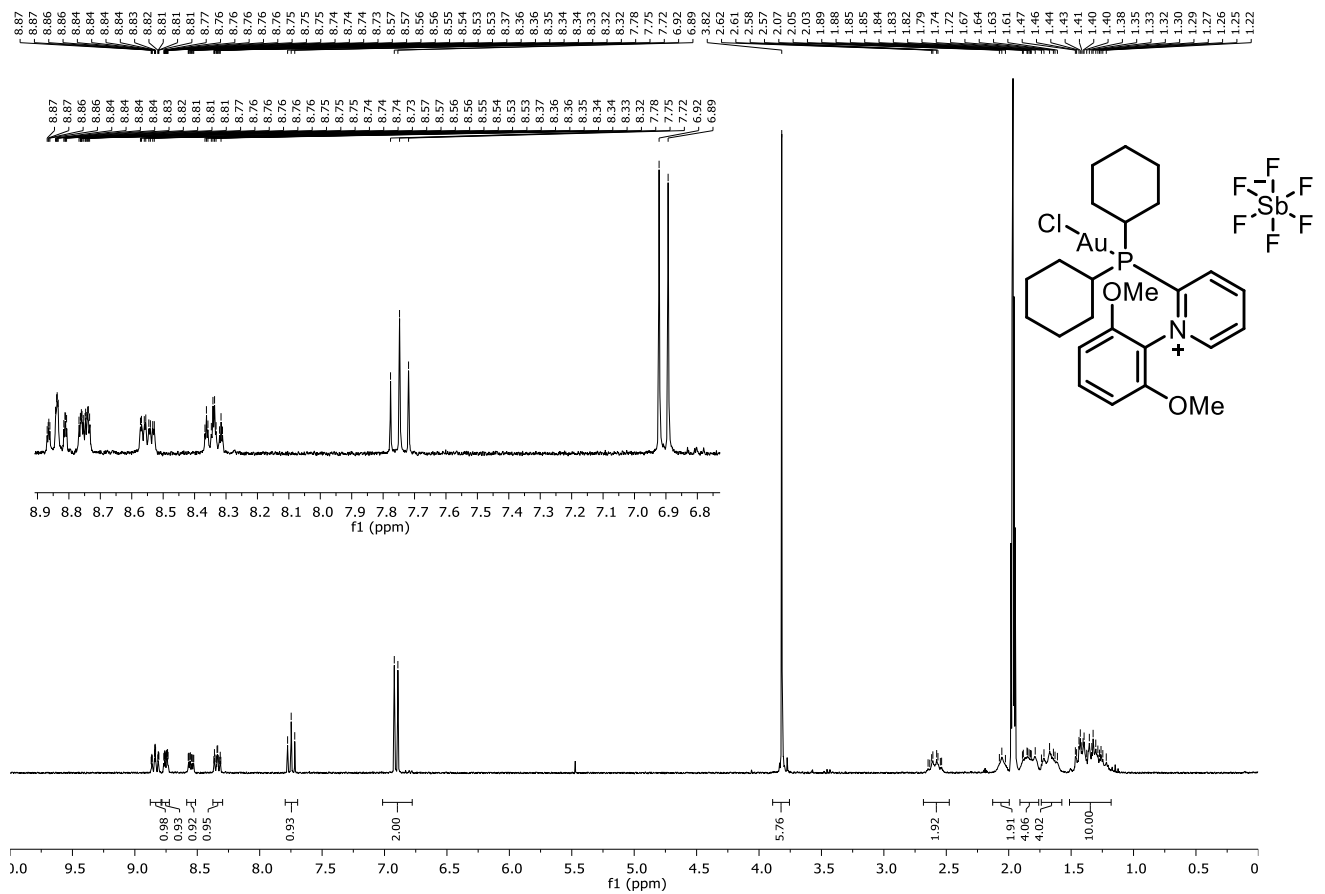
Compound 191d: ^{13}C NMR (101 MHz, CD_3CN)



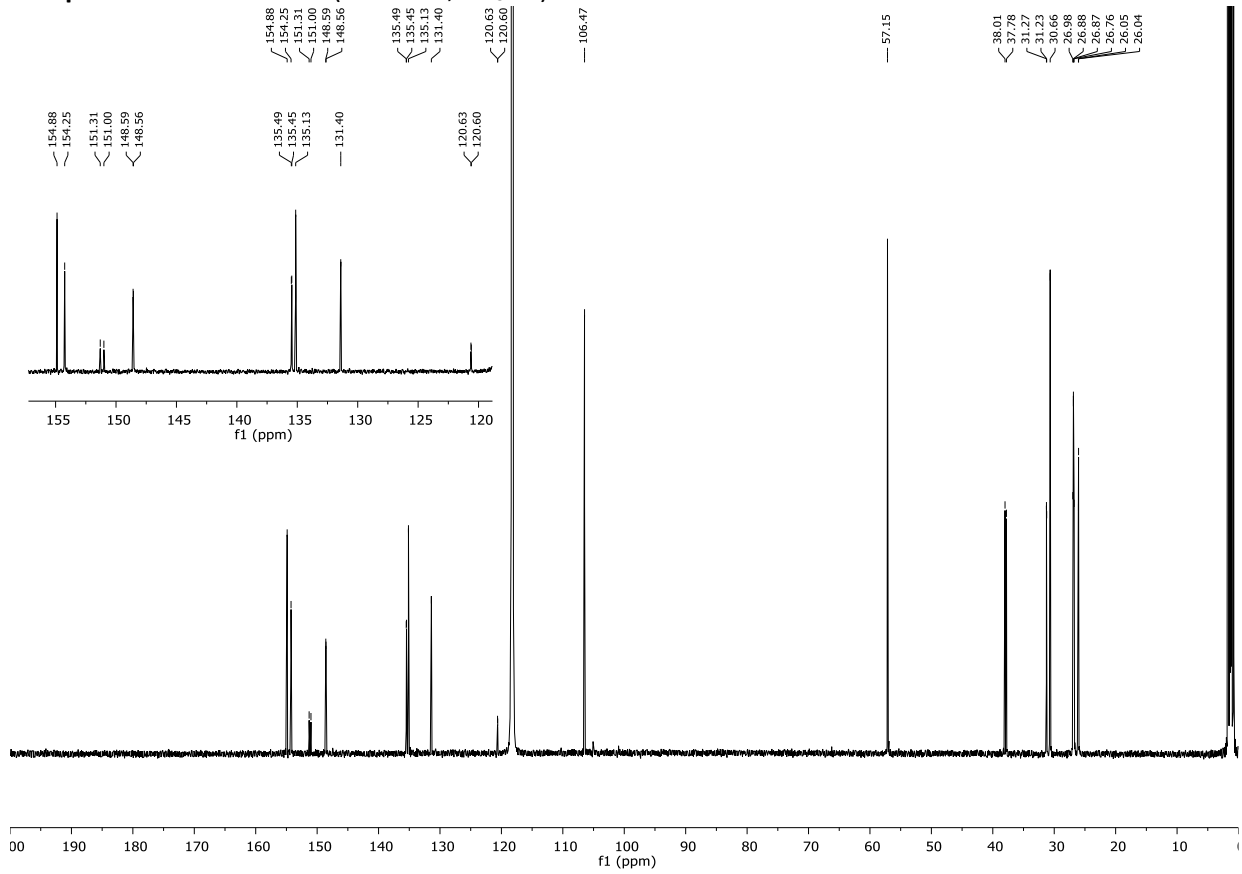
Compound 191d: ^{31}P NMR (121 MHz, CD_3CN)



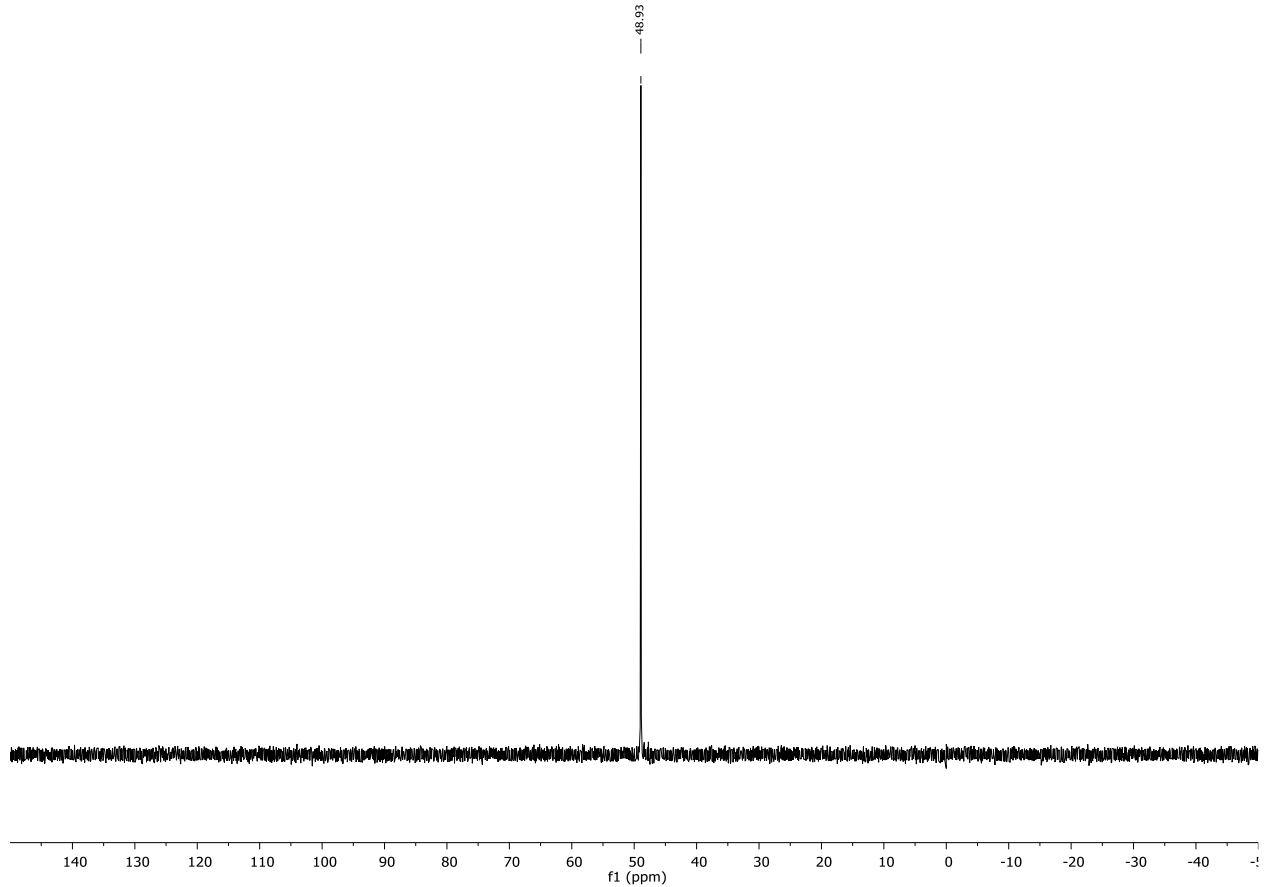
Compound 191e: ^1H NMR (400 MHz, CDCl_3)



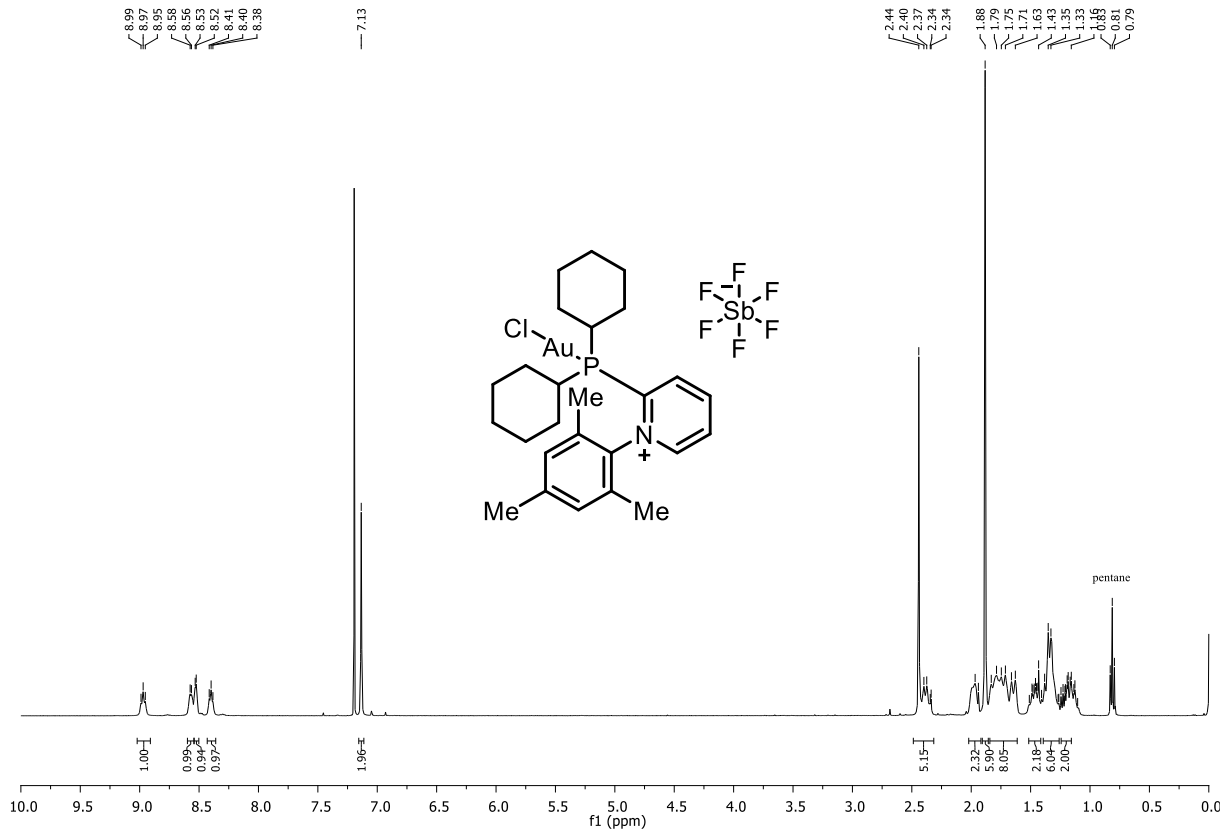
Compound 191e: ^{13}C NMR (101 MHz, CD_3CN)



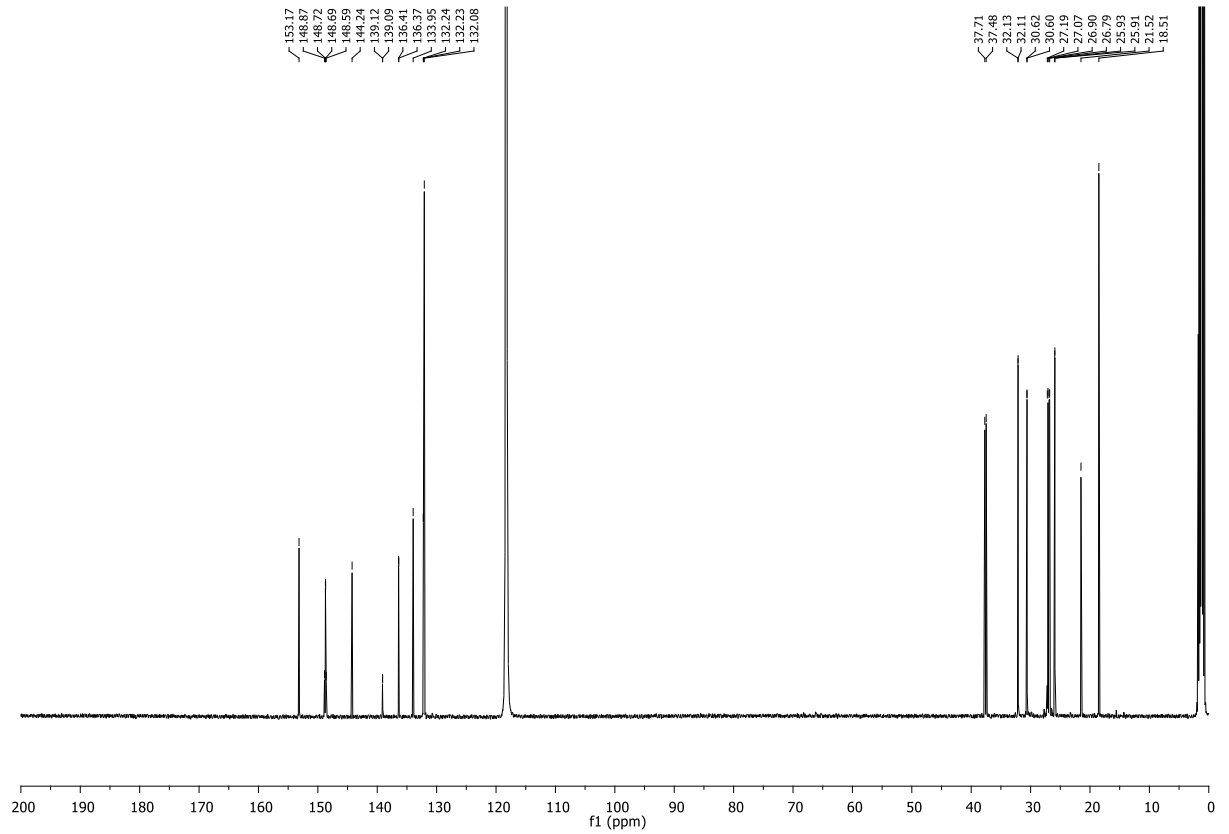
Compound 191e: ^{31}P NMR (121 MHz, CDCl_3)



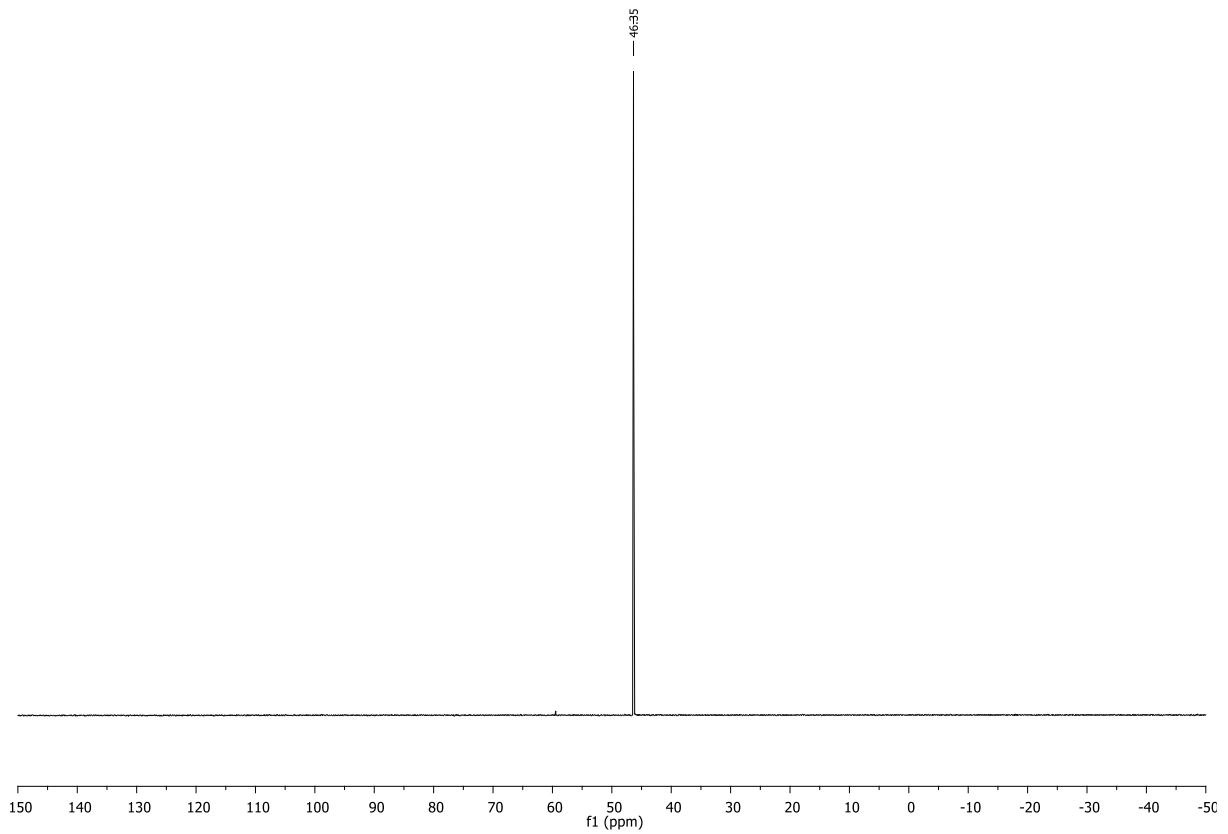
Compound 191f: ^1H NMR (400 MHz, CDCl_3)



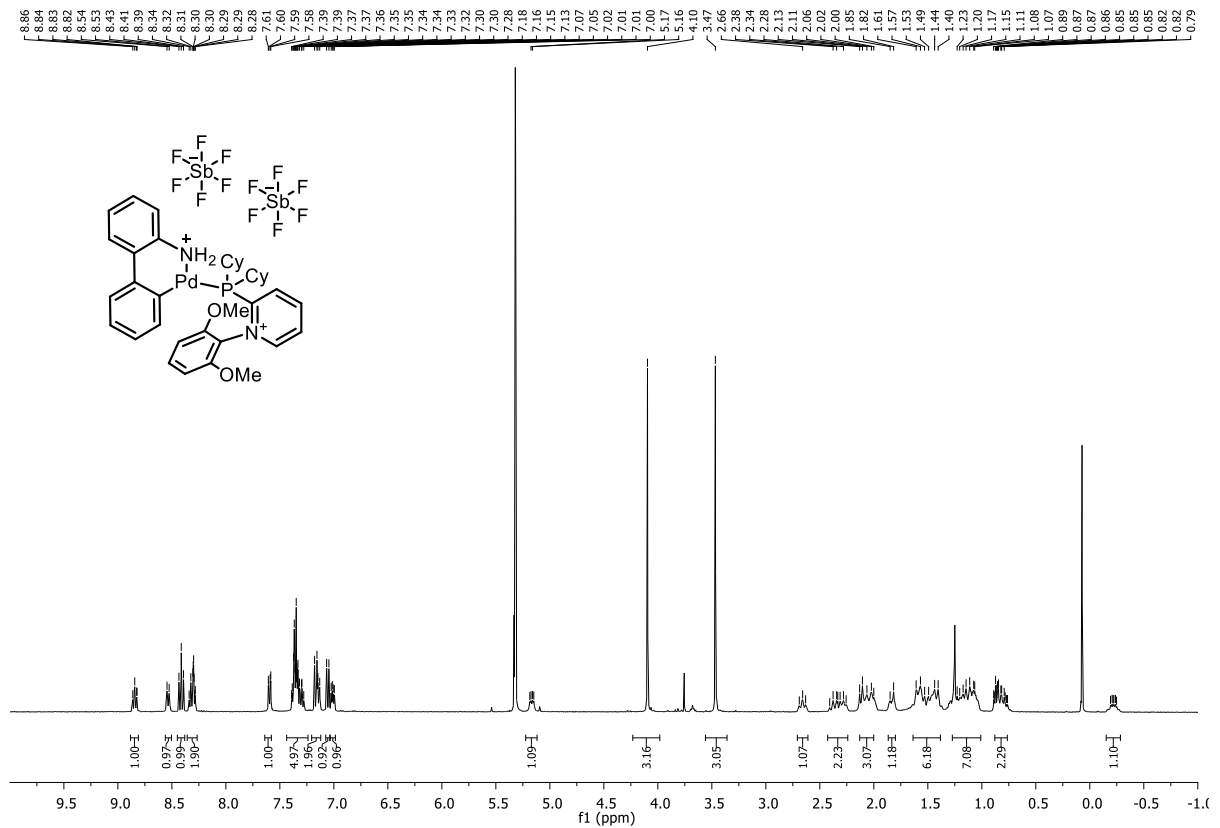
Compound 191f: ^{13}C NMR (126 MHz, CD_3CN)



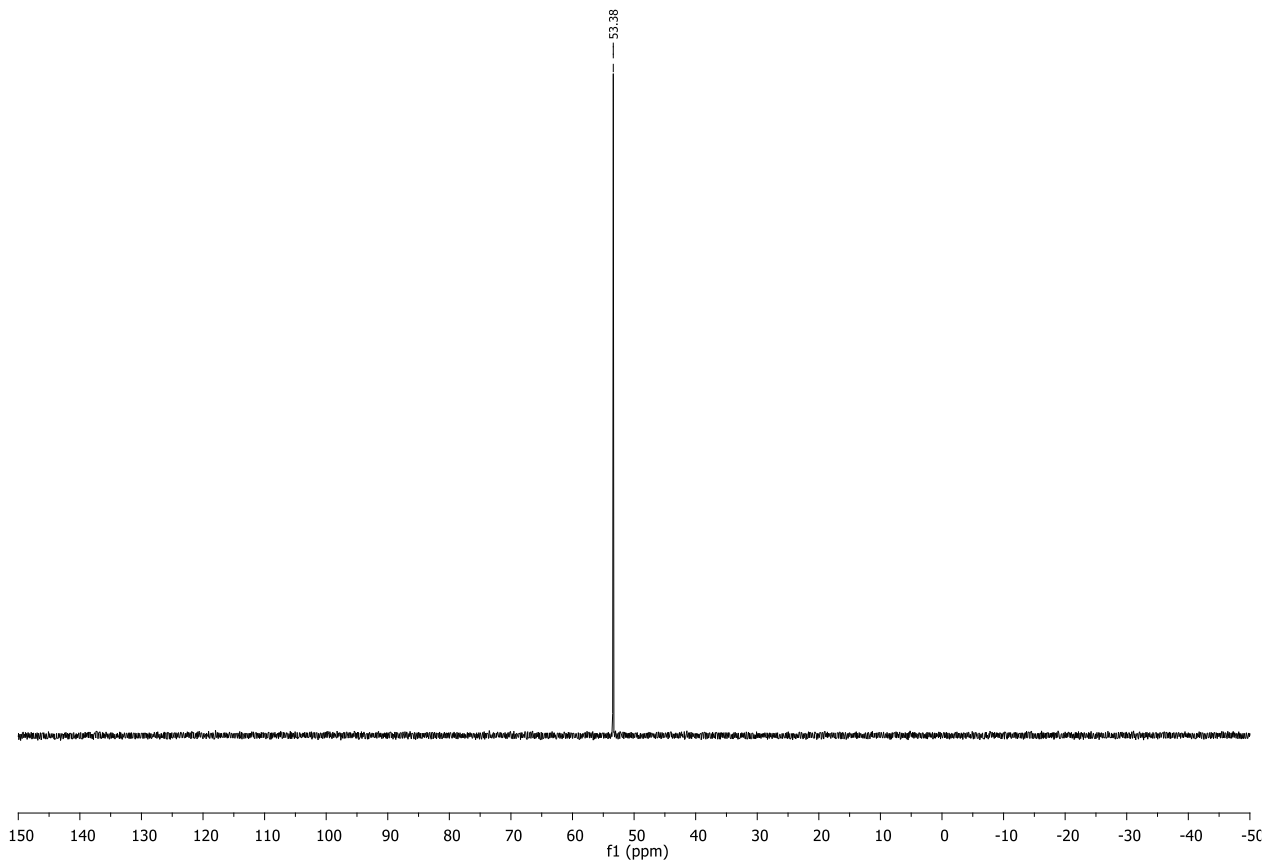
Compound 191f: ^{31}P NMR (121 MHz, CDCl_3)



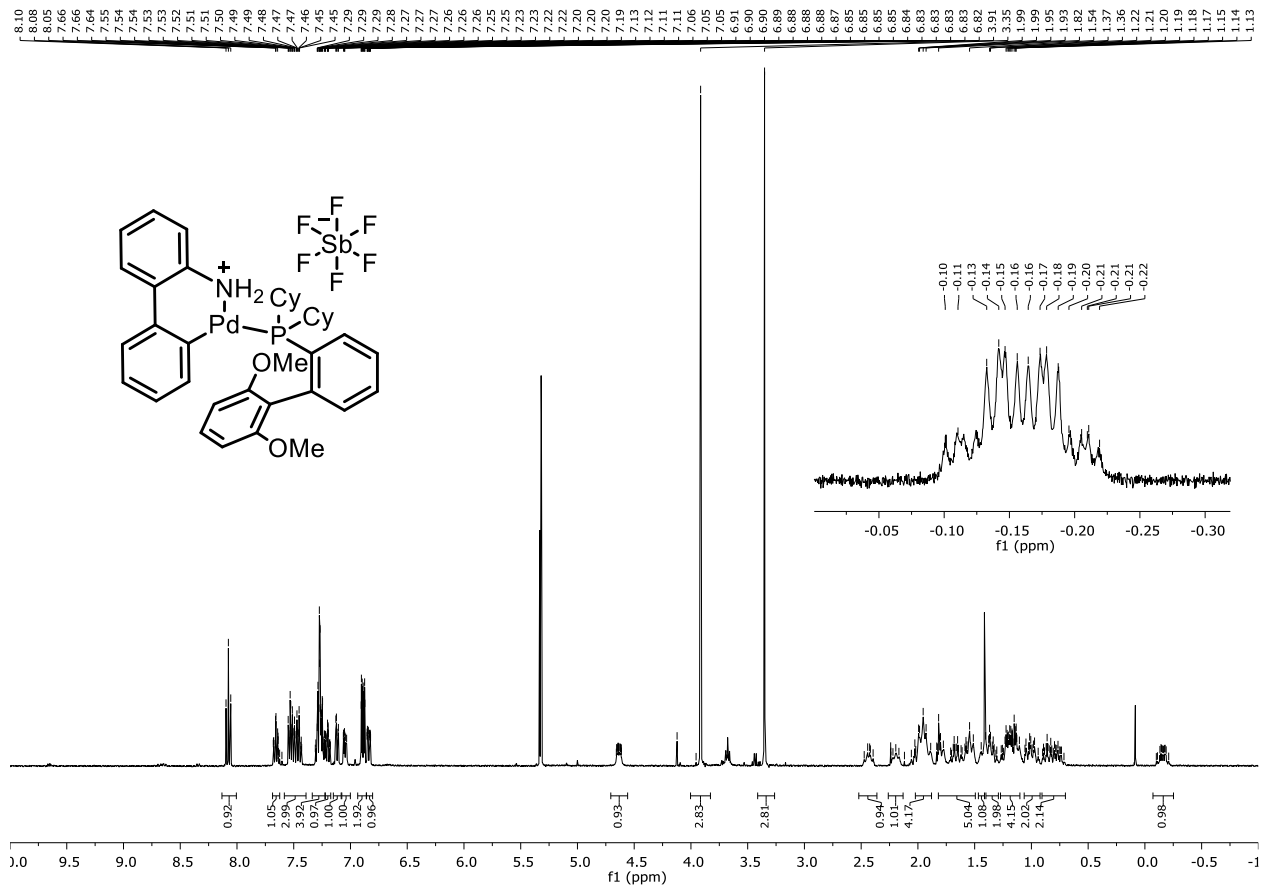
Compound 196: ^1H NMR (400 MHz, CD_2Cl_2)



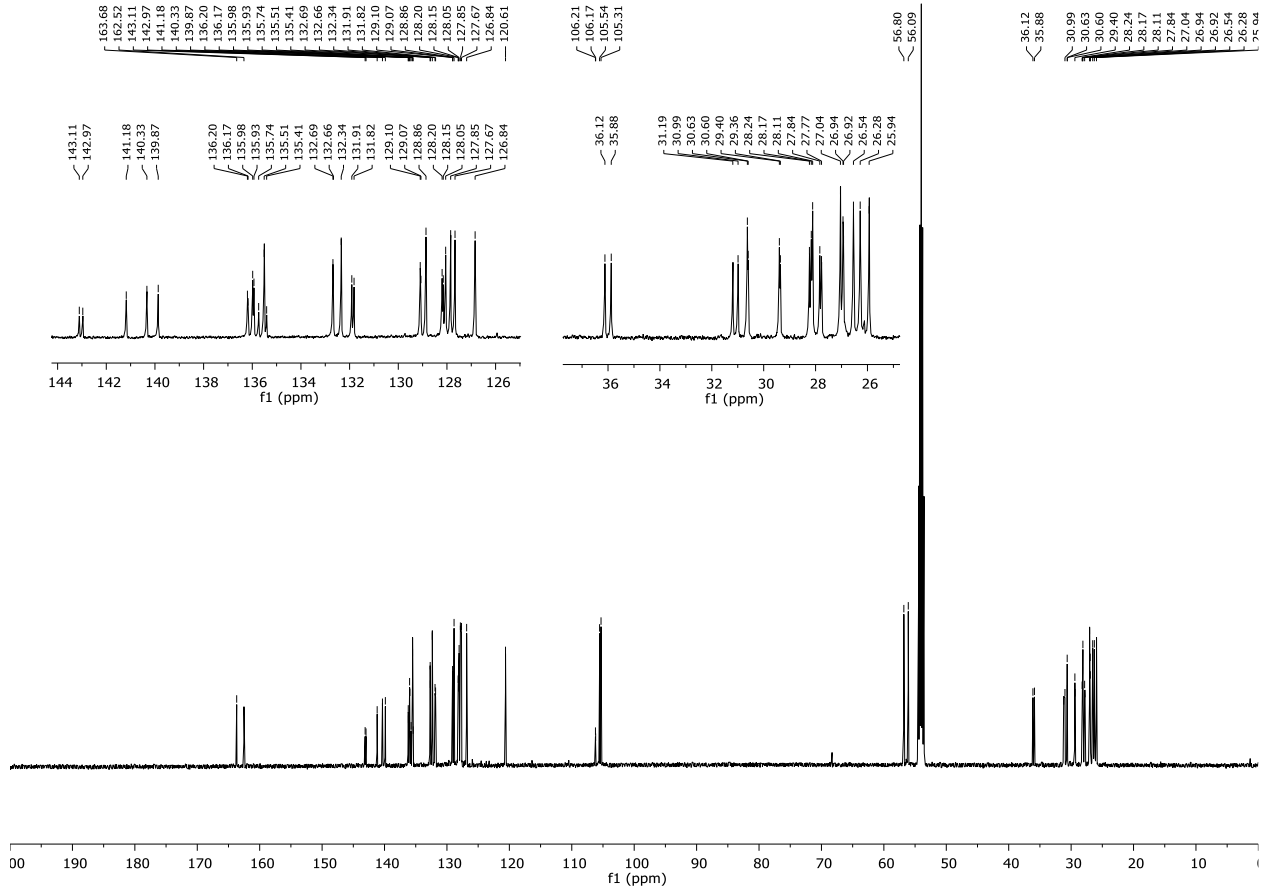
Compound 196: ^{31}P NMR (121 MHz, CD_2Cl_2)



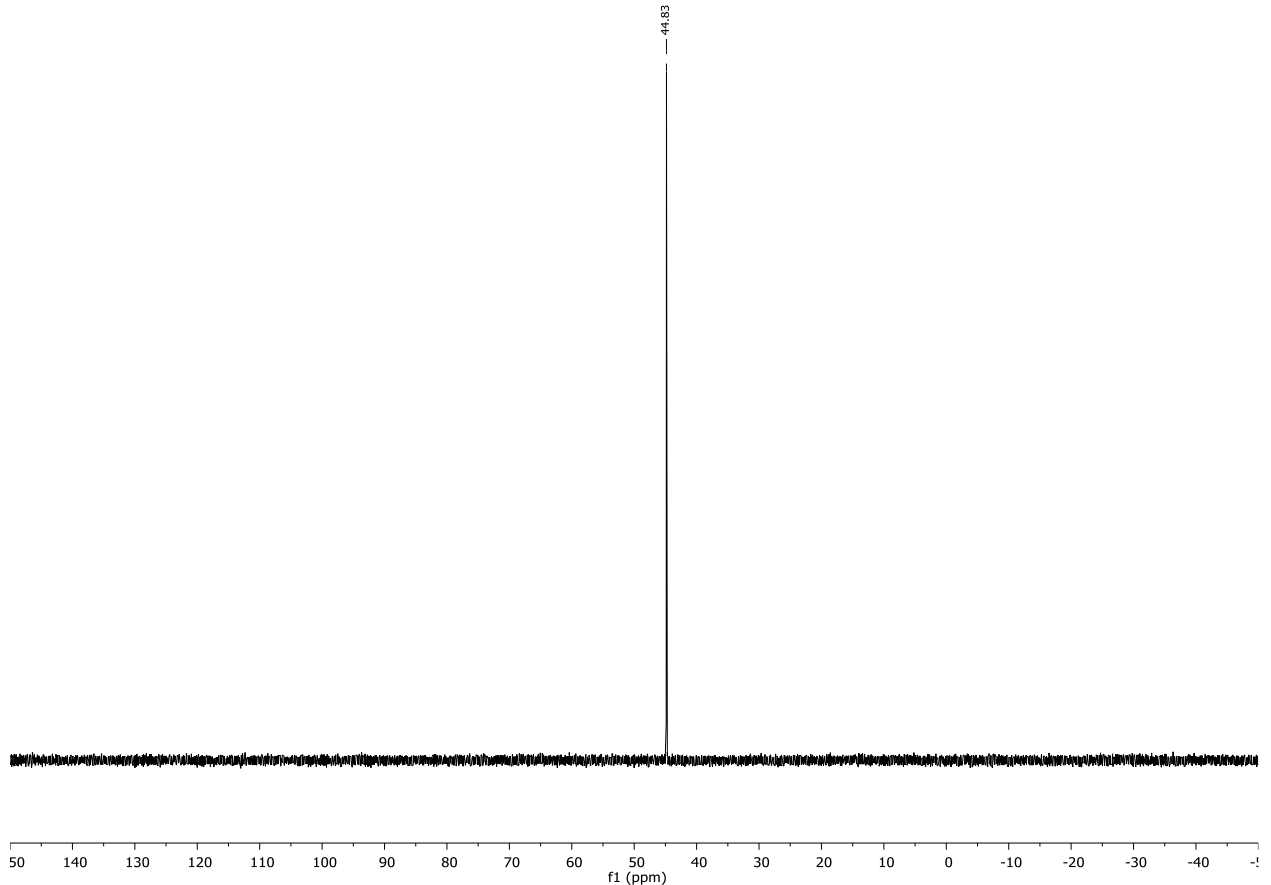
Compound 197: ^1H NMR (400 MHz, CD_2Cl_2)



Compound 197: ^{13}C NMR (121 MHz, CD_2Cl_2)

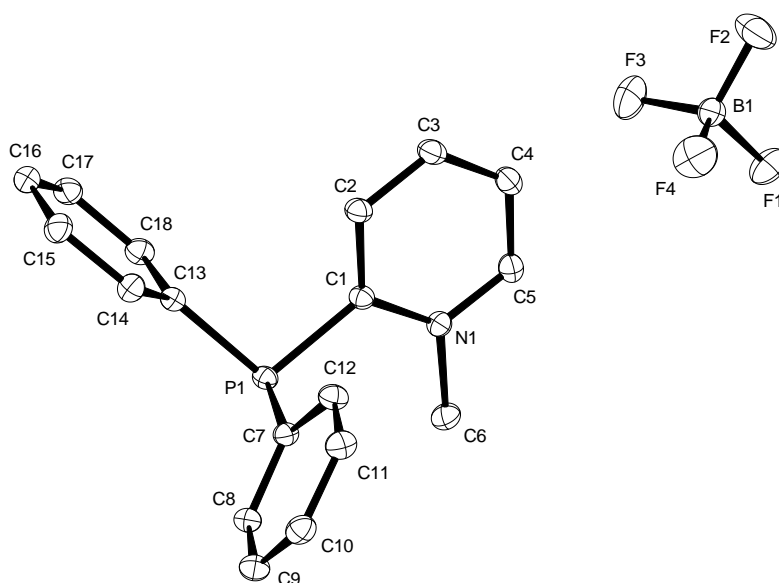


Compound 197: ^{31}P NMR (121 MHz, CD_2Cl_2)



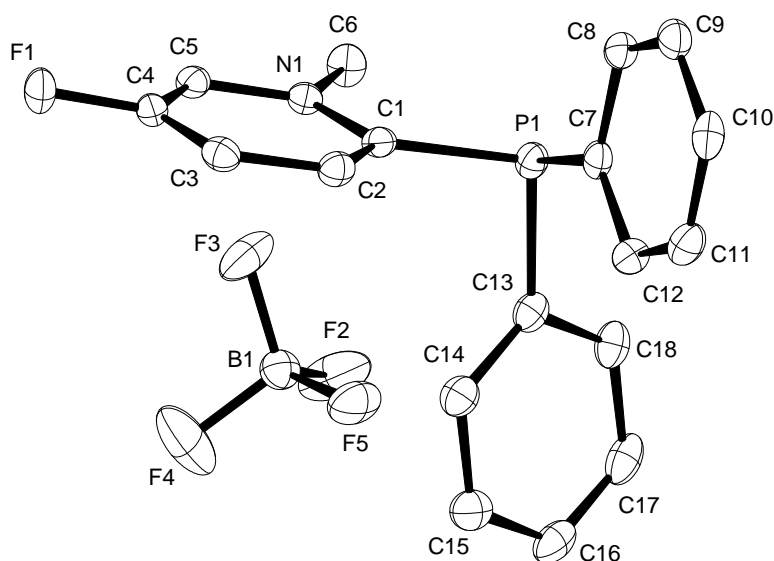
10.3 Solid State Structures

Crystal Data and Structure Refinement of Compound 124a

**Table 1. Crystal data and structure refinement.**

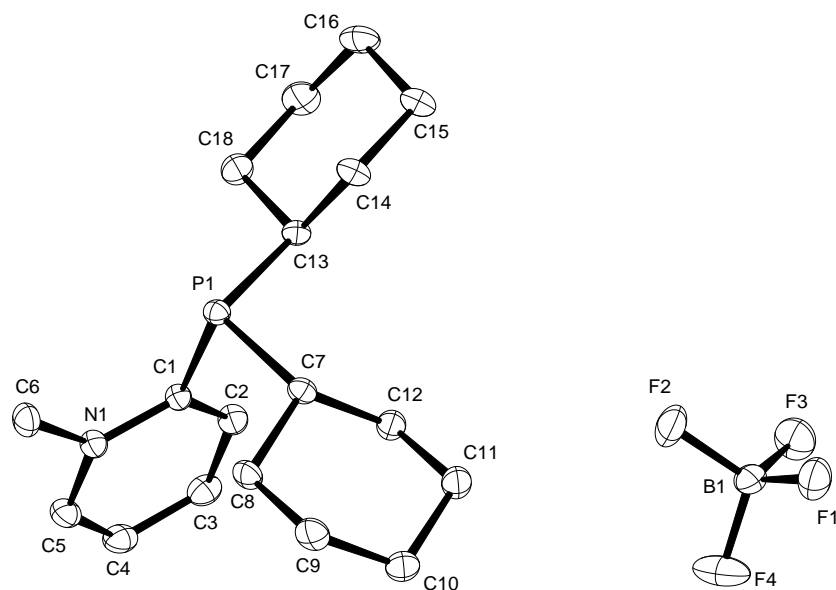
Identification code	8265	
Empirical formula	$C_{18}H_{17}BF_4NP$	
Color	colorless	
Formula weight	$365.11 \text{ g} \cdot \text{mol}^{-1}$	
Temperature	100 K	
Wavelength	0.71073 \AA	
Crystal system	MONOCLINIC	
Space group	$P2_1/n$, (no. 14)	
Unit cell dimensions	$a = 8.1868(10) \text{ \AA}$	$\alpha = 90^\circ$.
	$b = 17.678(2) \text{ \AA}$	$\beta = 98.430(2)^\circ$.
	$c = 11.6245(15) \text{ \AA}$	$\gamma = 90^\circ$.
Volume	$1664.2(4) \text{ \AA}^3$	
Z	4	
Density (calculated)	$1.457 \text{ Mg} \cdot \text{m}^{-3}$	
Absorption coefficient	0.207 mm^{-1}	
F(000)	752 e	
Crystal size	$0.28 \times 0.11 \times 0.05 \text{ mm}^3$	
θ range for data collection	2.11 to 37.05° .	
Index ranges	$-13 \leq h \leq 13$, $-29 \leq k \leq 29$, $-19 \leq l \leq 19$	
Reflections collected	63349	
Independent reflections	8167 [$R_{\text{int}} = 0.0195$]	
Reflections with $I > 2\sigma(I)$	7368	
Completeness to $\theta = 27.50^\circ$	100.0 %	
Absorption correction	Gaussian	
Max. and min. transmission	0.99 and 0.93	
Refinement method	Full-matrix least-squares on F^2	
Data / restraints / parameters	8167 / 0 / 227	
Goodness-of-fit on F^2	1.053	
Final R indices [$I > 2\sigma(I)$]	$R_1 = 0.0327$	$wR^2 = 0.0921$
R indices (all data)	$R_1 = 0.0368$	$wR^2 = 0.0955$
Largest diff. peak and hole	0.699 and $-0.508 \text{ e} \cdot \text{\AA}^{-3}$	

Crystal Data and Structure Refinement of Compound 124b

**Table 1. Crystal data and structure refinement.**

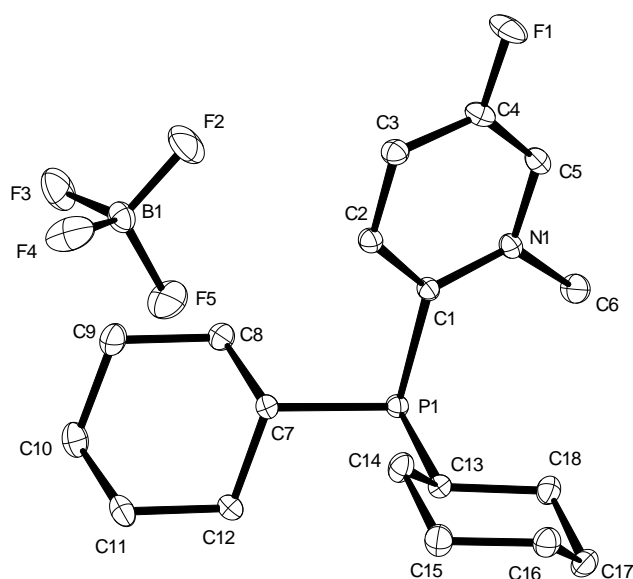
Identification code	8292	
Empirical formula	$C_{18}H_{16}BF_5NP$	
Color	yellow	
Formula weight	$383.10 \text{ g} \cdot \text{mol}^{-1}$	
Temperature	100 K	
Wavelength	1.54178 \AA	
Crystal system	MONOCLINIC	
Space group	$P2_1/n$, (no. 14)	
Unit cell dimensions	$a = 8.2324(6) \text{ \AA}$	$\alpha = 90^\circ$
	$b = 18.2784(13) \text{ \AA}$	$\beta = 101.487(3)^\circ$
	$c = 11.8087(8) \text{ \AA}$	$\gamma = 90^\circ$
Volume	$1741.3(2) \text{ \AA}^3$	
Z	4	
Density (calculated)	$1.461 \text{ Mg} \cdot \text{m}^{-3}$	
Absorption coefficient	1.887 mm^{-1}	
F(000)	784 e	
Crystal size	$0.33 \times 0.32 \times 0.05 \text{ mm}^3$	
θ range for data collection	4.522 to 66.982°	
Index ranges	$-9 \leq h \leq 9$, $-21 \leq k \leq 21$, $-14 \leq l \leq 14$	
Reflections collected	53683	
Independent reflections	3045 [$R_{\text{int}} = 0.0444$]	
Reflections with $I > 2\sigma(I)$	2964	
Completeness to $\theta = 67.679^\circ$	96.9 %	
Absorption correction	Gaussian	
Max. and min. transmission	0.91 and 0.57	
Refinement method	Full-matrix least-squares on F^2	
Data / restraints / parameters	3045 / 0 / 236	
Goodness-of-fit on F^2	1.050	
Final R indices [$I > 2\sigma(I)$]	$R_1 = 0.0315$	$wR^2 = 0.0784$
R indices (all data)	$R_1 = 0.0321$	$wR^2 = 0.0788$
Largest diff. peak and hole	0.4 and $-0.4 \text{ e} \cdot \text{\AA}^{-3}$	

Crystal Data and Structure Refinement of Compound 124e

**Table 1. Crystal data and structure refinement.**

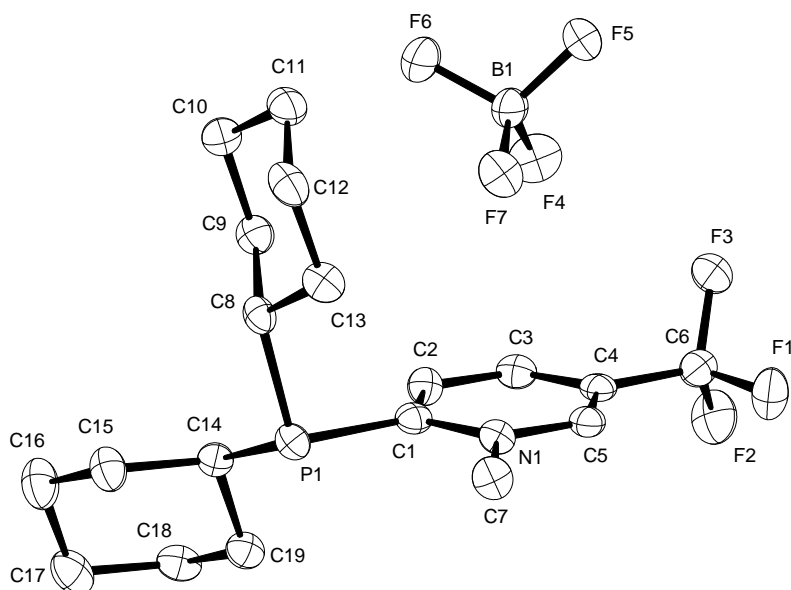
Identification code	8242	
Empirical formula	C ₁₈ H ₂₉ B ₄ F ₄ N ₁ P	
Color	colorless	
Formula weight	377.20 g · mol ⁻¹	
Temperature	100 K	
Wavelength	0.71073 Å	
Crystal system	ORTHORHOMBIC	
Space group	P2₁2₁2, (no. 18)	
Unit cell dimensions	a = 9.7816(12) Å	α = 90°.
	b = 30.483(4) Å	β = 90°.
	c = 6.4504(8) Å	γ = 90°.
Volume	1923.3(4) Å ³	
Z	4	
Density (calculated)	1.303 Mg · m ⁻³	
Absorption coefficient	0.180 mm ⁻¹	
F(000)	800 e	
Crystal size	0.28 x 0.26 x 0.18 mm ³	
θ range for data collection	2.19 to 31.12°.	
Index ranges	-14 ≤ h ≤ 14, -44 ≤ k ≤ 44, -9 ≤ l ≤ 9	
Reflections collected	56947	
Independent reflections	6190 [R _{int} = 0.0382]	
Reflections with I > 2σ(I)	5987	
Completeness to θ = 31.12°	99.7 %	
Absorption correction	Gaussian	
Max. and min. transmission	0.97 and 0.96	
Refinement method	Full-matrix least-squares on F ²	
Data / restraints / parameters	6190 / 0 / 227	
Goodness-of-fit on F ²	1.088	
Final R indices [I > 2σ(I)]	R ₁ = 0.0305	wR ² = 0.0788
R indices (all data)	R ₁ = 0.0320	wR ² = 0.0798
Absolute structure parameter	0.45(5)	
Largest diff. peak and hole	0.5 and -0.3 e · Å ⁻³	

Crystal Data and Structure Refinement of Compound 124f

**Table 1. Crystal data and structure refinement.**

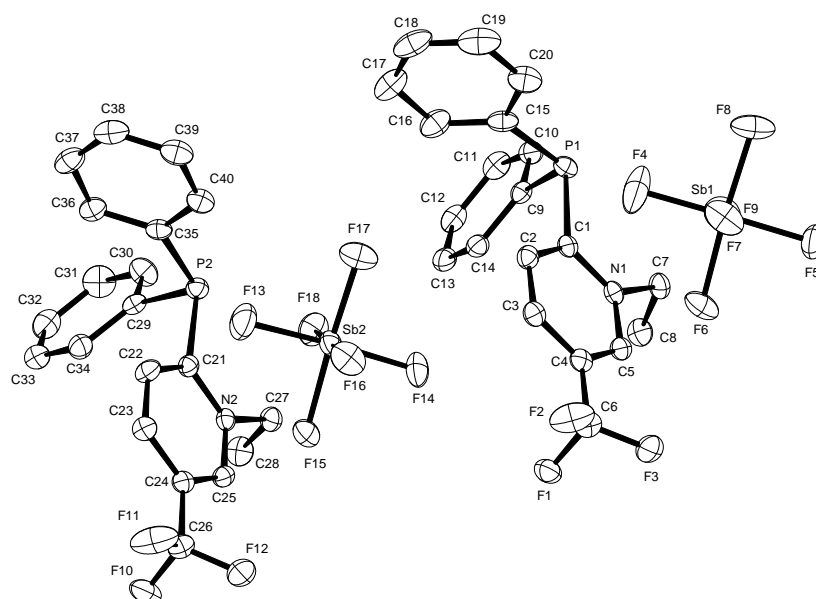
Identification code	8277	
Empirical formula	$C_{18}H_{28}BF_5NP$	
Color	colourless	
Formula weight	$395.19 \text{ g} \cdot \text{mol}^{-1}$	
Temperature	100 K	
Wavelength	0.71073 \AA	
Crystal system	MONOCLINIC	
Space group	$P2_1/n$, (no. 14)	
Unit cell dimensions	$a = 9.7832(10) \text{ \AA}$	$\alpha = 90^\circ$.
	$b = 12.5194(6) \text{ \AA}$	$\beta = 91.707(7)^\circ$.
	$c = 15.7945(12) \text{ \AA}$	$\gamma = 90^\circ$.
Volume	$1933.6(3) \text{ \AA}^3$	
Z	4	
Density (calculated)	$1.358 \text{ Mg} \cdot \text{m}^{-3}$	
Absorption coefficient	0.190 mm^{-1}	
F(000)	832 e	
Crystal size	$0.32 \times 0.32 \times 0.07 \text{ mm}^3$	
θ range for data collection	2.643 to 33.130° .	
Index ranges	$-15 \leq h \leq 15$, $-19 \leq k \leq 19$, $-24 \leq l \leq 24$	
Reflections collected	45003	
Independent reflections	7352 [$R_{\text{int}} = 0.0296$]	
Reflections with $I > 2\sigma(I)$	6219	
Completeness to $\theta = 25.242^\circ$	99.8 %	
Absorption correction	Gaussian	
Max. and min. transmission	0.99 and 0.95	
Refinement method	Full-matrix least-squares on F^2	
Data / restraints / parameters	7352 / 0 / 236	
Goodness-of-fit on F^2	1.054	
Final R indices [$I > 2\sigma(I)$]	$R_1 = 0.0345$	$wR^2 = 0.0826$
R indices (all data)	$R_1 = 0.0455$	$wR^2 = 0.0893$
Largest diff. peak and hole	0.697 and $-0.586 \text{ e} \cdot \text{\AA}^{-3}$	

Crystal Data and Structure Refinement of Compound 124g

**Table 1. Crystal data and structure refinement.**

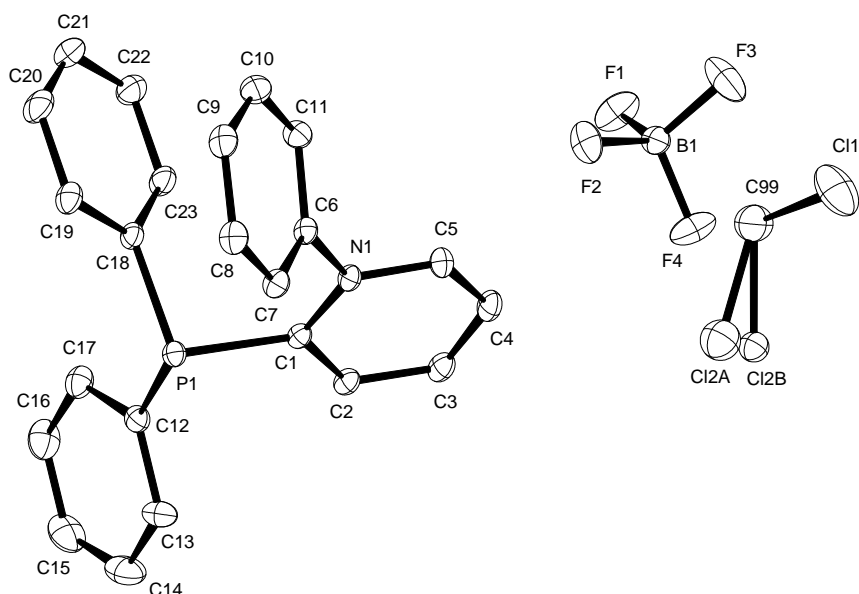
Identification code	8286	
Empirical formula	$C_{19}H_{28}BF_7NP$	
Color	colorless	
Formula weight	445.20 $g \cdot mol^{-1}$	
Temperature	100 K	
Wavelength	1.54178 Å	
Crystal system	ORTHORHOMBIC	
Space group	$P2_1 2_1 2_1$, (no. 19)	
Unit cell dimensions	$a = 8.2411(4)$ Å	$\alpha = 90^\circ$
	$b = 9.6509(5)$ Å	$\beta = 90^\circ$
	$c = 26.3708(12)$ Å	$\gamma = 90^\circ$
Volume	2097.38(18) Å ³	
Z	4	
Density (calculated)	1.410 $Mg \cdot m^{-3}$	
Absorption coefficient	1.775 mm^{-1}	
F(000)	928 e	
Crystal size	0.30 x 0.14 x 0.11 mm ³	
θ range for data collection	3.352 to 63.686°.	
Index ranges	$-9 \leq h \leq 9, -11 \leq k \leq 11, -30 \leq l \leq 29$	
Reflections collected	35051	
Independent reflections	3348 [$R_{int} = 0.0613$]	
Reflections with $I > 2\sigma(I)$	3062	
Completeness to $\theta = 67.679^\circ$	90.0 %	
Absorption correction	Gaussian	
Max. and min. transmission	0.83 and 0.67	
Refinement method	Full-matrix least-squares on F^2	
Data / restraints / parameters	3348 / 0 / 263	
Goodness-of-fit on F^2	1.119	
Final R indices [$I > 2\sigma(I)$]	$R_1 = 0.0306$	$wR^2 = 0.0707$
R indices (all data)	$R_1 = 0.0415$	$wR^2 = 0.0769$
Absolute structure parameter	0.004(12)	
Largest diff. peak and hole	0.4 and -0.5 $e \cdot \text{Å}^{-3}$	

Crystal Data and Structure Refinement of Compound 124h

**Table 1. Crystal data and structure refinement.**

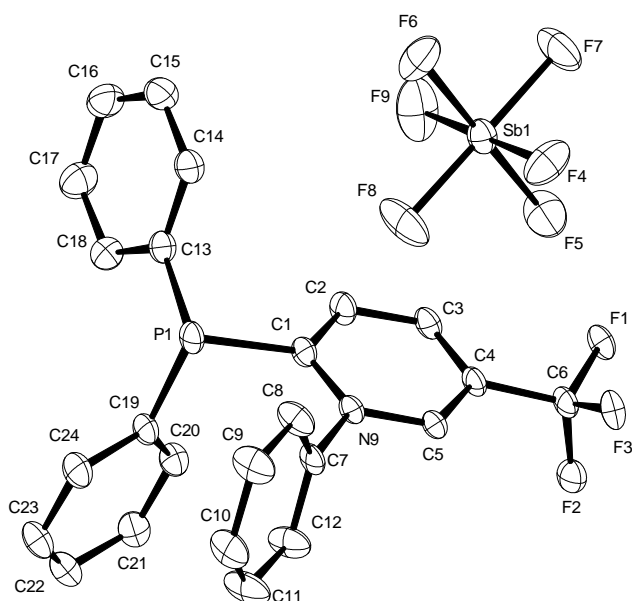
Identification code	8631	
Empirical formula	$C_{40}H_{36}F_{18}N_2P_2Sb_2$	
Color	yellow	
Formula weight	1192.15 $g \cdot mol^{-1}$	
Temperature	100 K	
Wavelength	1.54178 Å	
Crystal system	MONOCLINIC	
Space group	$P2_1/n$, (no. 14)	
Unit cell dimensions	$a = 13.5380(4)$ Å	$\alpha = 90^\circ$.
	$b = 11.1079(3)$ Å	$\beta = 101.3476(9)^\circ$.
	$c = 30.2418(9)$ Å	$\gamma = 90^\circ$.
Volume	$4458.8(2)$ Å ³	
Z	4	
Density (calculated)	1.776 $Mg \cdot m^{-3}$	
Absorption coefficient	11.276 mm^{-1}	
F(000)	2336 e	
Crystal size	0.34 x 0.17 x 0.17 mm^3	
θ range for data collection	2.981 to 67.578°.	
Index ranges	$-16 \leq h \leq 15$, $-13 \leq k \leq 13$, $-36 \leq l \leq 36$	
Reflections collected	99679	
Independent reflections	7995 [$R_{int} = 0.0394$]	
Reflections with $I > 2\sigma(I)$	7764	
Completeness to $\theta = 67.679^\circ$	99.1 %	
Absorption correction	Gaussian	
Max. and min. transmission	0.33 and 0.039	
Refinement method	Full-matrix least-squares on F^2	
Data / restraints / parameters	7995 / 0 / 579	
Goodness-of-fit on F^2	1.107	
Final R indices [$I > 2\sigma(I)$]	$R_1 = 0.0243$	$wR^2 = 0.0572$
R indices (all data)	$R_1 = 0.0252$	$wR^2 = 0.0577$
Largest diff. peak and hole	0.4 and $-0.7 e \cdot \text{Å}^{-3}$	

Crystal Data and Structure Refinement of Compound 124j

**Table 1. Crystal data and structure refinement.**

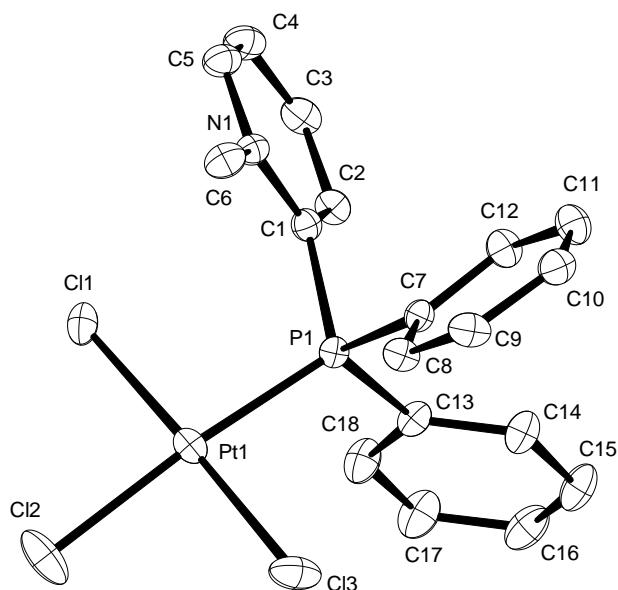
Identification code	8322	
Empirical formula	$C_{24}H_{21}BCl_2F_4NP$	
Color	colorless	
Formula weight	$512.10 \text{ g} \cdot \text{mol}^{-1}$	
Temperature	100 K	
Wavelength	0.71073 \AA	
Crystal system	MONOCLINIC	
Space group	$P2_1/c$, (no. 14)	
Unit cell dimensions	$a = 12.6094(17) \text{ \AA}$	$\alpha = 90^\circ$.
	$b = 6.1859(8) \text{ \AA}$	$\beta = 98.846(2)^\circ$.
	$c = 30.722(4) \text{ \AA}$	$\gamma = 90^\circ$.
Volume	$2367.8(5) \text{ \AA}^3$	
Z	4	
Density (calculated)	$1.437 \text{ Mg} \cdot \text{m}^{-3}$	
Absorption coefficient	0.386 mm^{-1}	
F(000)	1048 e	
Crystal size	$0.29 \times 0.08 \times 0.04 \text{ mm}^3$	
θ range for data collection	1.342 to 33.217° .	
Index ranges	$-19 \leq h \leq 19$, $-9 \leq k \leq 9$, $-47 \leq l \leq 47$	
Reflections collected	74779	
Independent reflections	8957 [$R_{\text{int}} = 0.0484$]	
Reflections with $I > 2\sigma(I)$	7241	
Completeness to $\theta = 25.242^\circ$	100.0 %	
Absorption correction	Gaussian	
Max. and min. transmission	0.99 and 0.97	
Refinement method	Full-matrix least-squares on F^2	
Data / restraints / parameters	8957 / 0 / 297	
Goodness-of-fit on F^2	1.017	
Final R indices [$I > 2\sigma(I)$]	$R_1 = 0.0538$	$wR^2 = 0.1259$
R indices (all data)	$R_1 = 0.0694$	$wR^2 = 0.1367$
Largest diff. peak and hole	1.9 and $-2.2 \text{ e} \cdot \text{\AA}^{-3}$	

Crystal Data and Structure Refinement of Compound 124m

**Table 1. Crystal data and structure refinement.**

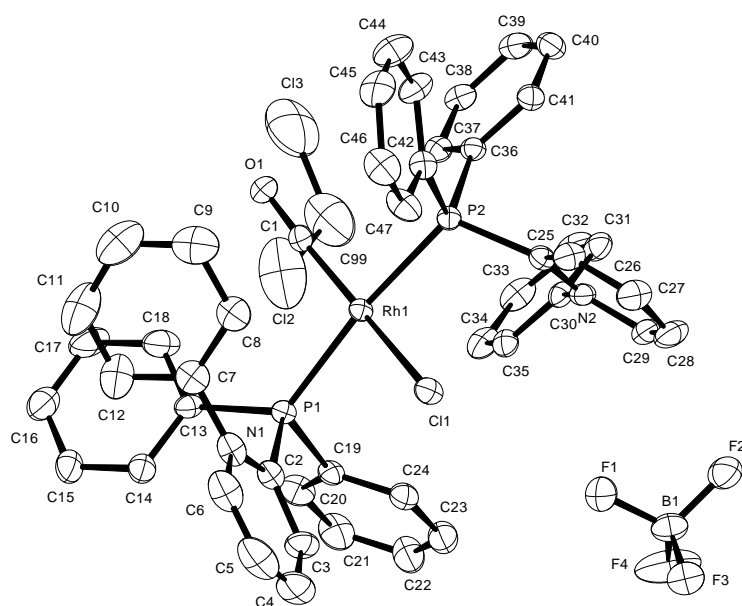
Identification code	8790	
Empirical formula	$C_{24}H_{18}F_9NP Sb$	
Color	yellow	
Formula weight	$644.11 \text{ g} \cdot \text{mol}^{-1}$	
Temperature	100.15 K	
Wavelength	0.71073 \AA	
Crystal system	ORTHORHOMBIC	
Space group	Pbca, (no. 61)	
Unit cell dimensions	$a = 15.656(2) \text{ \AA}$	$\alpha = 90^\circ$
	$b = 15.3839(9) \text{ \AA}$	$\beta = 90^\circ$
	$c = 20.5777(17) \text{ \AA}$	$\gamma = 90^\circ$
Volume	$4956.1(9) \text{ \AA}^3$	
Z	8	
Density (calculated)	$1.726 \text{ Mg} \cdot \text{m}^{-3}$	
Absorption coefficient	1.259 mm^{-1}	
F(000)	2528 e	
Crystal size	$0.16 \times 0.10 \times 0.07 \text{ mm}^3$	
θ range for data collection	2.714 to 34.051°	
Index ranges	$-24 \leq h \leq 24, -24 \leq k \leq 24, -32 \leq l \leq 32$	
Reflections collected	103241	
Independent reflections	10154 [$R_{\text{int}} = 0.0751$]	
Reflections with $I > 2\sigma(I)$	7835	
Completeness to $\theta = 25.242^\circ$	99.7 %	
Absorption correction	Gaussian	
Max. and min. transmission	0.92 and 0.83	
Refinement method	Full-matrix least-squares on F^2	
Data / restraints / parameters	10154 / 0 / 325	
Goodness-of-fit on F^2	1.070	
Final R indices [$I > 2\sigma(I)$]	$R_1 = 0.0655$	$wR^2 = 0.1618$
R indices (all data)	$R_1 = 0.0818$	$wR^2 = 0.1784$
Largest diff. peak and hole	3.1 and $-4.3 \text{ e} \cdot \text{\AA}^{-3}$	

Crystal Data and Structure Refinement of Compound 136a

**Table 1. Crystal data and structure refinement.**

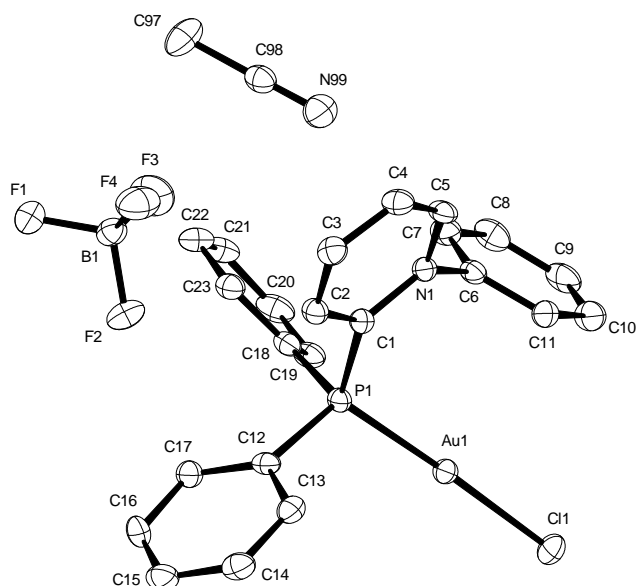
Identification code	8228	
Empirical formula	$C_{18}H_{17}Cl_3NPt$	
Color	yellow	
Formula weight	579.74 $g \cdot mol^{-1}$	
Temperature	100 K	
Wavelength	0.71073 Å	
Crystal system	MONOCLINIC	
Space group	$P2_1/n$, (no. 14)	
Unit cell dimensions	$a = 16.278(5)$ Å	$\alpha = 90^\circ$.
	$b = 9.206(3)$ Å	$\beta = 117.292(4)^\circ$.
	$c = 16.897(5)$ Å	$\gamma = 90^\circ$.
Volume	$2250.3(11)$ Å ³	
Z	4	
Density (calculated)	1.711 $Mg \cdot m^{-3}$	
Absorption coefficient	6.662 mm^{-1}	
F(000)	1104 e	
Crystal size	0.38 x 0.18 x 0.12 mm^3	
θ range for data collection	2.60 to 31.69°.	
Index ranges	$-23 \leq h \leq 23$, $-13 \leq k \leq 13$, $-23 \leq l \leq 24$	
Reflections collected	61879	
Independent reflections	7565 [$R_{int} = 0.0538$]	
Reflections with $I > 2\sigma(I)$	7217	
Completeness to $\theta = 27.50^\circ$	99.9 %	
Absorption correction	Gaussian	
Max. and min. transmission	0.60 and 0.12	
Refinement method	Full-matrix least-squares on F^2	
Data / restraints / parameters	7565 / 0 / 218	
Goodness-of-fit on F^2	1.069	
Final R indices [$I > 2\sigma(I)$]	$R_1 = 0.0280$	$wR^2 = 0.0693$
R indices (all data)	$R_1 = 0.0293$	$wR^2 = 0.0699$
Largest diff. peak and hole	3.6 and $-1.7 e \cdot \text{Å}^{-3}$	

Crystal Data and Structure Refinement of Compound 135c

**Table 1. Crystal data and structure refinement.**

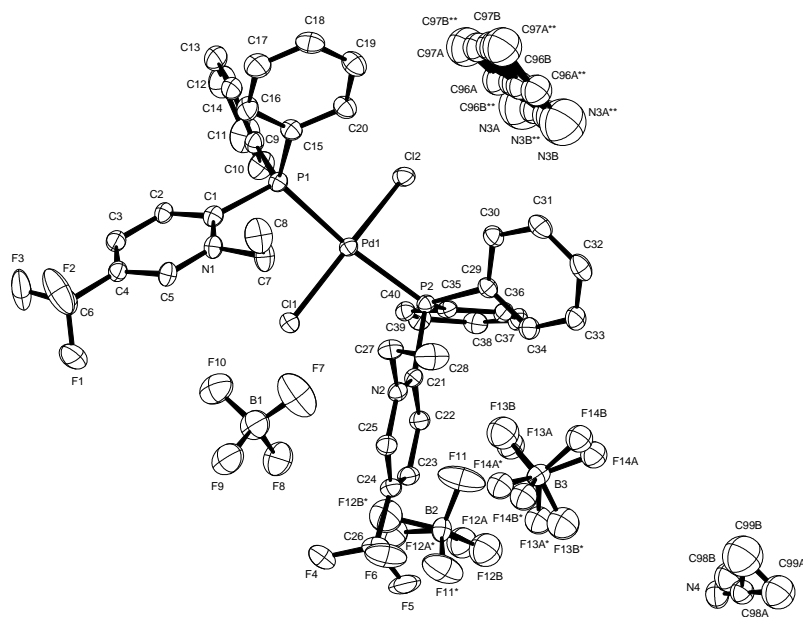
Identification code	8324	
Empirical formula	$C_{48}H_{40}BCl_3F_4N_2OP_2Rh$	
Color	orange	
Formula weight	1018.83 g · mol ⁻¹	
Temperature	100 K	
Wavelength	0.71073 Å	
Crystal system	TRICLINIC	
Space group	P1, (no. 2)	
Unit cell dimensions	$a = 14.350(3)$ Å	$\alpha = 69.336(16)^\circ$.
	$b = 14.805(3)$ Å	$\beta = 78.738(16)^\circ$.
	$c = 14.902(3)$ Å	$\gamma = 84.327(16)^\circ$.
Volume	2903.8(10) Å ³	
Z	2	
Density (calculated)	1.165 Mg · m ⁻³	
Absorption coefficient	0.531 mm ⁻¹	
F(000)	1034 e	
Crystal size	0.16 x 0.10 x 0.08 mm ³	
θ range for data collection	2.711 to 31.113°.	
Index ranges	$-20 \leq h \leq 20, -21 \leq k \leq 20, -21 \leq l \leq 21$	
Reflections collected	52379	
Independent reflections	18527 [$R_{int} = 0.0721$]	
Reflections with $I > 2\sigma(I)$	12816	
Completeness to $\theta = 25.242^\circ$	99.9 %	
Absorption correction	Gaussian	
Max. and min. transmission	0.99 and 0.97	
Refinement method	Full-matrix least-squares on F^2	
Data / restraints / parameters	18527 / 0 / 559	
Goodness-of-fit on F^2	1.052	
Final R indices [$I > 2\sigma(I)$]	$R_1 = 0.0649$	$wR^2 = 0.1704$
R indices (all data)	$R_1 = 0.0951$	$wR^2 = 0.1855$
Largest diff. peak and hole	1.1 and -2.1 e · Å ⁻³	

Crystal Data and Structure Refinement of Compound 137d

**Table 1. Crystal data and structure refinement.**

Identification code	8330	
Empirical formula	$C_{25}H_{22}AuBClF_4N_2P$	
Color	colourless	
Formula weight	$700.64 \text{ g} \cdot \text{mol}^{-1}$	
Temperature	100 K	
Wavelength	0.71073 \AA	
Crystal system	MONOCLINIC	
Space group	$P2_1/n$, (no. 14)	
Unit cell dimensions	$a = 9.4334(18) \text{ \AA}$	$\alpha = 90^\circ$.
	$b = 11.215(2) \text{ \AA}$	$\beta = 99.881(19)^\circ$.
	$c = 24.280(6) \text{ \AA}$	$\gamma = 90^\circ$.
Volume	$2530.6(9) \text{ \AA}^3$	
Z	4	
Density (calculated)	$1.839 \text{ Mg} \cdot \text{m}^{-3}$	
Absorption coefficient	6.029 mm^{-1}	
F(000)	1352 e	
Crystal size	$0.40 \times 0.04 \times 0.02 \text{ mm}^3$	
θ range for data collection	2.847 to 30.026° .	
Index ranges	$-13 \leq h \leq 13$, $-15 \leq k \leq 15$, $-34 \leq l \leq 34$	
Reflections collected	43300	
Independent reflections	7381 [$R_{\text{int}} = 0.0787$]	
Reflections with $I > 2\sigma(I)$	5691	
Completeness to $\theta = 25.242^\circ$	99.9 %	
Absorption correction	Gaussian	
Max. and min. transmission	0.95 and 0.85	
Refinement method	Full-matrix least-squares on F^2	
Data / restraints / parameters	7381 / 0 / 317	
Goodness-of-fit on F^2	1.060	
Final R indices [$I > 2\sigma(I)$]	$R_1 = 0.0388$	$wR^2 = 0.0820$
R indices (all data)	$R_1 = 0.0618$	$wR^2 = 0.0923$
Largest diff. peak and hole	2.2 and $-2.5 \text{ e} \cdot \text{\AA}^{-3}$	

Crystal Data and Structure Refinement of Compound 151b

**Table 1. Crystal data and structure refinement.**

Identification code	9100	
Empirical formula	$C_{86}H_{78}B_4Cl_4F_{28}N_7P_4Pd_2$	
Color	colorless	
Formula weight	2263.27 $g \cdot mol^{-1}$	
Temperature	100 K	
Wavelength	0.71073 Å	
Crystal system	HEXAGONAL	
Space group	P 32 2₁, (no. 154)	
Unit cell dimensions	$a = 14.8390(6)$ Å	$\alpha = 90^\circ$
	$b = 14.8390(6)$ Å	$\beta = 90^\circ$
	$c = 37.249(2)$ Å	$\gamma = 120^\circ$
Volume	$7103.1(7)$ Å ³	
Z	3	
Density (calculated)	1.587 $Mg \cdot m^{-3}$	
Absorption coefficient	0.664 mm^{-1}	
F(000)	3405 e	
Crystal size	0.08 x 0.08 x 0.04 mm^3	
θ range for data collection	2.701 to 33.169°.	
Index ranges	$-18 \leq h \leq 22, -22 \leq k \leq 14, -57 \leq l \leq 57$	
Reflections collected	113924	
Independent reflections	18115 [$R_{int} = 0.0631$]	
Reflections with $I > 2\sigma(I)$	13712	
Completeness to $\theta = 25.242^\circ$	99.8 %	
Absorption correction	Gaussian	
Max. and min. transmission	0.97 and 0.93	
Refinement method	Full-matrix least-squares on F^2	
Data / restraints / parameters	18115 / 0 / 619	
Goodness-of-fit on F^2	1.031	
Final R indices [$I > 2\sigma(I)$]	$R_1 = 0.0502$	$wR^2 = 0.1113$
R indices (all data)	$R_1 = 0.0848$	$wR^2 = 0.1275$
Absolute structure parameter	-0.025(7)	
Largest diff. peak and hole	1.0 and -1.6 $e \cdot \text{Å}^{-3}$	

Crystal Data and Structure Refinement of Compound 151c

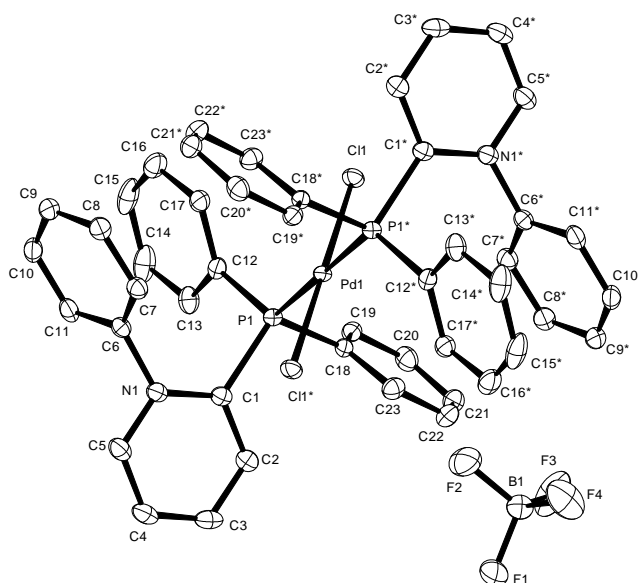
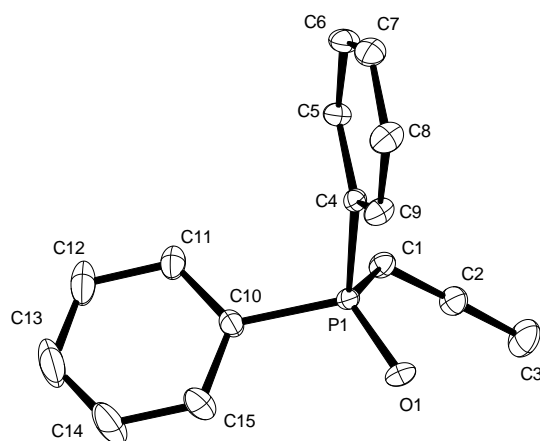


Table 1. Crystal data and structure refinement.

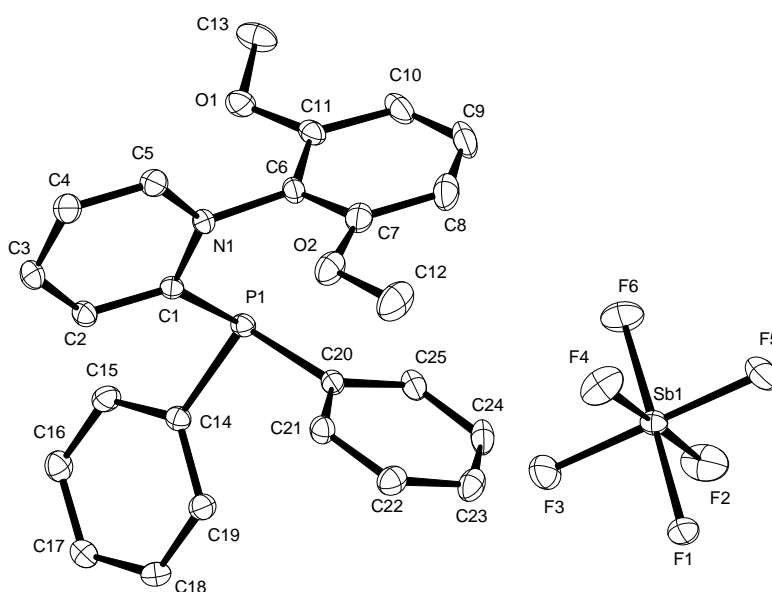
Identification code	8507	
Empirical formula	$C_{46}H_{38}B_2Cl_2F_8N_2P_2Pd$	
Color	yellow	
Formula weight	1031.64 $g \cdot mol^{-1}$	
Temperature	100 K	
Wavelength	0.71073 Å	
Crystal system	MONOCLINIC	
Space group	$P2_1/n$, (no. 14)	
Unit cell dimensions	$a = 10.647(3)$ Å	$\alpha = 90^\circ$.
	$b = 14.190(4)$ Å	$\beta = 106.680(5)^\circ$.
	$c = 14.951(4)$ Å	$\gamma = 90^\circ$.
Volume	$2163.7(10)$ Å ³	
Z	2	
Density (calculated)	1.583 $Mg \cdot m^{-3}$	
Absorption coefficient	0.698 mm^{-1}	
F(000)	1040 e	
Crystal size	0.10 x 0.06 x 0.02 mm^3	
θ range for data collection	2.020 to 29.128°.	
Index ranges	$-14 \leq h \leq 14$, $-18 \leq k \leq 19$, $-20 \leq l \leq 20$	
Reflections collected	55292	
Independent reflections	5682 [$R_{int} = 0.0962$]	
Reflections with $I > 2\sigma(I)$	4342	
Completeness to $\theta = 25.242^\circ$	100.0 %	
Absorption correction	Gaussian	
Max. and min. transmission	0.99 and 0.93	
Refinement method	Full-matrix least-squares on F^2	
Data / restraints / parameters	5682 / 0 / 286	
Goodness-of-fit on F^2	1.058	
Final R indices [$I > 2\sigma(I)$]	$R_1 = 0.0404$	$wR^2 = 0.0725$
R indices (all data)	$R_1 = 0.0662$	$wR^2 = 0.0804$
Largest diff. peak and hole	0.6 and $-0.5 e \cdot \text{Å}^{-3}$	

Crystal Data and Structure Refinement of Compound 161

**Table 1. Crystal data and structure refinement.**

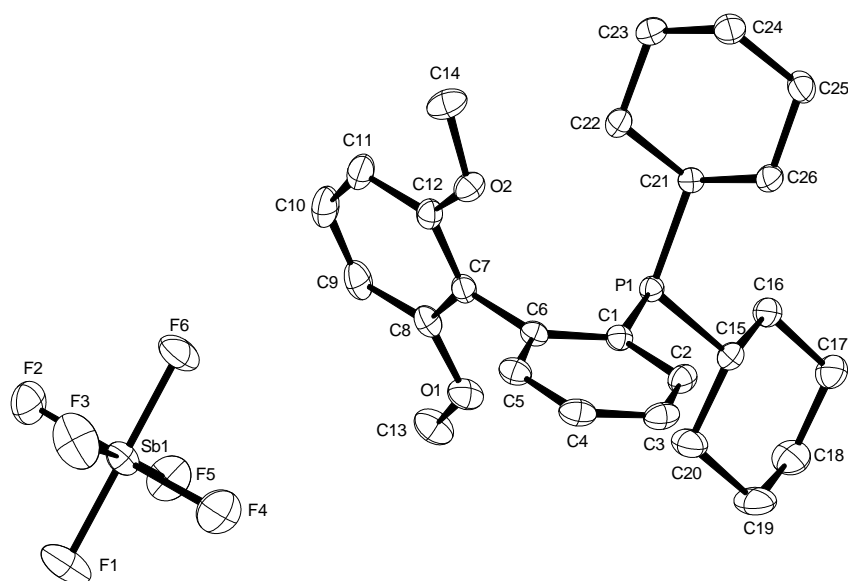
Identification code	8178	
Empirical formula	$C_{15}H_{13}OP$	
Color	colorless	
Formula weight	$240.22 \text{ g} \cdot \text{mol}^{-1}$	
Temperature	100 K	
Wavelength	0.71073 \AA	
Crystal system	MONOCLINIC	
Space group	$P2_1/n$, (no. 14)	
Unit cell dimensions	$a = 8.4948(7) \text{ \AA}$	$\alpha = 90^\circ$.
	$b = 10.5939(9) \text{ \AA}$	$\beta = 97.3440(10)^\circ$.
	$c = 14.6280(13) \text{ \AA}$	$\gamma = 90^\circ$.
Volume	$1305.62(19) \text{ \AA}^3$	
Z	4	
Density (calculated)	$1.222 \text{ Mg} \cdot \text{m}^{-3}$	
Absorption coefficient	0.191 mm^{-1}	
F(000)	504 e	
Crystal size	$0.24 \times 0.18 \times 0.12 \text{ mm}^3$	
θ range for data collection	2.38 to 36.72° .	
Index ranges	$-14 \leq h \leq 14$, $-17 \leq k \leq 17$, $-24 \leq l \leq 24$	
Reflections collected	49009	
Independent reflections	6384 [$R_{\text{int}} = 0.0192$]	
Reflections with $I > 2\sigma(I)$	5834	
Completeness to $\theta = 36.72^\circ$	98.0 %	
Absorption correction	Gaussian	
Max. and min. transmission	0.98 and 0.96	
Refinement method	Full-matrix least-squares on F^2	
Data / restraints / parameters	6384 / 0 / 162	
Goodness-of-fit on F^2	1.044	
Final R indices [$I > 2\sigma(I)$]	$R_1 = 0.0301$	$wR^2 = 0.0897$
R indices (all data)	$R_1 = 0.0331$	$wR^2 = 0.0922$
Largest diff. peak and hole	0.6 and $-0.2 \text{ e} \cdot \text{\AA}^{-3}$	

Crystal Data and Structure Refinement of Compound 190c

**Table 1. Crystal data and structure refinement.**

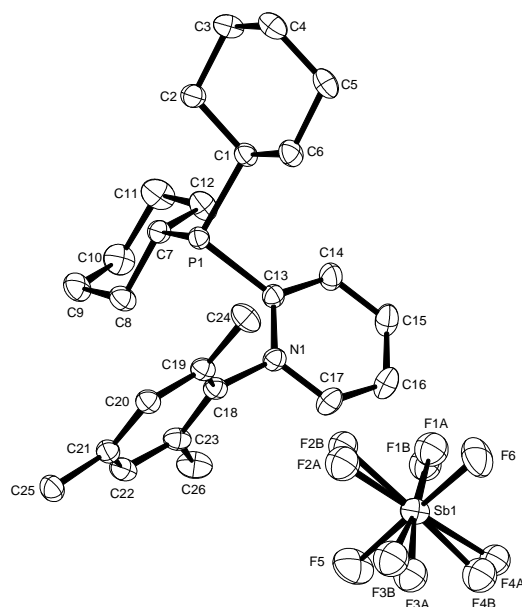
Identification code	9105	
Empirical formula	C ₂₅ H ₂₃ F ₆ N O ₂ P Sb	
Color	yellow	
Formula weight	636.16 g · mol ⁻¹	
Temperature	100 K	
Wavelength	0.71073 Å	
Crystal system	TRICLINIC	
Space group	P1, (no. 2)	
Unit cell dimensions	a = 8.3643(9) Å	α = 91.321(2)°.
	b = 11.8205(13) Å	β = 104.359(2)°.
	c = 13.1583(14) Å	γ = 99.991(2)°.
Volume	1238.2(2) Å ³	
Z	2	
Density (calculated)	1.706 Mg · m ⁻³	
Absorption coefficient	1.248 mm ⁻¹	
F(000)	632 e	
Crystal size	0.27 x 0.08 x 0.02 mm ³	
θ range for data collection	1.601 to 31.145°.	
Index ranges	-12 ≤ h ≤ 12, -17 ≤ k ≤ 17, -19 ≤ l ≤ 19	
Reflections collected	36828	
Independent reflections	7968 [R _{int} = 0.0306]	
Reflections with I > 2σ(I)	7317	
Completeness to θ = 25.242°	100.0 %	
Absorption correction	Gaussian	
Max. and min. transmission	0.98 and 0.79	
Refinement method	Full-matrix least-squares on F ²	
Data / restraints / parameters	7968 / 0 / 327	
Goodness-of-fit on F ²	1.127	
Final R indices [I > 2σ(I)]	R ₁ = 0.0229	wR ² = 0.0572
R indices (all data)	R ₁ = 0.0279	wR ² = 0.0693
Largest diff. peak and hole	0.7 and -0.8 e · Å ⁻³	

Crystal Data and Structure Refinement of Compound 190e

**Table 1. Crystal data and structure refinement.**

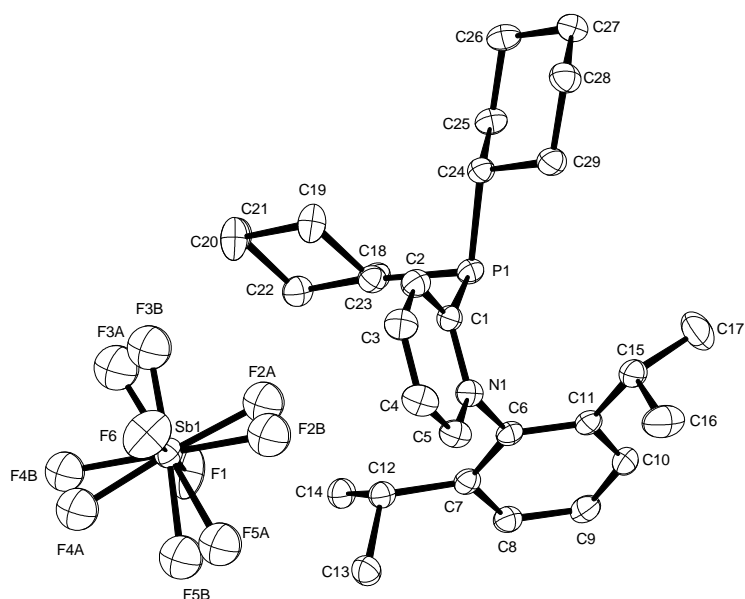
Identification code	9419sadabs	
Empirical formula	C ₂₆ H ₃₆ F ₆ O ₂ P Sb	
Color	yellow	
Formula weight	647.27 g·mol ⁻¹	
Temperature	100 K	
Wavelength	0.71073 Å	
Crystal system	Monoclinic	
Space group	P 1 2 ₁ /c 1, (no. 14)	
Unit cell dimensions	a = 10.6246(7) Å	α = 90°.
	b = 15.9949(10) Å	β = 95.037(8)°.
	c = 16.2938(17) Å	γ = 90°.
Volume	2758.3(4) Å ³	
Z	4	
Density (calculated)	1.559 Mg·m ⁻³	
Absorption coefficient	1.120 mm ⁻¹	
F(000)	1312 e	
Crystal size	0.11 x 0.07 x 0.05 mm ³	
θ range for data collection	2.706 to 33.086°.	
Index ranges	-16 ≤ h ≤ 16, -24 ≤ k ≤ 24, -25 ≤ l ≤ 25	
Reflections collected	86612	
Independent reflections	10448 [R _{int} = 0.0356]	
Reflections with I > 2σ(I)	9314	
Completeness to θ = 25.242°	99.7 %	
Absorption correction	Gaussian	
Max. and min. transmission	0.94895 and 0.89335	
Refinement method	Full-matrix least-squares on F ²	
Data / restraints / parameters	10448 / 0 / 327	
Goodness-of-fit on F ²	1.258	
Final R indices [I > 2σ(I)]	R ₁ = 0.0513	wR ² = 0.1687
R indices (all data)	R ₁ = 0.0584	wR ² = 0.1774
Extinction coefficient	n/a	
Largest diff. peak and hole	1.881 and -2.208 e·Å ⁻³	

Crystal Data and Structure Refinement of Compound 190f

**Table 1. Crystal data and structure refinement.**

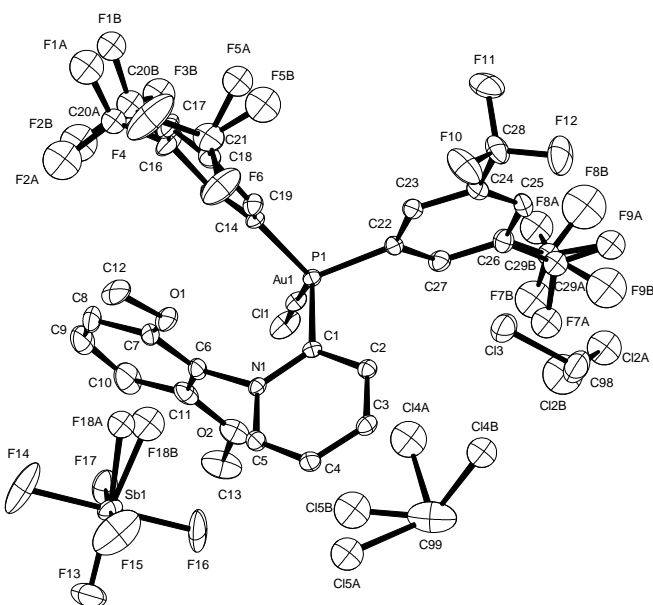
Identification code	9294sadabs	
Empirical formula	C ₂₆ H ₃₇ F ₆ NPSb	
Color	colourless	
Formula weight	630.28 g·mol ⁻¹	
Temperature	423.15 K	
Wavelength	0.71073 Å	
Crystal system	MONOCLINIC	
Space group	P2 ₁ /n, (no. 14)	
Unit cell dimensions	a = 13.8885(9) Å	α = 90°.
	b = 13.3919(6) Å	β = 112.626(6)°.
	c = 15.6069(18) Å	γ = 90°.
Volume	2679.4(4) Å ³	
Z	4	
Density (calculated)	1.562 Mg·m ⁻³	
Absorption coefficient	1.147 mm ⁻¹	
F(000)	1280 e	
Crystal size	0.14 x 0.08 x 0.05 mm ³	
θ range for data collection	2.927 to 35.059°.	
Index ranges	-22 ≤ h ≤ 22, -21 ≤ k ≤ 20, -25 ≤ l ≤ 25	
Reflections collected	56140	
Independent reflections	11816 [R _{int} = 0.0346]	
Reflections with I > 2σ(I)	10182	
Completeness to θ = 25.242°	99.2 %	
Absorption correction	Gaussian	
Max. and min. transmission	0.95096 and 0.87548	
Refinement method	Full-matrix least-squares on F ²	
Data / restraints / parameters	11816 / 0 / 315	
Goodness-of-fit on F ²	1.030	
Final R indices [I > 2σ(I)]	R ₁ = 0.0380	wR ² = 0.0948
R indices (all data)	R ₁ = 0.0458	wR ² = 0.1009
Largest diff. peak and hole	1.198 and -1.755 e·Å ⁻³	

Crystal Data and Structure Refinement of Compound 190h

**Table 1. Crystal data and structure refinement.**

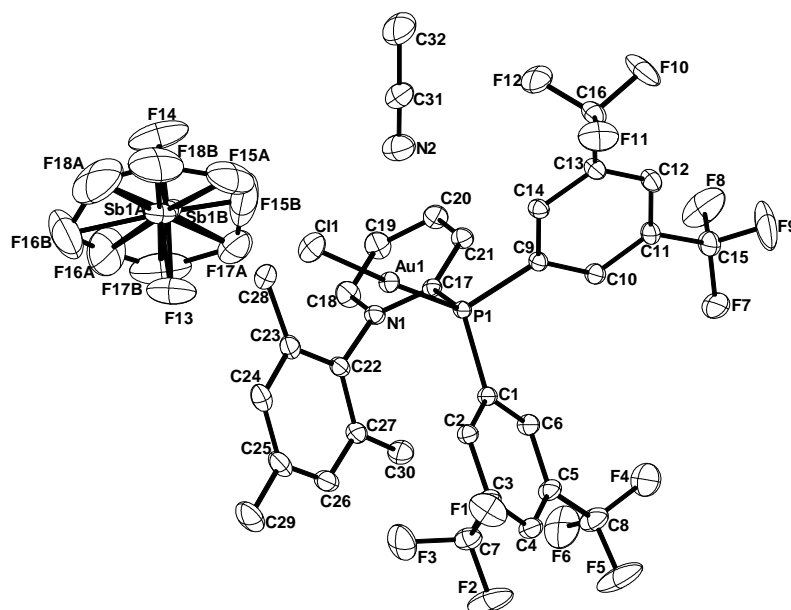
Identification code	9564sadabs	
Empirical formula	C ₂₉ H ₄₃ F ₆ N P Sb	
Color	colourless	
Formula weight	672.36 g·mol ⁻¹	
Temperature	100 K	
Wavelength	1.54178 Å	
Crystal system	ORTHORHOMBIC	
Space group	p b c a, (no. 61)	
Unit cell dimensions	a = 16.4612(8) Å	α = 90°.
	b = 13.7221(7) Å	β = 90°.
	c = 26.8500(13) Å	γ = 90°.
Volume	6064.9(5) Å ³	
Z	8	
Density (calculated)	1.473 Mg·m ⁻³	
Absorption coefficient	8.201 mm ⁻¹	
F(000)	2752 e	
Crystal size	0.59 x 0.30 x 0.16 mm ³	
θ range for data collection	3.292 to 67.520°.	
Index ranges	-19 ≤ h ≤ 19, -15 ≤ k ≤ 16, -32 ≤ l ≤ 32	
Reflections collected	133531	
Independent reflections	5453 [R _{int} = 0.0519]	
Reflections with I > 2σ(I)	5182	
Completeness to θ = 67.520°	99.6 %	
Absorption correction	Gaussian	
Max. and min. transmission	0.36282 and 0.05828	
Refinement method	Full-matrix least-squares on F ²	
Data / restraints / parameters	5453 / 0 / 343	
Goodness-of-fit on F ²	1.048	
Final R indices [I > 2σ(I)]	R ₁ = 0.0339	wR ² = 0.0890
R indices (all data)	R ₁ = 0.0356	wR ² = 0.0908
Extinction coefficient	n/a	
Largest diff. peak and hole	1.246 and -0.864 e·Å ⁻³	

Crystal Data and Structure Refinement of Compound 191a

**Table 1. Crystal data and structure refinement.**

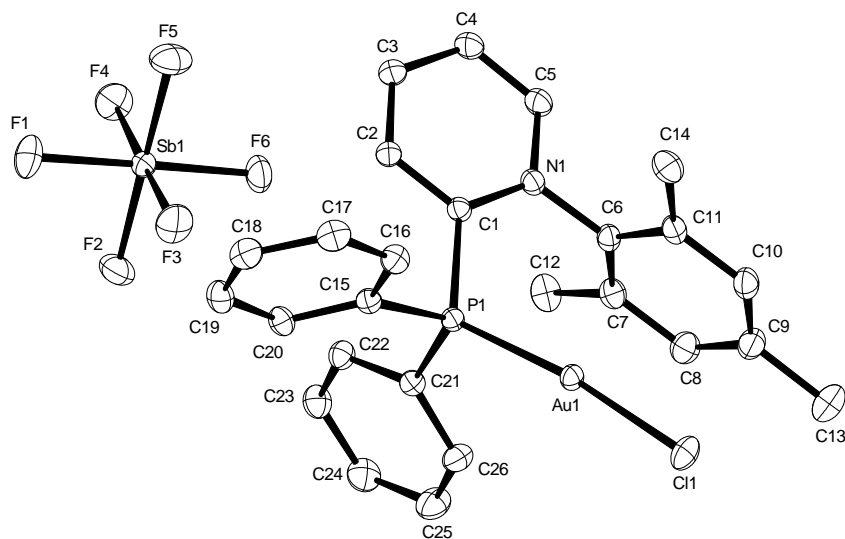
Identification code	8975	
Empirical formula	$C_{31} H_{23} Au Cl_5 F_{18} N O_2 P Sb$	
Color	colorless	
Formula weight	1310.44 $g \cdot mol^{-1}$	
Temperature	100 K	
Wavelength	0.71073 Å	
Crystal system	TRICLINIC	
Space group	P1, (no. 2)	
Unit cell dimensions	$a = 8.9106(12)$ Å	$\alpha = 73.397(2)^\circ$
	$b = 12.9646(17)$ Å	$\beta = 82.399(2)^\circ$
	$c = 19.744(3)$ Å	$\gamma = 85.849(2)^\circ$
Volume	$2165.1(5)$ Å ³	
Z	2	
Density (calculated)	2.010 $Mg \cdot m^{-3}$	
Absorption coefficient	4.462 mm^{-1}	
F(000)	1248 e	
Crystal size	0.22 x 0.10 x 0.07 mm^3	
θ range for data collection	1.084 to 30.507°	
Index ranges	$-12 \leq h \leq 12, -18 \leq k \leq 18, -28 \leq l \leq 28$	
Reflections collected	60001	
Independent reflections	13209 [$R_{int} = 0.0416$]	
Reflections with $I > 2\sigma(I)$	12312	
Completeness to $\theta = 25.242^\circ$	99.7 %	
Absorption correction	Gaussian	
Max. and min. transmission	0.64 and 0.20	
Refinement method	Full-matrix least-squares on F^2	
Data / restraints / parameters	13209 / 3 / 530	
Goodness-of-fit on F^2	1.120	
Final R indices [$I > 2\sigma(I)$]	$R_1 = 0.0546$	$wR^2 = 0.1266$
R indices (all data)	$R_1 = 0.0584$	$wR^2 = 0.1283$
Largest diff. peak and hole	3.2 and -3.2 $e \cdot \text{Å}^{-3}$	

Crystal Data and Structure Refinement of Compound 191b

**Table 1. Crystal data and structure refinement.**

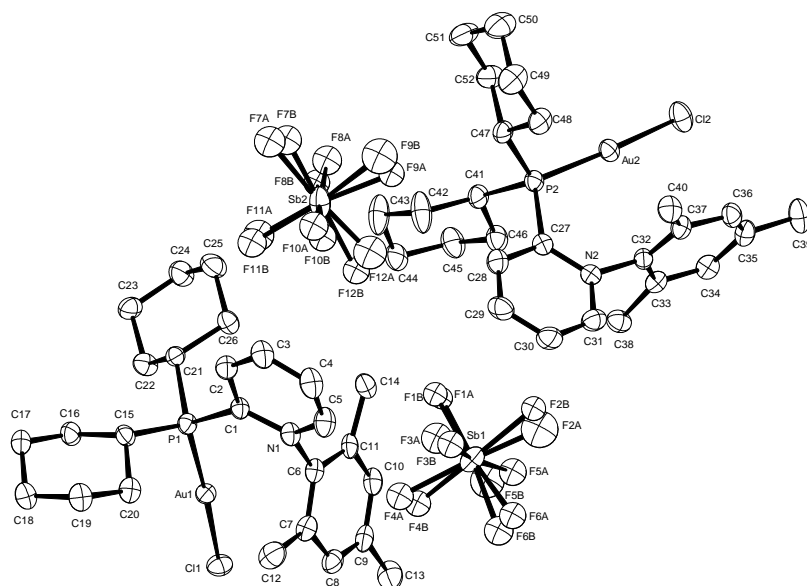
Identification code	8893sadabs	
Empirical formula	$C_{32} H_{24} Au Cl F_{18} N_2 P Sb$	
Color	colourless	
Formula weight	1163.67 g·mol ⁻¹	
Temperature	100.15 K	
Wavelength	0.71073 Å	
Crystal system	MONOCLINIC	
Space group	p 2 ₁ /n, (no. 14)	
Unit cell dimensions	a = 8.7962(6) Å	$\alpha = 90^\circ$.
	b = 27.1915(18) Å	$\beta = 103.535(9)^\circ$.
	c = 16.0760(14) Å	$\gamma = 90^\circ$.
Volume	3738.3(5) Å ³	
Z	4	
Density (calculated)	2.068 Mg·m ⁻³	
Absorption coefficient	4.875 mm ⁻¹	
F(000)	2216 e	
Crystal size	0.22 x 0.07 x 0.06 mm ³	
θ range for data collection	2.712 to 33.184°.	
Index ranges	-13 ≤ h ≤ 13, -41 ≤ k ≤ 41, -24 ≤ l ≤ 24	
Reflections collected	111778	
Independent reflections	14268 [$R_{int} = 0.0394$]	
Reflections with $I > 2\sigma(I)$	12884	
Completeness to $\theta = 25.242^\circ$	99.8 %	
Absorption correction	Gaussian	
Max. and min. transmission	0.76040 and 0.44907	
Refinement method	Full-matrix least-squares on F^2	
Data / restraints / parameters	14268 / 90 / 555	
Goodness-of-fit on F^2	1.110	
Final R indices [$I > 2\sigma(I)$]	$R_1 = 0.0252$	$wR^2 = 0.0601$
R indices (all data)	$R_1 = 0.0307$	$wR^2 = 0.0633$
Extinction coefficient	n/a	
Largest diff. peak and hole	1.037 and -1.904 e·Å ⁻³	

Crystal Data and Structure Refinement of Compound 191d

**Table 1. Crystal data and structure refinement.**

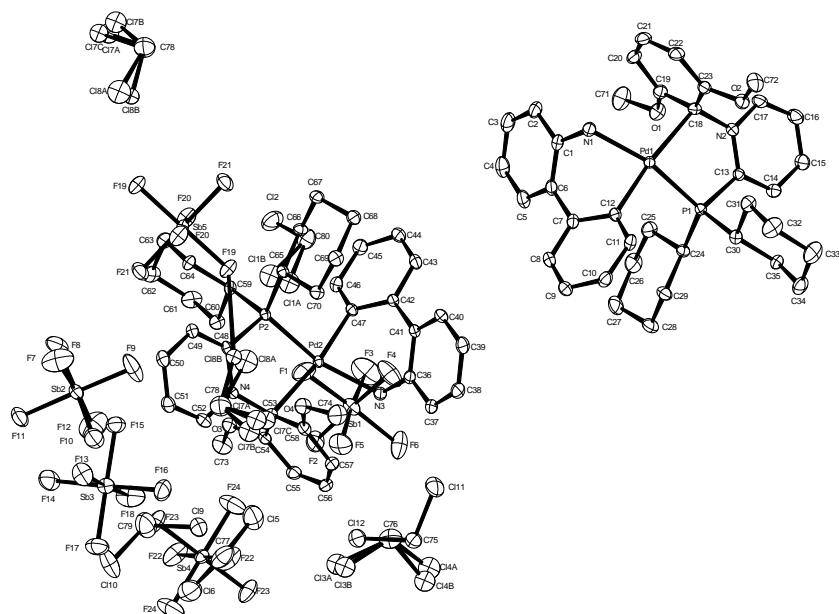
Identification code	8745A	
Empirical formula	$C_{26}H_{25}AuClF_6NP Sb$	
Color	colorless	
Formula weight	850.60 $g \cdot mol^{-1}$	
Temperature	100 K	
Wavelength	0.71073 Å	
Crystal system	TRICLINIC	
Space group	P1, (no. 2)	
Unit cell dimensions	$a = 10.0040(4)$ Å	$\alpha = 107.808(3)^\circ$.
	$b = 10.1489(4)$ Å	$\beta = 92.182(4)^\circ$.
	$c = 15.7193(9)$ Å	$\gamma = 112.364(3)^\circ$.
Volume	$1383.44(12)$ Å ³	
Z	2	
Density (calculated)	2.042 $Mg \cdot m^{-3}$	
Absorption coefficient	6.484 mm^{-1}	
F(000)	808 e	
Crystal size	0.13 x 0.10 x 0.06 mm^3	
θ range for data collection	2.765 to 36.026°.	
Index ranges	-16 ≤ h ≤ 16, -16 ≤ k ≤ 16, -25 ≤ l ≤ 25	
Reflections collected	69067	
Independent reflections	13039 [$R_{int} = 0.0246$]	
Reflections with $I > 2\sigma(I)$	12743	
Completeness to $\theta = 25.242^\circ$	98.4 %	
Absorption correction	Gaussian	
Max. and min. transmission	0.69 and 0.49	
Refinement method	Full-matrix least-squares on F^2	
Data / restraints / parameters	13039 / 0 / 337	
Goodness-of-fit on F^2	1.092	
Final R indices [$I > 2\sigma(I)$]	$R_1 = 0.0143$	$wR^2 = 0.0359$
R indices (all data)	$R_1 = 0.0154$	$wR^2 = 0.0365$
Largest diff. peak and hole	0.9 and -1.4 $e \cdot \text{Å}^{-3}$	

Crystal Data and Structure Refinement of Compound 191f

**Table 1. Crystal data and structure refinement.**

Identification code	9727sadabs	
Empirical formula	$C_{26}H_{37}AuClF_6NP_2Sb_2$	
Color	colourless	
Formula weight	862.70 $g \cdot mol^{-1}$	
Temperature	150 K	
Wavelength	0.71073 Å	
Crystal system	TRICLINIC	
Space group	$p-1$, (no. 2)	
Unit cell dimensions	$a = 10.6409(9)$ Å	$\alpha = 82.428(8)^\circ$
	$b = 16.737(2)$ Å	$\beta = 84.084(5)^\circ$
	$c = 17.0626(14)$ Å	$\gamma = 87.346(9)^\circ$
Volume	$2994.5(5)$ Å ³	
Z	4	
Density (calculated)	1.914 $Mg \cdot m^{-3}$	
Absorption coefficient	5.992 mm^{-1}	
F(000)	1664 e	
Crystal size	0.10 x 0.02 x 0.02 mm ³	
θ range for data collection	2.942 to 33.149°	
Index ranges	$-16 \leq h \leq 16$, $-25 \leq k \leq 25$, $-26 \leq l \leq 26$	
Reflections collected	80573	
Independent reflections	22772 [$R_{int} = 0.0760$]	
Reflections with $I > 2\sigma(I)$	16411	
Completeness to $\theta = 25.242^\circ$	99.8 %	
Absorption correction	Gaussian	
Max. and min. transmission	0.7155 and 0.3886	
Refinement method	Full-matrix least-squares on F^2	
Data / restraints / parameters	22772 / 0 / 661	
Goodness-of-fit on F^2	1.049	
Final R indices [$I > 2\sigma(I)$]	$R_1 = 0.0587$	$wR^2 = 0.1378$
R indices (all data)	$R_1 = 0.0899$	$wR^2 = 0.1562$
Extinction coefficient	n/a	
Largest diff. peak and hole	3.876 and -5.354 $e \cdot \text{Å}^{-3}$	

Crystal Data and Structure Refinement of Compound 196

**Table 1. Crystal data and structure refinement.**

Identification code	9360sadabs	
Empirical formula	$C_{40}H_{51}C_{16}F_{12}N_2O_2PPdSb_2$	
Color	yellow	
Formula weight	1413.40 g·mol ⁻¹	
Temperature	100 K	
Wavelength	0.71073 Å	
Crystal system	TRICLINIC	
Space group	p -1, (no. 2)	
Unit cell dimensions	a = 12.4480(19) Å	$\alpha = 98.570(3)^\circ$.
	b = 20.240(3) Å	$\beta = 94.337(3)^\circ$.
	c = 20.871(3) Å	$\gamma = 99.482(3)^\circ$.
Volume	5101.6(13) Å ³	
Z	4	
Density (calculated)	1.840 Mg·m ⁻³	
Absorption coefficient	1.826 mm ⁻¹	
F(000)	2776 e	
Crystal size	0.34 x 0.06 x 0.06 mm ³	
θ range for data collection	0.992 to 31.125°.	
Index ranges	-18 ≤ h ≤ 18, -29 ≤ k ≤ 29, -30 ≤ l ≤ 30	
Reflections collected	152306	
Independent reflections	32752 [$R_{int} = 0.0462$]	
Reflections with $I > 2\sigma(I)$	25368	
Completeness to $\theta = 25.242^\circ$	100.0 %	
Absorption correction	Gaussian	
Max. and min. transmission	0.93095 and 0.70139	
Refinement method	Full-matrix least-squares on F^2	
Data / restraints / parameters	32752 / 0 / 1195	
Goodness-of-fit on F^2	1.039	
Final R indices [$I > 2\sigma(I)$]	$R_1 = 0.0421$	$wR^2 = 0.1103$
R indices (all data)	$R_1 = 0.0631$	$wR^2 = 0.1262$
Extinction coefficient	n/a	
Largest diff. peak and hole	2.843 and -1.856 e·Å ⁻³	

Curriculum Vitae

Address: Sudetenweg 4d, 59065 Hamm, Germany

Areas of Interests:

Development and Improvement of Synthetic Methods, Catalyst Design, Total Synthesis

Education:

- 01/2016-11/2017 Georg-August-Universität, Göttingen, Germany
Degree: Dr. rer. nat. (finished)
Major: Metal Organic Chemistry
- 01/2015-12/2015 Max-Planck-Institut für Kohlenforschung, Mülheim, Germany
Major: X-Ray crystallography
- 11/2012-12/2015 Max-Planck-Institut für Kohlenforschung, Mülheim, Germany
Degree: Dr. rer. nat. (started)
Major: Metal organic Chemistry
- 09/2010- 09/2012 Technische Universität Dortmund, Germany
Degree: Master of Science
Major: Organic Chemistry
- 09/2007- 09/2010 Technische Universität Dortmund, Deutschland
Degree: Bachelor of Science
Major: Organic Chemistry

Academic Experience

Metal Organic Chemistry, Georg-August-Universität, Göttingen, Germany (Advisor: Prof. Alcarazo) and Max-Planck-Institut für Kohlenforschung, Mülheim, Germany (Advisor: Prof. Fürstner with Prof. Alcarazo)

- 11/2012-11/2016 ***Design, Synthesis and Applications of New Cationic Ligands of the 15th Main Group Elements***
- *Design, Synthesis and Applications of Pyridinium Based Phosphine Ligands*
 - *Single Crystal Structure Determination*

Organic Chemistry, Technische Universität Dortmund, Germany
(Advisor: Prof. Hiersemann)

09/2010- 09/2012 **To the Development of an Asymmetric Catalytic Kojic Acid Claisen Rearrangement**

- *μwave assisted or catalytic vinylogous Gosteli Claisen Rearrangement*

09/2007- 09/2010 **To the Total Synthesis of Menverin C and F**

- *intramolecular thermal Carbonyl En Reaction for the Synthesis of a Cyclopentane Fragment*

Publications

- "Synthesis and reactivity of α -cationic phosphines: the effect of imidazolium and amidinium substituents", E. Haldón, Á. Kozma, H. Tinnermann, L. Gu, R. Goddard, M. Alcarazo, *Dalton Trans.* **2016**, **45**, 1872.
- "Synthesis, Structure, and Applications of Pyridiniophosphines", H. Tinnermann, C. Wille, M. Alcarazo, *Angew. Chem. Int. Ed.* **2014**, **33**, 8732.
- "Synthese, Struktur und Anwendungen von Pyridiniumphosphanen", H. Tinnermann, C. Wille, M. Alcarazo, *Angew. Chem.* **2014**, **33**, 8877.

Technical Skills

- Mastered the Operation of MS, NMR, HPLC, GC, TLC, IR, UV, XRAY, CV
- Mastered the Procedures of Organic, Inorganic Synthesis and Schlenk Techniques
- Highly Proficient in Reading and Writing Research Paper in English

Personality

Responsible, Motivated, Cooperative, Conscientious

Hamm, 05.12.2017

Hendrik Tinnermann